TESIS DE LA UNIVERSIDAD DE ZARAGOZA

2023 237

Zainab Afailal

Exploring thermochemical routes for argan shells valorization

http://zaguan.unizar.es/collection/Tesis

Director/es
Sánchez Cebrián, José Luis
Gil Lalaguna, Noemí

ISSN 2254-7606

Prensas de la Universidad
Universidad Zaragoza

© Universidad de Zaragoza
Servicio de Publicaciones

ISSN 2254-7606

Universidad Zaragoza
1542

Tesis Doctoral

EXPLORING THERMOCHEMICAL ROUTES FOR ARGAN SHELLS VALORIZATION

Autor

Zainab Afailal

Director/es

Sánchez Cebrián, José Luis
Gil Lalaguna, Noemí

UNIVERSIDAD DE ZARAGOZA
Escuela de Doctorado

Programa de Doctorado en Ingeniería Química y del Medio Ambiente

2023

Repositorio de la Universidad de Zaragoza – Zaguan http://zaguan.unizar.es

Universidad Zaragoza

EXPLORING THERMOCHEMICAL ROUTES FOR ARGAN SHELLS VALORIZATION

Zainab Afailal

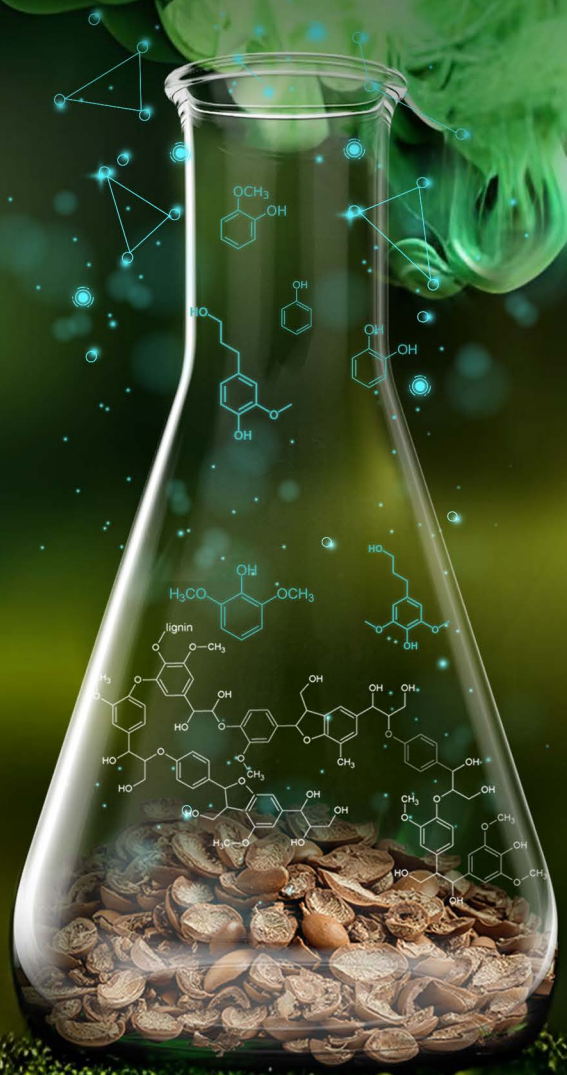

2023

Supervisors:

Dr. Noemí Gil Lalaguna / Dr. José Luis Sánchez Cebrián

Departamento de Ingeniería
Química y Tecnologías
del Medio Ambiente
Universidad Zaragoza

EXPLORING THERMOCHEMICAL ROUTES FOR ARGAN SHELLS VALORIZATION

This dissertation is presented to the Department of Chemical Engineering and Environmental Technologies at the University of Zaragoza, Spain, to qualify for the degree of Doctor.

Zainab Afailal

Supervisors
Dr. Noemí Gil Lalaguna
Dr. José Luis Sánchez Cebrián

Zaragoza, 2023

To my family

To Rachida

To those who supported me unconditionally in the most difficult moments

D. José Luis Sánchez Cebrián, Catedrático de Universidad, y **Dña. Noemí Gil Lalaguna**, Profesora Ayudante Doctor, ambos pertenecientes al Departamento de Ingeniería Química y Tecnologías del Medio Ambiente de la Universidad de Zaragoza,

INFORMAN

Que la presente memoria titulada:

EXPLORING THERMOCHEMICAL ROUTES FOR ARGAN SHELLS VALORIZATION

ha sido realizada bajo nuestra supervisión en el Grupo de Procesos Termoquímicos perteneciente al Instituto de Investigación en Ingeniería de Aragón (I3A), y en el Departamento de Ingeniería Química y Tecnologías del Medio Ambiente de la Universidad de Zaragoza, por **Dña. Zainab Afailal** y **AUTORIZAN** su presentación con la mención internacional en el título de Doctor, cumpliendo con las condiciones requeridas para que su autora pueda optar al grado de Doctor en el Programa de Doctorado de Ingeniería Química y del Medio Ambiente de la Universidad de Zaragoza.

Y para que así conste, lo firmamos en Zaragoza a 14 de abril de 2023.

D. José Luis Sánchez Cebrián

Dña. Noemí Gil Lalaguna

Professor **José Luis Sánchez Cebrián** and Assistant Professor **Noemí Gil Lalaguna**, both belonging to the Department of Chemical and Environmental Engineering of the University of Zaragoza,

REPORT that:

The Doctoral Thesis entitled:

EXPLORING THERMOCHEMICAL ROUTES FOR ARGAN SHELLS VALORIZATION

has been carried out under our supervision in the Thermo-Chemical Processes Group belonging to the Aragón Institute of Engineering Research (I3A), and in the Department of Chemical and Environmental Engineering of the University of Zaragoza, by **Ms. Zainab Afailal**, and we **AUTHORIZE and APPROVE** the presentation of this dissertation with the international citation on the doctoral certificate, fulfilling the requirements for the degree of Doctor.

And for the record, we sign this document in Zaragoza on 14th April 2023.

Dr. José Luis Sánchez Cebrián

Dr. Noemí Gil Lalaguna

قال رسول الله صلى الله عليه وسلم :

"لا يَشْكُرُ اللهَ مَنْ لا يَشْكُرُ النَّاسَ".

"Who is not grateful to people, is not grateful to Allah"

Prophet Muhammad peace be upon him .

Acknowledgments. شكر وعرفان Agradecimientos.

Siempre veía tan lejano llegar a escribir estas líneas y finalmente llegó el momento tan esperado.

Realizar una tesis doctoral no es nunca un trabajo individual y la presente tesis no hubiera sido posible sin el apoyo de muchas personas a las que quisiera mostrar mi agradecimiento.

En primer lugar, quiero dar mi más sincero agradecimiento a mis directores, la Dra. Noemí Gil Lalaguna y el Dr. José Luis Sánchez Cebrián, por su asesoría, paciencia y dedicación absoluta durante estos años; sin sus conocimientos y guías no hubiera sido posible que esta tesis saliera adelante. Además del aporte científico, quiero agradecer a Noe por ser una maravillosa amiga y hermana y a JL por su apoyo en los momentos más difíciles. Muchísimas gracias a los mejores jefes que he tenido en mi vida.

Quisiera igualmente mencionar a dos personas que tienen un lugar muy especial en mi corazón, el "*Bigboss*" Dr. Jesús Arauzo y mi Mami zaragozana la Dra. Ángela Millera, que desde mi primera llegada a Zaragoza me rodearon de cariño y amor. Recordando mi llegada a Zaragoza, quiero también dar las gracias al Dr. Alberto Gonzalo, quien me abrió las puertas y los brazos del GPT para hacer una estancia de investigación, que se pudo llevar a cabo gracias a la ayuda y los ánimos de mi primera "Jefamiga" la Dra. Isabel Fonts y de mi tutora la Dra. Gloria Gea. Lo que inicialmente iba a ser una estancia breve de investigación se fue alargando y ha terminado siendo una tesis doctoral.

Antes de cruzar el estrecho, quiero agradecer a todos los miembros de la familia "GPTiana", liderada por el profesor Dr. Rafael Bilbao. Gracias por vuestra amorosa acogida y apoyo incondicional, gracias por esos cafecitos y salidas inolvidables, gracias por animarme a hablar y aprender el castellano; a Olga, José Antonio, Javi, Lorena, María Ab., María At., Alicia, Maribeni, Uxue y Joaquín. También quiero dar las gracias a mis chicas del despacho africano, Rachel y África. Siempre he contado y contaré con vuestro apoyo vaya donde vaya.

I would also like to thank the researchers at the chemical and biochemical engineering department at the Technical University of Denmark for their welcome during the months of mobility. In particular, I thank Professor Dr. Anker Degn Jensen for his

advice and help. It was a real pleasure working under your supervision Anker, Tusind Tak.

Asimismo, quisiera dar las gracias al Dr. Alfonso Cornejo, de la Universidad Pública de Navarra, por su amabilidad y por su aporte científico en esta tesis.

No quiero olvidarme de dar las gracias a Pilar Borrajo, personal de administración y servicios de la universidad, por ayudarme con todo el tema del papeleo y de extranjería.

وأخيرا أعود إلى الضفة الجنوبية للمتوسط ، كي أقدم أسمى عبارات الإمتنان لمن لا ولن توفيهم كل كلمات الحب قدرهم :

إلى من لم ينضب معين دعائها يوما إلى عائشة أمي . و إلى الأب الفخور دائما ، عبد السلام .

إلى سندي أخي عمر ، وإلى قدوتي أختي حفصة ، كذلك إخوتي التي لم تلدهم أمي إنصاف وعبد العظيم .

إلى مصدر السعادة في حياتي ، يوسف وعالية و أمين وعايدة .

وإلى كل أفراد عائلتي . شكرا لكم وأتمنى أن أكون دائما مصدرا لفخركم .

شكرا خالتو خديجة .

شكر خاص للصديق مولاي ادريس الدباغ على ماقدمه لي من مساعدة ، وكذلك جزيل الشكر لكل ولوعي الموسيقى الأندلسية على حبهم ، فخرهم ودعمهم .

شكرا لمن أجدهم بجانبي دائما أصدقائي : عماد ، العربي ، عماد ، نجد ، بنيس ، د . عزيز ، Tunca and Sara .

Quisiera dar las gracias a mi amigo Imad Azaouyat por el diseño de la portada de esta tesis.

Por último, quisiera agradecer a todas aquellas personas que me apoyaron y que no pude nombrar.

شكرا جزيلا

Muchísimas gracias

Thank you very much

Tak rigtig meget

çok teşekkür ederim

ACRONYMS

I3A	Aragón Institute of Engineering Research.
GPT	Thermochemical Processes Group.
CHEC	Center for Combustion and Harmful Emission Control.
DTU	Technical University of Denmark.
MINECO	Spanish Ministry of Economic Affairs.
AbFINE	Advanced bioFuels with Integrated Negative Emissions.
JCR	Journal of Citation Reports.
AS	Argan Shells.
P	Pine forest residues.
WS	Wheat Straw.
RCF	Reductive Catalytic Fractionation.
HHV	Higher Heating Value.
DCM	Dichloromethane.
ICP-MS	Inductively Coupled Plasma combined with a Mass Spectrometer.
GC/MS	Gas Chromatograph–Mass Spectrometer.
TGA	Thermogravimetric analysis.
DTG	Derivative thermogravimetry.
ATR-FTIR	Attenuated Total Reflection-Fourier Transform Infra-Red.
GC	Gas Chromatography.
FID	Flame Ionization Detector.
MSD	Mass Selective Detector.
ECN	Effective Carbon Numbers.
STP	Standard Temperature and Pressure.
TP220	Torrefied Pine at 220 °C.
TP250	Torrefied Pine at 250 °C.
TAS220	Torrefied Argan Shells at 220 °C.
TAS250	Torrefied Argan Shells at 250 °C.
PAHs	Polycyclic Aromatic Hydrocarbons.
S/C	Steam to Carbon mass ratio.
ER	Equivalent Ratio.
WGS	Water-Gas Shift.
LHV	Lower heating value.
HT	Hydrothermal Treatment.
OXY	Oxidation time.
ΔOXY	Oxidation stability improvement rate.
$Char_{AS}$	Biochar obtained from AS pyrolysis at 450 °C.
AC	Activated Carbon.
AC90	Activated Carbon obtained after 90 min of activation.
AC120	Activated Carbon obtained after 120 min of activation.
AC150	Activated Carbon obtained after 150 min of activation.
BET	Brunauer, Emmett and Teller theory.
NLDFT	Non-Local Density Functional Theory.
FESEM	Field Emission Scanning Electron Microscope.
MB	Methylene Blue.
IUPAC	International Union of Pure and Applied Chemistry.
BHT	butylated hydroxytoluene.
TBHQ	tert-butyl hydroxyquinone.
BHA	3-tert-butyl-4-hydroxyanisole.
ASL_f	Lignin-rich fraction from argan shells.

GPC or SEC	Gel Permeation Chromatography or Size Exclusion Chromatography.
ANOVA	Analysis of variance.
OP	Organic Phase.
BKF	2,2′-Methylenbis(4-methyl-6-tert-butylphenol.
BSO	n-butanol-soluble oil.
RAP	Remaining in the aqueous phase.
EAP	Extracted from aqueous phase.
MSO	Methanol-soluble oil.
NMR	Nuclear Magnetic Resonance spectroscopy.
FAME	Fatty Acids Methyl Esters.
THF	tetrahydrofuran.
RID	Refractive Index Detector.
DMSO-d_6	Dimethyl sulfoxide-d6.
HSQC	Heteronuclear Single Quantum Coherence spectroscopy.
HSQC-TOCSY	Heteronuclear Single Quantum Coherence-Total Correlation spectroscopy.
PrOH-G	4-n-propanolguaiacol.
PrOH-S	4-n-propanolsyringol.
G	Guaiacol
S	Syringol.
DOSY-NMR	Diffusion-ordered NMR spectroscopy.
PS	Polystyrene.
PEGP	Polyethylene glycol and monomeric phenols.
LCA	Life Cycle Assessment.
PCS	Poder Calorífico Superior
PCI	Poder Calorífico Inferior
FCR	Fraccionamiento Catalítico Reductivo

TABLE OF CONTENT

PREFACE 1
PRÓLOGO 7
1. INTRODUCTION 15
1.1. Argania 15
1.2. General objectives and motivations 18
1.3. Thermochemical conversion of biomass 22
1.4. Lignocellulosic biomass 22
2. MATERIALS AND CHARACTERIZATION METHODS 27
2.1. Argan shells 27
2.2. Forest pine residues 34
2.3. Wheat straw 37
3. TORREFACTION 43
3.1. Introduction 43
3.2. Experimental method 44
3.3. Results and discussion 47
3.4. Conclusions 56
4. GASIFICATION 61
4.1. Introduction 61
4.2. Experimental methods 63
4.3. Results and discussion 66
4.4. Conclusions 80
5. PYROLYSIS 85
5.1. Introduction 85
5.2. Experimental methods 87
5.3. Results and discussion 91
5.4. Conclusions 102
6. ACTIVATION 107
6.1. Introduction 107
6.2. Experimental methods 108
6.3. Results and discussion 110
6.4. Conclusions 119
7. HYDROTHERMAL TREATMENT 123
7.1. Introduction 123
7.2. Experimental methods 126
7.3. Results and discussion 131
7.4. Conclusions 154

8. REDUCTIVE CATALYTIC FRACTIONATION 159
8.1. Introduction 159
8.2. Experimental methods 161
8.3. Results and discussion 165
8.4. Conclusions 195
SUMMARY, CONCLUSIONS AND FUTURE WORK 199
RESUMEN Y TRABAJOS FUTUROS 203
REFERENCES 211
APPENDIX I: PUBLICATIONS. 227
APPENDIX II: Complementary information of Chapter 2. 262
APPENDIX III: Complementary information of Chapter 3 265
APPENDIX IV: Complementary information of Chapter 4. 269
APPENDIX V: Complementary information of Chapter 5. 270
APPENDIX VI: Complementary information of Chapter 7. 271
APPENDIX VII: Complementary information of Chapter 8. 273

LIST OF FIGURES

Figure 1.1. Argan tree (region of Essaouira, Morocco) (own photography). 15
Figure 1.2. Components of the whole argan nut. 16
Figure 1.3. Goats feeding from an Argan tree (own photography). 16
Figure 1.4. Shells from argan nut in the entrances of some argan cooperatives (Essaouira, Morocco) (own photography). 18
Figure 1.5. Summary of the studies developed in this work. 21
Figure 1.6. Composition of the macro-components of the lignocellulosic biomass. 24
Figure 2.1. Organic compounds identified in the extractives from AS: (1) Vanillin; (2) n-Hexadecanoic acid; (3) Oleic acid; (4) Oleic acid amide; (5) cis-13-Docosenamide; (6) 3β-acetoxyolean-12-en-27-oic acid; (7) Lupenyl acetate. 31
Figure 2.2. TGA-DTA thermograms of AS (a) N_2 atmosphere, (b) air atmosphere. 33
Figure 2.3. FT-IR spectra of AS. 34
Figure 2.4. Organic compounds identified in the extractives from P: (1) 2-pentadecanone; (2) n-hexadecanoic acid; (3) 9-octadecenamide; (4) heptadecane; (5) trans-3,5-dimethoxystilbene; (6) methyl dehydroabietate; (7) 4'-methoxy-2-hydroxystilbene; (8) dehydroabietic acid; (9) 7-oxodehydroabietic acid, methyl ester; (10) cis-13-docosenamide; (11) β-saccharostenone; (12) Stigmast-4-en-3-one, (24S); (13) β-Sitosterol. 35
Figure 2.5. TGA-DTA thermograms of P (a); N_2 atmosphere (b); air atmosphere. 36
Figure 2.6. FT-IR spectra of P. 37
Figure 2.7. Organic compounds identified in the extractives from WS: (1) hexahydrofarnesyl acetone; (2) 2-heptadecanone, (3) n-hexadecanoic acid; (4) cis-9-octadecenamide; (5) hexacosane; (6) octacosane; (7) cis-13-docosenamide; (8) octacosanal; (9) 14,16-hentriacontanedione. 38
Figure 2.8. TGA-DTG thermograms of WS (a); N_2 atmosphere (b); air atmosphere. .. 39
Figure 2.9. FT-IR spectra of WS. 39
Figure 3.1. Diagram of the experimental torrefaction setup. 45
Figure 3.2. Schematic flowsheet of mass (M) balance and approach to energy (E) balance in the torrefaction processes of AS and P at 220 °C (A) and 250 °C (B). 48
Figure 3.3. Appearance of AS and P before and after the torrefaction at 220 °C and 250 °C. 49
Figure 3.4. DTG plots of AS and P before and after the torrefaction at 220 °C and 250 °C. 53
Figure 3.5. FTIR spectra of AS and P before and after the torrefaction at 220 °C and 250 °C. 54
Figure 4.1. Diagram of the experimental gasification setup. 64
Figure 4.2. General view of AS, P, TAS220 and TAS250 gasification simulation results. 68
Figure 4.3. Theoretical production of $CO+H_2$ (red surface) and CO_2 (blue surface) at different temperatures and S/C ratios for the gasification of: AS (A), P (B), TAS220 (C) and TAS250 (D). 70
Figure 4.4. Theoretical and experimental concentrations of H_2, CO, CO_2 and CH_4 (vol.%) in the gasification gas. 76
Figure 4.5. Theoretical and experimental LHV of the syngas (MJ/m^3_{STP}). 77
Figure 5.1. Diagram of the experimental pyrolysis setup. 88
Figure 5.2. Diagram of the experimental hydrothermal treatment setup. 89
Figure 5.3. Gas composition from pyrolysis of AS and WS. 94
Figure 5.4. Additive yields produced from AS and WS bio-oils. 96

Figure 5.5. Concentration of the phenolic monomers in the additives produced from AS and WS bio-oils. 99
Figure 5.6. OXY time and real dosage of the additives produced from AS and WS bio-oils. 100
Figure 5.7. Improvement of oxidation stability of biodiesel dopped by additives produced from AS and WS bio-oils. 101
Figure 6.1. Diagram of the experimental for physical activation setup..... 108
Figure 6.2. N_2 isotherm at 77 K (adsorption/desorption branches) of the activated carbons produced from argan shells biochar..... 113
Figure 6.3. Pore size distribution determined from N_2 adsorption isotherms using NLDFT calculations. 114
Figure 6.4. Pore size distribution determined for AC120 from CO_2 adsorption isotherm using NLDFT calculations with a slit pore model (the fitting error between the model and the sample was 1.7 %). 115
Figure 6.5. FESEM micrograph of the biochar before and after CO_2-activation during 120 min. 116
Figure 6.6. Boehm titration for the AC150. 116
Figure 6.7. Retention capacities of different compounds for the activated carbons prepared from argan shells biochar: (a) adsorption of methylene blue and (b) adsorption of phenolic compounds..... 118
Figure 6.8. Methylene blue adsorption. 119
Figure 7.1. Diagram of the experimental semi-chemical pulping setup. 127
Figure 7.2. Experimental steps: lignin extraction, lignin depolymerization, additive preparation and mixture with biodiesel and oxidation stability tests. 131
Figure 7.3. Residual gas pressure in the reactor (measured at 20 °C). 133
Figure 7.4. Joint yield of soluble and insoluble solids from depolymerization experiments (Y_{SS}+Y_{IS}). 133
Figure 7.5. Effect of the temperature and the reaction medium on the production of insoluble solid during lignin depolymerization: (a) H_2-experiments, (b) HCOOH-experiments, (c) CO_2-experiments. 137
Figure 7.6. Effect of the temperature and the reaction medium on the C/H ratio of the insoluble solid product: (a) H_2-experiments, (b) HCOOH-experiments, (c) CO_2-experiments..... 138
Figure 7.7. Effect of the temperature and the reaction medium on the production of soluble solid during lignin depolymerization: (a) H_2-experiments, (b) HCOOH-experiments, (c) CO_2-experiments. 139
Figure 7.8. Effect of the temperature and the reaction medium on the C/H ratio of the soluble solid product: (a) H_2-experiments, (b) HCOOH-experiments, (c) CO_2-experiments..... 140
Figure 7.9. Effect of the temperature and the reaction medium on the production of additive: (a) H_2-experiments, (b) HCOOH-experiments, (c) CO_2-experiments..... 141
Figure 7.10. Effect of the temperature and the reaction medium on the additive solubility in biodiesel (wt.%). (a) H_2-experiments, (b) HCOOH-experiments. 143
Figure 7.11. FT-IR spectra of the additives prepared after ASL_f depolymerization. .. 147
Figure 7.12. Molecular weight distribution (GPC plots) of the additives and their biodiesel insoluble fractions. 149
Figure 7.13. Oxidation stability times of neat and doped biodiesels..... 150
Figure 7.14. Effect of the depolymerization temperature and the reaction medium on the antioxidant performance of the additives (improvement of biodiesel oxidation stability): (a) H_2-experiments, (b) HCOOH-experiments, (c) CO_2-experiments..... 152

Figure 7.15. Improvement of the biodiesel oxidation stability as a function of the concentration of (a) catechol, (b) guaiacol, (c) syringol and (d) BKF dimer. 154
Figure 8.1. Summary of the product distribution in RCF experiments. 166
Figure 8.2. Effect of the temperature and the catalyst load on the product distribution (yields of solid, oil and gas) when using n-butanol/water (a, c, e) and methanol (b, d, f) as reaction media. 169
Figure 8.3. Production of phenolic monomers and carbohydrates-derived compounds in the RCF experiments. 171
Figure 8.4. Effect of the temperature and the catalyst load on the yield of phenolic monomers (wt.% over AS lignin): (a) n-butanol/water-experiments; (b) methanol-experiments..... 172
Figure 8.5. Mass yields (over AS lignin) of the main phenolic monomers identified in the oils. 174
Figure 8.6. Lignin depolymerization mechanisms to phenolic monomers (adapted from (Renders et al., 2018)). 175
Figure 8.7. Effect of the temperature and the catalyst load on the yield of carbohydrate-derived fraction (wt.% over AS holocellulose): (a) n-butanol/water-experiments, (b) methanol-experiments. 176
Figure 8.8. GC/MS spectra of (a) BSO before drying (liquid organic phase). (b) BSO redissolved in n-butanol. 177
Figure 8.9. Mass yields (over AS hollocelulose) of the main carbohydrate-derived families identified in the oils. 178
Figure 8.10. SEC plots of MSO and BSO. 180
Figure 8.11. Effect of the temperature and the catalyst load on the average molecular weight (M_w) (Da) of oils: (a) n-butanol/water-experiments (BSO); (b) methanol-experiments (MSO). 181
Figure 8.12. ^{1}H-DOSY NMR spectra of oils obtained at 300 °C: (a) Exp.#2, BSO without Pd/C; (b) Exp.#4, BSO with Pd/C; (c) Exp.#9, MSO without Pd/C and (d) Exp.#11, MSO with Pd/C. Red and blue numbers correspond to molecular weights obtained with PEGP and PS calibration, respectively. The numbers in the boxes represent the selected value according to the corresponding calibration. 186
Figure 8.13. ^{1}H-DOSY NMR spectra of MSO obtained at 250 °C: (a) Exp. #8, without Pd/C and (b) Exp. #10, with Pd/C. 187
Figure 8.14. HSQC spectra in the aliphatic region of oils obtained at 275 °C, 1 g Pd/C: (a) Exp. #12, MSO; (b) Exp. #5, BSO; and HSQC spectra in the aromatic region of oils obtained at 275 °C, 1 g Pd/C: (c) Exp. #12, MSO; (d) Exp. #5, BSO..... 189
Figure 8.15. HSQC spectra for the samples obtained in: (a) Exp. #5 (BSO at 275 °C; 1g Pd/C) and (b) Exp. #11 (MSO at 300 °C; 2g Pd/C). 190
Figure 8.16. HSQC-TOCSY in the aliphatic region of oils obtained at 275 °C, 1 g Pd/C: (a) Exp.#12, MSO; (b) Exp.#5, BSO..... 190
Figure 8.17. ^{31}P NMR after derivatization with TMDP of the samples obtained in: (a) Exp. #11: (MSO at 275 °C; 1g Pd/C) and (b) Exp. #4 (BSO at 300 °C; 2g Pd/C). 192
Figure 8.18. Entire FT-IR spectra from 4000 to 400 cm^{-1} of BSO and MSO samples prepared at different operational conditions. 194
Figure 8.19. Detailed FT-IR spectra of: (a) BSO samples and (b) MSO samples in the most characteristic fingerprint region. 195

LIST OF TABLES

Table 2.1. Ultimate and proximate analyses, HHV and macro-components composition of AS and lignocellulosic materials. 29
Table 2.2. Characterization of AS ash. 30
Table 2.3. Ultimate and proximate analyses, HHV and macro-components composition of the materials used for the comparison with AS. 35
Table 3.1. Ultimate and proximate analyses, HHV, and chemical composition of AS and P before and after torrefaction at 220 °C and 250 °C. 52
Table 3.2. Concentration of organic compounds in the torrefaction liquids (mg/g liquid, quantified by GC/FID). 56
Table 4.1. Operational conditions in the gasification experimental runs. 65
Table 4.2. Experimental results from the gasification at 850 °C of AS, P and TAS220. 73
Table 4.3. Tar production in the gasification experiments and composition of tar samples (GC/MS/FID). 79
Table 5.1. Distribution and characteristics of the products obtained in the pyrolysis of AS and WS. 93
Table 6.1. Characterization of argan shells biochar before and after CO_2 activation during different treatment times. 112
Table 7.1. Experimental design planned for the depolymerization experiments. 129
Table 7.2. Characterization of the lignin-rich fraction extracted from AS. 132
Table 7.3. Product distribution, pH of the reactional mixture, C/H ratio in the solids and additive yield. 135
Table 7.4. Concentration of monomeric phenolic compounds in the additives obtained from lignin depolymerization. 145
Table 7.5. Molecular weight (Mn, Mw, Mw/Mn) of the whole additives and of their insoluble fractions in biodiesel. 148
Table 8.1. Experimental conditions in the RCF tests (2^k full factorial design). 163
Table 8.2. Gas composition (vol. %) from the RCF experiments. 170
Table 8.3. Molecular average weights (M_n, M_w, M_w/M_n) of BSO and MSO. 181
Table 8.4. Estimated apparent masses using DOSY for the aromatic, methoxy and aliphatic regions using PS for calibration. 183
Table 8.5. Quantitative $HSQC_0$ of the produced oils (MSO and BSO). 188
Table 8.6. Estimated concentration of hydroxy group in MSO and BSO samples. 191

Preface/Prólogo

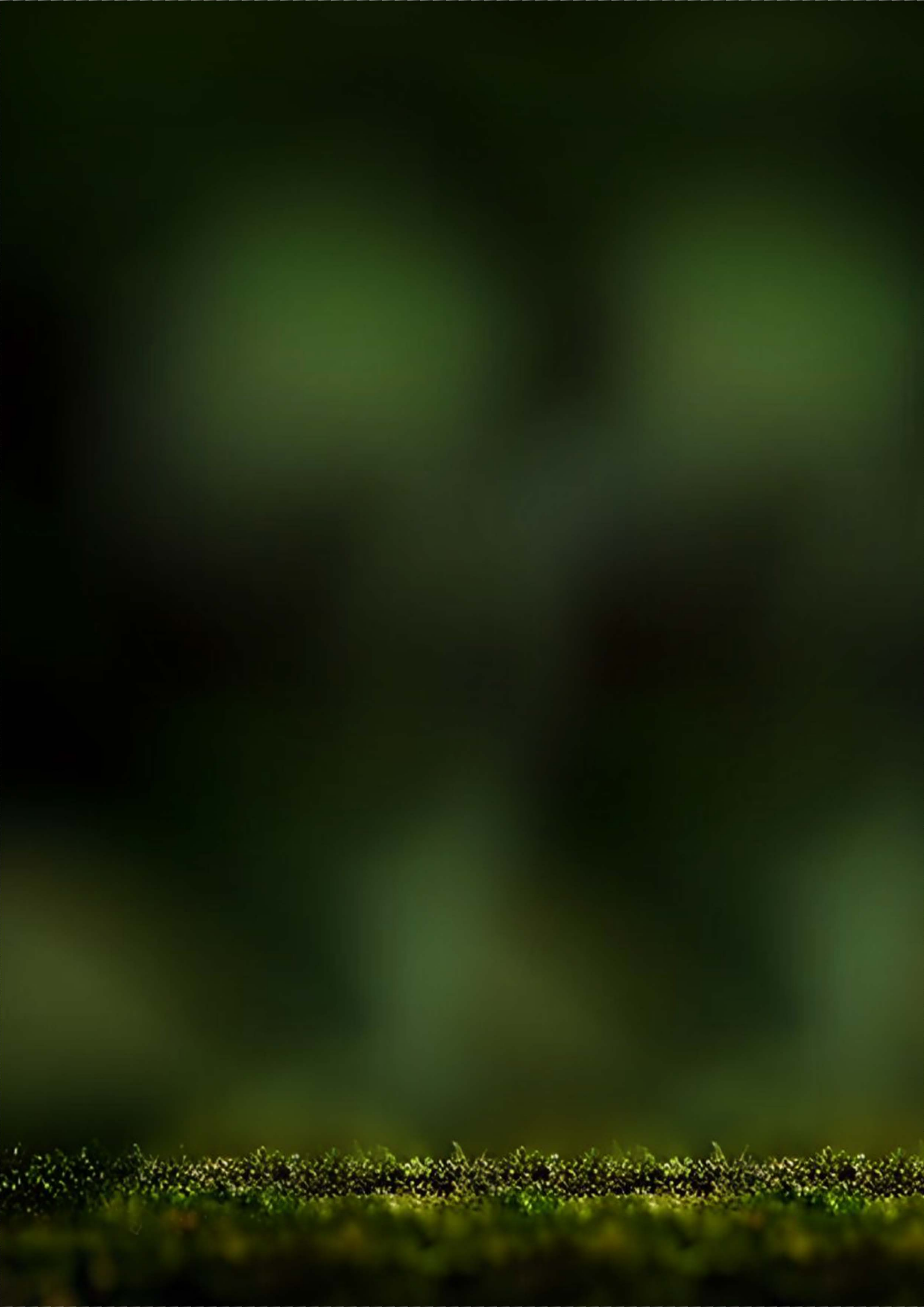

PREFACE

The present thesis addresses, as indicated in the title, the valorization of an agricultural waste, argan shells, via the thermochemical pathway.

This Ph.D. study has been developed at the Aragón Institute of Engineering Research (I3A), affiliated with the Universidad de Zaragoza-Spain, in the Thermochemical Processes Group (GPT). The topics investigated at the GPT can be divided into two main lines: (i) the fuel conversion and minimization of pollutant emissions and (ii) the production of biofuels and bioproducts from biomass and waste, where the current work is framed. In this research area, the main objective consists of finding the appropriate means for sustainable upgrading of industrial and agroforestry residues into add-valued products.

During the last three decades, the group has worked on the thermochemical processing of many types of materials, such as sewage sludge, animal manure, wood, plastics, meat and bone meal, as well as some agricultural wastes like wheat straw, sugar cane bagasse and fruit shells, by torrefaction, pyrolysis, gasification or hydrotreatment. For instance, almond shells, an abundant waste in Spain, were gasified, and their behavior was outlined in a previous work of the GPT (Bilbao et al., 1995). In the same way, the pyrolysis of cashew nutshells has more recently been studied at the facilities of the GPT, showing the great fuel potential of the charcoal and the liquid produced (Ábrego et al., 2018). The process prototype was scaled up into a 50 kg fixed-bed reactor mounted in Bobo-Dioulasso, Burkina Faso (Plaza et al., 2019), thus providing new avenues for the sustainable development of the mentioned region. Hence, the idea of valorizing another kind of fruit shell, specifically argan shells, emerged from the same perspective of promoting its use locally in the Moroccan region where the argan tree grows. Unlike other nutshells, such as almond or cashew, there were very few bibliographical antecedents about argan shells characterization and its thermochemical conversion when this Ph.D. project was started (by February 2018), except for some studies about activated carbon production and hard carbon for batteries (Boujibar et al., 2018; Dahbi et al., 2017; Elmouwahidi et al., 2012; Ennaciri et al., 2014). More recently, some of the thermal characteristics and the combustion behavior of this residue were involved in other studies developed by Moroccan researchers (Rahib et al., 2019a; Rahib et al., 2019b).

In the present Ph.D. work, the argan shells were characterized in depth, and their thermochemical treatment was experimentally studied through different routes in order to explore different potential alternatives for the valorization of this waste.

Torrefaction appears as the softest thermochemical treatment in terms of the temperature range applied to the material. In most cases, this treatment is used to increase the energetic value, improve the carbon content and ease the grinding of the raw material for the sake of storage and transportation (Brachi et al., 2017; Medic et al., 2012). In the present study, the torrefaction of argan shells was performed in an auger reactor under two different temperatures, with an exhaustive characterization of the products. Afterward, air-steam gasification of raw shells and of the torrefied material was experimentally tested in a fluidized-bed at the operational conditions pre-established by chemical thermodynamic equilibrium calculations. The behavior of argan shells in both processes was experimentally compared to another biomass more used and explored in thermochemical processes (pine residues).

In order to extend the knowledge on the thermochemical upgrading of argan shells, the pyrolysis process was also experimentally studied at three different temperatures in a fixed-bed reactor. The process was followed by other post-treatments intending to find sustainable applications and end-uses for the generated products. In particular, the produced biochar was used as feedstock to produce high-quality activated carbon (by physical activation in two different reactors using CO_2 as an agent). On the other hand, the bio-oil obtained from the pyrolysis process, as well as the lignin fraction extracted from the shells by a soda semi-chemical pulping process, were hydrothermally processed. The liquid products were further upgraded to obtain potential antioxidant additives, whose activity was tested by blending with biodiesel and measuring the improvement of its oxidation stability.

To complete the doctoral program, the candidate realized a research stay at the Center for Combustion and Harmful Emission Control (CHEC) of the Technical University of Denmark (DTU). An Erasmus + grant for student mobility partially financed the stay expenses. During the stay at DTU, a one-pot process known as reductive catalytic fractionation, was studied for the extraction and depolymerization of lignin from argan shells to produce phenolic monomers directly. The effect of the reaction medium, temperature and catalyst load was investigated.

The part of the work related to the production of renewable additives was framed within the projects “ENE2017-85040-R: Renewable additives for biofuels”, funded by the Spanish Ministry of Economic Affairs (MINECO) and “PID2020-114936RB-I00: Advanced bioFuels with Integrated Negative Emissions (AbFINE)” financed by the Spanish Investigation Agency.

The major part of the work presented in the current Ph.D. dissertation has been published in JCR-indexed journals under the following references:

– Zainab Afailal, Noemí Gil-Lalaguna, Robert J. Macías, José Luis Sánchez (2023). "*Pyrolysis of argan shells: towards a circular economy biorefinery concept*". **Submitted to Journal of Cleaner Production** (IF 2021: 11.072; Quartile: Q1- Chemical Engineering).

– Zainab Afailal, Noemí Gil-Lalaguna, Martin Høj, Alfonso Cornejo, José Luis Sánchez, Anker Degn Jensen (2023). "*Production of phenolic compounds from argan nutshells waste by reductive catalytic fractionation*". **Submitted to Industrial & Engineering Chemistry Research.** (IF 2021: 4.326; Quartile: Q2- Chemical Engineering).

– Zainab Afailal, Noemí Gil-Lalaguna, Isabel Fonts, Alberto Gonzalo, Jesús Arauzo, José Luis Sánchez (2023). "*Thermochemical valorization of argan nutshells: torrefaction and air-steam gasification*". **Fuel**, 332, 125970, DOI: 10.1016/j.fuel.2022.125970. (IF 2021: 8.035; Quartile: Q1- Chemical Engineering). **Published**.

– Zainab Afailal, Noemí Gil-Lalaguna, María Teresa Torrijos, Alberto Gonzalo, Jesús Arauzo Pérez, José Luis Sánchez (2021). "*Antioxidant additives produced from argan shells lignin depolymerization*". **Energy and fuels**, 35 (21), 17149–17166, DOI: 10.1021/acs.energyfuels.1c01705. (IF 2021: 4.565; Quartile: Q2- Chemical Engineering). **Published**.

Part of the work involved in this Ph.D. dissertation has been presented as a draft of a patent to the Moroccan Office of Industrial and Commercial Property (January 2021, register number 52330) under the title: "Procédé de valorisation des coques du fruit de l'argan". **Under consideration.**

Moreover, to disseminate the results obtained throughout this Thesis, the doctoral candidate has participated in several national and international congresses:

- **Zainab Afailal**, Noemí Gil-Lalaguna, Jesús Arauzo, Høj Martin, Alfonso Cornejo, José Luis Sánchez, Anker Degn Jensen. *Reductive catalytic fractionation as conversion process of argan nutshells*. **5th Doctoral colloquium bioenergy.** Leipzig (Germany), September 2022. Oral presentation.

- **Zainab Afailal**, Noemí Gil-Lalaguna, Jesús Arauzo, Høj Martin, Alfonso Cornejo, José Luis Sánchez, Anker Degn Jensen. *One-pot Catalytic conversion of argan nutshells in n-butanol/water over Pd/C*. **9th International conference on engineering for waste and biomass valorization – WasteEng22**. Lyngby (Denmark), June 2022. Oral presentation.

- **Zainab Afailal**, Noemí Gil-Lalaguna, Robert J. Macías, Alberto Gonzalo, José Luis Sánchez. *CO_2 activation of chars from two different materials: a comparative study*. **9th International conference on engineering for waste and biomass valorization – WasteEng22**. Lyngby (Denmark), June 2022. Poster presentation.

- **Zainab Afailal**, Noemí Gil-Lalaguna, Andrea Vanzella, Jesús Arauzo, José Luis Sánchez. *The influence of AC and Ni/AC catalyst in the antioxidant additives production from argan shells lignin*. **XI Jornadas de jóvenes investigadores I3A**. Zaragoza (Spain), June 2022. Poster presentation.

- **Zainab Afailal**, Noemí Gil-Lalaguna, Alberto Gonzalo, Jesús Arauzo, José Luis Sánchez. *Thermochemical valorization of Argan nutshells*. **Reunión de la red en biorrefinería sostenible.** Madrid (Spain), December 2021. Flash oral presentation.

- **Zainab Afailal**, Noemí Gil-Lalaguna, Robert J. Macías, Alberto Gonzalo, Jesús Arauzo, José Luis Sánchez. *CO_2 activation of char from argan nutshells pyrolysis: a preliminary study*. **X Jornadas de jóvenes investigadores I3A.** Zaragoza (Spain), October 2021. Oral presentation.

- **Zainab Afailal**, Noemí Gil-Lalaguna, Isabel Fonts, Alberto Gonzalo, José Luis Sánchez. *Air-steam gasification of raw and torrefied Argan nutshells*. **5th International conference on alternative fuels, energy and environment: future and challenges (virtual).** October 2021. Oral presentation.

– **Zainab Afailal**, Noemí Gil-Lalaguna, José Luis Sánchez. *Valorization of Argan nutshells via thermochemical processes*. **VII Jornadas doctorales del campus iberus.** Jaca (Spain), October 2021. Flash oral presentation.

– Noemí Gil-Lalaguna, **Zainab Afailal**, Alberto Gonzalo, Jesús Arauzo, José Luis Sánchez. *Antioxidant potential of wheat straw bio-oil*. **8th International conference on engineering for waste and biomass valorization – WasteEng20 (virtual).** June 2021. Oral presentation.

– Jean-Michel Lavoie, Jèrèmie Damay, Theirry Ghislain, Jesús Arauzo, Noemí Gil-Lalaguna, Alberto Gonzalo, **Zainab Afailal**, José Luis Sanchez. *Production of antioxidant additives from biorefiney lignin*. **8th International conference on engineering for waste and biomass valorization – WasteEng20 (virtual).** June 2021. Flash oral presentation.

– **Zainab Afailal**, Noemí Gil-Lalaguna, María Teresa Torrijos, Alberto Gonzalo, Jesús Arauzo, José Luis Sánchez. *Antioxidant additives for biodiesel obtained from Argan's nutshells lignin*. **Thermal & catalytic sciences TCS 2020 -virtual symposium.** October 2020. Oral presentation.

– Iciar Serrano, **Zainab Afailal**, Pablo González, Ana Bautista, Noemí Gil-Lalaguna, Alberto Gonzalo; Jesús Arauzo, Cristina Crespo, José Luis Sánchez. *Production of nanocellulose from argan's nutshells as reinforcement material for paper produced from secondary fibers*. **Thermal & catalytic sciences TCS 2020 -virtual symposium.** October 2020. Poster presentation.

– **Zainab Afailal**, Noemí Gil-Lalaguna, Alberto Gonzalo, Jesús Arauzo, José Luis Sánchez. *Torrefaction of argan's nutshells and pine forest residues in an auger reactor*. **Thermal & catalytic sciences TCS 2020 -virtual symposium.** October 2020. Poster presentation.

– Iván Valencia, **Zainab Afailal**, Noemí Gil-Lalaguna, Alberto Gonzalo, Jesús Arauzo, José Luis Sánchez. *Antioxidant effect on biodiesel of lignin fractions of different polarity*. **Thermal & catalytic sciences TCS 2020 -virtual symposium.** October 2020. Poster presentation.

– **Zainab Afailal**, Noemí Gil-Lalaguna, Isabel Fonts, Alberto Gonzalo, José Luis Sánchez. *Preliminary study of torrefaction of Argan's nutshells in auger reactor*.

XXXVI Jornadas nacionales de ingeniería química. Zaragoza (Spain), September 2019. Flash oral presentation.

– **Zainab Afailal**, Noemí Gil-Lalaguna, Alberto Gonzalo, José Luis Sánchez, Isabel Fonts. *Gasificación de las cáscaras de Argán con aire y vapor de agua en un reactor de lecho fluidizado*. **II Congreso nacional/ IV Jornadas de investigadores en formación.** Granada (Spain), June 2019. Flash oral presentation.

– **Zainab Afailal**, Noemí Gil-Lalaguna, Isabel Fonts. *Preliminary study of gasification of Argan's nutshells in a fluidized bed gasifier*. **VII Jornadas de jóvenes investigadores I3A.** Zaragoza (Spain), June 2018. Poster presentation.

– Isabel Fonts, **Zainab Afailal**, Noemí Gil-Lalaguna, José Antonio Mateo-Román, María Atienza-Martínez, Javier Ábrego. *Gasification of pine forest residues as first stage for the production of jet fuel via Fisher-Tropsch*. **25th European biomass conference & exhibition**. Stockholm (Sweden). June 2017. Oral presentation.

PRÓLOGO

La presente tesis aborda, como indica el título, la valorización de un residuo agrícola poco explorado hasta el momento, las cáscaras de las semillas de argán, utilizando procesos termoquímicos.

Este estudio de doctorado ha sido desarrollado en el Instituto de Investigación en Ingeniería de Aragón (I3A), afiliado a la Universidad de Zaragoza, en concreto en el Grupo de Procesos Termoquímicos (GPT). La investigación que se realiza en el GPT se divide en dos líneas fundamentales: (i) la conversión de combustibles y minimización de emisiones contaminantes y (ii) la producción de biocombustibles y bioproductos a partir de biomasa y residuos, en la que se enmarca el trabajo actual. En este ámbito de investigación, el objetivo principal consiste en encontrar los medios adecuados para la transformación sostenible de los residuos industriales y agroforestales en productos de alto valor añadido.

Durante las últimas tres décadas, el grupo ha trabajado en la conversión y aprovechamiento de muchos tipos de residuos, como lodos de depuradoras, purines, maderas, plásticos, harinas carnicas, así como algunos materiales agrícolas como paja de trigo, bagazo de caña de azúcar y cáscaras de frutos, mediante los procesos de torrefacción, pirólisis, gasificación e hidrotratamiento. Por citar algunos ejemplos más concretos en el caso de las cáscaras de frutos, se trabajó en la gasificación de cáscaras de almendra, residuo muy abundante en España (Bilbao et al., 1995). o, más recientemente, en la pirólisis de cáscaras de nuez de anacardo, mostrando el gran potencial combustible de los productos sólido y líquido (Ábrego et al., 2018). El proceso ensayado a escala de laboratorio fue escalado a un reactor de mayor tamaño (50 kg) y montado en la ciudad de Bobo-Dioulasso, en Burkina Faso (Plaza et al., 2019), proporcionando así una nueva vía para el desarrollo sostenible de la región.

La idea de estudiar alternativas para la valorización de la cáscara del fruto del argán surgió desde la misma perspectiva de impulsar su aprovechamiento, a nivel local, en la región marroquí donde crece el árbol del argán. Cuando se comenzó con la presente tesis doctoral (Febrero 2018), apenas existían antecedentes bibliográficos sobre la caracterización de las cáscaras del fruto del argán y su conversión termoquímica, a excepción de algunos estudios sobre la producción de carbón activado y carbón duro para baterías (Boujibar et al., 2018; Dahbi et al., 2017; Elmouwahidi et al., 2012; Ennaciri et

al., 2014). Posteriormente, han ido surgiendo algunos trabajos más centrados en el estudio de sus características térmicas y su comportamiento como combustible (Rahib et al., 2019a; Rahib et al., 2019b).

Para completar la información disponible en la literatura sobre esta biomasa, el trabajo desarrollado en la presente tesis se ha centrado en caracterizarla en profundidad y se ha planteado su valorización termoquímica a través de diferentes rutas, comparando los resultados obtenidos con otros materiales más ampliamente estudiados en la literatura.

La torrefacción es, entre los diferentes tratamientos termoquímicos, el que se realiza en un tramo más suave de temperatura. En general, este tratamiento se realiza para aumentar el contenido energético y de carbono de un material, facilitar su molienda y mejorar las condiciones de almacenamiento y transporte (Brachi et al., 2017; Medic et al., 2012). En el presente estudio, se realizó la torrefacción de las cáscaras de argán en un reactor de tornillo sinfin a dos temperaturas diferentes, realizando una exhaustiva caracterización de los productos obtenidos Posteriormente, se llevó a cabo un proceso de gasificación en lecho fluidizado con mezclas de aire y vapor de agua tanto para las cáscaras de argán originales como para el material torrefactado, estableciendo las condiciones de operación según cálculos termodinámicos. Para completar los estudios de torrefacción y gasificación, y con un propósito comparativo, se realizaron también ensayos con otra biomasa lignocelulósica más habitual y explorada en este tipo de procesos (residuos de pino).

Otro de los procesos termoquímicos estudiados experimentalmente fue la pirólisis de las cáscaras de argán, realizada a tres temperaturas diferentes en un reactor de lecho fijo. Tras la pirólisis, se realizaron otros post-tratamientos con la intención de encontrar aplicaciones sostenibles para los productos generados. En particular, el biochar obtenido se utilizó como materia prima para producir carbón activado de alta calidad (por activación física con CO_2 en dos reactores diferentes). El bio-oil del proceso de pirólisis, así como la lignina extraída de las cáscaras mediante pasteado semiquímico a la sosa, se procesaron hidrotérmicamente. Del producto líquido se extrajeron fracciones de compuestos fenólicos con potencial antioxidante, que se evaluó mediante su mezcla, en pequeñas dosis, con biodiésel, y posterior análisis de su estabilidad a la oxidación.

Para completar su formación pre-doctoral, la doctoranda realizó una estancia de investigación en el Centro de Combustión y Control de Emisiones Nocivas (CHEC) del

departamento de Ingeniería Química y Bioquímica de la Universidad Técnica de Dinamarca (DTU). Una beca Erasmus + para la movilidad de estudiantes de doctorado cubrió parcialmente los gastos de la misma. Durante la estancia en la DTU, se estudió el fraccionamiento catalítico reductivo para la extracción y despolimerización de la lignina contenida en las cáscaras de argán para producir monómeros fenólicos a partir de un proceso de una sola etapa. En dicho proceso se analizó el efecto del medio de reacción, la temperatura y la cantidad de catalizador añadido.

La parte del trabajo de esta tesis relacionada con la producción de aditivos se ha realizado en el marco de los proyectos "ENE2017-85040-R: Aditivos renovables para biocombustibles", financiado por el Ministerio de Economía español (MINECO). y "PID2020-114936RB-I00: Biocombustibles avanzados con emisiones negativas integradas (AbFINE)", financiado por la Agencia Estatal de Investigación.

La mayor parte del trabajo realizado en la presente tesis se ha publicado en revistas indexadas en el *Journal Citation Report (JCR)*:

– Zainab Afailal, Noemí Gil-Lalaguna, Robert J. Macías, José Luis Sánchez (2023). "*Pyrolysis of argan shells: towards a circular economy biorefinery concept*". **Enviado** a la revista **Journal of Cleaner production** (IF 2021: 11.072; Quartil: Q1- Ingeniería Química). Pendiente de revisión.

– Zainab Afailal, Noemí Gil-Lalaguna, Martin Høj, Alfonso Cornejo, José Luis Sánchez, Anker Degn Jensen (2023). "*Production of phenolic compounds from argan nutshells waste by reductive catalytic fractionation*". **Enviado** a la revista **Industrial & Engineering Chemistry Research.** (IF 2021: 4.326; Quartil: Q2- Ingeniería Química). Pendiente de revisión.

– Zainab Afailal, Noemí Gil-Lalaguna, Isabel Fonts, Alberto Gonzalo, Jesús Arauzo, José Luis Sánchez (2023). "*Thermochemical valorization of argan nutshells: torrefaction and air-steam gasification*". **Fuel**, 332, 125970, DOI: 10.1016/j.fuel.2022.125970. (FI 2021: 8.035; Quartil: Q1- Ingeniería Química). **Publicado**.

– Zainab Afailal, Noemí Gil-Lalaguna, María Teresa Torrijos, Alberto Gonzalo, Jesús Arauzo Pérez, José Luis Sánchez (2021). "*Antioxidant additives produced from argan shells lignin depolymerization*". **Energy and fuels**, 35 (21), 17149–17166,

DOI: 10.1021/acs.energyfuels.1c01705. (IF 2021: 4.565; Quartil: Q2- Ingeniería Química). **Publicado**.

Parte del trabajo involucrado en esta tesis doctoral se ha presentado como borrador de patente a la Oficina Marroquí de Propiedad Industrial y Comercial (enero de 2021, número de registro 52330) bajo el título: "Procédé de valorisation des coques du fruit de l'argan". **En proceso de revisión.**

Además, para la difusión científica de los resultados obtenidos, la doctoranda ha participado en varios congresos de ámbito nacional e internacional:

- **Zainab Afailal**, Noemí Gil-Lalaguna, Jesús Arauzo, Høj Martin, Alfonso Cornejo, José Luis Sánchez, Anker Degn Jensen. *Reductive catalytic fractionation as conversion process of argan nutshells*. **5th Doctoral colloquium bioenergy.** Leipzig (Alemania), Septiembre 2022. Presentación oral.

- **Zainab Afailal**, Noemí Gil-Lalaguna, Jesús Arauzo, Høj Martin, Alfonso Cornejo, José Luis Sánchez, Anker Degn Jensen. *One-pot Catalytic conversion of argan nutshells in n-butanol/water over Pd/C*. **9th International conference on engineering for waste and biomass valorization – WasteEng22**. Lyngby (Dinamarca), Junio 2022. Presentación oral.

- **Zainab Afailal**, Noemí Gil-Lalaguna, Robert J. Macías, Alberto Gonzalo, José Luis Sánchez. *CO_2 activation of chars from two different materials: a comparative study*. **9th International conference on engineering for waste and biomass valorization – WasteEng22**. Lyngby (Dinamarca), Junio 2022. Presentación Póster.

- **Zainab Afailal**, Noemí Gil-Lalaguna, Andrea Vanzella, Jesús Arauzo, José Luis Sánchez. *The influence of AC and Ni/AC catalyst in the antioxidant additives production from argan shells lignin*. **XI Jornadas de jóvenes investigadores I3A**. Zaragoza (España), Junio 2022. Presentación Póster.

- **Zainab Afailal**, Noemí Gil-Lalaguna, Alberto Gonzalo, Jesús Arauzo, José Luis Sánchez. *Thermochemical valorization of Argan nutshells*. **Reunión de la red en biorrefinería sostenible.** Madrid (España), Diciembre 2021. Presentación Flash oral.

- **Zainab Afailal**, Noemí Gil-Lalaguna, Robert J. Macías, Alberto Gonzalo, Jesús Arauzo, José Luis Sánchez. *CO_2 activation of char from argan nutshells pyrolysis:*

a preliminary study. **X Jornadas de jóvenes investigadores I3A.** Zaragoza (España), Octubre 2021. Presentación oral.

– **Zainab Afailal**, Noemí Gil-Lalaguna, Isabel Fonts, Alberto Gonzalo, José Luis Sánchez. *Air-steam gasification of raw and torrefied Argan nutshells*. **5th International conference on alternative fuels, energy and environment: future and challenges (virtual).** Octubre 2021. Presentación oral.

– **Zainab Afailal**, Noemí Gil-Lalaguna, José Luis Sánchez. *Valorization of Argan nutshells via thermochemical processes*. **VII Jornadas doctorales del campus iberus.** Jaca (España), Octubre 2021. Presentación Flash oral.

– Noemí Gil-Lalaguna, **Zainab Afailal**, Alberto Gonzalo, Jesús Arauzo, José Luis Sánchez. *Antioxidant potential of wheat straw bio-oil*. **8th International conference on engineering for waste and biomass valorization – WasteEng20 (virtual).** Junio 2021. Presentación oral.

– Jean-Michel Lavoie, Jèrèmie Damay, Theirry Ghislain, Jesús Arauzo, Noemí Gil-Lalaguna, Alberto Gonzalo, **Zainab Afailal**, José Luis Sanchez. *Production of antioxidant additives from biorefiney lignin*. **8th International conference on engineering for waste and biomass valorization – WasteEng20 (virtual).** Junio 2021. Presentación Flash oral.

– **Zainab Afailal**, Noemí Gil-Lalaguna, María Teresa Torrijos, Alberto Gonzalo, Jesús Arauzo, José Luis Sánchez. *Antioxidant additives for biodiesel obtained from Argan's nutshells lignin*. **Thermal & catalytic sciences TCS 2020 -virtual symposium.** Octubre 2020. Presentación oral.

– Iciar Serrano, **Zainab Afailal**, Pablo González, Ana Bautista, Noemí Gil-Lalaguna, Alberto Gonzalo; Jesús Arauzo, Cristina Crespo, José Luis Sánchez. *Production of nanocellulose from argan's nutshells as reinforcement material for paper produced from secondary fibers*. **Thermal & catalytic sciences TCS 2020 -virtual symposium.** Octubre 2020. Presentación Póster.

– **Zainab Afailal**, Noemí Gil-Lalaguna, Alberto Gonzalo, Jesús Arauzo, José Luis Sánchez. *Torrefaction of argan's nutshells and pine forest residues in an auger reactor*. **Thermal & catalytic sciences TCS 2020 -virtual symposium.** Octubre 2020. Presentación Póster.

- Iván Valencia, **Zainab Afailal**, Noemí Gil-Lalaguna, Alberto Gonzalo, Jesús Arauzo, José Luis Sánchez. *Antioxidant effect on biodiesel of lignin fractions of different polarity*. **Thermal & catalytic sciences TCS 2020 -virtual symposium.** Octubre 2020. Presentación Póster.

- **Zainab Afailal**, Noemí Gil-Lalaguna, Isabel Fonts, Alberto Gonzalo, José Luis Sánchez. *Preliminary study of torrefaction of Argan's nutshells in auger reactor*. **XXXVI Jornadas nacionales de ingeniería química.** Zaragoza (España), Septiembre 2019. Presentación Flash oral.

- **Zainab Afailal**, Noemí Gil-Lalaguna, Alberto Gonzalo, José Luis Sánchez, Isabel Fonts. *Gasificación de las cáscaras de Argán con aire y vapor de agua en un reactor de lecho fluidizado*. **II Congreso nacional/ IV Jornadas de investigadores en formación.** Granada (España), Junio 2019. Presentación Flash oral.

- **Zainab Afailal**, Noemí Gil-Lalaguna, Isabel Fonts. *Preliminary study of gasification of Argan's nutshells in a fluidized bed gasifier*. **VII Jornadas de jóvenes investigadores I3A.** Zaragoza (España), Junio 2018. Presentación Póster.

- Isabel Fonts, **Zainab Afailal**, Noemí Gil-Lalaguna, José Antonio Mateo-Román, María Atienza-Martínez, Javier Ábrego. *Gasification of pine forest residues as first stage for the production of jet fuel via Fisher-Tropsch*. **25th European biomass conference & exhibition**. Stockholm (Suecia). Junio 2017. Presentación oral.

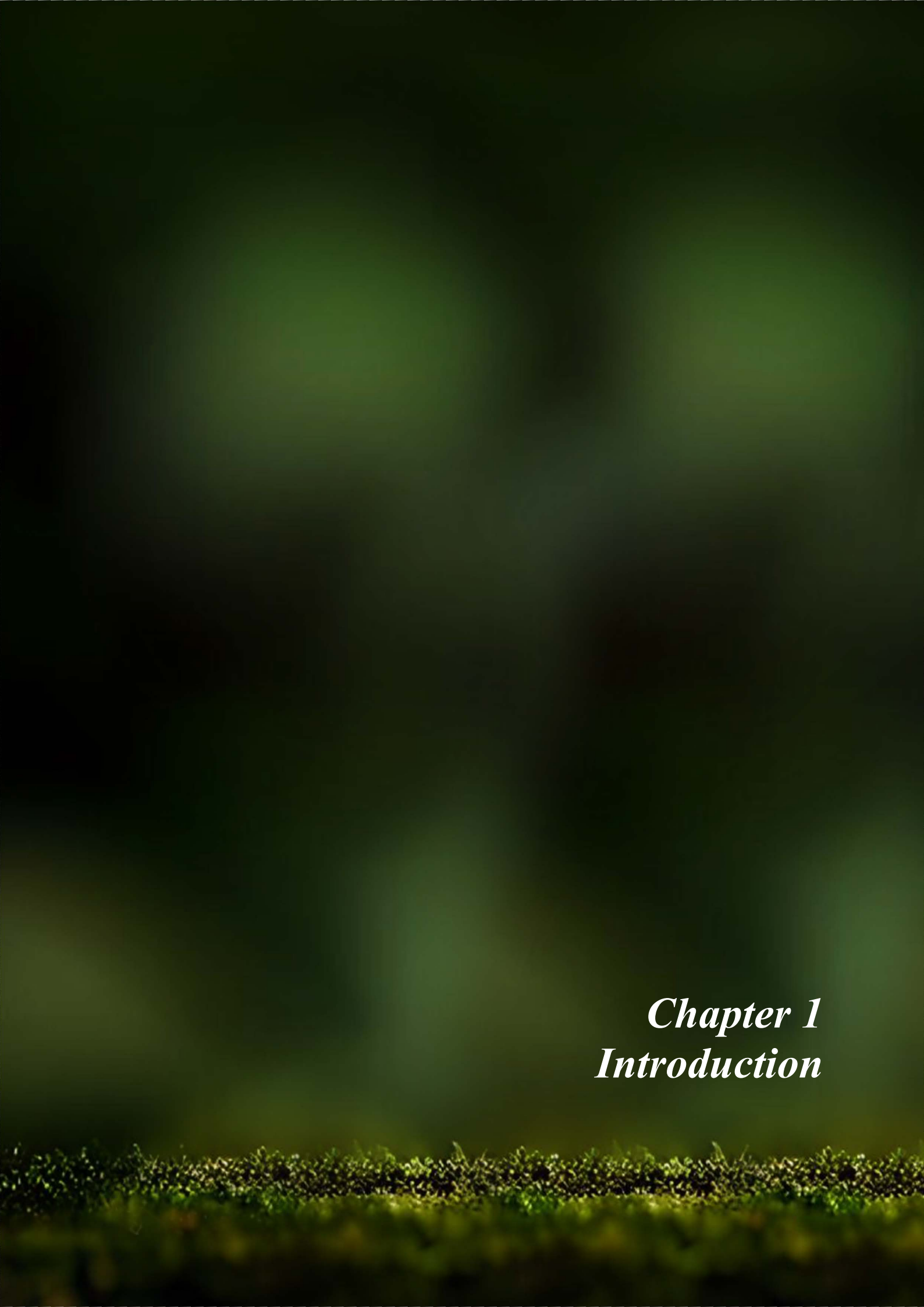

Chapter 1
Introduction

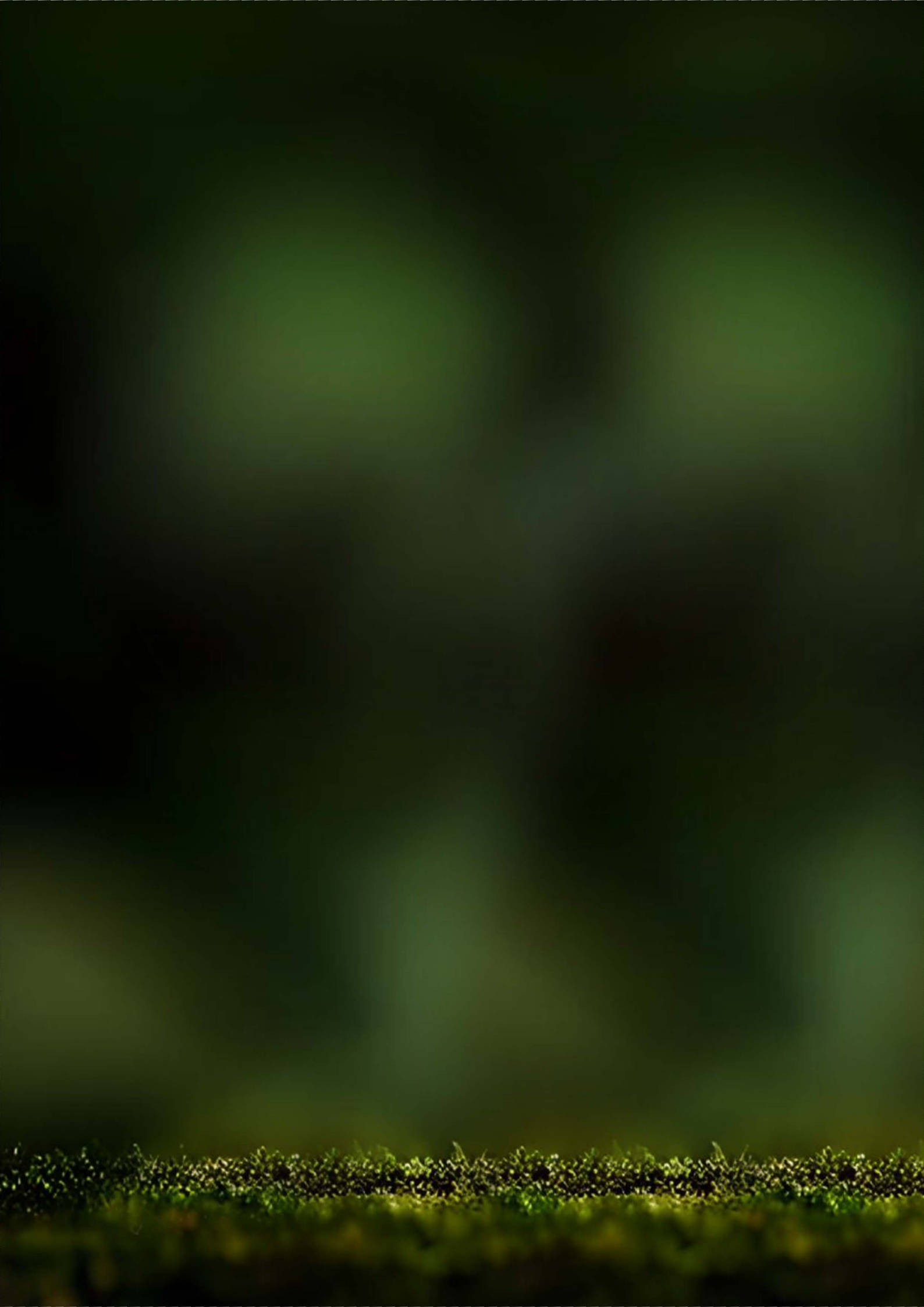

1. INTRODUCTION

1.1. Argania

The argan tree or *Argania Spinosa (L.) Skeels* belongs to the family Sapotaceae (Figure 1.1). It is an endemic tree of Morocco, growing wildly in the southwestern of the country and covering up to 870,000 ha of forest zones in the Anti-Atlas foothill mountains, the coastal region between Essaouira and Agadir and an important area in Souss-valley (Kamal et al., 2019). In a favorable atmosphere, this spiny tree can measure up to 10 m in height and can live more than 200 years (Charrouf and Guillaume, 2008). The most outstanding features of this tree are its adaptation to extreme climate, saline water, light irrigation and marginal soils (Guillaume and Charrouf, 2011; Solowey, 2001). Thanks to its roots, deeply introduced into the soil, the argan tree plays a crucial role in protecting against the superficial earth erosion and desertification. The argania tree, according to many authors (Charrouf and Guillaume, 2008; Faouzi, 2012), is on the way to extinction if the behavior of the local dwellers is not ameliorated. The consecutive arid years and the overuse of argan wood as fuel were responsible for many hectares of argan forest deterioration. Hence, the Moroccan agricultural authorities were engaged in reimplanting the argan tree as part of the *Green Morocco Plan,* estimated at 200,000 ha by 2025 (Charrouf and Guillaume, 1999; Montero, 2017). The sustainable valorization of the different products and residues coming from this tree could also be a great step to protect this species from a possible risk of extinction. As an example, the use of Argania wood as a fuel could be replaced by the exploitation of waste materials derived from the argan oil production industry.

Figure 1.1. Argan tree (region of Essaouira, Morocco) (own photography).

The Argania produces annually two harvests of nuts. The argan nut is called in the Amazigh language (local language) *Afiyach,* which is composed of the fleshy outer layer within a leathery skin *(Alig)* and a hard stone *(Akkay)*. This hard stone includes the kernel *(Zenin)* and the shell *(Argourech)*. All of these components of the argan nut are shown in Figure 1.2. The fleshy outer layer is a tasty food for camels and goats (seeing the goats up the argan tree is nowadays a touristic attraction, Figure 1.3).

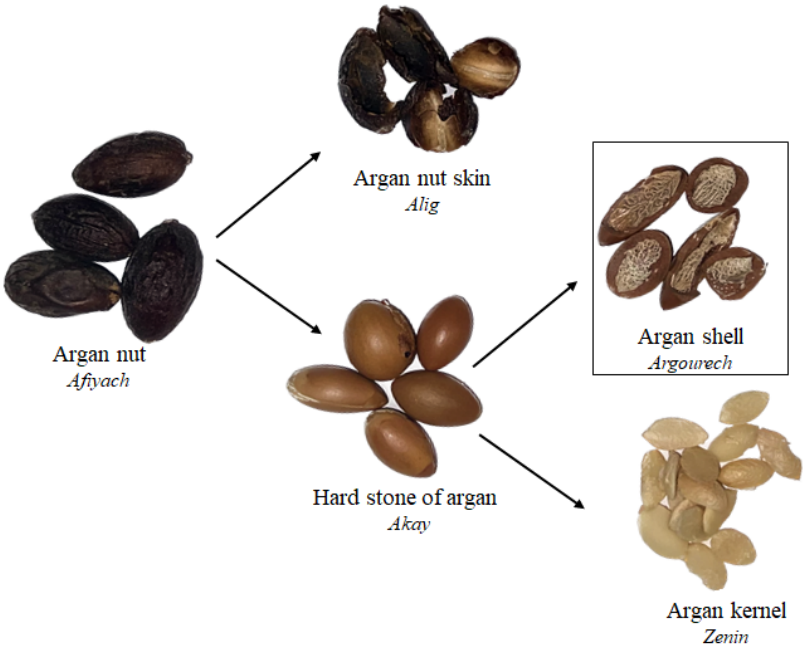

Figure 1.2. Components of the whole argan nut.

Figure 1.3. Goats feeding from an Argan tree (own photography).

The worldwide marketed argan oil, known for its nutritional composition and therapeutic and dermatologic benefits, is extracted from the kernels after removing the shell by crushing (mainly carried out manually, using stones or with scratching machines in modern cooperatives). The edible argan oil can be extracted from roasted kernels (Charrouf and Guillaume, 2008), either with traditional manual millstones or mechanic cold pressing methods (Kamal et al., 2019). The oil intended for cosmetology uses (one of the highest-priced vegetable oils in the world, up to 200 €/liter) can be directly extracted from the unroasted kernels by cold-pressing (manually or semi-mechanized), with lipophilic solvents or by flash distillation (Charrouf and Guillaume, 1999). On the other hand, the pulp (press cake) obtained after argan oil extraction, which contains up to 10 wt.% of oil (Charrouf and Guillaume, 2008), is used for soap production (from unroasted kernels) or as fodder (from roasted kernels).

The annual production of argan oil is over 4,000 tons, which leaves behind 20 tons of non-valorized waste (shells) per ton of oil produced (Dahbi et al., 2017). Some cooperatives have been using the shells obtained after extracting the kernels as gravel for the ground (Figure 1.4, left panel). While other local people have tried to employ this waste as a fuel for traditional heating furnaces (Rahib et al., 2019a), but its hardness, rigidity and difficulty in being ignited (delayed ignition and flame extinction (Rahib et al., 2019b)) prevent its easy and safe use in such a traditional way.

As the argan oil industry is considered a crucial lever for the socioeconomic development of the poor rural population (especially women) of southwestern Morocco, many efforts in the modernization of the argan oil sector to increase the production yield and to improve the oil quality control and storage conditions, as well as to protect the geographical origin, are being carried out either by the local cooperatives or the agricultural authorities. However, up to date, no serious attempts have been made to ensure the sustainable valorization of these shells, despite the great potential that these shells, as many other lignocellulosic materials, have to substitute fossil resources for the production of biofuels or biochemicals.

Figure 1.4. Shells from argan nut in the entrances of an argan cooperative (Essaouira, Morocco) (own photography).

1.2. General objectives and motivations

Moving from a limited local market to an extended worldwide market of argan oil provides a significant economic opportunity for the region. Nevertheless, it must be ensured that this economic development also has positive effects in preserving the argan tree and sustainable management of the environment. In this regard, valuable valorization of the unexploited components of argan nut, specifically the kernel shells, towards producing biofuels and add-value chemicals, can contribute to the socioeconomic development of the concerned areas of Morocco. On the other hand, involving local users in a green oil production strategy by managing their own wastes in a circular economy concept could be beneficial both economically and environmentally.

Accordingly, the main motivation of the present doctoral thesis is to contribute to finding a sustainable approach for valorizing this agricultural waste (the argan shells, AS from now on), exploring thermochemical routes such as torrefaction, pyrolysis, gasification, hydrothermal treatment, char activation and reductive catalytical fractionation. Hence, the global objectives of the present study are:

(i) To characterize in-depth argan shells as a potential raw material for thermochemical processes.

(ii) To examine the technical feasibility of different thermochemical processes for obtaining valuable products from argan wastes, which could be implemented on-site by the local producers towards a more sustainable argan oil production. To accomplish this second objective, the experimental work was divided into five fundamental tasks or experimental blocks consisting in:

1. Torrefaction: Characterization of the products obtained in the torrefaction of argan shells, which was conducted in an auger reactor operated at two different temperatures, with a particular focus on how the solid fuel properties were affected by the process. For comparative purposes, torrefaction of another type of lignocellulosic biomass (pine residues), more common in thermochemical processes, was also investigated.

2. Gasification: Characterization of the products obtained in the gasification of argan shell, which was conducted in a fluidized-bed reactor operated with air or air/steam as a gasifying agent. The main point of interest was evaluating the syngas composition and the effect of torrefying the material before gasifying it. For comparative purposes, gasification of another type of lignocellulosic biomass (pine residues), more common in thermochemical processes, was investigated.

3. Pyrolysis: Characterization of the products obtained in the pyrolysis of argan shells, which was conducted in a fixed-bed reactor operated at three different temperatures. For comparative purposes, pyrolysis of another type of lignocellulosic biomass (wheat straw), more common in thermochemical processes, was investigated. The potential use of bio-oil as an antioxidant additive for biofuels, and the feasibility of using biochar as an adsorbent material after physical activation (using CO_2) were investigated.

4. Hydrothermal treatment of the lignin extracted from argan shells (by semi-chemical pulping with NaOH) aiming at obtaining antioxidant additives. The effects of the temperature and the reaction media (N_2, H_2, CO_2 and HCOOH) on the lignin depolymerization were investigated. The hydrothermal treatment was also extended to pyrolysis bio-oil to check if it could improve its antioxidant potential.

5. Reductive catalytic fractionation (RCF) of argan shells: the main objective was to produce phenolic monomers, focusing on the effect of the temperature, the catalyst load and the reaction media (n-butanol/water or methanol).

Figure 1.5 shows graphically all the studies carried out in this doctoral thesis, including the reaction media, the raw materials and the different products obtained in each studied process.

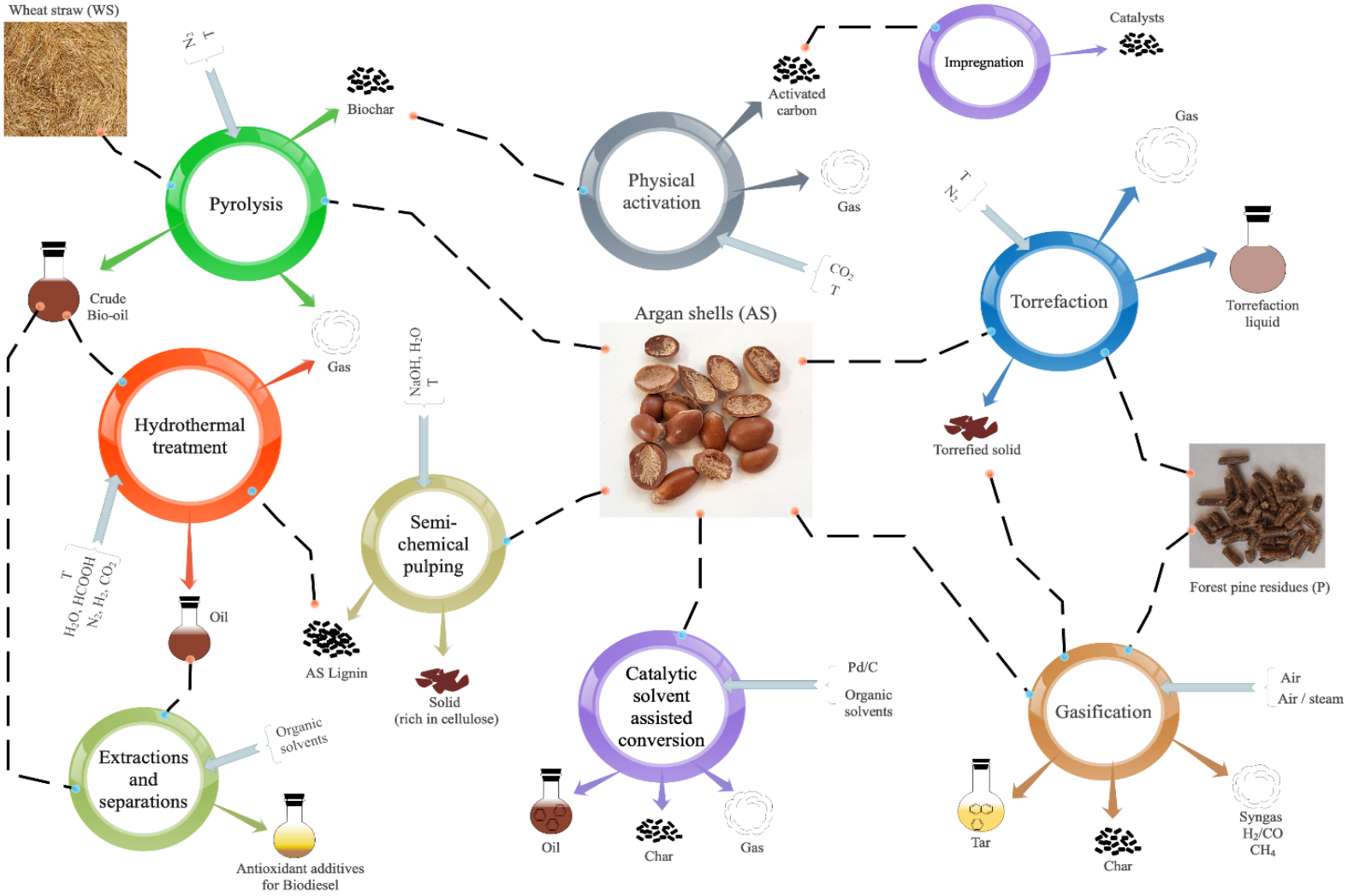

Figure 1.5. Summary of the studies developed in this work.

1.3. Thermochemical conversion of biomass

Biomass was the first energy source used by humans. Its use is still vital and occupies an increasingly prominent position in the current energetic panorama because of the vast potential to reduce emissions if biomass is well-used and valorized. Many pathways have been developed to valorize biomass from different origins, not only as a source of energy but also in producing chemicals and products with noticeable economic added value. With this purpose, biochemical processes, such as fermentation or anaerobic digestion using enzymes or microorganisms, have been studied for biomass conversion into gaseous or liquid fuels (Elgarahy et al., 2021). On the other hand, thermochemical processes, such as pyrolysis, gasification, hydrothermal treatment, etc., have also been researched in producing fuels and value-added chemicals using biomass instead of fossil derivatives which had traditionally been the unique suppliers. As a basic definition, these processes involve heat and/or catalysts to convert organic resources into solids, liquids, gases or thermal energy (Brown and Brown, 2014b). Thermochemical processes have proven to be effective and efficient in biomass valorization due to their diversity and broader technology choice. During these treatments, the chemical bonds between carbon, hydrogen and oxygen are destroyed, and the chemical energy stored during the plant's photosynthesis gets released (Ram and Mondal, 2022). Thermochemical upgrading can be carried out under inert or oxidative atmospheres at a large temperature interval.

Many types of biomasses, such as algae, municipal waste or lignocellulosic materials, could be used as feedstock for thermochemical processes. As the present study is dedicated to upgrading argan shells, which is a lignocellulosic biomass, the following sections are focused on explaining the composition of this kind of biomass and its thermochemical conversion.

1.4. Lignocellulosic biomass

Lignocellulosic materials, either herbaceous, woody or fruit shells, are the most abundant biomass on earth. Those materials are essentially composed of hemicellulose, cellulose and lignin, with smaller amounts of pectins, proteins, extractives and ash. This polymer repartition can differ from one plant to another (Bajpai, 2016) and strongly affects the product distribution and characteristics resulting from thermochemical conversion (Nunes et al., 2018).

Generally, cellulose is the most significant fraction, representing about 40 to 50 wt.% of the biomass; hemicellulose represents 10 to 40 wt.% and lignin between 10 and 40 wt.% (Amen-Chen et al., 2001; Effendi et al., 2008; Pandey and Kim, 2011; Yang et al., 2007).

Cellulose is a homopolymer of high molecular weight (Figure 1.6), consisting of a long linear chain of β D-glucopyranose moieties denoted as $(C_6H_{10}O_5)_n$, where, depending on the material source, "n" could range from 10,000 to 15,000 (Moon et al., 2011). These units are linked together by β-(1,4) bonds (McKendry, 2002). Cellulose is characterized by its noticeable stability (compared to hemicellulose) and its packed microfibrils structure due to the hydrogen and the Van der Waals bonds (Bajpai, 2016).

Unlike cellulose, hemicellulose is not chemically homogeneous as it is formed from several structural varieties and is distinguished by shorter chains and lower molecular weight (Figure 1.6). This biopolymer is principally formed from pentoses (xylose, rhamnose and arabinose), hexoses (glucose, mannose and galactose) and uronic acids (D-glucuronic, D-galacturonic and 4-O-methyl glucuronic acids). The hemicellulose composition differs from one biomass to another; for instance, softwoods mainly contain glucomannan, while straw and grasses contain xylan (Bajpai, 2016). Moreover, this biopolymer is known as the more reactive constituent during the thermochemical conversion as it degrades at lower treatment temperatures (below 250 °C) (Tumuluru et al., 2011).

No less important than the previous two macro-components, lignin appears as one of the fundamental components of lignocellulosic materials (Figure 1.6). Lignin is a complex phenolic biopolymer with a recalcitrant structure composed of phenyl propanoid groups (named as guaiacyl, syringyl and hydroxyphenyl) linked together with condensed linkages (meaning C-C bonds) as 5-5, β-β, β-5 and β-1 and/or ether linkages as α-O-4, 5-O-4 and β-O-4 (Gillet et al., 2017; Ma et al., 2021). Lignin presents a kind of rigidity and resistance to microbial attack and oxidative stress in plant cell walls and is considered the adhesive of the other components of the material (Bajpai, 2016). One of the main issues to be addressed during lignin thermal upgrading is the subsequent repolymerization. During these treatments, condensation reactions occur after the cleavage of the ether bonds and their substitution by more resistant and stable C-C bonds (Abu-Omar et al., 2021), making its thermal conversion challenging.

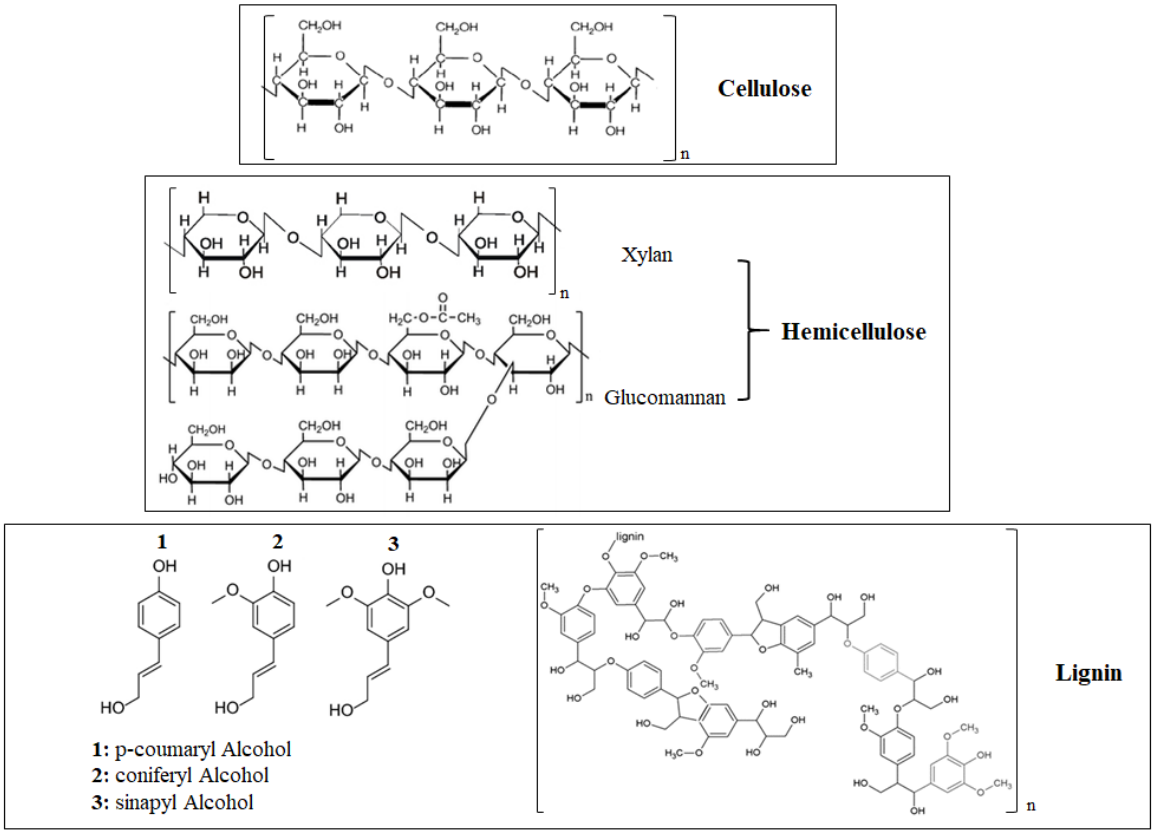

Figure 1.6. Composition of the macro-components of the lignocellulosic biomass.

Chapter 2
Materials and characterization methods

2. MATERIALS AND CHARACTERIZATION METHODS

As addressed previously, argan shells (AS) are the principal raw material used to feed the different thermochemical processes involved in the present work. At the same time, other raw materials such as forest pine residues (P from now on) in the torrefaction and gasification studies and wheat straw (WS from now on) in the pyrolysis study were also investigated to be able to compare them with the experimental behavior of AS under the same operational conditions and laboratory setups. Hence, this section resumes the main characteristics of the materials handled throughout the experimental study.

2.1. Argan shells

Argan shells collected in the Essaouira region were kindly supplied by a Moroccan cooperative after argan kernel extraction. Before an in-depth characterization, AS was crushed and sieved in order to obtain a particle size ranging from 200 μm to 1 cm (the particle size depended on the further use, either for analysis or process feeding purposes). The proximate analysis, involving ash, moisture and volatile matter contents, was determined according to standardized procedures (EN 14775:2010, EN 14774-3:2010 and EN 15148-2010, respectively), while the higher heating value (HHV) was measured using a calorific bomb IKA model C2000 basic. The elemental analysis was explored using a LECO CHN628 Analyzer combined with the sulfur add-on module 628-S. Concerning the macro-components distribution in the AS, hemicellulose, cellulose, and lignin contents were determined by the Van Soest analysis. This method consists of succeeding digestion steps using three different detergents (neutral detergent, acid detergent, and sulfuric acid 72 %) (Godin et al., 2011). On the other hand, the organic extractives content was determined by the Soxhlet extraction method using dichloromethane (DCM) as a solvent for 6 h (this solvent was chosen after some previous tests using a variety of solvents with different polarities such as hexane, methanol and water). More details about macro-component determination methods are shown in Appendix II.

Table 2.1 summarizes the results of AS characterization together with other data reported in the literature for other types of biomass in order to situate AS in the panorama of agricultural wastes and lignocellulosic biomasses used as feedstock for thermochemical upgrading. As can be seen, the outstanding characteristics of AS were its low ash content (0.2 wt. %), the high volatile matter content of around 75 wt.% and the considerable energetic content with a HHV of 19 MJ/kg. The contents of lignin and

cellulose (on a dry basis) were both pretty similar in AS (around 38 wt. %), as well as the elemental carbon and oxygen contents. Comparing the AS characteristics with other residues, as a whole, the fruit shells had quite similar characteristics: HHV ranging between 16 and 20 MJ/kg, C content around 47 wt.% and volatile matter content between 64 and 75 wt.%. In general terms, among all the residues considered, AS characterization was closer to that of almond shells, although with a notable difference in holocellulose distribution. In fact, AS differed from the other shells mainly in the macro-components distribution with the highest cellulose content and the second higher lignin content after the hazelnut shells. Lignin content was also higher in AS compared to woods or herbaceous biomass (these were more studied materials for thermochemical upgrading). For most parameters, AS fitted between the characteristics of softwood (pine in this case) and hardwood (eucalyptus).

Table 2.1. Ultimate and proximate analyses, HHV and macro-components composition of AS and lignocellulosic materials.

Parameter	Argan shells (Current study)	Almond shells (Rapagnà and Latif, 1997)	Coconut shells (Razvigorova et al., 1994)	Hazelnut shells	Peanut shells	Softwood Pine	Hardwood Eucalyptus[f] (ECN Phyllis data basis)	Bagasse	Wheat straw
Proximate analysis (wt. % ar. basis)									
Ash	0.20 ± 0.04	1.1	0.5	0.6[c]	7.5[e]	0.5[g]	0.8	7.1[i]	7.6[j]
Moisture	8.74 ± 0.03	8.8	5.6	12.8[c]	8.0[e]	12.0[g]	4.0	8.4[i]	15.1[j]
Volatile matter	74.6 ± 0.3	72.5	71.8	63.7[c]	65.9[e]	73.2[g]	77.2	73.0[i]	62.3[j]
Fixed Carbon[a]	16.5 ± 0.4	17.6	22.1	22.9[c]	18.7[e]	14.3[g]	18.0	11.6[i]	15.0[j]
Ultimate analysis (wt. % ar. basis)									
C	47.5 ± 0.2	45.3	49.4	41.1[c]	43.8[e]	45.3[g]	49.2	41.4[i]	37.3[j]
H	6.6 ± 0.1	5.5	6.2	4.8[c]	4.9[e]	5.4[g]	5.8	5.0[i]	4.7[j]
N	0.177 ± 0.003	n.d	2.3	0.1[c]	1.5[e]	0.1[g]	0.2	0.2[i]	0.7[j]
S	0.044 ± 0.001	n.d	0.8	0.8[c]	0.2[e]	0.04[g]	0.02	0.02[i]	0.2[j]
O	45.5[a] ± 0.2	38.7	37.3	39.9[a,c]	37.1[a,e]	36.6[a,g]	40.0[a]	38.3[i]	34.3[a,j]
HHV (MJ/kg)	18.61 ± 0.04	18.0[a]	20.6[a]	15.6[a,c]	17.1[a,e]	18.2[a,g]	19.5[a]	16.0[a,i]	14.6[a,j]
Macro-components composition (wt.% dry basis)									
Extractives	0.2 ± 0.1	n.d	n.d	3.3[b,d]	n.d	n.d	n.d	n.d	8.1[f]
Hemicellulose	23 ± 1	30.6	48.8	30.4[d]	18.7[f]	27.0[h]	31.8	47.0[h]	24.0[f]
Cellulose	39 ± 2	31.7	20.0	26.8[d]	35.7[f]	50.0[h]	43.3	36.0[h]	40.0[f]
Lignin	38 ± 2	38.2	30.0	42.9[d]	30.2[f]	23.0[h]	24.7	17.0[h]	21.0[f]

[a] Calculated by difference
[b] Dry and extractives-free basis
n.d not determined
[c] (Dogru et al., 1999)
[d] (Demirbaş, 2002)
[e] (Lu et al., 2006)
[f] (ECN Phyllis database)
[g] (Feldman et al., 1981)
[h] (Miller and Bellan, 1997)
[i] (Gabra et al., 2001)
[j] (Livingston, 1991)

In addition to the AS characteristics listed in Table 2.1, metal content in AS ash was investigated by inductively coupled plasma combined with a mass spectrometer (ICP-MS) through a Perkin Elmer Elan DRC-e spectrometer (kindly analyzed by the Chemical Analysis Service of the Universidad de Zaragoza). The ash sample was acid digested, assisted by microwave in a CEM MARS-X reaction system. Table 2.2 resumes the obtained results. As seen, the principal metals identified by ICP in the AS ash were K with the highest content of 252 mg/g of ash, Na with up to 142 mg/g, and Ca and Mg with 42 and 13 mg/g, respectively. Traces of less than 2 mg/g of Fe, Al and Si were also detected. A relatively similar value of K content was reported in the literature for almond shells ash with a content of K_2O of 310 mg/g of ash and lower Na content (4.9 mg/g) (Fernández Llorente et al., 2006). In contrast, almond shells ash had higher contents of other minerals, such as Ca (160 mg/g).

Table 2.2. Characterization of AS ash.

Metal content (mg/g $_{Ash}$)	(Average value ± standard deviation)
Na	142.2 ± 0.5
Mg	12.6 ± 0.2
Al	1.46 ± 0.02
Si	1.4 ± 0.2
K	252 ± 2
Ca	42.3 ± 0.4
Fe	1.30 ± 0.02

The dry extractives from AS (yielding 0.2 wt.%) were redissolved in DCM and analyzed by gas chromatograph–mass spectrometer (GC/MS). In general, the extractives from biomass consist of a mixture of lipids, phenolic compounds, terpenoids, fatty acids, resin acids, steryl esters, sterol, and waxes (Dorado et al., 2000; Fernandez et al., 2001; Sebio-Puñal et al., 2012), while the relative fraction of each group changed from one biomass to another. Figure 2.1 shows the chromatogram (by GC/MS) and lists the identified compounds in the extractives from AS. The main peaks identified corresponded to fatty acids such as oleic acid ($C_{18}H_{34}O_2$) and n-hexadecanoic acid ($C_{16}H_{32}O_2$), amides of long-chain fatty acids, such as oleic acid amide ($C_{18}H_{35}NO$) and *cis*-13-docosenamide ($C_{22}H_{43}NO$), and other molecules with high molecular weight, such as lupenyl acetate ($C_{32}H_{52}O_2$) and 3β-acetoxyolean-12-en-27-oic acid ($C_{32}H_{50}O_4$).

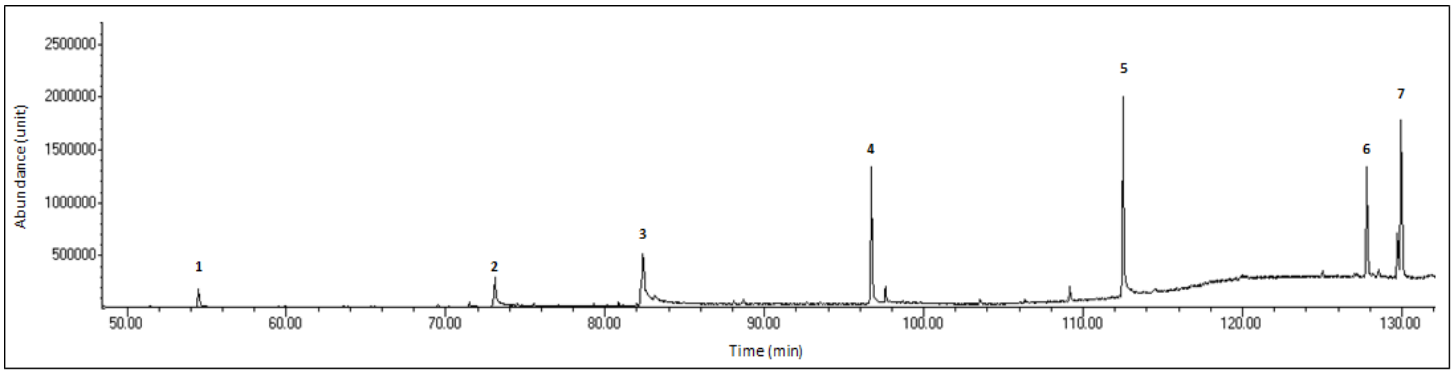

Figure 2.1. Organic compounds identified in the extractives from AS: (1) Vanillin; (2) n-Hexadecanoic acid; (3) Oleic acid; (4) Oleic acid amide; (5) cis-13-Docosenamide; (6) 3β-acetoxyolean-12-en-27-oic acid; (7) Lupenyl acetate.

On the other hand, the AS thermal behavior was investigated by thermogravimetric analysis (TGA-DTG, Proteus STA 449 F1 Jupiter-Netzsch). The thermogravimetric analysis (TGA) curves represent the instantaneous weight loss of the material during its thermal decomposition as a function of the applied temperature. This analysis was carried out under inert (N_2) and oxidative (air) media to have a preliminary view of the material behavior during the thermal degradation before testing its conversion in the lab-scale torrefaction, pyrolysis and gasification plants. In both atmospheres, around 50 mg of the solid sample was heated up at a constant heating rate of 5 °C/min from ambient temperature to 750 °C. The gas flow was fixed for both media at 100 mL/min. It is worth indicating that TGA-DTG runs, especially under air atmosphere, showed unusual and unrepeatable results when AS particles of up to 1 mm size were used, thus showing an unstable behavior of AS during combustion. Hence, smaller particles (up to 200 μm) were used to perform the analysis properly.

Figure 2.2 depicts the TGA-DTG analysis results of AS under N_2 (Figure 2.2a) and air (Figure 2.2b) atmospheres. As displayed in Figure 2.2a, most of torrefaction/pyrolysis conversion occurred at temperatures below 500 °C. The AS weight trace curve can be partitioned into three consecutive stages; the first mass decay (around 10 wt.%) observed at low temperatures (roughly 20-150 °C) was attributed to the AS moisture elimination and the release of light volatiles (moisture content determined at 105 °C according to standard EN 14774-3:2010 was 8.74 wt.%). The second mass loss stage could be related to the fingerprint zone of holocellulose degradation, starting at around 200 °C and finishing at temperatures lower than 350 °C, with a noticeable change in the TGA curve

slope between 270 and 285 °C. This slope variation may correspond to the simultaneous degradation of hemicellulose in the first place and the starting of cellulose decomposition. A minor part of lignin degradation may also be included in this 60 wt.% mass loss, as lignin decomposition has been proven to start from 200 °C (Nunes et al., 2018). The last mass loss stage (corresponding to the carbonization) was observed at higher temperatures (T > 350 °C), attributed to the slow lignin degradation extended until 600 °C. Finally, a residual mass estimated by 26 wt.% remained at 750 °C, which could be assigned principally to the fixed carbon content in AS (16.5 wt.% when calculated by difference using the results of proximate analyses) since AS is poor on ashes (0.2 wt.%).

On the other hand, in the presence of air, three stages of degradation were also observed from TGA-DTG curves (Figure 2.2b). The dehydration step (1st stage) was identical in both media, but some differences were observed in the other stages. Although the TGA curves related to the second stage were pretty similar in both cases, the DTG curves showed an inversed trend in the mass loss rate between hemicellulose and cellulose from one medium to another. For AS pyrolysis, slight differences in mass loss rate were observed between both peaks (Figure 2.2a), ranging between 2.7 and 3 wt.%/min for hemicellulose and cellulose, respectively. However, when using air, the mass loss rate peak of hemicellulose reached its highest value of 3.2 wt.%/min and became thinner, and the cellulose one reached its lowest value of 2.4 wt.%/min. As expected, the most visual difference between both atmospheres was during the third stage (the carbonization or combustion stage), with a total mass loss of 14 wt.% for N_2 vs. 43 wt.% for air, obviously explained by the residual char burning in the presence of oxygen.

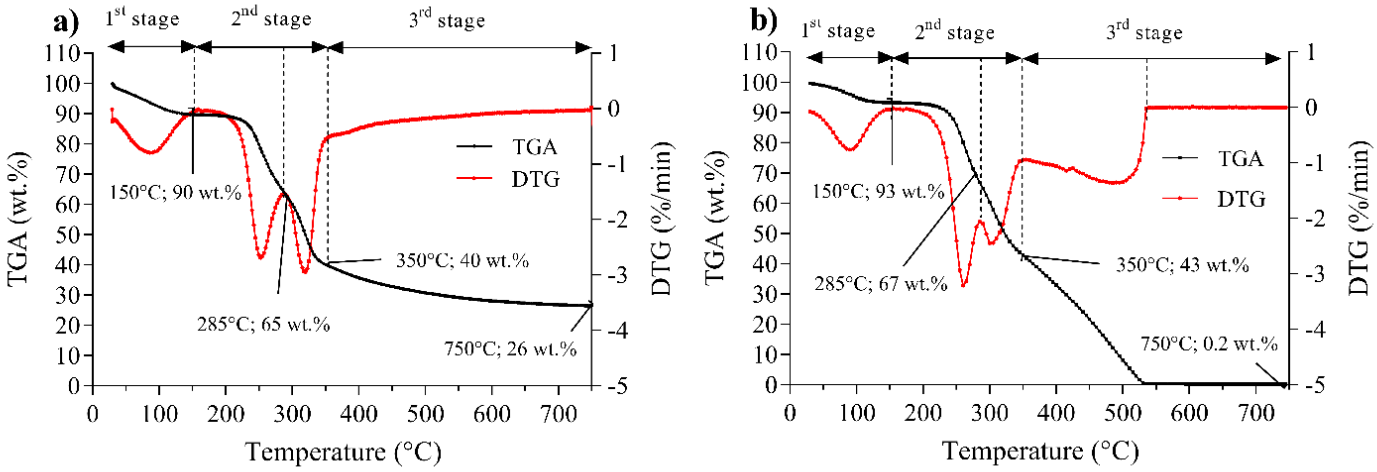

Figure 2.2. TGA-DTA thermograms of AS (a) N_2 atmosphere, (b) air atmosphere.

To finish the characterization of AS, the surface functional groups were examined by Attenuated Total Reflection-Fourier Transform Infra-Red (ATR-FTIR) spectroscopy analysis, using an Agilent Cary 630 FTIR spectrometer with a resolution of 4 cm^{-1} in the wavenumber range of 4000 – 400 cm^{-1} (medium IR region). Figure 2.3 presents the FTIR spectra of AS, the absorbance signal was normalized, and its baseline was corrected in order to facilitate the visual comparison of the peaks' particularities (Faix, 1992; Zhou et al., 2011). As can be seen, the most intense peak was situated in the region 1050 - 1000 cm^{-1} (concretely at 1030 cm^{-1}). This peak could be assigned to the primary alcohol C-O stretch (present in hemicellulose and cellulose), and it could also point to a higher presence of guaiacol units in the material lignin (Coates, 2006; Faix, 1992). Additionally, a shoulder at wavenumber 990 cm^{-1} was observed pointing to –HC=CH- out-of-plane deformation. The peak intensity observed between 1300 - 1200 cm^{-1} might be associated with C-O and C-O-C bonds stretching vibration in xylan and cellulose (Bakhattar et al., 2021; Shi et al., 2012). At the fingerprint region of the aromatic skeletal vibrations (between 1600 and 1430 cm^{-1}) (Faix, 1992; Nandiyanto et al., 2019; Zhou et al., 2011), many peaks with considerable intensities were observed, concretely at wavenumbers 1516, 1460, and 1429 cm^{-1}. In addition to the aromatic ring vibrations at these peaks, C-H deformation (-CH_3 and –CH_2-) could occur. The peak observed at wavenumbers in the range of 1770 - 1700 cm^{-1} assigned to the C=O stretch in acids, aldehydes, esters and ketones of carbohydrate origin (Coates, 2006; Faix, 1992). Finally, at the left of the FTIR spectra, two high-intensity peaks were observed (at

3000 - 2800 cm^{-1} and 3600 - 3100 cm^{-1}), corresponding to aliphatic C-H stretching and O-H stretching, respectively.

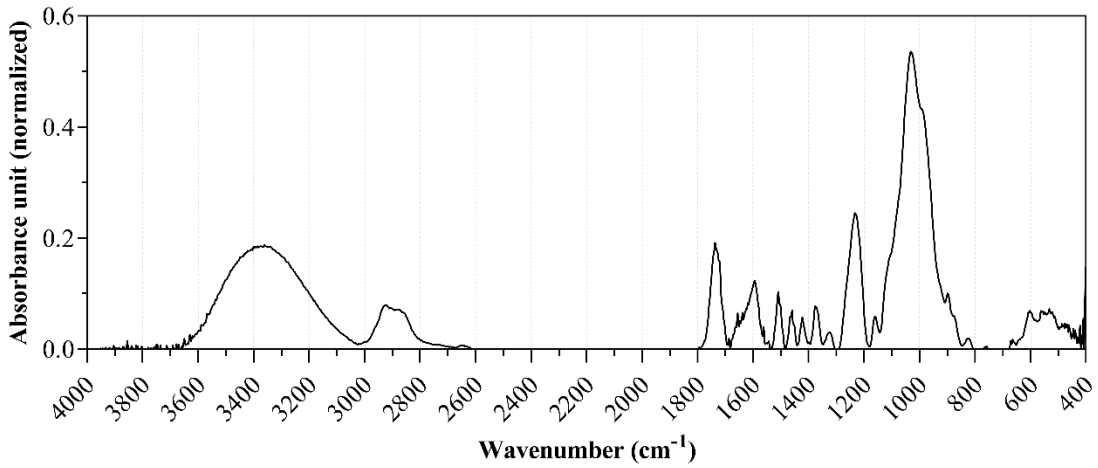

Figure 2.3. FT-IR spectra of AS.

2.2. Forest pine residues

The pine residues (P) used in this work for comparative purposes were wastes from pine forest cleaning. They were provided in the form of pellets from a Spanish cooperative in the region of Tauste (north of Spain, N41°55'24.46" O1°11'22.09"). This residue was mainly composed of pine wood and contained minor fractions of needles, roots, pinecones and some additives used for pelletization. As well as AS, P was characterized in terms of ultimate and proximate analyses, HHV and macro-components distribution. The P characteristics are depicted in Table 2.3. Overall, P and AS were pretty similar regarding elemental composition, HHV (18.5 MJ/kg for P vs. 18.6 MJ/kg for AS), moisture and volatile matter contents. However, they significantly differed in the ash content (0.2 wt.% for AS and 1.8 wt.% for P) and macro-components distribution (extractives, holocellulose and lignin). The hemicellulose and lignin contents of AS were relatively higher than those of P, while the extractives and cellulose of P exceeded the ones measured in AS.

Table 2.3. Ultimate and proximate analyses, HHV and macro-components composition of the materials used for the comparison with AS.

Parameter		P	WS
Proximate analysis (wt. % ar. basis)			
	Ash	1.8 ± 0.2	3.9 ± 0.2
	Moisture	7.7 ± 0.2	4.2 ± 0.1
	Volatile matter	77 ± 2	84 ± 2
	Fixed Carbon	13 ± 2	7.9 ± 0.5
Ultimate analysis (wt. % ar. basis)			
	C	46.74 ± 0.02	45.2 ± 0.2
	H	6.28 ± 0.04	6.5 ± 0.2
	N	0.093 ± 0.001	0.29 ± 0.05
	S	0.050 ± 0.001	0.130 ± 0.002
	O*	45.04	44.0
HHV (MJ/kg)		18.5 ± 0.1	17.2 ± 0.1
Macro-components composition (wt. % dry. basis)			
	Extractives	4 ± 1	0.4 ± 0.2
	Hemicellulose	13 ± 1	19 ± 4
	Cellulose	50 ± 3	55 ± 1
	Lignin	31 ± 1	26 ± 5

*Calculated: %O=100-C-H-N-S-Ash.

Concerning the nature of the organic compounds extracted from P (yielding 4 wt.%), Figure 2.4 shows the GC/MS of the redissolved extractives. Apart from some extractives already identified for AS, such as oleic acid, n-hexadecanoic acid, oleic acid amide and *cis*-13-docosenamide, others such as dehydroabietic acid ($C_{20}H_{28}O_2$) and some derivatives of stigmastane hydride were also detected in the extractives from P.

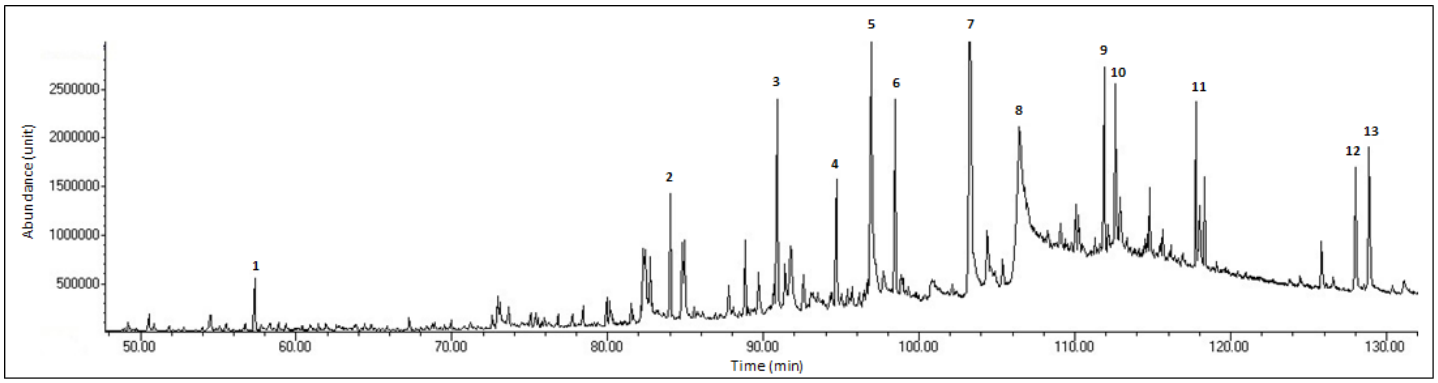

Figure 2.4. Organic compounds identified in the extractives from P: (1) 2-pentadecanone; (2) n-hexadecanoic acid; (3) 9-octadecenamide; (4) heptadecane; (5) trans-3,5-dimethoxystilbene; (6) methyl dehydroabietate; (7) 4'-methoxy-2-hydroxystilbene; (8) dehydroabietic acid; (9) 7-oxodehydroabietic acid, methyl ester; (10) cis-13-docosenamide; (11) β-saccharostenone; (12) Stigmast-4-en-3-one, (24S); (13) β-Sitosterol.

On the other hand, Figure 2.5 displays the TGA-DTG analysis results of P under inert and oxidative atmospheres. As well as AS, the thermal degradation of P in both media presented three stages. However, the repartition of those stages vis-à-vis the temperature was quite different in the case of P; for example, the first stage for P finished at 136 °C (vs. 150 °C in the case of AS), presenting a mass loss of 8 wt.%. In the second stage, many differences between P and AS could be observed; the holocellulose degradation of P presented just one peak with a high mass loss rate (4.6 wt.%/min) with the presence of a tiny shoulder at 285 °C. The different shape of the curves in this region of the thermogram points to differences in hemicellulose and cellulose distribution in both materials (even if the holocellulose content was about 50-57 wt.% in both of them), which supports the results obtained by the Van Soest extraction method. Eventually, in the third stage, the carbonization of P (N_2 atmosphere) left behind a residual solid of 21 wt.% (13 wt.% was the fixed carbon content, and 1.8 wt.% was the ash content determined by proximate analyses). In the presence of air, it can be observed that the P char combustion occurred between 350 and 490 °C, while AS char combustion was shifted to higher temperatures (between 350 and 555 °C).

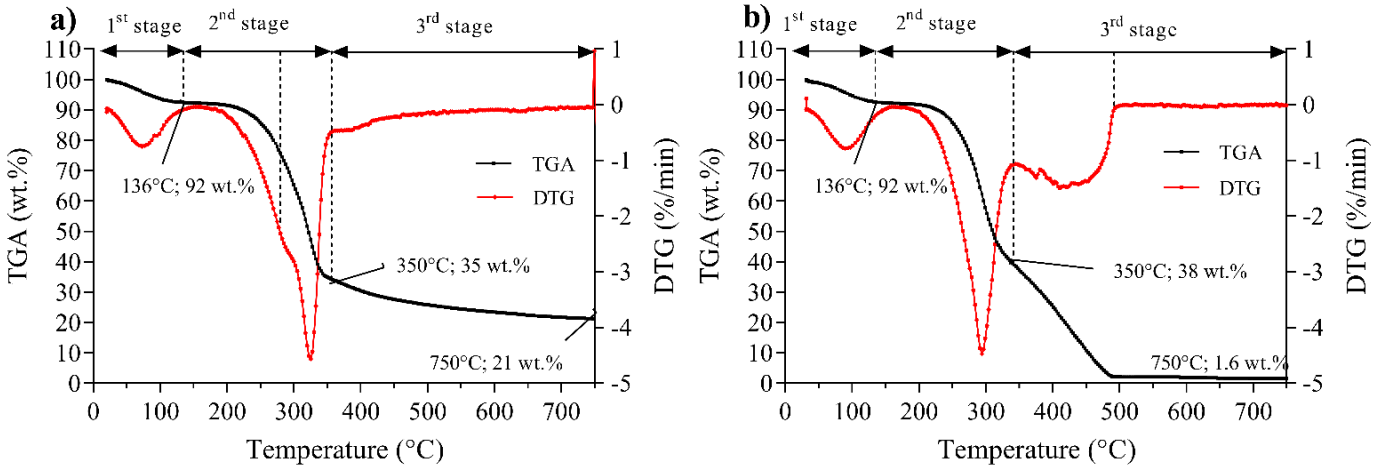

Figure 2.5. TGA-DTA thermograms of P (a); N_2 atmosphere (b); air atmosphere.

Concerning FT-IR spectra (Figure 2.6), the functional groups found on the P surface were quite similar to those on AS surface, especially in the region 1050 - 1000 cm^{-1}, with the absence of the shoulder observed at 990 cm^{-1} in the case of AS. Two peaks of lower intensities at regions between 1770 - 1700 cm^{-1} and 1300 - 1200 cm^{-1} were observed for P, although less noticeable than in the AS spectra, as these peaks were assigned to

carbohydrate origin components, such as C-O, C-O-C and C=O stretching vibration in hemicellulose; the higher hemicellulose content in AS could be an explanation for such difference. Moreover, it is to highlight that the peaks corresponding to aliphatic C-H stretching (3000 - 2800 cm^{-1}) were more pronounced on the P surface than in AS. Finally, peaks that appeared at the right of the FT-IR spectra (700 -400 cm^{-1}) were more noticeable for P than for AS, which the higher ash content could explain, as this zone of the spectra region is usually attributed to some metal-oxides (Fernández-Carrasco et al., 2012).

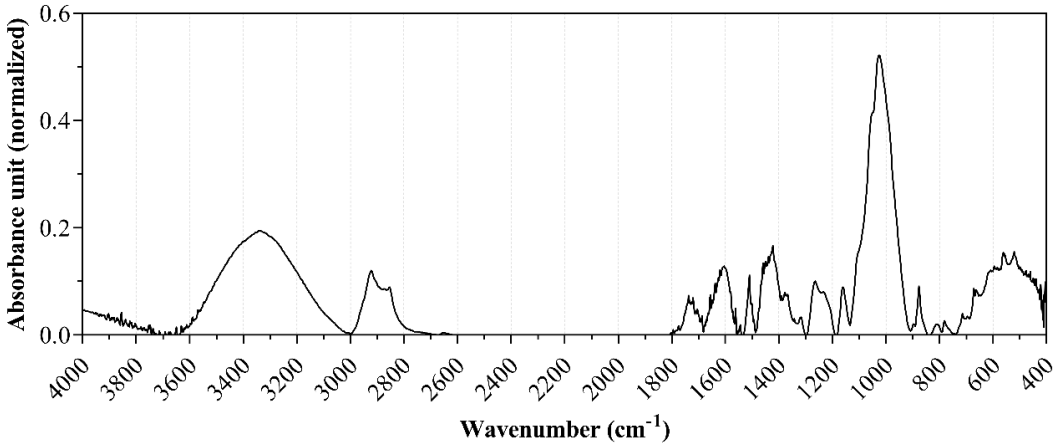

Figure 2.6. FT-IR spectra of P.

2.3. Wheat straw

In the study of pyrolysis, wheat straw (WS) was used as raw material to be compared with AS. This raw material proceeded from Sabiñánigo (northeast of Spain, 42°31′07″N 0°21′52″O). Before the thermochemical treatment, it was washed and dried at ambient temperature for 96 h before being cut to a smaller size of around 5 mm. The WS was subjected to different characterization procedures, which are resumed in Table 2.3, Figure 2.8 (TGA-DTG analysis) and Figure 2.9 (FT-IR spectra). The results obtained from the characterization of WS in the current work were somewhat different from those in Table 2.1 reviewed from the literature (Gabra et al., 2001; Livingston, 1991). Among the outstanding features of WS was its higher volatile matter content (up to 84 wt.%), which could be related to the high cellulose content of 55 wt.% (Zhao et al., 2017); this high volatile content was expected to lead to great bio-oil and gas yields during pyrolysis. Additionally, the WS ash content was relatively higher compared with those in AS and P (up to 4 wt.% in WS vs. 1.8 wt.% for P and 0.2 wt.% for AS). However, this

value is still lower than other data reported in the literature (Table 2.1), which could be explained by the removal of dust and minerals in the washing step before characterization. Both the C content and the HHV were slightly lower in WS than in P or AS, as seen in Tables 2.1 and 2.3.

In terms of extractives (representing 0.4 wt.% of WS), the GC/MS revealed the existence of some components (Figure 2.7), such as n-hexadecanoic acid and cis-9-octadecenamide, already existing in AS or P, in addition to some chain-long alkane and diketone like hexacosane ($C_{26}H_{54}$), octacosane ($C_{28}H_{58}$), hexatriacontane ($C_{36}H_{74}$) and 14,16-hentriacontanedione ($C_{31}H_{60}O_2$).

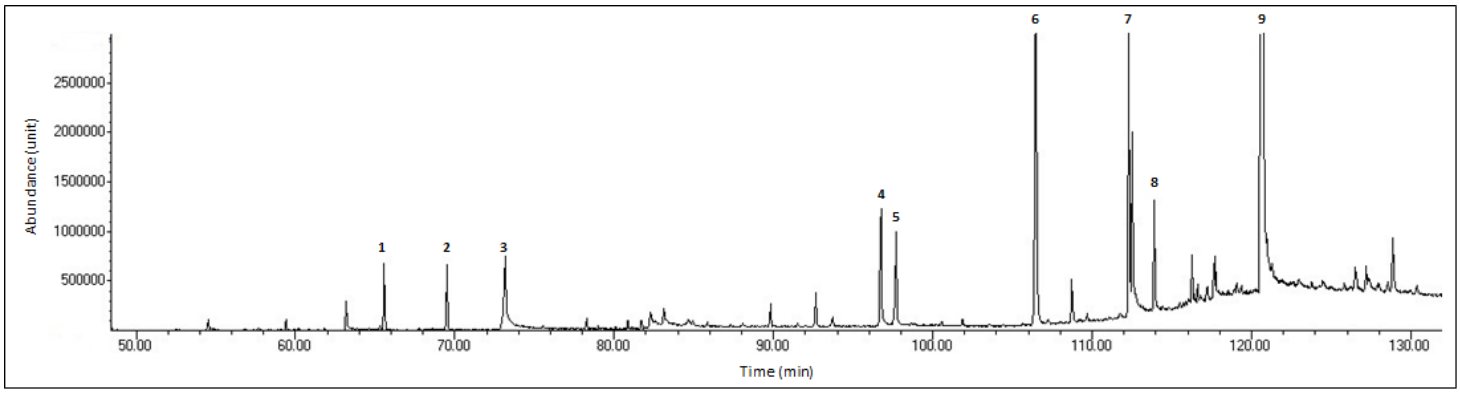

Figure 2.7. Organic compounds identified in the extractives from WS: (1) hexahydrofarnesyl acetone; (2) 2-heptadecanone, (3) n-hexadecanoic acid; (4) cis-9-octadecenamide; (5) hexacosane; (6) octacosane; (7) cis-13-docosenamide; (8) octacosanal; (9) 14,16-hentriacontanedione.

Respecting the thermal behavior of WS, as shown in Figure 2.8, the first stage of WS degradation finished at 120 °C with a mass loss of 7 wt. %. The second stage showed a mass decay of 55 wt.%, with a similar TGA shape to P. As the hemicellulose content in WS was higher than in P and lower than in AS, it can be seen that the shoulder at 266 °C was more pronounced than the one observed in the DTG curve of P (Figure 2.8a). Concerning the mass loss rate, the WS degradation was slightly faster than AS; the peak observed in the DTG plot at 320 °C showed a maximum rate of 3.6 wt.%/min (vs. 3 wt.%/min for AS). After the carbonization of both WS and AS, the residual solid was similar in both cases (25-26 wt.%), so that similar biochar yields could be predicted for the pyrolysis of both materials. In the oxidative atmosphere, the DTG curve of WS was moved toward a lower temperature, reaching the entire degradation of the material at 460 °C.

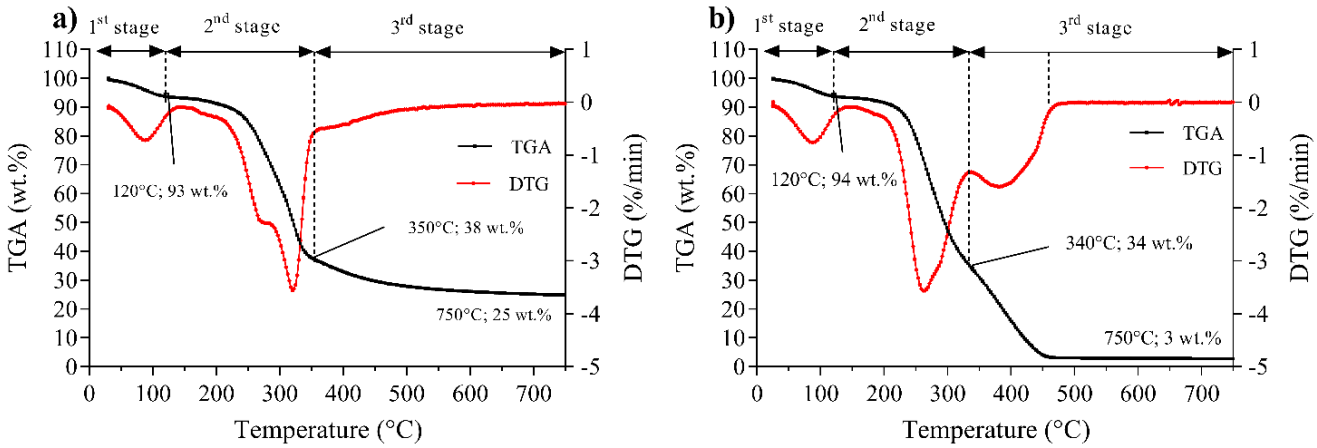

Figure 2.8. TGA-DTG thermograms of WS (a); N_2 atmosphere (b); air atmosphere.

In relation to the FT-IR spectra (Figure 2.9), the functional groups on the surface of WS were also analogous to those in AS and P. However, the peaks corresponding to the primary alcohol C-O stretching present in holocellulose (at a wavenumber around 1030 cm^{-1}) were more pronounced in WS, which its highest holocellulose content could explain (75 wt.% in WS vs. 63 and 62 wt.% for P and AS, respectively). The intensity of the peaks at wavenumbers between 700 and 400 cm^{-1} was also higher than in the other materials, which confirms the connection between the material ash content and this region of the spectra.

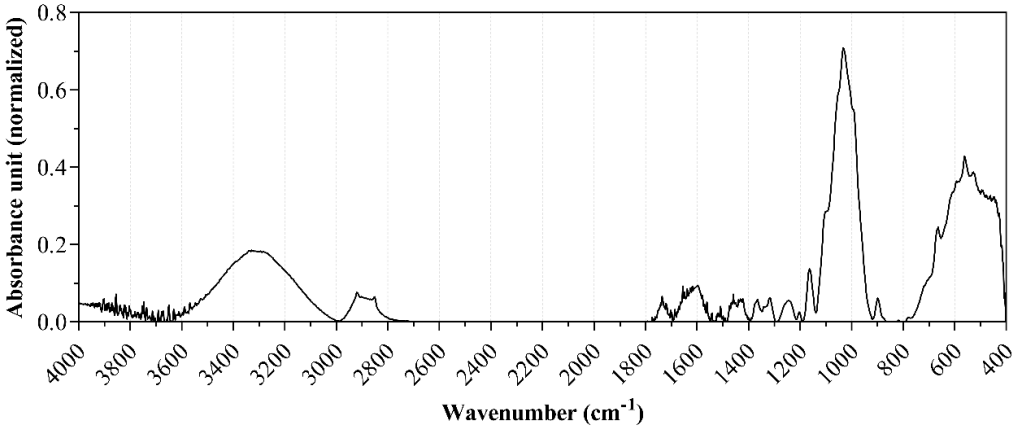

Figure 2.9. FT-IR spectra of WS.

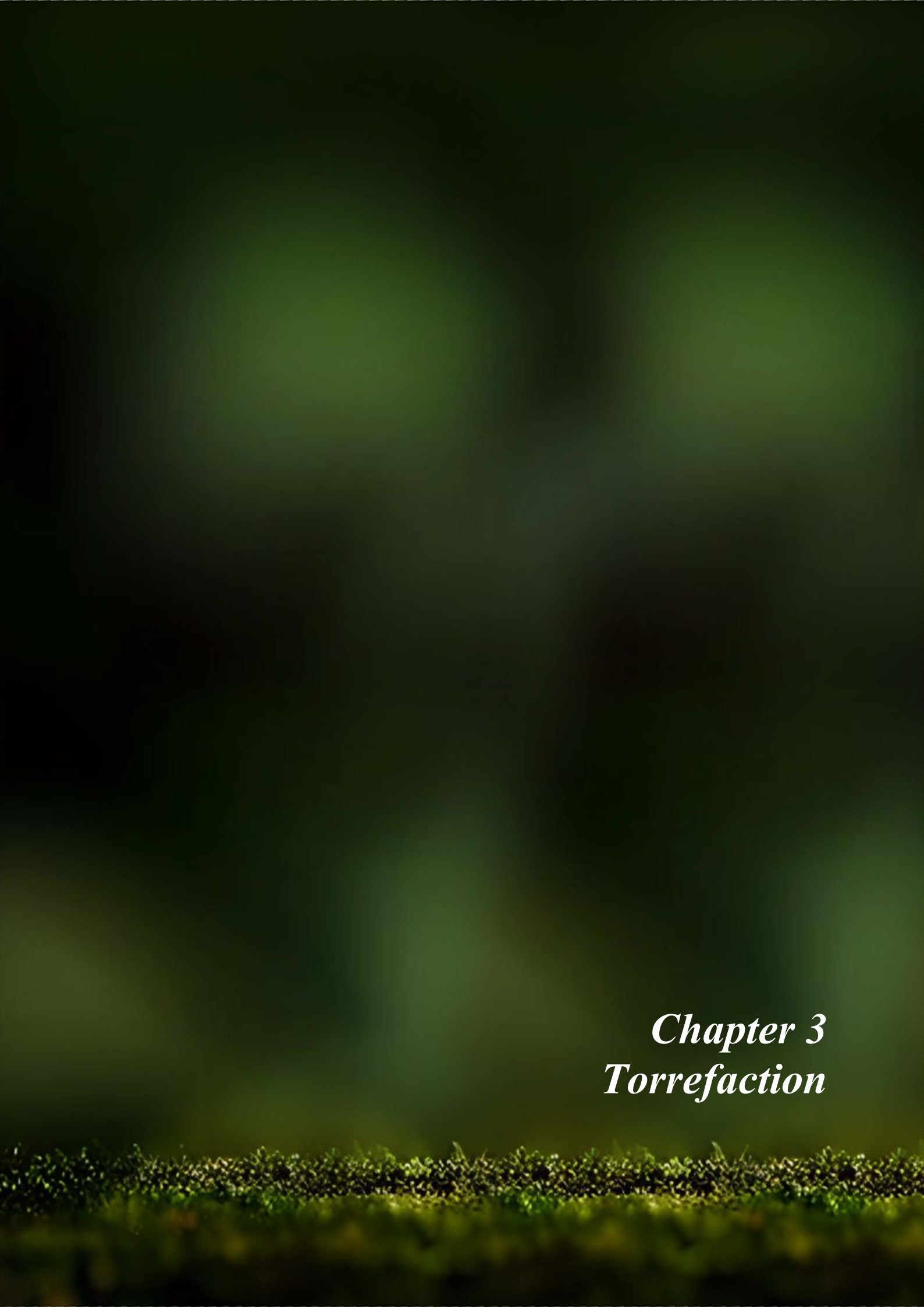

Chapter 3
Torrefaction

3. TORREFACTION

3.1. Introduction

The current chapter shows the results of the torrefaction of AS and P at a lab-scale auger reactor at two temperatures, 220 and 250 °C.

Torrefaction is one of the main thermochemical processes applied to biomass to produce a hydrophobic solid with increased energy density and reduced moisture content. This soft treatment runs at a moderate temperature range, usually between 200 and 300 °C (Bergman and Kiel, 2005; Medic et al., 2012; Tumuluru et al., 2011; Van der Stelt et al., 2011), with a slow heating rate and under an inert atmosphere. The degradation of hemicellulose, cellulose and lignin (partially) in biomass occurs in such temperature range. Hemicellulose, as said above, is the more reactive constituent; it starts to decompose at about 200 °C (Nunes et al., 2018; Tumuluru et al., 2011), while it is subjected to extensive devolatilization and even carbonization at temperatures above 250 °C (Bergman and Kiel, 2005). On the other hand, the first weight loss in the case of cellulose starts around 280 °C (Rao and Sharma, 1998), while lignin decomposition begins around 200 °C, but with slower kinetics than hemicellulose (Nunes et al., 2018; Rao and Sharma, 1998; Tumuluru et al., 2011). Removal of oxygen from the raw material is also one of the main torrefaction goals (Van der Stelt et al., 2011), thus obtaining a hydrophobic solid product with a higher calorific value and a lower O/C ratio compared to the raw material (Cerone et al., 2016; Couhert et al., 2009; Van der Stelt et al., 2011) and reduced moisture content (between 1 and 6 %) (Bergman and Kiel, 2005; Tumuluru et al., 2011). Depending on the torrefaction conditions, the heating value of the biomass can be increased from·17-19 MJ/kg to 19-23 MJ/kg (Couhert et al., 2009; Medic et al., 2012; Mišljenović et al., 2014; Van der Stelt et al., 2011). The oxygen removal from the solid is confirmed by the composition analyses of the gas and liquid products also obtained in the torrefaction process (Nunes et al., 2018). The non-condensable gas product contains a considerable amount of atomic oxygen in the form of CO_2 and CO (Medic et al., 2012), with a small quantity of CH_4 and H_2 (Chen et al., 2018; Nunes et al., 2018; Prins et al., 2006a; Van der Stelt et al., 2011). On the other hand, the liquid product is mainly composed of water coming from biomass dehydration and also from the breaking of hydroxyl groups in the organic material (Nunes et al., 2018), but also contains different organic products such as acetic acid, methanol, furfural, phenol and

hydroxyacetone, produced in the degradation of hemicellulose, cellulose and lignin (Chen et al., 2018; Medic et al., 2012; Nunes et al., 2018; Prins et al., 2006b).

3.2. Experimental method

3.2.1. Torrefaction experiments

The torrefaction of AS and P was carried out in a laboratory-scale auger reactor (800 mm in length with an internal diameter of 55 mm) surrounded by an electrical furnace; the furnace is composed of three zones controlled separately (to control the reactor temperature during the experiments better, avoiding temperature profiles). The schematic diagram of this system is presented in Figure 3.1. The auger reactor operated with continuous solid feeding and removal of volatiles using a flow of N_2 (1 L_{STP}/min) as inert carrier gas. This reactor has already been successfully used in previous works of the GPT for sewage sludge torrefaction (Atienza-Martínez et al., 2015). The solid residence time (27 min) was adjusted by changing the screw rotation frequency (with the highest rotation frequency of the screw). In each P experiment, 1000 g of raw material were processed (particle size of 1-4 mm), while in AS runs, 500 g were employed (particle size between 2 and 4 mm). The torrefied solid produced was collected in the recovering hopper situated at the bottom of the reactor (Figure 3.1). A glass wool filter heated to the same reactor temperature was used to retain the small solid particles swept by the gas without condensing the vapors at this stage. Then, two condensers refrigerated with a water-ethylene glycol recirculating chiller (0.5 °C) were employed to collect the condensable vapors released during the reaction (water and organic compounds), followed by a cotton filter to finish cleaning the gas from traces of humidity and organics (1-2 % of the produced liquid was retained in the cotton filter). The volume of clean and dried gas (free of particles and vapors) was continuously measured using a volumetric gas meter (Gallus G4). The gas composition was analyzed online (semi-continuos analysis, with one measurement every 3 min) by a micro-gas chromatograph (Agilent 3000A), previously calibrated using a standard gas mixture of nine components (H_2, CH_4, CO, CO_2, C_2H_2, C_2H_4, C_2H_6, H_2S). The mass of each produced gas was roughly calculated by combining the composition data registered for different times and the corresponding gas volume measured for each elapsed time.

Two different torrefaction temperatures (220 and 250 °C) were tested for both materials. As has already been reported in the literature, the torrefaction temperature has

a more remarkable effect on the product distribution than other operational factors, such as residence time (Nunes et al., 2018; Pinto et al., 2017). For this reason, the temperature was the only operational factor studied (besides the biomass nature). For both treatment temperatures, good reproducibility and consistent results were observed when repeating the experiments twice, with an experimental error of less than 10 % (coefficient of variability) for each product yield.

Once the torrefaction experiment had finished, the mass of the liquid product was determined by the weight difference between the condensers and the cotton filter before and after the experiment. To ensure the total recovery of the liquid collected in the condensers, whose composition was analyzed in a subsequent step, the condensers were washed with a weighted amount of solvent (methanol). On the other hand, the amount of torrefied solid was determined by the weight difference of the collecting hopper before and after the experiment (the reactor was emptied at the end of the experiment).

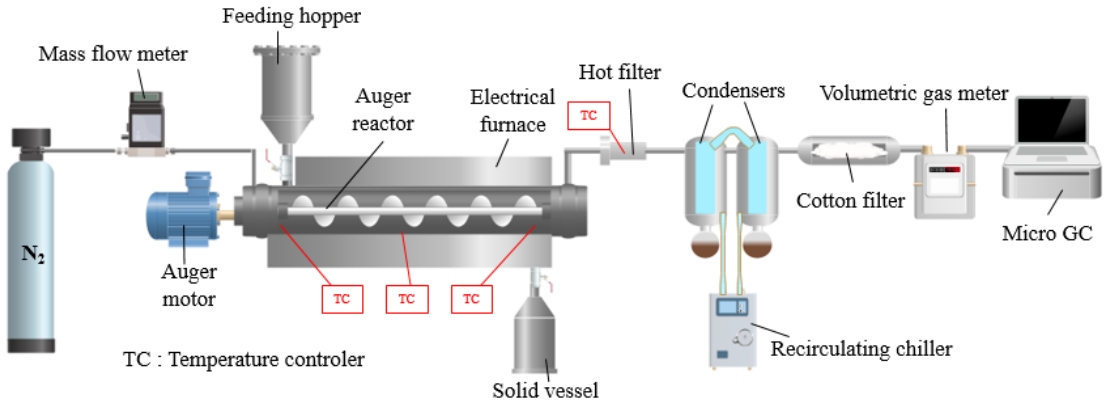

Figure 3.1. Diagram of the experimental torrefaction setup.

The mass yields of gas, liquid and solid products ($Y_{m,i}$) were calculated with respect to biomass fed (Equation 3.1). The total mass of biomass for these calculations was expressed on an as-received basis.

$$Y_{m,i} = \frac{\text{Mass of solid, liquid or gas product (g)}}{\text{Total mass of biomass fed (g)}} \cdot 100 \qquad \text{(Eq. 3.1)}$$

Besides the mass balance, an approach to the energy balance has been calculated, as shown in Equation 3.2. This first approach shows how the initial energetic content of biomass (expressed as its HHV) was distributed into the different products ($Y_{e,i}$) (Bergman et al., 2005; Bergman and Kiel, 2005; Nunes et al., 2018). It must be noticed

that neither the energy externally supplied nor the heat losses were included in the calculation, so this balance was only a first simple approach.

$$Y_{e,i} = Y_{m,i} \cdot \frac{HHV_{\text{torrefaction product}}}{HHV_{\text{biomass}}} \cdot 100 \qquad \text{(Eq. 3.2)}$$

The HHV of the gas product was calculated as a weighted average of the HHV of the gas components, while the HHV of the liquid product was calculated using Dulong's formula (Equation 3.3) based on the results of its elemental analysis expressed on a dry weight basis.

$$HHV = 8{,}140 \,.\frac{\%C}{100} + 34{,}400 \,.\left(\frac{\%H}{100} - \frac{\%O}{800}\right) + 2{,}220.\frac{\%S}{100} \qquad \text{(Eq. 3.3)}$$

3.2.2. Products characterization

As well as the original raw materials (AS and P), the torrefied solids were characterized in terms of ultimate and proximate analyses and HHV. In addition, the thermogravimetric and FT-IR spectroscopy analyses were conducted on the torrefied solids to further study the changes that occurred after this treatment.

The liquid product obtained in the torrefaction experiments was also examined. The water content was analyzed using the Karl Fischer titration method (Mettler Toledo V-20 analyzer), and its density was measured with a portable densimeter Mettler Toledo Densito 30px. On the other hand, the composition of the organic matter in the torrefaction liquid (also referred to as tar) was analyzed by gas chromatography (GC) using an Agilent 7890A GC chromatograph equipped with a flame ionization detector (FID) and combined with an Agilent 5975C mass selective detector (MSD). The detailed operating parameters employed in this characterization are listed in Appendix III. The compounds identification and quantification were performed based on the peaks with more significant areas (more than 92 % of the total area). Firstly, the identification of condensed organic compounds was performed using the MS signal by means of NIST MS Search Program 2.2. Afterward, the quantification of those compounds was based on integrating the peaks of the FID signal. Six standard solutions with 12 compounds each (acetol, furfural, 5-methylfurfural, 2-furanmethanol, guaiacol, creosol, phenol, 4-ethylguaiacol, eugenol, phenol 2,6-dimethoxy, vanillin, and acetic acid) were prepared in a concentration range of 240 - 4600 µg/mL, except for the acetic acid whose concentration range was higher (13323 - 91143 µg/mL). These standards were used for calibrating the FID signal. The

FID response factors of other compounds, that had been identified by GC/MS but not calibrated with the prepared standards, were calculated from the response factor of the most similar standard compound, applying a correction factor following the methodology based on the Effective Carbon Numbers (ECN) (Scanlon and Willis, 1985). More details about the ECN calculations can be found in Appendix III.

3.3. Results and discussion

3.3.1. Product distribution

The results of the product distribution and the energy balance for the torrefaction experiments are summarized in Figure 3.2 (scheme adapted from the bibliography (Bergman et al., 2005; Nunes et al., 2018)). TP220 in Figure 3.2 refers to torrefied pine at 220 °C, TP250 is the torrefied pine at 250 °C, TAS220 is the torrefied argan shells at 220 °C and TAS250 is the torrefied argan shells at 250 °C.

According to the calculated product yields, the mass balance closed fairly well, between 98 % and 102 % in all the experiments. The mass loss in the raw material increased with the torrefaction temperature as the devolatilization process promoted the formation of liquid and gas, thus decreasing the remaining solid yield. The temperature was the main factor affecting the occurrence of the decomposition reactions (Nunes et al., 2018), playing a pivotal role in kinetics, as can be seen in the strong effect that it had on the product yields even with an increase of only 30 °C. For P torrefaction, the solid yield decreased from 69.8 to 61.8 wt.% by increasing the temperature from 220 to 250 °C. While in the case of AS, the reduction was even more accentuated, and the solid yield dropped from 65.8 to 49.7 wt.%. This points to the higher reactivity of AS. Hence, in addition to the temperature effect, hemicellulose, cellulose, and lignin contents in each type of biomass can also affect the torrefaction products distribution, even working under the same operational conditions (Bergman and Kiel, 2005).

Water was the following most abundant product of the torrefaction after the torrefied solid. It was formed, as mentioned before, from the material's moisture evaporation and dehydration reactions occurring due to the loss of hydroxyl groups (Nunes et al., 2018). The yield of water in P torrefaction (on an as-received basis) was 13.9 wt.% at 220 °C and 19.1 wt.% at 250 °C, while in the case of AS it was higher, reaching 19.2 and 23.7 wt.% at 220 °C and 250 °C, respectively. On the other hand, the yield of condensable organics with respect to biomass fed increased from 7.6 to 9.2 wt.%

in the case of P and from 7.8 to 15.7 wt.% in the case of AS when raising the temperature from 220 to 250 °C. The same upward trend was observed for non-condensable gas, which increased from 5.4 to 10.4 wt.% for AS and from 10.8 to 12.3 wt.% for P. From these results, it can be concluded that AS tended to generate more condensable organics than non-condensable gas in the torrefaction process and vice versa for P, especially at higher temperatures.

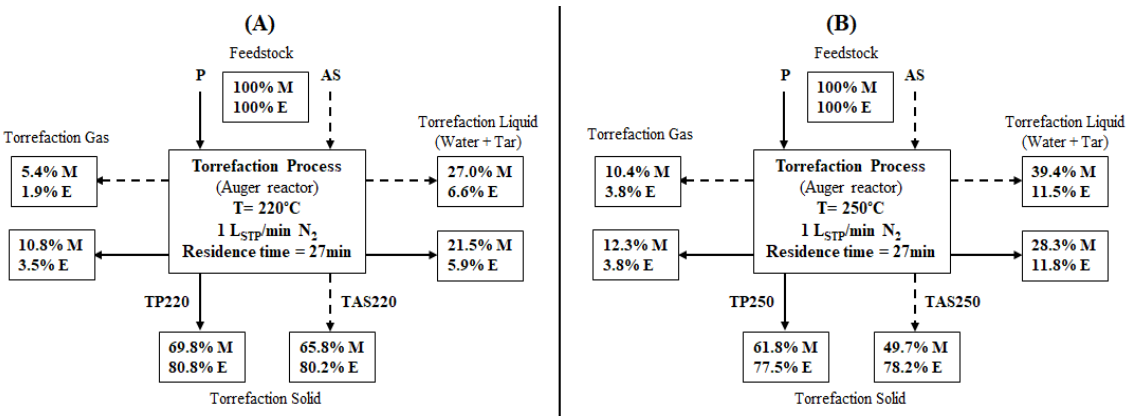

Figure 3.2. Schematic flowsheet of mass (M) balance and approach to energy (E) balance in the torrefaction processes of AS and P at 220 °C (A) and 250 °C (B).

Other studies in the literature showed a wide range of product yields (see Appendix III). For example, in the study of Brachi et al. (Brachi et al., 2017), the torrefaction of sugar beet pulp (smaller particle size between 1 and 2 mm and ash content up to 4 wt.%) at 250 °C in a fixed bed reactor led to the same yield of solid product (49 wt.%) as TAS250 but different production of gas (34.4 wt.% for sugar beet pulp vs. 10.4 wt.% for AS) and liquid product (16.6 wt.% for sugar beet pulp vs. 39.4 wt.% for AS) when operating at similar conditions but in different reactor type and particle size. For a shorter residence time (15 min vs. 27 min in this work), higher torrefied solid yield (up to 83 wt.%) was reported in the study of Asadullah et al. when torrefying palm kernel shell (bigger particle size between 7 and 15 mm and ash content of 3 wt.%) in a fixed bed reactor (Asadullah et al., 2014).

The 89-94 % of the calorific value of the raw materials remains as energetic content in the torrefaction products. Regarding the effect of torrefaction temperature on the energy distribution (calculations shown in Appendix III), the most remarkable impact was observed on the energy remaining in the form of tar, which was higher at 250 °C (6.6 %

at 220 °C and 11.5 % at 250 °C in the case of AS). As shown in Figure 3.2, the energy balance was hardly affected by the biomass nature, especially at 250 °C.

3.3.2. Solid product characterization

The torrefied solid is the product of interest in the torrefaction process, which should have improved fuel properties compared with the raw material. The obtained solids (see their appearances in Figure 3.3) became darker with the increased temperature because of the caramelization of cellulose and hemicellulose components and the formation of quinones (Boonstra, 2008; Zheng et al., 2012). In addition, the high initial hardness of AS was noticeably reduced (the torrefied material was easily crushed).

Figure 3.3. Appearance of AS and P before and after the torrefaction at 220 °C and 250 °C.

The characterization results are summarized in Table 3.1 (for an easier comparison, the characterization results of the raw AS and P are listed again in the same table). The HHV of AS increased from 18.6 to 22.7 MJ/kg in TAS220 and to 27.0 MJ/kg in TAS250, which means respective increases of 22 % and 45 %. In the case of P, this increase was slightly lower, from 18.5 to 21.4 MJ/kg in TP220 and up to 23.2 MJ/kg in TP250 (increases of 16 % and 25 %, respectively). On the other hand, the fraction of fixed carbon was more than doubled after torrefaction at 250 °C: from 13 % in P to 28 % in TP250 and from 16.5 % in AS to 45 % in TAS250. For both materials, this energy density gain was ascribed to the release of volatiles (Grigiante and Antolini, 2014) and the increase in the fixed carbon content, and also consistent with the observed decrease in the O/C molar

ratio in the torrefied solid due to the important release of CO_2 (section 3.3.3) and H_2O because of dehydration reactions.

Table 3.1 also lists the evolution of the macro-components composition of the material after torrefaction. The hemicellulose content dropped from 12 % in P to 3 % in TP250 and from 21.2 % in AS to 0.6 % in TAS250. These results attested that hemicellulose was, in both materials, the major decomposed component during torrefaction, being almost totally degraded, especially in the case of AS, which agrees with other results found in the literature (Kulkarni et al., 2016; Pinto et al., 2017). The diminution of cellulose content was also significant in both materials, regardless of the temperature of the treatment. This decrease appeared more acute in the case of P (from 46 % to 33 % in TP220) than in AS (from 35.2 % to 31.3 % in TAS220). In terms of degraded mass, the effect of the torrefaction temperature on the cellulose degradation rate was more significant in AS than in P: 41 % of cellulose in AS was degraded at 220 °C and 52 % at 250 °C, while in the case of P, the results at both temperatures were more similar (50 % of cellulose was degraded at 220 °C and 53 % at 250 °C).

Regarding lignin, data in the literature showed that its decomposition starts at 200 °C (Kawamoto, 2017; Nunes et al., 2018). Therefore, during torrefaction at 220-250 °C, lignin depolymerization should be expected to occur to some extent. In fact, as will be discussed below, the presence of some phenolic compounds in the torrefaction liquid points to the degradation of lignin. However, as shown in Table 3.1, the lignin content increased from 29 % in P to 53 % in the case of TP250 and from 34 % in AS to 62 % in the case of TAS250. This increase was not only observed in the percentage data but also in the net weight of lignin produced. This increase could be explained by the formation of complex structures from the condensation and repolymerization processes of lignin itself during the torrefaction process (after breaking the ether bonds and forming C-C ones) (Kulkarni et al., 2016) or from the decomposition of polysaccharides and subsequent condensation reactions, which were insoluble in sulfuric acid (72 %) and therefore quantified as lignin by the Van Soest analysis procedure (considered as technical lignin).

As commented before and shown in Table 3.1, the extractives content of P and AS were found to be around 4 % and 0.2 %, respectively. After torrefaction, the extractives content in P dropped from 4 % to around 0.87 % in TP220 and 1.67 % in TP250, while in the case of AS, the fraction of extractives increased slightly to 0.4-0.5 %. For a better

understanding, the extractives from the torrefied materials were dissolved in DCM and analyzed by GC/MS. In general, the composition of the extractives in both materials significantly changed after the torrefaction treatment. Firstly, the concentration of the heaviest molecules, which were initially present in the raw materials, was significantly reduced after torrefaction, showing lower peak areas in the chromatograms or even totally disappeared as the torrefaction temperature increased. This result highlights that torrefaction eliminated the extractives from the treated biomass. Some other works in the literature have reported the same result (Nunes et al., 2018), but others contradict it (Pinto et al., 2017). Therefore, the apparent increase observed in the extractive content of AS after torrefaction may be related to other volatile compounds, mainly phenol-derived compounds. These compounds did not appear in the extractives obtained from the untreated raw materials but were present in the torrefaction liquids (see section 3.3.3), indicating that the tar produced during torrefaction was adsorbed on the surface the torrefied solids, thus justifying the relative increase in the extractives amount.

Table 3.1. Ultimate and proximate analyses, HHV, and chemical composition of AS and P before and after torrefaction at 220 °C and 250 °C.

	AS	TAS220	TAS250	P	TP220	TP250
Proximate analysis (wt. % ar. basis)						
Ash	0.20 ± 0.04	0.4 ± 0.1	0.73 ± 0.01	1.8 ± 0.2	3.4 ± 0.4	4.9 ± 0.2
Moisture	8.74 ± 0.03	1.4 ± 0.4	2.0 ± 0.4	7.7 ± 0.2	1.99 ± 0.09	2.2± 0.2
Volatile matter	74.6 ± 0.3	69 ± 2	52.6 ± 0.8	77 ± 2	72.2 ± 0.6	64.4 ± 0.7
Fixed Carbon	16.5 ± 0.4	30 ± 2	45 ± 1	13 ± 2	22 ± 1	28 ± 1
Ultimate analysis (wt. % ar. basis)						
C	47.5 ± 0.2	59.8 ± 0.2	68.9 ± 0.1	46.74 ± 0.02	55.51 ± 0.08	58.5 ± 0.2
H	6.55 ± 0.08	5.5 ± 0.1	4.75 ± 0.04	6.28 ± 0.04	6.03 ± 0.06	5.26 ± 0.06
N	0.177 ± 0.003	0.243 ± 0.005	0.33 ± 0.01	0.093 ± 0.001	0.15 ± 0.01	0.21 ± 0.02
S	0.044 ± 0.001	0.040 ± 0.001	0.040 ± 0.001	0.050 ± 0.001	0.044 ± 0.001	0.04 ± 0.01
O[a]	45.5 ± 0.2	33.9 ± 0.3	25.2 ± 0.1	45.04 ± 0.02	34.7 ± 0.1	31.0 ± 0.3
O/C molar ratio	0.58	0.43	0.28	0.72	0.47	0.4
H/C molar ratio	1.65	0.78	0.43	1.61	1.3	1.08
HHV (MJ/kg)	18.61 ± 0.04	22.67 ± 0.04	26.97 ± 0.05	18.5 ±0.1	21.44 ± 0.03	23.2 ± 0.2
Macro-components composition (wt. % ar. basis)						
Extractives	0.2 ± 0.1	0.4±0.01	0.5 ± 0.1	4 ± 1	0.87 ± 0.02	1.67 ± 0.03
Hemicellulose	21 ± 1	5 ± 0.2	0.60 ± 0.03	12 ± 1	7 ± 1	3 ± 1
Cellulose	35 ± 2	31 ± 2	34 ± 2	46 ± 3	33 ± 2	35.1 ± 0.1
Lignin	34 ± 2	61 ± 3	62 ± 3	29 ± 1	53 ± 1	53 ± 1

[(a)] Calculated by difference (wt.%): O=100-C-H-N-S-Ash.

Figure 3.4 shows the comparative DTG plots of AS and P before and after torrefaction at 220 °C and 250 °C. In the torrefied materials, a noticeable diminution and/or disappearance of peaks in the temperature interval between 30 and 300 °C was observed. This fact can be correlated with the differences in moisture and hemicellulose contents, as commented above. The area of the peak situated between 200 and 300 °C was significantly reduced in TAS220 and TAS250, which agrees with the almost complete removal of hemicellulose found in the torrefied materials with the Van Soest analysis (degradation of 85 % and 98.6 % of hemicellulose in AS after torrefaction at 220 °C and 250 °C, respectively). The reduction of these peak areas was more pronounced as the torrefaction temperature increased, indicating a lower hemicellulose content in TAS250.

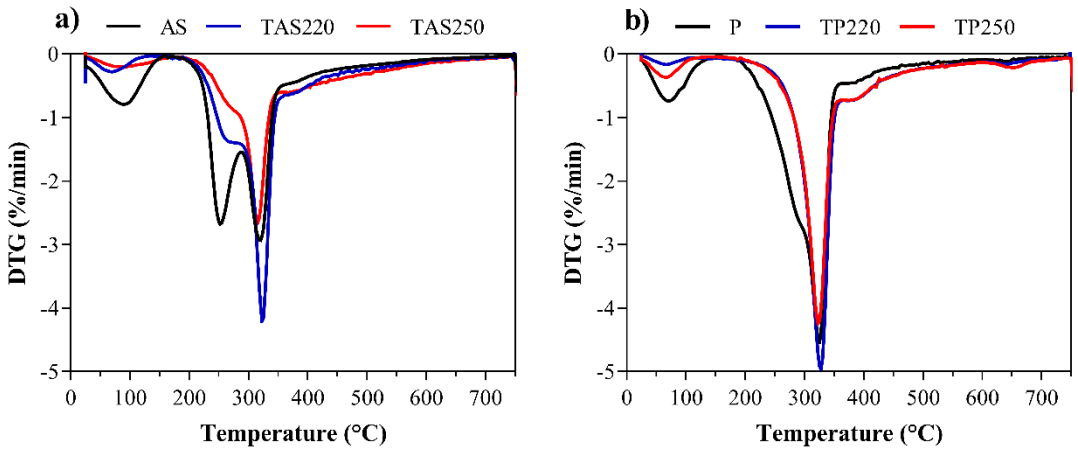

Figure 3.4. DTG plots of AS and P before and after the torrefaction at 220 °C and 250 °C.

The FT-IR spectra of the two materials before and after the torrefaction treatment are represented in Figure 3.5. In general, the FT-IR spectrum of AS changed more significantly than that of P after torrefaction. The peaks at wavenumbers ranging between 3600 and 3100 cm^{-1} and between 3000 - 2800 cm^{-1} decreased with the increase of torrefaction temperature, corresponding to the disappearance of hydroxyl groups (formation of water and alcohols) and alkyl groups in the torrefied solids. The peak at wavenumbers from 1760 to 1700 cm^{-1}, which corresponds to C=O band assigned to acids, esters, aldehydes and ketones, was reduced during the torrefaction of AS. This fact could be correlated with the important release of acetic acid in the torrefaction liquid during the

experiments with AS, which may likely be due to the cleavage of acetyl radicals ($COCH_3$), especially in hemicellulose (Nunes et al., 2018) (see section 3.3.3). Peaks at wavenumbers around 1640-1500 cm^{-1} indicate aromatic links, and its intensity in TAS220 and TAS250 was slightly increased compared to the raw AS. Finally, it should also be noted that the reduction of the peaks at 1250 and 1050 cm^{-1} after the torrefaction of both materials corresponds to the reduction of ether bonds (C-O-C) in lignin, xylan and cellulose (Shi et al., 2012).

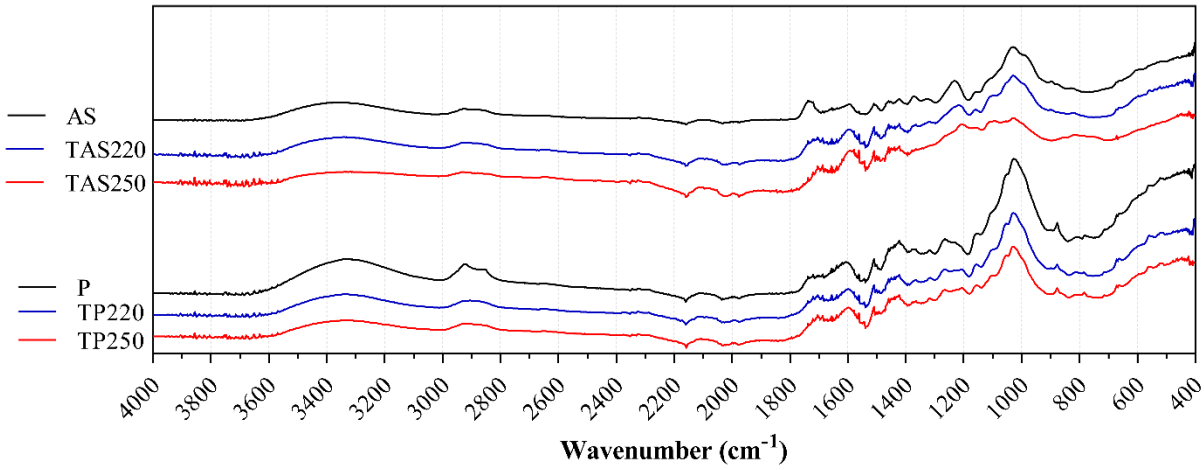

Figure 3.5. FTIR spectra of AS and P before and after the torrefaction at 220 °C and 250 °C.

3.3.3. Characterization of liquid and gas products

The liquid produced in the torrefaction process mainly comprised water and oxygen-containing organic compounds. The GC/MS/FID analysis (Table 3.2) allowed identifying and quantifying around 59-67 % of the mass of organic compounds in the case of AS and 32 % for P. Methanol is known to be one of the most abundant organic products in the torrefaction liquid product (Medic et al., 2012) due to the degradation of xylan or from the methoxyl groups of uronic acid (Demirbaş, 2000). In fact, methanol was clearly identified in the chromatograms, but as it had been used as a solvent for recovering the liquid from the condensers, its actual production during torrefaction could not be estimated. This fact, together with the presence of oligomeric compounds (with high molecular weight) undetectable by GC (Fonts et al., 2021; Pinheiro Pires et al., 2019), may fit the remaining fraction of organics that could not be quantified by GC/MS/FID. Most of the identified organic compounds belonged to the families of carboxylic acids,

alcohols, ketones, aldehydes, furans and phenol monomers. Acids, alcohols, ketones, and furans are typical products of the thermal degradation of hemicellulose (Zheng et al., 2012), but they can also be produced during cellulose degradation (Demirbaş, 2000). More specifically, acids have been found to be produced as soon as the temperature threshold for the thermal decomposition of cellulose (around 270 °C in the case of some woody biomass) is exceeded (Melkior et al., 2012). On the other hand, the production of phenols is known to result from lignin decomposition.

Table 3.2 presents the individual GC/FID quantification results of the main compounds identified in the torrefaction liquids. As can be seen, the most abundant compound was acetic acid. Its concentration increased slightly with the torrefaction temperature from 146 to 159 mg/g liquid in the case of AS, while the opposite trend was observed for P (dropped from 48 to 27 mg/g). Several studies related the formation of acetic acid in torrefaction with the thermolysis of acetyl radicals linked to the hemicellulose pentosans (Demirbaş, 2000; Nunes et al., 2018). On the other hand, the content of acetol was higher in the liquids produced from P, which could be explained by the higher content of cellulose in P, which was partially degraded during torrefaction. Moreover, furfural content, which was also one of the major compounds in the torrefaction liquids, was not affected by the torrefaction temperature. Its formation was related to the dehydration of the xylose unit (hemicellulose component) (Demirbaş, 2005) or the degradation of cellulose via the dehydration of the formed levoglucosan followed by formaldehyde degradation (Van der Stelt, 2011). Among phenolic compounds, guaiacol and syringol were the most abundant in AS torrefaction liquids, which were derived from coniferyl alcohol (G) and sinapyl alcohol (S), respectively. In contrast, phenols in P tar were mainly derived from p-coumaryl alcohol (H) and coniferyl alcohol, such as phenol, eugenol and guaiacol. Temperature promoted the production of most of the identified phenols.

Non-condensable gas was the minority product (by weight) in the torrefaction of both AS and P. On an N_2-free basis, CO_2 (62 - 65 vol.% for AS and 61 - 64 % for P) and CO (25 - 30 vol.% for AS and 32 - 34 % for P) were the main gases produced. Other gases were detected in smaller percentages, such as CH_4 (6 - 7 vol.% for AS and 3 % for P) and H_2 (1 vol.% for both AS and P). The formation of CO_2 (at this relatively low temperature range) is due to the decarboxylation reaction of the carboxyl group in hemicellulose (Atienza-Martínez et al., 2015; Yang et al., 2007), while CO is the result of carbonyl,

carboxyl and ether groups cracking (Yang et al., 2007). Such volumetric concentration data match with the following mass yields calculated with respect to the mass of AS and P fed, respectively: 4 - 8 wt.% (AS) and 8 - 9 wt.% (P) for CO_2, 1 - 2 wt.% (AS) and 3 wt.% (P) for CO, 0.2 - 0.3 wt.% (AS) and 0.2 wt.% (P) for CH_4 and 0.003 - 0.005 wt.% (AS) and 0.004 - 0.1 wt.% (P) for H_2 (the higher the torrefaction temperature, the higher yield of each individual gas).

Table 3.2. Concentration of organic compounds in the torrefaction liquids (mg/g liquid, quantified by GC/FID).

	Concentration in the torrefaction liquid (mg/g torrefaction liquid)			
Compound	**AS, 220 °C**	**AS, 250 °C**	**P, 220 °C**	**P, 250 °C**
Furan, tetrahydro-2,5-dimethoxy-	-	1.9	-	1.8
Acetol	6	11	23.6	28.9
1-Hydroxy-2-butanone	9	11	9.6	11.6
Acetic acid	146	159	48	27
Furfural	14	14	8.7	9
Propanoic acid	5.90	9.3	6.4	4.8
5-methyl furfuryl	0.500	0.7	0.928	1.1
2-Furanmethanol	1.7	2.9	5.0	5.6
2-Cyclopenten-1-one, 2-hydroxy	0.6	1.30	0.69	0.46
2-Cyclopenten-1-one, 2-hydroxy-3-methyl-	0.6	1.80	1.26	1.71
Guaiacol	1.5	3.7	1.61	2.4
Creosol	0.6	2.3	0.8	1.4
Phenol			0.21	
4-Ethylguaiacol	0.5	1.4	0.5	0.9
Cyclopentanol	-	0.7	1.7	2.0
Eugenol	-	0.3	0.53	0.6
4-Vinylguaiacol	0.3	0.6	0.61	0.6
Syringol	1.7	4.9	-	-
Trans-Isoeugenol	1	1.4	1.8	2.2
Methoxyeugenol	1	3.4	-	-
Benzene, 1,2,3-trimethoxy-5-methyl-	0.5	1.8	-	-
Vanillin	0.4	0.6	0.87	-
Guaiacylacetone	-	0.4	0.48	0.5
Total	192.0	235.3	113.1	102.0

3.4. Conclusions

The torrefaction treatment of argan shells and forest pine residues has been investigated in a lab-scale auger reactor (temperature of 220-250 °C and residence time of 27 min). The main conclusions drawn from this study are the following:

- Torrefaction can be a promising pretreatment for argan shells valorization, attaining an important increase in the solid HHV (up to 45 % higher), a significant reduction of O/C ratio (by more than half) and an increase in the percentage of fixed

carbon (almost threefold higher). Hence, the torrefied solid could be used as a better-quality fuel.

- A small change in the torrefaction temperature of only 30 °C strongly affected the distribution and properties of the products, showing, for example, a solid yield decrease from 69.8 to 61.8 % in the case of P and from 65.8 to 49.7 % in the case of AS.

- Even though having similar percentages of C, H, N, O and the same HHV, the behavior of AS and P during torrefaction was quite different. This means that differences in the material macro-components composition strongly affect both the thermal behavior of biomass and the properties of the torrefaction products.

- DTG and Van Soest analyses revealed that hemicellulose in the torrefied argan shells was almost totally removed even at the lowest torrefaction temperature (220 °C), while forest pine residues required more severe treatment.

- Besides the torrefied solid, water and CO_2 were also important products in the torrefaction of both materials, as well as oxygen-containing tar compounds.

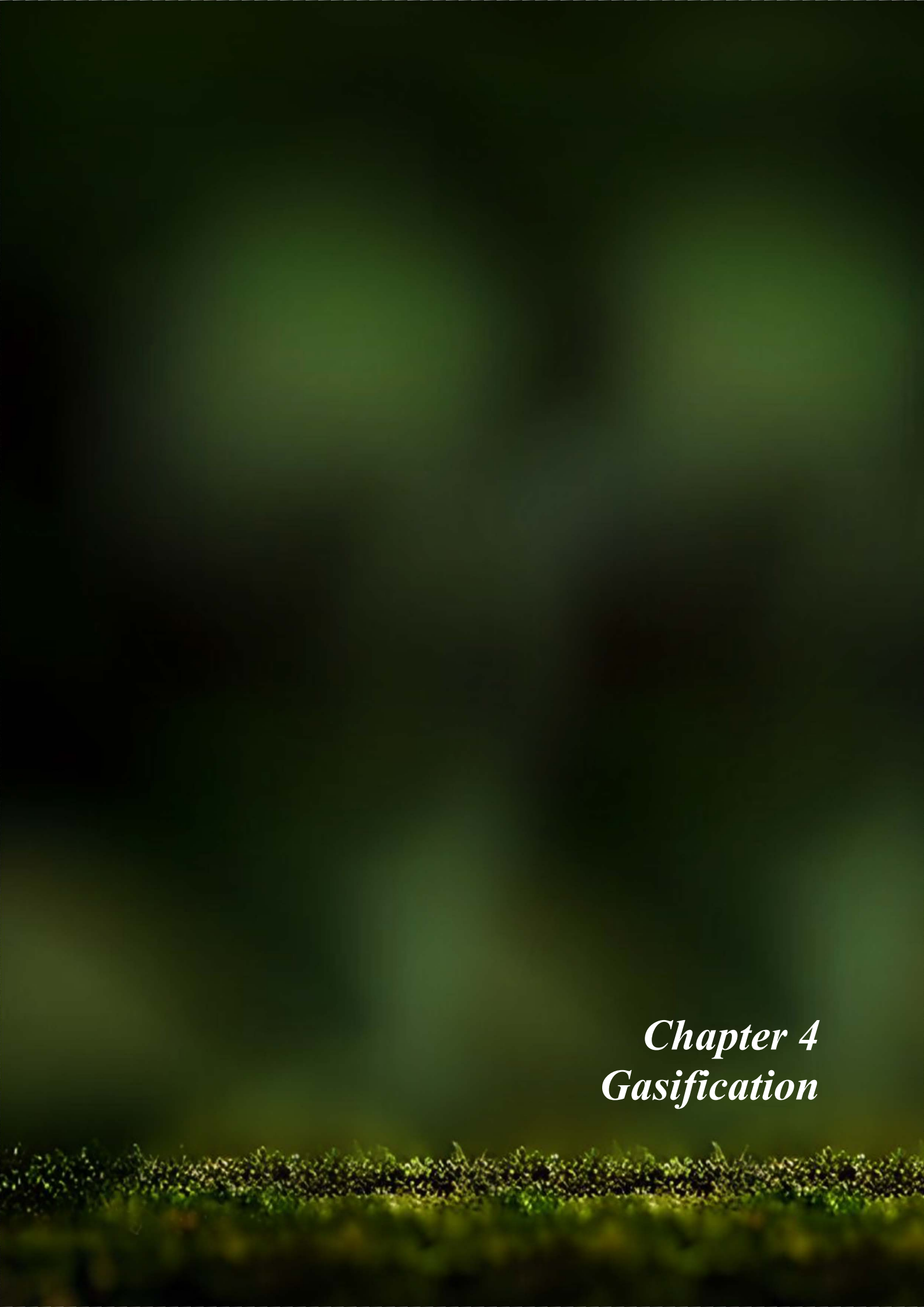

Chapter 4
Gasification

4. GASIFICATION

4.1. Introduction

This chapter presents the results of the study about the air and air-steam gasification of argan shells (AS), forest pine residues (P) and torrefied argan shells at 220 °C (TAS220). This part of the work is not only focused on comparing the gasification behavior of AS and P but also on investigating the effect of torrefaction as a pretreatment stage.

Gasification is the conversion of a carbonaceous feedstock into a gaseous fuel at high temperatures (typically in the range of 800-1200 °C) using an oxidative medium, such as air, oxygen or steam (Knoef, 2005). The main product of gasification is the gas (usually referred to as syngas), which consists of a mixture of hydrogen (H_2), carbon monoxide (CO), carbon dioxide (CO_2), nitrogen (N_2) (if using air or enriched air as gasifying agent), methane (CH_4) and other light hydrocarbons. Clean syngas could be used as a fuel for heat and/or power production due to its reasonably high energy density (Cerone et al., 2020). However, it seems even more attractive to evaluate its potential use as a feedstock for Fisher-Tropsch-based processes to produce a great variety of liquid biofuels and biochemicals, such as methanol, ethanol, higher alcohols or dimethyl ether (Dayton et al., 2019). The synthesis of these biochemicals requires specific H_2/CO molar ratios, ranging from 2 for methanol to 1 for higher alcohols (Spath and Dayton, 2003).

The quality of syngas in terms of the H_2/CO ratio can be improved by using steam in the mixture of gasification agents, as has been highlighted by research works dealing with wood gasification (Cerone et al., 2020; Nguyen et al., 2020). However, this trend has scarcely been corroborated in works involving lignin-rich materials such as fruit shells.

In addition to syngas, char (carbonaceous solid) and tar (mixture of heavy and condensable hydrocarbons) are also generated as by-products in this conversion process, thus constraining the gas production rate. Moreover, the existence of tar in the syngas negatively impacts its subsequent utilization by causing difficulties associated with condensation in downstream equipment, formation of aerosols and polymerization (Gil-Lalaguna et al., 2014), and contributing to the deactivation of the catalysts used in the subsequent gas upgrading stages. In this regard, several studies in the literature outline that gasification accompanied by a previous torrefaction pretreatment of woody biomass

could provide benefits such as reducing tar concentration in the gas (Cerone et al., 2016; Chen et al., 2013; Kulkarni et al., 2016), as the torrefied material has a decreased O/C ratio and volatile content, and a higher energy density and carbon content (Nguyen et al., 2020). It has been stated that gasification of torrefied Eucalyptus (at 280 °C) wood chips resulted in a five-fold lower tar concentration in the syngas (164 g/m^3 for the raw Eucalyptus wood chips vs. 34 g/m^3 for the torrefied one) and a noticeable increment of the thermal power of the plant (Cerone et al., 2016). On the other hand, in the study of Kulkarni et al., a similar trend was observed in the gasification of torrefied pine, producing less than half of tar yield (8 g/ kg of raw dried pine vs. 3.9 g/kg of torrefied pine) (Kulkarni et al., 2016). The effect of torrefaction pretreatment on tar production in gasifying such types of lignocellulosic materials seems clear. However, this effect has been scarcely studied for lignin-rich biomass, such as nutshells, and conclusions should not be directly extrapolated to these materials since lignin is known to be less affected by torrefaction than the carbohydrate fraction of lignocellulosic biomass (Li et al., 2016).

In the last decade, some studies have been dedicated to investigating the use of fruit shells in the gasification process using different reactors (Barco-Burgos et al., 2021; Cerone et al., 2020; Menon et al., 2021; Yahaya et al., 2019; Zubair Yahaya et al., 2020). For instance, Yahaya et al. studied air gasification of coconut and palm kernel shells at 700-900 °C, producing syngas with an H_2/CO ratio of 0.63-0.84 for coconut shells and 0.6-0.75 for palm kernel shells (Yahaya et al., 2019). On the other hand, Macrì et al. stated that almond shells gasification theoretically exhibited a higher gas yield but lower cold gas efficiency compared with other feedstocks with higher moisture content (microalgae, digestate and sludge) (Macrì et al., 2020).

In the present chapter, the gasification of torrefied argan shells, using air and air-steam mixtures as a gasifying agents, has been experimentally evaluated and compared with the raw AS gasification in order to define the impact of such pretreatment on important gasification quality parameters. Additionally, P gasification was also tested to compare, at identical operation conditions, the effect of the biomass on the syngas characteristics.

4.2. Experimental methods

4.2.1. Gasification experiments

Gasification experiments of AS, P and TAS220 were performed operating at atmospheric pressure in a laboratory-scale fluidized bed reactor (Figure 4.1). Regarding the torrefied material, TAS220 was chosen as gasification feedstock because of its higher production yield in the torrefaction stage compared to the material torrefied at 250 °C (as shown in Chapter 3).

The gasifier was a refractory steel tubular reactor composed of a bed zone of 40 mm inner diameter and a freeboard zone with an inner diameter of 63 mm. An initial bed (100 g) of calcined dolomite (at 900 °C) with a particle size of 350 to 500 μm was initially introduced into the reactor. The use of calcined dolomite as bed material has been proven to report benefits in catalytic cracking of the generated tar (Berrueco et al., 2014). The feedstock (AS, P or TAS220) was fed semi-continuously into the reactor as pulses of 3.5 g per minute through a double-valve system located on top of the reactor. When the solid inside the reactor (mixture of dolomite and char) exceeded the available bed height, set by a lateral pipe, it overflowed into a closed container.

On the other hand, the gasifying agent, air or a mixture of air and steam, entered the reactor below the distributor plate and passed through the dolomite bed. Vapors and gases passed through a cyclone and a glass wool filter (both heated to 450 °C), where the smallest solid particles (char and dolomite) were retained. Then, the condensation and analysis systems were similar to those used in the torrefaction process (see Chapter 3, section 3.2).

Each gasification experiment took 60 min, and the AS and P gasification runs were repeated twice to estimate the experimental variability.

The lower heating value of the obtained gas and the cold gas efficiency were calculated according to Equations 4.1 and 4.2, respectively.

$$LHV_{gas} = \sum (x_i \cdot LHV_i) \qquad \text{(Eq. 4.1)}$$

$$\text{Cold gas efficiency } (\%) = \frac{LHV_{gas} \cdot V_{gas}}{LHV_{feedstock} \cdot m_{feed}} \cdot 100 \qquad \text{(Eq. 4.2)}$$

where LHV_i (MJ/m^3_{STP}) is the lower heating value of each gaseous component and x_i its volumetric fraction (measured experimentally online through the micro-gas

chromatograph), V_{gas} is the total volume of produced gas (m^3_{STP}), $LHV_{feedstock}$ is the lower heating value of the biomass fed (AS, P or TAS220), and m_{feed} is the total mass of biomass fed during the experiment (kg).

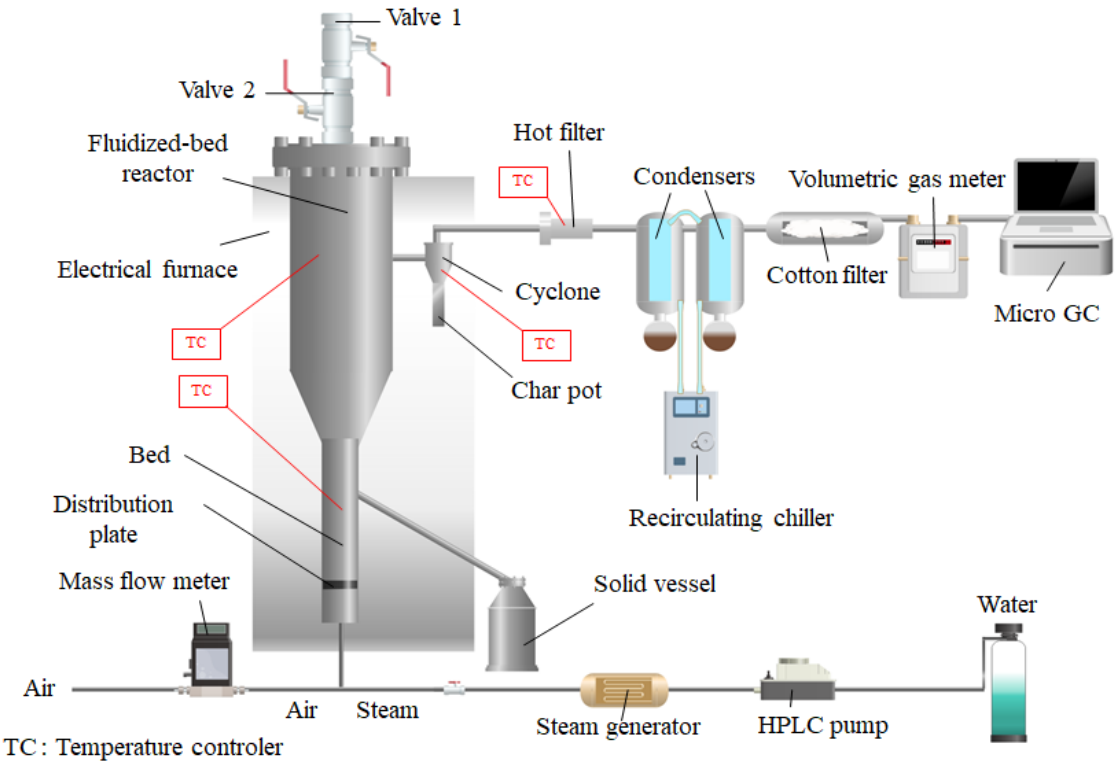

Figure 4.1. Diagram of the experimental gasification setup.

4.2.2. Products characterization

In addition to the gas analysis followed online during the experiment, the produced solid and the condensed liquid from AS, P and TAS220 gasification were offline analyzed. The generated char was characterized in terms of ultimate and proximate analyses, while the liquid fraction was analyzed by Karl Fischer titration and GC/MS/FID (more details about the operational parameter are shown in Appendix IV). The FID signal was calibrated for the gasification samples using five calibration solutions prepared in concentrations ranging between 10 and 500 µg/mL from different dilutions of a commercial standard (PAH Mix 3 Supelco) containing 11 polycyclic aromatic hydrocarbons (naphthalene, acenaphthylene, acenaphthene, fluorene, phenanthrene, anthracene, fluoranthene, pyrene, benz[a]anthracene, chrysene, benzo[b]fluoranthene).

4.2.3. Thermodynamic equilibrium model

Before performing the gasification runs, the process was theoretically modeled by studying the chemical equilibrium using HSC 9.0 software add-in in Excel. The calculations were based on three statements: i) minimization of the Gibbs free energy of the system, ii) compliance with the atomic balance in the whole process, and iii) establishment of an auto-thermal gasification reaction by introducing enough amount of air for reaching a required temperature (the energy balance was accomplished without considering the energy recovery from the products streams and taking into account 5 % of heat losses). By entering the characteristics of the raw material (mass flow, elemental analysis, ash and moisture contents and HHV), the gasification atmosphere composition (including S/C: steam to carbon mass ratio) and the expected gasification temperature, as well as other parameters related to the energy balance (calorific capacities and standard enthalpies of formation of reagents and products), the calculation procedure determined the required equivalent ratio (ER) in the gasification process for getting an auto-thermal reaction at a specific temperature. This simulation model also calculated the gas production and composition, fulfilling the conditions mentioned earlier. This model was run in a wide range of temperatures (750 - 1100 °C) and S/C ratios (up to 1.1 g H_2O/g biomass), and the results are detailed in section 4.3.1.

The operational conditions for the experimental gasification runs were set based on these simulation results and summarized in Table 4.1. It is to outline that in the experiments in which the gasifying agent was only air (runs # 1, 2, 5, 6 and 9), the S/C ratio is not zero as it does not only refer to the added flow of steam, but also includes the steam provided by the material moisture (g of moisture/ g of C). When feeding steam together with air as gasifying agent (runs # 3, 4, 7, 8 and 10), the S/C ratio of 0.5 comprises both the material moisture and the steam added.

Table 4.1. Operational conditions in the gasification experimental runs.

Run #	Feedstock	Gasifying agent	T (ºC)	S/C	ER (%)
1, 2	AS	Air	850	0.184	31.1
3, 4	AS	Air-steam	850	0.5	32.2
5, 6	P	Air	850	0.165	28.86
7, 8	P	Air-steam	850	0.5	29.97
9	TAS220	Air	850	0.024	33.4
10	TAS220	Air-steam	850	0.5	35.0

4.3. Results and discussion

4.3.1. Thermodynamic equilibrium model results

As commented before, the gasification model described in the previous section was run under a wide range of operational conditions (T=750 - 1100 °C and S/C=0 - 1.1) to determine the ER required for auto-thermal gasification and to evaluate the gas composition once chemical equilibrium was reached for the studied materials (AS, P, TAS220 and TAS250). Figure 4.2 shows the results of these simulations for the raw AS, P and the torrefied materials at different temperatures and S/C values. As expected, the higher the temperature, the higher the ER required for operation. In general, ER for auto-thermal and chemical equilibrium conditions ranged between 28 % and 45 %. Note that the equilibrium calculation in the case of TAS250 showed lower ER values, especially at the lowest studied temperatures, and also incomplete solid conversion.

The gas quality can be evaluated through the H_2/CO ratio. As expected, the increase of the S/C ratio led to a higher H_2/CO ratio in all cases, regardless of the temperature evaluated, due to the shift of the water-gas shift reaction (R4.1) to the products side, which was one of the most representative reactions of the gasification process. The H_2/CO ratio was reduced with increasing the temperature (shift of R4.1 towards the left side because of its exothermic character), and this reduction was even more pronounced with the incorporation of steam in the gasification atmosphere, as steam could help to increase H_2/CO at lower temperatures, but its effect was much less significant as increasing the temperature because the equilibrium constant became more and more lower.

Water-gas shift (WGS):

$$CO(g) + H_2O(g) \leftrightarrow CO_2(g) + H_2(g) \qquad \Delta H_{r,\,298K} = -41.16 \text{ kJ/mol} \qquad \text{(R4.1)}$$

Oxidation:

$$C(s) + O_2(g) \leftrightarrow CO_2(g) \qquad \Delta H_{r,\,298K} -393.509 \text{ kJ/mol} \qquad \text{(R4.2)}$$

Although higher S/C ratios led to improved H_2/CO ratios in the producer gas, syngas production (considering this only as the joint production of CO and H_2) was not always favored at such conditions, as a higher ER was, in turn, required to reach auto-thermal conditions, thus promoting the complete oxidation of C into CO_2 (complete combustion, R4.2).

Similar H_2/CO ratios were predicted for raw AS and P, with 0.61 as the minimal value (at S/C=material moisture and T=1100 °C) and 1.62 as the maximal (at S/C=1.1 and T=750 °C). Both materials had similar elemental composition and HHV, which justified these similar results. Nevertheless, lower values were obtained for both torrefied materials, at similar conditions, with minimal values of 0.45 and 0.38 and maximal values of 1.42 and 1.23 for TAS220 and TAS250, respectively.

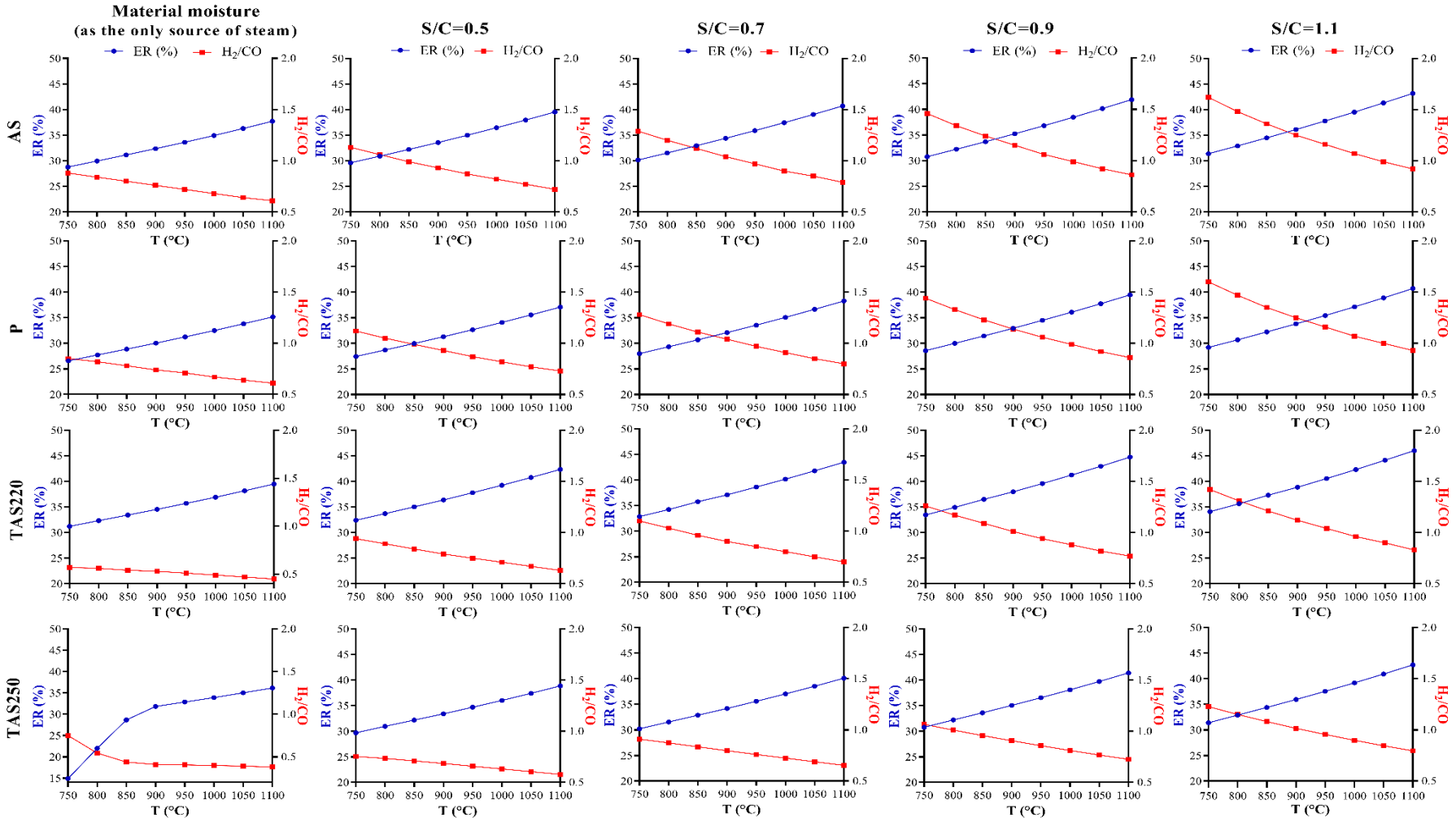

Figure 4.2. General view of AS, P, TAS220 and TAS250 gasification simulation results.

Figure 4.3 shows the production of $CO+H_2$ and CO_2 (m^3_{STP}/kg material) at the different temperatures and S/C values for all the studied materials. The production of $CO+H_2$, in general, enhanced at lower S/C ratios and lower temperatures (involving lower ER), occurring at the expense of CO_2 generation. However, this trend was not observed for TAS250 gasification at the lowest S/C ratios (S/C < 0.5) and temperatures (< 850 °C), as the total conversion of the carbonaceous material was not reached. For example, syngas production in AS gasification at 850 °C fell from 1.12 to 1.04 m^3_{STP}/kg when the S/C ratio varied from 0.184 to 1.1, while CO_2 production almost doubled its value (Figure 4.3A). Analogous values and tendencies were observed in P gasification, as the syngas production at 850 °C dropped from 1.14 to 1.06 m^3_{STP}/kg when the S/C ratio increased from 0.165 to 1.1 and the CO_2 production also doubled its value (Figure 4.3B). Higher syngas production and lower CO_2 generation have been obtained for the torrefied materials with respect to the gasification of raw AS. For instance, syngas production reached 1.43 m^3_{STP}/kg for TAS220 at S/C of 0.024 (only air as gasifying agent) and 850 °C (Figure 4.3C), which means an increase of 22 % with respect to raw AS. This increase was even higher for TAS250 gasification (Figure 4.3D) when operating at temperatures above 850 °C and with enough amount of gasifying agent (1.82 m^3_{STP}/kg at S/C=0.5 and 750 °C). Hence, if taking into account the elemental composition of the four materials, it can be concluded that the production of syngas at auto-thermal and equilibrium conditions was favored by lower O/C and H/C ratios in the feedstock (as long as the material can be gasified entirely), but not so the H_2/CO ratio in the syngas, which followed the opposite trend.

In summary, these theoretical results from the equilibrium model indicated that increasing the S/C ratio was favorable for a higher H_2/CO in the produced gas (Figure 4.2) but not for maximizing syngas production (Figure 4.3). In addition, too low temperatures could leave behind unconverted solids, especially in the case of torrefied AS. Hence, an intermediate value of S/C ratio (0.5) was set for the gasification experiments, as an agreement between the studied parameters was required to obtain a syngas rich in H_2. Moreover, kinetic aspects usually hinder reaching chemical equilibrium in the process, so tar formation and incomplete conversion of solid carbon may be expected from the actual gasification process. This motivated us to set the gasification temperature for the experiments at a relatively high value (850 °C). According to the equilibrium model, such

a combination of temperature and S/C ratio allowed operating at an ER lower than 35 % in all cases.

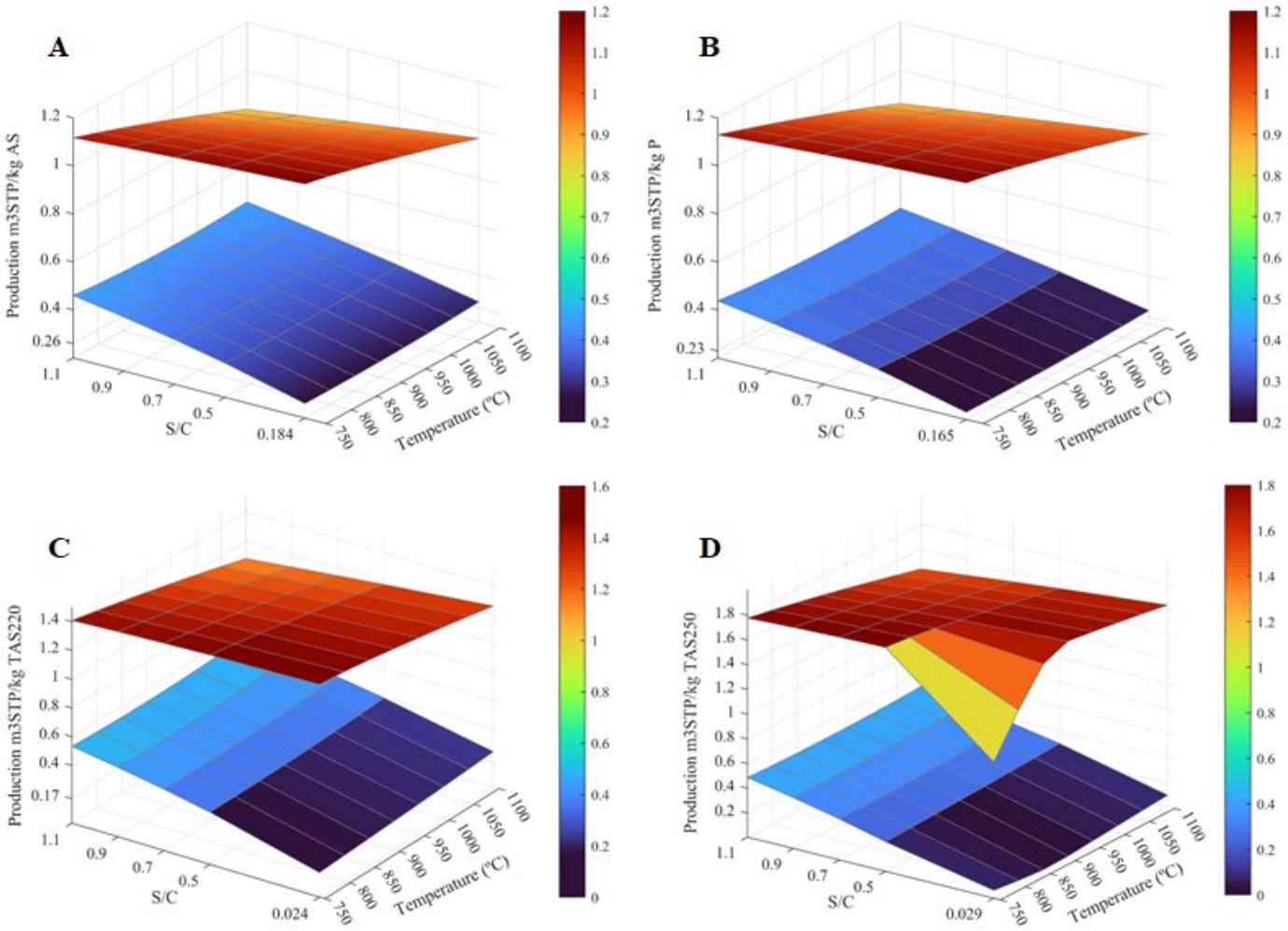

Figure 4.3. Theoretical production of $CO+H_2$ (red surface) and CO_2 (blue surface) at different temperatures and S/C ratios for the gasification of: AS (A), P (B), TAS220 (C) and TAS250 (D).

4.3.2. Product distribution

Mass balance closed fairly well, between 92 % and 97 %, in all the experiments.

Experimental results for the distribution of products in the gasification of AS, P and TAS220 are summarized in Table 4.2. The char yield obtained from AS gasification was lower than that obtained from P (2.3 vs. 5.4 wt.% when using only air as a gasification medium and 1.8 vs. 5.05 wt.% when using air-steam). Taking into account the ash content

of these solid products (Table 4.2), the char yield on an ash-free basis was 2.1 and 4.3 wt.% for AS and P, respectively. These data indicated that the higher ash content in P could not be the unique responsible for obtaining more solid product during P gasification but also the raw material's nature. On the other hand, the most significant increase in the char generation was observed in the case of TAS220 gasification if compared with the raw AS (10.6 vs. 2.3 wt.% when using only air and 7.5 vs. 1.8 wt.% when using air-steam). As the ash content is even lower in the char obtained from TAS220 (Table 4.2), this noticeable increase in the amount of char must be related to the reduced reactivity of the raw material after torrefaction. A similar finding has already been reported in the study of Fisher et al. using raw and torrefied short-rotation coppice willow (Fisher et al., 2012). In fact, the carbon content in the remaining solid after TAS220 gasification was found to be significantly higher, while oxygen content was much lower, thus leading to a reduced O/C ratio. Using a mixture of air and steam as the gasifying agent instead of only air slightly decreased the production of char in all cases (AS, P and TAS220) due to the enhancement of the water-gas reaction (R4.3) that could further generate CO and H_2, but also due to favored combustion of char (R4.2), as the addition of steam involves higher ER for auto-thermal operation.

$$C(s) + H_2O(g) \leftrightarrow CO(g) + H_2(g) \qquad \Delta H_{r,\,298K} = 131.30\ kJ/mol \qquad (R4.3)$$

The yield of liquid product (including tar and condensed water) was found to increase when adding steam as gasifying agent (from 22 to 30 wt.% for AS gasification, from 23 to 32 wt.% for P and from 17.9 to 34 wt.% for TAS220). Such a rough increase in the liquid yield may not necessarily mean a higher tar formation (see section 4.3.4), as unconverted or produced water was also included in this yield. Anyway, the liquid yield was quite similar for both AS and P, while it was 20 % lower in the case of TAS220 due to the dehydration reaction and tar elimination during the previous torrefaction step.

On the other hand, the fact of having gas yields above 100 % was only a matter of the calculation basis (as the reference was only biomass, without including the gasifying agent). The volumetric gas production is usually preferred in gasification studies as a more representative factor of syngas generation. As shown in Table 4.2, this factor has shown values of around 2.4 m^3_{STP}/kg for both AS and P, while increased up to 2.7-2.9 m^3_{STP}/kg for TAS220. These gas production data included N_2 coming from the air, so, as TAS220 gasification involved higher ER values (see Table 4.1), it means that the N_2 fed was also greater. Considering a N_2-free basis for gas production, such differences

between all the materials practically disappeared (1.1 - 1.2 m^3_{STP}/kg material). As expected, if gas production in TAS220 gasification was calculated with respect to the original amount of AS fed to the torrefaction stage, it fell by around 25 % (0.7 - 0.8 m^3_{STP}/kg AS). The N_2-free gas produced in the torrefaction stage (0.08 m^3_{STP}/kg AS) did not offset such a difference.

Table 4.2. Experimental results from the gasification at 850 °C of AS, P and TAS220.

Run	**1 & 2**	**3 & 4**	**5 & 6**	**7 & 8**	**9**	**10**
Material	**AS**	**AS**	**P**	**P**	**TAS220**	**TAS220**
Reaction medium	Air	Air-steam	Air	Air-steam	Air	Air-steam
Product yield (wt. %)*						
Char	2.3 ± 0.4	1.8 ± 0.6	5.4 ± 0.2	5.05 ± 0.05	10.6	7.5
Liquid (tar + water)	22 ± 1	30.24 ± 0.02	22.8 ± 0.4	32 ± 1	18	34
Gas (N_2-free basis)	135 ± 2	133 ± 7	122 ± 2	130 ± 1	138	148
Syngas composition (vol. %)						
H_2	9.7 ± 0.9	11 ± 2	10.7 ± 0.1	12.28 ± 0.01	7	9
CO	14 ± 1	12 ± 1	13.2 ± 0.3	11.6 ± 0.2	11	10
CO_2	17.3 ± 0.3	18.2 ± 0.2	17.02 ± 0.01	18.2 ± 0.1	17.0	16.9
CH_4	4.0 ± 0.2	3.9 ± 0.4	3.3 ± 0.1	3.20 ± 0.02	3.1	3.0
C_2H_6	0.14 ± 0.02	0.12 ± 0.03	0.07 ± 0.01	0.06 ± 0.01	0.1	0.1
C_2H_4	0.9 ± 0.1	0.9 ± 0.1	0.79 ± 0.01	0.72 ± 0.06	0.6	0.5
C_2H_2	0.07 ± 0.05	0.08 ± 0.01	0.023 ± 0.005	0.018 ± 0.002	0.1	0.03
H_2S	0.10 ± 0.05	0.10 ± 0.01	0.0050 ± 0.0001	0.0050 ± 0.0001	0.01	0.1
N_2	54 ± 2	54 ± 3	54.8 ± 0.4	53.9 ± 0.1	62	57
H_2/CO ratio	0.69 ± 0.04	0.90 ± 0.04	0.81 ± 0.01	1.06 ± 0.02	0.64	0.94
CO/CO_2 ratio	0.81 ± 0.04	0.7 ± 0.1	0.78 ± 0.02	0.64 ± 0.01	0.63	0.57
Cold gasification efficiency (%)	66 ± 4	66 ± 9	56.8 ± 0.3	58 ± 1	45 (37)	49 (40)
LHV_{gas} (MJ/m^3_{STP})	4.7 ± 0.3	4.5 ± 0.5	4.3 ± 0.1	4.16 ± 0.04	3.6	3.6
Gas production (m^3_{STP}/kg material)	2.37±0.01	2.4 ± 0.1	2.2 ± 0.1	2.37 ± 0.01	2.7 (1.8)	2.9 (1.9)
Gas production N_2_free basis (m^3_{STP}/kg material)	1.1 ± 0.4	1.1 ± 0.1	1.01 ± 0.02	1.09 ± 0.01	1.1 (0.7)	1.2 (0.8)
Carbon yield to gas phase (%)	100 ± 2	97 ± 7	91 ± 2	94 ± 1	79	83
Concentration of tar in syngas, g/m^3_{STP} (GC/MS quantification)	0.7 ± 0.1	0.6 ± 0.1	0.7 ± 0.1	0.57 ± 0.02	0.7	0.3
Char characterization (elemental analysis and ash content, wt. %)						
C	83 ± 7	79.9	76.6 ± 0.1	75 ± 1	93	93
H	2 ± 1	1.3	1.3 ± 0.2	1.28 ± 0.02	1	1
N	0.7 ± 0.1	0.8	0.55 ± 0.03	0.499 ± 0.001	1.0	0.9
O	8.1	11.1	1.5	0.2	2.9	2.8
Ash	6.2 ± 0.1	6.9	20 ± 1	23 ± 1	2.4	2.5

*Calculated considering the amount of biomass fed without including the gasifying agent.

The values shown in brackets for TAS220 gasification represent the analogous results obtained if considering for the calculations the original amount of AS that was torrefied instead of the amount of TAS220 that was gasified.

4.3.3. Syngas composition and properties

Besides the reactions previously commented on, a wide range of exothermic and endothermic reactions occur during the different stages taking place in the gasification process:

Partial oxidation: $C(s) + 1/2O_2(g) \leftrightarrow CO(g)$ $\Delta H_{r,\,298K} = -110.53$ kJ/mol (R4.4)

Boudouard: $C(s) + CO_2(g) \leftrightarrow 2CO(g)$ $\Delta H_{r,\,298K} = 172.45$ kJ/mol (R4.5)

Methanation: $C(s) + 2H_2(g) \leftrightarrow CH_4(g)$ $\Delta H_{r,\,298K} = -74.85$ kJ/mol (R4.6)

Steam reforming: $C_xH_y(g) + xH_2O(g) \leftrightarrow xCO(g) + (y/2+x)\,H_2(g)$ $\Delta H>0$ (R4.7)

Dry reforming: $C_xH_y(g) + xCO_2(g) \leftrightarrow 2xCO(g) + (y/2)\,H_2(g)$ $\Delta H>0$ (R4.8)

Cracking: $C_xH_y(g) \leftrightarrow xC(s) + (y/2)\,H_2(g)$ $\Delta H>0$ (R4.9)

According to the results exposed in Table 4.2, the gasification of AS, P and TAS220 produced significant amounts of H_2, CO, CO_2, light hydrocarbons (predominantly CH_4) and H_2S (detected and quantified by micro-GC). As predicted by the equilibrium calculations, the experimental data confirmed that adding steam to the gasifying agent improved the gas quality. H_2 concentration was increased from 9.7 vol.% to 11 vol.% when adding steam (S/C=0.5) in the case of AS gasification, while it reached 12.3 vol.% when using an S/C of 0.5 in P gasification (vs. 10.7 vol.% with only air). Accordingly, the H_2 concentration was slightly higher in P gasification when compared with AS, regardless of the gasifying agent used. Lower H_2 concentrations were obtained in the case of TAS220 gasification: 7 vol.% when gasifying with only air and 9 vol.% at S/C=0.5.

The opposite behavior was found for the concentration of CO, which decreased when steam was added. This reverse relation between H_2 and CO concentrations directly affected the H_2/CO ratio, which was enhanced from 0.69 to 0.9 by adding steam in the case of AS, from 0.81 to 1.06 in the case of P and from 0.64 to 0.94 for TAS220. Therefore, the torrefaction of AS did not further improve the H_2/CO ratio in the syngas, as even if the CO concentration slightly decreased, the H_2 concentration was not improved (the same trend was predicted by the equilibrium calculations, Figure 4.2). In any case, these H_2/CO values were greater than those reported in the literature for the gasification of similar materials, such as almond shells gasification in an updraft reactor at 850 °C, for which the H_2/CO ratio ranged between 0.46 (S/C=0) and 0.75 (S/C=0.2) (Cerone et al., 2020). On the other hand, it is to outline the fact that the H_2/CO in P gasification was slightly better than AS due to the high H_2 concentration and the lower CO concentration. Regarding the concentration of CO_2, a slight increase was observed

for the raw AS and P when adding steam (up to 18.2 vol.%), which could boost either the water-gas shift reaction or the combustion reactions because of the simultaneous increase of the ER (needed to keep the reaction at 850 °C). The concentration of CO_2 in the gasification gas was not affected by the previous torrefaction stage, as it was maintained at around 17 vol.%, but CO_2 production in terms of m^3_{STP}/kg material was increased when gasifying the torrefied materials, especially when adding steam (0.43 m^3_{STP}/kg of AS vs. 0.51 m^3_{STP}/kg of TAS220). As expected, the production of light hydrocarbons during gasification was also significantly affected by the previous torrefaction stage. The concentration of CH_4 was around 25 % lower in the TAS220 gas and the production in terms of m^3_{STP}/kg material was 11 % lower. This fact seems to be directly related to the volatile matter released during the torrefaction process (the volatile matter content in the raw material was reduced from 75 wt.% in AS to 69 wt.% in TAS220). A similar trend was observed by other authors when comparing the gasification of raw and torrefied woody residues (Strandberg, 2015). As mentioned in that work, the main reason for the presence of CH_4 in the gasification syngas is an unconverted fraction of pyrolysis products coming from the volatile components in the raw biomass. On the contrary, CH_4 production was also lower for P gasification, even if the volatile matter content in P was slightly higher than in AS (77 vs. 75 wt.%). It is to highlight that the CH_4 content was not affected by the composition of the gasifying agent for both materials (no significant effect of steam addition was observed).

Figure 4.4 compares the experimental gas composition obtained at the different operating conditions with the theoretical data predicted by the equilibrium model (only including the four main gas products). Theoretical and experimental data are noticeably different. The equilibrium calculations for all the materials predicted higher concentrations of H_2 and CO (about double) than those experimentally obtained in the lab setup, while the experimental content of CO_2 almost doubled the simulation prediction in some cases. The model expected only traces of CH_4 (< 0.01 vol.%), while actual concentrations obtained in the gasification experiments were between 3 and 4 vol.%. This divergence between the theoretical and experimental data means that the equilibrium was not reached during the experiments at these operational conditions. Although the vol.% were different, the observed trend when increasing the S/C ratio was the same as the predicted by the equilibrium model.

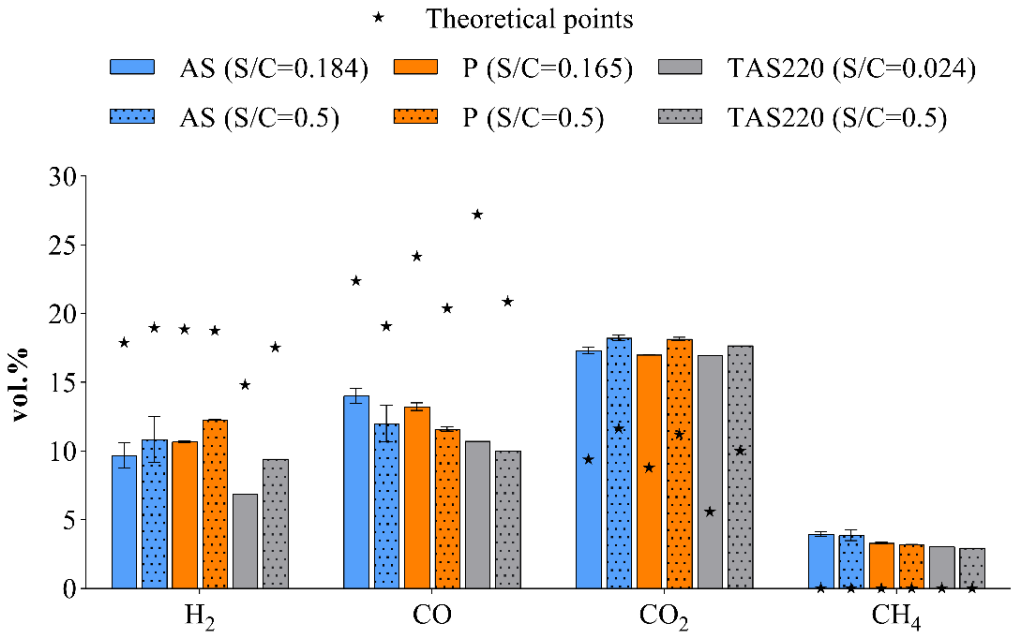

Figure 4.4. Theoretical and experimental concentrations of H_2, CO, CO_2 and CH_4 (vol.%) in the gasification gas.

Besides composition, other important characteristics of the produced syngas, such as its lower heating value (LHV_{gas}), the carbon conversion to the gas phase and the cold gas efficiency, were also included in Table 4.2. The addition of steam to the gasification atmosphere did not significantly affect the LHV of the gas obtained from any of the materials gasified. Typical values between 3 and 5 MJ/m^3 were reported in the literature for the LHV of the syngas obtained in the air gasification of many lignocellulosic materials (woody, herbaceous or fruit-shells (Karatas and Akgun, 2018; Kulkarni et al., 2016; Sarkar et al., 2014). For instance, the LHV of the syngas was 5.2 MJ/m$^3_{STP}$ for pine gasification (Kulkarni et al., 2016). For walnut and pistachio shells, LHV values of up to 5 MJ/m^3 were reported at lower ER values (Karatas and Akgun, 2018). The ER played a significant role in the LHV of the gas because of the N_2 dilution effect. In this work (Table 4.2), the LHV_{gas} from AS gasification was somewhat higher than that from P, which could be mainly attributed to the higher CH_4 content in AS syngas. Even if the H_2 content in the syngas from P was higher, the LHV of CH_4 was more than three times greater than H_2, which could explain this difference in the LHV_{gas}. Concerning the effect of torrefaction, significant differences were found in the LHV_{gas} when comparing the gases from AS and TAS220, as it was reduced by around 1 MJ/m$^3_{STP}$ when feeding the torrefied material. This reduction may be related to the lower content of combustible gases such as CH_4, H_2 and CO and the increased fraction of N_2 in the syngas from TAS220. A similar trend was

observed in other work in the literature for the gasification of raw and torrefied switchgrass, for which the LHV_{gas} decreased in 0.4 - 0.6 MJ/m^3 depending on torrefaction temperature (230 and 270 °C) (Sarkar et al., 2014). In other work, a decrease of 0.7 MJ/m^3_{STP} in LHV_{gas} after the gasification of torrefied pine was reported (Kulkarni et al., 2016).

As shown in Figure 4.5, the equilibrium-based model used to simulate the gasification of AS, P and TAS220, either with air or air-steam, predicted minor differences between the values of LHV_{gas} obtained from the three materials, all of them ranging between 4.5 and 5.1 MJ/m^3_{STP}. The experimental values of LHV_{gas} obtained in the case of AS and P gasification were quite similar to the model estimations (except when gasifying P using only air as gasifying agent), while in the case of TAS220, the theoretical values were higher.

The theoretical model did not consider the nature of the chemical bonds in the original materials. However, the kinetics of the gasification process has been experimentally proved to be affected by the chemical transformations occurring in the previous torrefaction stage (as shown by the higher char yield obtained in the gasification of TAS220), which in turn resulted in important differences in the composition and the LHV of the syngas.

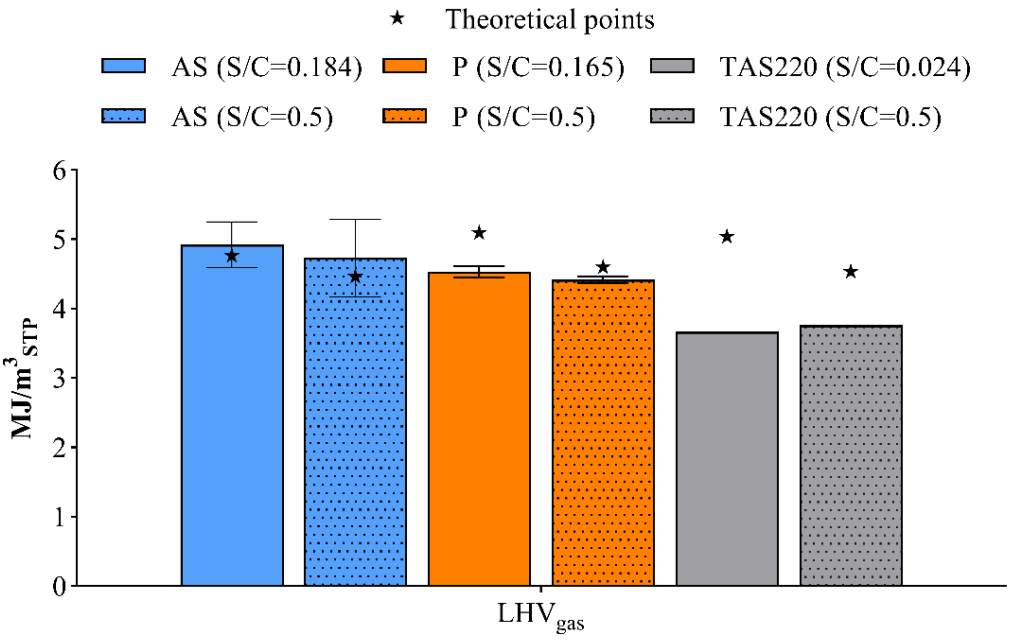

Figure 4.5. Theoretical and experimental LHV of the syngas (MJ/m^3_{STP}).

The LHV of the syngas directly affects the cold gas efficiency (Equation 4.5). The gasification of AS showed a cold gas efficiency between 66 and 68 %; in the case of P, this parameter was up to 60 %, while in the case of TAS220 gasification, it reached 49 % as the

maximum value. The cold gas efficiency for the gasification of the torrefied material was even lower (37 - 40 %) if considering the initial amount of AS that was torrefied as the calculation reference. However, gas from the torrefaction step (LHV=0.6 MJ/m^3_{STP}) could also be included to calculate a global cold gas efficiency for the two-stage process, obtaining a result of 40 - 43%. From this point of view, the two-stage process was less efficient than the direct gasification of the raw AS.

Another interesting parameter to assess the gasification performance is the carbon yield to the gas phase, which is the ratio between the mass of carbon contained in the syngas and the mass of carbon in the material fed (fraction of carbon converted to gaseous compounds). In all cases (except for the softest conditions for TAS250), this ratio was estimated to be 100 % at equilibrium conditions. However, lower values were obtained experimentally (Table 4.2), especially for TAS220 (79 and 83 % for air and air-seam gasification, respectively). This difference pointed to slower kinetics for the gasification of the torrefied material. Comparing the AS and P, it could be observed that this parameter was slightly higher for AS, especially when gasifying with air (100 % vs. 91 %).

4.3.4. Production of tar

The production of tar in the gasification runs was quantified by GC/MS/FID analysis. Table 4.2 shows the concentration of tar in the produced syngas, which was quite similar in most cases, between 0.6 and 0.7 g/m^3_{STP} (with a minimal decrease when adding steam), except when gasifying TAS220 at a S/C ratio of 0.5, for which a decrease of 50 % was observed. This was also confirmed in terms of tar yield with respect to the material fed, which ranged around 1.5 - 1.7 g/kg for AS, 1.4 - 1.7 g/kg for P and 1.9 - 0.9 g/kg for TAS220 gasification (Table 4.3). It was observed in the literature that the gasification of torrefied pine (at a temperature of 935 °C and ER of 25 %) reduced by half the production of tar compared to the original material (from 8 to 3.9 g/kg dried biomass) (Kulkarni et al., 2016). In the present work, we used calcined dolomite as bed material, which has been proven to be efficient in tar cracking at analogous operating conditions (temperature and use of steam) (Berrueco et al., 2014), which might be the reason for the lower values of tar production obtained for all the materials, regardless the biomass nature or the torrefaction pretreatment.

Tar is mainly composed of polycyclic aromatic hydrocarbons (PAHs). Table 4.3 summarizes the composition of the identified tar compounds (mass fractions), including 11 different PAHs detected in the condensed liquids. As shown, naphthalene, acenaphthylene and

phenanthrene were the main tar compounds, accounting for 56 - 70 % of the produced tar. The formation of these aromatic tar species without substituent groups is favored in the temperature range of 750 to 900 °C (Devi et al., 2005). Such types of aromatics are considered the most challenging tar fraction to destroy because of their stability (Devi et al., 2005).

The addition of steam to the gasification atmosphere contributed to decreasing the individual production of some of these PAHs. For example, naphthalene yield dropped from 0.8 to 0.6 g/kg in the case of AS, from 0.7 to 0.5 g/kg for P and from 0.8 to 0.3 g/kg in the case of TAS220 by increasing the S/C ratio up to 0.5. Steam reforming reactions (R4.7) may be involved in such observed reduction (Haimiao et al., 2014). In summary, biomass nature did not significantly affect tar production or composition, as similar values were generally observed in both AS and P gasification. In addition, tar production during the gasification of AS or TAS220 with air was hardly affected by the torrefaction stage previously undergone by the solid, while a reduction in tar production was observed when adding steam to the TAS220 gasification atmosphere. However, tar composition was hardly impacted by the torrefaction stage, as the same PAHs (naphthalene, acenaphthylene and phenanthrene) were identified as the majority ones.

Table 4.3. Tar production in the gasification experiments and composition of tar samples (GC/MS/FID).

Run **Material, S/C**	**1 & 2** **AS, 0.184**	**3 & 4** **AS, 0.5**	**5 & 6** **P, 0.165**	**7 & 8** **P, 0.5**	**9** **TAS220, 0.024**	**10** **TAS220, 0.5**
Production of tar (g/kg material)	1.7 ± 0.2	1.5 ± 0.2	1.6 ± 0.2	1.34 ± 0.05	1.9	0.9
Tar composition (%)*						
Naphthalene	46 ± 1	35 ± 6	43 ± 1	38.7 ± 0.1	43.2	34.9
Acenaphthylene	13 ± 1	11 ± 2	12.1 ± 0.4	11.9 ± 0.4	12.9	12.1
Acenaphthene	2.3 ± 0.4	2.9 ± 0.1	2.4 ± 0.2	2.6 ± 0.2	2.6	3.9
Fluorene	5.9 ± 0.2	5.7 ± 0.6	5.2 ± 0.2	5.324 ± 0.003	6.1	6.5
Phenanthrene	9.9 ± 0.4	9 ± 2	15 ± 1	17.5 ± 0.5	9.2	10.3
Anthracene	4.0 ± 0.2	4.2 ± 0.5	3.9 ± 0.1	4.22 ± 0.02	4.1	4.9
Fluoranthene	4.068 ± 0.004	4.3 ± 0.5	4.0 ± 0.1	4.30 ± 0.01	4.2	5.2
Pyrene	3.92 ± 0.01	4.2 ± 0.6	3.5 ± 0.1	3.8 ± 0.1	4.2	5.1
Benz[a]anthracene	3.8 ± 0.5	5.0 ± 0.4	4.1 ± 0.3	4.3 ± 0.2	4.7	5.9
Chrysene	3.8 ± 0.6	4.8 ± 0.3	3.8 ± 0.3	4.0 ± 0.3	4.5	5.8
Benzo[b]fluoranthene	3.3 ± 0.5	4.5 ± 0.3	3.6 ± 0.3	3.7 ± 0.2	4.2	5.4

*Percentage of each tar element in the condensed tar.

4.4. Conclusions

An experimental study was conducted at a lab-scale reactor to understand the performance of argan shells and torrefied argan shells as gasification raw materials. Forest pine residues were also tested in this study for comparison purposes. Both raw materials (AS and P) showed quite similar characterization results of elemental analyses and calorific value, although there were noticeable differences in the composition of the macro-components. The main conclusions drawn from this chapter are the following:

– The experimental study (designed for operating at auto-thermal conditions), as well as the chemical equilibrium model implemented for auto-thermal operation, revealed that the addition of steam to the gasification atmosphere has a beneficial effect on the syngas composition by improving its H_2/CO ratio.

– The theoretical model pointed out that the lower O/C and H/C ratios found in the torrefied solid (TAS220) should leave behind a higher production of syngas (CO+H_2) and a lower H_2/CO ratio in the syngas, but this result was not observed experimentally, pointing that the chemical equilibrium was not achieved in the experimental runs.

– The residual char formation differed from the gasification of one material to another; AS led to lower char yield and higher carbon to gas phase conversion compared to P, while torrefaction pretreatment turned the material less reactive after, thus resulting in higher char formation and lower conversion of carbon to the gas phase, also with a lower CO/CO_2 distribution ratio.

– Gas production was hardly affected by the biomass nature or the gasifying agent (1 - 1.2 m^3_{STP}/kg material on a N_2-free basis in all cases).

– Gas characteristics were clearly different when comparing AS with P; the H_2/CO ratio was higher in the syngas from P, regardless of the gasifying agent, while its LHV was somewhat lower. Concerning the torrefaction pretreatment effect, the LHV of the gas from TAS220 was noticeably reduced mainly because of its lower CH_4 content (4.7 MJ/m^3_{STP} for AS gasification vs. 3.6 MJ/m^3_{STP} for TAS220 gasification).

– Tar reduction was one of the major expected advantages of including torrefaction as a pretreatment step before argan shells gasification. However, in the presence of dolomite, tar production was virtually the same for all the materials (AS, P or TAS220). Tar reduction

was only observed to some extent when adding steam into the TAS220 gasification atmosphere (0.7 g/m^3_{STP} for AS gasification vs. 0.3 g/m^3_{STP} for TAS220).

– Torrefaction as a pretreatment stage has not brought many benefits in terms of syngas production and quality for the gasification of argan shells.

– The gasification of the forest pine residues showed many similarities to argan shells; both could be promising materials to feed this process.

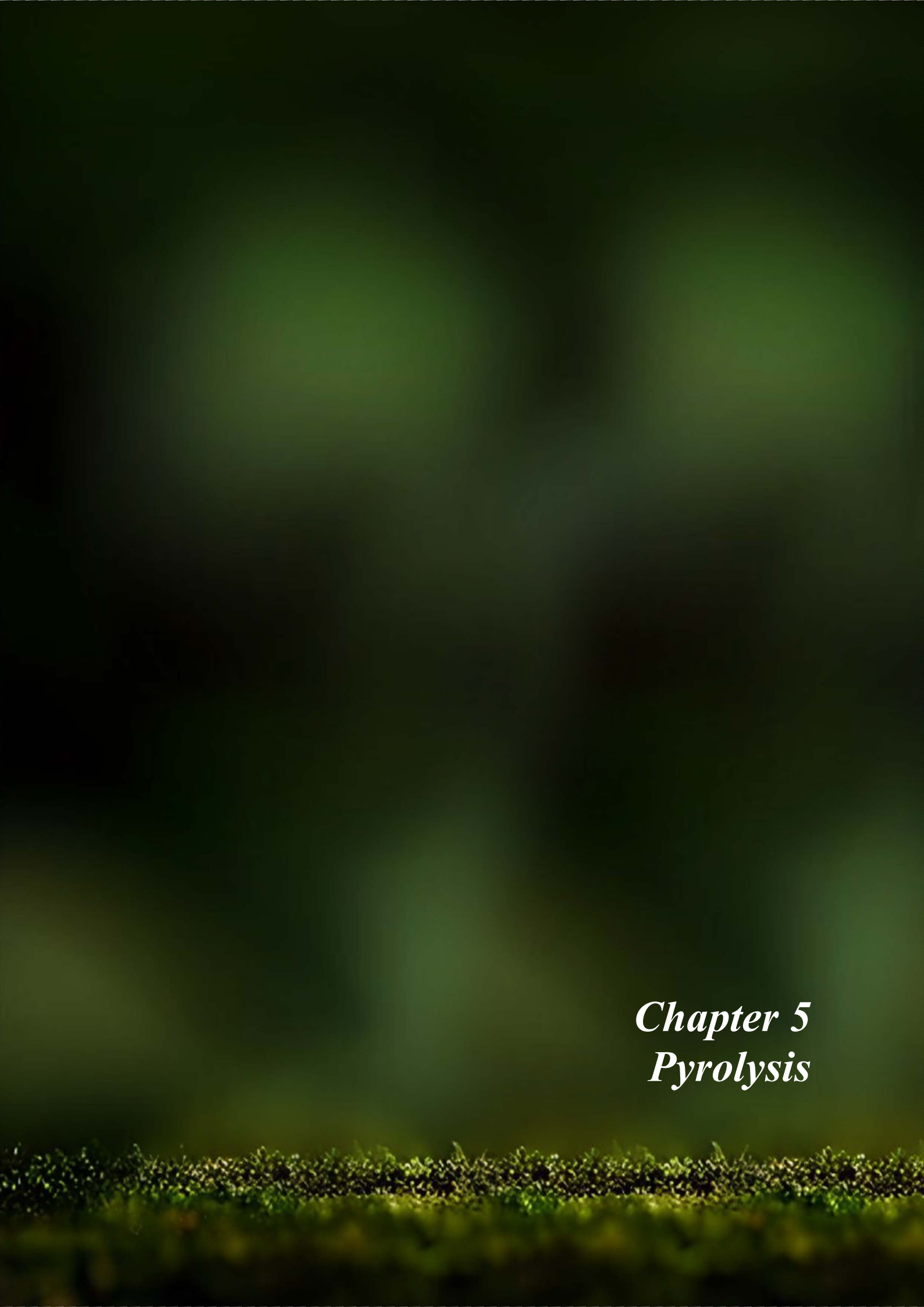

Chapter 5
Pyrolysis

5. PYROLYSIS

5.1. Introduction

This chapter addresses the pyrolysis behavior of argan shells compared with wheat straw. Both residues were pyrolyzed at three different temperatures. This part of the work is not limited to exploring the performance of the pyrolysis process of both biomasses but also to finding out sustainable applications and end-uses for the obtained bio-oil product.

The same as torrefaction, pyrolysis also involves the thermochemical decomposition of organic matter in the absence of oxygen (Brown and Brown, 2014a; Koppejan and Loo, 2007), but in this case, at more severe temperatures, between 350 and 600 °C (Adhikari et al., 2018). Pyrolysis appears as a promising technology for biomass valorization because of the end-use versatility and potentially high value of the products, specially bio-oil (liquid product) and biochar (solid product) (Adhikari et al., 2018), which could substitute petroleum-based products as fuels or in producing chemicals, polymers and activated carbons (Adhikari et al., 2018). The pyrolysis products distribution and their characteristics are affected by many factors, such as the feedstock particle size, operational temperature, heating rate, residence time, reactor type and raw material nature. Therefore, setting the proper operation conditions plays a crucial role in the final end-use of the product of interest.

Biochar is a carbonaceous residue mainly composed of elemental carbon, which also contains some amount of ash (mineral content) coming from the original raw material. Because of its reasonably high energy density, homogeneity, hydrophobicity and proper pulverous form (Adhikari et al., 2018), biochar is a prime candidate as a solid biofuel. Moreover, other valuable biochar applications can be further developed, including its use as a soil amendment (Ranguin et al., 2020; Sun et al., 2021) or as a precursor for electrode materials and supercapacitors (Abioye and Ani, 2015; Sundriyal et al., 2021; Taer et al., 2021), catalyst supports (Iwanow et al., 2020; Liew et al., 2018), fuel cell (Yu et al., 2014) or adsorbent material for pollutants in gases or liquids (Jin et al., 2014; Xiong et al., 2013).

On the other hand, bio-oil is collected from the condensation of organic vapors, aerosols and steam released during pyrolysis (Brown and Brown, 2014a). Commonly, this dark liquid product (usually yielding between 50 and 75 wt.% in the fast pyrolysis of lignocellulosic materials) is described as an emulsion of lignin-derived phenolic compounds in an aqueous phase enriched with holocellulose-derived compounds (Brown and Brown, 2014a; Fonts et al., 2021). The lignin-derived phenolic fraction consists of phenolic oligomers and other minor

phenolic monomers, dimers and trimers. Depending on the main monolignols (p-coumaryl alcohol lignin (H), coniferyl alcohol lignin (G) or sinapyl alcohol lignin (S) shown in Figure 1.6) that build lignin in the raw material, different branching and functional groups can be found in the phenolic fraction (alkyl, methoxy, vinyl, etc.). Bio-oil can be used in power generation or transport fuels after upgrade (Adhikari et al., 2018; Chiaramonti et al., 2007). The use of the crude bio-oil without any further treatment is a challenge due to its high oxygen content, high water content (which causes phase separation) and its tendency to polymerize. Alternatively, thanks to its wide diversity of chemicals (that can be higher than 300), bio-oil is also considered a promising source of many chemical products with different structures and uses (alcohols, acids, phenols, etc.). Many works have been dedicated to studying different upgrading routes for pyrolysis bio-oil in order to extract and purify the small organic acids (Brueckner et al., 2020; Sarchami et al., 2021; Teella et al., 2011), mainly acetic acid, which could represent between 2.5 to 15 wt.% of the bio-oil, depending on the raw material (Sarchami et al., 2021). In addition to the acetic acid, ketones and phenols could also be recovered from pyrolysis bio-oil at increased amounts after catalytic upgrading (Mansur et al., 2014). Furthermore, bio-oil contains compounds with antioxidant effects, which could also be a promising way for its valorization (Chandrasekaran et al., 2016; García et al., 2017; Gil-Lalaguna et al., 2017). Incorporating extracted fractions from lignocellulosic bio-oil into biodiesel was found to improve its oxidation stability by up to 500 % even with small dosages of bio-oil compounds (< 8 wt.%) (García et al., 2017).

Regarding the feedstock type, most of the pyrolysis studies in the literature involve conventional woody biomasses. Nevertheless, some publications studied the pyrolysis of agricultural wastes, such as corn cob, wheat straw, rice straw, rice husk (Biswas et al., 2017) or even fruit shells. The fruit shells performance on pyrolysis showed promising results either for bio-oil or biochar production (Demirbaş, 2006; Gunasekar et al., 2021; Kumar et al., 2021; Shagali et al., 2021). Most of the studies were focused on studying the effect of the operational conditions on product distribution and characteristics. For example, the pyrolysis of four different shells (walnut, hazelnut, almond and sunflower) was compared at an extensive temperature range (500 - 1200 K), and it was concluded that pyrolysis temperatures between 700 and 800 K were optimal to maximize the bio-oil yield in the range of 40 wt.% (Demirbaş, 2006). The effect of particle size (1.18, 2.36 and 5 mm) and treatment temperature (350, 400, 450, 500 and 550 °C) on products distribution for palm kernel shell pyrolysis was also studied. (Ogunkanmi et al., 2018). The highest bio-oil yield of 38.7 wt.% was obtained for the smaller

particle size at 450 °C. More recently, regarding to bio-oil applications, coconut shells bio-oil pyrolysis was successfully used as a co-fuel for diesel; the authors stated that bio-oil blends at 20 wt.% with diesel could reduce 28 % and 24 % the unburned hydrocarbon and carbon monoxide emissions, respectively, comparing it against the diesel combustion (Gunasekar et al., 2021).

As mentioned before, in addition to studying the pyrolysis performance of AS and WS, the products were tested for some applications. The impact of a hydrothermal post-treatment of bio-oil on its antioxidant properties has been included as part of this work, as preliminary results in GPT with other types of bio-oil showed promising results in terms of improving the oxidation stability of biodiesel with small additions of bio-oil hydrothermally treated (Botella et al., 2018; Gil-Lalaguna et al., 2017).

5.2. Experimental methods

5.2.1. Pyrolysis experiments

Pyrolysis experiments were performed in a fixed-bed reactor (total volume of 0.7 L) heated by means of an electric furnace (Figure 5.1). In a typical run, 150 g of AS or up to 80 g of WS was loaded into the reactor (the amount of biomass fed changed from AS to WS because of each material density). Once the reactor was sealed, a continuous flow of N_2 (1.5 L_{STP}/min) was introduced, allowing the volatiles removal and ensuring an inert atmosphere for thermal decomposition. The pyrolysis temperatures studied were 350, 450 and 550 °C (set according to the TGA thermograms of AS and WS, ensuring the release of most volatiles at the highest temperature). The reactor was heated at a heating rate of 5 °C/min. Each experiment took about 4 h, and all the pyrolysis runs were repeated twice for the experimental variability estimation. The bio-oil condensation system and the analysis of non-condensable gas were similar to those described in the previous chapters for other processes. However, in this process, two different solvents were employed to recover bio-oil from the condensers depending on the subsequent use of bio-oil. In one of the repetitions of each experiment, the liquid was recovered using isopropyl acetate, which was later used as extraction agent (1:7 mass ratio bio-oil: isopropyl acetate in the case of WS and 1:3 in the case of AS), and in the other repetition bio-oil was recovered using a weighted amount of acetone, which could be more easily removed from bio-oil by evaporation. The recovered bio-oils were analyzed in terms of water content by Karl Fischer titration. More details about the further treatment of bio-oil and its potential end-use as a source of antioxidants are given below.

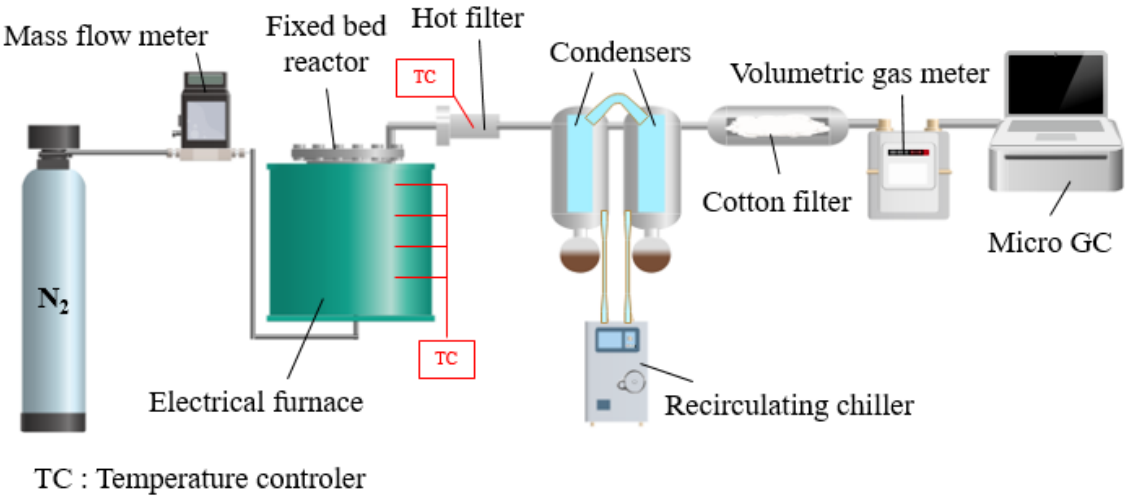

Figure 5.1. Diagram of the experimental pyrolysis setup.

5.2.2. Hydrothermal treatment of the pyrolysis bio-oil

The bio-oil samples recovered from the condensers using acetone were distillated in a rotary evaporator (550 mbar; 40 °C) to remove the solvent. Then, the acetone-free bio-oil samples were hydrothermally processed in an autoclave Parr reactor model 4575 (Figure 5.2). For the hydrothermal treatment (HT), bio-oil was initially mixed with distilled water at a 1:1 mass ratio, and the mixture was loaded into the reactor. Once the reactor was properly closed, the air remaining inside was evacuated using a vacuum pump, and the system was purged three times with pressurized N_2. The hydrothermal treatment of bio-oil was performed at 300 °C and autogenous pressure (8.5 MPa maximum) for 1 h under continuous stirring at 1000 rpm. Once the reaction time had elapsed, the reactor was removed from the heating jacket and quickly cooled by circulating tap water in the built-in cooling coil and using an ice bath outside. Then, at room temperature, the remaining gas in the reactor (0.2 - 0.32 MPa) was recovered in a gas bag and analyzed by a micro-GC.

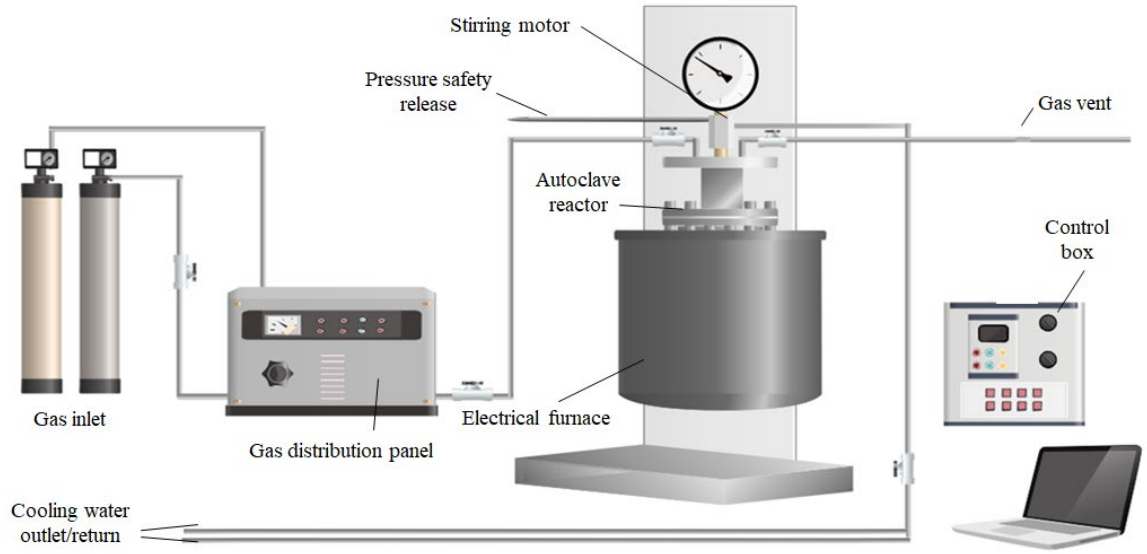

Figure 5.2. Diagram of the experimental hydrothermal treatment setup.

The liquid product was directly collected from the reactor, using methanol to recover the water-insoluble organic fraction from the reactor walls and stirrer. Then, both liquids were blended and filtered under vacuum conditions (using a pre-weighed filter paper). The water-insoluble organic fraction remaining in the filter was dried overnight at 105 °C and, once dried, it was weighed to determine its yield according to Equation 5.1.

$$\text{Insoluble fraction yield (wt.\%)} = \frac{W_{Ins}}{W_{org-biooil}} \cdot 100 \qquad \text{(Eq. 5.1)}$$

where W_{Ins} is the amount (g) of the insoluble fraction weighted after filtration of the liquid from HT and $W_{org\text{-}biooil}$ is the mass (g) of the water-free bio-oil fraction (only organic matter) initially loaded into the rector; this organic fraction in bio-oil was estimated by difference with its water content (determined by Karl Fischer titration).

5.2.3. Analysis of composition and antioxidant potential of bio-oil

The liquid products obtained produced in the pyrolysis of both materials, AS and WS, and after hydrothermal treatment of bio-oil, were further handled to obtain antioxidant additives. Pristine bio-oil directly obtained in the pyrolysis stage (recovered from the condensers using isopropyl acetate) was undergone an extraction process adding an extra amount of isopropyl acetate. The mixture was vigorously shaken for 10 min and kept in a decantation funnel. After that, two phases (aqueous phase and organic phase soluble in isopropyl acetate) were separated. The antioxidant additives were prepared from the organic

phase. Similarly, the filtered aqueous liquid obtained in the HT of bio-oil was also extracted with the same solvent (1:2 HT liquid: isopropyl acetate mass ratio).

The same as for tar characterization, the composition of these organic phases was qualitatively and quantitatively examined using GC/MS/FID. FID signal was previously calibrated with standards used in the torrefaction study (see section 3.2.2) in addition to other standards containing (guaiacol, creosol, catechol, 3-methoxycatechol, syringol and 2-methoxy-4-vinylphenol) at the concentration range of 838 - 41000 µg/mL. More information about the operating parameters can be found in Appendix V.

To evaluate the potential of these organic phases to be used as antioxidant additives, each one was firstly distilled in a rotary evaporator (60 °C, 10 mbar) to remove the solvent (note that light organic compounds, such as acetic acid, were also lost during this stage). From now on, this dried organic fraction will be referred to as "additive" throughout this chapter. The additive yield obtained from bio-oil can be calculated according to Equation 5.2.

$$\text{Additive yield (\%)} = \frac{W_{extr-biooil}}{W_{org-biooil}} \cdot 100 \qquad \text{(Eq. 5.2)}$$

where $W_{extr\text{-}biooil}$ is the amount (g) of extracted compounds remaining after distillation and $W_{org\text{-}biooil}$ is the organic matter initially present in the bio-oil.

5.2.4. Blend of biodiesel and additives and measurement of oxidation stability

The biodiesel used in this study was synthesized in the laboratory using sunflower oil and methanol as reagents (molar ratio methanol/oil of 6:1) and potassium hydroxide as catalyst (1 % of oil mass). The biodiesel production process has been described in greater detail elsewhere (García et al., 2017; Gil-Lalaguna et al., 2017; Lavoie et al., 2019; Palomo et al., 2019).

To start the procedure of incorporating the additives into biodiesel, the additive was weighed, so the appropriate amount of neat biodiesel could be added to the same flask, adjusting it to an initial additive dosage of 1 wt.%. In order to enhance the additive dissolution in the biodiesel, methanol was used as a co-solvent (with a mass ratio methanol/biodiesel of 1:1) and the mixture was sonicated for several minutes in an ultrasound bath. Then, methanol was distilled in a rotary evaporator. The final mixture of biodiesel and additive was centrifuged to separate the additive insoluble fraction. The homogeneous mixture of doped biodiesel was recovered from the upper part of the centrifugation tube, while the insoluble fraction remaining at the bottom was thoroughly washed with hexane (with sonication) in order to solve and remove biodiesel traces. Then, the washed solid was dried overnight at 50 °C and weighed to

determine the fraction of insoluble additive by difference. Hence, the real dosage of the soluble additive was determined after centrifugation and separation of the insoluble fraction according to Equation 5.3.

$$\text{Real dosage of soluble additive (\%)} = \frac{W_{\text{initial additive}} - W_{\text{insoluble additive}}}{W_{\text{biodiesel}} + (W_{\text{initial additive}} - W_{\text{insoluble additive}})} \cdot 100 \quad \text{(Eq. 5.3)}$$

where $W_{\text{initial additive}}$ is the weight (g) of additive initially added to biodiesel, $W_{\text{insoluble additive}}$ is the weight (g) of insoluble additive quantified after centrifugation, hexane-washing and drying, and $W_{\text{biodiesel}}$ is the weight (g) of neat biodiesel used for the mixture.

Finally, the oxidation stability of both neat and doped biodiesel samples was measured according to EN 16091 and ASTM D7545 methods through a PetroOXY Tester device (Petrotest Instruments GmbH & Co.). The oxidation stability was measured as the time required by a biodiesel sample (5 mL) to reduce by 10 % the oxygen pressure initially loaded in the measurement vessel. Hence, a longer oxidation time means a more stable biodiesel sample. These oxidation times (OXY) measured for neat and doped samples of biodiesel were compared in order to calculate an oxidation stability improvement rate (ΔOXY) (Equation 5.4).

$$\Delta\text{OXY}(\%) = \frac{\text{OXY}_{\text{Doped biodiesel}} - \text{OXY}_{\text{Neat biodiesel}}}{\text{OXY}_{\text{Neat biodiesel}}} \cdot 100 \quad \text{(Eq. 5.4)}$$

5.3. Results and discussion

5.3.1. Distribution and characteristics of the pyrolysis products

Table 5.1 summarizes the results of the distribution and some characteristics of the products obtained in the pyrolysis of both materials (AS and WS) at the three temperatures studied (350, 450 and 550 °C). The mass balance closure reached more than 90 % in all cases. The biochar yield ranged between 28.5 and 34 wt.% for AS and between 28.2 and 32 wt.% for WS, decreasing with the final pyrolysis temperature. Bio-oil production from AS was slightly increased at 550 °C (up to 55 wt.%) and gas generation reached up to 15 wt.% at 450 °C. On the contrary, for WS, the bio-oil and gas yields increased more significantly with the temperature (from 41 to 49 wt.% for the bio-oil and from 14 to 20 wt.% for the gas). It is to outline that WS tends to generate more gas and less bio-oil than AS; this residue's highest volatile matter could explain it. Lower bio-oil yields have been reported in the literature when using other fruit shells. Bio-oil produced at 550 °C from *Parinari polyandra Benth* fruit shell yielded up to 40 wt.% (Odetoye et al., 2014), while yields of 37.2, 39.4, 38.3 and 34.2 wt.% were obtained at pyrolysis temperatures between 427 and 527 °C for hazelnut, walnut, almond and sunflower shells, respectively (Demirbaş, 2006).

According to the thermogravimetric analysis (Chapter 2, sections 2.1 and 2.3), the holocellulose in both materials was almost degraded entirely under the N_2 atmosphere at temperatures under 350 °C, thus accounting for a loss weight of 58 - 60 %, which points to a similar reactivity of both AS and WS even at mild temperatures. Above 350 °C, the degradation kinetic of both AS and WS became slower, mainly involving lignin degradation. Only 7.3 %, 3.6 % and 2.8 % weight losses were observed at the temperature intervals of 350 - 450 °C, 450 - 550 °C and 550 - 750 °C, respectively, for AS. While for WS, the weight losses at the same temperature intervals were 8.1 %, 2.9 % and 1.9 %. This fact could explain the minor differences found in the product distribution obtained in the pyrolysis experiments carried out at 350-550 °C since most of the volatiles (condensable and non-condensable) release occurred at the heating stage under 350 °C, which was common in all experiments, and the relatively similar biochar yield for both materials.

The biochar obtained in the pyrolysis of AS was characterized by its increased calorific value, with a HHV ranging between 30 and 33 MJ/kg (vs. 19 MJ/kg for the original AS), while the HHV of WS char ranged from 25 to 27 MJ/kg (vs. 17 MJ/kg for the original WS). The increase of the pyrolysis temperature from 350 to 550 °C led to a significant reduction in the molar O/C ratio contained in the biochar (from 0.13 to 0.07 for AS and 0.15 to 0.1 for WS), as well as in the H/C ratio (from 0.6 - 0.7 to 0.4 for both materials).

Table 5.1. Distribution and characteristics of the products obtained in the pyrolysis of AS and WS.

Material	**AS**			**WS**		
Pyrolysis temperature (°C)	350	450	550	350	450	550
Product yield (wt. %)						
Biochar	34 ± 1	31 ± 1	28.5 ± 0.1	32 ± 1	29.5 ± 0.4	28.2 ± 0.5
Bio-oil	51 ± 1	51 ± 3	55 ± 1	41 ± 1	49 ± 1	48.2 ± 0.4
Gas	13 ± 4	14.8 ± 0.1	13 ± 2	14 ± 2	16.9 ± 0.4	19.92 ± 0.05
Biochar characterization						
HHV (MJ/kg)	30.0 ± 0.4	31 ± 1	33.3 ± 0.3	25.4 ± 0.2	27 ± 1	27.1 ± 0.3
C (wt.%)	81 ± 2	85 ± 2	88 ± 3	68 ± 1	72 ± 2	74 ± 1
H (wt.%)	4.0 ± 0.2	3.5 ± 0.2	2.9 ± 0.1	3.8 ± 0.2	3.2 ± 0.2	2.2 ± 0.2
N (wt.%)	0.3 ± 0.1	0.4 ± 0.1	0.6 ± 0.1	1.1 ± 0.03	1.1 ± 0.1	1.17 ± 0.04
O[a] (wt.%)	14 ± 1	10 ± 2	7.8 ± 3	13 ± 1	12 ± 1	10 ± 1
Ash (wt.%)	1.2 ± 0.1	1.1± 0.1	0.8 ± 0.1	13.5 ± 0.6	11.9 ± 0.04	12.3 ± 0.3
O/C	0.13	0.09	0.07	0.15	0.13	0.10
H/C	0.6	0.5	0.4	0.7	0.5	0.4
Bio-oil characterization						
Water content (wt.%)	63 ± 2	66 ± 2	62 ± 1	68	69	71
Gas composition (vol.%)						
H_2	0.043 ± 0.003	0.06 ± 0.01	0.23 ± 0.02	0.010 ± 0.02	0.08 ± 0.03	0.4 ± 0.1
CO	1.8 ± 0.3	1.35 ± 0.05	1.4 ± 0.5	0.6 ± 0.3	1.1 ± 0.1	1.11 ± 0.01
CO_2	4 ± 1	2.6 ± 0.1	1.8 ± 0.5	1.2 ± 0.1	1.7 ± 0.1	1.8 ± 0.1
CH_4	0.6 ± 0.2	0.5 ± 0.1	0.52 ± 0.03	0.03 ±	0.3 ± 0.1	0.5 ± 0.2
C_2H_6	0.07 ± 0.01	0.056 ± 0.003	0.05 ± 0.01	0.011 ± 0.002	0.026 ± 0.003	0.028 ± 0.003
C_2H_4	0.03 ± 0.01	0.023 ± 0.001	0.027 ± 0.001	0.004 ± 0.001	0.004 ± 0.001	0.004 ± 0.001
C_2H_2	0.0042 ±0.0004	0.004 ±0.001	0.002 ±0.001	0.02 ± 0.01	0.052 ± 0.003	0.10 ± 0.05
H_2S	0.009 ± 0.001	0.010± 0.002	0.012± 0.005	0.007 ± 0.001	0.007 ± 0.001	0.007 ± 0.001
N_2	93 ± 2	91 ± 6	95 ± 3	98.1 ± 0.5	96.8 ± 0.3	96.0 ± 0.4

[(a)] Calculated by difference (wt.%): O=100-C-H-N-Ash.

The pyrolysis gas was mainly composed of CO_2, CO, CH_4 and H_2, besides the N_2 used to inert the atmosphere. Increasing the pyrolysis temperature improved the content of H_2 and CH_4 in the gases derived from both materials (Figure 5.3). A similar trend was observed for the CO concentration in the gas from AS pyrolysis, while no clear trend was observed in the gas from WS (CO concentration was slightly higher at 450 °C). CO_2 concentration dropped from 59 vol.% at 350 °C to 46 vol.% at 550 °C in the gas obtained from AS and from 67 to 44 vol.% for WS gas, being the principal component in the pyrolysis gas. In terms of production, between 84 and 104 g of CO_2 per kg of AS and between 104 and 130 g of CO_2 per kg of WS were produced during pyrolysis experiments. For CO production, amounts ranging between 29 and 40 g of CO per kg of AS and between 30 and 51 g of CO per kg of WS were obtained.

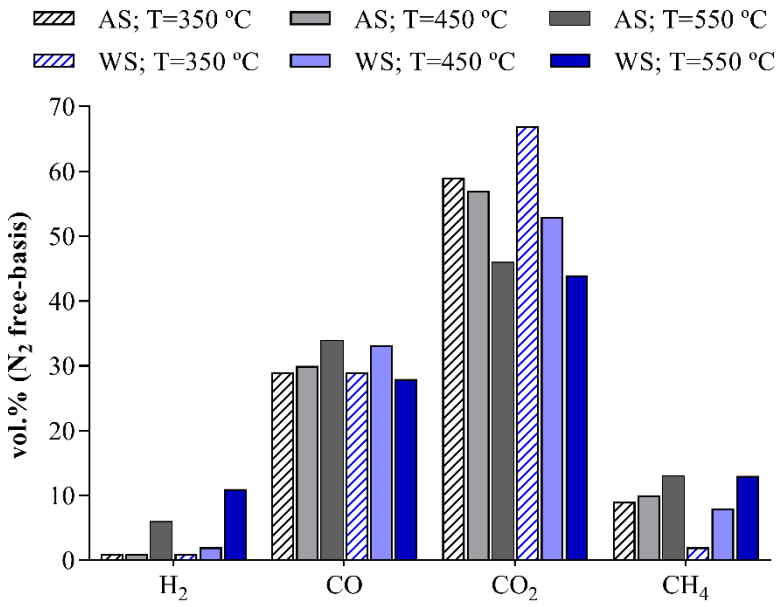

Figure 5.3. Gas composition from pyrolysis of AS and WS.

5.3.2. Distribution of products in the hydrothermal treatment of bio-oil

The mass balance in the hydrothermal treatment of bio-oils produced from both materials closed between 91 and 94 %. The production of the insoluble fraction (calculated using Eq. 5.1) yielded 3, 8 and 2 wt.% when treating the bio-oils obtained from AS at 350, 450 and 550 °C, respectively. When treating bio-oils from WS, less insoluble fraction was produced, with yields ranging between 0.7 and 1 wt.%. The gas generated in the HT yielded between 3 and 4 wt.% for bio-oils from AS and between 1 and 2 wt.% for bio-oil from WS. In all cases, the gas product mainly comprised CO_2 (around 80 vol.% on a N_2 free-basis) and lower contents of CO and H_2.

The product of interest in this HT process was the aqueous filtered liquid, which underwent liquid-liquid extraction/separation to obtain the antioxidant additives following the procedure detailed in section 5.2.4.

5.3.3. Production and characterization of antioxidant additives derived from bio-oil

Figure 5.4 compares the yields of the additives produced through both pathways: those directly extracted from the original bio-oil and those extracted from the hydrothermally treated bio-oil. It is worth saying that these data of additive yields do not include the fraction of the most volatile compounds that could be present in the liquids (such as acetic acid and some short-chain alcohols), as they were lost together with the solvent during the evaporation step and/or retained in the separated aqueous phases. The production of additives directly extracted from AS bio-oils was more than two times greater than that from WS bio-oil, with additive yields ranging between 28 - 33 wt.% in the case of AS and 11 - 15 wt.% in the case of WS. This means that AS bio-oil contained more compounds extractable by isopropyl acetate.

Regarding the effect of the HT treatment, a slight improvement in the additive yield was observed when preparing the additives from the AS hydrothermally treated bio-oil (30 - 36 wt.%) compared to each corresponding original bio-oil. This improvement could be due to further fractionation of the phenolic oligomeric fraction in bio-oil occurring during the HT treatment, thus enhancing the subsequent extraction process using isopropyl acetate. A maximal additive yield of 36 wt.% was obtained after the HT of the AS bio-oil produced at 450 °C. On the contrary, the HT treatment of the bio-oils produced from WS slightly decreased the additive production (10 – 11 wt.%).

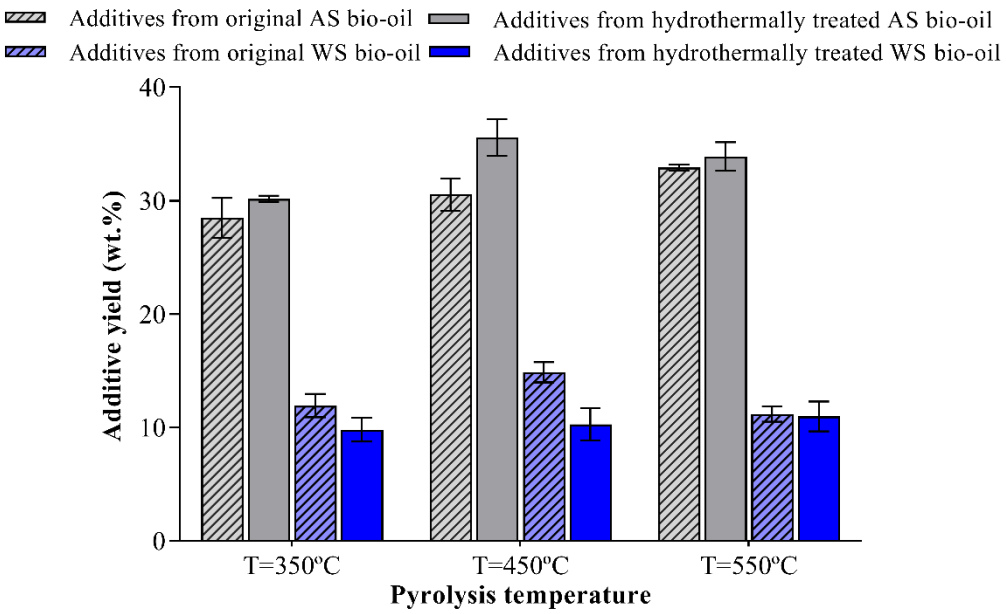

Figure 5.4. Additive yields produced from AS and WS bio-oils.

In terms of composition, Figure 5.5 depicts the concentration of the phenolic monomers in the dried additives prepared from the original and the hydrothermally treated bio-oils, analyzed by GC/MS/FID. Generally, the additives prepared from original AS bio-oils were much more concentrated on phenolic monomers than WS bio-oils. The total content of phenolic monomers in the additives directly extracted from AS bio-oils produced at 350, 450 and 550 °C (pyrolysis temperature) was found to be 63, 58 and 53 wt.%, respectively, while this concentration of monomers was reduced to 26, 25 and 36 wt.% in the additives directly extracted from WS bio-oils produced at 350, 450 and 550 °C. On the other hand, the additives prepared from the hydrothermally treated AS bio-oils were less concentrated on monomers (34 - 37 wt.%) than those directly extracted from the original bio-oils. This could be due to the competition between the depolymerization and the condensation reactions occurring during the HT treatment, which could finally lead to the formation of phenolic molecules bigger than monomers (dimers or trimers) undetectable through GC/MS/FID analysis but extractable by isopropyl acetate. This trend was not observed in the case of hydrothermally treated bio-oils from WS, as the total concentration of phenolic monomers was maintained around 28 and 34 wt.%. Concerning the effect of pyrolysis temperature, no clear trend was observed on the total concentration of monomers in the additives, except for those directly extracted from AS bio-oils, in which the monomers concentration was increased when reducing the pyrolysis temperature.

After the HT treatment, the concentration of each individual monomer detected in the additives was reduced or even disappeared (Figure 5.5), except for some specific compounds: catechol and 4-methylcatechol in AS bio-oils and guaiacol and 4-methylcatechol in WS bio-oils. The concentration of 4-methylcatechol was doubled or even tripled in the additives prepared from hydrothermally treated AS bio-oils and it became between 4 and 7 times in those additives prepared from the hydrothermally treated WS bio-oils. The increase in the catechol concentration in AS additives was relatively lower, ranging between 0.4 and 1.2 wt.% more in the HT additives from AS, while catechol was not detected in the hydrothermally treated WS additives.

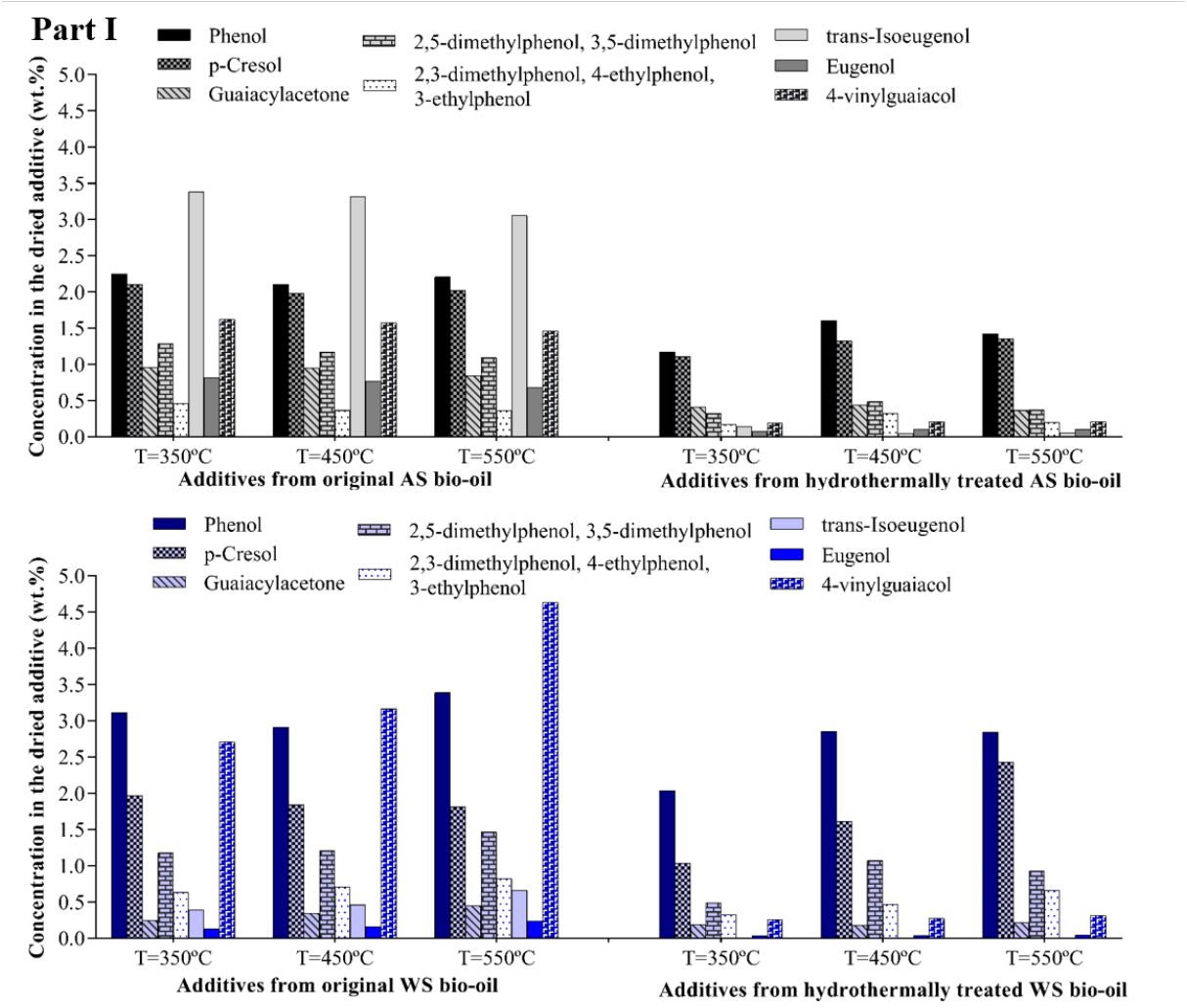

Part II

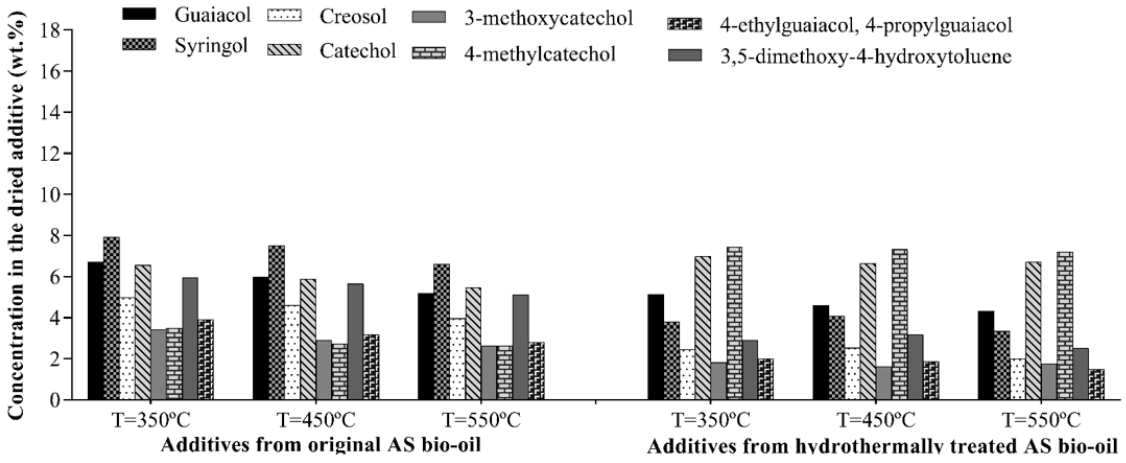
Guaiacol
Creosol
3-methoxycatechol
4-ethylguaiacol, 4-propylguaiacol
Syringol
Catechol
4-methylcatechol
3,5-dimethoxy-4-hydroxytoluene
Concentration in the dried additive (wt.%)
T=350ºC
T=450ºC
T=550ºC
T=350ºC
T=450ºC
T=550ºC
Additives from original AS bio-oil
Additives from hydrothermally treated AS bio-oil

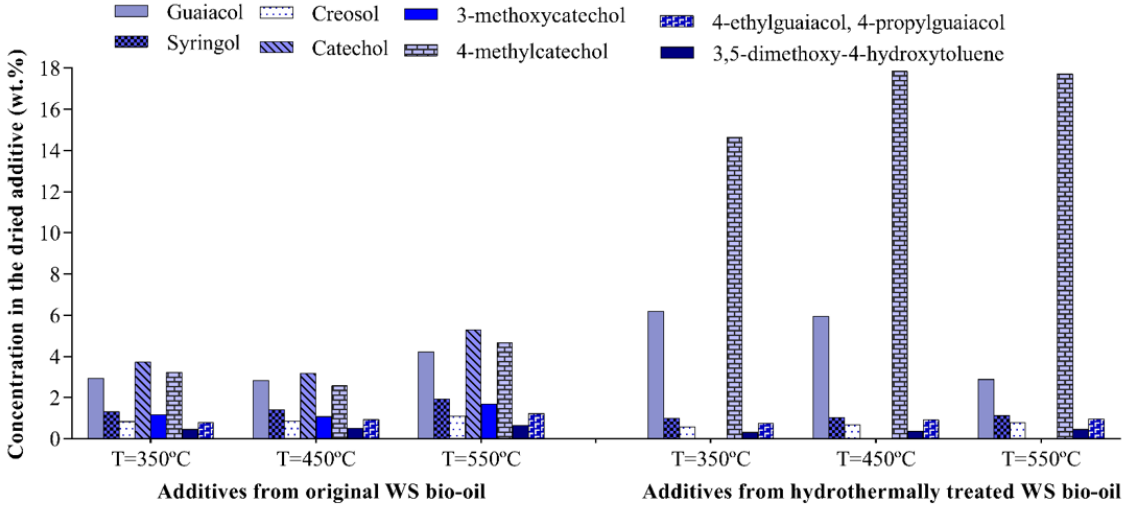
Guaiacol
Creosol
3-methoxycatechol
4-ethylguaiacol, 4-propylguaiacol
Syringol
Catechol
4-methylcatechol
3,5-dimethoxy-4-hydroxytoluene
Concentration in the dried additive (wt.%)
T=350ºC
T=450ºC
T=550ºC
T=350ºC
T=450ºC
T=550ºC
Additives from original WS bio-oil
Additives from hydrothermally treated WS bio-oil

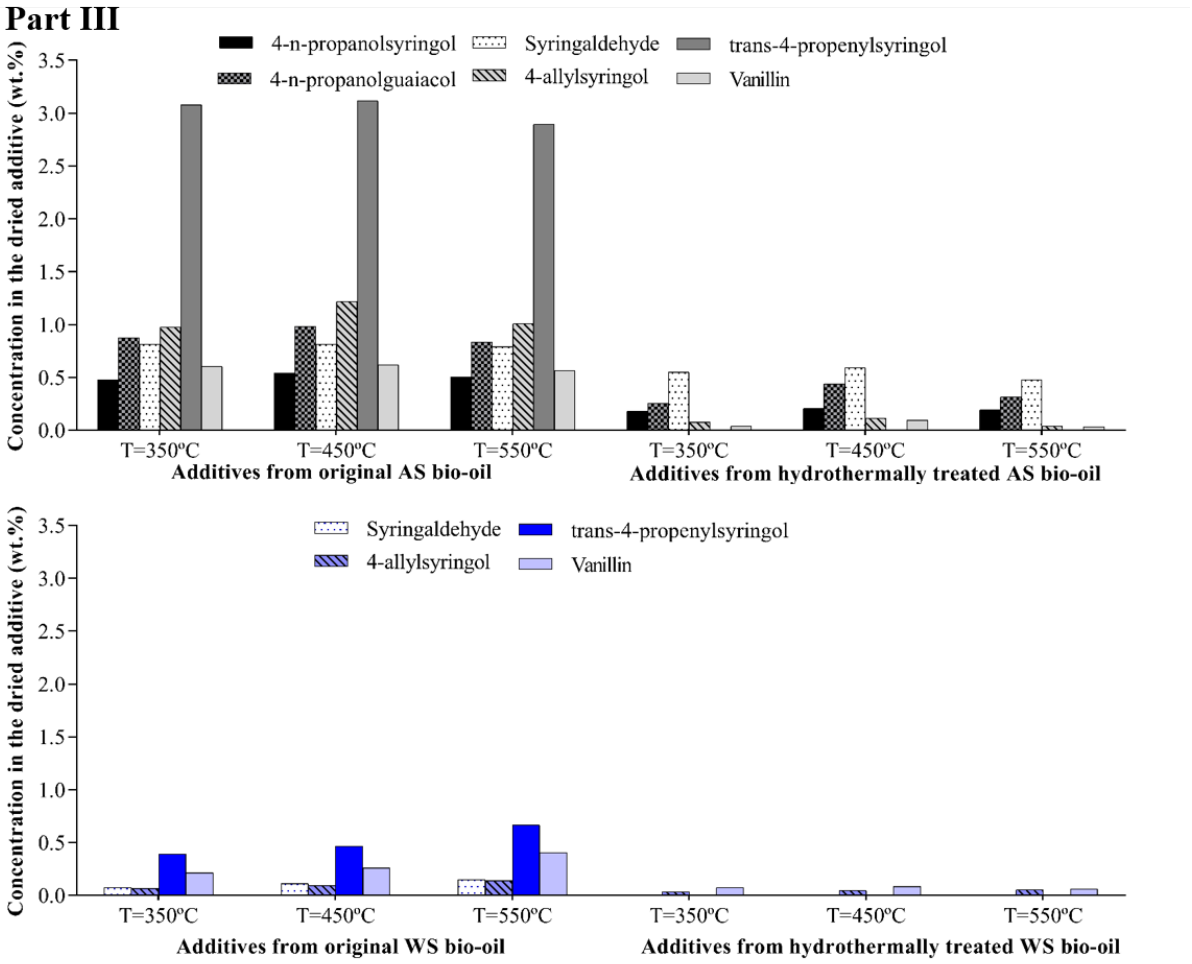

Figure 5.5. Concentration of the phenolic monomers in the additives produced from AS and WS bio-oils.

5.3.4. Antioxidant potential of bio-oil additives

The real dosage of each additive solved in biodiesel, as well as the OXY time measured for each sample of doped biodiesel, are exposed in Figure 5.6. The real dosage of soluble additive incorporated into biodiesel ranged between 0.82 and 0.92 wt.% in the case of original bio-oils and between 0.80 and 0.91 wt.% for HT bio-oils, so all the additives were relatively well solubilized in biodiesel, regardless of the bio-oil used for their preparation. Minimal differences were observed when comparing the original bio-oil samples and those hydrothermally treated. The bio-oil prepared at 550 °C (original and hydrothermally treated) led to less soluble additives than those prepared at 350 °C.

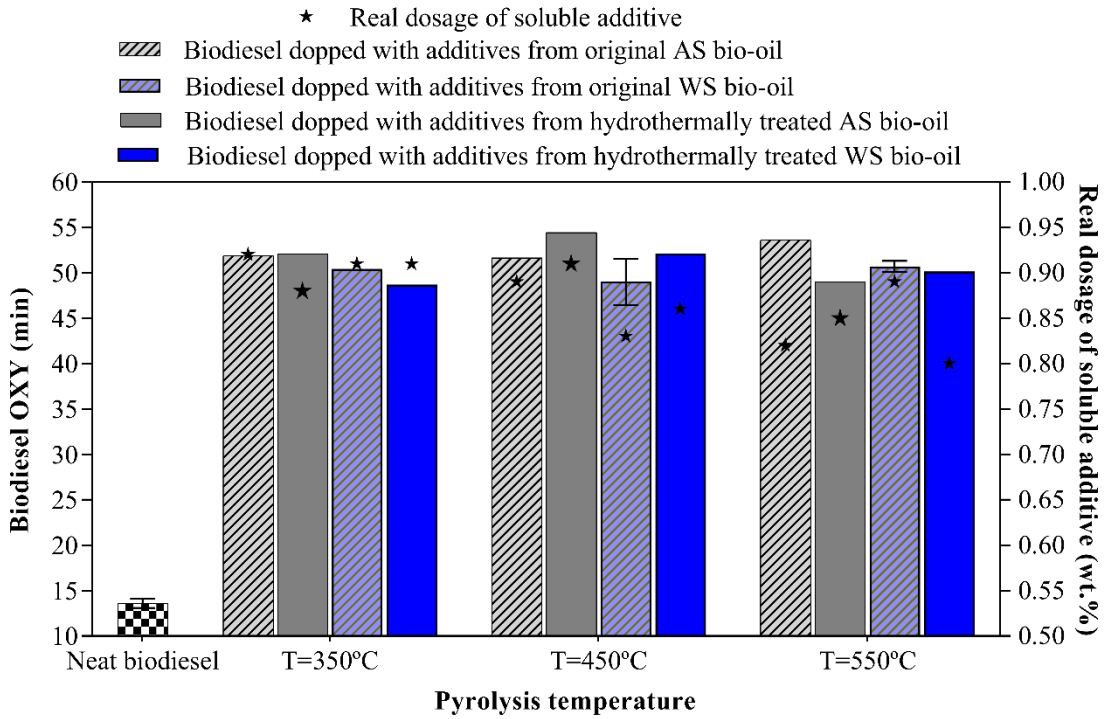

Figure 5.6. OXY time and real dosage of the additives produced from AS and WS bio-oils.

The neat biodiesel involved in the study showed an average oxidation stability time of 13.6 ± 0.5 min. Generally, the biodiesel OXY time was drastically improved when adding different fractions extracted from bio-oil, either from AS or WS, and with or without posterior hydrothermal treatment (49 - 54 min). The HT only slightly improved the performance of the additives prepared at 450 °C, especially in the case of AS bio-oil (55 min for the HT bio-oil vs. 52 min for the original one).

Although in a previous study carried out in GPT (Gil-Lalaguna et al., 2017), it was proved that the HT of pinewood bio-oil significantly improved its antioxidant potential to be used as biodiesel additive (ΔOXY of 404 % for HT bio-oil vs. 132 % for original bio-oil), such an important effect was not found in this work conducted with bio-oils prepared from other types of raw materials.

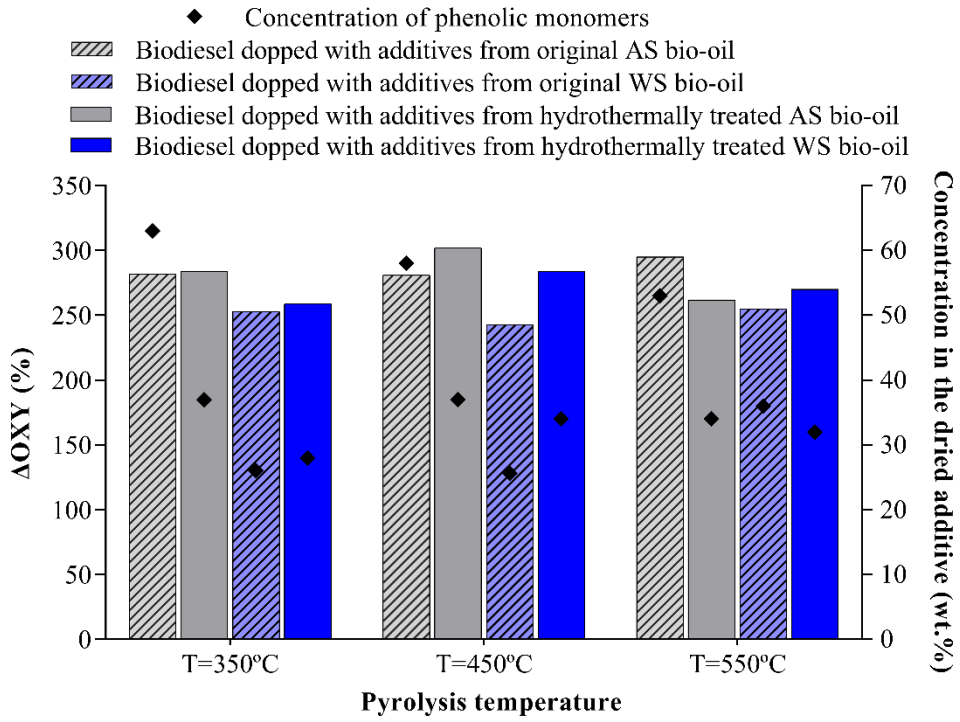

Figure 5.7. Improvement of oxidation stability of biodiesel dopped by additives produced from AS and WS bio-oils.

The results from GC/MS/FID analysis (section 5.3.3) and OXY time analysis were inconclusive concerning the relationship between the phenolic monomeric content and the OXY improvement (Figure 5.7). On the one hand, the total concentration of phenolic monomers was higher in the additives prepared from the original bio-oils than in those derived from the hydrothermally treated bio-oils, especially in the case of AS. On the other hand, the presence of some monomers with particularly good antioxidant performance, such as catechol and 4-methylcatechol, was more significant in the hydrothermally treated bio-oils. Therefore, it seems to indicate that not only these compounds affect the final antioxidant performance of the additives, but other monomers, or even heavier compounds, may have an effect on it.

In fact, as shown in the next Chapter 7 (Afailal et al., 2021), it was proved that other phenolic monomers detected by GC/MS/FID analysis had a positive effect on the biodiesel oxidation stability, but bigger molecules could also have the same effect (undetected dimers and oligomers). This fact was also supported by the study of Larson et al. (Larson et al., 2017). To corroborate this statement, synthetic additives were prepared containing the same phenolic monomeric composition as that detected by GC/MS/FID in some of the additives (specifically those extracted from the original bio-oils prepared at 550 °C from both materials). More

information about the composition of these synthetic additives can be found in Appendix V. Their antioxidant performance when blended with biodiesel at a dosage of 1 wt.% was measured and compared with the results shown by the original bio-oil additives. The OXY improvement of the biodiesel dopped with the synthetic additive simulating the one from AS was up to 144 ± 15 %, which was significantly lower (almost half) than the improvement obtained when biodiesel was dopped with the original additive extracted from AS bio-oil (295 %). The synthetic additive simulating the one from WS showed an OXY improvement of 89 ± 8 % vs. 249 % for its corresponding original bio-oil additive. This difference in the OXY improvement supported that not only the monomeric phenolic fraction is responsible for the antioxidant activity of the additive, but other compounds not included in the synthetic additives may have an important role.

5.4. Conclusions

The pyrolysis treatment of argan shells (AS) and wheat straw (WS) has been investigated in a lab-scale fixed-bed reactor at three different final temperatures (350, 450 and 550 °C). The obtained bio-oils were hydrothermally treated in an autoclave reactor at 300 °C. Antioxidant additives were prepared by extraction (with isopropyl acetate) of both original and hydrothermally treated bio-oils. The main conclusions drawn from this study are the following:

- The change in the pyrolysis temperature from 350 to 550 °C hardly affected the distribution of the products, showing solid yields ranging between 28 - 34 wt.% for both raw materials.

- Argan shells tend to generate more bio-oil and less gas than wheat straw, with a maximal bio-oil yield of 55 wt.% in the case of AS and 49 wt.% in the case of WS, and a maximal gas yield of 14 wt.% for AS and 20 wt.% for WS.

- Producing antioxidant additives from bio-oil could be an interesting added-value application for this liquid fraction. The production of additives from AS bio-oils doubled the yield of those from WS bio-oils. In terms of composition, the concentration of phenolic monomers in the additives ranged between 53 - 63 wt.% for AS bio-oils and 25 - 36 wt.% for WS bio-oils.

- The oxidation stability of biodiesel was improved by 250-300 % with small dosages (< 1 wt.%) of all the additives prepared from the bio-oils of AS and WS.

- Pyrolysis temperature did not significantly affect the antioxidant performance of the additives when being blended with biodiesel. Around 80-90 % of the amount of additive

blended with biodiesel was really soluble, regardless of the bio-oil used for preparing the additive.

– Despite increasing the content of some phenolic monomers with good antioxidant abilities (such as catechol or 4-methylcatechol), the hydrothermal treatment of bio-oil only slightly improved the antioxidant performance of the additives in some specific conditions. Therefore, this small improvement does not support the hydrothermal treatment as a bio-oil upgrading treatment to produce antioxidants from AS or WS.

– The antioxidant activity of the additive is not related only to the presence of phenolic monomers, but other bigger molecules (dimers and oligomers) could also be responsible.

Chapter 6
Activated carbon production

6. ACTIVATION

6.1. Introduction

The current chapter shows the results of the activation step of the char produced from AS.

Historically, in ancient Egypt, porous carbons were used as adsorbents in water purification and liquid filtration even before creating the nomenclature of adsorption (Tadda et al., 2016). This latter was investigated systematically by Scheele in 1774 (Robens, 1994), but the term "adsorption" was employed for the first time in Kayser's work dedicated to the capture of ammonia vapors in the 1881 (Kayser, 1881; Robens, 1994). At the beginning of the 20th century, several processes were established to enhance the performance of the porous carbons, where the notion of activated carbon appeared, and the two basic methods of activation (chemical and physical activation) were explained (Ostrejko, 1920). Since then, the production of activated carbons or activated charcoals has been developed worldwide via different processes and using raw materials such as wood, peat or by-products from the paper industry. The quality and performance of activated carbons depend principally on the raw material chemical structure and the preparation method used. Feedstocks employed in this production can be provided from fossil origin, such as lignite and petrol residues, or from sustainable sources, such as biomass.

Nowadays, activated carbons (especially from sustainable sources) are involved in many important fields and industries. Liew et al. studied the performance of activated biochar from palm kernel shells as a catalyst support, comparing the effect of chemical and physical activation methods in the catalytic performance of methane dry reforming process (Liew et al., 2018). Concerning the use as supercapacitor electrodes, excellent results were reported in the work of Xu et al. when using apricot shells as feedstock to prepare chemically activated carbon (Xu et al., 2010). As an adsorbent, activated carbon from almond shells was tested in the study of Omri et al. (Omri et al., 2013) and showed great results in the adsorption of iodine and methylene blue from aqueous solutions and in the elimination of total organic carbon during the phosphoric acid production.

In this context, the main objective of this part of the work is the production, characterization and evaluation of possible uses of the activated carbon prepared via physical activation (with CO_2) of argan shells biochar. Among the few studies published in the literature about this residue, it appears the production of activated carbons prepared from argan shells, using NaOH, KOH and H_3PO_4 as chemical activation agents, which showed excellent results

concerning the porosity characteristics of the produced material (Boujibar et al., 2019; Boujibar et al., 2018; Elmouwahidi et al., 2012). Ennaciri et al. reported that high-quality activated carbon could also be obtained from argan shells biochar by using steam as an activation agent (Ennaciri et al., 2014). Hence, in this part of the work, physical activation with other cheaper agents, such as CO_2, has been conducted, evaluating the potential uses of the activated solid.

6.2. Experimental methods

6.2.1. Activation experiments

The physical activation of biochar was conducted in a quartz horizontal lab-scale fixed bed reactor with an inner diameter of 22 mm and 70 cm in length (Figure 6.1). The biochar obtained in the AS pyrolysis at 450 °C (from now on, $Char_{AS}$) was crushed and sieved to a particle size between 1 and 1.6 mm. During the activation process, the reactor was heated from room temperature to 900 °C at 15 °C/min under N_2 atmosphere; once the temperature reached the setpoint, the N_2 flow (0.5 L_{STP}/min) was substituted by a CO_2 flow (0.5 L_{STP}/min). The experiments were carried out for three different activation times: t_1=90 min, t_2=120 min and t_3=150 min, thus producing three different activated carbons (AC90, AC120 and AC150, respectively). Once the set time finished, the reactor was left to cool down to room temperature under an inert atmosphere of N_2. Then the activated carbon (AC) produced was weighted (W_{AC}) to calculate its production yield (Equation 6.1) with respect to the amount of $Char_{AS}$ fed (W_{CharAS}).

$$\text{AC yield (\%)} = \frac{W_{AC}}{W_{CharAS}} \cdot 100 \qquad \text{(Eq. 6.1)}$$

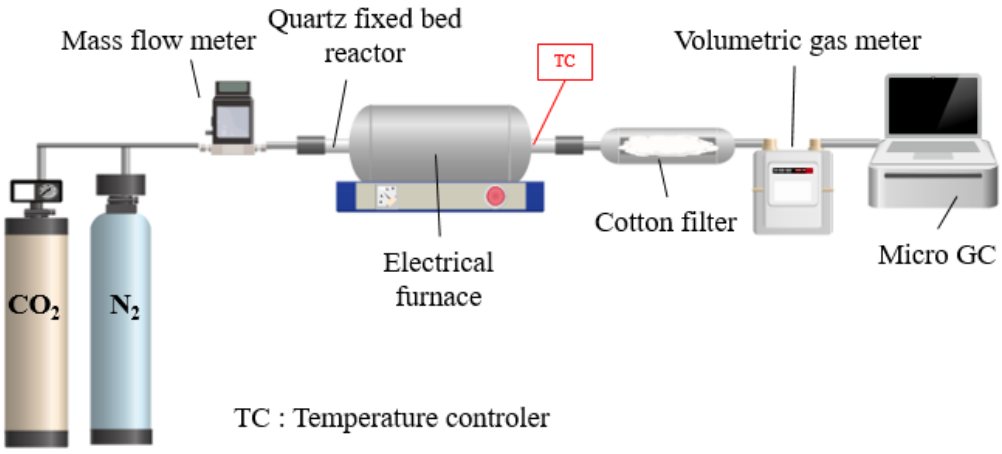

Figure 6.1. Diagram of the experimental for physical activation setup.

6.2.2. Biochar and activated carbon characterization

The biochar obtained in the pyrolysis of AS at 450 °C ($Char_{AS}$) and the three samples of activated carbons (AC90, AC120 and AC150) were characterized in terms of elemental analysis, proximate analysis and calorific value. In addition, the textural properties of these solids were examined through N_2 adsorption isotherms (measured at 77 K) acquired with a Quantachrome Autosorb 6 instrument. Before determining the material porosity, all the samples were vacuum outgassed at 523 K for 15 h to remove moisture and impurities adsorbed on the material surface. The multi-point BET surface area (S_{BET}) was determined by fitting the data of N_2 isotherms to Brunauer, Emmett and Teller (BET) theory. The average pore size and the total pore volume (V_T) were calculated from N_2 isotherms at a relative pressure (P/P_0) of 0.99. Non-local density functional theory (NLDFT) was also applied, assuming slit porosity, in order to determine the pore size distribution and the micropore specific surface area (S_{micro}). In addition, to complete the information about the microporous structure (pore size between 0.35 and 1.5 nm), CO_2 adsorption isotherm at lower relative pressures ($P/P_0 < 0.029$) were also examined for AC120 using the same equipment. The results obtained were modeled by the NLDFT approach based on slit pores. The morphology of the samples was observed by Field Emission Scanning Electron Microscope (FESEM) carried out by Carl Zeiss MERLIN.

Further analyses, such as Boehm titration and pH, were performed to characterize the AC samples. To determine the pH of the activated carbons, 1 g of the AC was added to 150 mL of distilled water (pH of 7.03), the mixture was left for 24 h at room temperature under stirring (700 rpm). After this time, the pH of the water was measured by means of a Thermo Orion Star A215 pH/conductivity benchtop multiparameter meter. In order to determine the nature of the functional groups present on the activated carbon surface, the Boehm procedure was followed (Boehm, 2008; Tsechansky and Graber, 2014). In a typical test, 500 mg of AC150 was added to 50 mL of each of the following aqueous solutions (0.05 M): (i) sodium bicarbonate ($NaHCO_3$) to neutralize the carboxylic acid sites; (ii) sodium carbonate (Na_2CO_3) to neutralize lactonic and carboxylic acid sites; (iii) sodium hydroxide (NaOH) to determine the total acidity and (iv) hydrochloric acid (HCl) to determine the total alkalinity. Each mixture was left under stirring (700 rpm) and after 24 h each solution was filtered to remove the AC. The aqueous solutions of NaOH and HCl were directly titrated by HCl (0.05 M) and NaOH (0.05 M), respectively. On the other hand, the solutions of $NaHCO_3$ and Na_2CO_3 were back-titrated: a known excess of HCl was added and then the mixture was flushed by a flow of N_2 to evacuate

the formed CO_2 before being titrated by NaOH. The detailed calculations of this procedure can be found in the study of Wu et al. (Wu et al., 2020).

6.2.3. Activated carbon end-uses

The performance of the AC samples as an adsorbent material for different compounds was studied: methylene blue (MB), phenol, catechol, vanillin and CO_2. For liquid phase adsorption tests, four aqueous solutions were prepared with a known initial concentration of methylene blue (MB), phenol, catechol or vanillin (125 mg/L of MB and 100 mg/L of the phenolic compounds). AC was added to 50 mL of each solution (250 mg of AC in the MB solution and 50 mg in each phenolic solution). The adsorbed fraction of each compound was continuously monitored through UV-Visible absorbance measurements and a retention capacity rate was calculated (Equation 6.2).

$$\text{Retention (\%)} = \frac{C_{initial} - C_t}{C_{initial}} \cdot 100 \qquad \text{(Eq. 6.2)}$$

where $C_{initial}$ is the initial concentration of each adsorbate in the solution before being in contact with the activated carbons, and C_t is the concentration after a specific contact time of t hours.

On the other hand, the CO_2 adsorption experimental setup consists of a quartz tube in which a fixed-bed of approximately 1 g of adsorbent material (AC120) was loaded and supported by glass wool on the sides. The device was placed inside an oven, where the system temperature was controlled. Before starting the adsorption test, a degassing step of the sample was done at 150 °C under an inert atmosphere of N_2. Then, the sample was cooled down and the adsorption test was performed at 25 °C by feeding a gas mixture of CO_2 (50 %) diluted with N_2 (50 %). The total gas flow into the system remained fixed at 70 $mL_{(STP)}$/min (adjusted with mass flow controllers). After passing through the AC bed, a mass spectrometer (Hiden QIC-20) continuously analyzed the gas composition at the exit. Considering the composition evolution over time, the CO_2 flow at the output and its adsorbed amount were calculated using the N_2 flow as an internal standard.

6.3. Results and discussion

6.3.1. Production and characteristics of the activated carbon

Depending on the treatment time, the production of activated carbon after the CO_2 physical activation step (900 °C) ranged between 38 wt.% (150 min) and 68 wt.% (90 min) with respect to the biochar fed into the activation step, which means a reductionby almost half

when increasing the treatment time from 90 to 150 min. These relatively highyields of AC can be explained by the high conten of fixed carbon in $Char_{AS}$ (78.8 ± 0.2 wt.%). In general, lower activated carbon yields have been reported in the literature for biochars from different origins. According to Gonçalves et al. (Gonçalves et al., 2017), solid yields between 17 and 19.5 wt.% were obtained after CO_2 activation of a mixture of brewer's spend grain and surplus yeast (at 850 °C and 2 - 4 h). In other work, Zhao et al. reported solid yields between 16.7 and 21.2 wt.% after CO_2 activation of walnut shells at 900 °C and holding times of 1 and 2 h (Zhao et al., 2020).

Considering the yield of biochar in the pyrolysis of AS, (31 wt.% at 450 °C), the overall production of activated carbon with respect to the initial amount of AS which was pyrolyzed yielded 20, 16 and 11 wt.% when extending the activation step for 90, 120 and 150 min, respectively.

Table 6.1 compares some characterization results of biochar before and after the activation step during the three different treatment times. As can be seen, the carbon content in the solids increased from 85 wt.% in raw biochar to around 95 wt.% in the activated ones, regardless of the treatment time; the hydrogen content in the activated carbons was up to 0.5 wt.% instead of 3 wt.% in $Char_{AS}$. Ash content ranged between 1.3 wt.% and 2 wt.% in all the solids. Similar ash contents were obtained in other works when biochar from AS was activated using steam (Ennaciri et al., 2014). This low ash content in the activated carbon is, in turn, related to the low mineral content in the raw material (ash content of AS is up to 0.3 wt.%) and the absence of chemical precursors in the activation process. This could be one of the highlighted characteristics of these activated carbons, as higher contents are unwelcomed because of reducing the mechanical strength and adsorption capacity (Ekpete et al., 2017). In particular, the activated carbons produced from fruit residues usually showed low ash contents, such as those from almond shells (up to 3 wt.%), apricot stones (2 wt.%) (Savova et al., 2001) and pistachio shells (Lua et al., 2004). However, woody materials led to activated carbons characterized by a relatively higher ash content ranging between 5 and 20 wt.%, mainly depending on the type of raw material and the activation method (Ekpete et al., 2017; Girods et al., 2009). The activated carbons produced from AS biochar were neutral or slightly alkaline, with a pH ranging between 7.8 and 8. According to Ahmedna et al., the pH and the ash content in activated carbons are positively correlated (Ahmedna et al., 2000). Generally, carbons with a pH of 6–8 are characterized by their low ash contents (less than 5 wt.%).

Table 6.1. Characterization of biochar from argan shells before and after CO_2 activation during different treatment times.

	$Char_{AS}$	AC90	AC120	AC150
Ultimate analysis (wt.% ar. basis)				
C	85 ± 2	95.1 ± 0.2	94.9 ± 0.3	94.3 ± 0.1
H	3.5 ± 0.2	0.7 ± 0.1	0.55 ± 0.04	0.505 ± 0.004
N	0.3 ± 0.1	1.02 ± 0.03	1.0 ± 0.1	1.12 ± 0.02
S	< 0.05	< 0.05	< 0.05	< 0.05
O[a]	10 ± 2	1.9 ± 0.1	2.0 ± 0.1	1.9 ± 0.2
Ash (wt.%)	1.1 ± 0.1	1.3 ± 0.1	1.5 ± 0.2	2.1 ± 0.3
Textural properties (N_2 adsorption isotherms)				
S_{BET} (m^2/g)[a]	282 ± 20	838 ± 80	1138 ± 78	1544
S_{micro} (m^2/g)[b]	295 ± 36	698 ± 122	927 ± 18	1101
V_T (cm^3/g)[c]	0.18 ± 0.01	0.37 ± 0.03	0.49 ± 0.04	0.68
V_p (cm^3/g)[b]	0.152 ± 0.004	0.33 ± 0.03	0.44 ± 0.04	0.60
Average pore size (nm)[c]	2.5 ± 0.1	1.8 ± 0.1	1.73 ± 0.23	1.76
Pore size (nm)[b]	1.476 ± 0.001	1.45 ± 0.04	1.411 ± 0.001	1.48

[a] Determined by BET theory
[b] Calculated from the NLDFT equation with slit pore model: the fitting error between the model and all the activated carbons ranged between 0.03 and 0.05 % and for the $Char_{AS}$ between 0.04 and 0.08%.
[c] Calculated at P/P_0=0.99.

Textural properties of the AS biochar and the activated carbons were investigated through N_2 isotherms (measured at 77 K). According to the IUPAC classification, the isotherms of the three samples of AC (Figure 6.2) were characterized as type IV, outlining a microporous solid with the presence of a hysteresis loop (H4), which also reveals the presence of a small number of mesopores (more significant when increasing the treatment time). The activation treatment was successfully in terms of significantly increasing the BET surface area of biochar (Table 6.1, 282 m^2/g for $Char_{AS}$). Increasing the activation time improved the BET surface area, which reached 838 m^2/g in AC90, 1138 m^2/g in AC120 and attained its maximal value of 1544 m^2/g in AC150. Higher values of BET surface area (up to 2250 m^2/g) were reported in the study of Boujibar et al., who used the same feedstock (AS) to obtain activated carbons via impregnation or physical mixing with KOH after AS carbonization (Boujibar et al., 2018).

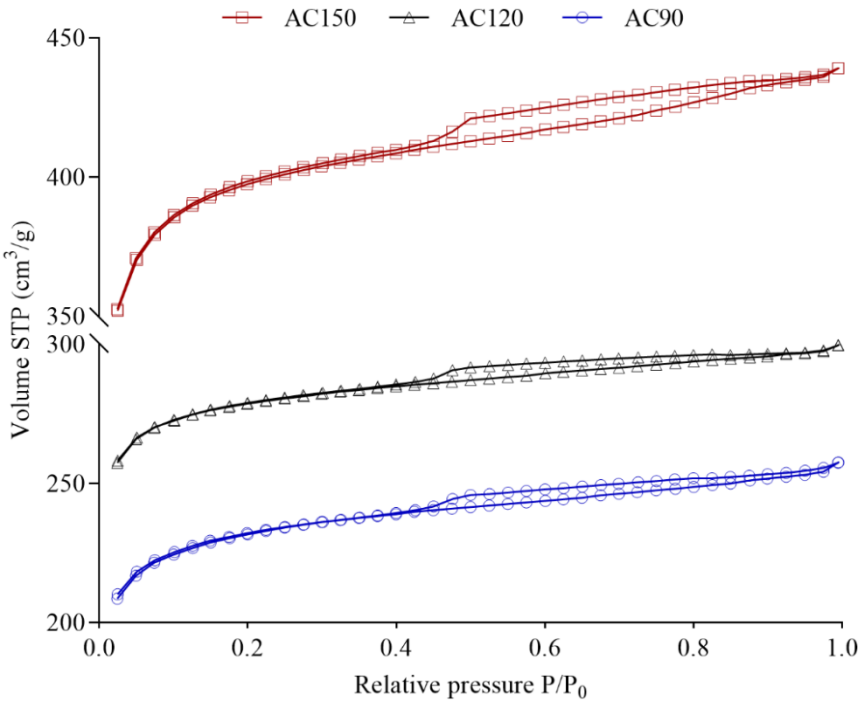

Figure 6.2. N_2 isotherm at 77 K (adsorption/desorption branches) of the activated carbons produced from argan shells biochar.

The AC samples produced in the present work showed total pore volumes (V_T) ranging between 0.37 and 0.68 cm^3/g. This parameter showed the same tendency as S_{BET}, since it was further developed at longer activation treatment times. The average pore width was up to 1.7 nm for all the AC produced (both V_T and the average pore width were calculated at P/P_0 of 0.99). The pore size distribution resulting from applying the NLDFT method on N_2 adsorption isotherms (Figure 6.3) showed that N_2 adsorption occurred principally at a pore width zone between 1.2 and 2 nm size. Accordingly, as shown in Table 6.1, S_{micro} (estimated by NLDFT) ranged between 698 and 1101 m^2/g when increasing the activation time from 90 to 150 min, representing between 71 and 83 % of the BET surface area (ratio directly calculated as S_{micro}/S_{BET}). The cumulative pore volume determined by NLDFT (V_P) ranged between 0.33 and 0.6 cm^3/g, slightly lower than the values of V_T, but following the same trend: the longer activation time, the higher the pore volume. In addition to micropores, a noticeable shoulder in the distribution (Figure 6.3) was observed at pore widths ranging between 3.4 and 4.4 nm, outlining the further development of small mesopores, in which the activation time clearly had an influence.

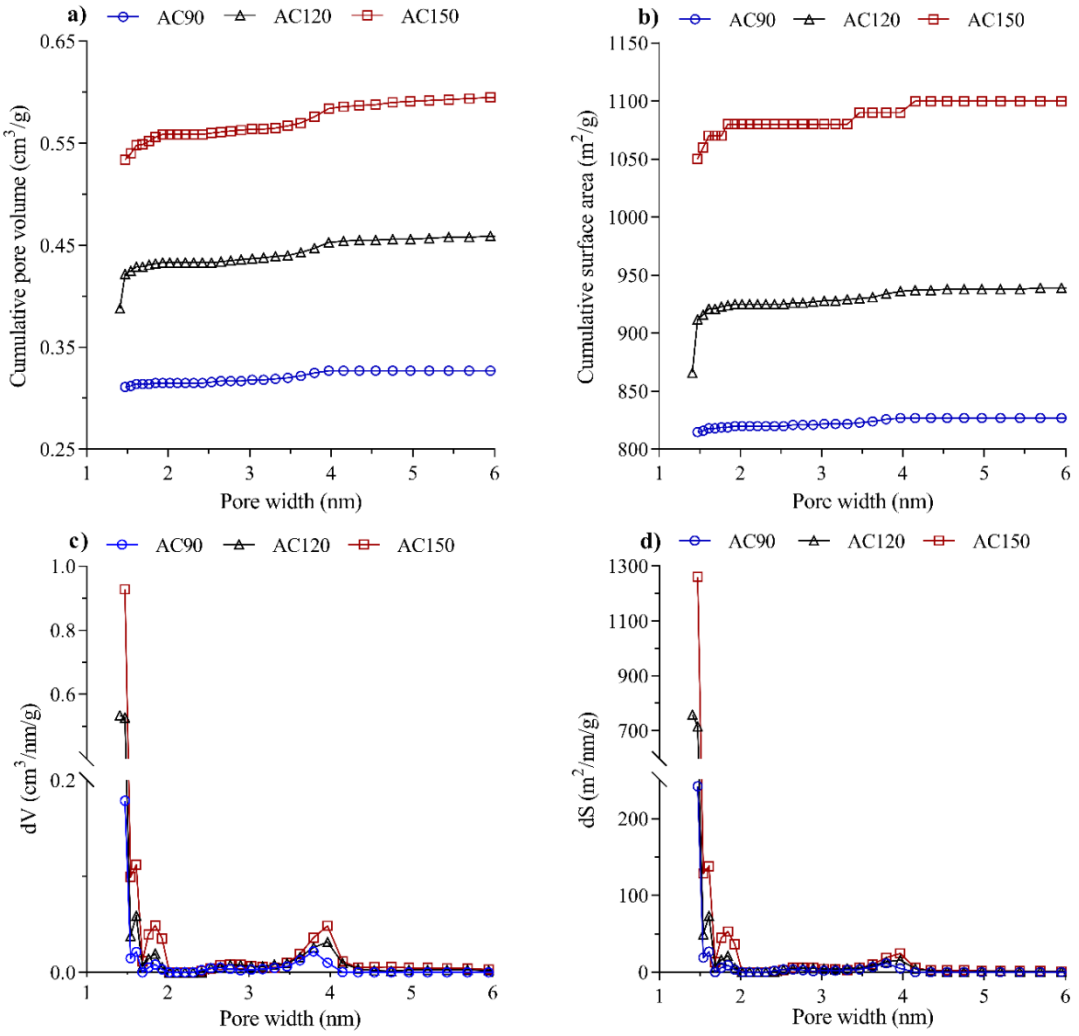

Figure 6.3. Pore size distribution determined from N_2 adsorption isotherms using NLDFT calculations.

Microporous materials are better characterized with CO_2 adsorption isotherms evaluated at lower relative pressures because of the no-limitation of CO_2 to penetrate the narrower micropores (Lozano-Castelló et al., 2004). CO_2 adsorption isotherm analyzed for AC120 (temperature of 0 °C and $P/P_0 < 0.029$) suggests the existence of ultramicropores with pore widths less than 0.7 nm and small micropores with pore sizes ranging between 0.8 and 1 nm (Figure 6.4). According to NLDFT calculations based on a slit pore model applied to this CO_2 adsorption isotherm (fitting error between the model and the sample of 1.7 %), the micropores surface area was estimated to be 1002 m^2/g, the average pore width was 0.35 nm and the cumulative pore volume was 0.3 cm^3/g. Similar values and trends concerning the porosity

nature of the activated carbons were observed when char from AS was activated using chemical precursors in the study of Boujibar et al. (Boujibar et al., 2018).

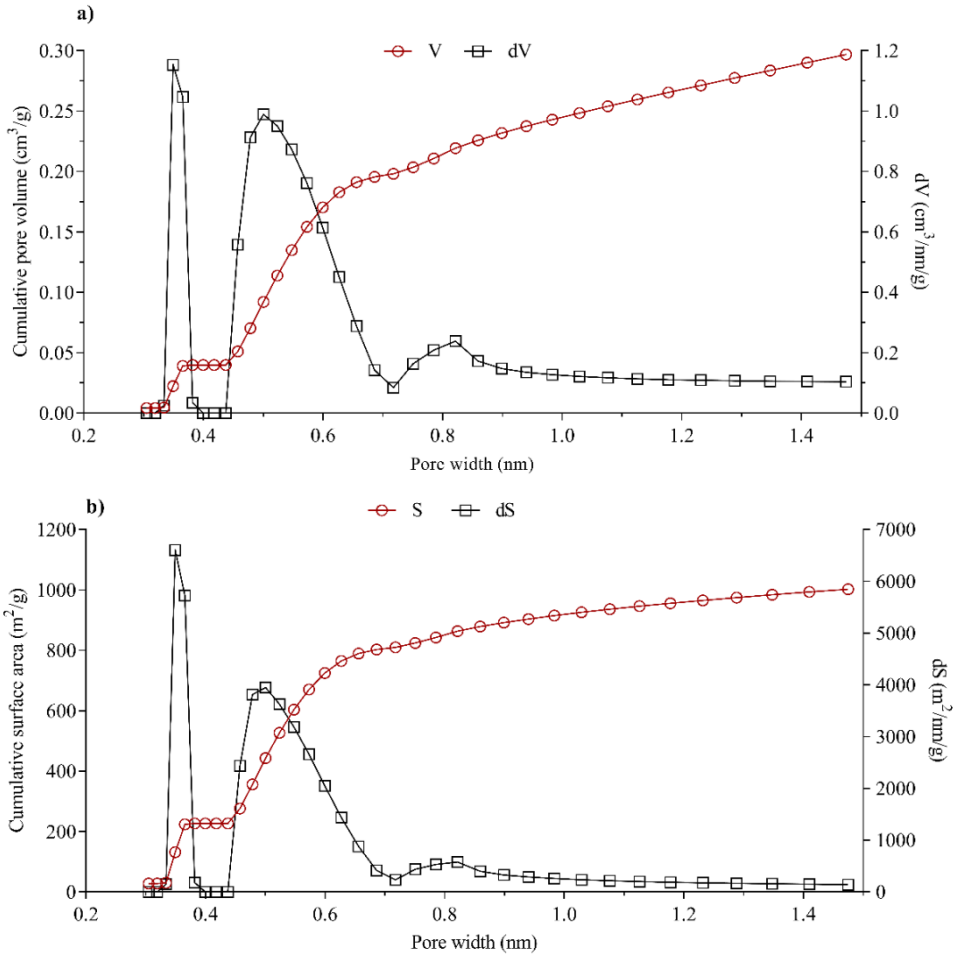

Figure 6.4. Pore size distribution determined for AC120 with NLDFT calculations from CO_2 adsorption isotherm data.

Figure 6.5 shows the Field-Emission Scanning Electron Microscopy (FESEM) results for both the original biochar ($Char_{AS}$) and the AC120. The $Char_{AS}$ micrograph presents a honeycomb-like structure with large spherical cavities and a relatively smooth external surface, while a foam cluster structure has appeared in the activated carbon AC120. This structure was attributable to the selective effect of CO_2 during the activation (Herzog et al., 2006).

Finally, the Boehm titration of AC150 (Figure 6.6) showed that the total amount of acid sites on the surface was almost the same as the total alkaline sites (around 4100 µmol/g). The acid sites identified were mainly carboxyls (up to 2340 µmol/g), lactones (up to 935 µmol/g) and phenolics (up to 830 µmol/g).

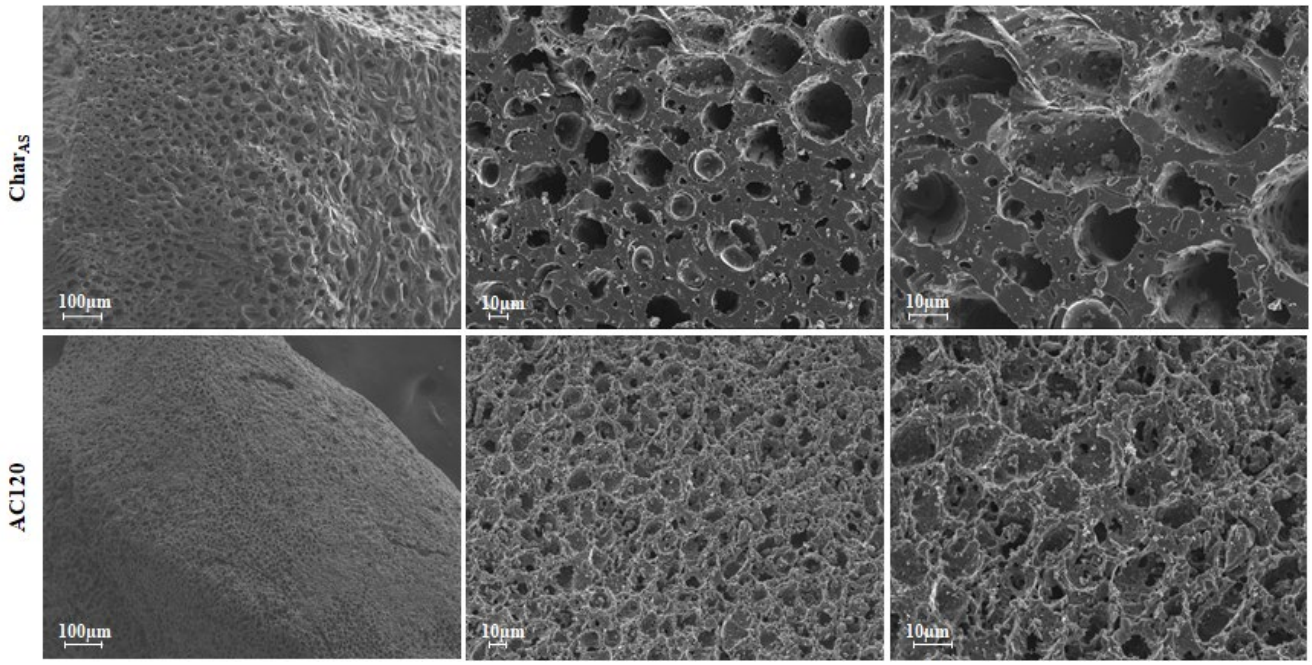

Figure 6.5. FESEM micrograph of AS biochar before and after CO_2-activation during 120 min.

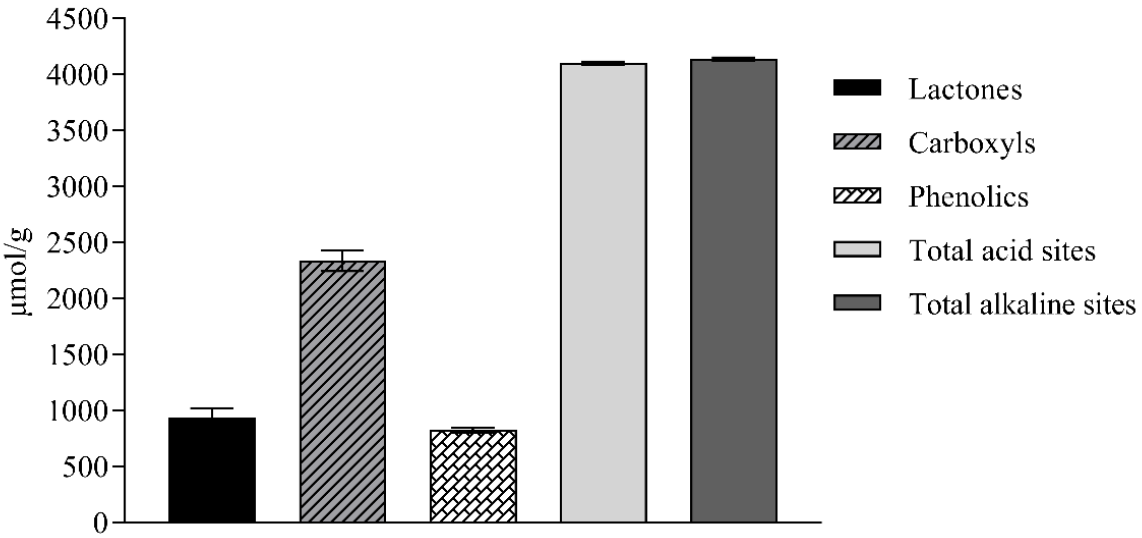

Figure 6.6. Boehm titration for the AC150.

6.3.2. Use of the activated carbon as an adsorbent material

The adsorption capacities of the three activated carbons produced from AS biochar were investigated after leaving the solid in contact with different aqueous solutions containing

methylene blue (MB) and various phenolic compounds (phenol, vanillin and catechol), respectively.

Figure 6.7 shows the results of the retention capacity of AC90, AC120 and AC150. Generally, all the activated carbons showed an excellent retention capacity of these potential contaminants. MB was almost completely removed from the aqueous solution after 24 h of contact time with any of the three samples of AC, although the retention rate in the case of AC90 was slightly slower (as shown in Figure 6.7 and Figure 6.8). Regarding the adsorption of phenolic compounds, vanillin was entirely removed from the aqueous solution after 4 h of contact time with both tested materials (AC90 and AC150). Lower retention percentages were observed for phenol and catechol for the same contact time. After 24 h, phenol was totally adsorbed, while 95 wt.% of the initial amount of catechol was retained. It is to highlight that AC150 required less contact time to achieve total adsorption of the contaminants thanks to its greater porosity (surface area and pore volume).

Finally, the feasibility of adsorbing CO_2 on this type of AC was also evaluated at 25 °C (fixed-bed adsorption reactor), finding an adsorption capacity of 125 mg of CO_2 per gram of AC120. Similar CO_2 retention capacities have been reported in the literature for activated carbons prepared from other biomasses. Yang et al. found relatively closer values of CO_2 uptakes (between 111 and 135 mg/g at 25 °C) with activated carbons prepared from walnut shells via chemical activation with $NaNH_2$ at 450 °C (Yang et al., 2019). In other work (Khuong et al., 2021), physical activation (with CO_2 at 900 °C) of the solid residue from hydrothermal treatment of bamboo led to slightly higher CO_2 uptakes (150 mg/g); this solid was characterized by a S_{BET} of 1316 m^2/g and a V_T of 0.55 cm^3/g. In contrast, lower values were reported for activated carbons prepared by monoethanolamine impregnation of coconut shells and sawdust chars, showing CO_2 adsorption capacities of 36 and 45 mg/g, respectively (Ghani et al., 2015; Madzaki et al., 2016).

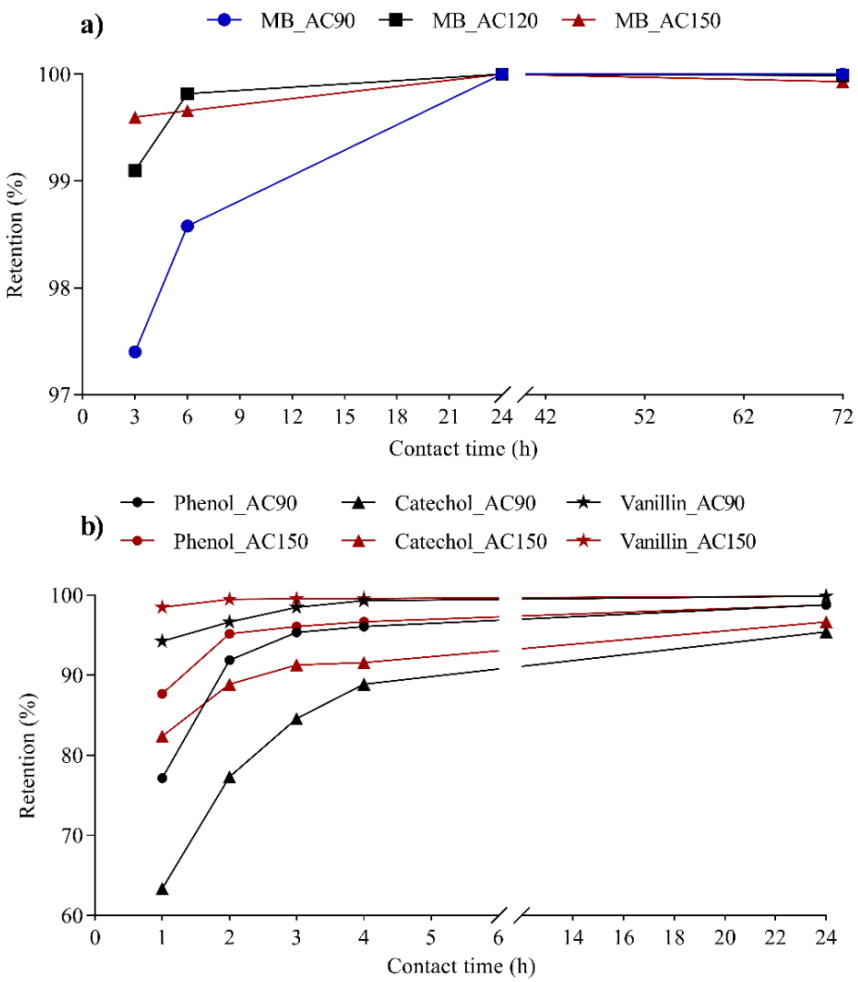

Figure 6.7. Retention capacities of different compounds for the activated carbons prepared from argan shells biochar: (a) adsorption of methylene blue and (b) adsorption of phenolic compounds.

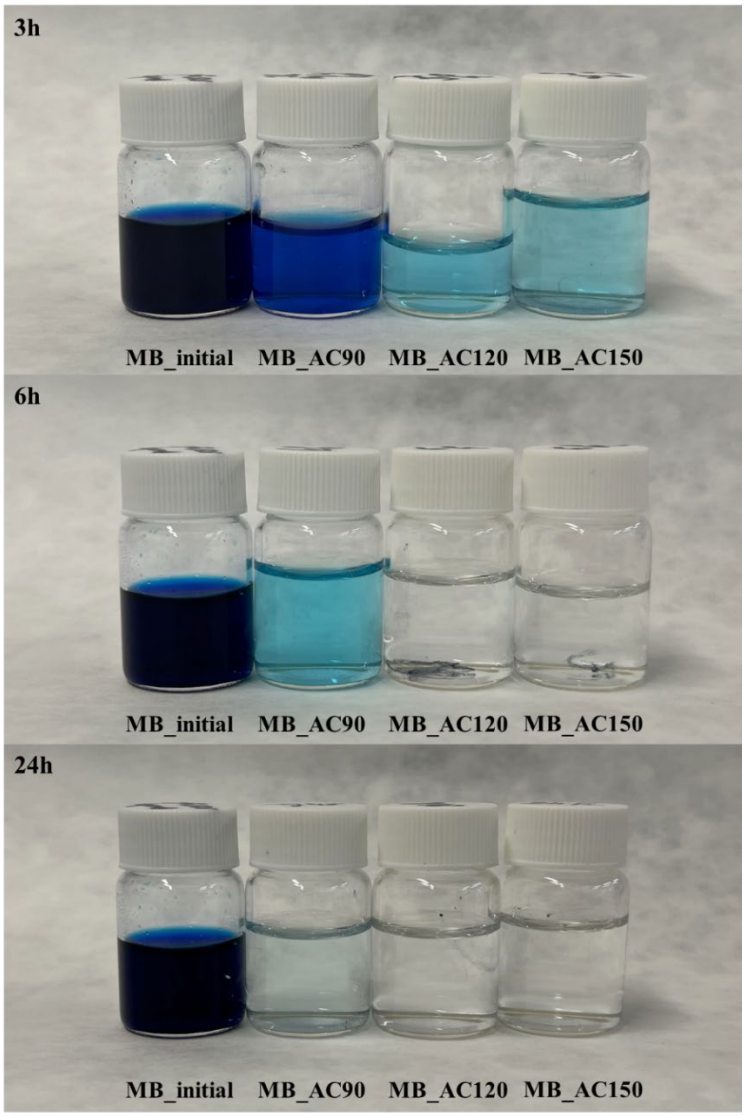

Figure 6.8. Methylene blue adsorption.

6.4. Conclusions

The physical activation treatment (with CO_2) of argan shells biochar has been investigated in a lab-scale fixed-bed reactor at 900 °C and three different treatment times (90, 120 and 150 min). The main conclusions drawn from this study are the following:

– A high-quality activated carbon can be obtained via this treatment characterized by pH slightly alkaline (around 8), high carbon content (up to 95 wt.%), and low ash content (around 2 wt.%).

– The textural properties of the produced activated carbons were proportionally affected by the activation time: reaching 838 m^2/g and 0.3 cm^3/g in AC90, 1138 m^2/g and

0.4 cm^3/g in AC120 and attaining its maximal value of 1544 m^2/g and 0.6 cm^3/g in AC150, for BET surface area and average pore volume, respectively.

– Existence of ultramicropores with pore widths less than 0.7 nm in the produced activated carbons.

– The activated carbons showed considerable potential as contaminants adsorbent material from aqueous solutions, such as phenols and methylene blue.

– Noticeable CO_2 uptakes were obtained when using the activated carbons from argan shells biochar.

Chapter 7
Hydrothermal treatment

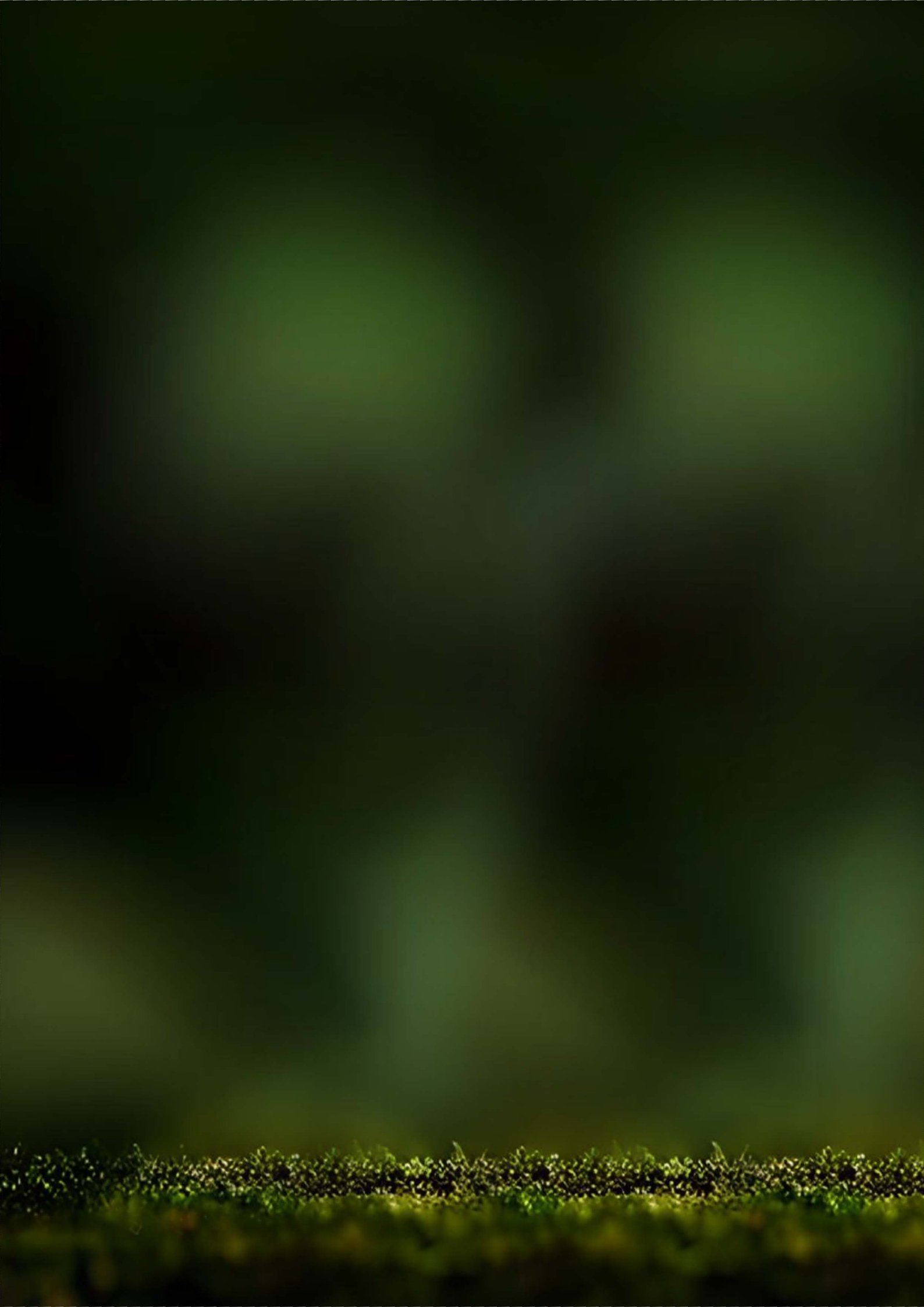

7. HYDROTHERMAL TREATMENT

7.1. Introduction

As mentioned in the general introduction section, this chapter is dedicated to the extraction of lignin from AS and its further treatment to produce antioxidant additives.

Lignin is considered one of the most abundant biopolymers in the world. It can be extracted from the lignocellulosic biomass by classical chemical methods (such as Kraft and sulfite processes) and semi-chemical methods (organosolv and soda processes), in addition to other new promising methods involving the use of ammonia (Da Costa Sousa et al., 2016) or imidazole (Morais et al., 2016). However, due to its complex structure, the extraction of an unaltered native lignin is still not possible (Gillet et al., 2017). Semi-chemical pulping process using soda has been a historically typical process in the production of pulp and paper from non-woody materials such as crops (miscanthus, kenaf) or agricultural residues (straw, bagasse) (Gonzalo et al., 2017). This process entails separating pulp with high cellulose content from the original lignocellulosic material, leaving behind a black liquor, rich in lignin content, as a problematic by-product to be managed (Gonzalo et al., 2017; Marín et al., 2009).

Lignin conversion could be considered a potential alternative to the petrochemical industry, especially for fuel and chemicals production (Gillet et al., 2017). For its chemical valorization, lignin fragmentation can be implemented via various technologies such as biological depolymerization, homogeneous and heterogeneous catalysis and thermochemical treatments (Ragauskas et al., 2014). Fragmentation means the cleavage of condensed (C-C) or/and ether linkages (Huang et al., 2014; Lavoie et al., 2019; Tolbert et al., 2014). Generally, the main depolymerization products in thermochemical treatments of lignin are a gas stream (mainly CO_2), small organic compounds, up to 10 wt.% of phenolic monomers and 45-70 wt.% of oligomers (Beauchet et al., 2012), all of them with an important add-value.

Among thermochemical treatments, hydrothermal processes are defined as chemical and physical transformations at high pressure and moderate temperature [200 - 400 °C] in an aqueous solution (Cao et al., 2018; Kang et al., 2013). These processes are considered as an effective and environmental-friendly technology for the chemical valorization of lignocellulosic biomass (Akhtar and Amin, 2011; Cao et al., 2018; Garrote et al., 1999; Kang et al., 2013) with the advantages of high conversion rate and short holding time (Cao et al., 2018). Several studies were dedicated to lignin fragmentation by hydrothermal treatment for chemicals production (Gosselink et al., 2012; Otromke et al., 2019). During this treatment,

oxygen content in the organic material can decrease from 40 % to 15 % through its release in the form of CO_2, H_2O and CO (He et al., 2008). Additionally, many reactions occur during the hydrothermal process, such as demethoxylation, alkylation, condensation and breakage of ether and carbon-carbon bonds (Cao et al., 2018; Chandrasekaran et al., 2016). Regarding the reaction medium, some works were focused on the performance of H_2 and hydrogen donors (such as formic acid or alcohols) on stabilizing the free radicals formed during the hydrothermal depolymerization of lignin (Davoudzadeh et al., 1985) and its effectivity in increasing the yield of depolymerized lignin (Huang et al., 2014; Kleinert et al., 2009) by hindering repolymerization reactions and promoting demethoxylation (Kim et al., 2014). Other gaseous reaction media have been studied, such as CO_2 (Cao et al., 2018), whose incorporation in the aqueous solution was found to be favorable because of carbonic acid formation, which enhanced the quality of the substrates produced during enzymatic hydrolysis reactions of lignin (Scanlon and Willis, 1985). Other researches were focused on the effect of base catalysts (such as $Ca(OH)_2$, K_2CO_3, LiOH, KOH or NaOH) on lignin depolymerization (Erdocia et al., 2014; Mahmood et al., 2013; Toledano et al., 2014). In general, the use of basic catalysts prevents coke formation and favors the production of monomers and dimers, but the type of catalyst clearly affects the nature of the phenolic products obtained and the yields of organic compounds (Toledano et al., 2012). NaOH was considered as the best option to catalyze the hydrothermal depolymerization of lignin (Toledano Zabaleta, 2012).

The lignin-derived chemical products from hydrothermal depolymerization are mainly based on phenolic compounds. In general, phenolic compounds are usually considered to have good antioxidant properties (Kähkönen et al., 1999). In this field, some research works have tested the production of antioxidants from renewable phenolic sources such as pyrolysis bio-oil of birch wood or black liquor; these antioxidants have been proven to be effective in, for example, the improvement of the oxidation stability of biodiesel (Chandrasekaran et al., 2016; Lavoie et al., 2019).

Biodiesel is an environmentally friendly fuel composed of fatty acid esters; it is usually synthesized through triglyceride transesterification with short-chain alcohols (Yaakob et al., 2014). Biodiesel can replace fossil diesel in conventional engines (decreasing the unburned carbon monoxide and smoke emissions by 30 % and 50 %, respectively (Tabatabaei and Aghbashlo, 2020), but keeping in mind essential issues related to the low storage stability of biodegradable fuels. Biodiesel is less resistant to oxidative degradation due to the instability caused by the unsaturation of fatty acid chains (Pullen and Saeed, 2012). Its oxidation process

begins by forming peroxyl radical (from fatty acid radical in O_2 presence). Then, this unstable radical starts the self-sustaining chain-reaction abstracting the most reactive hydrogen atoms. To avert this problem, synthetic antioxidants are usually incorporated into biofuels with the role of interrupting the subsequent chain reaction of peroxyl radicals by substituting them with new and less reactive radicals (such as phenolic radicals) in order to stop or retard the chain degradation (Larson et al., 2017; Pullen and Saeed, 2012; Yaakob et al., 2014). According to several studies, the use of commercial antioxidants such as butylated hydroxytoluene (BHT), tert-butyl hydroxyquinone (TBHQ) and 3-tert-butyl-4-hydroxyanisole (BHA) shows an efficient way to improve biodiesel oxidation stability (Domingos et al., 2007; Focke et al., 2012). However, these compounds are produced from fossil resources, so the production of antioxidant additives from renewable materials appears as a potential field to be investigated in the development of new energetic strategies (Chandrasekaran et al., 2016; Gil-Lalaguna et al., 2017; Larson et al., 2017).

During the last years, the Thermochemical Processes Research Group (University of Zaragoza, Spain) has been focused on using different lignocellulosic feedstocks for the production of natural antioxidants additives for biodiesel (Botella et al., 2018; García et al., 2017; Gil-Lalaguna et al., 2017; Lavoie et al., 2019; Palomo et al., 2019). The incorporation of bio-based antioxidant additives, such as bio-oil fractions, has led to excellent biodiesel oxidation stability improvements (Gil-Lalaguna et al., 2017). The present study continues in the same investigation field by processing argan shells.

Considering the great social and economic impact that the valorization of agricultural wastes will take on a biorefinery concept (Manzanares, 2020), this part of the work focuses on the valorization of lignin contained in AS, which was extracted through a semi-chemical process (Gonzalo et al., 2017). The resulting black liquor contained a high amount of lignin, as well as some hemicellulose and inorganic matter (Gillet et al., 2017) from the chemicals used in the pulping treatment (NaOH) (Lavoie et al., 2019). The solid contained in the black liquor (from now on, ASL_f: lignin-rich fraction from argan shells) was depolymerized under hydrothermal conditions (aqueous solution) at a temperature interval between 250 and 350 °C, and involving different reaction media: formic acid (HCOOH), H_2 and CO_2 (both gases being the decomposition products of HCOOH in hydrothermal conditions). The impact of these factors on the lignin hydrothermal treatment performance and on the products characteristics, specially the antioxidant potential of the liquid product, was investigated.

7.2. Experimental methods

7.2.1. Extraction and characterization of the lignin fraction

Before extracting the lignin fraction, AS, in its original size, was washed to remove dust and impurities and dried at room temperature overnight. Then, lignin was extracted via a semi-chemical pulping process, in which the material was digested for 4 h in an aqueous solution of sodium hydroxide (9.5 wt.% of NaOH with respect to the dry weight of the material) in a batch stirred reactor of 50 L (Figure 7.1) at 98 °C and atmospheric pressure (Gonzalo et al., 2017; Lavoie et al., 2019; Marín et al., 2009). The produced black liquor was separated from the remaining shells by filtration (mesh size 100 μm) and kept in an oven at 105 °C until getting a dried solid, which was maintained at such temperature during storage to prevent rehydration. The dried lignin-rich fraction (ASL_f) was characterized in terms of molecular weight distribution, acid-lignin insoluble content, ash content (EN 14775:2010), HHV (calorific bomb IKA model C2000 basic) and elemental analysis (LECO CHN628 Analyzer). Acid-insoluble lignin was gravimetrically quantified after precipitation of the raw solid dissolved in water (Beauchet et al., 2012). HCl 0.5 N was added to the aqueous solution to decrease the pH to 2. The solution was heated to approximately 70 ºC during 20 min and then filtered with a Büchner funnel to separate the acid-insoluble lignin.

The molecular weight distribution was measured by gel permeation chromatography (GPC) using HPLC Agilent 1200 equipment. The equipment consists of two columns (ultrahydrogel 250 by Waters) and UV-vis (280 nm and 250 nm)/RI detectors. The columns and detectors were maintained at 40 °C under operation. An aqueous solution (pH 12) of NaOH: methanol (1:1 wt.) with 0.1 vol% of LiBr and 0.05 vol% of NaN_3 was used as mobile phase (flow rate of 0.8 mL/min). For the analysis, the solid was dissolved at a concentration of around 1 g/L. 13 different polyethylene glycol standards ranging from 106 to 100900 Da were used for calibration (more information is exposed in Appendix VI). The results of GPC were expressed in terms of average molecular weight in number (Mn), in weight (Mw) and polydispersity.

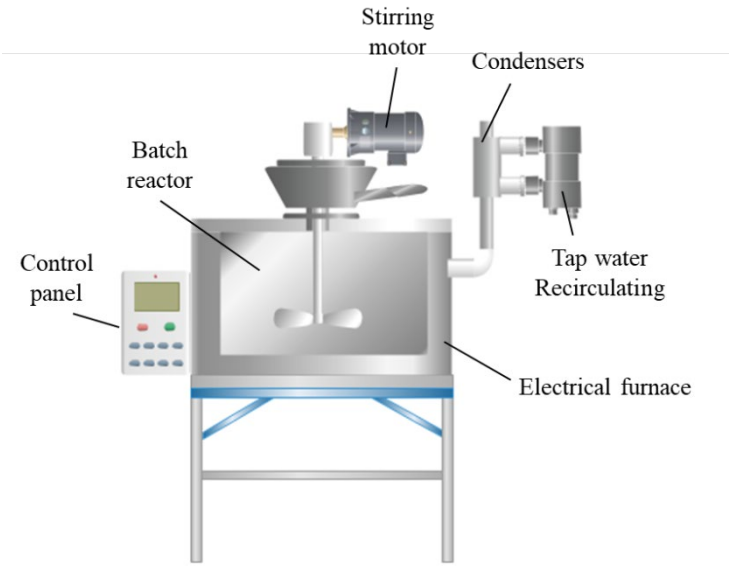

Figure 7.1. Diagram of the experimental semi-chemical pulping setup.

7.2.2. Lignin depolymerization experiments: hydrothermal treatment

The depolymerization experiments were conducted in a 500 mL Parr reactor (Parker Inc. USA) operating in a discontinuous system (see Figure 5.2). In a typical run, an aqueous solution of 200 g with 7 wt.% of ASL_f was homogeneously prepared and loaded into the reactor. Different liquid and gas media were selected for the depolymerization process. On the one hand, HCOOH was added to the aqueous solution as a hydrogen donor. On the other hand, H_2 and CO_2 atmospheres were also tested, aiming at evaluating their individual effect on the products distribution and the antioxidant activity of the liquid one, as these gases are the major products of HCOOH decomposition under the experimental conditions set (Huang et al., 2014).

In the HCOOH-experiments, the selected amount of acid (14 g or 28 g, leading to a mass ratio between HCOOH and ASL_f of 1 or 2, respectively) was slowly added to the aqueous mixture before closing the reactor. The pH of the reactional mixture (as well as that in the final mixture after the experiment) was measured with a Thermo Orion Star A215 pH/conductivity benchtop multiparameter meter. It is to highlight that the initial pH of the reactional mixture decreased from 10.5 to around 3 with the addition of HCOOH, which indicates neutralization of the NaOH by HCOOH before heating.

Once the reactor was sealed, the air was evacuated using a vacuum pump and purged with pressurized N_2 (a common step in all experiments to check leakage and remove air). Moreover,

in the experiments using H_2 or CO_2, some further purges involving the pressurized reagent gas were required. After the purge step, the reactor was finally loaded with the selected pressure of H_2 or CO_2 (25 or 50 bar) just before starting the heating. The reactor temperature was raised to the specified temperature (250, 300 or 350 ºC) at a heating rate of 5 °C/min and held constant for one hour. The stirring was fixed at 1000 rpm throughout the experiment and during the reactor cooling. Once the experiment had finished, the reactor was quickly cooled by flowing tap water through the built-in cooling coil. The produced gas phase was collected in a gas bag and analyzed with a micro-gas chromatograph.

The aqueous liquid product was recovered from the reactor, and the reactor walls and stirrer were washed with methanol, filtering both liquids together under vacuum conditions (using a pre-weighed filter paper). Methanol was used as a washing solvent in order to ensure the recovery of the water-insoluble organic phase that remained stuck on the walls, stirrer and cooling coil. After filtration, the solid remaining in the filter was dried at 105 °C overnight and, once dried, weighted to determine the yield of insoluble solid (Y_{IS}) according to Equation 7.1. An aliquot of the filtered liquid was also dried at 105 °C (three replicates) to determine the yield of soluble solid (Y_{SS}, Equation 7.2). It should be noted that the distribution of the solid product into the soluble or insoluble fractions could be affected by the amount of methanol used in washing the reactor and the filtered solid, as methanol plays a co-solvent role and can enhance the dissolution of some water-insoluble compounds into the aqueous-methanol phase. Therefore, the amount of methanol used for washing was similar in all the experiments.

Although some volatile organics can be lost during drying, the organic compounds considered of interest as an antioxidant (mainly phenolics) have vapor pressures that are low enough to be hardly affected.

$$Y_{IS}\ (\text{wt.}\%) = \frac{W_{IS}}{W_{ASLf}} \cdot 100 \qquad \text{(Eq. 7.1)}$$

$$Y_{SS}\ (\text{wt.}\%) = \frac{X_{SS} \cdot W_{FL}}{W_{ASLf}} \cdot 100 \qquad \text{(Eq. 7.2)}$$

where W_{IS} is the weight of the insoluble filtered solid (g), W_{ASLf} is the weight of the dried lignin-rich fraction initially loaded in the rector (about 14 g), W_{FL} is the weight (g) of the total filtered liquid (aqueous reaction product + washing methanol) and X_{SS} is the content of soluble solid in this liquid (wt.%) (quantified by drying some aliquots of this filtered liquid).

A full factorial design 2^k with two factors and two levels was established for each reaction medium (H_2, CO_2 and HCOOH) to study the influence of the temperature (250 - 350 °C) and

the initial amount of reagent (0 - 50 bar of H_2 or CO_2 / 0 - 28 g of HCOOH) on the production and characteristics of the antioxidant additives. Three replicates in the central point of the factor levels (300 °C, 25 bar of H_2 or CO_2 / 14 g of HCOOH) were performed to evaluate the experimental error. In the end, a total of 17 runs were performed. Table 7.1 summarizes the experimental conditions tested (factors and levels).

Some experimental data such as the production of insoluble solid (Equation 7.1) and soluble solid (Equation 7.2) after ASL_f depolymerization, the C/H ratio in each solid, the additive yield (see section 7.3.5), the solubility of the additives in biodiesel (see section 7.3.6) and its performance as antioxidants additives for biodiesel (see section 7.3.8) were analyzed through analysis of variance (ANOVA) with a confidence level of 90 %, and the least significant difference was calculated. Hence, the significant effects of the factors, as well as their interactions, were highlighted.

Table 7.1. Experimental design planned for the depolymerization experiments.

Experiment#	Reaction medium	T (°C)	Initial gas (H_2/CO) pressure (bar) /HCOOH weight (g)
1	Inert atmosphere experiments	250	0
2		350	0
3	H_2 experiments	250	50
4		350	50
5		300	25
6		300	25
7		300	25
8	CO_2 experiments	250	50
9		350	50
10		300	25
11		300	25
12		300	25
13	HCOOH experiments	250	28
14		350	28
15		300	14
16		300	14
17		300	14

7.2.3. Additives preparation and characterization

An aliquot of the filtered liquid (about half of it) was extracted using twice the weight of isopropyl acetate (chosen as extracting solvent according to a previous study in which a large variety of solvents were evaluated (García et al., 2017)). The mixture was shaken for 10 min in a funnel and then left to decant at room temperature. The decanted aqueous phase was separated and discarded, while the organic phase (OP) was filtered using silicone-treated filter paper to remove the aqueous phase particles that remained in suspension. Three aliquots of OP (15 g

each) were dried during 48 h at 50 °C to determine the concentration of extracted compounds and from this value, the additive yield ($Y_{additive}$) was calculated according to Equation 7.3 (from now on, the dried OP will be referred as "additive" throughout this paper).

$$Y_{additive}\ (wt.\%) = \frac{X_{OP} \cdot W_{OP} \cdot W_{FL}}{W_{EL} \cdot W_{ASLf\ (ash\ free)}} \cdot 100 \quad \text{(Eq. 7.3)}$$

where X_{OP} is the concentration (wt. %) of the lignin-derived compounds in the OP, W_{OP} is the weight (g) of OP obtained after the extraction, and W_{EL} is the weight (g) of the aqueous liquid subjected to extraction and W_{FL} is the weight (g) of the total filtered liquid (aqueous reaction product + washing methanol). Here, W_{ASLf} is expressed on an ash-free basis involving only the organic fraction in the raw material.

For the chemical characterization, the additives were redissolved in methanol and analyzed by gas chromatography GC/MS/FID. The operating parameters are detailed in Appendix VI. For the calibration of the FID signal, 8 standards solutions, including the most abundant phenolic components in the samples (guaiacol, creosol, 2,4,6-trimethyl phenol, phenol, 4-ethylguaiacol, 2,5-dimethylphenol, p-creosol, eugenol, 4-ethylphenol, syringol, 3-methoxycatechol, 4-Allylsyringol, vanillin, apocynin, guaiacylacetone, catechol, homovanillyl alcohol and hydroquinone) were prepared using dichloromethane-methanol (1:1 vol.) as eluent. The concentration of each compound in the standard solutions ranged between 50 and 3000 µg/mL.

The structural composition of the additives was also investigated using a Fourier Transform Infrared spectrometer (Agilent Cary 630 FT-IR).

For further characterization, the molecular weight distribution of the additives, as well as their biodiesel-insoluble fractions, was measured by GPC following the same procedure detailed for the raw lignin.

To incorporate the additives into biodiesel, a portion of the OP extracted was evaporated in a rotary evaporator at 60 °C and vacuum conditions (10 mbar absolute pressure) to remove the solvent (isopropyl acetate). The remaining dried solid (i.e., the additive itself) was weighed, and the appropriate amount of neat biodiesel was added to the same flask in order to obtain an initial additive dosage of 1 wt.%. The detailed procedure is explained in section 5.2.4 in Chapter 5.

Figure 7.2 summarizes all the steps in the experimental procedure developed in this part of the work, from the initial stage of lignin extraction from AS to the last step of measurement of the oxidation stability of biodiesel after incorporating the antioxidant additives.

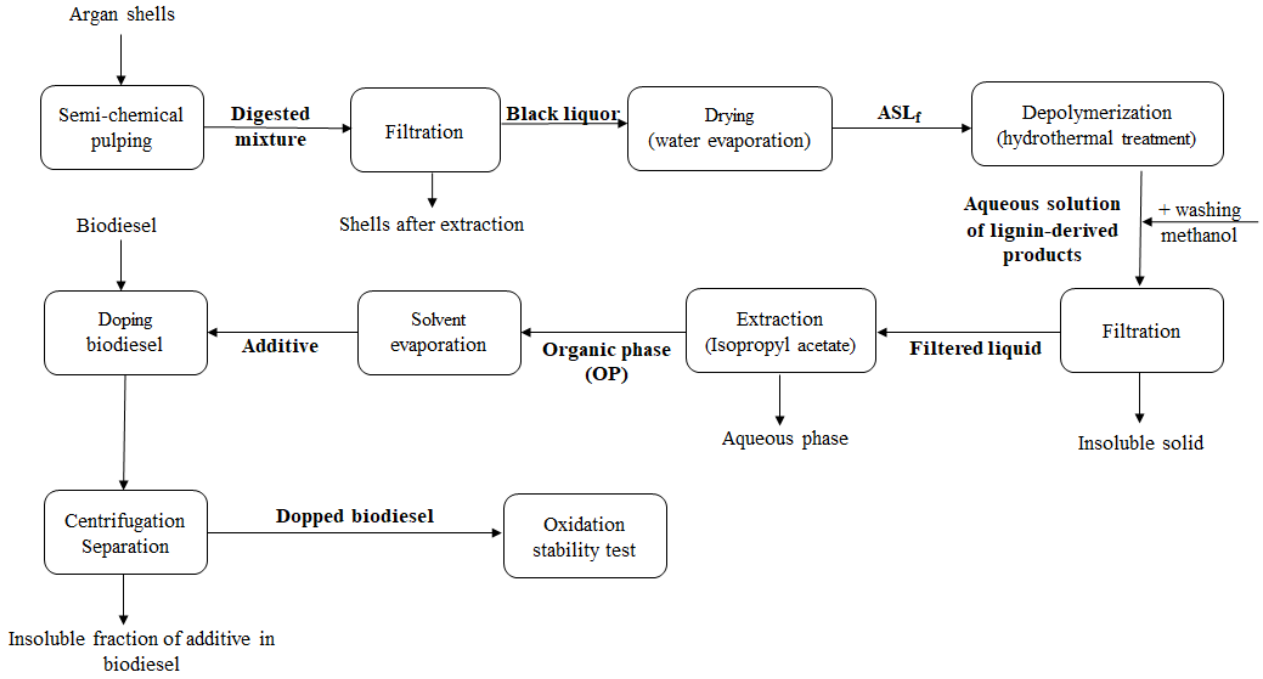

Figure 7.2. Experimental steps: lignin extraction, lignin depolymerization, additive preparation and mixture with biodiesel and oxidation stability tests.

7.3. Results and discussion

7.3.1. Characterization results of the lignin-rich fraction extracted from argan shells

The yield of the lignin fraction extracted from AS by semi-chemical pulping treatment was up to 22 % with respect to the initial lignin contained in the raw material (ash-free basis). As commented before, the content of acid-insoluble lignin in this extracted fraction was determined gravimetrically, accounting for 43 wt.% of the organic fraction in the solid. The ash content in ASL_f was much higher (up to 60 wt.%) than the initial ash content in AS (0.3 %). This high ash content could be explained by the presence of much of the NaOH used in the pulping treatment (Gillet et al., 2017; Lavoie et al., 2019), which, a priori, will benefit the subsequent depolymerization process, as NaOH could be considered a good base catalyst in the hydrothermal process (Otromke et al., 2019; Toledano et al., 2014). Table 7.2 exposes other characterization results of the extracted and dried ASL_f.

Table 7.2. Characterization of the lignin-rich fraction extracted from AS.

Parameter	Average value
Ultimate analysis (wt.%, ash-free basis)	
C	75.2 ± 0.1
H	7.78 ± 0.04
N	0.58 ± 0.02
S	<0.05
O[a]	16.4 ± 0.2
HHV (MJ/kg)	10.33 ± 0.04

[a] by difference.

Regarding the molecular weight distribution of ASL_f, Mw was found to be 37900 Da, Mn was 24200 Da and polydispersity was 1.6.

7.3.2. Product distribution in the hydrothermal treatment

During depolymerization, the ASL_f has been mainly converted to water-soluble and insoluble solid compounds (or liquids in the case of some specific soluble compounds). Only a minimal amount of gases was generated in the process. Mass balance (excluding the few produced gas) was closed fairly well (between 86 and 100.8 %). Regarding the produced gas, Figure 7.3 exposes the residual gas pressure in the reactor after cooling (at 20 °C). As shown, at the inert atmosphere reaction medium, only up to 0.4 bar of gas was generated after the experiment at 250 °C, a value that increased to 2 bar at 350 °C. In both cases, the gas product was essentially composed of CO_2 and traces of H_2. In the case of the H_2-experiments conducted at 350 and 300 °C, the amount of residual gas was lower than the initial pressure loaded in the reactor, which points to a net consumption of H_2 during the reaction. However, a slight increase in the total amount of gas was detected at 250 °C as a consequence of a higher CO_2 production, thus hiding the H_2 consumption. In the case of CO_2-experiments, residual gas (around 5 bar) was only generated when initially loading the highest pressure of CO_2 in the reactor (at both 250 and 350 °C). As expected, the composition of this residual gas was essentially CO_2 (between 90 and 98 vol.%). Lastly, a drastic increase in pressure was observed in HCOOH-experiments due to the formic acid decomposition into H_2, CO_2 and CO at this temperature range according to two possible pathways (R7.1 and R7.2) (Tedsree et al., 2011).

$$HCOOH \leftrightarrow CO_2 + H_2 \qquad \Delta G = -48.4 \text{ kJ mol}^{-1} \qquad \text{(R7.1)}$$

$$HCOOH \leftrightarrow CO + H_2O \qquad \Delta G = -28.5 \text{ kJ mol}^{-1} \qquad \text{(R7.2)}$$

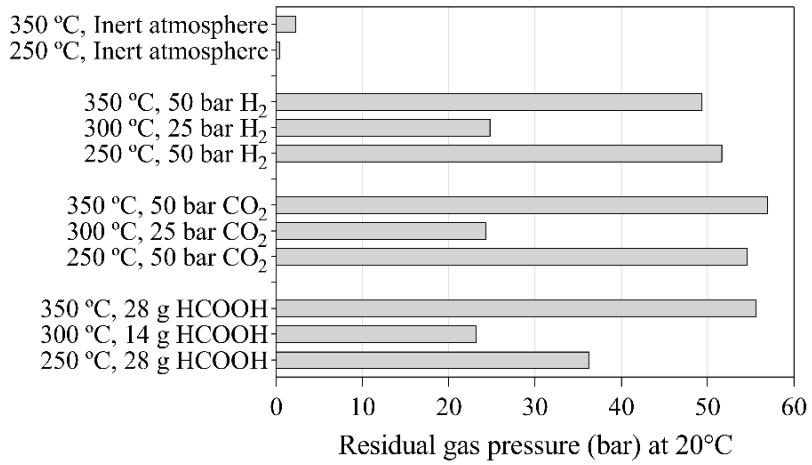

Figure 7.3. Residual gas pressure in the reactor (measured at 20 °C).

As regards other products formed in the hydrothermal treatment of ASL_f, the joint yield of soluble and insoluble solids ($Y_{SS}+Y_{IS}$), exposed in Figure 7.4, ranged between 88 % and 96 % in most experiments, except in some of those experiments carried out with HCOOH, in which this joint yield exceeded 100 %, reaching values even up to 110 %. Such high values could be due to the precipitation of sodium bicarbonate ($NaHCO_3$), which may be formed in the reaction between the dissociated CO_2 from HCOOH decomposition and Na^+ from NaOH present in the ASL_f.

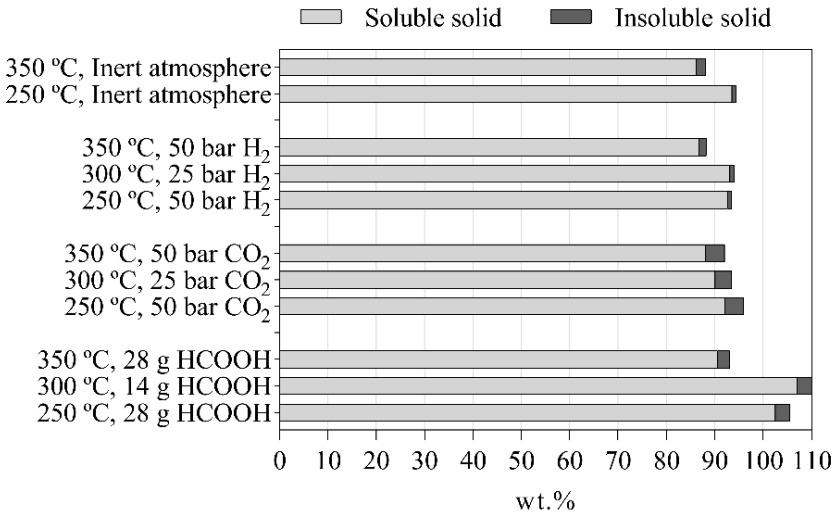

Figure 7.4. Joint yield of soluble and insoluble solids from depolymerization experiments ($Y_{SS}+Y_{IS}$).

Table 7.3 summarizes other important product distribution results and some of their characteristics. As shown, an alkaline reaction medium was maintained throughout the experiments in the cases of the initial inert atmosphere and H_2 medium, while in the case of CO_2-experiments, the pH of the reactional mixture was neutralized. However, different pH values were measured after the experiments in the case of HCOOH medium: 4.8, 6.3 and 7.6 at 250, 300 and 350 °C, respectively, which correlates with the decomposition extent of HCOOH.

A more detailed discussion about the effect of the temperature and the reaction medium on each response variable is included below.

Table 7.3. Product distribution, pH of the reactional mixture, C/H ratio in the solids and additive yield.

Reaction medium	T (°C)	Initial gas (H_2, CO) pressure (bar) / HCOOH weight (g)	pH		Y_{IS} (wt.%)	Y_{SS} (wt.%)	C/H ratio		$Y_{additive}$ (wt.%)
			before experiment	after experiment			C/H (IS)	C/H (SS)	
Inert atmosphere	250	0	10.5	9.9	0.86	93.58	9.2 ± 0.1	8.0 ± 0.6	6.42
	350	0	10.5	8.4	2.01	86.18	15.1 ± 0.1	9.1 ± 0.3	21.29
H_2	250	50	10.6	10.4	0.81	92.70	9.8 ± 0.1	7.6 ± 0.1	13.18
	350	50	10.5	10	1.38	86.88	12.9 ± 0.1	7.4 ± 0.4	20.50
	300	25	10.4	9.9	1.04	92.27	12.13 ± 0.04	7.5 ± 0.3	13.49
	300	25	10.3	10.1	0.80	95.17	12.3 ± 0.05	6.89 ± 0.02	19.13
	300	25	10.4	10.1	0.76	92.20	12.3 ± 0.2	7.9 ± 0.1	17.94
CO_2	250	50	10.4	7	3.90	92.10	13.4 ± 0.2	8.5 ± 0.1	18.48
	350	50	10.5	7.4	3.92	88.17	16.3 ± 0.6	9.4 ± 0.4	24.38
	300	25	10.7	7.3	3.26	89.24	16.0 ± 0.2	8.36 ± 0.01	14.49
	300	25	10.5	7.1	3.32	89.44	15.8 ± 1.4	9.3 ± 0.2	17.54
	300	25	10.6	6.9	3.58	91.78	16.1 ± 0.1	8.7 ± 0.3	17.09
HCOOH	250	28	2.8	4.8	2.98	102.60	10.4 ± 0.1	6.8 ±0.3	38.80
	350	28	2.8	7.6	2.46	90.63	10.6 ± 0.2	7.1 ± 0.2	28.08
	300	14	3.3	6.3	2.72	112.16	11.3 ± 0.5	4.6 ± 0.2	18.24
	300	14	3.1	6.4	3.36	109.96	10.9 ± 0.2	4.5 ± 0.1	24.11
	300	14	3	6.4	3.58	-	11.2 ± 0.1	5.828 ± 0.001	21.06

7.3.3. Insoluble solid

Among other results, Table 7.3 shows the yield of insoluble solid obtained under different operational conditions. To better interpret the results, Figure 7.5 plots the ANOVA statistical analysis of this response parameter (error bars correspond to the least significant difference at a confidence level of 90 %). Both the experimental data (denoted in the figures as filled symbols) and the theoretical values resulting from the one-way ANOVA (denoted in the figures as "Mean ANOVA value") have been included in the graphs, thus giving a first approach of the good or bad fitting of the models in the high and low levels of the experimental design. If the mean ANOVA value does not appear in a figure, it means that experimental and theoretical values are just the same.

As seen in Figure 7.5a, the depolymerization temperature showed a significant increasing effect on the production of insoluble solid when operating under an inert atmosphere or with H_2 as a reaction medium. According to other studies in the literature, this increase in the insoluble solid yield was interpreted by the condensation or repolymerization reactions that could occur at temperatures higher than 300 °C (Huang et al., 2014; Long et al., 2014; Yuan et al., 2010). The repolymerization/condensation reaction has been reported by several studies and explicated as the reaction between unstable lignin fragments and original lignin (James E. Miller et al., 2002; Toledano et al., 2012). According to Li et al. (Li et al., 2007), the key point of these reactions is the carbenium ion generated at the α-carbon atom. After the ether bond cleavage, this ion can be attacked by an adjacent aromatic ring forming a stable carbon-carbon bond that increases the molecular weight (Erdocia et al., 2014; Toledano et al., 2012) and could change the molecular structure. On the other hand, the presence of H_2 only significantly impacted the insoluble solid yield at the highest temperature, while hydrogenation did not occur efficiently to prevent repolymerization/condensation reactions at a temperature of 250 °C (Figure 7.5a). According to other studies in the literature, other H-donating reaction media (such as alcohols) have been proven to reduce char formation (Gosselink et al., 2012; Kleinert and Barth, 2008). However, this effect was not observed in the present work when using HCOOH, which can also be considered an H-donor. In fact, the opposite effect was even observed, as the production of insoluble solid was augmented in comparison with the inert atmosphere results (Figure 7.5b). The same trend was observed in the case of CO_2-experiments (Figure 7.5c), as the presence of CO_2 had a remarkable effect on increasing the insoluble solid yield, which was maintained stable at around 4 % throughout the entire temperature range (and P_{CO2} = 50 bar). A significant interaction between both factors has been observed: the temperature showed a

positive effect on the production of insoluble yield in the absence of CO_2, while that effect disappeared by initially feeding CO_2 or HCOOH. Therefore, acidification of the reaction medium by adding either HCOOH or CO_2 played a key role in producing a water-insoluble solid.

In short, the most unfavorable operating conditions for generating such insoluble solid, which is an undesirable by-product of the process, involve high amounts of CO_2 in the reaction medium. To minimize its production, the optimal working conditions would be the most moderate reaction temperature (250 °C) and either inert or H_2 atmospheres (Y_{IS} of around 0.8 wt.%).

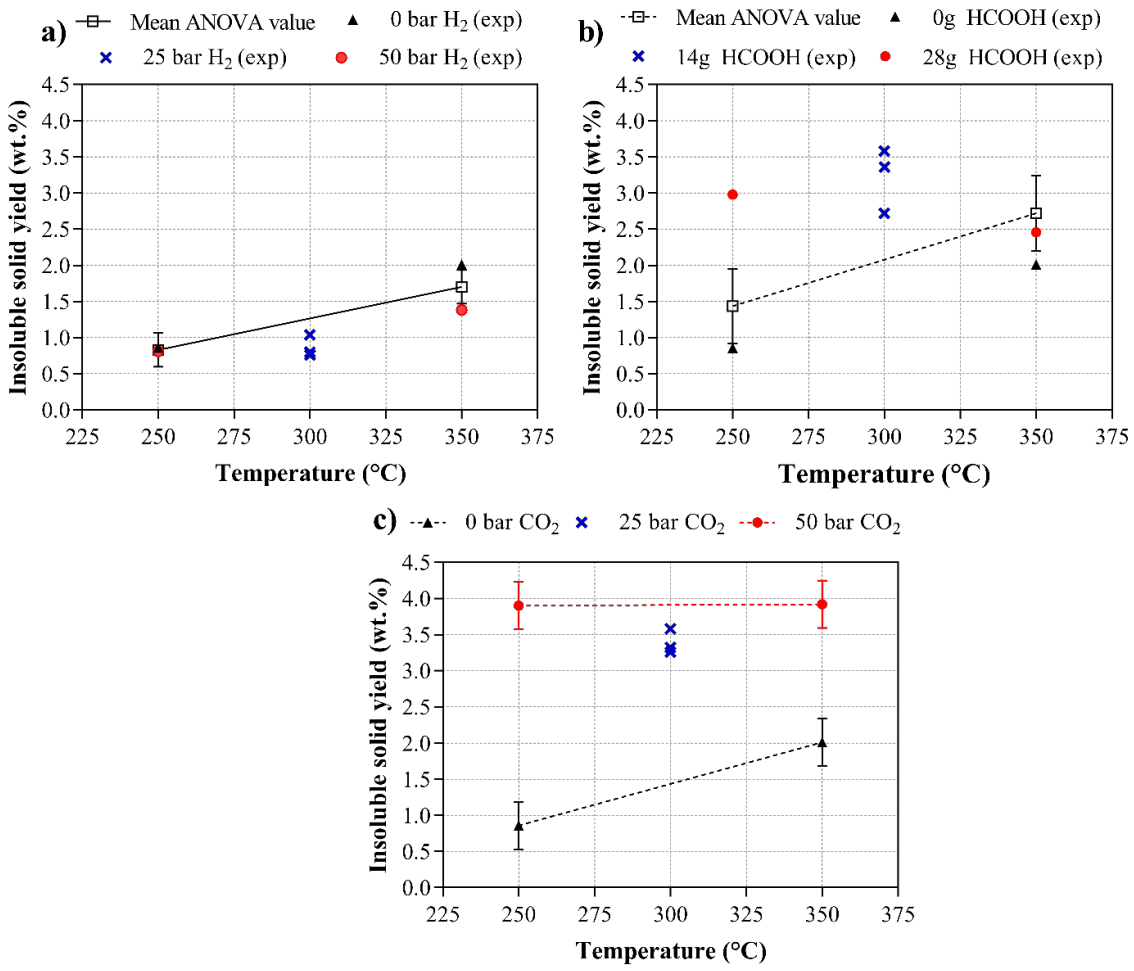

Figure 7.5. Effect of the temperature and the reaction medium on the production of insoluble solid during lignin depolymerization: (a) H_2-experiments, (b) HCOOH-experiments, (c) CO_2-experiments.

The C/H ratio in both the insoluble and the soluble solids was calculated using the elemental analysis data summarized in Appendix VI. The ANOVA analysis of this parameter is exposed in Figure 7.6. The temperature, the reaction medium and the interaction between them had a significant effect on this C/H ratio. The presence of CO_2 positively affected the C/H ratio in the entire temperature interval, while the presence of H_2 or HCCOH contributed to an increase in the fraction of H in the solid formed at the highest temperature (the C/H ratio was reduced).

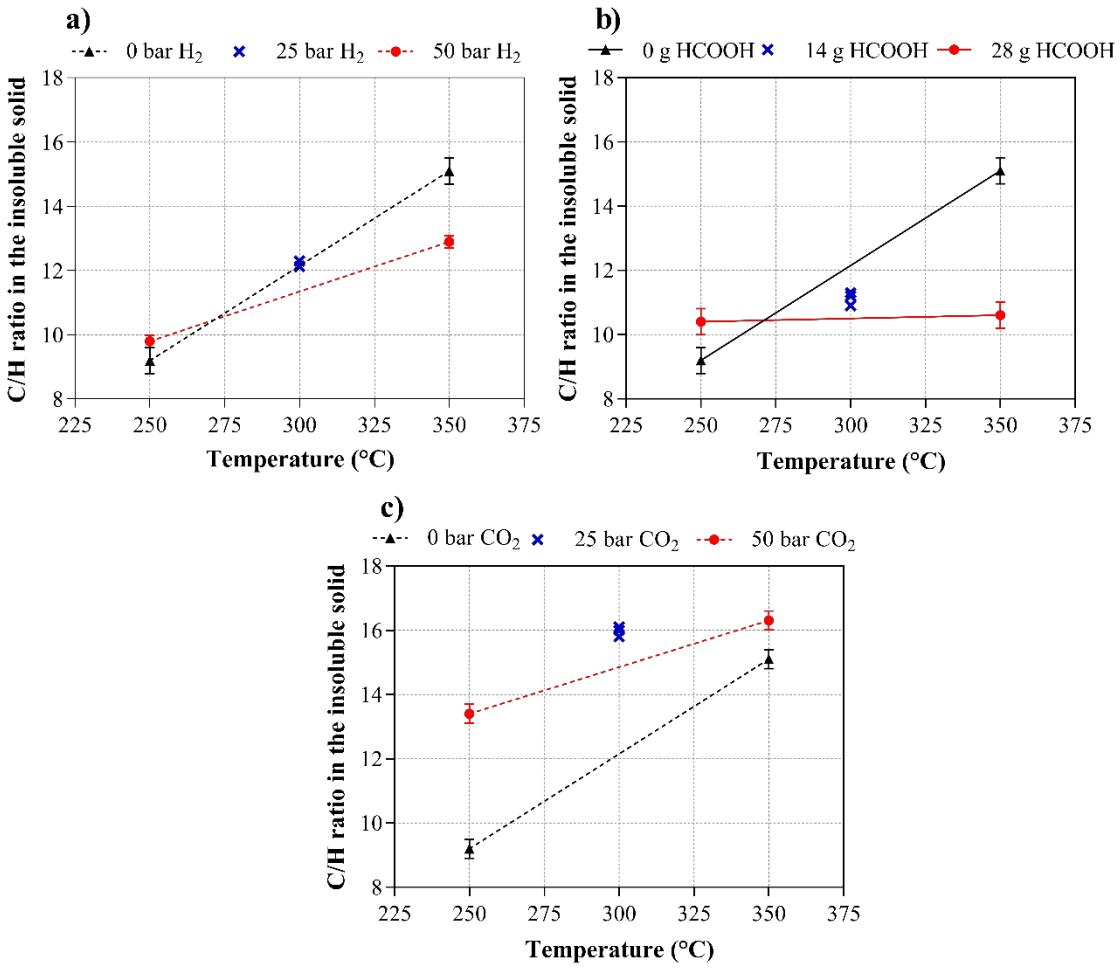

Figure 7.6. Effect of the temperature and the reaction medium on the C/H ratio of the insoluble solid product: (a) H_2-experiments, (b) HCOOH-experiments, (c) CO_2-experiments.

7.3.4. Soluble solid

Figure 7.7 exposes the ANOVA of the results obtained for the yield of soluble solids produced under the different reaction media and temperatures (Table 7.3). The temperature increase led to a significant reduction in the soluble solid yield regardless of the reaction media.

Changing the reaction media did not affect the soluble solid yield. In the case of H_2-experiments and HCOOH-experiments, data did not fit a linear model (significant curvature), which may be related to the temperature profile, as the amount of reagent present in the reaction medium was found to have a non-significant effect.

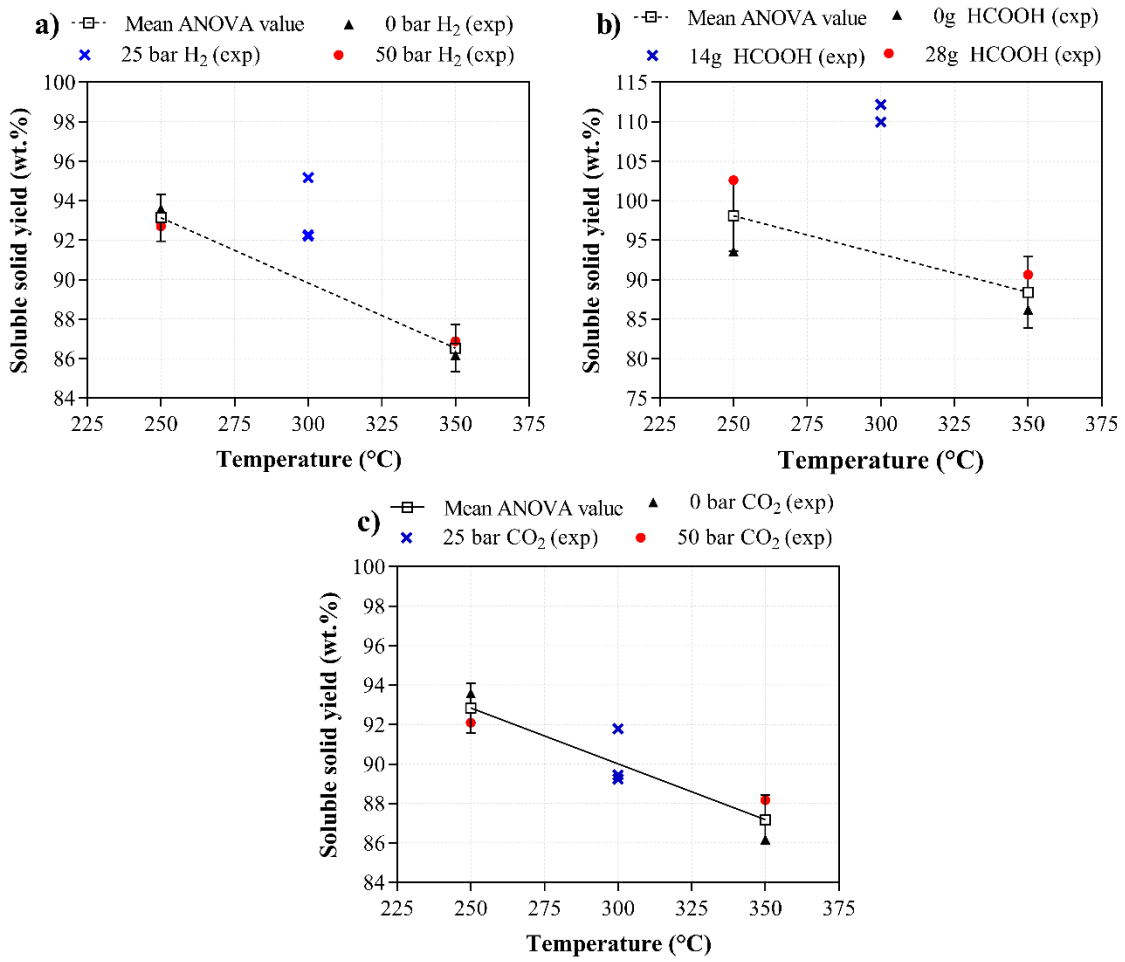

Figure 7.7. Effect of the temperature and the reaction medium on the production of soluble solid during lignin depolymerization: (a) H_2-experiments, (b) HCOOH-experiments, (c) CO_2-experiments.

Figure 7.8 exposes the ANOVA analysis of the C/H ratio in the soluble solid. The increase of temperature under inert atmosphere led to an increase in the C/H ratio of the soluble solid (Figure 7.8). This ratio was not affected by changing the reaction medium by CO_2 (Figure 7.8c). However, the presence of H_2 or HCOOH reduced the C/H ratio in the soluble solid, especially at the highest temperature (Figures 7.8a and 7.8b); the temperature effect disappeared at both

reaction media, although data showed a non-linear model (with significant curvature) and a clear minimum in the C/H ratio was found when operating at 300 °C and with 14 g of HCOOH.

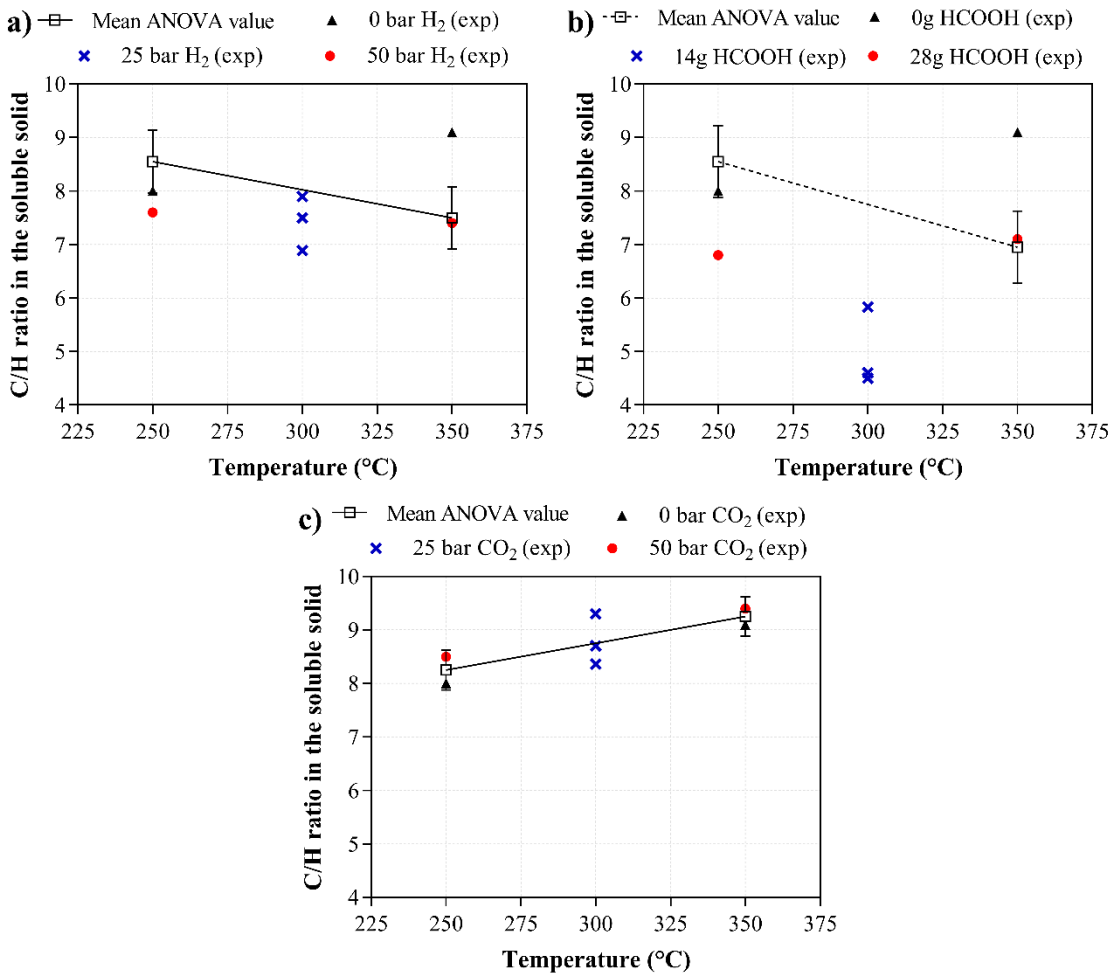

Figure 7.8. Effect of the temperature and the reaction medium on the C/H ratio of the soluble solid product: (a) H_2-experiments, (b) HCOOH-experiments, (c) CO_2-experiments.

7.3.5. Additive yield

Table 7.3 reports the yields of the produced additives under different experimental conditions. The ANOVA of the results (Figure 7.9) shows that both the temperature and the reaction medium significantly affected the additive yield. The temperature showed a clear positive effect in the case of the inert atmosphere, H_2-experiments and CO_2-experiments, while it showed a negative effect in the case of HCOOH-experiments (with a linear trend in all cases). Regarding the influence of each reaction medium, H_2 presence did not significantly affect the additive production yield with respect to the inert medium. In contrast, the presence of CO_2 was

favorable for the additive production; more additive was extracted as more CO_2 was initially fed into the reactor. The same occurred in the case of HCOOH-experiments, although this drastic positive effect was only reported at the lowest temperature (250 °C), as the interaction between both factors was found to be significant at this reaction medium. The use of HCOOH was the most favorable reagent from the point of view of maximizing the additive production, especially when operating at 250 °C and with an initial dosage of 28 g of HCOOH (HCOOH/ASL_f mass ratio of 2), which led to a maximum additive yield of around 39 wt.%.

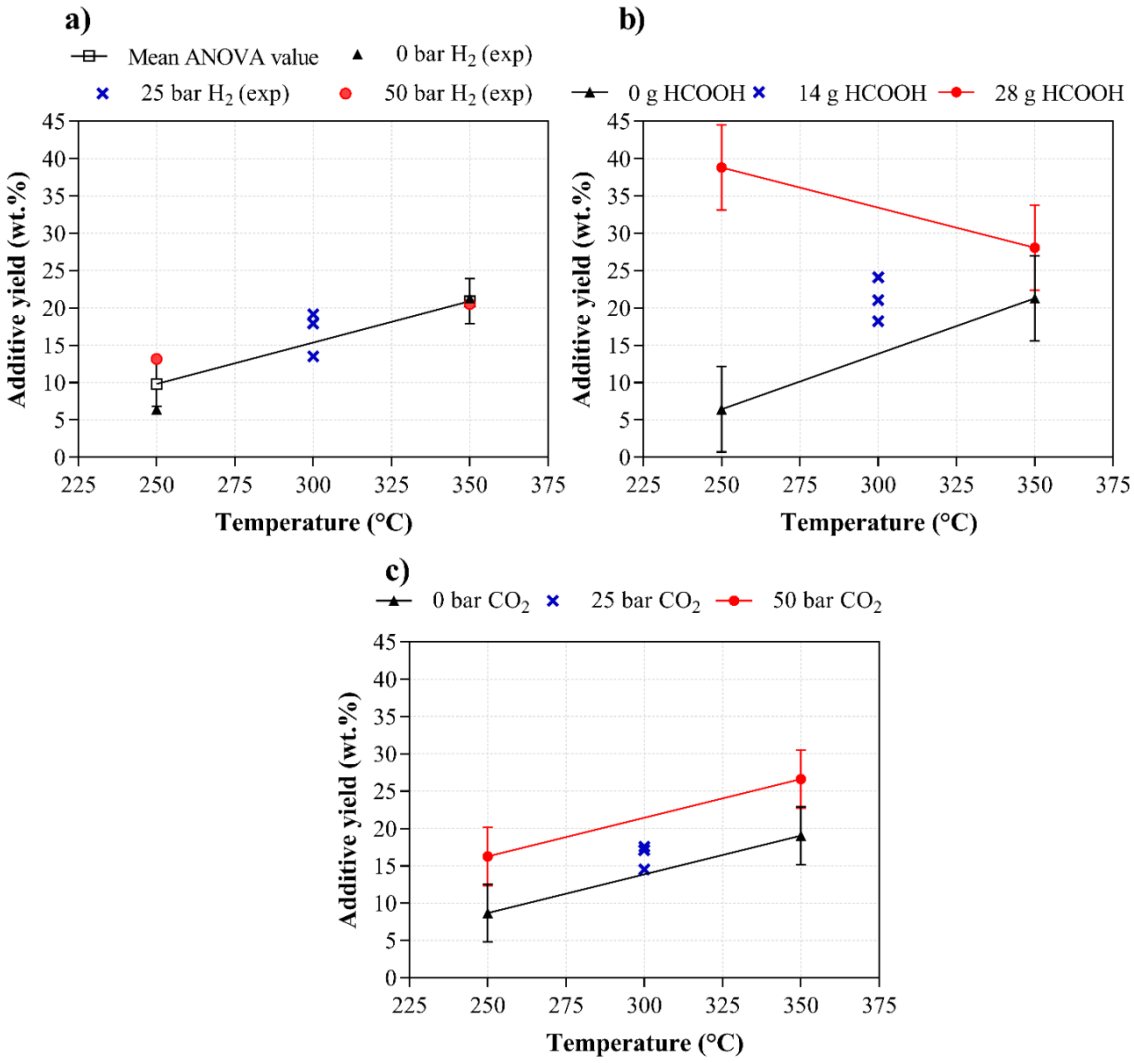

Figure 7.9. Effect of the temperature and the reaction medium on the production of additive: (a) H_2-experiments, (b) HCOOH-experiments, (c) CO_2-experiments.

7.3.6. Additive solubility in biodiesel

As mentioned previously, the real dosage of the soluble additive was determined after centrifugation and separation of the insoluble fraction (Equation 5.3).

Figure 7.10 shows the effect of both the temperature and the amount of reagent used in the depolymerization experiments on the additive solubility in biodiesel. As shown, at the lowest temperature (250 °C), the presence of H_2 (50 bar initially) led to a much less soluble additive than that obtained when operating with an inert atmosphere. This difference in the solubility of both additives was considerably reduced at 350 °C. Moreover, the solubility of the additives produced under an inert atmosphere was decreased with temperature, while it improved under H_2-medium (a significant interaction between both factors was observed). The same trend was observed for the solubility of the additives obtained under HCOOH-medium, although these data were noticeably better than those obtained for H_2-medium. The most soluble additive (actual additive dosage incorporated into biodiesel of 0.8 wt.%) was obtained under HCOOH-medium at 350 °C. The solubility of the additive was not affected by changing the inert medium by CO_2 at 350 °C, while similarly to H_2-experiments and HCOOH-experiments, at 250 °C the presence of CO_2 led to less soluble additive than obtained at inert atmosphere

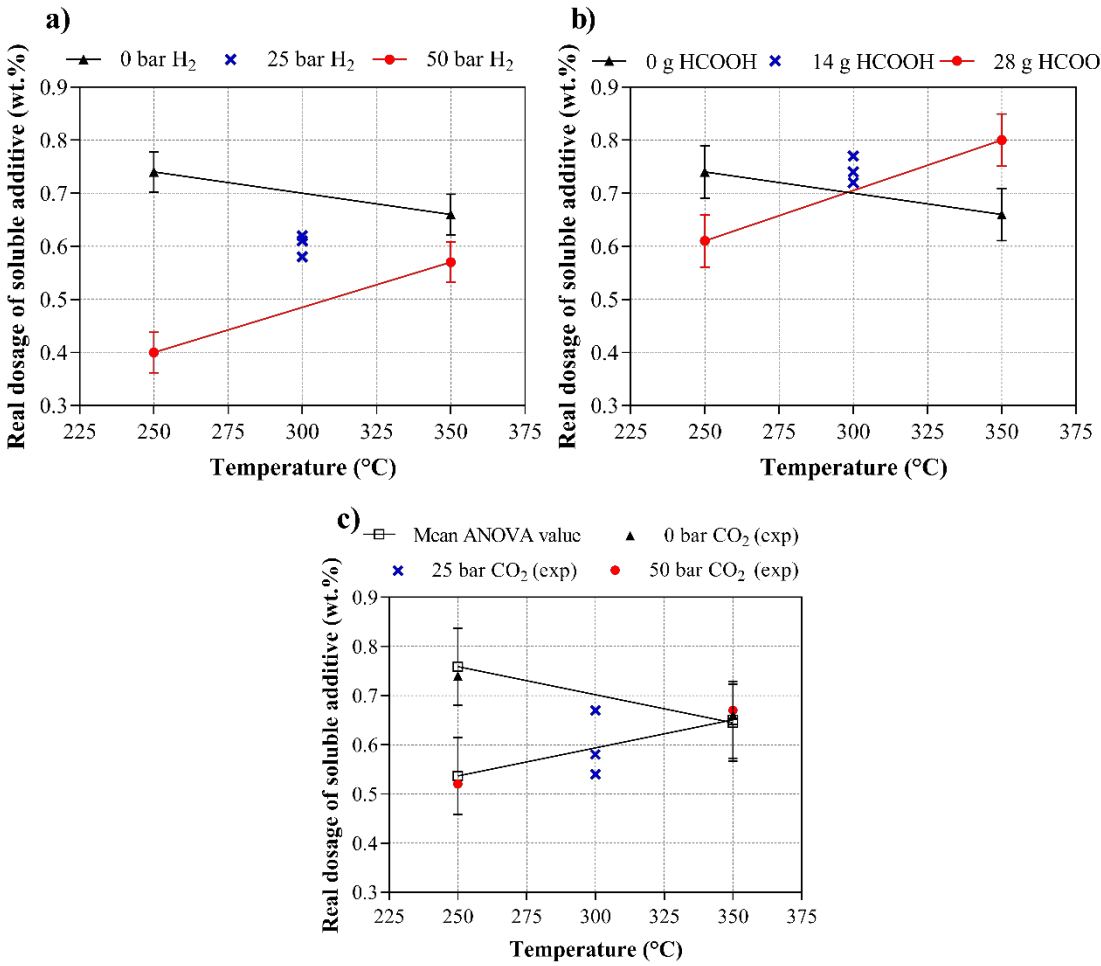

Figure 7.10. Effect of the temperature and the reaction medium on the additive solubility in biodiesel (wt.%). (a) H_2-experiments, (b) HCOOH-experiments.

7.3.7. Additives characterization

7.3.7.1. GC/MS/FID analysis of the additives

The GC/MS/FID analysis revealed the presence of a wide variety of monomeric phenolic compounds, as well as acetic acid, aldehydes and furans. Table 7.4 exposes the concentration of the monomeric phenolic compounds expressed as mg per g of additive. Some of the major phenolic compounds identified were phenol, guaiacol, syringol and catechol, as well as their alkyl and methoxy-substituted derivates. Catechol was identified as the predominant compound at 300 °C regardless of the reaction medium, while syringol was the main phenolic product at 250 °C, especially when using an inert medium. In general (except for the HCOOH medium), the increase in the depolymerization temperature led to a reduction in the concentration of syringol and guaiacol, while catechol and catechol derivatives increased their concentrations.

However, when using HCOOH as a reaction medium, only traces of guaiacol were detected in the additive produced at 250 °C, which increased proportionally with temperature, while no apparent effect of the temperature was detected on the syringol concentration. In this reaction medium (HCOOH), a wider variety of phenolic monomers was observed, especially at high temperatures. In addition to catechol and catechol derivatives, the presence of other monomers such as hydroquinone, 4-hydroxybenzeneethanol, 4-hydroxy-3-methoxybenzeneethanol and homovanillyl alcohol has been found at a level comparable to guaiacol or syringol.

According to several studies in the literature (James E. Miller et al., 2002; Toledano et al., 2012; Toledano Zabaleta, 2012), at severe conditions of temperature (at least 300 °C) and in the presence of base catalysts, both guaiacol and syringol directly coming from lignin fragmentation are intermediate products that could undergo demethylation, demethoxylation or dealkylation reactions to produce advantageous products such as phenol, catechol, catechol derivatives and creosol. This finding is in agreement with the observations found in this work for inert, H_2 and CO_2 atmospheres, as ASL_f contains an important amount of NaOH used for the extraction of lignin from AS. Trends were not so clear for the HCOOH medium, which could be due to the acidic character of this reactional mixture.

It should be stressed that the GC/MS/FID analysis allowed identifying and quantifying around 47 % of the organic mass of the additive produced in the case of the inert atmosphere at 250 °C, a value that dropped to only 5 % at 350 °C. The identified and quantified fraction in the additives obtained in the H_2-experiments dropped from 20 % at 250 °C to 10 % at higher temperatures and did not exceed 10 % in the remaining cases. The identified fraction of additives was constituted of phenolic compounds (Table 7.4) and no phenolic compounds such as hexadecanoic acid methyl ester, acetic acid and cyclopentenone derivatives.

The most important part of the GC/FID unquantified components could be related to undetectable phenolic dimers, trimers and oligomers with mass-to-charge index (m/z) higher than 500, also including repolymerized fractions of lignin with a very high molecular weight. For further characterization, the molecular weight distribution of the additives was analyzed (section 7.3.7.3).

Table 7.4. Concentration of monomeric phenolic compounds in the additives obtained from lignin depolymerization.

	Concentration in the additives (mg/g)																
	Inert atmosphere experiments		H_2 experiments					CO_2 experiments					HCOOH experiments				
Compound	250°C	350°C	250 °C, 50 bar	350 °C, 50 bar	300 °C, 25 bar			250 °C, 50 bar	350 °C, 50 bar	300 °C, 25 bar			250 °C, 28 g	350 °C, 28 g	300 °C, 14 g		
Guaiacol	18	1	24	1	2	3	3	8	0.3	11	4	2	0.2	6	1	1	3
2,6-dimethylphenol	-	-	0.5	1	0.5	0.3	0.5	-	-	-	-	-	0.1	0.4	0.3	-	-
Creosol	2	0.3	2	-	1	1	1	0.3	0.2	3	1	1	0.1	1	0.5	0.4	1
1,2,3-Trimethoxybenzene	2	0.1	2	-	-	-	0.2	0.3	0.2	-	-	-	0.3	-	-	-	-
2,4,6-trimethylphenol	-	-	-	0.5	-	-	-	-	0.1	-	-	-	0.2	0.2	0.5	-	-
Phenol	2	0.4	3	6	1	1	2	1	1	5	1	1	1	3	1	0.5	1
4-ethylguaiacol	2	0.1	2	-	0.4	0.5	0.4	1	0.03	2	1	0.3	-	2	1	1	2
3-ethylphenol	-	1	-	0.5	-	-	-	-	0.1	-	-	-	-	-	-	-	-
p-Cresol	-	3	-	3	0.2	0.4	0.3	-	1	1	0.3	0.1	1	0.4	-	0.1	0.3
2-methoxy-4-propylphenol	-	-	-	-	-	-	-	0.2	-	1	-	0.3	0.3	2	1	1	1
4-ethylphenol	-	-	0.2	1	0.5	0.4	0.3	0.1	0.5	1	-	0.2	1	1	0.2	0.2	0.4
3,4-dimethylphenol	-	-	-	0.5	-	-	-	0.2	1	1	1	0.2	0.3	-	-	-	-
Syringol	148	0.2	71	0.4	1	1	1	27	-	3	2	1	5	3	6	4	9
3,5-Dimethoxy-4-hydroxytoluene	39	0.1	20	-	0.5	0.3	0.4	2	-	1	1	1	-	1	0.5	0.3	1
1,2,3-trimethoxy-5-methylbenzene	16	0.4	8	-	0.3	1	0.2	3	-	1	0.5	0.2	-	4	-	-	-
m-Guaiacol	1	1	0.4	-	-	0.3	-	0.1	0.3	-	-	-	-	-	-	-	-
2-Allyl-4-methylphenol	-	-	-	-	-	-	-	-	-	-	-	-	0.3	-	-	-	-
Vanillin	4	-	1	1	0.5	-	1	0.3	0.4	-	0.5	0.2	-	-	-	-	-
4-butyl-1,2-dimethoxybenzene	4	-	2	1	0.3	0.3	-	1	1	-	-	-	0.5	-	-	-	-
Apocynin	8	-	4	-	2	1	2	1	-	1	2	0.6	-	0.5	-	-	-
Guaiacylacetone	8	0.5	5	-	-	-	-	4	0.4	-	1	0.4	-	15	2	1.2	-
Catechol	35	-	18	30	51	64	36	16	-	54	32	19	-	11	15	12	24
3-methylcatechol	-	-	-	-	6	-	13	-	-	12	9	-	3	-	-	-	13
Homovanillyl alcohol	2	0.2	-	-	-	-	-	1	-	-	-	-	-	9	5	3	4
4-Ethylcatechol	-	-	-	-	-	-	-	-	-	-	-	-	-	-	4	3	6
4-hydroxy-3-methoxy benzenepropanol	-	-	9	1	1	0.5	0.3	5	-	1	2	1	-	4	3	2	3
4-hydroxy benzeneethanol	-	-	-	-	-	-	-	-	-	-	-	-	0.3	1	4	3	3
Desaspidinol	4	-	3	-	-	-	-	1	-	-	1	1	-	4	-	-	-
Hydroquinone	-	-	-	-	-	-	-	-	-	1	1	0.2	-	2	5	3	6

7.3.7.2. FT-IR analysis of the additives

FT-IR spectra of the produced additives, as well as that of ASL_f, are represented in Figure 7.11. In general, the spectra show some significant differences according to the reaction medium and the lignin processing temperature. The peak intensity corresponding to the hydroxyl group (at wavenumbers in the range of 3600 - 3100 cm^{-1}) was not strongly affected by the medium and/or the temperature, but it was slightly more pronounced in the case of CO_2 and HCOOH medium. Peaks corresponding to alkyl groups (wavenumber between 3000 and 2900 cm^{-1}) appeared in the spectra of the additives produced at the lowest temperatures but almost completely disappeared in the additives obtained at 350 °C regardless of the reaction medium. No peaks were detected throughout the interval 3600 - 2900 cm^{-1} in the spectra of the original ASL_f. On the other hand, the two clear peaks observed in the original raw material at wavenumbers in the range of 1700 - 400 cm^{-1} have undergone several changes compared with the spectra of the additives obtained at 250 °C. Some of these peaks were reduced or disappeared, while others appeared when increasing the depolymerization temperature up to 300 °C, indicating the ASL_f depolymerization by the cleavage of many functional groups and restructuration into other bonds. At 350 °C, the spectra of all the additives became similar to char and activated carbons plots with fewer peaks representing functional groups, which could indicate the condensation of phenolic compounds forming a residual or repolymerized lignin at this severe treatment temperature. It is to note that, in the additives produced at 250 and 300 °C (regardless of the reaction medium), an important peak appeared at wavenumbers around 1300 - 1150 cm^{-1}, with a significant shoulder at 1250 cm^{-1}. The peaks at these wavenumbers are usually attributed to aromatic links and tertiary/secondary alcohols, which could be explained by the presence of catechol, alkyls catechol, syringol, guaiacol and hydroquinone in the additives prepared at 300 °C (Table 7.4). The peak intensity observed in the spectra of ASL_f at a wavenumber of around 1400 cm^{-1} (corresponding to O-CH_3 links) started to decrease in the additives prepared at 250 °C in the presence of H_2 and CO_2, and almost completely disappeared at 300 °C. According to Li et al. (Li et al., 2007), the linkages β-O-4 are the first to be cleaved during the hydrothermal treatment. This peak reappeared again in the additives produced at 350 °C under CO_2 medium and inert atmosphere, which might be due to repolymerization reactions involving linkages between phenolic rings, similar to those present in the original feedstock. No peaks were detected at this wavenumber (1400cm^{-1}) in the

additives produced at the highest temperature in the presence of HCOOH and H_2, which seems to indicate that these H-donating reaction media led to other types of products.

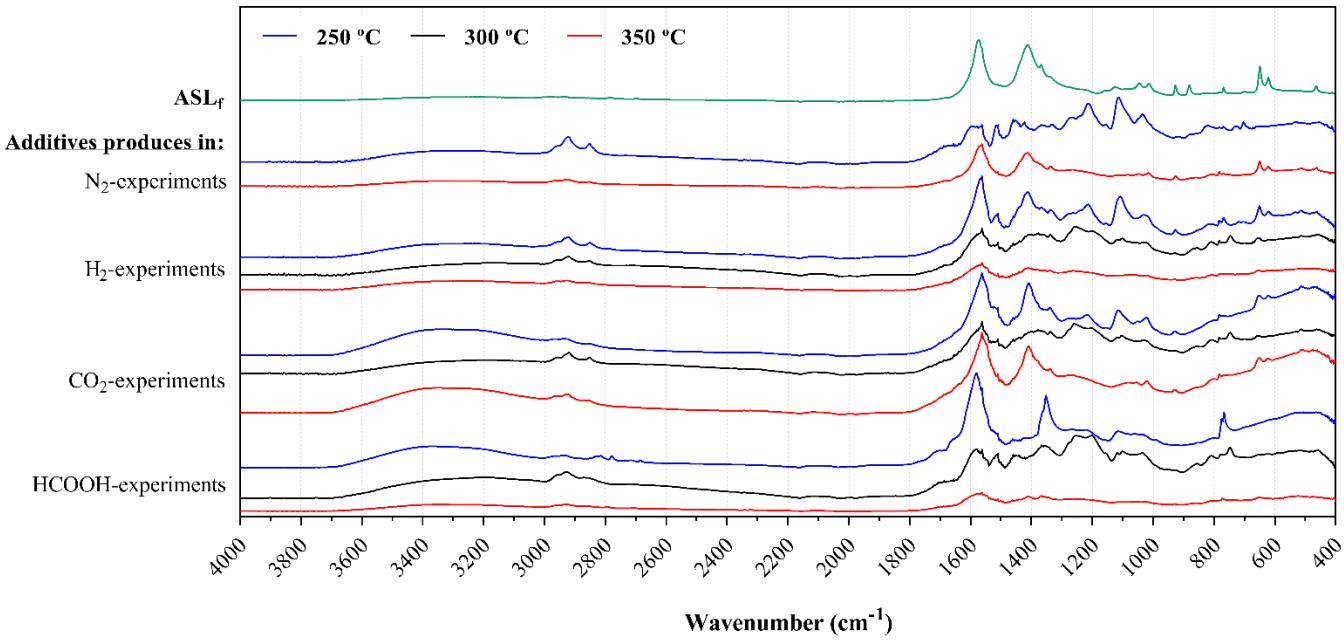

Figure 7.11. FT-IR spectra of the additives prepared after ASL_f depolymerization.

7.3.7.3. Molecular weight distribution of the additives

The GPC chromatograms of the entire additives and the insoluble fractions remaining after blending with biodiesel are reported in Figure 7.12. Table 7.5 summarizes final results, such as the number-average molecular weight (Mn), weight-average molecular weight (Mw) and polydispersity (Mw/Mn) of the analyzed samples. As exposed in Figure 7.12, up to four different peaks (or shoulders) were observed for the additives. The peaks eluted at lower retention times could be related to a part of unconverted lignin, higher molecular weight fragments of lignin as well as repolymerized lignin, while the peaks observed at higher retention time (from 21 min) are associated to lower molecular weight (<1400 Da), thus meaning that depolymerization reaction had occurred to a greater or lesser extent (Toledano et al., 2012). It is to note the significant increase in the first peak eluted at a retention time of around 17 min in the additives produced at 300 °C regardless of the reaction atmosphere, which indicates a higher molecular weight compared with those obtained at 250 and 350 °C. This tendency was also observed in the biodiesel insoluble fraction. Comparing the GPC plots of the entire additives and their respective insoluble fractions in biodiesel highlights a noticeable

decrease in the intensities of the peaks at retention times of 18.5, 20.2 and 21.48, which is related to the fraction of the additive that was mainly dissolved in biodiesel.

Concerning the average data of Mn and Mw, higher values were obtained for either the entire additive or the biodiesel insoluble fraction, depending on the depolymerization operating conditions. Moreover, it is to note that incorporating H_2, CO_2 or HCOOH into the reaction medium had a noticeable effect on increasing the molecular weight of the additives, especially at 250 °C.

Table 7.5. Molecular weight (Mn, Mw, Mw/Mn) of the whole additives and of their insoluble fractions in biodiesel.

			Additives			**Insoluble fraction of the additives in biodiesel**		
	T (°C)	Initial gas pressure (bar) / HCOOH weight (g)	Mn (Da)	Mw (Da)	Mw/Mn	Mn (Da)	Mw (Da)	Mw/Mn
Inert atmosphere Experiments	250	0	6700	13000	1.9	10600	16800	1.6
	350	0	8200	15900	2.0	10700	18600	1.8
H_2 Experiments	250	50	10000	18900	1.9	11800	18500	1.6
	350	50	9200	18400	2.0	9200	15900	1.7
	300	25	13200	22000	1.7	15600	23600	1.5
CO_2 Experiments	250	50	12600	24700	2.0	9800	14600	1.5
	350	50	8100	16300	2.0	9300	15400	1.6
	300	25	15200	27300	1.8	14200	20700	1.4
HCOOH Experiments	250	28	10000	16400	1.6	12600	17800	1.4
	350	28	9300	15100	1.6	10800	18700	1.7
	300	14	12000	19600	1.6	14600	20600	1.4

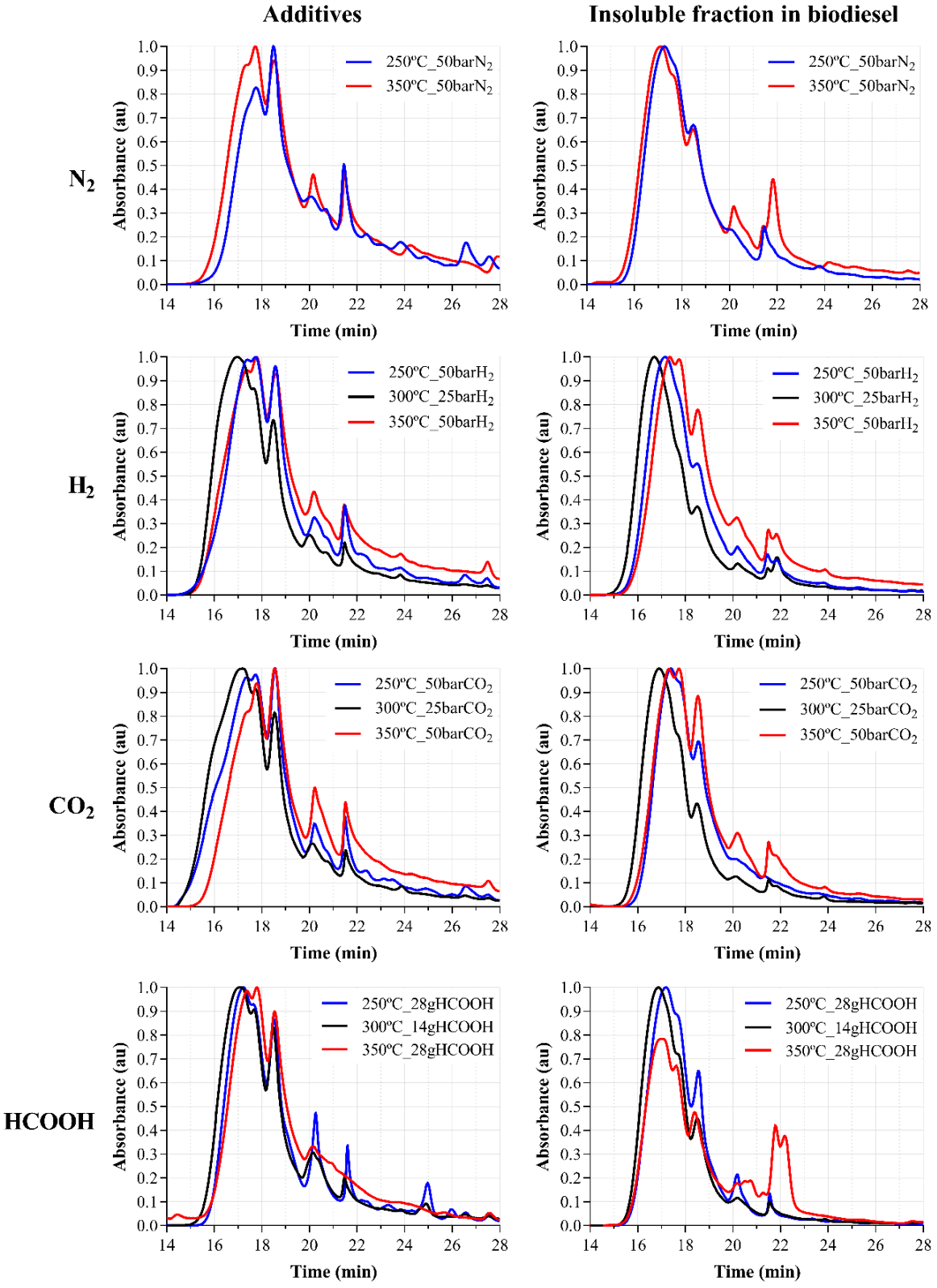

Figure 7.12. Molecular weight distribution (GPC plots) of the additives and their biodiesel insoluble fractions.

7.3.8. Oxidation stability of biodiesel

Figure 7.13 shows a comparison of all the results of biodiesel oxidation stability time (PetroOXY tests). The average oxidation stability time (OXY) of neat biodiesel was 14.8 ± 1.1 min. As a general result, doping biodiesel with AS lignin-based additives has been demonstrated to achieve an excellent improvement in the OXY time. The temperature of 300 °C is clearly the optimal temperature for producing the most active additives. In fact, only slight differences were observed due to the reaction medium for ASL_f depolymerization at this temperature, while the performance of the additives obtained at 250 and 350 °C was more affected by the reaction medium.

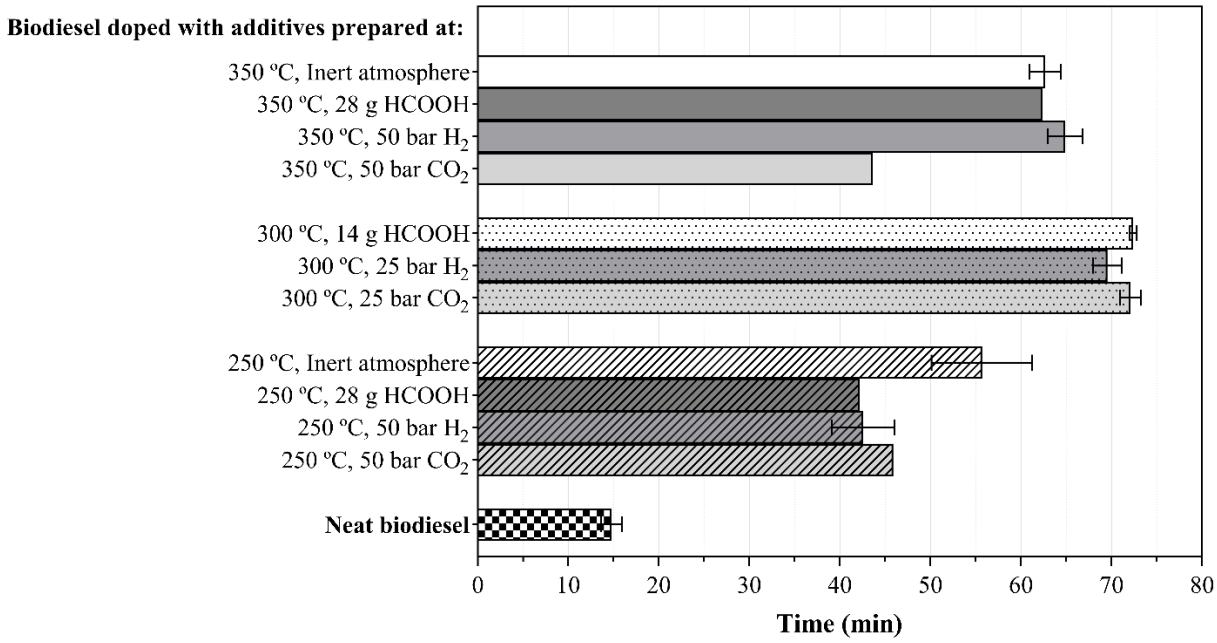

Figure 7.13. Oxidation stability times of neat and doped biodiesels.

The ANOVA performed to the results of oxidation improvement rate, ΔOXY, (Figure 7.14) indicates that both the temperature and the reaction medium, as well as the interaction between them, were significant terms in the analysis. The increase in the reaction temperature from 250 to 350 °C had a positive impact on the biodiesel oxidation stability achieved with the additives prepared under inert atmosphere and under H_2 or HCOOH media, but not in the presence of CO_2 (similar results for both temperatures). However, experimental data did not fit linear models, but a strong curvature was detected at 300 °C regardless of the nature of the reagent incorporated (quadratic effect of temperature). On the other hand, it should be noted that introducing H_2 or HCOOH in the

process was not advantageous for the antioxidant performance of the additives, as no substantial differences were found at the highest temperature (ΔOXY ranged between 323 % and 340 % for the three reaction media at 350 °C) or even a negative effect was observed at the lowest temperature (250 °C) when comparing their data with those reported for inert atmosphere.

These results seem to be connected with the observed decrease in the additive solubility in biodiesel, which dropped from an actual soluble dosage of 0.74 wt.% for the additive produced at 250 °C under inert atmosphere to 0.4 wt.% and 0.61 wt.% for the additives produced under H_2 and HCOOH media, respectively. On the other hand, adding 50 bar of CO_2 to the reaction medium led to additives that achieved lower ΔOXY than those obtained in the N_2 inert atmosphere. Concretely, the improvement of oxidation stability decreased dramatically from 334 % (for additive obtained in N_2 atmosphere at 350 °C) to 196 % (for additive produced at 350 °C and 50 bar of CO_2). In summary, the most favorable operating conditions from the point of view of maximizing the improvement of biodiesel oxidation stability were those corresponding to the central points of the experimental design: 391 % (300 °C and 28 g HCOOH), 389 % (300 °C and 25 bar CO_2) and 371 % (300 °C and 25 bar H_2).

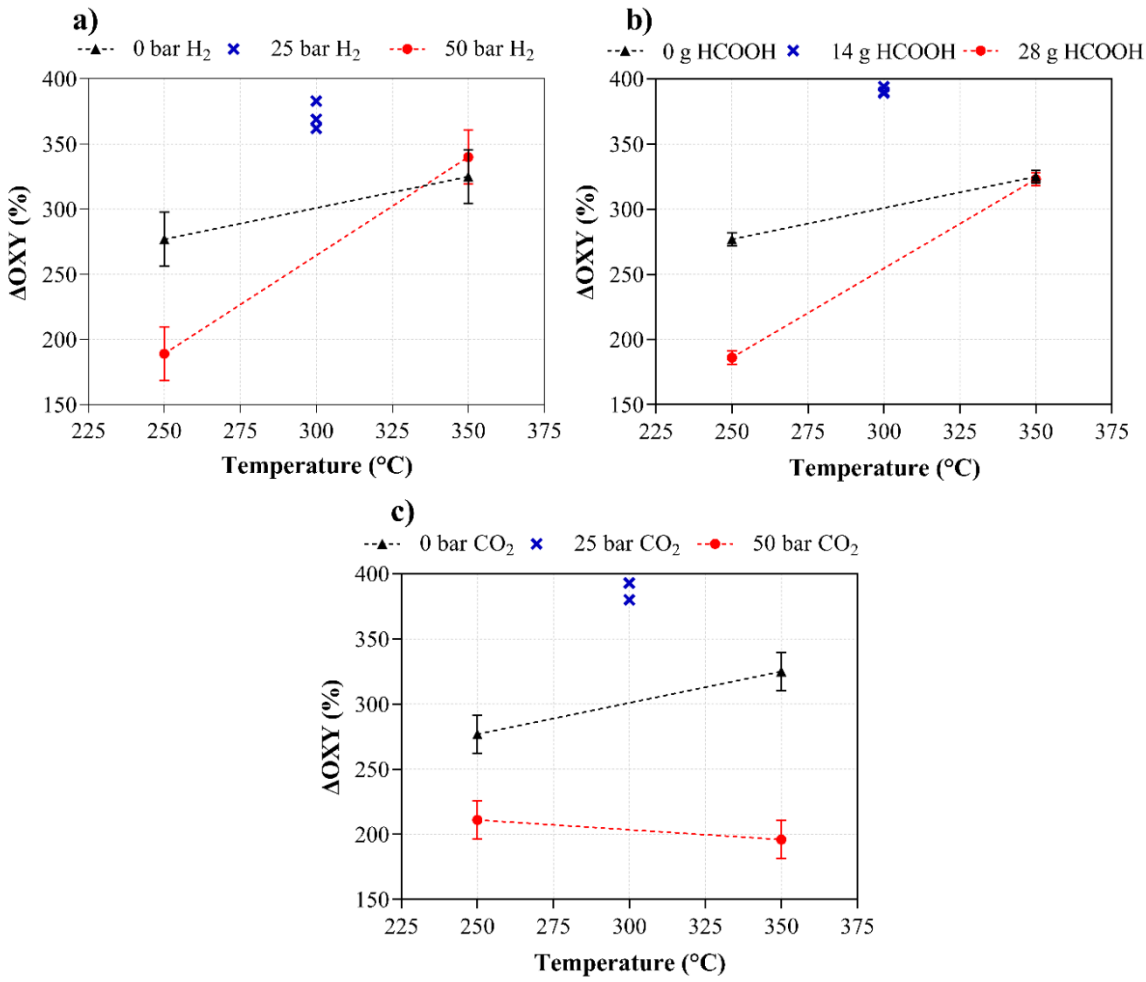

Figure 7.14. Effect of the depolymerization temperature and the reaction medium on the antioxidant performance of the additives (improvement of biodiesel oxidation stability): (a) H_2-experiments, (b) HCOOH-experiments, (c) CO_2-experiments.

The composition of the additives analyzed by GC/MS/FID (Table 7.4) can partially help to explain the trends observed in the antioxidant potential of the additives. For instance, the highest catechol concentration was obtained at a treatment temperature of 300 °C, regardless of the reaction medium. This finding could also be related to obtaining the maximum improvement rate of the oxidation stability with the additives produced at 300 °C. Catechol has been reported to show a high antioxidant potential even at lower dosages (Botella et al., 2014; Larson et al., 2017), much higher than other phenolic monomers derived from lignin, such as guaiacol or alkylated guaiacols, that not only do not have an antioxidant effect but instead, may have a pro-oxidant effect (Larson et al.,

2017). This means that the presence of guaiacols could play a role in diluting the antioxidant activity of other active components present in the additives, such as catechol.

Additionally, Larson et al. reported that not only monomers but also dimers and oligomers obtained from lignin fractionation can show great antioxidant activity (Larson et al., 2017). Hence, the antioxidant capacity of the additives produced in this study could also be affected by the presence of dimers and oligomers, which are non-detected by GC/MS. Some of these compounds could be lignin-derived dimers of catechol or guaiacol, such as α,ω-dicatechols or α,ω-diguaiacols, which have been proven to have an important antioxidant activity (Larson et al., 2017).

Aiming at studying the individual effect of some of the phenolic compounds identified in the additives, biodiesel was blended with catechol, syringol, guaiacol and a dimer commercially named as BKF antioxidant (2,2′-Methylenbis(4-methyl-6-tert-butylphenol) at different concentrations; OXY tests were conducted to these biodiesel samples according to the same methodology used before. Figure 7.15 shows the results of ΔOXY as a function of the concentration of each phenolic compound. As shown, both catechol and BKF positively affected the oxidation stability even at a low concentration. In contrast, the inverse trend was shown in the case of guaiacol, which negatively affected the oxidation stability of biodiesel, thus confirming the pro-oxidant effect of this component. As guaiacol, syringol negatively affected the oxidation stability of biodiesel at the lowest concentration, but it slightly improved it at higher dosages. These results correlate with the finding that the additives with higher catechol content and lower guaiacol/guaiacol derivates content led to the most remarkable OXY improvements.

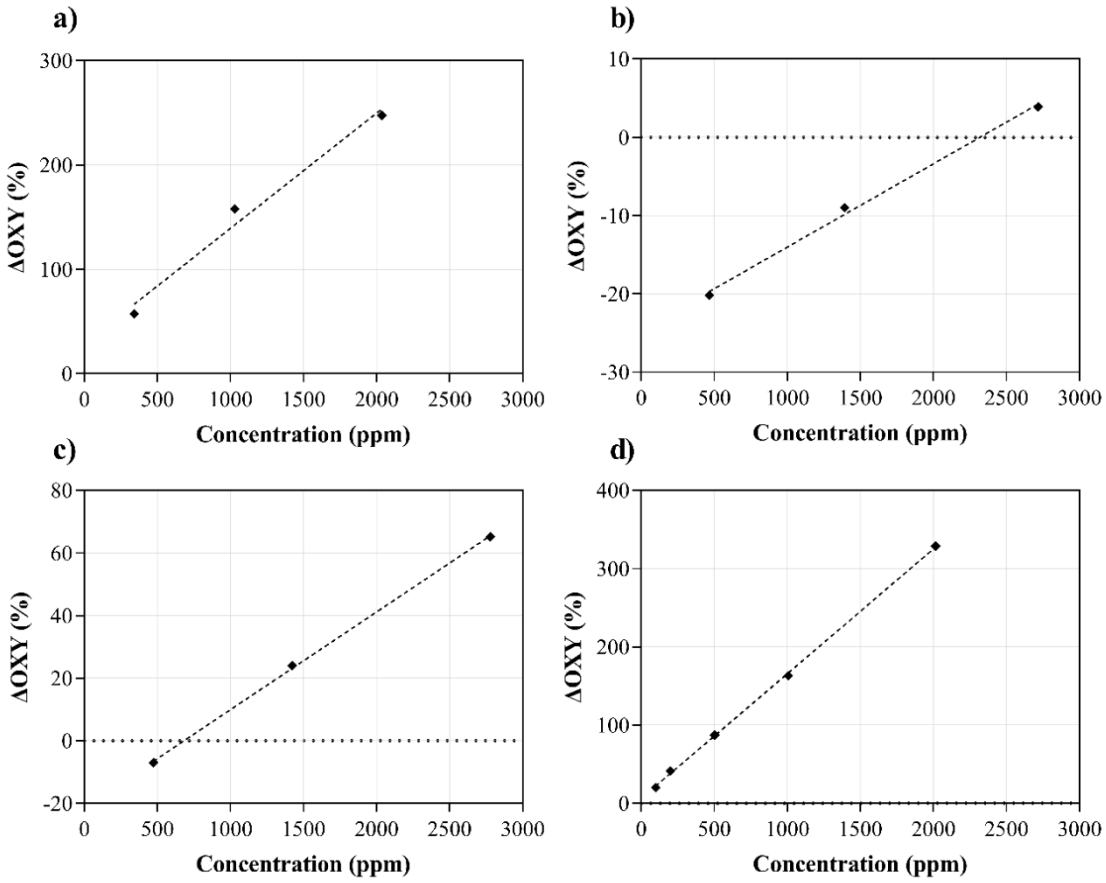

Figure 7.15. Improvement of the biodiesel oxidation stability as a function of the concentration of (a) catechol, (b) guaiacol, (c) syringol and (d) BKF dimer.

7.4. Conclusions

The depolymerization of lignin extracted from argan shells to produce add-value chemicals, specifically antioxidant additives, has been studied. Lignin from argan shells was processed in hydrothermal conditions under N_2, H_2, CO_2 or HCOOH as reaction medium at temperatures ranging from 250 - 350 °C. For the purpose of producing antioxidant additives for biofuels, such as biodiesel, the depolymerization temperature was a critical factor in both the production and the antioxidant potential and solubility of the additives. The main conclusions drawn from this study are the following:

– This experimental study has shown the technical feasibility of producing efficient antioxidant additives from an underused waste, such as argan shells.

– Biodiesel oxidation stability was significantly improved (up to 400 %) with small dosages (< 1 wt.%) of the additives produced at 300 °C, regardless of the reaction medium.

– In the conditions tested, lignin depolymerization yielded 15 - 20 % of the additive.

– The presence of catechol and catechol derivates in the additives obtained at 300 °C could be partially responsible for these good results of oxidation stability.

Chapter 8
Reductive catalytic fractionation

8. REDUCTIVE CATALYTIC FRACTIONATION

8.1. Introduction

The work included in the current chapter was realized during a research stay at the CHEC Research Centre at the Technical University of Denmark. It is focused on the reductive catalytic fractionation process as a one-pot valorization process of AS.

Nowadays, replacing fossil-based products with more sustainable resources, such as lignocellulosic biomass, for the production of fuels, chemicals and materials has become a worldwide challenge (Abu-Omar et al., 2021). In the past 50 years, the obtention of chemicals and biofuels from lignocellulose has mainly focused on converting the carbohydrate fraction, leaving behind the lignin as a subordinate constituent (Abu-Omar et al., 2021; Renders et al., 2018; Renders et al., 2017). By contrast, the conversion of lignin as a principal major component of interest in biomass has recently gained ground in the biorefinery community, thus giving birth to the lignin-first concept (Abu-Omar et al., 2021; Renders et al., 2017). This concept is mainly based on a reductive catalytic fractionation process (RCF) that, ideally, dissolves the lignin and leaves the holocellulose fraction intact. As commented above, many industrial processes can be used to isolate lignin from the lignocellulosic biomasses, such as kraft, sulfite, organosolv or soda processes. However, the lignin obtained from these processes (technical lignin) differs from the native lignin structure in biomass (Lan and Luterbacher, 2019; Sturgeon et al., 2014; Van den Bosch et al., 2017). This alteration or modification of the native lignin structure is due to the condensation reactions occurring after the cleavage of the ether and ester bonds and their substitution by more resistant and stable C-C bonds that render technical lignin more recalcitrant than native lignin (Abu-Omar et al., 2021). As a result, the subsequent depolymerization and upgrading stages of the isolated lignin to obtain phenolics of smaller molecular size (monomers and dimers) become a more challenging issue (Lan and Luterbacher, 2019). To address this condensation problem, the lignin-first approach proposes to combine, in a one-pot process, biomass fractionation with lignin disassembly and stabilization, also preserving the carbohydrate pulp (Renders et al., 2018; Renders et al., 2017). This methodology comprises a solvent-based lignin extraction process under a hydrogen atmosphere in the presence of a transition metal-based catalyst. The metal sites in the catalyst stabilize the reactive intermediates generated in the solvolysis and depolymerization of lignin by hydrogenation of broken ether and C-C bonds (Abu-Omar et al., 2021). The effect of using different types of solvents and

catalysts in RCF has been carefully reported in the literature involving different woody materials (Renders et al., 2018; Renders et al., 2017; Schutyser et al., 2018; Schutyser et al., 2015; Van den Bosch et al., 2017; Van den Bosch et al., 2015) (Ferrini et al., 2017; Ferrini and Rinaldi, 2014; Rinaldi et al., 2016) or herbaceous biomasses such as corn stover (Anderson et al., 2016) or wheat straw (Brienza et al., 2022). Among the catalysts that have been successfully tested in RCF, it can be mentioned Pd/C (Van den Bosch et al., 2015), Ru/C (Yan et al., 2008), Ni/C (Ferrini et al., 2017) and Ni-Al_2O_3 (Van den Bosch et al., 2017). The type of catalyst principally affects the product selectivity; for example, arylpropanes are the main products in the case of Ru and arylpropanols in the case of Pd catalysts (Abu-Omar et al., 2021; Lan and Luterbacher, 2019; Van den Bosch et al., 2015), even though quite similar yields of total oil could be obtained with different catalysts (Van den Bosch et al., 2015). The solvent choice also has a significant role, especially in the delignification step. Schutyser et al. (Schutyser et al., 2015) studied, in the presence of a Pd/C catalyst, the effect of a large variety of bio-based solvents (within a wide polarity range) on the delignification degree and monophenolics yield. They concluded that polar solvents showed a higher delignification capability. However, an overly polar solvent, such as water, caused a significant dissolution of carbohydrates fraction instead of being retained in the pulp.

As detailed in Chapter 7 (Afailal et al., 2021), the production of antioxidants from the lignin contained in argan shells was successfully demonstrated through a two-step process: (i) lignin extraction via a semi-chemical pulping process and (ii) subsequent depolymerization under subcritical hydrothermal conditions. In an attempt to simplify the process, AS underwent a one-pot conversion process based on the RCF methodology in order to investigate and compare how the production of small phenolic compounds is affected by the conversion process. Up to date, and to the best of our knowledge, this methodology has only been applied to woody and herbaceous feedstocks, and no research works can be found in the literature concerning the use of fruit shells (a priori, richer in lignin). Hence, this chapter of the doctoral thesis evaluates the potential of argan shells as a raw material for this process. The degree of depolymerization and product selectivity to phenolic compounds have been evaluated in either a non-catalytic pathway or using a Pd/C catalyst for depolymerization and stabilization.

8.2. Experimental methods

8.2.1. RCF experiments

Two different series of experiments were performed depending on the reaction medium used: (i) 1:1 vol. n-butanol/water and (ii) pure methanol. In both cases, the RCF experiments were conducted in a stainless steel Parr reactor 4575 (Figure 5.2). In a typical run, 20 g of AS was mixed first with the selected amount of Pd/C catalyst (0, 1 or 2 g); then, 200 mL of the solvent (n-butanol/water mixture or methanol) was added to the mixture. The reactor vessel was placed in the experimental setup, and once sealed, it was flushed with N_2 to remove air, and a leakage test was performed. Further purges involving pressurized H_2 were then carried out to evacuate the remaining N_2. Finally, the system was pressurized to 26 bars with H_2 before starting the stirring and heating. The reactor was heated up to the specified temperature (250, 275 or 300 °C) at a heating rate of up to 10 °C/min, and the final temperature was maintained for two hours. Once the experiment had finished, the reactor was quickly cooled by immersing it in an ice bath. After reaching the room temperature, a gas sample was collected in a Tedlar gas bag to be analyzed using a Thermo Scientific Trace 1300 gas chromatograph, pre-calibrated with an external standard. The gas yield (on a H_2 and N_2 free-basis) was calculated according to Equation 8.1. The remaining gas-phase was discharged by flushing the reactor with N_2 for 15 min. Once the reactor was open, the produced liquid and solid phases were gravimetrically quantified to determine the mass balance. A weighted amount of the same solvent used as the reaction medium was employed to wash the reactor and recover the sticky organic fraction remaining on the reactor stirrer, walls and coils. The mixture of liquid, solid and washing solvent was filtered (with additional flushing of the filter cake using the same solvent). The filtered solid was dried in a Büchner funnel under vacuum conditions for at least 4 h (for safety reasons, a flow of N_2 was kept on the top of the Büchner funnel, as shown in Appendix VII, to prevent any possible autoignition of the spent catalyst (Pd/C) with the adsorbed hydrogen (Chandra and Zebrowski, 2016)). Then, the filtered solid was left overnight in a desiccator under vacuum. The dried solid was weighed and the solid yield was calculated according to Equation 8.2.

$$\text{Gas yield (wt.\%)} = \frac{\sum m_{g-GC}}{W_{AS}} \cdot 100 \qquad \text{(Eq. 8.1)}$$

$$\text{Solid yield (wt.\%)} = \frac{W_S - W_{Cat}}{W_{AS}} \cdot 100 \qquad \text{(Eq. 8.2)}$$

where $m_{g\text{-}GC}$ is the mass of each individual gas compound quantified through GC, W_S is the weight (g) of the dried filtered solid, W_{Cat} is the weight (g) of the Pd/C loaded in the reactor, W_{AS} is the weight (g) of the AS fed (as-received basis).

In the n-butanol/water-experiments, the two immiscible phases of the filtrate were separated using a decantation funnel. Three aliquots from the organic phase were dried for 18 h at 117 °C (boiling point of n-butanol) to determine the corresponding yield of n-butanol-soluble oil (BSO) according to Equation 8.3.

Because of the higher temperature required for removing n-butanol, other volatile compounds, apart from butanol, can be lost during the drying stage. In order to quantify such losses, another aliquot from the organic phase was distilled at the softest conditions in a rotary evaporator (60 °C and 150 mbar) to separate the lightest organic compounds from the heaviest n-butanol soluble oil (n-butanol could not be evaporated at 150 mbar and 60 °C) and to estimate the organic volatiles losses during the drying process.

Subsequently, the previously decanted aqueous phase was extracted with 50 mL of n-butanol and then separated again to extract the remaining depolymerized lignin products. After this second extraction, aliquots from the two phases were dried for 18 h at 105 °C and 117 °C to evaporate water and n-butanol, respectively, resulting in two more fraction products: RAP (remaining in the aqueous phase) and EAP (extracted from aqueous phase).

No separation or extraction steps were performed in the runs where methanol was used as the reaction medium. In this case, the filtered liquid was the unique liquid product, which was dried during 18 h at 70 °C to determine the yield of methanol-soluble oil (MSO) (Equation 8.3).

$$\text{BSO / MSO yield (wt.\%)} = \frac{X_{DO} \cdot W_{OF}}{W_{AS}} \cdot 100 \qquad \text{(Eq. 8.3)}$$

where W_{OF} is the weight (g) of the filtered organic liquid collected in each experiment, X_{DO} is the content of dried matter (MSO or BSO) in this filtered liquid (wt.%, determined in the drying procedure) and W_{AS} is the weight (g) of the AS fed (as-received basis).

8.2.2. Experimental design

A full factorial experimental design 2^k with two factors and two levels was established for each reaction medium (n-butanol/water and methanol) in order to evaluate

the effect of both the temperature (250 - 300 °C) and the catalyst load (0 - 2 g, which led to a maximum catalyst/AS mass ratio of 0.1 g/g) on the yields and the characteristics of the produced oils. To evaluate the experimental error, three replicates at the central point of the factor levels were conducted (for each reaction medium). Hence, a total of 14 experiments were performed (Table 8.1). The experimental results were evaluated through an analysis of variance (ANOVA) with a confidence level of 95 %, including the following response variables: (i) product distribution: solid, gas and oil yields, differentiating between the production of lignin-monomers and carbohydrate-fraction in the oil; (ii) characterization of the oils, including the results of the average molecular weight, the composition determined by gas chromatography, Attenuated Total Reflection-Fourier transform infra-red spectroscopy (ATR-FTIR) and nuclear magnetic resonance spectroscopy (NMR).

Table 8.1. Experimental conditions in the RCF tests (2^k full factorial design).

Exp.#	Reaction medium	T (°C)	Pd/C amount (g)
1	n-butanol/water (1:1 vol.)	250	0
2		300	0
3		250	2
4		300	2
5		275	1
6		275	1
7		275	1
8	Methanol	250	0
9		300	0
10		250	2
11		300	2
12		275	1
13		275	1
14		275	1

8.2.3. Products characterization

The composition of the filtered organic liquids dissolved in methanol and n-butanol, respectively, was analyzed by GC/MS/FID. The FID signal was calibrated for the quantification of some phenolic compounds using 8 standard solutions prepared with concentrations ranging between 50 and 3000 μg/mL. For the carbohydrate-derived compounds, 5 standard solutions with concentrations ranging between 100 and 5000 μg/mL were prepared. All the standards were prepared using a mixture of dichloromethane-methanol (1:1 vol.) as solvent. Finally, a commercial standard (Supelco 37 Comp. FAME mix) was used to calibrate the FID signal for fatty acids methyl esters

(FAME) and other aliphatic esters. More information about the GC/MS/FID operating parameters, standards composition and calibration can be found in Appendix VII.

The phenolic monomers yields were calculated from GC/FID data (Equation 8.4). Similarly, the yields of carbohydrate-derived compounds (furan, alcohols, C5 and C6 ketones, linear esters and ethers) were calculated using the GC/FID composition data (Equation 8.5).

$$Y_{Monomers}\ (wt.\%) = \sum\left(\frac{m_{i-GC}}{W_{AS}}\right) \cdot 100 \qquad (Eq.\ 8.4)$$

$$Y_{carbohydrate-derived}\ (wt.\%) = \sum\left(\frac{m_{j-GC}}{W_{AS}}\right) \cdot 100 \qquad (Eq.\ 8.5)$$

where $m_{i\text{-}GC}$ is the individual mass of each phenolic monomer identified and quantified through GC/MS/FID, and $m_{j\text{-}GC}$ is the individual mass of each carbohydrate-derived compound determined through GC/MS/FID and W_{AS} is the weight (g) of the AS fed (as-received basis).

To get more information about the degree of lignin depolymerization, the molecular weight distribution of BSO and MSO was measured via size exclusion chromatography (SEC). The measurements were performed with an Agilent 1100 HPLC using two coupled HR-5 and HR-1 Styragel (Waters) columns as the stationary phase at 30 °C and with tetrahydrofuran (THF) as a mobile phase. The dried samples (MSO and BSO) were dissolved in the eluent with a concentration of 10 mg/mL in THF; 25 µL of the sample was injected for each analysis at an elution flow rate of 1 mL/min. Two detectors were used for the analysis: UV-vis detector (λ_{abs}= 254 nm) and refractive index detector (RID). The wavelength of 254 nm in the UV-visible detector is suitable for detecting aromatic species, while the RID detects, in addition to aromatics, other compounds, such as saccharides and compounds derived from the degradation of the solvents (methanol and n-butanol), which are transparent to UV radiation. The molecular weight was calibrated against the retention time using polystyrene standards prepared at a concentration of 10 mg/mL in THF, thus allowing the calculation of the number average molecular weight, M_n, and the mass average molecular weight, M_w, expressed in Da.

NMR measurements were made at 300 K on a Bruker Ascend III spectrometer equipped with a PABBO 5 mm probe at 400 MHz and 101 MHz for ^{1}H and ^{13}C, respectively and were processed using Bruker Topspin 3.6.2 software. NMR samples were prepared in DMSO-*d*$_6$ and referenced using the residual signal at 2.50 ppm and

39.52 ppm for ^{1}H and ^{13}C measurements (Fulmer et al., 2010). ^{1}H experiments were run using the *zg30* pulse program at 16 scans. The two-dimensional ^{1}H-^{13}C correlation was carried out using Heteronuclear Single Quantum Coherence spectroscopy (HSQC) and Heteronuclear Single Quantum Coherence-Total Correlation spectroscopy (HSQC-TOCSY) that run *hsqcetgpsi2* and *hsqcdietgpsisp.2* pulse programs in an echo-antiecho acquisition mode with D1= 1.48 s and D1= 2.0 s, respectively. More details about the applied procedures can be found in Appendix VII. Finally, ^{31}P measurements were made using a proton-decoupled experiment running the *zgpg30* pulse program. Derivatization of MSO and BSO prior to ^{31}P measurements followed the protocol described by Pu et al. (Pu et al., 2011) using 2–chloro–4,4,5,5–tetramethyl–1,3,2– dioxaphospholane (TMDP) as a derivatizing agent in $CHCl_3$/pyridine medium and N-hydroxy-5-norbornene-2,3-dicarboximide as internal standard.

To complete the information provided by the different analytical methods, the presence of surface characteristic functional groups was investigated by ATR-FTIR spectroscopy analysis.

8.3. Results and discussion

8.3.1. Product distribution

The mass balance in most of the experiments closed between 90 and 99 % (calculated directly from the mass of reactants loaded into the reactor and the product mixture recovered just after the reaction, before the separation procedure). The one-pot conversion of argan shells into oil and gas (calculated as 100 % minus the solid yield) widely ranged depending on the operational conditions: 79 - 97 % for n-butanol/water-experiments and 33 - 89 % for methanol-experiments.

Figure 8.1 summarizes the product distribution in each experiment, including most of the fractions recovered and quantified. The sum of the product yields does not fit with the overall mass balance because of the volatiles lost during the drying stage required for removing the solvent and quantifying the MSO or BSO yields. This difference was more pronounced in the case of n-butanol/water-experiments than in methanol-experiments as a consequence of the higher evaporation temperature (117 °C for n-butanol and 70 °C for methanol). According to the estimation of these losses obtained in the distillation procedure, the light fraction (volatiles) in the organic phase of n-butanol/water-experiments ranged between 28 and 40 wt.%, which matches with the missing fraction to

close the mass balance. For this reason, the GC/MS/FID characterization was carried out on the filtered organic liquids (samples before drying) to gain insight into the nature of the volatiles in this fraction.

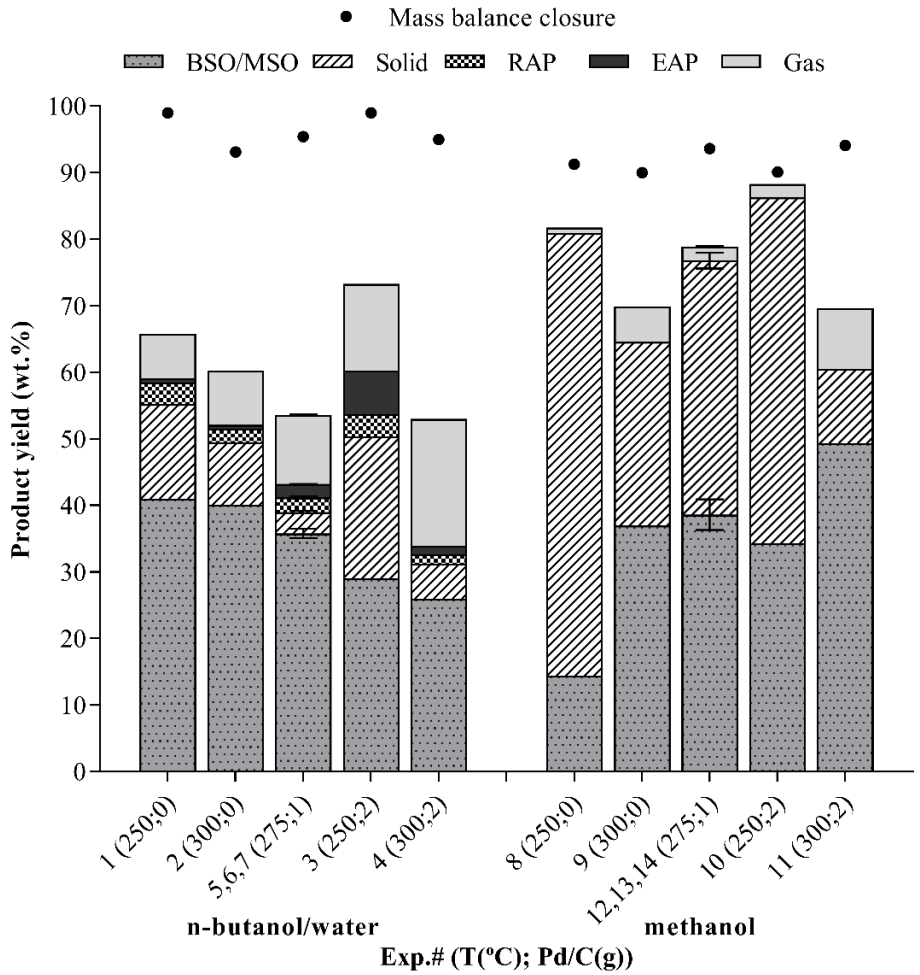

Figure 8.1. Summary of the product distribution in RCF experiments.

For a better understanding and interpretation of the experimental results, Figure 8.2 plots the ANOVA of the yields of solid, gas and oil (BSO or MSO) (error bars correspond to the least significant difference at a confidence level of 95 %). As can be seen, the increase of the treatment temperature from 250 to 300 °C significantly reduced the amount of remaining solid, regardless of the catalyst load or reaction medium. Furthermore, less solid was obtained when using the mixture of n-butanol/water (Figure 8.2a) compared to the use of methanol (Figure 8.2b). On the other hand, the highest Pd/C load minimized the solid yield to 11 % when using methanol (300 °C; 2 g Pd/C) (both factors, temperature and catalyst load, affected the solid yield in a linear trend

with no interaction between them). The lowest solid yield when using the n-butanol/water mixture was only 3 % at the central point (275 °C; 1 g Pd/C), pointing to a significant interaction between the factors and a non-linear trend. Surprisingly, in this solvent medium, the solid yield obtained at 250 °C increased from 14 % in the non-catalytic condition to 21 % with catalyst.

As shown in Figures 8.2c and 8.2d, higher oil yields were obtained in the catalytic methanol pathway. The ANOVA shows that both the temperature and the catalyst load positively affected, in a linear trend, the production of MSO. However, for n-butanol/water, the presence of catalyst adversely affected BSO production, dropping from 40 wt.% in non-catalytic conditions (Exp.#1 and #2) to around 26 wt.% in the catalytic ones (Exp.#3 and #4) regardless of the reaction temperature. A similar trend was reported in the literature (Parto et al., 2020) when processing beech wood in ethanol at 300 °C over sulfided NiMo/ɣ-Al_2O_3, where the oil yield decreased from 50 wt.% (non-catalytic process) to 44 wt.% (in the presence of catalyst). That could be explained by the fact that using the catalyst caused a more significant fractionation, producing more volatiles (higher gas release) and decreasing the oil yield. The effect of the temperature on the recovered fraction of oil was much more significant when using methanol. Saccharides may be partially responsible for this difference in the effect of the temperature. It is well known that the decomposition of holocellulose to produce saccharides is promoted when increasing the temperature (Parto et al., 2020). Since no phase separation was made in the case of using methanol (being a one-phase system), the increased fraction of saccharides remained in the MSO and contributed to increasing its yield. However, when the reaction was performed in n-butanol/water, part of these saccharides was solved in the aqueous phase and the other part figured as a light organic fraction in the BSO that was evaporated in the drying process at 117 °C, therefore, were not included in the BSO yield, leading to a more or less constant BSO yield with the temperature.

On the other hand, the gas yield (Figures 8.2e and 8.2f) was affected by both the temperature and the catalyst load in a non-linear trend for both reaction media. More gas was produced when using the catalyst, with maximal yields of 9 wt.% and 19 wt.% at 300 °C and 2 g of Pd/C in methanol and n-butanol/water, respectively. Table 8.2 exposes the gas composition obtained in each experiment (vol.% on a H_2 and N_2 free-basis). Essentially, in the non-catalytic conditions for both solvents, CO_2 was the main component in the produced gas (up to 90 vol.% in the case of n-butanol/water and

56 vol.% in the case of methanol). This trend changed when introducing Pd/C in the reaction medium, and CO was turned to be the principal produced gas (more than 60 vol.% in most cases) with a significant simultaneous increase of CH_4 and C_2H_6 concentrations. This trend could be explained by the decarbonylation reactions of the released carboxylic acids, promoted by the Pd catalyst, rather than decarboxylation reactions (Deng et al., 2021) or the catalytic reduction of CO_2 to CO via reverse water gas shift reaction in the presence of H_2 (Zhu et al., 2020).

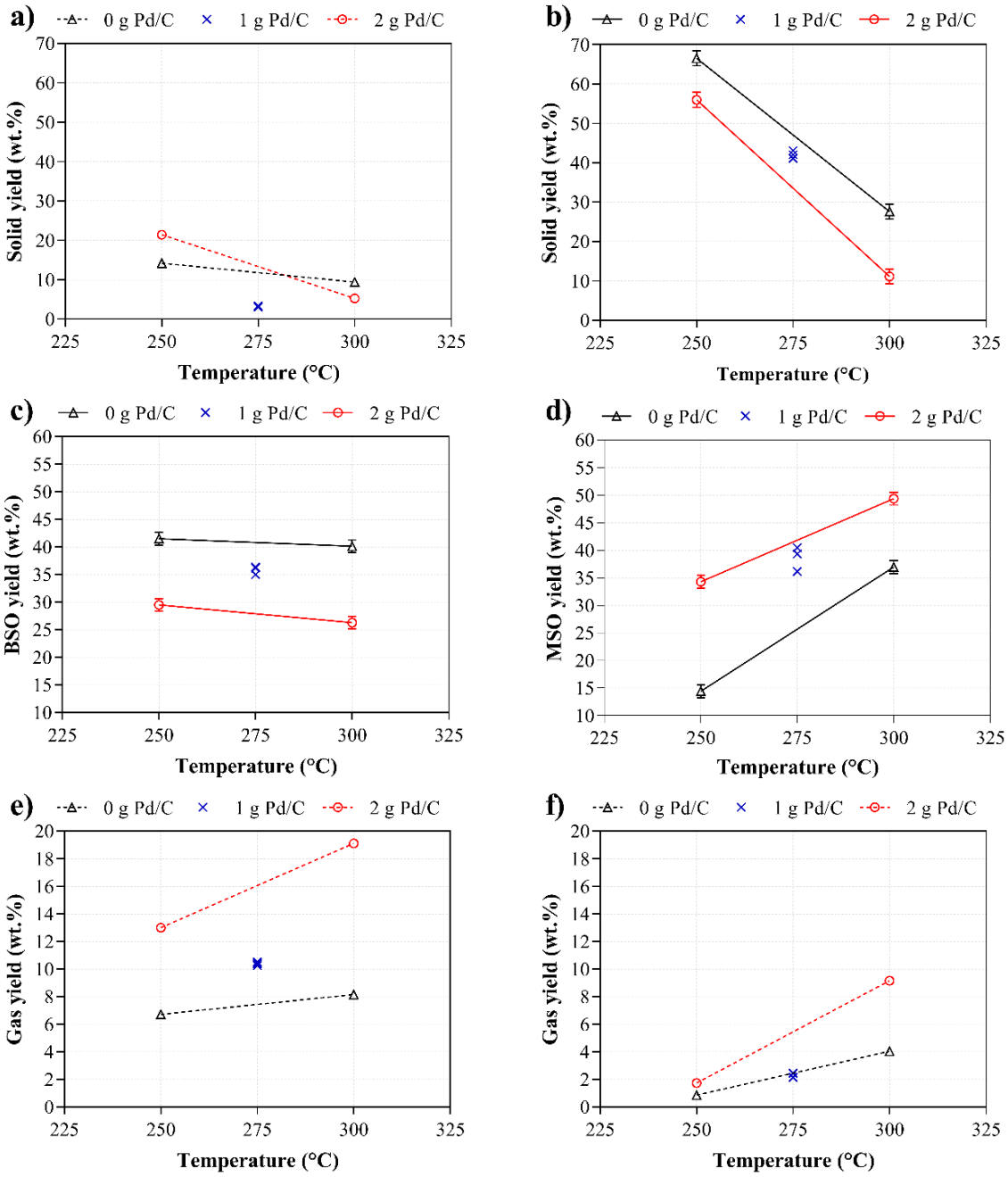

Figure 8.2. Effect of the temperature and the catalyst load on the product distribution (yields of solid, oil and gas) when using n-butanol/water (a, c, e) and methanol (b, d, f) as reaction media.

Table 8.2. Gas composition (vol. %) from the RCF experiments.

Exp. #	1	2	3	4	5,6,7	8	9	10	11	12,13,14
CH_4	0.5	2.0	6.9	6.5	2.8 ± 0.2	3	7	16	23	22 ± 1
CO	8	14	69	71	63 ± 1	40	66	67	59	59 ± 1
CO_2	90	82	17	16	32 ± 1	56	27	17	18	19.0 ± 0.4
C_2H_4	0.1	0.1	0.1	0.1	0.1 ± 0.01	0.1	0.1	-	-	-
C_2H_6	0.5	0.2	3.4	3.1	0.9 ± 0.1	0.1	0.1	0.5	0.3	0.150 ± 0.004
C_3H_8	0.5	0.2	2.6	2.3	0.78 ± 0.05	0.1	0.026	-	-	-
C_3H_6	0.2	0.3	0.2	0.2	0.28 ± 0.02	0.1	-	-	-	-
C_3H_4	0.6	0.2	0.4	0.4	0.12 ± 0.02	0.1	-	-	-	-
C_4H_8	0.1	0.1	0.03	0.03	0.020 ± 0.004	0.02	-	-	-	-
Iso-C_4H_8	0.2	0.8	0.02	0.04	0.010 ± 0.001	0.01	-	-	-	-

8.3.2. GC/MS/FID of the produced oils

The composition of the filtered organic liquids (MSO, BSO and EAP before drying) was analyzed using GC/MS/FID. Final yields of compounds in the n-butanol experiments were calculated involving both BSO and EAP phases. The identification and quantification of the produced oils (more than 88 % of the total area in the chromatograms) revealed the presence of 81 compounds from different families: monomeric phenols, aliphatic acids, alcohols, esters, furans and ketones. Figure 8.3 summarizes the total yields (over AS fed) of the compounds derived from lignin and holocellulose decomposition, which were identified and quantified by GC/MS/FID. In general, the production of phenolic monomers when using methanol in the RFC experiments was more significant than the carbohydrate-derived fraction, while the opposite was observed in the n-butanol/water-experiments. More details about the composition of each fraction are given below.

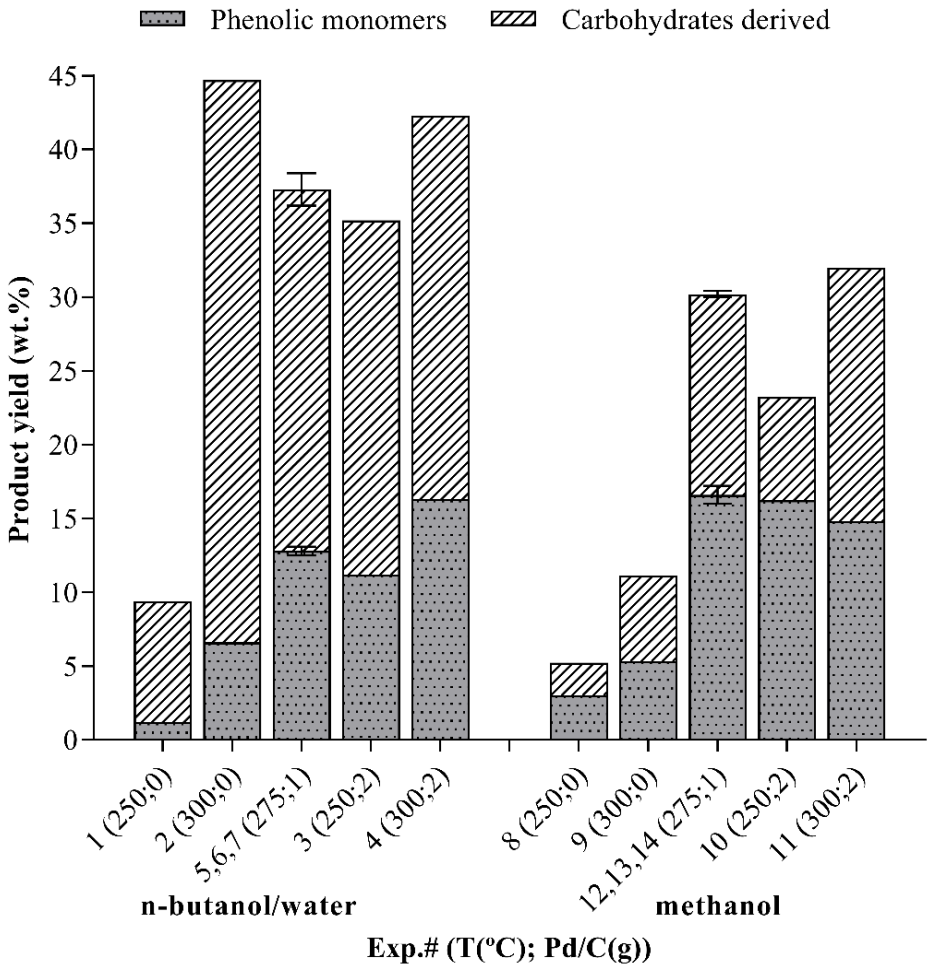

Figure 8.3. Production of phenolic monomers and carbohydrates-derived compounds in the RCF experiments.

8.3.2.1. Phenolic monomers

As phenolic monomers are known to be directly produced from the lignin fraction in biomass, Figure 8.4 summarizes again the total yields of phenolic monomers, but now calculated over the lignin fraction in AS, which was estimated to be around 34 wt.% (Afailal et al., 2021). Methanol appears as the best solvent to enhance the production of lignin monomers at lower temperatures (250 and 275 °C), while this yield was slightly higher in the n-butanol/water-experiments at 300 °C (up to 48 wt.% in the presence of 2 g of Pd/C). For both solvents, the monomers yield was less than 10 wt.% in the non-catalytic runs at 250 °C (4 wt.% in BSO and 9 wt.% in MSO), which means that this temperature was not enough to fractionate the lignin at this relatively short reaction time (2 h). Repolymerization reactions between the unsaturated intermediates (coniferyl and

sinapyl alcohols) could also be occurring after the solvolytic β-O-4 bond cleavage (Erdocia et al., 2014; Kumaniaev et al., 2017; Toledano et al., 2012). The ANOVA results indicate that both the temperature and the Pd/C load were significant factors in the n-butanol/water experiments (Figure 8.4a), showing a non-linear effect on the monomers yield. Within the conditions tested, the maximal yield of BSO when using n-butanol/water (48 wt.%) was obtained at the highest temperature (300 °C) and with the greatest load of catalyst (2 g), which means more than double that obtained at the same temperature and without catalyst (19 wt.% of BSO). In the case of methanol-experiments, no significant changes in the monomers yield were observed when varying the temperature, obtaining the highest yield of 44 - 49 wt.% with either 1 or 2 g of catalyst, which means a five-fold increase, from 9 to 48 wt.%, in the monomers yield obtained at 250 °C.

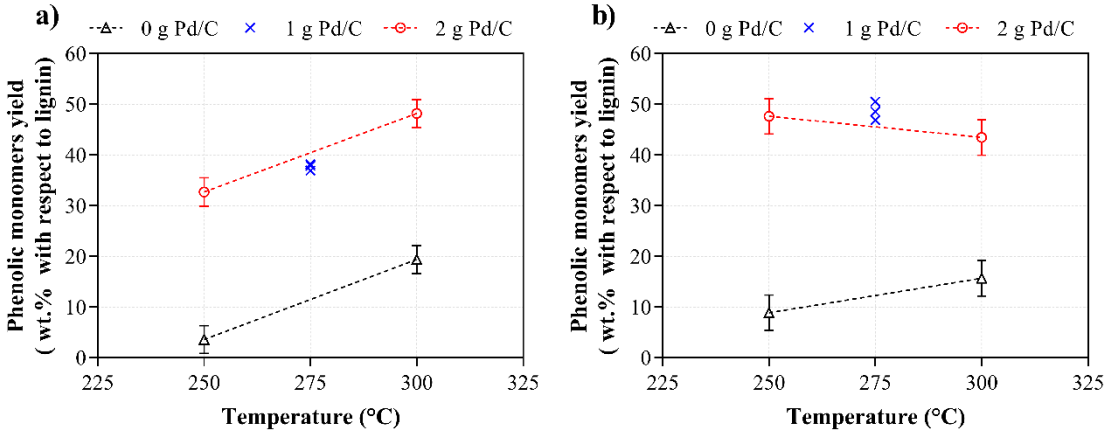

Figure 8.4. Effect of the temperature and the catalyst load on the yield of phenolic monomers (wt.% over AS lignin): (a) n-butanol/water-experiments; (b) methanol-experiments.

In spite of the lower values of AS conversion obtained when using methanol, the production of monomers from lignin was not negatively affected in this reaction medium, which points to good efficiency and selectivity into lignin fractionation during the solvolytic step of the process. Among other linear alcohols, methanol has been pointed out in the literature as a suitable solvent for lignin depolymerization due to its highest polarity and hydrogen bonding ability (Kouris et al., 2020).

To keep such high yields of aromatic monomers, the catalytic hydrogenation/hydrogenolysis of unsaturated intermediates plays a crucial role in

avoiding repolymerization/condensation reactions and stabilizing the final products (Van den Bosch et al., 2017). Renders et al. (Renders et al., 2018) found that operating under 10-30 bars of H_2, as done in this work (26 bars), allowed keeping high monomers yields. According to the literature (Lan and Luterbacher, 2019), the RCF of hardwood using catalysts supported on activated carbon led to yields of aromatic monomers ranging between 40 and 50 wt.% (superior to those supported on metal oxide), which was close to the theoretical yield (calculated assuming that only the ether bonds linking the monomers in the lignin polymer could be broken). The empirical calculation reported in the literature (Yan et al., 2008) supposed that ether bonds in the native lignin could represent between 2/3 to 3/4 of the total linkages; hence this theoretical maximum yield of monomers (calculated as the square of ether bonds fraction) could range between 45 and 56 wt.%. Therefore, the results obtained in this study for the RCF of AS suggest a behavior similar to that of hardwood. In fact, AS chemical characterization is closer to hardwood than softwood (hemicellulose content up to 20 wt.%, cellulose content slightly lower than 40 wt.% and lignin content higher than 25 wt.% (Roger et al., 2012)).

For further characterization of the lignin-derived fraction, Figure 8.5 shows the individual yield (wt.% over the amount of lignin in AS) of the main phenolic compounds identified and quantified by GC/MS/FID in the produced oils. More detailed information about the individual yields of the main phenolic compounds can be found in Table B in Appendix VII. Although the same catalyst was employed in both reaction media, the product distribution was strikingly different. In the case of n-butanol/water, the catalytic pathway led to an increased selectivity to 4-n-propanolguaiacol (PrOH-G) and 4-n-propanolsyringol (PrOH-S), accompanied by the formation of other monomers at lower concentrations, such as guaiacol (G), syringol (S) or catechol. According to the ANOVA analysis, the catalyst load had an apparent positive effect on the yields of PrOH-G and PrOH-S, while the treatment temperature did not significantly affect it. Several studies reported that propanol-substituted syringol and guaiacol are characteristic products of Pd catalysts, that tune the OH content of the lignin-derived compounds, concretely the phenolic monomers (Renders et al., 2018; Van den Bosch et al., 2015). Other catalysts such as Ru/C or sulfided NiMo/ɣ-Al_2O_3 tend to favor the generation of the hydrodeoxygenated propyl guaiacol and syringol (Parto et al., 2020; Van den Bosch et al., 2015). Figure 8.6 exposes the different pathways proposed during the lignin solvolysis

and hydrogenation/hydrogenolysis of the unstable unsaturated intermediates (Renders et al., 2018).

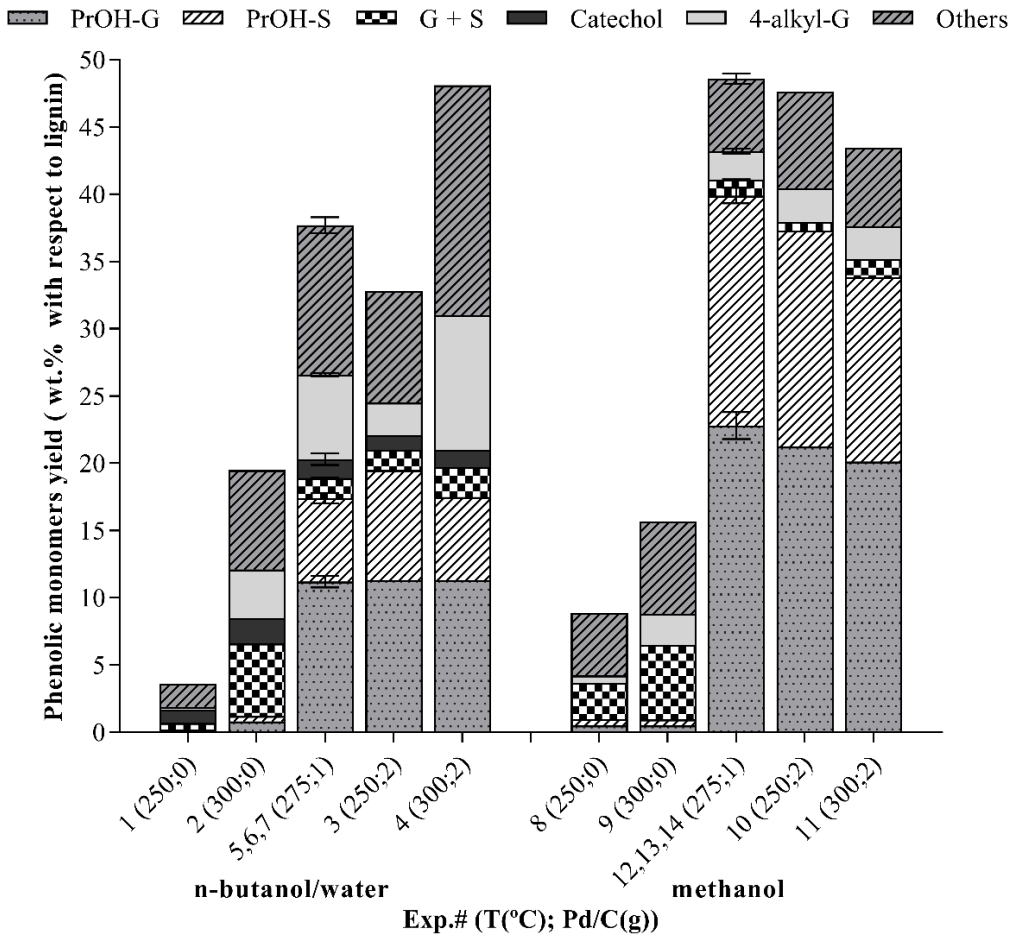

Figure 8.5. Mass yields (over AS lignin) of the main phenolic monomers identified in the oils.

The selectivity to PrOH-G and PrOH-S was also considerably increased when operating in methanol. For example, in terms of composition, at 300 °C and a catalyst load of 2 g, PrOH-G and PrOH-S jointly accounted for 78 wt.% of the identified monomers (in the methanol-experiments) vs. 36 wt.% (in n-butanol/water-experiments). However, non-substituted guaiacol and syringol were mainly observed in the non-catalytic runs. Their production increased with temperature in both reaction media but dropped when the catalyst Pd/C was added. The inverse trend was observed for the presence of alkyl-G compounds (4-methyl, 4-ethyl and 4-propyl guaiacol), which was enhanced in the presence of the catalyst, especially in n-butanol/water-experiments. Maximizing PrOH-G and PrOH-S in methanol may likely be related to the direct

hydrogenation of the intermediates (direct hydrogenation route in Figure 8.6). In contrast, in the case of n-butanol/water-experiments, the important presence of alkyl-G could point to G/S alcohol hydrogenolysis followed by hydrogenation of C_α and C_β bounds (hydrogenolysis plus hydrogenation route in Figure 8.6). Finally, it is to highlight that catechol and phenol were exclusively identified in the oil from n-butanol/water-experiments; in this reaction medium, the production of catechol could be promoted by the presence of water through guaiacol protonation (Cui et al., 2017; Wahyudiono et al., 2007; Yang et al., 2013), while phenol could be produced by deoxygenation of the generated catechol.

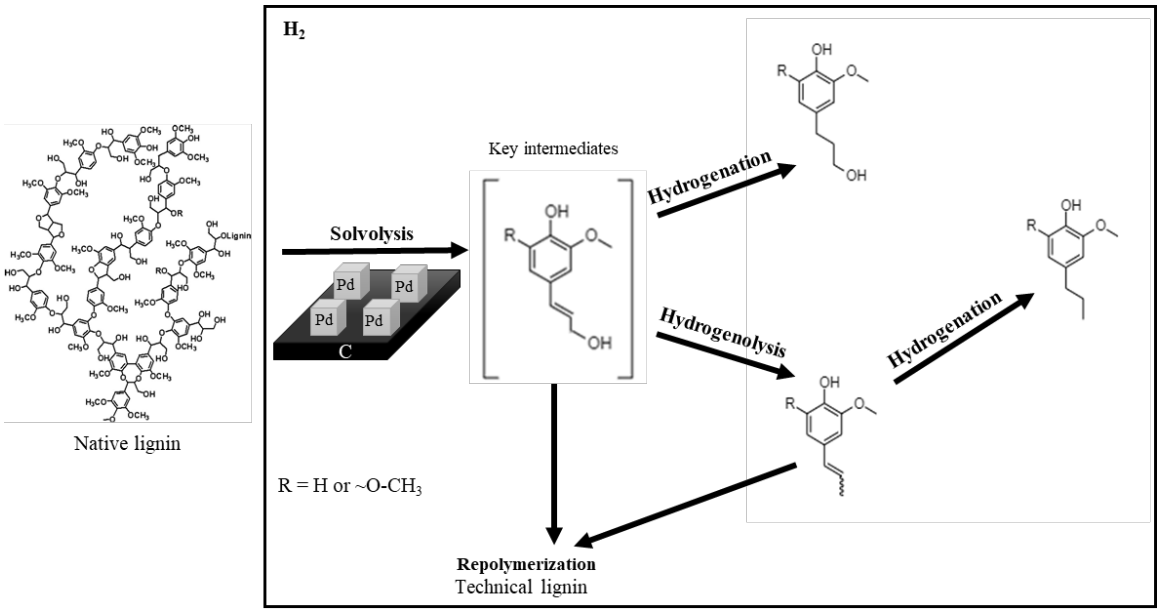

Figure 8.6. Lignin depolymerization mechanisms to phenolic monomers (adapted from (Renders et al., 2018)).

8.3.2.2. Carbohydrate-derived compounds

In addition to the phenolic monomers fraction, the GC/MS/FID analysis of the produced oils revealed the presence of carbohydrate-derived compounds. As these compounds are directly produced from hemicellulose and cellulose fractions in biomass, the production of this type of compound has been now calculated over holocellulose content in AS, which was estimated to be 57 wt.% (Afailal et al., 2021). These data are shown in Figure 8.7. The ANOVA showed that both factors and the interaction between them affect (in a non-linear way) the production of carbohydrate-derived compounds in

the methanol reaction medium (Figure 8.7b): increasing the temperature in the presence or absence of the catalyst was favorable to enhance the holocellulose degradation with a maximal yield of 17 wt.% of carbohydrate-derived compounds (at 300 °C and 2 g of Pd/C). However, in the case of n-butanol/water-experiments (Figure 8.7a), the temperature only played a significant positive role in the carbohydrate-derived yield when operating in the absence of the Pd/C catalyst, but no significant changes were observed when increasing the temperature in the presence of the catalyst.

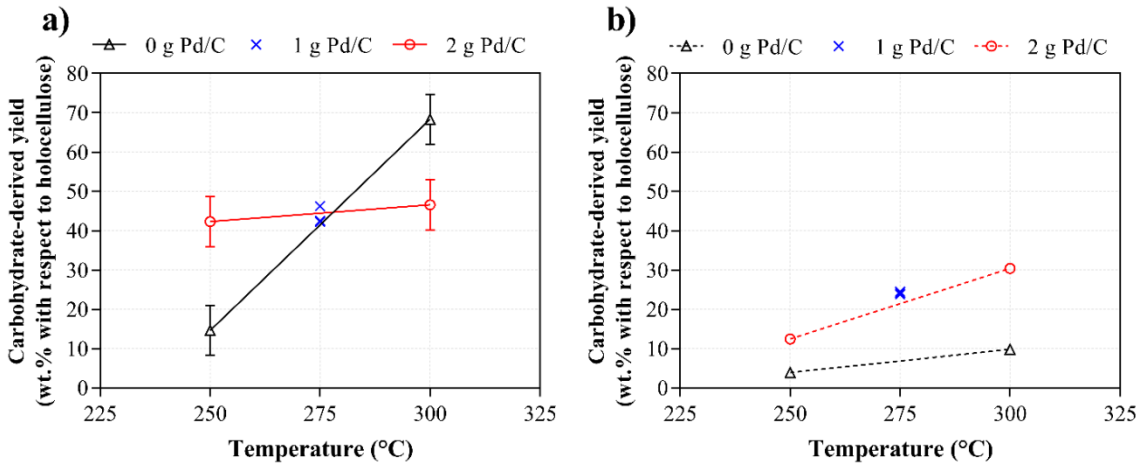

Figure 8.7. Effect of the temperature and the catalyst load on the yield of carbohydrate-derived fraction (wt.% over AS holocellulose): (a) n-butanol/water-experiments, (b) methanol-experiments.

Overall, the conversion of holocellulose into oil was enhanced more in n-butanol/water-experiments than in methanol-experiments, which agrees with the lower unconverted solid yields found in the former reaction medium. While most of the carbohydrate-derived compounds were not included when calculating the BSO yield (Section 8.3.1, Figure 8.1 and Figure 8.2c) as part of them was evaporated in the drying stage at the n-butanol evaporation temperature (117 °C) and the other part remained in the aqueous phase (RAP before the drying at 105 °C). This fact was confirmed by comparing the GC/MS spectra of the original n-butanol organic phase and the dried BSO (for the GC analysis, BSO was redissolved at the same concentration as the initial solution) (Figure 8.8). These chromatograms showed how the peaks eluted at relatively low retention times, corresponding to volatile compounds such as acetic acid, butyl ester,

1-hydroxy-2-butanone, butane, 1,1-dibutoxy, etc., only appeared in the original sample, but not in the dried and redissolved sample (BSO).

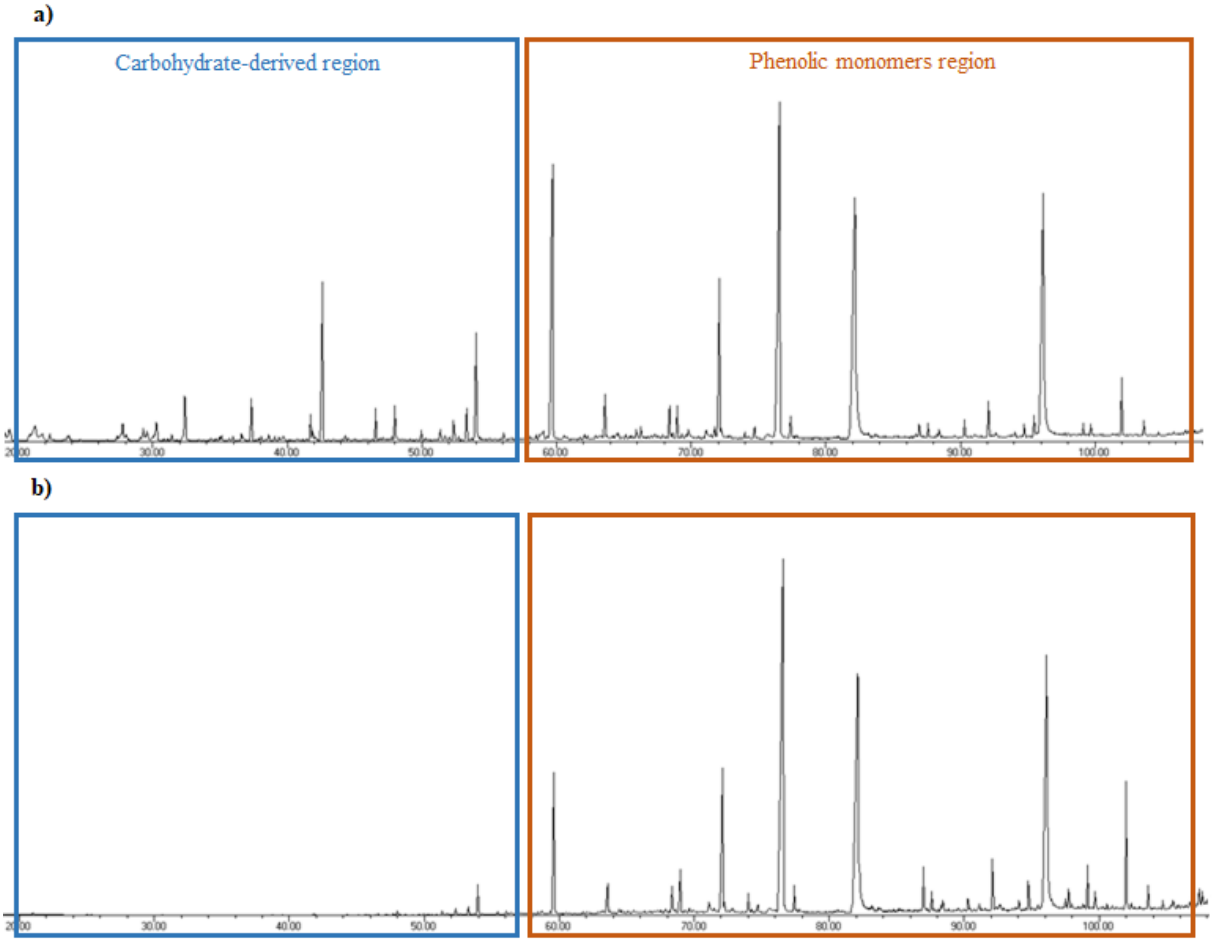

Figure 8.8. GC/MS spectra of (a) BSO before drying (liquid organic phase). (b) BSO redissolved in n-butanol.

For further details about the production of carbohydrate-derived compounds, Figure 8.9 shows how the yields (wt.% over holocellulose) are distributed into the main chemical families. More detailed information about the individual yields of the main carbohydrate-derived compounds can be found in Table C in Appendix VII. Aliphatic esters are the most prominent family of compounds detected due to the esterification reactions occurring between the carboxylic acids (mainly acetic acid) released during the holocellulose degradation and the alcohol used as a solvent for RCF (especially for n-butanol/water runs). Carboxylic acid–methyl ester was the major compound when operating in methanol and carboxylic acid–butyl ester in n-butanol/water. The production of these compounds (in terms of mass yield) was more significant in the case of n-

butanol/water-experiments. It is evident that the butyl ester branching is heavier than the methyl ester one, thus increasing the weight of this chemical family. However, the lower yield of the carbohydrate-derived fraction found in the methanol reaction medium may also be explained by the reduced conversion of AS (higher yield of unconverted solid) and the remarkable selectivity of methanol to lignin (aromatic) solvolysis. In addition, the noticeable production of ethers in n-butanol/water-experiments, mainly 1,1-di-butoxybutane (Table C in Appendix VII), probably points to a Guerbet condensation and co-condensation of the solvent, which is favored at this temperature range (250 to 300 °C) in the presence of H_2 (Larina et al., 2019). In the case of methanol-experiments, the aliphatic ketones were the main carbohydrate-derived family, followed by aliphatic alcohols (polyols) and furans coming from hemicellulose processing, especially when the catalyst Pd/C was added.

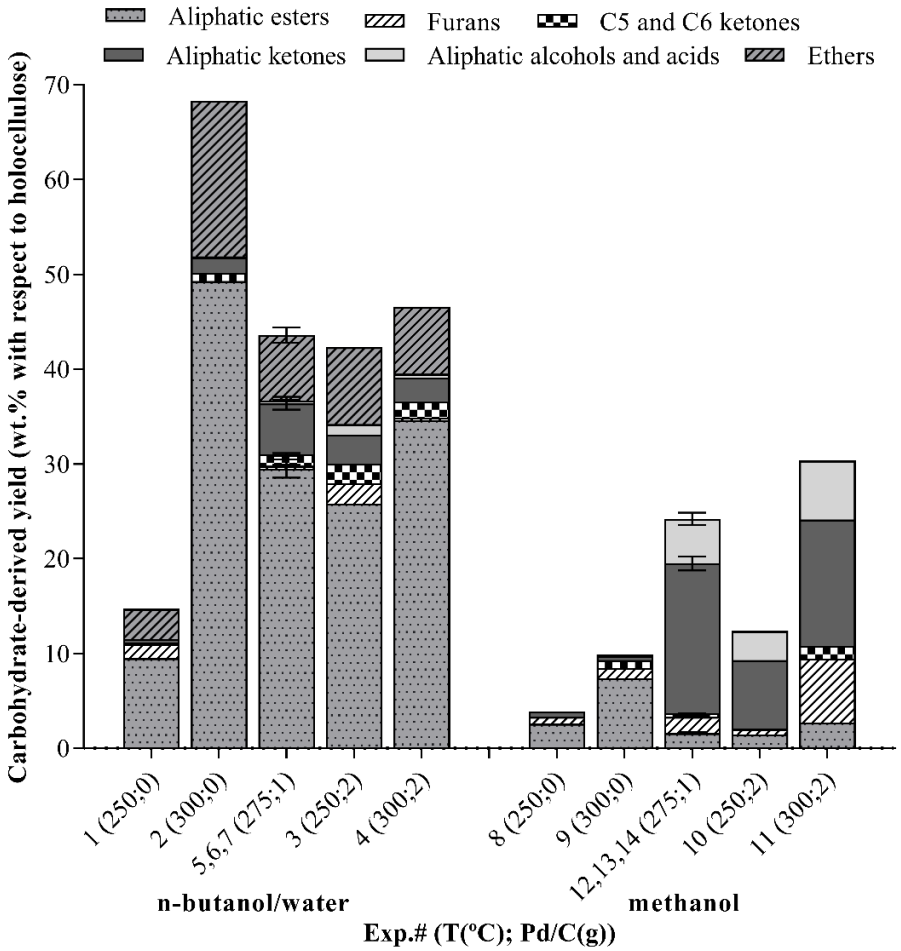

Figure 8.9. Mass yields (over AS hollocelulose) of the main carbohydrate-derived families identified in the oils.

8.3.3. Molecular weight distribution of the produced oils

Figure 8.10 displays the size exclusion chromatograms of all the produced oils (BSO and MSO) using a UV-detector at $\lambda = 254$ nm, which allows ruling out the aliphatic species coming from saccharide or solvent degradation. The plots for BSO (left panels) and MSO (right panels) show different molecular weight distributions. As expected, in the non-catalytic pathway (Exp.#1, 2, 8, 9), the molecular weight distribution is wider and shifted towards higher molecular weights. These data agree with the lower monomers yield obtained via GC/MS/FID in the case of n-butanol/water-experiments (Exp.#1 vs. Exp.#8) and could be explained by repolymerization reactions producing heavy oligomers instead of smaller molecules. The oils produced in the presence of the Pd/C catalyst showed a narrower size distribution and shifted to lower molecular weights, which evidenced the role of the catalyst in the lignin fractionation. It can be observed that the MSO from Exp.#10-14 showed a significant shoulder between 100 and 200 Da and between 200 and 300 Da, which could be related to the high selectivity to PrOH-G (182.2 Da) and PrOH-S (212.2 Da). The effect of the solvent in the catalytic experiments can also be observed in the SEC chromatograms. Thus, when the reactions were run in methanol using Pd/C, the SEC curves of MSO were shifted to lower molecular weights and presented lower average M_n (Table 8.3) than BSO obtained under the same conditions (675 Da for Exp. # 10 vs. 847 Da for Exp.#3; 727 Da and 997 Da for Exp. #12 and #5). Shoulders in the range of 100 - 200 Da and 200 - 300 Da were much less significant in BSO than in MSO. In short, the SEC analyses show the efficiency of the Pd/C catalyst in stabilizing the produced aromatic monomers and preventing condensation reactions in both media, but this effect was more pronounced when methanol was used as a solvent.

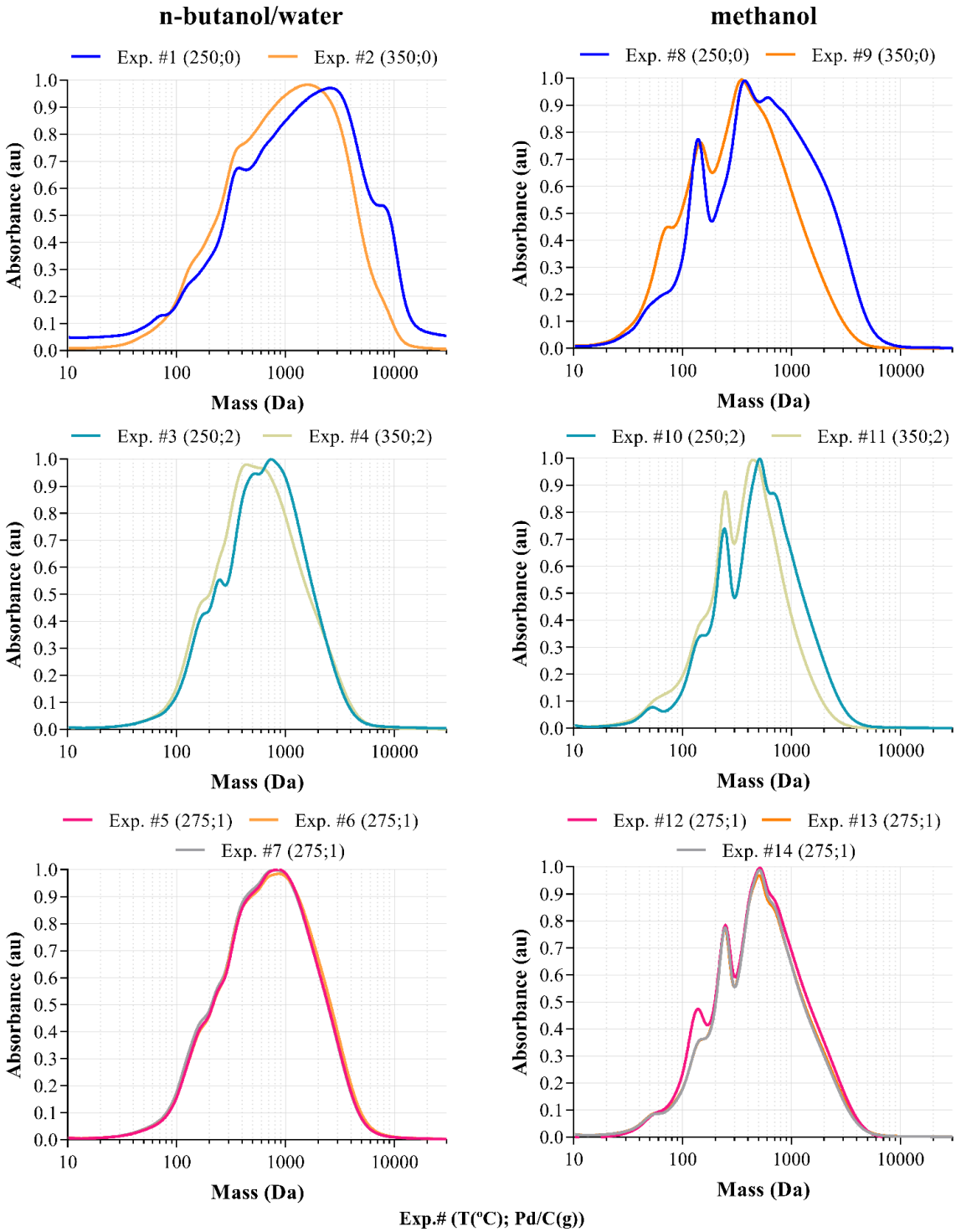

Figure 8.10. SEC plots of MSO and BSO.

The operational conditions significantly affected the molecular weight distribution of the produced oils. Generally, comparing the reaction media, lower values of M_w and M_n were obtained when methanol was used, regardless of whether the catalyst was present

or not (Table 8.3). For example, at 250 °C in non-catalytic conditions, the M_w of BSO was up to 5839 Da, but it was almost three times lower (1975 Da) in the case of MSO. The results from the ANOVA of the M_w (Figure 8.11) indicated that the temperature, the catalyst load and their interaction were significant factors for both reaction media. The M_w of MSO and BSO decreased with the reaction temperature when operating in non-catalytic conditions, but the effect of the temperature turned into non-significant when using 2 g of Pd/C in both reaction media. Furthermore, in methanol-experiments, the effect of using the catalyst was removed by increasing the temperature up to 300 °C.

Table 8.3. Molecular average weights (M_n, M_w, M_w/M_n) of BSO and MSO.

Exp #	Reaction medium	T (°C)	Catalyst load (g)	M_w (Da)	M_n (Da)	M_w/M_n
1	n-butanol/water (1:1 vol.)	250	0	5839	2707	2.2
2		300	0	3132	1576	2.0
3		250	2	1503	847	1.8
4		300	2	1565	802	2.0
5,6,7		275	1	1870 ± 56	997 ± 28	1.87 ± 0.01
8	Methanol	250	0	1975	895	2.2
9		300	0	1187	531	2.2
10		250	2	1245	675	1.8
11		300	2	961	501	1.9
12,13,14		275	1	1468 ±66	727 ± 13	2.0 ± 0.1

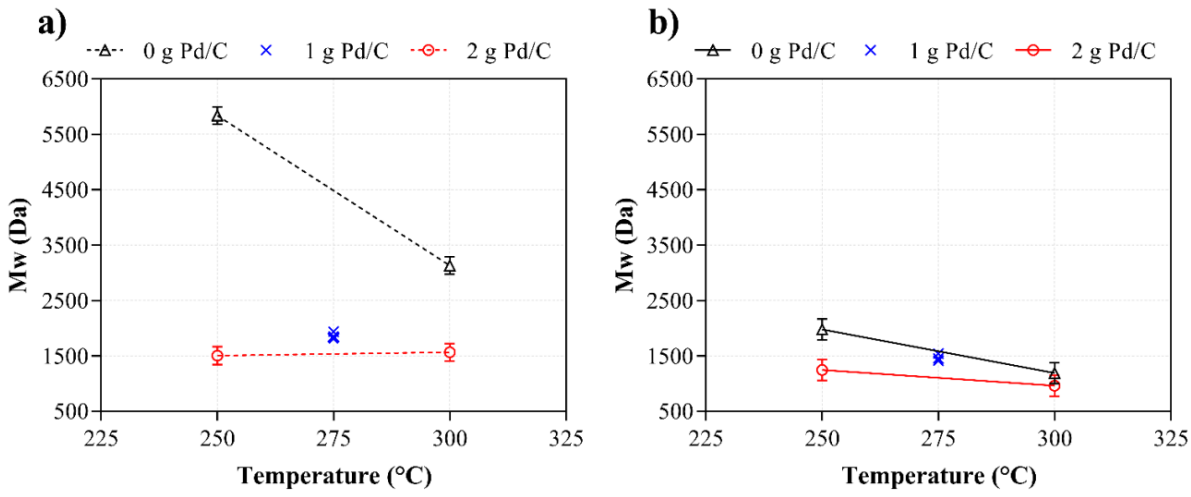

Figure 8.11. Effect of the temperature and the catalyst load on the average molecular weight (M_w) (Da) of oils: (a) n-butanol/water-experiments (BSO); (b) methanol-experiments (MSO).

8.3.4. NMR analysis of the produced oils

Diffusion-ordered NMR spectroscopy (DOSY-NMR) can be extremely useful in estimating the molecular weight in depolymerization reaction mixtures (Cornejo et al., 2020a; Cornejo et al., 2020b). The most important feature of DOSY spectroscopy is that any chemical shift in the ^{1}H NMR spectrum can be directly correlated with the diffusion coefficient of the corresponding molecule. The diffusion coefficient is directly associated with the hydrodynamic radius of the molecule via the Stokes-Einstein equation (Li et al., 2009) and, consequently, with its molecular weight (Pu et al., 2011). The DOSY-NMR spectroscopy can be therefore seen as a pseudo-SEC technique that allows the estimation of the masses according to their chemical structure. Average diffusion coefficients were obtained for different regions of all the spectra using the integral values for different regions (7.16 ppm to 6.01 ppm for the aromatic region, 3.91 ppm to 3.51 ppm for the methoxy and the saccharide region, whereas the aliphatic region was divided into two intervals, 2.40 ppm - 1.80 ppm and 1.73 ppm - 0.72 ppm). The calibration of the diffusion coefficient of polystyrene (PS) and polyethylene glycol and monomeric phenols (PEGP) standards and their corresponding molecular weights was performed (Cornejo et al., 2020a; Cornejo et al., 2020b). This calibration was successfully used to determine the masses of the aromatic and aliphatic fractions arising from lignin depolymerization. As previously reported, the calibration made with PS standards provided higher accuracy for higher apparent masses, thus corresponding to more hydrophobic oligomers, whereas values calculated with PEGP standards were more suitable for low molecular weight and, therefore, more polar fragments (Cornejo et al., 2020b). The average apparent masses estimated by DOSY-NMR using the two different calibration curves are gathered in Table 8.4.

Table 8.4. Estimated apparent masses using DOSY for the aromatic, methoxy and aliphatic regions using PS for calibration.

					PS calibration				PEGP calibration			
Exp.#	Reaction medium	T (°C)	Catalyst load (g)	Mn (Da)*	Aromatic region [a]	Methoxy region [b]	Aliphatic region [c]	Aliphatic region 2[d]	Aromatic region [a]	Methoxy region [b]	Aliphatic region [c]	Aliphatic region 2[d]
1	n-butanol/water (1:1 vol.)	250	0	1797	1080	1320	604	426	801	1001	419	284
2		300	0	1379	725	1008	435	410	514	741	290	272
3		250	2	763	589	663	n.d	430	407	465	n.d	287
4		300	2	716	447	520	317	397	300	354	204	262
5,6,7		275	1	870	595	706	433	495	412	498	289	335
8	Methanol	250	0	813	646	503	363	392	451	342	238	259
9		300	0	566	462	403	323	295	311	267	144	188
10		250	2	629	549	539	363	423	377	369	237	282
11		300	2	505	492	474	249	316	333	320	156	203
12,13,14		275	1	625	470	457	308	361	317	307	198	236

* SEC (RID detector), n.d: not detected, [a] from 7.16 to 6.01 ppm, [b] from 3.91 to 3.51 ppm, [c] from 2.40 to 1.85 ppm, [d] from 1.72 to 0.72 ppm

The average apparent masses for the aromatic region calculated using the PS calibration did not match perfectly in the case of Exp.#1 and #2 with those determined by SEC, although a much better match was achieved for the rest of the experiments. It is noteworthy that the apparent masses for the aromatic region estimated using DOSY are lower than those determined by SEC using RID (Table 8.4), which may be due to species that are not considered upon integration as, for instance, some oligosaccharides, for which the presence of lower diffusion coefficient species has been detected. Overall, a similar trend can be observed in the apparent mass determined either by DOSY or by SEC.

For BSO samples, the apparent mass (by DOSY) for the aromatic fraction decreased when increasing the temperature in non-catalytic conditions (1080 vs.725 Da for Exp.#1 and #2, respectively). The catalyst load had an apparent positive effect on the depolymerization, as adding 2 g of Pd/C at 300 °C caused a decrease from 725 Da to 447 Da (Exp.#2 vs. Exp.#4) in the aromatic fraction. A similar effect was observed when 2 g of Pd/C was added at 250 °C, with a decrease in the apparent mass from 1080 to 589 Da (Exp.#1 vs. Exp.#3).

DOSY spectra (Figures 8.12 and 8.13) also provided valuable information about the composition of the different fractions and the formation of reaction products derived from other side reactions than lignin depolymerization. The calculated apparent masses for the first calibration (using PS standards) can be seen on the left side of the DOSY spectra (blue numbers), and the second calibration (using PEGP standards) is shown on the right side (red numbers). The most accurate mass is in the blue or red square, considering the mass and the calibration curve. DOSY spectra of the BSO samples obtained at 300 °C without or with catalyst (Figures 8.12a and 8.12b) show that most of the aromatic fractions from the RCF reaction carried out at 300 °C without catalyst (Exp.#2) could be found in mass ranges between 266 and 756 Da. In contrast, when the reaction was performed at the same temperature with the catalyst (2 g), the aromatic masses ranged from 198 to 527 Da, evidencing the positive effect of the catalyst in the depolymerization of lignin.

On the other hand, for MSO samples, the effect of Pd/C load was less important. The apparent masses ranged between 462 and 646 Da in all experiments, whatever the reaction conditions (Table 8.4), which corroborates the results obtained by SEC for this reaction medium. DOSY spectra of the MSO produced with and without catalyst at 300 °C (Exp.#9 and Exp.#11, Figures 8.12c and 8.12d) presented diffusion traces in the

aromatic region ranging from 230 to 450 Da in both cases, showing that the effect of the catalyst was not important in the average apparent mass when using methanol at high temperatures, although it could also be observed that the size distribution was also narrower when the catalyst was used. However, the effect of the catalyst was of paramount importance in the apparent masses when the experiment was run at 250 °C (Exp.#8, no catalyst, Exp. #10, 2 g Pd/C, Figure 8.13). Thus, when the reaction was run in the absence of the catalyst, apparent masses ranged from 315 to 1116 Da (Figure 8.13a), while in the presence of the catalyst, the apparent masses were in the 223-635 Da range (Figure 8.13b).

Concerning the carbohydrates-derived compounds, as can also be observed in Figures 8.12a and 8.12b, the intense diffusion traces present in the aliphatic region (0.7 ppm - 2.0 ppm) corresponded to apparent masses ranging from 175 to 266 Da in Exp.#2 and from 198 to 250 Da in Exp.#4. Therefore, the apparent mass for the aliphatic compounds was noticeably lower than for the aromatic region in the non-catalytic reaction, for example, in Exp.#2. This means that most of these aliphatics may come from side reactions of n-butanol, such as the Guerbet reaction or directly from saccharide degradation products, giving rise to aliphatic esters and ethers, as was pointed out previously (Section 8.3.2.2). A similar observation can be made for Exp.#4 (at 300 °C with 2 g of Pd/C), but the difference in the estimated apparent mass was much lower in this case. In addition, the diffusion traces of the aliphatic compounds (Figure 8.12b) presented similar masses to those in the aromatic region, which agrees with the significant presence of 4-alkyl-G or PrOH-G and PrOH-S units in the reaction mixture (see Figure 8.5); these aliphatic compounds may correspond to the propanol units of the PrOH-G and PrOH-S monomers. DOSY spectra for MSO obtained in the absence or presence of Pd/C (Figures 8.12c and 8.12d) presented diffusion traces in the aliphatic region with similar apparent masses as in the aromatic region, showing that some aliphatic chains were connected to the aromatic compounds, although other aliphatic traces presented lower apparent masses than the corresponding aromatic region, as in the MSO sample of Exp.#11.

Besides the diffusion traces corresponding to the methoxy moiety at 3.75 ppm, in all the experiments carried out in methanol (Exp.#8 - 12), diffusion traces can be observed in the range of 3.0 ppm to 5.5 ppm. These traces could correspond to saccharides, which was confirmed by the traces at 4.5 ppm, which may correspond to the anomeric carbon

with the same diffusion coefficient (Figures 8.12c, 8.12d and 8.13). These diffusion traces attributed to saccharides were not observed in the DOSY spectra of BSO (Figures 8.12a, 8.12b), which could be explained by the retention of these saccharides in the aqueous phase separated in the earlier step of the process or because of the drying process at 117 °C.

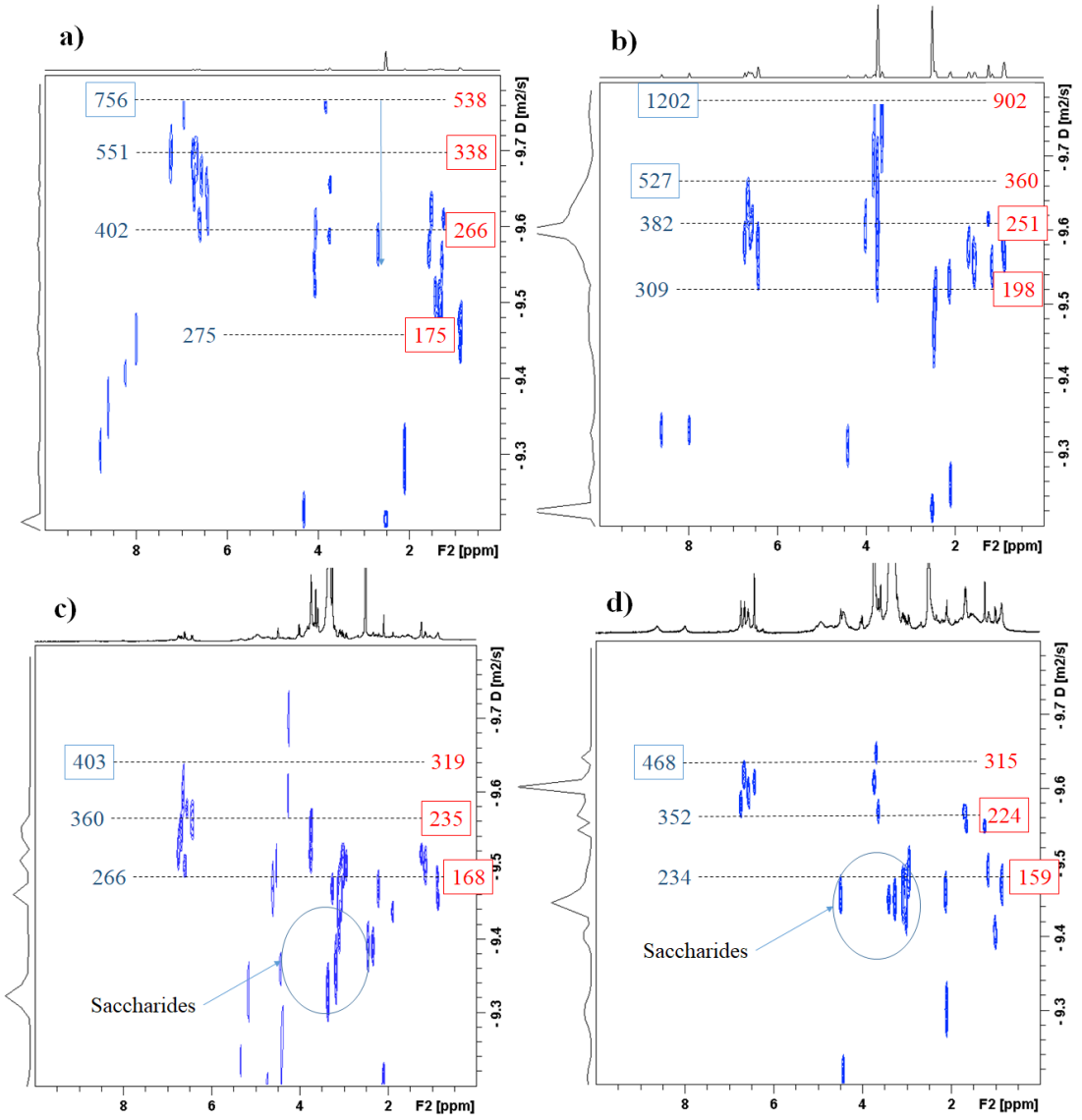

Figure 8.12. ^{1}H-DOSY NMR spectra of oils obtained at 300 °C: (a) Exp.#2, BSO without Pd/C; (b) Exp.#4, BSO with Pd/C; (c) Exp.#9, MSO without Pd/C and (d) Exp.#11, MSO with Pd/C. Red and blue numbers correspond to molecular weights obtained with PEGP and PS calibration, respectively. The numbers in the boxes represent the selected value according to the corresponding calibration.

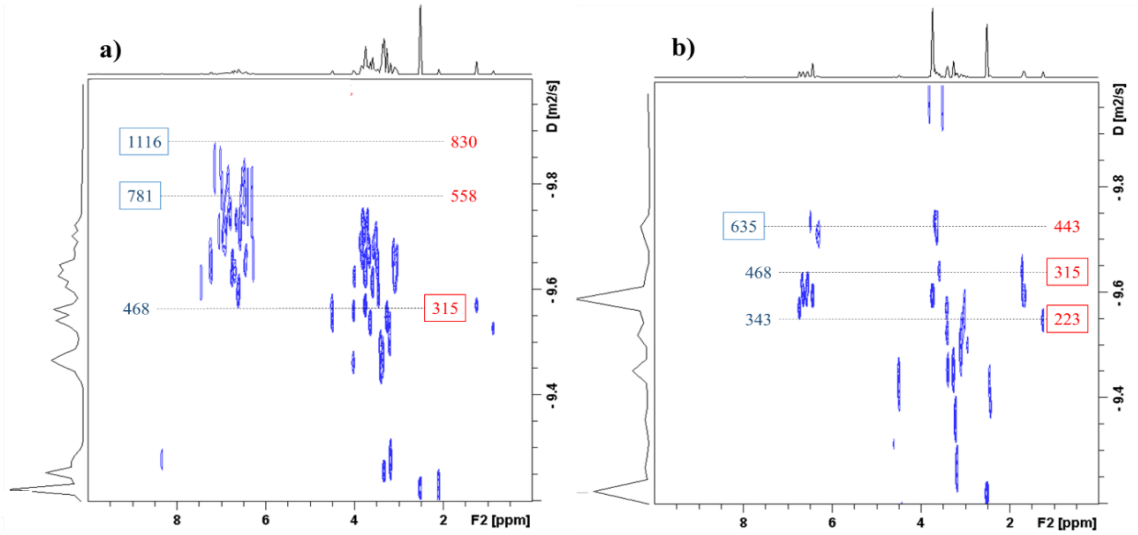

Figure 8.13. ^{1}H-DOSY NMR spectra of MSO obtained at 250 °C: (a) Exp. #8, without Pd/C and (b) Exp. #10, with Pd/C.

MSO and BSO samples were analyzed using HSQC-NMR. The main difference between these samples was the presence of intense cross signals (δ_H-δ_C) at 4.49 - 99.97 ppm, 4.24 - 101.75 ppm and 4.01 - 104.55 ppm in the HSQC spectra of MSO samples (Figure 8.14a) that were hardly detected in BSO samples (Figures 8.14b and 8.15a). The HSQC-TOCSY spectroscopy allowed unequivocally assigning these signals to anomeric carbon atoms as they presented a strong correlation with signals at 3.21 and 3.11 ppm, evidencing the presence of such saccharides or phenyl glycosides as pointed in the literature (see Figure 8.16a for Exp.#12) (Rencoret et al., 2009). The most intense cross-signal in the aliphatic region of the HSQC spectra (Figure 8.14a) corresponded in all cases to the methoxy moiety (3.71 - 55.6 ppm). Besides this signal, HSQC contour at 4.03 - 63.2 ppm in BSO samples presented a noticeable intensity (Figure 8.14b). The HSQC-TOCSY showed that this cross-signal correlated well with three alkyl signals, and therefore these signals were assigned to butyl esters, produced upon the esterification reactions occurring between the carboxylic acids (mainly acetic acid) released during the holocellulose degradation and the degraded butanol solvent. Additionally, three signals presented remarkable intensity (3.41 - 60.1 ppm, 2.50 - 31.1 ppm and 1.68 - 34.41 ppm). The HSQC-TOCSY spectroscopy could assign them to the propyl chains presented in PrOH-G and PrOH-S. Concerning the aromatic region, HSQC contours corresponding to guaiacyl, syringyl and hydroxyphenyl units could be detected as the main signals in all the experiments (Figures 8.14c and 8.14d),

showing very similar patterns for BSO and MSO samples (related with the raw material used), and assigned according to the use of literature data (Hu et al., 2012; Wen et al., 2013).

It has been shown that extrapolated time-zero ^{13}C-HSQC ($HSQC_0$) enables simultaneous quantification and identification of chemicals in metabolite mixtures (Hu et al., 2011) and recently, $HSQC_0$ has proven to be a reliable methodology for the quantitative analysis of lignin using HSQC (Sette et al., 2013). The $HSQC_0$ was carried out for both BSO and MSO (Table 8.5) using the integration of the HSQC contours cited in the literature (Hu et al., 2012; Wen et al., 2013). Regarding the relative composition of the aromatics, syringyl and guaiacyl units presented similar amounts both in BSO and MSO, with a slight increase in syringyl units in methanol-experiments (50 % in MSO vs. 44 % in BSO). Finally, even if the signals corresponding to the inter-unit linkages presented low intensity, it was tried to evaluate the amount of the most common linkages, phenylcoumarane, resinol and β-O-4. More noticeable differences were found in the inter-unit linkages. On average, 64 % of these linkages corresponded to β-O-4 moieties in the BSO mixtures, whereas only 55 % were found in the MSO, which could confirm the higher efficiency of methanol in the hydrogenolysis process of β-O-4 linkages, as was also evidenced by the results of the other characterization methods (SEC and GC/MS/FID).

Table 8.5. Quantitative $HSQC_0$ of the produced oils (MSO and BSO).

Exp.#	1	2	3	4	5,6,7	Average of BSO samples	8	9	10	11	12,13,14	Average of MSO samples
%β-O-4	64	68	62	67	62	64	52	54	62	46	62	55
% Phenylcoumarans	24	26	35	30	33	30	38	42	35	49	34	40
% Resinols	12	6	3	3	5	6	10	3	3	5	4	5
% Syringyl units	41	36	47	46	47	44	54	51	49	46	50	50
% Guaiacyl units	51	56	51	50	50	51	45	48	51	54	49	49
% Hydroxyphenyl units	3	3	0	1	0	1	1	1	0	1	0	1

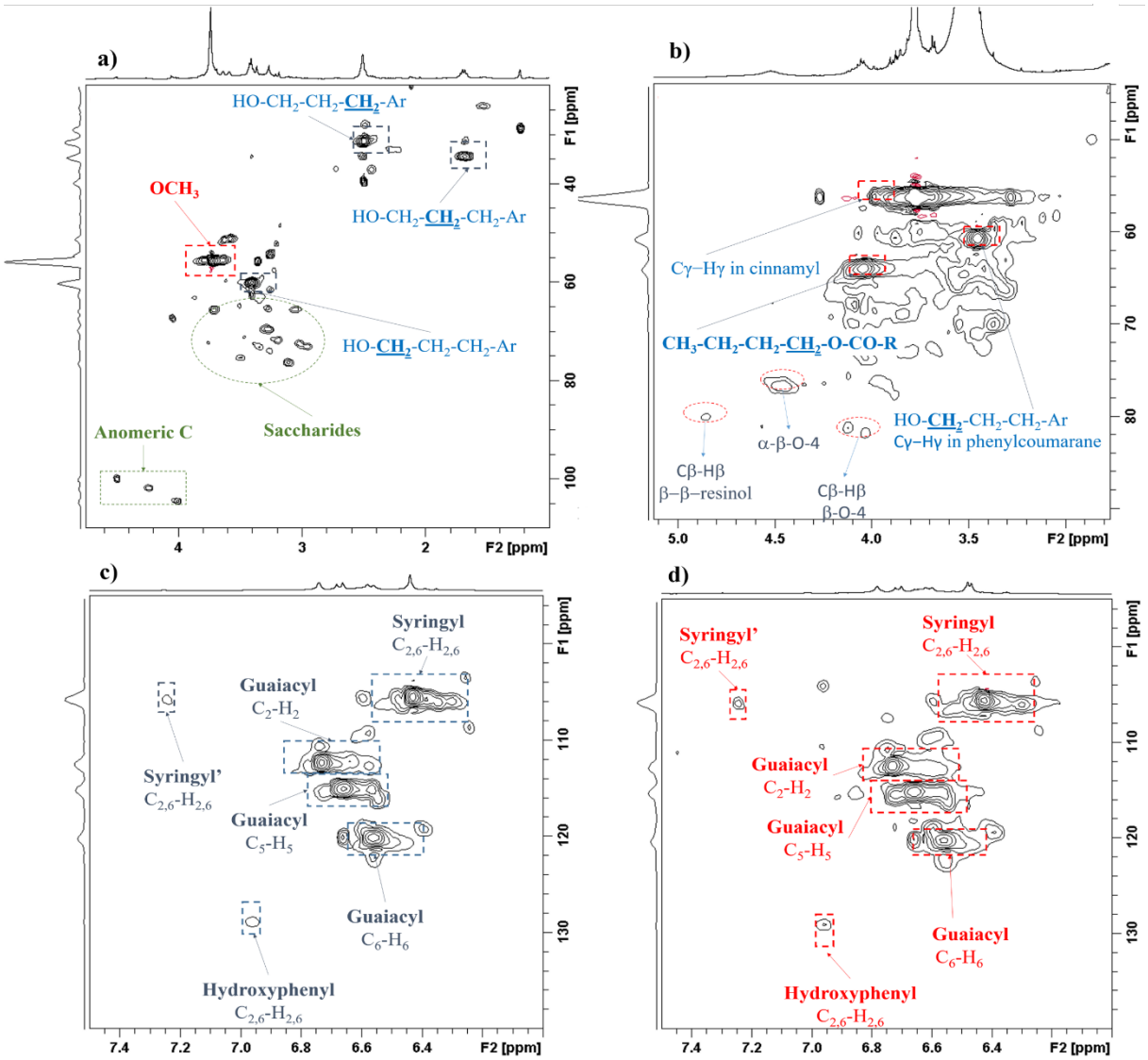

Figure 8.14. HSQC spectra in the aliphatic region of oils obtained at 275 °C, 1 g Pd/C: (a) Exp. #12, MSO; (b) Exp. #5, BSO; and HSQC spectra in the aromatic region of oils obtained at 275 °C, 1 g Pd/C: (c) Exp. #12, MSO; (d) Exp. #5, BSO. Syringyl'= oxidized syringyl unit.

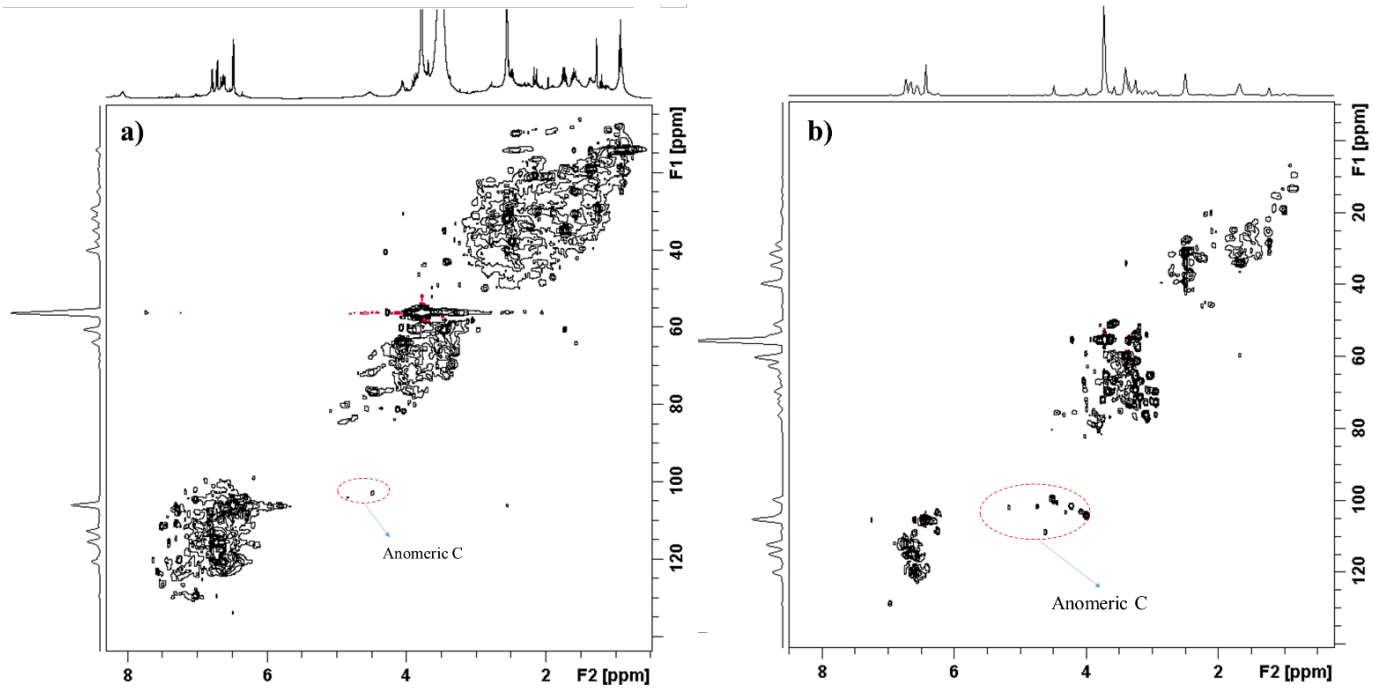

Figure 8.15. HSQC spectra for the samples obtained in: (a) Exp. #5 (BSO at 275 °C; 1g Pd/C) and (b) Exp. #11 (MSO at 300 °C; 2g Pd/C).

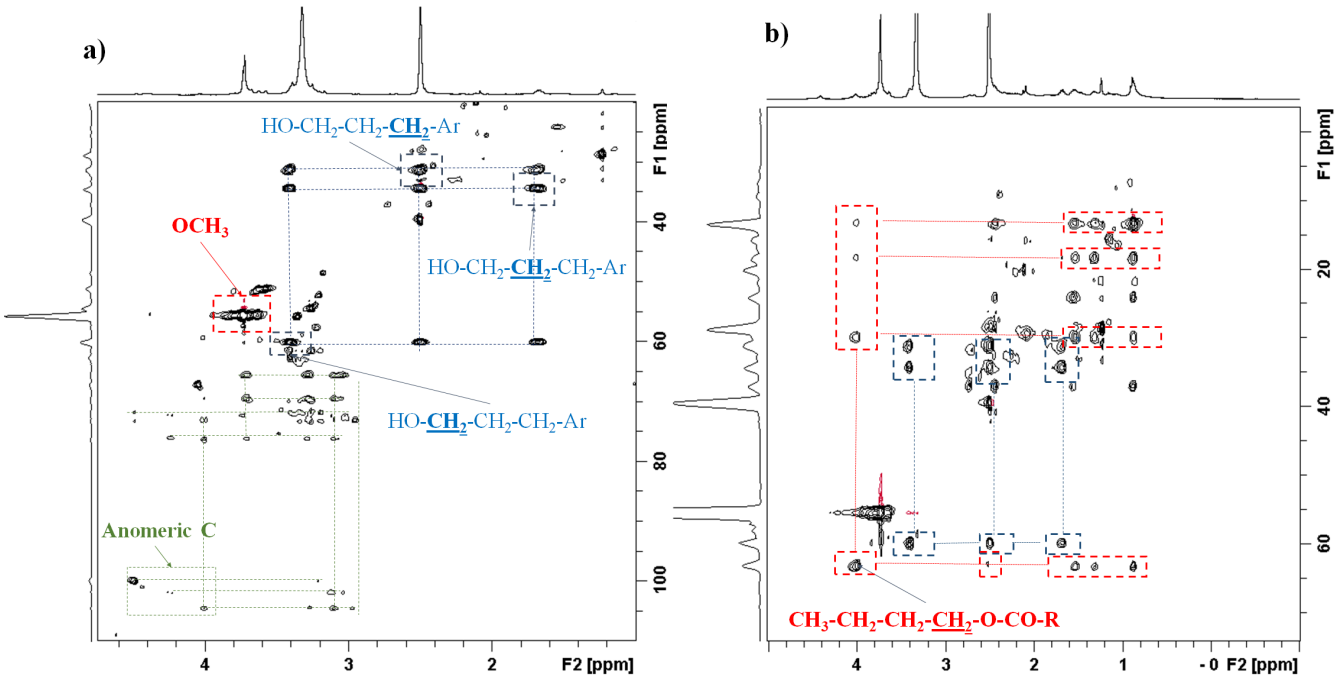

Figure 8.16. HSQC-TOCSY in the aliphatic region of oils obtained at 275 °C, 1 g Pd/C: (a) Exp.#12, MSO; (b) Exp.#5, BSO.

The ^{31}P NMR of the MSO and BSO samples provided valuable information about their content on hydroxy groups (Table 8.6 and Figure 8.17). It was observed that the

overall number of hydroxy groups was noticeably higher in the MSO samples (6.2 - 7.8 mmol/g) than in the BSO samples (2.9 - 5.3 mmol/g) obtained for all the reaction conditions, being the main difference in the content of aliphatic hydroxy groups, that was much higher in the MSO samples (0.6 - 1.9 mmol/g for BSO vs. 3.8 - 5.9 mmol/g in MSO). The presence of saccharides in the MSO, evidenced by the DOSY and HSQC spectroscopies, was the origin of this much higher amount of hydroxy groups in the MSO samples. It could also be deduced that some of these aliphatic groups corresponded to PrOH-S and PrOH-G. Indeed, the content in alkyl hydroxy groups in the MSO increased with the reaction temperature regardless of the catalyst presence (4.5 - 4.7 mmol/g for reactions at 250 °C and 5.9 mmol/g when the reaction was run at 300 °C). However, the amount of PrOH-G and PrOH-S was almost constant in catalytic reactions, which evidences that the increase in aliphatic hydroxy groups was related to more efficient solvolysis of the holocellulose fraction at higher temperatures. Aliphatic hydroxy groups in the BSO samples can be mostly ascribed to the presence of propanol side chains. Concerning the aromatic hydroxy groups, the effect of the catalyst was clearly evidenced in the BSO samples, whose content of aromatic hydroxy groups was noticeably higher in the experiments run in the presence of catalyst either at 250 °C (Exp. #1, 2.2 mmol/g; Exp.#3, 3.4 mmol/g) or 300 °C (Exp.#2, 2.3 mmol/g; Exp.#4, 3.9 mmol/g). A similar trend was observed in the MSO samples, in which the presence of the aromatic hydroxy group was higher when the reaction was run in the presence of Pd/C at 250 °C (1.8 mmol/g for Exp.#8 vs. 2.4 mmol/g for Exp.#10), whereas it remained constant at 300 °C (up to 1.9 mmol/g). On the other hand, the content of aromatic hydroxy groups was remarkably higher in the BSO samples, which could be related to the enhanced formation of catechol because of the presence of water in the reaction media.

Table 8.6. Estimated concentration of hydroxy group in MSO and BSO samples.

Exp. #	Reaction medium	T (°C)	Catalyst load (g)	Total OH/g	Aromatics (mmol/g)	Aliphatics (mmol/g)	S/G
1		250	0	3.2	2.2	1.1	1.0
2	n-	300	0	2.9	2.3	0.6	0.9
3	butanol/water	250	2	5.3	3.4	1.9	1.4
4	(1:1 vol.)	300	2	4.9	3.9	1.0	1.6
5,6,7		275	1	4.4	3.2	1.1	1.6
8		250	0	6.2	1.8	4.5	1.5
9		300	0	7.6	1.8	5.9	1.1
10	Methanol	250	2	7.1	2.4	4.7	0.8
11		300	2	7.8	1.9	5.9	1.0
12,13,14		275	1	6.2	2.5	3.8	0.8

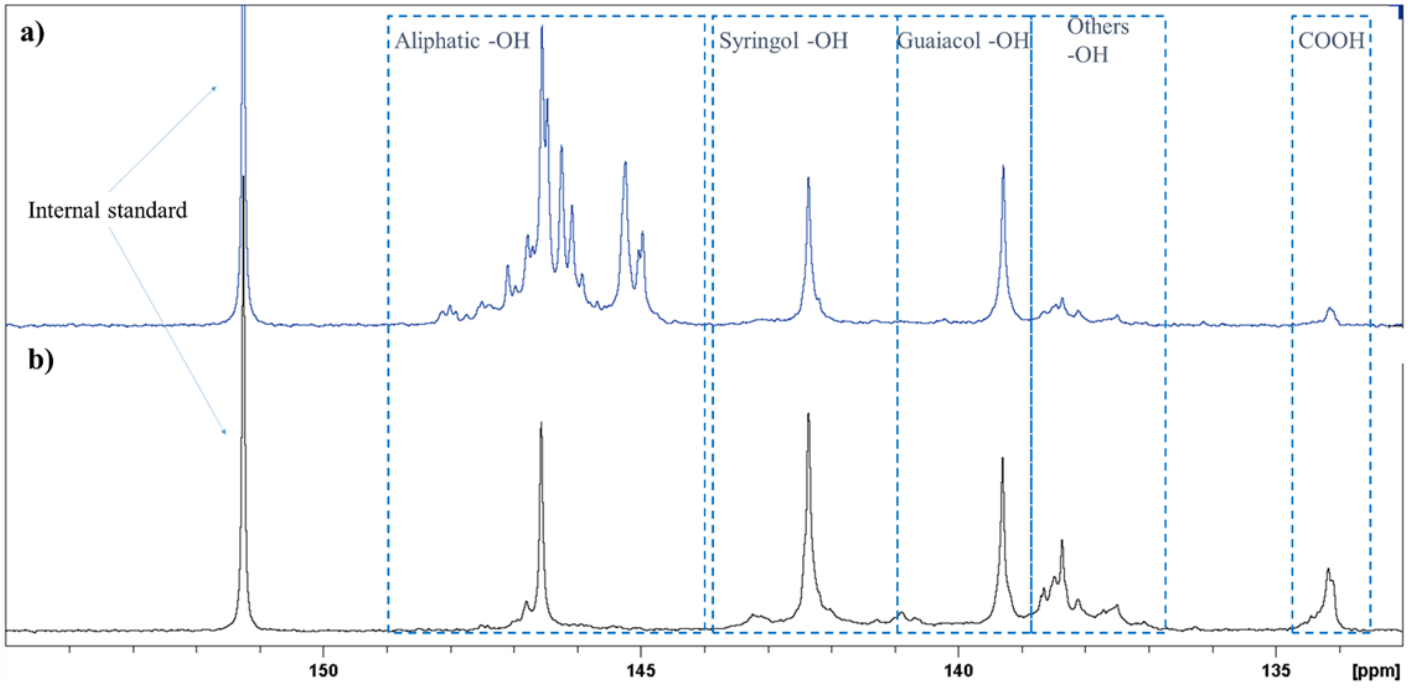

Figure 8.17. ^{31}P NMR after derivatization with TMDP of the samples obtained in: (a) Exp. #11: (MSO at 275 °C; 1g Pd/C) and (b) Exp. #4 (BSO at 300 °C; 2g Pd/C).

In short, DOSY-NMR results corroborated the trends observed in GC/MS/FID and SEC analyses concerning the effect of the treatment temperature and Pd/C addition in both reaction media. DOSY-NMR revealed that adding the catalyst or increasing the temperature in non-catalytic conditions decreased the apparent masses of the aromatic region in BSO. However, such effect of the catalyst was only observed in MSO at the lowest temperature (250 °C). DOSY-NMR indicated the presence of aliphatic compounds (diffusion traces at apparent masses lower than aromatic region) proceeding from saccharide or solvent degradation in both reaction media. In addition, this analysis indicated the presence of diffusion traces in similar apparent masses as the aromatics pointing to the aliphatic chains connected to phenolic rings (alkyl and propanyl chains). HSQC-NMR and HSQC-TOCSY also confirmed this fact.

8.3.5. FT-IR analysis of the produced oils

The FT-IR spectra of the MSO and the BSO in the whole measurement interval 4000 - 400 cm^{-1} are represented in Figure 8.18. All the signals were normalized and their baselines were corrected (Faix, 1992; Zhou et al., 2011) to easily compare the peaks particularities and intensities. Figure 8.19 focuses on the most characteristic bands in the

fingerprint region (between 1800 and 800 cm^{-1}). The peaks in the range of 1740 - 1650 cm^{-1} were more pronounced in the BSO (Figure 8.19a) than in the MSO (Figure 8.19b). This region is attributed to C=O stretch in the non-conjugated ketones and esters and C=O stretch in the conjugated acids and aldehydes of carbohydrate origin (Faix, 1992), which corroborates the results discussed in Section 8.3.2.2, as the yields of carbohydrate-derived compounds were higher when n-butanol/water was used as a solvent. At the wavenumbers corresponding to the aromatic skeletal vibrations (between 1600 and 1430 cm^{-1}) (Faix, 1992; Nandiyanto et al., 2019; Zhou et al., 2011), all the oil samples produced in both media showed significant peaks with slight differences in their intensities. At wavenumbers of 1516, 1460 and 1429 cm^{-1}, a slight increase in the intensities of the peaks could be seen when the Pd/C catalyst was used. These peaks could also be related with C-H deformation (-CH_3 and –CH_2-) (Faix, 1992). This could be explained by the higher content of alkyl-G in the catalytic pathway, while S and G were most abundant in the non-catalytic samples. In the region between 1400 and 1300 cm^{-1}, no clear peaks were observed in the samples obtained in n-butanol/water-experiments, contrary to those from methanol-experiments, in which two significant peaks appeared at 1360 and 1330 cm^{-1}, which in the literature were related to aliphatic C-H stretch, phenolic-OH, and the condensed C-C in S and G units (Coates, 2006; Faix, 1992). This finding corroborates the higher selectivity to PrOH-G and PrOH-S observed in methanol-experiments.

The most important difference between the two media was found in the 1112 - 1030 cm^{-1} region. The peak intensity observed at 1112 cm^{-1}, assigned to C-H in-plane deformation typical for S units and to secondary alcohols, increased when Pd/C was used in both media (at 250 and 275 °C), which agrees with the higher PrOH-S yield found in such samples. In addition, two lower intensity peaks at wavenumber between 830 and 800 cm^{-1} appeared when Pd/C was added. These peaks could be assigned to the vibration of the hydrogen atoms in positions 2, 5 and 6 in the benzene ring (especially in the G unit) (Faix, 1992).

Finally, in the region corresponding to O-H stretching (from 3600 to 3000 cm^{-1}), higher intensity peaks were observed in the catalytic pathway with methanol, while more pronounced ones were observed at 3000 - 2800 cm^{-1} (aliphatic C-H stretching) in the catalytic pathway with n-butanol/water (Figure 8.18). This fact could be explained by the alkyl radical highly present in the catalytic BSO vs. propanol radicals in the MSO.

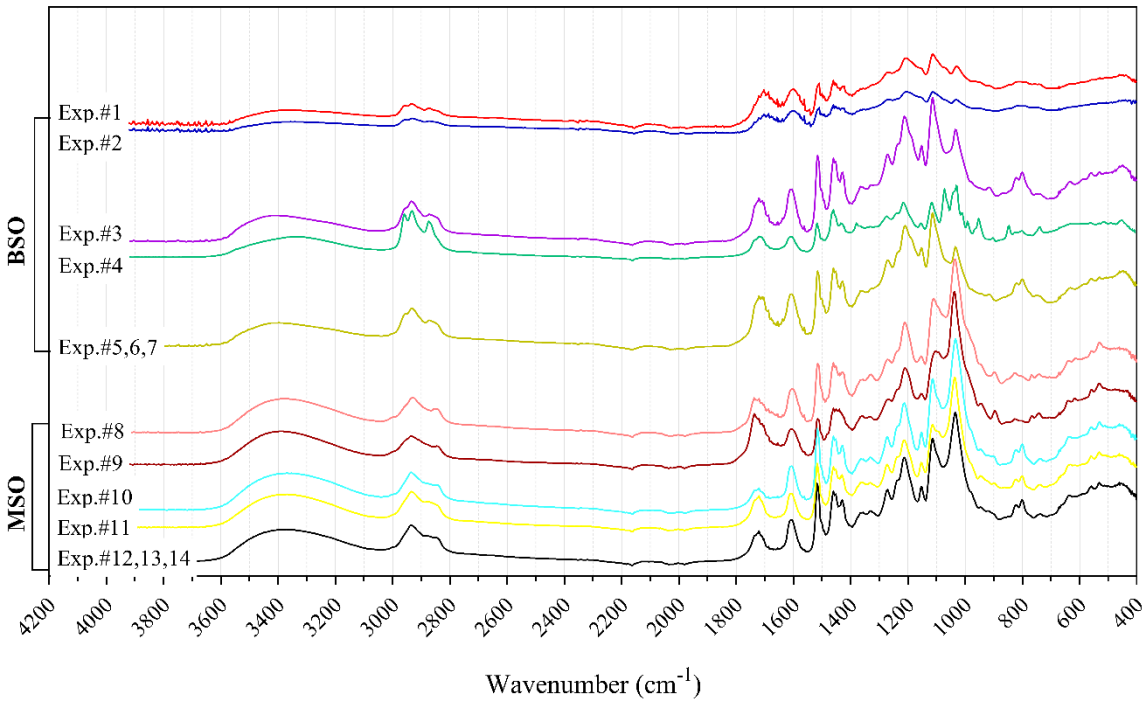

Figure 8.18. Entire FT-IR spectra from 4000 to 400 cm^{-1} of BSO and MSO samples prepared at different operational conditions.

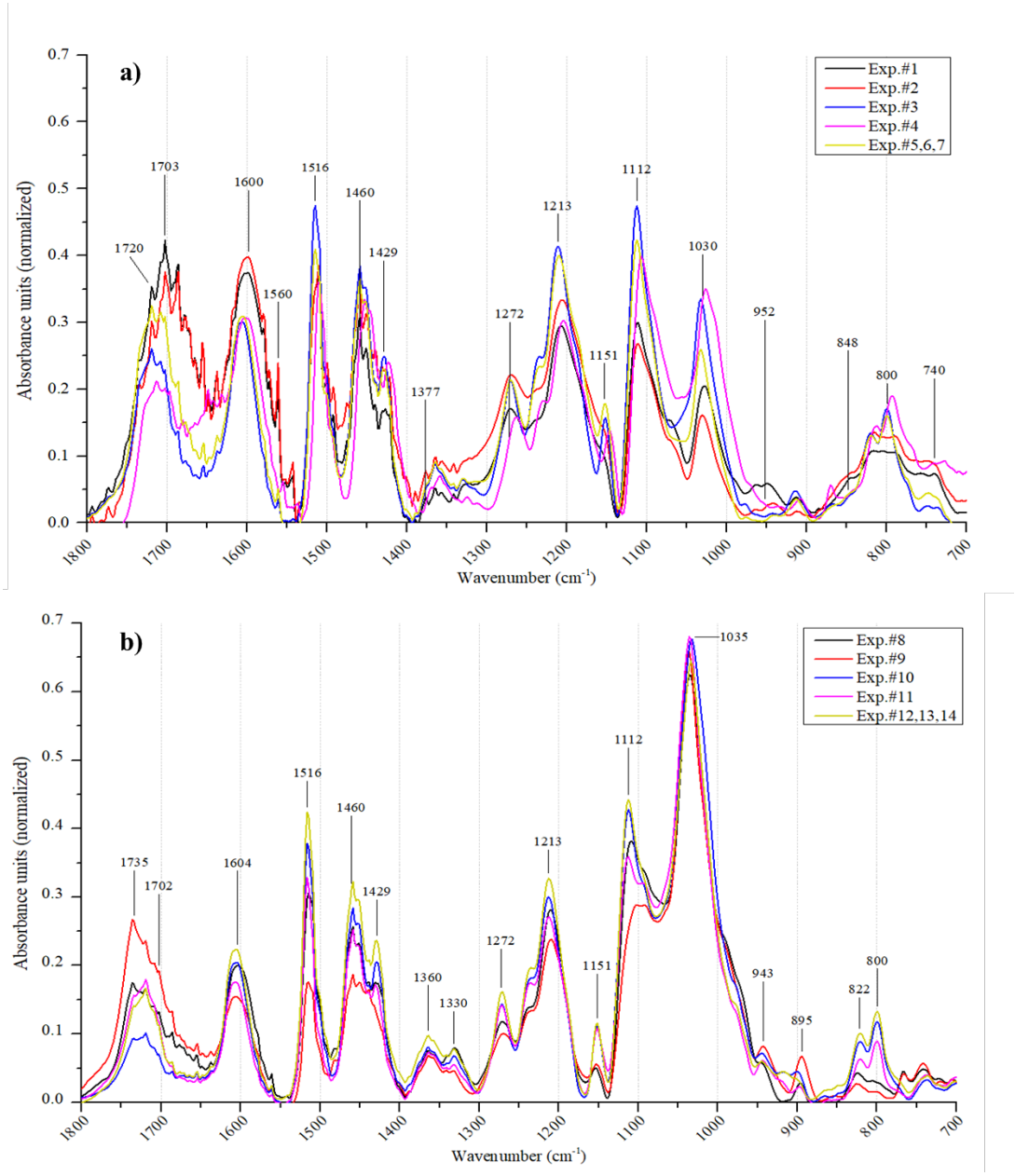

Figure 8.19. Detailed FT-IR spectra of: (a) BSO samples and (b) MSO samples in the most characteristic fingerprint region.

8.4. Conclusions

The reductive catalytic fractionation of argan shells was studied at different temperatures using methanol and n-butanol/water as solvents and Pd/C as a catalyst to evaluate the performance of this unexplored biomass. The main conclusions drawn from this study are the following:

– The solvent nature, the catalyst load (0, 1 or 2 g) and the temperature significantly impacted the products distribution and their characteristics.

– Less solid remained after the RCF process when using the mixture of n-butanol/water (from 3 to 21 wt.%) compared to the use of methanol (from 11 to 67 wt.%), while the Pd/C catalyst was quite effective in producing more gas in both reaction media.

– Lower operating temperatures are recommended (<250 °C) when using the mixture of n-butanol/water; as for the lignin-first concept, the carbohydrate pulp from biomass should be preserved, while this fraction was severely affected under the tested conditions.

– The production of lignin-derived oil, which is the main interest product, was enhanced with the use of the catalyst Pd/C, obtaining a yield of phenolic monomers up to 49 wt.% over the lignin content when using methanol as reaction medium and up to 48 wt.% when using the mixture n-butanol/water. Methanol performance was better in terms of selectivity (4-n-propanolguaiacol and 4-n-propanolsyringol) and lower molecular weights (narrower size distributions and lower values of M_w).

– Complementary and corroborating results from the different characterization techniques (GC/MS/FID, SEC, NMR, and FTIR) were obtained, indicating the efficiency of the Pd/C catalyst in stabilizing the produced aromatic monomers and preventing repolymerization reactions. This thorough characterization may pave the way for further utilization of the phenolic and polyphenolic fractions obtained from argan shells.

Conclusions and future work

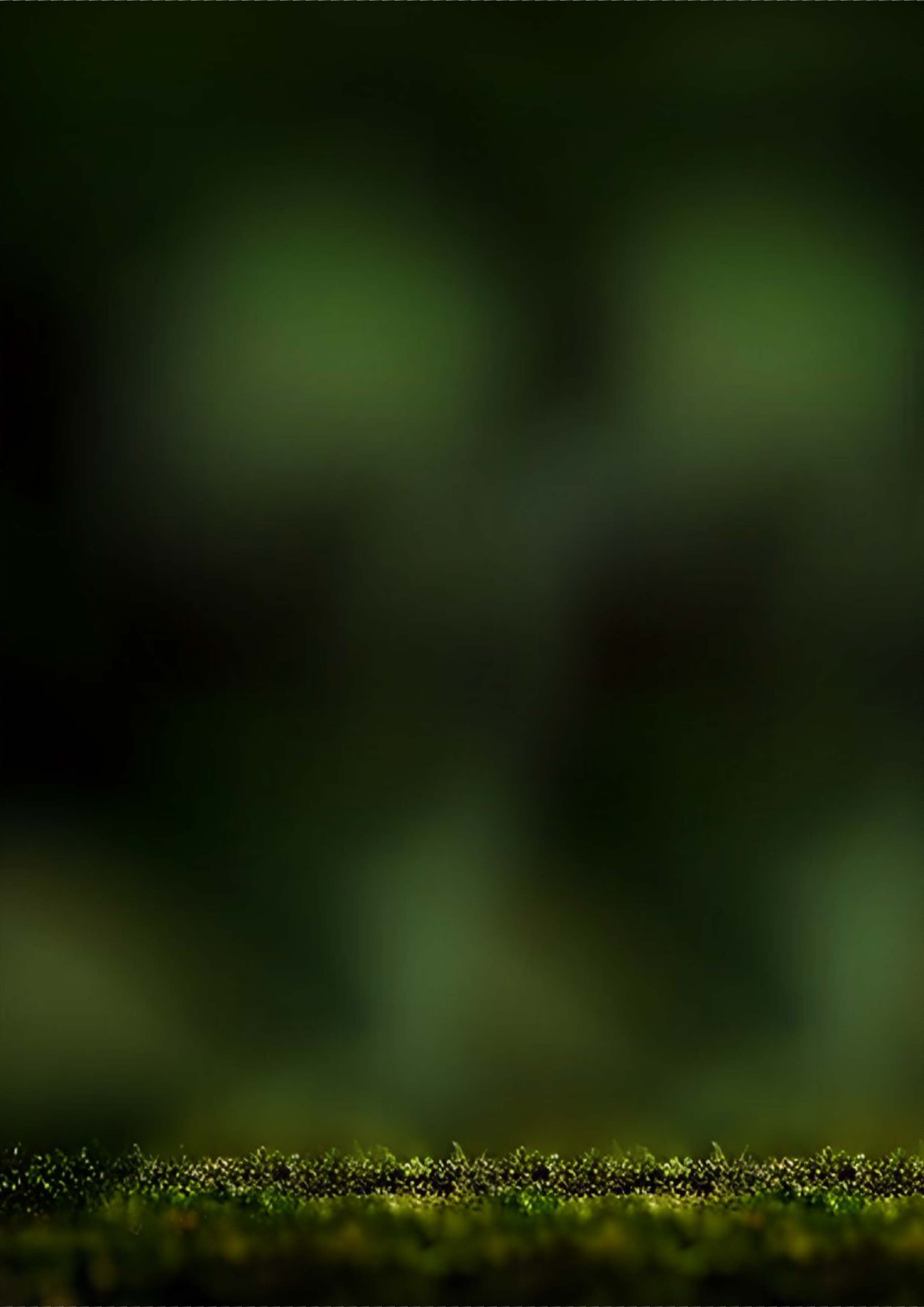

SUMMARY, CONCLUSIONS AND FUTURE WORK

In the present thesis, the valorization of argan shells (agricultural waste scarcely studied in the literature) via thermochemical processes has been experimentally investigated to evaluate the feasibility of obtaining different added-value outputs, including bio-oil, syngas, biochar and chemicals. Besides analyzing the effect of important operational factors in the different processes, some of them were combined together to study the potential of a pre/post-treatment to enhance the yield and the quality of the desirable products.

Torrefaction of argan shells to upgrade the properties of the solid as fuel:

The torrefaction treatment could be an interesting option to valorize argan shells, especially in the case of using the torrefied solid as fuel. The torrefied argan shells attained a significant increase in the higher heating value (> 45 %), as well as in the fixed carbon content, that was triplicated after the torrefaction. Other important changes in the composition of the solid were the reduction, by more than half, of the O/C ratio due to the total elimination of hemicellulose, releasing water, CO_2 and some oxygenated organic compounds. Concerning the physical properties, the hardness of argan shells, which is one of the critical points for safe use in traditional combustion furnaces, was significantly reduced after torrefaction.

Another interesting observation of the torrefaction study was that the behavior of biomass materials with a similar elemental analysis and the same energy content (as is the case of argan shells and forest pine residues) might show significant differences in the distribution and characteristics of the torrefaction products. This is principally attributed to important differences in the distribution of the main macro-components of biomass (cellulose, hemicellulose and lignin), which strongly affects the thermal behavior of biomass.

Gasification of argan shells and torrefied argan shells to produce syngas:

Gasification appears as another interesting pathway for converting argan shells into syngas. Regarding product distribution, the gasification of the raw argan shells led to a low char yield (2 wt.%) and a high carbon conversion to gas phase (97 - 100 %). The gas production was up to 1.1 m^3_{STP}/kg of solid (N_2-free basis) with a calorific value of around 4.7 MJ/m^3_{STP}, that is to say, with an energy content suitable for use in boilers or turbines, although for the latter case, the main limitation would be the tar content (0.7 g/m^3_{STP}).

Adding steam as a gasifying agent did not affect the gas production or its LHV, but improved the H_2/CO ratio (up to 0.9) and slightly decreased the tar content (0.6 g/m^3_{STP}). However, these values are still unsuitable for the direct use of gas in the main chemical synthesis routes in which it could be involved, so posterior stages of gas conditioning would be necessary.

Comparing the gasification of argan shells with forest pine residues, slightly higher char formation and lower carbon conversion to gas phase were obtained in the case of pine residues. The gas production was similar for both materials (1 -1.1 m^3_{STP}/kg of solid), while the H_2/CO ratio of the syngas was higher (0.8 - 1) and the LHV was slightly lower in the case of pine residues gasification.

Torrefaction, as a pretreatment stage, was not favorable for improving the syngas yield or its quality, as the torrefied material was less reactive, leading to a higher char formation (10 wt.%) and lower conversion of carbon to the gas phase (79 %). The LHV of the gas was noticeably reduced to 3.6 MJ/m^3_{STP} for the torrefied solid. The only improvement observed, using the torrefaction as a pretreatment, was the tar reduction when gasifying using steam (0.7 g/m^3_{STP} for the raw argan shells vs. 0.3 g/m^3_{STP} for the torrefied argan shells).

Pyrolysis of argan shells and bio-oil and biochar applications:

For the studied operational conditions (350-550 °C, fixed bed reactor, heating rate of 10 °C/min approximately), the pyrolysis of argan shells led to biochar yields in the range of 28 - 34 wt.%, gas yields around 14 wt.% and bio-oil yields higher than 50 wt.%. This product distribution was hardly affected by the final operating temperature because most of the material decomposition occurred in the common heating range of up to 350 °C. Comparing the pyrolysis of argan shells with the pyrolysis of wheat straw, the main difference observed was the greater tendency to generate gaseous compounds in the case of wheat straw.

Regarding the applications of the products obtained in the pyrolysis of argan shells, the potential use of bio-oil as a source of antioxidant additives (due to its content in phenolic compounds) was studied. The bio-oil was extracted with an organic solvent (isopropyl acetate), and the extracted fraction showed a phenolic monomer concentration of 53-63 wt.%. Incorporating a small dosage (< 1 wt.%) of this extracted fraction into biodiesel improved its oxidation stability by about 300 %. Neither the pyrolysis

temperature nor a subsequent bio-oil treatment (hydrothermal treatment) significantly affected the antioxidant behavior of the fraction extracted from bio-oil.

The solid product in the pyrolysis of argan shells (biochar) underwent a physical activation process (with CO_2) to achieve a high-quality adsorbent material. The activated carbon obtained was characterized by a slightly alkaline pH, a high fixed carbon content (95 wt.%) and a low ash content (less than 2 wt.%). Concerning its textural properties, the best results were obtained for the material produced after the longest activation time, 150 min (BET surface of 1544 m^2/g and average pore volume of 0.6 cm^3/g). This solid also showed good behavior in the adsorption of pollutants present in aqueous solutions (different phenols and methylene blue), as well as in the retention of CO_2.

Hydrothermal treatment of lignin extracted from argan shells to produce antioxidant additives:

The lignin contained in the argan shells was extracted through semi-chemical pulping and processed by hydrothermal treatment to carry out its depolymerization and obtain phenolic compounds with antioxidant properties. The liquid product of the process was extracted with an organic solvent (isopropyl acetate). Small doses of this extracted fraction (< 1 wt.%) were blended with biodiesel, whose oxidation stability improved significantly by up to 400 %. The best antioxidant additives were obtained when lignin depolymerization was carried out at 300 °C, regardless of the reaction medium (N_2, H_2, CO_2 or HCOOH). These additives were mainly characterized by an important catechol content and some of its derivatives, whose antioxidant properties are known. One of the main limitations of this process could be its low production rate, since the additives yields ranged between 15 and 20 wt.% of the processed lignin.

Reductive catalytic fractionation of the argan shells to produce phenolic monomers:

Reductive catalytic fractionation (RCF) is a "*lignin-first approach*" strategy for bio-refineries aiming at producing depolymerized lignin with almost theoretical amounts of phenolic monomers. The RCF of the argan shells was carried out in two different reaction media (methanol and n-butanol/water) using Pd/C as a catalyst.

Methanol performance was generally better in terms of selectivity to 4-n-propanolguaiacol and 4-n-propanolsyringol, and also in terms of reducing the molecular size of the obtained phenolic compounds. In addition, using the catalyst in both reaction media led to high yields of phenolic monomers (up to 49 wt.% over lignin content). Under

the operating conditions studied (250-350 °C), the conversion of argan shells to liquid and gaseous compounds was significantly higher in the n-butanol/water reaction medium than in the case of methanol, suggesting that, to keep the carbohydrate fraction intact in the process, the operating temperature in the case of n-butanol/water should be lower. Therefore, studying a lower temperature range for this reaction medium (n-butanol/water) would be interesting.

The RCF proved to be an interesting pathway for valorizing argan shells to phenolic monomers. However, it would be interesting to continue studying the process involving cheaper catalysts and solvents, analyzing the catalyst's life cycle and possible reuse.

Future work

According to the results obtained throughout this doctoral thesis, some future work can be proposed to continue the research line and to have an overview of the most suitable technology for the valorization of argan shells that could be implemented in the areas producing the argan fruit:

– To perform a life cycle assessment (LCA) for each studied process to evaluate the overall environmental impact and identify areas for improvement, including the analysis of energy inputs and outputs, as well as possible emissions and byproducts generated by each process.

– To evaluate the scaling-up of the processes considering the LCA data, as well as a SWOT (Strengths, Weaknesses, Opportunities and Threats) analysis.

– Once the most appropriate process has been selected, the final objective would be to propose a pilot plant project to be implemented and tested on-site in one of the argan oil cooperatives in the region of Essaouira - Morocco. Therefore, establishing some training plans on the importance of recovering waste for the rural community where significant amounts of argan shells are generated would be an important task to be considered, not only for the use of the waste but also to support sustainable energy sources, create jobs and improve the quality of life of their community.

"The journey of a thousand miles begins with one step". Lao Tzu

Here is our first step...

RESUMEN Y TRABAJOS FUTUROS

En la presente tesis se ha investigado experimentalmente la valorización de las cáscaras de argán (un residuo agrícola poco estudiado a día de hoy) a través de diferentes procesos termoquímicos para evaluar la viabilidad de obtener diferentes productos, incluyendo bio-combustibles, gas de síntesis, biochar y productos químicos de valor. Además de analizar el efecto de importantes factores de operación en los diferentes procesos, algunos de ellos se combinaron para estudiar el potencial de las etapas de pre- y post-tratamiento para mejorar la calidad y el rendimiento de los productos deseados.

Torrefacción de cáscaras de argán para mejorar las propiedades combustibles del sólido:

El tratamiento de torrefacción puede ser una opción interesante para valorizar las cáscaras de argán, especialmente en el caso de usar el sólido torrefactado como combustible. Las cáscaras de argán torrefactadas experimentaron un aumento significativo (> 45 %) en el poder calorífico del sólido, así como en el contenido en carbono fijo, que se triplicó después de la torrefacción. Otros cambios importantes en la composición del sólido fueron la reducción, en más de la mitad, de la relación O/C debido a la eliminación total de la hemicelulosa, liberando agua, CO_2 y algunos alquitranes oxigenados. En cuanto a sus propiedades físicas, la dureza de las cáscaras de argán, que es uno de los puntos críticos para su uso en los hornos tradicionales de combustión, se redujo notablemente después de la torrefacción.

Otra observación interesante del estudio de torrefacción realizado fue que el comportamiento de materiales biomásicos con un análisis elemental muy similar y un mismo contenido energético (como es el caso de las cáscaras de argán y los residuos forestales de pino) pueden manifestar diferencias importantes en la distribución y las características de los productos de la torrefacción. Esto se atribuye fundamentalmente a diferencias significativas en la distribución de los principales macrocomponentes de la biomasa (celulosa, hemicelulosa y lignina), que afectan fuertemente al comportamiento térmico de la biomasa.

Gasificación de cáscaras de argán y cáscaras de argán torrefacadas para la obtención de gas de síntesis:

La gasificación es otra vía interesante para la conversión de las cáscaras de argán en gas de síntesis. En cuanto a la distribución de productos, en la gasificación de las

cáscaras de argán originales se obtuvo un bajo rendimiento a char (2 % en masa) y una alta conversión de carbono a fase gas (97 - 100 %); la producción de gas fue de aproximadamente 1,1 m^3N/kg sólido (en base libre de N_2), con un poder calorífico inferior (PCI) de alrededor de 4,7 MJ/m^3N, es decir con un contenido energético suficiente para su uso en calderas o turbinas, aunque para este último caso la principal limitación sería el contenido de alquitranes (0,7 g/m^3N). El uso de vapor de agua como agente gasificante no afectó a la producción de gas ni a su PCI, pero mejoró la relación H_2/CO (hasta valores de 0,9) y disminuyó ligeramente el contenido de alquitranes (0,6 g/m^3N). Sin embargo, estos valores siguen sin ser adecuados para el aprovechamiento directo del gas en las principales rutas de síntesis química en las que podría utilizarse, por lo que serían necesarias etapas posteriores de acondicionamiento del gas.

Al comparar la gasificación de las cáscaras de argán con la de los residuos forestales de pino, se obtuvo más char y menor conversión de carbono a fase gas en el segundo caso. La producción de gas fue similar en ambos casos (1-1.1 m^3_{STP}/kg de sólido), mientras que la relación H_2/CO en el gas fue mayor (0,8 - 1) y el PCI del gas fue ligeramente inferior en el caso de la gasificación de los residuos de pino.

La torrefacción como etapa de previa a la gasificación no fue favorable para el rendimiento ni para la calidad del gas síntesis, ya que el material torrefactado fue menos reactivo, lo que resultó en una mayor formación de char (10 % en masa) y una menor conversión de carbono a fase gas (79 %). El PCI del gas también se redujo notablemente (de 4,7 MJ/m^3N para las cáscaras originales a 3,6 MJ/m^3N para el material torrefactado). La única mejora observada al incluir la torrefacción como pretratamiento fue la reducción de los alquitranes al gasificar con vapor de agua (0,7 g/m^3N para las cáscaras originales vs. 0,3 g/m^3N para el material torrefactado).

Pirólisis de las cáscaras de argán y aplicaciones del bio-oil y el bio-char:

En las condiciones de operación estudiadas (350-550 °C, reactor de lecho fijo, calentamiento de 10 °C/min aproximadamente), la pirólisis de las cáscaras de argán condujo a rendimientos de biochar en el rango de 28 - 34 % en masa, rendimientos de gas en torno a 14 % en masa y rendimientos de bio-oil superiores a 50 % en masa. Esta distribución de productos apenas se vio afectada por la temperatura final de operación debido a que la mayor parte de la descomposición del material se produjo en el tramo de calentamiento común hasta alcanzar los 350 °C. Comparando la pirólisis de cáscaras de

argán con la pirólisis de paja de trigo, la principal diferencia observada fue la mayor tendencia a generar compuestos gaseosos en el caso de la paja de trigo.

En cuanto a las aplicaciones de los productos obtenidos en la pirólisis de las cáscaras de argán, se estudió el posible uso del bio-oil como fuente de aditivos antioxidantes (debido a su contenido en compuestos fenólicos). El bio-oil se extrajo con un disolvente orgánico (acetato de isopropilo), y la fracción extraída mostró una concentración de monómeros fenólicos de 53-63 % en masa. La incorporación a un biodiésel de una pequeña dosis de esta fracción extraída (< 1% en masa) supuso una mejora de su estabilidad a la oxidación de aproximadamente un 300 %. Ni la temperatura de pirólisis ni el hecho de someter al bio-oil a un tratamiento posterior (solvólisis con agua) tuvieron un efecto significativo en el comportamiento antioxidante de la fracción extraída del bio-oil.

El producto sólido de la pirólisis de las cáscaras de argán (biochar) se sometió a un proceso de activación física (con CO_2) para tratar de conseguir un material adsorbente de alta calidad. El carbón activo obtenido se caracterizó por tener un pH ligeramente alcalino, un alto contenido en carbono (95% en masa) y un bajo contenido en cenizas (inferior a 2 % en masa). En cuanto a sus propiedades texturales, los mejores resultados se obtuvieron para el material obtenido tras el mayor tiempo de activación, 150 min (superficie BET de 1544 m^2/g y volumen de poro de 0,6 cm^3/g). Dicho sólido mostró además un buen comportamiento en la adsorción de contaminantes presentes en disoluciones acuosas (diferentes fenoles y azul de metileno), así como en la retención de CO_2.

Tratamiento hidrotermal (solvólisis) de la lignina extraída de las cáscaras de argán para producir aditivos antioxidantes:

La lignina contenida en las cáscaras de argán se extrajo mediante pasteado semiquímico y se procesó mediante tratamiento hidrotermal con el objetivo de llevar a cabo su despolimerización y obtener compuestos fenólicos con propiedades antioxidantes. El producto líquido del proceso se extrajo con un disolvente orgánico (acetato de isopropilo). Pequeñas dosis de dicha fracción (< 1 % en masa) se mezclaron con biodiésel, cuya estabilidad a la oxidación mejoró significativamente hasta en un 400 %. Los mejores aditivos antioxidantes se obtuvieron cuando la despolimerización de la lignina se llevó a cabo a 300 °C, independientemente del medio de reacción utilizado (N_2, H_2, CO_2 ó HCOOH). Estos aditivos se caracterizaron principalmente por un

importante contenido de catecol y algunos de sus derivados, cuyas propiedades antioxidantes son conocidas. Una de las principales limitaciones de este proceso podría ser su baja tasa de producción, ya que los rendimientos a aditivo oscilaron entre un 15 y un 20 % sobre la masa de lignina procesada.

Fraccionamiento catalítico reductivo de las cáscaras de argán para producir monómeros fenólicos:

El fraccionamiento catalítico reductivo (FCR) es una estrategia en el ámbito de las biorrefinerías que busca el aprovechamiento directo de lignina contenida en la biomasa para despolimerizarla y obtener cantidades casi teóricas de monómeros fenólicos. El FCR de las cáscaras de argán se llevó a cabo en dos medios de reacción diferentes (metanol y n-butanol/agua) utilizando Pd/C como catalizador.

El uso del metanol fue mejor en términos de selectividad a 4-n-propanolguaiacol y 4-n-propanolsyringol, y también para obtener compuestos fenólicos de menor tamaño molecular. El uso del catalizador en ambos medios de reacción condujo a altos rendimientos a monómeros fenólicos (hasta 49 % en masa sobre el contenido de lignina). En las condiciones de operación estudiadas (250-350 °C), la conversión de las cáscaras de argán a productos líquidos y gaseosos fue notablemente mayor en el medio de reacción n-butanol/agua que en el caso del metanol, lo que parece indicar que, para mantener intacta la fracción de carbohidratos en el proceso, la temperatura de operación en el caso del n-butanol/agua debería ser más baja. Por lo tanto, sería interesante estudiar un intervalo inferior de temperatura para este medio de reacción (n-butanol/ agua).

El FCR demostró ser una vía interesante para la valorización de las cáscaras de argán a monómeros fenólicos. Sin embargo, sería interesante seguir estudiando el proceso involucrando catalizadores y disolventes más baratos, y analizando también el ciclo de vida del catalizador y su posible reutilización.

Trabajos futuros

De acuerdo con los resultados obtenidos a lo largo de esta tesis doctoral, se pueden proponer algunos trabajos futuros para continuar con la línea de investigación y llegar a tener una visión general de la tecnología más adecuada para la valorización de las cáscaras de argán que pudiese llegar a implementarse en las zonas productoras del fruto del argán:

– Plantear un análisis de ciclo de vida para cada proceso estudiado con el fin de evaluar el impacto ambiental global e identificar áreas de mejora; el análisis debería

incluir entradas y salidas de energía, así como posibles emisiones y subproductos generados por cada proceso.

- Evaluar la escalabilidad de los procesos teniendo en cuenta los datos del análisis de ciclo de vida, así como un análisis DAFO (Debilidades, Amenazas, Fortalezas y Oportunidades).

- Una vez seleccionado el proceso más adecuado, el objetivo final sería proponer un proyecto de planta piloto para ser implantado y probado in situ en una de las cooperativas de aceite de argán presentes en la región Essaouira de Marruecos. Para ello, establecer planes de formación para la comunidad rural donde se generan importantes cantidades de cáscaras de argán sobre la importancia de valorizar sus residuos sería un punto importante a considerar, no solo para el aprovechamiento de los residuos, sino también para apoyar las fuentes de energía sostenible, crear empleo y mejorar la calidad de vida de su comunidad.

"Un viaje de mil millas comienza con el primer paso". Lao Tzu

Aquí va nuestro primer pasito…

References

REFERENCES

Abioye, A. M., & Ani, F. N. (2015). Recent development in the production of activated carbon electrodes from agricultural waste biomass for supercapacitors: A review. Renewable and Sustainable Energy Reviews, 52, 1282-1293.

Ábrego, J., Plaza, D., Luño, F., Atienza-Martínez, M., & Gea, G. (2018). Pyrolysis of cashew nutshells: Characterization of products and energy balance. Energy, 158, 72-80.

Abu-Omar, M. M., Barta, K., Beckham, G. T., Luterbacher, J. S., Ralph, J., Rinaldi, R., Román-Leshkov, Y., Samec, J. S. M., Sels, B. F., & Wang, F. (2021). Guidelines for performing lignin-first biorefining. Energy & Environmental Science, 14(1), 262-292.

Adhikari, S., Nam, H., & Chakraborty, J. P. (2018). Chapter 8 - Conversion of solid wastes to fuels and chemicals through pyrolysis. In: T. Bhaskar, A. Pandey, S. V. Mohan, D.-J. Lee & S. K. Khanal (Eds.), Waste Biorefinery. pp. 239-263: Elsevier.

Afailal, Z., Gil-Lalaguna, N., Torrijos, M. T., Gonzalo, A., Arauzo, J., & Sánchez, J. L. (2021). Antioxidant additives produced from argan shell lignin depolymerization. Energy & Fuels, 35(21), 17149–17166.

Ahmedna, M., Marshall, W. E., & Rao, R. M. (2000). Production of granular activated carbons from select agricultural by-products and evaluation of their physical, chemical and adsorption properties. Bioresource Technology, 71(2), 113-123.

Akhtar, J., & Amin, N. A. S. (2011). A review on process conditions for optimum bio-oil yield in hydrothermal liquefaction of biomass. Renewable and Sustainable Energy Reviews, 15(3), 1615-1624.

Amen-Chen, C., Pakdel, H., & Roy, C. (2001). Production of monomeric phenols by thermochemical conversion of biomass: a review. Bioresource Technology, 79(3), 277-299.

Anderson, E. M., Katahira, R., Reed, M., Resch, M. G., Karp, E. M., Beckham, G. T., & Román-Leshkov, Y. (2016). Reductive catalytic fractionation of corn stover lignin. ACS Sustainable Chemistry & Engineering, 4(12), 6940-6950.

Asadullah, M., Adi, A. M., Suhada, N., Malek, N. H., Saringat, M. I., & Azdarpour, A. (2014). Optimization of palm kernel shell torrefaction to produce energy densified bio-coal. Energy Conversion and Management, 88, 1086-1093.

Atienza-Martínez, M., Mastral, J. F., Ábrego, J., Ceamanos, J., & Gea, G. (2015). Sewage sludge torrefaction in an auger reactor. Energy & Fuels, 29(1), 160-170.

Bajpai, P. (2016). Pretreatment of lignocellulosic biomass for biofuel production (1st ed.): Springer Singapore.

Bakhattar, I., Asbik, M., Chater, H., El Alami, K., Adnan, I., Zegaoui, O., Mouaky, A., Koukouch, A., & Benzaouak, A. (2021). Physicochemical and thermal characterization of olive pomace (biomass). Paper presented at the 9th International Renewable and Sustainable Energy Conference (IRSEC), Morocco.

Barco-Burgos, J., Carles-Bruno, J., Eicker, U., Saldana-Robles, A. L., & Alcántar-Camarena, V. (2021). Hydrogen-rich syngas production from palm kernel shells (PKS) biomass on a downdraft allothermal gasifier using steam as a gasifying agent. Energy Conversion and Management, 245, 114592.

Beauchet, R., Monteil-Rivera, F., & Lavoie, J. M. (2012). Conversion of lignin to aromatic-based chemicals (L-chems) and biofuels (L-fuels). Bioresource Technology, 121, 328-334.

Bergman, P. C. A., Boersma, A., Zwart, R., & Kiel, J. H. A. (2005). Torrefaction for biomass co-firing in existing coal-fired power stations (pp. 72). Petten, Netherlands: Energy research Centre of the Netherlands ECN

Bergman, P. C. A., & Kiel, J. H. A. (2005). Torrefaction for biomass upgrading. Paper presented at the 14th European Biomass Conference & Exhibition, Paris.

Berrueco, C., Montané, D., Matas Güell, B., & Del Alamo, G. (2014). Effect of temperature and dolomite on tar formation during gasification of torrefied biomass in a pressurized fluidized bed. Energy, 66, 849-859.

Bilbao, R., García Bacaicoa, P., & Usón, C. (1995). Gasification of almond shells for electricity production: A real case. In: P. Chartier, A. Beenackers & G. Grassi (Eds.), Biomass for energy, environment, agriculture and industry. Vol. 1-3, pp. 1819-1824.

Biswas, B., Pandey, N., Bisht, Y., Singh, R., Kumar, J., & Bhaskar, T. (2017). Pyrolysis of agricultural biomass residues: Comparative study of corn cob, wheat straw, rice straw and rice husk. Bioresource Technology, 237, 57-63.

Boehm, H.-P. (2008). Chapter 13 - Surface chemical characterization of carbons from adsorption studies. In: E. J. Bottani & J. M. D. Tascón (Eds.), Adsorption by Carbons. pp. 301-327: Elsevier Science.

Boonstra, M. (2008). A two-stage thermal modification of wood. Doctoral thesis, Doctor of Philosophy in wood science, Ghent University, Henri Poincaré University, Ghent, Belgium.

Botella, L., Bimbela, F., Martín, L., Arauzo, J., & Sánchez, J. L. (2014). Oxidation stability of biodiesel fuels and blends using the Rancimat and PetroOXY methods. Effect of 4-allyl-2,6-dimethoxyphenol and catechol as biodiesel additives on oxidation stability. Frontiers in Chemistry, 2(43).

Botella, L., Stankovikj, F., Sánchez, J. L., Gonzalo, A., Arauzo, J., & Garcia-Pérez, M. (2018). Bio-oil hydrotreatment for enhancing solubility in biodiesel and the oxydation stability of resulting blends. Frontiers in chemistry, 6, 83-83.

Boujibar, O., Ghosh, A., Achak, O., Chafik, T., & Ghamouss, F. (2019). A high energy storage supercapacitor based on nanoporous activated carbon electrode made from Argan shells with excellent ion transport in aqueous and non-aqueous electrolytes. Journal of Energy Storage, 26, 100958.

Boujibar, O., Souikny, A., Ghamouss, F., Achak, O., Dahbi, M., & Chafik, T. (2018). CO2 capture using N-containing nanoporous activated carbon obtained from argan fruit shells. Journal of Environmental Chemical Engineering, 6(2), 1995-2002.

Brachi, P., Riianova, E., Miccio, M., Miccio, F., Ruoppolo, G., & Chirone, R. (2017). Valorization of sugar beet pulp via torrefaction with a focus on the effect of the preliminary extraction of pectins. Energy & Fuels, 31(9), 9595-9604.

Brienza, F., Van Aelst, K., Devred, F., Magnin, D., Sels, B. F., Gerin, P. A., Cybulska, I., & Debecker, D. P. (2022). Reductive catalytic fractionation of wheat straw biomass. ACS Sustainable Chemistry & Engineering, 10(34), 11130–11142.

Brown, R. C., & Brown, T. R. (2014a). Biorenewable resources : Engineering new products from agriculture (2nd ed.). Iowa state: John Wiley & sons, Inc.

Brown, R. C., & Brown, T. R. (2014b). Chapter 8 - Thermochemical processing of lignocellulosic biomass. In: W. Blackwell (Ed.), Biorenewable Resources: Engineering New Products from Agriculture. Second ed., pp. 195-236. Iowa state: John Wiley & sons, Inc.

Brueckner, T. M., Pickup, P. G., & Hawboldt, K. A. (2020). Improvement of bark pyrolysis oil and value added chemical recovery by pervaporation. Fuel Processing Technology, 199, 106292.

Cao, L., Yu, I. K. M., Liu, Y., Ruan, X., Tsang, D. C. W., Hunt, A. J., Ok, Y. S., Song, H., & Zhang, S. (2018). Lignin valorization for the production of renewable chemicals: State-of-the-art review and future prospects. Bioresource Technology, 269, 465-475.

Cerone, N., Zimbardi, F., Contuzzi, L., Baleta, J., Cerinski, D., & Skvorčinskienė, R. (2020). Experimental investigation of syngas composition variation along updraft fixed bed gasifier. Energy Conversion and Management, 221, 113116.

Cerone, N., Zimbardi, F., Villone, A., Strjiugas, N., & Kiyikci, E. G. (2016). Gasification of wood and torrefied wood with air, oxygen, and steam in a fixed-bed pilot plant. Energy & Fuels, 30(5), 4034-4043.

Coates, J. (2006). Interpretation of infrared spectra, A practical approach. Encyclopedia of Analytical Chemistry.

Cornejo, A., Bimbela, F., Moreira, R., Hablich, K., García-Yoldi, Í., Maisterra, M., Portugal, A., Gandía, L. M., & Martínez-Merino, V. (2020a). Production of aromatic compounds by catalytic depolymerization of technical and downstream biorefinery lignins. Biomolecules, 10(9), 1338.

Cornejo, A., García-Yoldi, Í., Alegria-Dallo, I., Galilea-Gonzalo, R., Hablich, K., Sánchez, D., Otazu, E., Funcia, I., Gil, M. J., & Martínez-Merino, V. (2020b). Systematic Diffusion-Ordered Spectroscopy for the selective determination of molecular weight in real lignins and fractions arising from base-catalyzed depolymerization reaction mixtures. ACS Sustainable Chemistry & Engineering, 8(23), 8638-8647.

Couhert, C., Salvador, S., & Commandré, J.-M. (2009). Impact of torrefaction on syngas production from wood. Fuel, 88(11), 2286–2290.

Cui, K., Yang, L., Ma, Z., Yan, F., Wu, K., Sang, Y., Chen, H., & Li, Y. (2017). Selective conversion of guaiacol to substituted alkylphenols in supercritical ethanol over MoO3. Applied Catalysis B: Environmental, 219, 592-602.

Chandra, T., & Zebrowski, J. P. (2016). Hazards associated with laboratory scale hydrogenations. Journal of Chemical Health and Safety, 23(4), 16-25.

Chandrasekaran, S. R., Murali, D., Marley, K. A., Larson, R. A., Doll, K. M., Moser, B. R., Scott, J., & Sharma, B. K. (2016). Antioxidants from slow pyrolysis bio-oil of birch wood: Application for biodiesel and biobased lubricants. ACS Sustainable Chemistry & Engineering, 4(3), 1414-1421.

Charrouf, Z., & Guillaume, D. (1999). Ethnoeconomical, ethnomedical, and phytochemical study of Argania spinosa (L.) Skeels. Journal of Ethnopharmacology, 67(1), 7-14.

Charrouf, Z., & Guillaume, D. (2008). Argan oil: Occurrence, composition and impact on human health. European Journal of Lipid Science and Technology, 110(7), 632-636.

Chen, D., Gao, A., Cen, K., Zhang, J., Cao, X., & Ma, Z. (2018). Investigation of biomass torrefaction based on three major components: Hemicellulose, cellulose, and lignin. Energy Conversion and Management, 169, 228-237.

Chen, W.-H., Chen, C.-J., Hung, C.-I., Shen, C.-H., & Hsu, H.-W. (2013). A comparison of gasification phenomena among raw biomass, torrefied biomass and coal in an entrained-flow reactor. Applied Energy, 112, 421-430.

Chiaramonti, D., Oasmaa, A., & Solantausta, Y. (2007). Power generation using fast pyrolysis liquids from biomass. Renewable and Sustainable Energy Reviews, 11(6), 1056-1086.

Da Costa Sousa, L., Jin, M., Chundawat, S. P. S., Bokade, V., Tang, X., Azarpira, A., Lu, F., Avci, U., Humpula, J., Uppugundla, N., Gunawan, C., Pattathil, S., Cheh, A. M., Kothari, N., Kumar, R., Ralph, J., Hahn, M. G., Wyman, C. E., Singh, S., Simmons, B. A., Dale, B. E., & Balan, V. (2016). Next-generation ammonia pretreatment enhances cellulosic biofuel production. Energy & Environmental Science, 9(4), 1215-1223.

Dahbi, M., Kiso, M., Kubota, K., Horiba, T., Chafik, T., Hida, K., Matsuyama, T., & Komaba, S. (2017). Synthesis of hard carbon from argan shells for Na-ion batteries. Journal of Materials Chemistry A, 5(20), 9917-9928.

Davoudzadeh, F., Smith, B., Avni, E., & Coughlin, R. W. (1985). Depolymerization of lignin at low pressure using lewis acid catalysts and under high pressure using H2 donor solvents. Holzforschung, 39(3), 159 -166.

Dayton, D. C., Turk, B., & Gupta, R. (2019). Chapter 5 - Syngas cleanup, conditioning, and utilization. In: R. C. Brown (Ed.), Thermochemical Processing of Biomass: Conversion into Fuels, Chemicals and Power. Second ed., pp. 125-174.

Demirbaş, A. (2000). Mechanisms of liquefaction and pyrolysis reactions of biomass. Energy Conversion and Management, 41(6), 633-646.

Demirbaş, A. (2002). Fuel characteristics of olive husk and walnut, hazelnut, sunflower, and almond shells. Energy Sources, 24(3), 215-221.

Demirbaş, A. (2005). Pyrolysis of ground beech wood in irregular heating rate conditions. Journal of Analytical and Applied Pyrolysis, 73(1), 39-43.

Demirbaş, A. (2006). Effect of temperature on pyrolysis products from four nut shells. Journal of Analytical and Applied Pyrolysis, 76(1), 285-289.

Deng, F., Huang, J., Ember, E. E., Achterhold, K., Dierolf, M., Jentys, A., Liu, Y., Pfeiffer, F., & Lercher, J. A. (2021). On the mechanism of catalytic decarboxylation of carboxylic acids on Carbon-supported Palladium hydride. ACS Catalysis, 11(23), 14625-14634.

Devi, L., Ptasinski, K. J., & Janssen, F. J. J. G. (2005). Pretreated olivine as tar removal catalyst for biomass gasifiers: investigation using naphthalene as model biomass tar. Fuel Processing Technology, 86(6), 707-730.

Dogru, M., Malik, A. A., Howarth, C. R., & Olgun, H. (1999). Use of bio-nut shells for gasification. Paper presented at the 4th Biomass Conference of the Americas: A Growth Opportunity in Green Energy and Value-added Products, Oakland.

Domingos, A. K., Saad, E. B., Vechiatto, W. W. D., Wilhelm, H. M., & Ramos, L. P. (2007). The influence of BHA, BHT and TBHQ on the oxidation stability of soybean oil ethyl esters (biodiesel). Journal of the Brazilian Chemical Society, 18, 416-423.

Dorado, J., Claassen, F. W., van Beek, T. A., Lenon, G., Wijnberg, J. B. P. A., & Sierra-Alvarez, R. (2000). Elimination and detoxification of softwood extractives by white-rot fungi. Journal of Biotechnology, 80(3), 231-240.

Effendi, A., Gerhauser, H., & Bridgwater, A. V. (2008). Production of renewable phenolic resins by thermochemical conversion of biomass: A review. Renewable and Sustainable Energy Reviews, 12(8), 2092-2116.

Ekpete, O. A., Marcus, A. C., & Osi, V. (2017). Preparation and characterization of activated carbon obtained from Plantain (Musa paradisiaca) fruit stem. Journal of Chemistry, 2017, 8635615.

Elgarahy, A. M., Hammad, A., El-Sherif, D. M., Abouzid, M., Gaballah, M. S., & Elwakeel, K. Z. (2021). Thermochemical conversion strategies of biomass to biofuels, techno-economic and bibliometric analysis: A conceptual review. Journal of Environmental Chemical Engineering, 9(6), 106503.

Elmouwahidi, A., Zapata-Benabithe, Z., Carrasco-Marín, F., & Moreno-Castilla, C. (2012). Activated carbons from KOH-activation of argan (Argania spinosa) seed shells as supercapacitor electrodes. Bioresource Technology, 111, 185-190.

Ennaciri, K., Baçaoui, A., Sergent, M., & Yaacoubi, A. (2014). Application of fractional factorial and Doehlert designs for optimizing the preparation of activated carbons from Argan shells. Chemometrics and Intelligent Laboratory Systems, 139, 48-57.

Erdocia, X., Prado, R., Corcuera, M. Á., & Labidi, J. (2014). Base catalyzed depolymerization of lignin: Influence of organosolv lignin nature. Biomass and Bioenergy, 66, 379-386.

Faix, O. (1992). Chapter 4 - Fourier Transform Infrared Spectroscopy. In: S. Y. Lin & C. W. Dence (Eds.), Methods in Lignin Chemistry. pp. 83-109. Berlin, Heidelberg: Springer.

Faouzi, H. (2012). Impact des coopératives féminines sur la préservation et la valorisation de l'arganeraie : cas de la coopérative Tafyoucht (confédération des Ait Baamrane, Anti-Atlas, Maroc). Confins, 14.

Feldman, H. F., Paisley, M. A., Folsom, D. W., & Kim, B. C. (1981). Conversion of forest residues to a methane-rich gas in a high-throughput gasifier (Vol. 83, pp. 13601). Springfield, Virginia: Pacific Northwest Laboratory, U.S. Department of Energy

Fernández-Carrasco, L., Torrens-Martín, D., Morales, L., & Martínez-Ramírez, S. (2012). Infrared spectroscopy in the analysis of building and construction materials Infrared Spectroscopy - Materials Science. Engineering and Technology. IntechOpen.

Fernández Llorente, M. J., Escalada Cuadrado, R., Murillo Laplaza, J. M., & Carrasco García, J. E. (2006). Combustion in bubbling fluidised bed with bed material of limestone to reduce the biomass ash agglomeration and sintering. Fuel, 85(14), 2081-2092.

Fernandez, M. P., Watson, P. A., & Breuil, C. (2001). Gas chromatography–mass spectrometry method for the simultaneous determination of wood extractive compounds in quaking aspen. Journal of Chromatography A, 922(1), 225-233.

Ferrini, P., Chesi, C., Parkin, N., & Rinaldi, R. (2017). Effect of methanol in controlling defunctionalization of the propyl side chain of phenolics from catalytic upstream biorefining. Faraday Discussions, 202(0), 403-413.

Ferrini, P., & Rinaldi, R. (2014). Catalytic biorefining of plant biomass to non-pyrolytic lignin bio-oil and carbohydrates through hydrogen transfer reactions. Angewandte Chemie International Edition, 53(33), 8634-8639.

Fisher, E. M., Dupont, C., Darvell, L. I., Commandré, J. M., Saddawi, A., Jones, J. M., Grateau, M., Nocquet, T., & Salvador, S. (2012). Combustion and gasification characteristics of chars from raw and torrefied biomass. Bioresource Technology, 119, 157-165.

Focke, W. W., Westhuizen, I. v. d., Grobler, A. B. L., Nshoane, K. T., Reddy, J. K., & Luyt, A. S. (2012). The effect of synthetic antioxidants on the oxidative stability of biodiesel. Fuel, 94, 227-233.

Fonts, I., Atienza-Martínez, M., Carstensen, H.-H., Benés, M., Pinheiro Pires, A. P., Garcia-Perez, M., & Bilbao, R. (2021). Thermodynamic and physical property estimation of compounds derived from the fast pyrolysis of lignocellulosic materials. Energy & Fuels, 35(21), 17114-17137.

Fulmer, G. R., Miller, A. J. M., Sherden, N. H., Gottlieb, H. E., Nudelman, A., Stoltz, B. M., Bercaw, J. E., & Goldberg, K. I. (2010). NMR chemical shifts of trace impurities: common laboratory solvents, organics, and gases in deuterated solvents relevant to the organometallic chemist. Organometallics, 29(9), 2176-2179.

Gabra, M., Nordin, A., Öhman, M., & Kjellström, B. (2001). Alkali retention/separation during bagasse gasification: a comparison between a fluidised bed and a cyclone gasifier. Biomass and Bioenergy, 21(6), 461-476.

García, M., Botella, L., Gil-Lalaguna, N., Arauzo, J., Gonzalo, A., & Sánchez, J. L. (2017). Antioxidants for biodiesel: Additives prepared from extracted fractions of bio-oil. Fuel Processing Technology, 156, 407-414.

Garrote, G., Domínguez, H., & Parajó, J. C. (1999). Hydrothermal processing of lignocellulosic materials. Holz als Roh- und Werkstoff, 57(3), 191-202.

Ghani, W. A. W. A. K., Rebitanim, N. Z., Salleh, M. A. M., & Alias, A. B. (2015). Chapter 51 - Carbon dioxide adsorption on coconut shell biochar. In: I. Dincer, C. O. Colpan, O. Kizilkan & M. A. Ezan (Eds.), Progress in Clean Energy. Vol. 1, pp. 683-693: Springer International Publishing.

Gil-Lalaguna, N., Bautista, A., Gonzalo, A., Sánchez, J. L., & Arauzo, J. (2017). Obtaining biodiesel antioxidant additives by hydrothermal treatment of lignocellulosic bio-oil. Fuel Processing Technology, 166, 1-7.

Gil-Lalaguna, N., Sánchez, J. L., Murillo, M. B., Rodríguez, E., & Gea, G. (2014). Air–steam gasification of sewage sludge in a fluidized bed. Influence of some operating conditions. Chemical Engineering Journal, 248, 373-382.

Gillet, S., Aguedo, M., Petitjean, L., Morais, A. R. C., Da Costa Lopes, A. M., Łukasik, R. M., & Anastas, P. T. (2017). Lignin transformations for high value applications: towards targeted modifications using green chemistry. Green Chemistry, 19(18), 4200-4233.

Girods, P., Dufour, A., Fierro, V., Rogaume, Y., Rogaume, C., Zoulalian, A., & Celzard, A. (2009). Activated carbons prepared from wood particleboard wastes: Characterisation and phenol adsorption capacities. Journal of Hazardous Materials, 166(1), 491-501.

Godin, B., Agneessens, R., Gofflot, S., Lamaudière, S., Sinnaeve, G., Gerin, P. A., & Delcarte, J. (2011). Revue bibliographique sur les méthodes d'analyse des polysaccharides structuraux des biomasses lignocellulosiques. Biotechnologie, Agronomie, Société et Environnement, 15(1), 165-182.

Gonçalves, G. d. C., Nakamura, P. K., Furtado, D. F., & Veit, M. T. (2017). Utilization of brewery residues to produces granular activated carbon and bio-oil. Journal of Cleaner Production, 168, 908-916.

Gonzalo, A., Bimbela, F., Sánchez, J. L., Labidi, J., Marín, F., & Arauzo, J. (2017). Evaluation of different agricultural residues as raw materials for pulp and paper production using a semichemical process. Journal of Cleaner Production, 156, 184-193.

Gosselink, R. J. A., Teunissen, W., van Dam, J. E. G., de Jong, E., Gellerstedt, G., Scott, E. L., & Sanders, J. P. M. (2012). Lignin depolymerisation in supercritical carbon dioxide/acetone/water fluid for the production of aromatic chemicals. Bioresource Technology, 106, 173-177.

Grigiante, M., & Antolini, D. (2014). Experimental results of mass and energy yield referred to different torrefaction pathways. Waste and Biomass Valorization, 5(1), 11-17.

Guillaume, D., & Charrouf, Z. (2011). Argan oil and other argan products: Use in dermocosmetology. European Journal of Lipid Science and Technology, 113(4), 403-408.

Gunasekar, N., Mohan, C. G., Prakash, R., & Saravana Kumar, L. (2021). Utilization of coconut shell pyrolysis oil diesel blends in a direct injection diesel engine. Materials Today: Proceedings, 45, 713-717.

Haimiao, Y., Ze, Z., Zeshen, L., & Dezhen, C. (2014). Characteristics of tar formation during cellulose, hemicellulose and lignin gasification. Fuel, 118, 250-256.

He, W., Li, G., Kong, L., Wang, H., Huang, J., & Xu, J. (2008). Application of hydrothermal reaction in resource recovery of organic wastes. Resources, Conservation and Recycling, 52(5), 691-699.

Herzog, A., Reznik, B., Chen, T., Graule, T., & Vogt, U. (2006). Structural changes in activated wood-based carbons: correlation between specific surface area and localization of molecular-sized pores. Holzforschung, 60(1), 85-92.

Hu, G., Cateto, C., Pu, Y., Samuel, R., & Ragauskas, A. J. (2012). Structural characterization of switchgrass lignin after ethanol organosolv pretreatment. Energy & Fuels, 26(1), 740-745.

Hu, K., Westler, W. M., & Markley, J. L. (2011). Simultaneous quantification and identification of individual chemicals in metabolite mixtures by two-dimensional extrapolated time-zero 1H−13C HSQC (HSQC0). Journal of the American Chemical Society, 133(6), 1662-1665.

Huang, S., Mahmood, N., Tymchyshyn, M., Yuan, Z., & Xu, C. (2014). Reductive de-polymerization of kraft lignin for chemicals and fuels using formic acid as an in-situ hydrogen source. Bioresource Technology, 171, 95-102.

Iwanow, M., Gärtner, T., Sieber, V., & König, B. (2020). Activated carbon as catalyst support: precursors, preparation, modification and characterization. Beilstein Journal of Organic Chemistry, 16, 1188-1202.

James E. Miller, Evans, L. R., Littlewolf, A. E., & Trudell, D. E. (2002). Batch microreactor studies of lignin depolymerization by bases. 2. Aqueous solvents. New Mexico, California: Sandia National Laboratories, U.S. Department of Energy

Jin, H., Capareda, S., Chang, Z., Gao, J., Xu, Y., & Zhang, J. (2014). Biochar pyrolytically produced from municipal solid wastes for aqueous As(V) removal: Adsorption property and its improvement with KOH activation. Bioresource Technology, 169, 622-629.

Kähkönen, M. P., Hopia, A. I., Vuorela, H. J., Rauha, J.-P., Pihlaja, K., Kujala, T. S., & Heinonen, M. (1999). Antioxidant activity of plant extracts containing phenolic compounds. Journal of Agricultural and Food Chemistry, 47(10), 3954-3962.

Kamal, R., Kharbach, M., Vander Heyden, Y., Doukkali, Z., Ghchime, R., Bouklouze, A., Cherrah, Y., & Alaoui, K. (2019). In vivo anti-inflammatory response and bioactive compounds' profile of polyphenolic extracts from edible Argan oil (Argania spinosa L.), obtained by two extraction methods. Journal of Food Biochemistry, 43(12), 13066.

Kang, S., Li, X., Fan, J., & Chang, J. (2013). Hydrothermal conversion of lignin: A review. Renewable and Sustainable Energy Reviews, 27, 546-558.

Karatas, H., & Akgun, F. (2018). Experimental results of gasification of walnut shell and pistachio shell in a bubbling fluidized bed gasifier under air and steam atmospheres. Fuel, 214, 285-292.

Kawamoto, H. (2017). Lignin pyrolysis reactions. Journal of Wood Science, 63(2), 117-132.

Kayser, H. (1881). Ueber die verdichtung von gasen an oberflächen in ihrer abhängigkeit von druck und temperatur. Annalen der Physik, 248(4), 526-537.

Khuong, D. A., Nguyen, H. N., & Tsubota, T. (2021). Activated carbon produced from bamboo and solid residue by CO2 activation utilized as CO2 adsorbents. Biomass and Bioenergy, 148, 106039.

Kim, K. H., Brown, R. C., Kieffer, M., & Bai, X. (2014). Hydrogen-donor-assisted solvent liquefaction of lignin to short-chain qlkylphenols using a micro reactor/gas chromatography system. Energy & Fuels, 28(10), 6429-6437.

Kleinert, M., & Barth, T. (2008). Phenols from lignin. Chemical Engineering and Technology, 31(5), 736-745.

Kleinert, M., Gasson, J. R., & Barth, T. (2009). Optimizing solvolysis conditions for integrated depolymerisation and hydrodeoxygenation of lignin to produce liquid biofuel. Journal of Analytical and Applied Pyrolysis, 85(1), 108-117.

Knoef, H. A. M. (2005). Handbook biomass gasification. Enschede, Netherlands: BTG Biomass Technology Group.

Koppejan, J., & Loo, S. v. (2007). The handbook of biomass combustion and co-firing (1st ed.). London: Routledge.

Kouris, P. D., van Osch, D. J. G. P., Cremers, G. J. W., Boot, M. D., & Hensen, E. J. M. (2020). Mild thermolytic solvolysis of technical lignins in polar organic solvents to a crude lignin oil. Sustainable Energy & Fuels, 4(12), 6212-6226.

Kulkarni, A., Baker, R., Abdoulmomine, N., Adhikari, S., & Bhavnani, S. (2016). Experimental study of torrefied pine as a gasification fuel using a bubbling fluidized bed gasifier. Renewable Energy, 93, 460-468.

Kumaniaev, I., Subbotina, E., Sävmarker, J., Larhed, M., Galkin, M. V., & Samec, J. S. M. (2017). Lignin depolymerization to monophenolic compounds in a flow-through system. Green Chemistry, 19(24), 5767-5771.

Kumar, M., Rai, D., Bhardwaj, G., Upadhyay, S. N., & Mishra, P. K. (2021). Pyrolysis of peanut shell: Kinetic analysis and optimization of thermal degradation process. Industrial Crops and Products, 174, 114128.

Lan, W., & Luterbacher, J. S. (2019). Preventing lignin condensation to facilitate aromatic monomer production. CHIMIA, 73(7-8), 591.

Larina, O. V., Valihura, K. V., Kyriienko, P. I., Vlasenko, N. V., Balakin, D. Y., Khalakhan, I., Čendak, T., Soloviev, S. O., & Orlyk, S. M. (2019). Successive vapour phase Guerbet condensation of ethanol and 1-butanol over Mg-Al oxide catalysts in a flow reactor. Applied Catalysis A: General, 588, 117265.

Larson, R. A., Sharma, B. K., Marley, K. A., Kunwar, B., Murali, D., & Scott, J. (2017). Potential antioxidants for biodiesel from a softwood lignin pyrolyzate. Industrial Crops and Products, 109, 476-482.

Lavoie, J.-M., Ghislain, T., Bahl, E., Arauzo, J., Gonzalo, A., Gil-Lalaguna, N., & Sánchez, J. L. (2019). Renewable antioxidant additive for biodiesel obtained from black liquor. Fuel, 254, 115689.

Li, D., Kagan, G., Hopson, R., & Williard, P. G. (2009). Formula weight prediction by internal reference Diffusion-Ordered NMR Spectroscopy (DOSY). Journal of the American Chemical Society, 131(15), 5627-5634.

Li, J., Henriksson, G., & Gellerstedt, G. (2007). Lignin depolymerization/repolymerization and its critical role for delignification of aspen wood by steam explosion. Bioresource Technology, 98(16), 3061-3068.

Li, M.-F., Chen, L.-X., Li, X., Chen, C.-Z., Lai, Y.-C., Xiao, X., & Wu, Y.-Y. (2016). Evaluation of the structure and fuel properties of lignocelluloses through carbon dioxide torrefaction. Energy Conversion and Management, 119, 463-472.

Liew, R. K., Chong, M. Y., Osazuwa, O. U., Nam, W. L., Phang, X. Y., Su, M. H., Cheng, C. K., Chong, C. T., & Lam, S. S. (2018). Production of activated carbon as catalyst support by microwave pyrolysis of palm kernel shell: a comparative study of chemical versus physical activation. Research on Chemical Intermediates, 44(6), 3849-3865.

Livingston, W. R. (1991). Straw ash characteristics. Harwell, United Kingdom: AEA Environment and Energy.

Long, J., Xu, Y., Wang, T., Shu, R., Zhang, Q., Zhang, X., Fu, J., & Ma, L. (2014). Hydrothermal depolymerization of lignin: Understanding the structural evolution. BioResources, 9(4), 14.

Lozano-Castelló, D., Cazorla-Amorós, D., & Linares-Solano, A. (2004). Usefulness of CO2 adsorption at 273 K for the characterization of porous carbons. Carbon, 42(7), 1233-1242.

Lu, Y. J., Guo, L. J., Ji, C. M., Zhang, X. M., Hao, X. H., & Yan, Q. H. (2006). Hydrogen production by biomass gasification in supercritical water: A parametric study. International Journal of Hydrogen Energy, 31(7), 822-831.

Lua, A. C., Yang, T., & Guo, J. (2004). Effects of pyrolysis conditions on the properties of activated carbons prepared from pistachio-nut shells. Journal of Analytical and Applied Pyrolysis, 72(2), 279-287.

Ma, Z., Kasipandi, S., Wen, Z., Yu, L., Cui, K., Chen, H., & Li, Y. (2021). Highly efficient fractionation of corn stover into lignin monomers and cellulose-rich pulp over H2WO4. Applied Catalysis B: Environmental, 284, 119731.

Macrì, D., Catizzone, E., Molino, A., & Migliori, M. (2020). Supercritical water gasification of biomass and agro-food residues: Energy assessment from modelling approach. Renewable Energy, 150, 624-636.

Madzaki, H., KarimGhani, W. A. W. A. B., NurZalikhaRebitanim, & AzilBahariAlias. (2016). Carbon dioxide adsorption on sawdust biochar. Procedia Engineering, 148, 718-725.

Mahmood, N., Yuan, Z., Schmidt, J., & Xu, C. (2013). Production of polyols via direct hydrolysis of kraft lignin: Effect of process parameters. Bioresource Technology, 139, 13-20.

Mansur, D., Tago, T., Masuda, T., & Abimanyu, H. (2014). Conversion of cacao pod husks by pyrolysis and catalytic reaction to produce useful chemicals. Biomass and Bioenergy, 66, 275-285.

Manzanares, P. (2020). The role of biorefinering research in the development of a modern bioeconomy. Acta Innovations, 37, 47-56.

Marín, F., Sánchez, J. L., Arauzo, J., Fuertes, R., & Gonzalo, A. (2009). Semichemical pulping of Miscanthus giganteus. Effect of pulping conditions on some pulp and paper properties. Bioresource Technology, 100(17), 3933-3940.

McKendry, P. (2002). Energy production from biomass (part 1): overview of biomass. Bioresource Technology, 83(1), 37-46.

Medic, D., Darr, M., Shah, A., Potter, B., & Zimmerman, J. (2012). Effects of torrefaction process parameters on biomass feedstock upgrading. Fuel, 91(1), 147-154.

Melkior, T., Jacob, S., Gerbaud, G., Hediger, S., Le Pape, L., Bonnefois, L., & Bardet, M. (2012). NMR analysis of the transformation of wood constituents by torrefaction. Fuel, 92(1), 271-280.

Menon, S. D., Sampath, K., & Kaarthik, S. S. (2021). Feasibility studies of coconut shells biomass for downdraft gasification. Materials Today: Proceedings, 44, 3133-3137.

Miller, R. S., & Bellan, J. (1997). A generalized biomass pyrolysis model based on superimposed cellulose, hemicellulose and liqnin kinetics. Combustion Science and Technology, 126(1-6), 97-137.

Mišljenović, N., Bach, Q.-V., Tran, K.-Q., Salas-Bringas, C., & Skreiberg, Ø. (2014). Torrefaction influence on pelletability and pellet quality of norwegian forest residues. Energy & Fuels, 28(4), 2554-2561.

Montero, M. L. (2017). Aceite de argán, el oro marroquí, *El País*.

Moon, R. J., Martini, A., Nairn, J., Simonsen, J., & Youngblood, J. (2011). Cellulose nanomaterials review: structure, properties and nanocomposites. Chemical Society Reviews, 40(7), 3941-3994.

Morais, A. R. C., Pinto, J. V., Nunes, D., Roseiro, L. B., Oliveira, M. C., Fortunato, E., & Bogel-Łukasik, R. (2016). Imidazole: prospect solvent for lignocellulosic biomass fractionation and delignification. ACS Sustainable Chemistry & Engineering, 4(3), 1643-1652.

Nandiyanto, A. B. D., Oktiani, R., & Ragadhita, R. (2019). How to read and Interpret FTIR spectroscope of organic material. 2019, 4(1), 22.

Nguyen, N. M., Alobaid, F., May, J., Peters, J., & Epple, B. (2020). Experimental study on steam gasification of torrefied woodchips in a bubbling fluidized bed reactor. Energy, 202, 117744.

Nunes, L. J. R., De Oliveira Matias, J. C., & Da Silva Catalão, J. P. (2018). Chapter 3 - Biomass torrefaction process. In: L. J. R. Nunes, J. C. De Oliveira Matias & J. P. Da Silva Catalão (Eds.), Torrefaction of Biomass for Energy Applications. pp. 89-124: Academic Press.

Odetoye, T. E., Onifade, K. R., AbuBakar, M. S., & Titiloye, J. O. (2014). Pyrolysis of Parinari polyandra Benth fruit shell for bio-oil production. Biofuel Research Journal, 1(3), 85-90.

Ogunkanmi, J. O., Kulla, D. M., Omisanya, N. O., Sumaila, M., Obada, D. O., & Dodoo-Arhin, D. (2018). Extraction of bio-oil during pyrolysis of locally sourced palm kernel shells: Effect of process parameters. Case Studies in Thermal Engineering, 12, 711-716.

Omri, A., Benzina, M., & Ammar, N. (2013). Preparation, modification and industrial application of activated carbon from almond shell. Journal of Industrial and Engineering Chemistry, 19(6), 2092-2099.

Ostrejko, R. V. (1920). USA Patent No.

Otromke, M., White, R. J., & Sauer, J. (2019). Hydrothermal base catalyzed depolymerization and conversion of technical lignin – An introductory review. Carbon Resources Conversion, 2(1), 59-71.

Palomo, J., Moles, S., Salafranca, J., Gil-Lalaguna, N., Gonzalo, A., & Sánchez, J. L. (2019). Production of antioxidants for biodiesel from straw black liquor depolymerization. WIT Transactions on Ecology and the Environment, 237, 97-108.

Pandey, M. P., & Kim, C. S. (2011). Lignin depolymerization and conversion: A review of thermochemical methods. Chemical Engineering & Technology, 34(1), 29-41.

Parto, S. G., Jørgensen, E. K., Christensen, J. M., Pedersen, L. S., Larsen, D. B., Duus, J. Ø., & Jensen, A. D. (2020). Solvent assisted catalytic conversion of beech wood and organosolv lignin over NiMo/γ-Al2O3. Sustainable Energy & Fuels, 4(4), 1844-1854.

Pinheiro Pires, A. P., Arauzo, J., Fonts, I., Domine, M. E., Fernández Arroyo, A., Garcia-Perez, M. E., Montoya, J., Chejne, F., Pfromm, P., & Garcia-Perez, M. (2019). Challenges and opportunities for bio-oil refining: A Review. Energy & Fuels, 33(6), 4683-4720.

Pinto, F., Gominho, J., Manuel Neto Andre, R., Braz Gonçalves, D., Miranda, M., Telles Varela, F., Neves, D., Santos, J., Lourenço, A., & Pereira, H. (2017). Effect of rice husk torrefaction on syngas production and quality. Energy & Fuels, 31(5), 5183–5192.

Plaza, D., Artigas, J., Ábrego, J., Gonzalo, A., Sánchez, J. L., Dro, A. D., & Richardson, Y. (2019). Design and operation of a small-scale carbonization kiln for cashew nutshell valorization in Burkina Faso. Energy for Sustainable Development, 53, 71-80.

Prins, M. J., Ptasinski, K. J., & Janssen, F. J. J. G. (2006a). More efficient biomass gasification via torrefaction. Energy, 31(15), 3458-3470.

Prins, M. J., Ptasinski, K. J., & Janssen, F. J. J. G. (2006b). Torrefaction of wood: Part 2. Analysis of products. Journal of Analytical and Applied Pyrolysis, 77(1), 35-40.

Pu, Y., Cao, S., & Ragauskas, A. J. (2011). Application of quantitative 31P NMR in biomass lignin and biofuel precursors characterization. Energy & Environmental Science, 4(9), 3154-3166.

Pullen, J., & Saeed, K. (2012). An overview of biodiesel oxidation stability. Renewable and Sustainable Energy Reviews, 16(8), 5924-5950.

Ragauskas, A. J., Beckham, G. T., Biddy, M. J., Chandra, R., Chen, F., Davis, M. F., Davison, B. H., Dixon, R. A., Gilna, P., Keller, M., Langan, P., Naskar, A. K., Saddler, J. N., Tschaplinski, T. J., Tuskan, G. A., & Wyman, C. E. (2014). Lignin valorization: improving lignin processing in the biorefinery. Science, 344(6185), 1246843.

Rahib, Y., Boushaki, T., Sarh, B., Chaoufi, J., Ahmed, L., Sylvie, B., & Abdallah, E. (2019a). Combustion analysis of fixed beds of Argan nut shell (ANS) biomass in a batch type reactor. Paper presented at the 7th International Renewable and Sustainable Energy Conference (IRSEC), Agadir, Morocco.

Rahib, Y., Elorf, A., Sarh, B., Ezahri, M., Rahib, Y., & Bonnamy, S. (2019b). Experimental analysis on thermal characteristics of Argan nut shell (ANS) biomass as a green energy resource. International Journal of Renewable Energy Research, 9(4), 1606-1615.

Ram, M., & Mondal, M. K. (2022). Chapter 13 - Biomass gasification: a step toward cleaner fuel and chemicals. In: B. Gurunathan, R. Sahadevan & Z. A. Zakaria (Eds.), Biofuels and Bioenergy. pp. 253-276: Elsevier.

Ranguin, R., Jean-Marius, C., Yacou, C., Gaspard, S., Feidt, C., Rychen, G., & Delannoy, M. (2020). Reduction of chlordecone environmental availability by soil amendment of

biochars and activated carbons from lignocellulosic biomass. Environmental Science and Pollution Research, 27(33), 41093-41104.

Rao, T. R., & Sharma, A. (1998). Pyrolysis rates of biomass materials. Energy, 23(11), 973-978.

Rapagnà, S., & Latif, A. (1997). Steam gasification of almond shells in a fluidised bed reactor: the influence of temperature and particle size on product yield and distribution. Biomass and Bioenergy, 12(4), 281-288.

Razvigorova, M., Goranova, M., Minkova, V., & Cerny, J. (1994). On the composition of volatiles evolved during the production of carbon adsorbents from vegetable wastes. Fuel, 73(11), 1718-1722.

Rencoret, J., Marques, G., Gutiérrez, A., Nieto, L., Santos, J. I., Jiménez-Barbero, J., Martínez, Á. T., & Río, J. C. d. (2009). HSQC-NMR analysis of lignin in woody (Eucalyptus globulus and Picea abies) and non-woody (Agave sisalana) ball-milled plant materials at the gel state. Holzforschung, 63(6), 691-698.

Renders, T., Cooreman, E., Van den Bosch, S., Schutyser, W., Koelewijn, S. F., Vangeel, T., Deneyer, A., Van den Bossche, G., Courtin, C. M., & Sels, B. F. (2018). Catalytic lignocellulose biorefining in n-butanol/water: a one-pot approach toward phenolics, polyols, and cellulose. Green Chemistry, 20(20), 4607-4619.

Renders, T., Van den Bosch, S., Koelewijn, S. F., Schutyser, W., & Sels, B. F. (2017). Lignin-first biomass fractionation: the advent of active stabilisation strategies. Energy & Environmental Science, 10(7), 1551-1557.

Rinaldi, R., Jastrzebski, R., Clough, M. T., Ralph, J., Kennema, M., Bruijnincx, P. C. A., & Weckhuysen, B. M. (2016). Paving the way for lignin valorisation: recent advances in bioengineering, biorefining and catalysis. Angewandte Chemie, 55(29), 8164-8215.

Robens, E. (1994). Some intriguing items in the history of adsorption. In: J. Rouquerol, F. Rodríguez-Reinoso, K. S. W. Sing & K. K. Unger (Eds.), Studies in Surface Science and Catalysis. Vol. 87, pp. 109-118: Elsevier.

Roger, M. R., Roger, P., & Mandla, A. T. (2012). Chapter 1 - Structure and Chemistry: Cell Wall Chemistry. In: R. M. Rowell (Ed.), Handbook of Wood Chemistry and Wood Composites. 2nd ed.: CRC Press.

Sarchami, T., Batta, N., & Berruti, F. (2021). Production and separation of acetic acid from pyrolysis oil of lignocellulosic biomass: a review. Biofuels, Bioproducts and Biorefining, 15(6), 1912-1937.

Sarkar, M., Kumar, A., Tumuluru, J. S., Patil, K. N., & Bellmer, D. D. (2014). Gasification performance of switchgrass pretreated with torrefaction and densification. Applied Energy, 127, 194-201.

Savova, D., Apak, E., Ekinci, E., Yardim, F., Petrov, N., Budinova, T., Razvigorova, M., & Minkova, V. (2001). Biomass conversion to carbon adsorbents and gas. Biomass and Bioenergy, 21(2), 133-142.

Scanlon, J. T., & Willis, D. E. (1985). Calculation of flame ionization detector relative response factors using the effective carbon number concept. Journal of Chromatographic Science, 23(8), 333-340.

Schutyser, W., Renders, T., Van den Bosch, S., Koelewijn, S. F., Beckham, G. T., & Sels, B. F. (2018). Chemicals from lignin: an interplay of lignocellulose fractionation, depolymerisation, and upgrading. Chemical Society Reviews, 47(3), 852-908.

Schutyser, W., Van den Bosch, S., Renders, T., De Boe, T., Koelewijn, S. F., Dewaele, A., Ennaert, T., Verkinderen, O., Goderis, B., Courtin, C. M., & Sels, B. F. (2015). Influence of bio-based solvents on the catalytic reductive fractionation of birch wood. Green Chemistry, 17(11), 5035-5045.

Sebio-Puñal, T., Naya, S., López Beceiro, J., Tarrío-Saavedra, J., & Artiaga, R. (2012). Thermogravimetric analysis of wood, holocellulose, and lignin from five wood species. Journal of Thermal Analysis and Calorimetry, 109, 1163-1167.

Sette, M., Lange, H., & Crestini, C. (2013). Quantitative HSQC analyses of lignin: A practical comparison. Computational and Structural Biotechnology Journal, 6(7), e201303016.

Shagali, A. A., Hu, S., Wang, Y., Li, H., Wang, Y., Su, S., & Xiang, J. (2021). Comparative study on one-step pyrolysis activation of walnut shells to biochar at different heating rates. Energy Reports, 7, 388-396.

Shi, J., Xing, D., & Lia, J. (2012). FTIR studies of the changes in wood chemistry from wood forming tissue under inclined treatment. Energy Procedia, 16, 758-762.

Solowey, E. M. (2001). Upscaling the experimental planting of Argania Spinosa at Kibbutz Ketura, Israel. In: D. Pasternak & A. Schlissel (Eds.), Combating Desertification with Plants. pp. 257-261. Boston: Springer New York.

Spath, P. L., & Dayton, D. C. (2003). Preliminary Screening -- Technical and economic assessment of synthesis gas to fuels and chemicals with emphasis on the potential for biomass-derived syngas. United States: National Renewable Energy Lab. (NREL), Golden, CO (United States), US Department of Energy

Strandberg, M. (2015). From torrefaction to gasification pilot scale studies for upgrading of biomass. Doctoral thesis, Doctor of Philosophy in chemical process engineering, Umeå University, Umeå, Sweden.

Sturgeon, M. R., Kim, S., Lawrence, K., Paton, R. S., Chmely, S. C., Nimlos, M., Foust, T. D., & Beckham, G. T. (2014). A mechanistic investigation of acid-catalyzed cleavage of Aryl-Ether linkages: Implications for lignin depolymerization in acidic environments. ACS Sustainable Chemistry & Engineering, 2(3), 472-485.

Sun, Y., Xiong, X., He, M., Xu, Z., Hou, D., Zhang, W., Ok, Y. S., Rinklebe, J., Wang, L., & Tsang, D. C. W. (2021). Roles of biochar-derived dissolved organic matter in soil amendment and environmental remediation: A critical review. Chemical Engineering Journal, 424, 130387.

Sundriyal, S., Shrivastav, V., Pham, H. D., Mishra, S., Deep, A., & Dubal, D. P. (2021). Advances in bio-waste derived activated carbon for supercapacitors: Trends, challenges and prospective. Resources, Conservation and Recycling, 169, 105548.

Tabatabaei, M., & Aghbashlo, M. (2020). The critical role of advanced sustainability assessment tools in enhancing the real-world application of biofuels. Acta Innovations, 37, 67-73.

Tadda, M. A., Ahsan, A., Shitu, A., ElSergany, M., Arunkumar, T., Jose, B., Abdur Razzaque, M., & Nik Daud, N. N. (2016). A review on activated carbon: process, application and prospects. Journal of Advanced Civil Engineering Practice and Research.

Taer, E., Afdal Yusra, D., Amri, A., Awitdrus, Taslim, R., Apriwandi, Agustino, & Putri, A. (2021). The synthesis of activated carbon made from banana stem fibers as the supercapacitor electrodes. Materials Today: Proceedings, 44, 3346-3349.

Tedsree, K., Li, T., Jones, S., Chan, C. W. A., Yu, K. M. K., Bagot, P. A. J., Marquis, E. A., Smith, G. D. W., & Tsang, S. C. E. (2011). Hydrogen production from formic acid decomposition at room temperature using a Ag–Pd core–shell nanocatalyst. Nature Nanotechnology, 6(5), 302-307.

Teella, A., Huber, G. W., & Ford, D. M. (2011). Separation of acetic acid from the aqueous fraction of fast pyrolysis bio-oils using nanofiltration and reverse osmosis membranes. Journal of Membrane Science, 378(1), 495-502.

Tolbert, A., Akinosho, H., Khunsupat, R., Naskar, A. K., & Ragauskas, A. J. (2014). Characterization and analysis of the molecular weight of lignin for biorefining studies. Biofuels, Bioproducts and Biorefining, 8(6), 836-856.

Toledano, A., Serrano, L., & Labidi, J. (2012). Organosolv lignin depolymerization with different base catalysts. Journal of Chemical Technology & Biotechnology, 87(11), 1593-1599.

Toledano, A., Serrano, L., & Labidi, J. (2014). Improving base catalyzed lignin depolymerization by avoiding lignin repolymerization. Fuel, 116, 617-624.

Toledano Zabaleta, A. (2012). Lignin extraction, purification and depolymerization study. Doctoral thesis, Doctor of Philosophy in renewable materials engineering, Universidad del País Vasco, San Sebastián, Spain.

Tsechansky, L., & Graber, E. (2014). Methodological limitations to determining acidic groups at biochar surfaces via the Boehm titration. Carbon, 66, 730-733.

Tumuluru, J. S., Sokhansanj, S., Hess, J., Wright, C., & Boardman, R. (2011). A review on biomass torrefaction process and product properties for energy applications. Industrial Biotechnology, 7, 384-401.

Van den Bosch, S., Renders, T., Kennis, S., Koelewijn, S. F., Van den Bossche, G., Vangeel, T., Deneyer, A., Depuydt, D., Courtin, C. M., Thevelein, J. M., Schutyser, W., & Sels, B. F. (2017). Integrating lignin valorization and bio-ethanol production: on the role of Ni-Al2O3 catalyst pellets during lignin-first fractionation. Green Chemistry, 19(14), 3313-3326.

Van den Bosch, S., Schutyser, W., Koelewijn, S. F., Renders, T., Courtin, C. M., & Sels, B. F. (2015). Tuning the lignin oil OH-content with Ru and Pd catalysts during lignin hydrogenolysis on birch wood. Chemical Communications, 51(67), 13158-13161.

Van der Stelt, M. J. C. (2011). Chemistry and reaction kinetics of biowaste torrefaction.

Van der Stelt, M. J. C., Gerhauser, H., Kiel, J. H. A., & Ptasinski, K. J. (2011). Biomass upgrading by torrefaction for the production of biofuels: A review. Biomass and Bioenergy, 35(9), 3748-3762.

Wahyudiono, Kanetake, T., Sasaki, M., & Goto, M. (2007). Decomposition of a lignin model compound under hydrothermal conditions. Chemical Engineering & Technology, 30(8), 1113-1122.

Wen, J.-L., Sun, S.-L., Xue, B.-L., & Sun, R.-C. (2013). Recent advances in characterization of lignin polymer by solution-state nuclear magnetic resonance (NMR) methodology. Materials, 6(1), 359-391.

Wu, H., Lu, W., Chen, Y., Zhang, P., & Cheng, X. (2020). Application of Boehm titration for the quantitative measurement of soot oxygen functional groups. Energy & Fuels, 34(6), 7363-7372.

Xiong, Z., Shihong, Z., Haiping, Y., Tao, S., Yingquan, C., & Hanping, C. (2013). Influence of NH3/CO2 modification on the characteristic of biochar and the CO2 capture. BioEnergy Research, 6(4), 1147-1153.

Xu, B., Chen, Y., Wei, G., Cao, G., Zhang, H., & Yang, Y. (2010). Activated carbon with high capacitance prepared by NaOH activation for supercapacitors. Materials Chemistry and Physics, 124(1), 504-509.

Yaakob, Z., Narayanan, B. N., Padikkaparambil, S., Unni K, S., & Akbar P, M. (2014). A review on the oxidation stability of biodiesel. Renewable and Sustainable Energy Reviews, 35, 136-153.

Yahaya, A. Z., Somalu, M. R., Muchtar, A., Sulaiman, S. A., & Wan Daud, W. R. (2019). Effect of particle size and temperature on gasification performance of coconut and palm kernel shells in downdraft fixed-bed reactor. Energy, 175, 931-940.

Yan, N., Zhao, C., Dyson, P. J., Wang, C., Liu, L.-t., & Kou, Y. (2008). Selective degradation of wood lignin over noble-metal catalysts in a two-step process. ChemSusChem, 1(7), 626-629.

Yang, H., Yan, R., Chen, H., Lee, D. H., & Zheng, C. (2007). Characteristics of hemicellulose, cellulose and lignin pyrolysis. Fuel, 86(12), 1781-1788.

Yang, L., Zhou, W., Seshan, K., & Li, Y. (2013). Green and efficient synthesis route of catechol from guaiacol. Journal of Molecular Catalysis A: Chemical, 368-369, 61-65.

Yang, Z., Zhang, G., Xu, Y., & Zhao, P. (2019). One step N-doping and activation of biomass carbon at low temperature through NaNH2: An effective approach to CO2 adsorbents. Journal of CO2 Utilization, 33, 320-329.

Yu, J., Zhao, Y., & Li, Y. (2014). Utilization of corn cob biochar in a direct carbon fuel cell. Journal of Power Sources, 270, 312-317.

Yuan, Z., Cheng, S., Leitch, M., & Xu, C. (2010). Hydrolytic degradation of alkaline lignin in hot-compressed water and ethanol. Bioresource Technology, 101(23), 9308-9313.

Zhao, C., Jiang, E., & Chen, A. (2017). Volatile production from pyrolysis of cellulose, hemicellulose and lignin. Journal of the Energy Institute, 90(6), 902-913.

Zhao, H., Yu, Q., Li, M., & Sun, S. (2020). Preparation and water vapor adsorption of “green” walnut-shell activated carbon by CO2 physical activation. Adsorption Science & Technology, 38(1-2), 60-76.

Zheng, A., Zhao, Z., Chang, S., Huang, Z., He, F., & Li, H. (2012). Effect of torrefaction temperature on product distribution from two-staged pyrolysis of biomass. Energy & Fuels, 26(5), 2968-2974.

Zhou, G., Taylor, G., & Polle, A. (2011). FTIR-ATR-based prediction and modelling of lignin and energy contents reveals independent intra-specific variation of these traits in bioenergy poplars. Plant Methods, 7(1), 9.

Zhu, M., Ge, Q., & Zhu, X. (2020). Catalytic reduction of CO2 to CO via reverse water gas shift reaction: recent advances in the design of active and selective supported metal catalysts. Transactions of Tianjin University, 26(3), 172-187.

Zubair Yahaya, A., Rao Somalu, M., Muchtar, A., Anwar Sulaiman, S., & Ramli Wan Daud, W. (2020). Effects of temperature on the chemical composition of tars produced from the gasification of coconut and palm kernel shells using downdraft fixed-bed reactor. Fuel, 265, 116910.

Appendices

APPENDIX I: PUBLICATIONS.

- Zainab Afailal; Noemí Gil-Lalaguna; Isabel Fonts; Alberto Gonzalo; Jesús Arauzo; José Luis Sánchez (2023). "*Thermochemical valorization of argan nutshells: torrefaction and air-steam gasification*". **Fuel journal,** 332, DOI: 10.1016/j.fuel.2022.125970.

Fuel 332 (2023) 125970

Contents lists available at ScienceDirect

Fuel

journal homepage: www.elsevier.com/locate/fuel

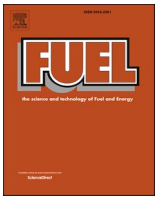

Thermochemical valorization of argan nutshells: Torrefaction and air–steam gasification

Zainab Afailal *, Noemí Gil-Lalaguna, Isabel Fonts, Alberto Gonzalo, Jesús Arauzo, José Luis Sánchez

Thermochemical Processes Group, Aragón Institute of Engineering Research (I3A), University of Zaragoza, C/Mariano Esquillor s/n, 50.018, Zaragoza, Spain

ARTICLE INFO

Keywords:
Argan nutshells
Waste valorization
Torrefaction
Air–steam gasification
Syngas quality

ABSTRACT

The upswing of argan's oil for the cosmetic industry has increased the farming of this plant and originated an unexplored residue of complex treatment, its nutshells. This work deals with the characterization of this feedstock, its pretreatment via torrefaction and its gasification either with or without the pretreatment stage. Torrefaction was carried out in a continuous auger reactor at two temperatures, 220 and 250 °C. Hemicellulose was almost totally removed from argan nutshells after torrefaction. Compared to the raw argan shells, the torrefied solids showed an increased content of fixed carbon, a noticeable reduction in the O/C ratio and a significant increase in the HHV, the higher the torrefaction temperature. Chemical thermodynamic equilibrium calculations were implemented to the gasification stage to calculate the equivalence ratio for auto-thermal operation and to assess the effect of temperature and steam-to-biomass ratio on gas yield and composition. Air-steam gasification was also experimentally tested for the raw and torrefied materials at the operational conditions drawn from the simulation results. The torrefied material gasification yielded four times more char than the raw material, while tar production from the torrefied material was only reduced in the presence of steam (anyway starting from a low value: 0.7 g/m^3_{STP} for raw argan shells vs 0.3 g/m^3_{STP} for the torrefied material). Nor gas production, neither the H_2/CO ratio nor the energy content in syngas were improved by gasifying the torrefied material, so torrefaction does not appear to be a profitable pretreatment stage for the gasification of argan nutshells from the point of view of syngas quality.

1. Introduction

Biomass is the most abundant and bio-renewable source of carbon and hydrogen on earth [1]. The transformation of biomass feedstocks is receiving growing attention as fundamental investigation lines in the field of sustainability and green energies, as well as on the finding of new sources and materials previously untapped. To benefit from biomass uses is a key point in the circular economy concept. It helps to reduce the generation of non-valorized residues and net emissions of greenhouse gases, and even the external energy dependence of particular regions, since the development of new strategies for the valorization of local biomasses could create new and clean industrial activities, thus contributing to the sustainable socio-economic development.

Argan's oil is increasingly highly valued directly or as an additive for cosmetic products, mainly produced by small rural cooperatives in Morocco. Its production is on the rise due to its boosting application in cosmetics and to its high price, up to 200 €/liter (2020). It is extracted from the fruit of the *Argania Spinosa (L.) Skeels*, an endemic tree of Morocco, covering about 870,000 ha in the country's south. The annual production of argan's oil is over 4,000 tons, leaving behind 20 tons of non-valorized waste (shells) per ton of oil produced [2]. Local people have tried to use this waste as a fuel for the traditional heating furnaces [3], but its hardness, rigidity, and difficulty in being ignited (delayed ignition and flame extinction [4]) prevent its easy and safe use in such a traditional way. The major macro-components of raw argan nutshells are cellulose, lignin, and hemicellulose, whereas minor ash and moisture contents are also present [3,5]. On a dry basis, the lignin content of this residue is up to 38 wt%. This high lignin content could be considered an intrinsic feature of most fruit shells, ranging between 38 and 45 wt% for almond and hazelnut shells [6,7]. Lower values of lignin content have usually been reported for hardwoods (18–25 wt%) and softwoods (25–35 wt%) [8].

* Corresponding author.
E-mail address: zainabafailal@unizar.es (Z. Afailal).

https://doi.org/10.1016/j.fuel.2022.125970
Received 29 January 2022; Received in revised form 26 August 2022; Accepted 8 September 2022
Available online 18 September 2022
0016-2361/© 2022 The Authors. Published by Elsevier Ltd. This is an open access article under the CC BY-NC-ND license (http://creativecommons.org/licenses/by-nc-nd/4.0/).

Among the different valorization routes developed to efficiently convert lignin-rich biomass into biochemicals and biofuels, thermochemical processes are considered the most attractive pathway thanks to their faster kinetics. One of these thermochemical processes is gasification, which offers an interesting possibility of treatment in terms of conversion efficiency [9]. During gasification, a carbonaceous feedstock is converted into a gaseous fuel at high temperatures (typically in the range 800–1200 °C), using an oxidative medium, such as air, oxygen or steam [10]. The main product of gasification is the gas (usually referred to as syngas), which consists of a mixture of hydrogen (H_2), carbon monoxide (CO), carbon dioxide (CO_2), nitrogen (N_2) (if using air or enriched air as gasifying agent), methane (CH_4) and other light hydrocarbons. Clean syngas could be used as fuel for heat and/or power production due to its reasonable high energy density [11], but it seems even more attractive to evaluate its potential as a feedstock for Fisher-Tropsch-based processes to produce a great variety of liquid biofuels and biochemicals, such as methanol, ethanol and higher alcohols and dimethyl ether [12].

The synthesis of these biochemicals requires specific H_2/CO molar ratios, ranging from 2 for methanol to 1 for higher alcohols [13]. Steam is considered the simplest way to tune the gas composition [9]. Hence, the quality of syngas in terms of the H_2/CO ratio can be improved by using steam in the mixture of gasification agents, as has been highlighted by research works dealing with wood gasification [9,11]. However, this trend has been scarcely corroborated by works focused neither on lignin-rich biomass nor with pretreated biomass.

In addition to syngas, char (carbonaceous solid) and tar (mixture of heavy and condensable hydrocarbons) are also generated as by-products in this conversion process, thus constraining the gas production rate. Moreover, the existence of tar in the syngas negatively impacts its subsequent utilization by causing difficulties associated with condensation in downstream equipments, formation of aerosols and polymerization [14], and contribution to the deactivation of the catalysts used in the subsequent gas upgrading stages. In this regard, several studies in the literature outline that gasification accompanied by a previous torrefaction pretreatment of woody biomass could provide benefits such as reducing tar concentration in the gas [15–17], as the torrefied material has a decreased O/C ratio and volatile content, and a higher energy density and carbon content [9]. Cerone et al. stated that the use of torrefied Eucalyptus wood chips resulted in a fivefold lower tar concentration in the syngas (164 g/m^3 for the raw Eucalyptus wood chips vs 34 g/m^3 for the torrefied one) and a noticeable increment of the thermal power of the plant [15]. On the other hand, in the study of Kulkarni et al., a similar trend was observed in the gasification of torrefied pine, producing less than half of tar yield (8 g/ kg of raw dried pine vs 3.9 g/kg of torrefied pine) [17]. The effect of the torrefaction pretreatment on the production of tar in the gasification of such type of lignocellulosic materials seems to be clear. However, this effect has been scarcely studied for lignin-rich biomass, such as nutshells, and conclusions should not be directly extrapolated to these materials since lignin is known to be less affected by torrefaction than the carbohydrate fraction of lignocellulosic biomass [18].

An interesting study concerning argan nutshells combustion has recently been published [19], but, from the best of our knowledge, nothing more related to argan nutshells torrefaction or gasification has been published before. Therefore, the motivation of the current work is, on the one hand, to fill the gap in the literature concerning the characterization and the thermochemical upgrading of this type of biomass. On the other hand, to investigate new applications and end-uses for this waste, as well as to evaluate the technical feasibility at lab-scale before scaling up the process to be used on-site by the local producers for sustainable argan oil production. Recently published studies from our research group showed promising results on producing antioxidant additives [5] and catalyst supports [20] from argan nutshells. Like other similar agricultural residues, this material has a relatively high-energy content, making it a good candidate for thermochemical valorization. In the last decade, some studies have been dedicated to investigate the use of fruit shells in the gasification process using different reactors [11,21–24]. Yahaya et al. [24] studied air gasification of coconut and palm kernel shells at 700–900 °C, producing syngas with an H_2/CO ratio of 0.63–0.84 for coconut shells and 0.6–0.75 for palm kernel shells. On the other hand, Macrì et al. [25] stated that almond shells gasification theoretically exhibited more gas yield but lower cold gas efficiency compared with other feedstocks with high moisture content (microalgae, digestate and sludge).

In the present work, the gasification of torrefied argan nutshells, using air and air–steam as a gasifying agent, has been experimentally evaluated and compared with the raw biomass gasification performance in order to define the impact of such pretreatment on important gasification parameters. The main experimental results obtained in the torrefaction stage are also reported in this study to further explain the results observed in the gasification steps.

2. Materials and methods

2.1. Materials and characterization equipment

2.1.1. Raw material

The raw material employed in this torrefaction/gasification study is argan nutshells (AS), collected in the region of Essaouira (southwest of Morocco). AS was supplied by a Moroccan cooperative after removing the argan's nut. AS was milled and sieved in order to have a particle size of around 5 mm. The main characteristics of AS (as shown in section 3.1.2) are its considerable higher heating value (HHV = 19 MJ/kg), its low ash content (0.3 wt%), pretty similar cellulose and lignin contents (up to 35 wt%) and carbon content of 47.5 wt%.

2.1.2. Characterization equipment for solid materials

The raw material, as well as the solid products obtained in the torrefaction and gasification experiments, were characterized in terms of elemental composition, macro-components distribution and calorific value. The elemental analysis was determined using a LECO CHN628 Analyzer combined with the sulfur add-on module 628-S, while the proximate analysis, involving ash content, moisture content and volatile matter, was determined according to standard procedures (EN 14775:2010, EN 14774–3:2010 and EN 15148–2010, respectively). The organic extractives content was determined by the Soxhlet's extraction method using dichloromethane (DCM) as a solvent for 6 h. Hemicellulose, cellulose, and lignin contents were determined by the Van Soest analysis, which is based on subsequent digestion stages in different detergents (neutral detergent, acid detergent, and sulfuric acid 72 %) [26]. The solids' higher heating value (HHV) was measured using the IKA model C2000 basic calorific bomb.

The thermal behavior of the raw material and the torrefied solids was also investigated by thermogravimetric analysis (TGA-DTG, Proteus STA 449 F1 Jupiter-Netzsch). The thermogravimetric analysis (TGA) curves represent the instantaneous weight loss of a material during its thermal decomposition as a function of the applied temperature. Hence, this analysis can be a helpful tool to compare the chemical decomposition behavior of different materials, for example, the raw material and its torrefied solids obtained at different temperatures. During these experiments, around 50 mg of the solid sample was heated at a constant heating rate of 5 °C/min from ambient temperature to 700 °C; N_2 was used as a purge gas with a flow rate of 100 mL/min.

Surface functional groups on both the raw AS and the torrefied solids were investigated by Attenuated Total Reflection-Fourier Transform Infra-Red (ATR-FTIR) spectroscopy analysis, using an Agilent Cary 630 FTIR spectrometer, with a resolution of 4 cm^{-1} in the wavenumber range of 4000 – 400 cm^{-1} (medium IR region).

2.1.3. Characterization of liquid products

The composition of the liquid products obtained from either

torrefaction or gasification was also analyzed. Water content in the condensable liquids was measured using the Karl Fischer titration method (Mettler Toledo V-20 analyzer), and their densities were measured with a portable densimeter Mettler Toledo Densito 30px.

The composition of volatile compounds in the liquids was analyzed by gas chromatography (GC), using an Agilent 7890A GC chromatograph equipped with a flame ionization detector (FID) and combined with an Agilent 5975C mass selective detector (MSD) (operating parameters are listed in Table S1 in the Supplementary Information Section). The compounds identification and quantification were performed based on the peaks with more significant areas (> 92 % of the total area). Firstly, the identification of condensed organic compounds was performed using the MS signal by means of NIST MS Search Program 2.2. The quantification of those compounds was based on integrating the peaks of the FID signal.

For the torrefaction liquids, six standard solutions with 12 compounds each (acetol, furfural, 5-methylfurfural, 2-furanmethanol, guaiacol, creosol, phenol, 4-ethylguaiacol, eugenol, phenol 2,6-dimethoxy, vanillin, and acetic acid) were prepared in the concentration range of 240–4600 μg/mL, except for the acetic acid whose concentration range was higher (13323–91143 μg/mL). These standards were used for calibrating the FID signal. The FID response factors of other compounds that were also identified by GC/MS but not calibrated as standards were calculated from the response factor of the most similar standard compound used and applying to it a correction factor according to the methodology based on the Effective Carbon Numbers (ECN) [27] (more details about the calculation can be found in the Supplementary Information Section).

In the same way as torrefaction liquids, the composition of condensables from the gasification experiments was further analyzed. In this case, for the calibration of the FID signal, five calibration solutions were prepared in the concentration range of 10–500 μg/mL from different dilutions of a commercial standard containing 16 polycyclic aromatic hydrocarbons (PAH Mix 3 Supelco).

2.2. Torrefaction experimental setup

The torrefaction of AS was carried out in a laboratory-scale auger reactor (800 mm in length with an internal diameter of 55 mm) surrounded by an electrical furnace composed of three zones controlled separately. The schematic diagram of this system is presented in Fig. 1. The Auger reactor operated with continuous solid feeding and removal of volatiles using a flow of N_2 (1 L_{STP}/min) as inert carrier gas. The solid feeding rate and the solid residence time were both adjusted by varying the screw rotation frequency. These parameters were maintained constant at 5.4 g/min and 27 min, respectively (maximal rotation frequency of the screw). In each experiment, a total of 500 g of AS (particle size between 2 and 4 mm) was processed. The torrefied solid produced was collected in a recovering hopper situated at the end of the reactor (Fig. 1). A glass wool filter heated at the reactor's temperature was used to retain the small solid particles swept by the gas without condensing the vapors in this stage. Then, two condensers refrigerated with a water-ethylene glycol recirculating chiller (0.5 °C) were employed to collect the condensable vapors released during the reaction (water and organic compounds), followed by a cotton filter to finish cleaning the gas from traces of humidity and organics (1–2 % of the produced liquid was retained in the cotton filter). The particle- and organics-free gas volume was continuously measured using a volumetric gas meter (Gallus G4). The gas composition was analyzed online by a micro-gas chromatograph (Agilent 3000A), previously calibrated using a standard gas mixture of nine components (H_2, CH_4, CO, CO_2, C_2H_2, C_2H_4, C_2H_6, H_2S). The mass of each produced gas was calculated based on the composition data and the gas volume produced throughout the experiment.

Two different torrefaction temperatures (220 and 250 °C) were tested. As has already been reported in the literature, the torrefaction temperature has a more remarkable effect on the product distribution than other operational factors, such as the residence time [28]. For this reason, the temperature was the only operational factor studied in this work. For both treatment temperatures, consistent results were observed by duplication, with a reproducibility of the results < 10 % in the products yields.

Once the experiment had finished, the mass of the liquid product was determined by the weight difference of the condensers and the cotton filter before and after the experiment. To ensure a total recovery of the liquid collected in the condensers, whose composition will be analyzed, the condensers were washed with a weighted amount of solvent (methanol). On the other hand, the amount of torrefied solid was determined by the collecting hopper's weight difference (the reactor was empty at the end of the experiment).

The mass yields of gas, liquid and solid products ($Y_{m,i}$) were calculated with respect to biomass fed (Equation (1)). The total mass of biomass for these calculations was expressed on an as-received basis.

$$Y_{m,i} = \frac{Mass\ of\ solid,\ liquid\ or\ gas\ product\ (g)}{Total\ mass\ of\ biomass\ fed\ (g)} \bullet 100 \quad (1)$$

2.3. Gasification experimental setup

Gasification experiments of AS and argan shells torrefied at 220 °C (TAS220) were performed operating at atmospheric pressure in a lab-scale fluidized bed reactor (Fig. 2). Besides AS, TAS220 was chosen as gasification feedstock because of its higher production yield compared to the material torrefied at 250 °C (as shown in section 3.1.1). As the final particle size of TAS220 ranged between 2 and 4 mm, the raw AS fed to the gasification process was also crushed and sieved to a similar particle size for comparison purposes. Biomass was semi-continuously introduced into the reactor in the form of pulses of 3.5 g per minute through a double valve system placed at the top of the reactor. An initial

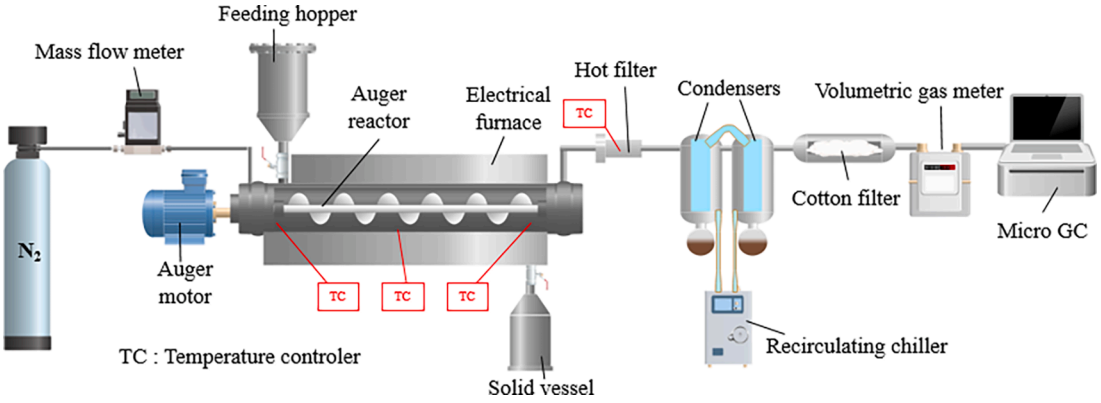

Fig. 1. Diagram of the torrefaction experimental setup.

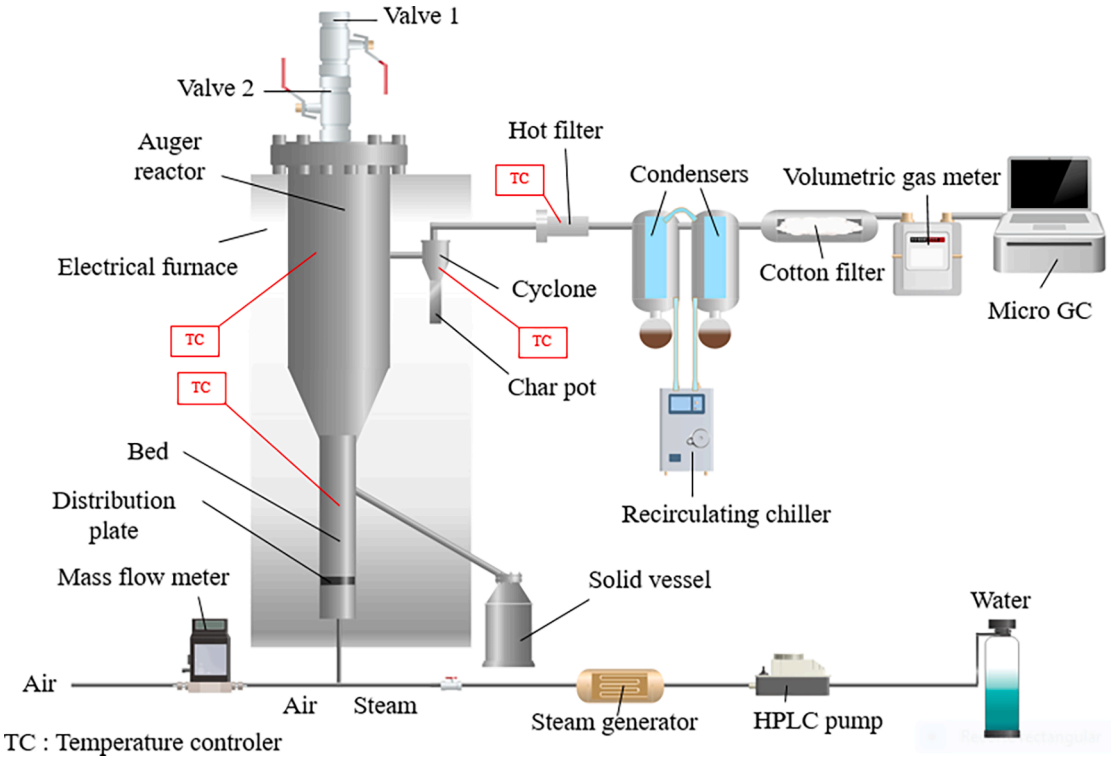

Fig. 2. Diagram of the gasification experimental setup.

bed (100 g) of calcined dolomite (at 900 °C) with a particle size of 350–500 μm was loaded. Using dolomite as bed material has been proved to report benefits in catalytic cracking of the generated tar [29]. The gasifying agent, composed of air or a mixture of air and steam, entered the reactor below the distributor plate and passed through the dolomite bed. Details about the reactor dimensions and the feeding systems for air and steam are explained elsewhere [14,30]. When solid in the reactor exceeded the available bed height, the solid (mixture of dolomite and char) left the bed overflowing to a solid container via a lateral pipe.

Vapors and gases passed through a cyclone and a glass wool filter (both heated to 450 °C), where the smallest solid particles (char and dolomite) were retained. Then, the condensing vapors and gas cleaning and analysis systems were similar to those in the torrefaction process (Section 2.2).

The lower heating value of the obtained syngas and the cold gas efficiency were calculated according to Equation (2) and Equation (3), respectively.

$$LHV_{gas} = \sum(x_i \cdot LHV_i) \quad (2)$$

where LHV_i (MJ/m^3_{STP}) is the lower heating value of each gaseous component and x_i its volumetric fraction (experimentally measured with the micro-gas chromatograph).

$$\text{Cold gas efficiency}\ (\%) = \frac{LHV_{gas} \bullet V_{gas}}{LHV_{feedstock} \bullet m_{feed}} \bullet 100 \quad (3)$$

where V_{gas} is the total volume of produced gas (m^3_{STP}), $LHV_{feedstock}$ is the lower heating value of the biomass fed (AS or TAS220), and m_{feed} is the total mass of biomass fed during the experiment (kg).

Each experiment was carried out for 60 min and, to estimate the experimental variability, each gasification run was repeated twice in the case of AS gasification.

2.4. Theoretical model for gasification

The gasification process has been theoretically modeled by studying the chemical equilibrium using HSC 9.0 software add-in in Excel. The calculations using the HSC 9.0 software were based on three conditions: i) minimization of the Gibbs free energy of the system, ii) compliance with the atomic balance in the whole process, and iii) establishment of an auto-thermal gasification reaction by accomplishing the energy balance without considering energy recovery from the products streams and taking into account 5 % of heat losses. By entering the characteristics of the raw material (mass flow, elemental analysis, ash and moisture contents and HHV), the gasification atmosphere composition (including S/C: steam to carbon mass ratio) and the expected gasification temperature, as well as other parameters related to the energy balance (calorific capacities and standard enthalpies of formation of reagents and products), the calculation procedure determined the required ER (equivalence ratio) in the gasification process for getting an auto-thermal reaction at a specific temperature. This simulation model also calculated the gas production and composition, fulfilling the aforementioned conditions. This model was run in a wide range of temperatures (750–1100 °C) and S/C ratios (up to 1.1 g H_2O/g biomass), and the results are detailed in Section 3.2.1.

The operational conditions for the experimental gasification runs were set based on these simulations results (Section 3.2.1) and are summarized in Table 1. Note that in the experiments in which the

Table 1
Operational conditions in the gasification experimental runs.

Run #	Feedstock	Gasifying agent	T (°C)	S/C	Added steam (L_{STP}/min)	ER (%)	Air flow (L_{STP}/min)
1, 2	AS	Air	850	0.184	0	31.1	6.2
3, 4	AS	Air-steam	850	0.5	0.7	32.2	6.4
5	TAS220	Air	850	0.024	0	33.4	7.9
6	TAS220	Air-steam	850	0.5	1.2	35.0	8.3

gasifying agent was only air (runs # 1, 2 and 5), the S/C ratio is not zero as it does not only refer to the added flow of steam but also includes the steam provided by the material moisture (g of moisture/ g of C). When feeding steam together with air as gasifying agent (runs # 3, 4 and 6), the S/C ratio of 0.5 includes both the material moisture and the flow of steam added.

3. Results and discussion

3.1. Torrefaction results

3.1.1. Products distribution

Mass balance closed fairly well, between 98 % and 99 %, in all the torrefaction experiments. Figure S1 in the Supplementary Information Section shows the distribution of the torrefaction products at 220 and 250 °C. Mass loss in the raw material increased with the torrefaction temperature as the devolatilization process promoted the formation of liquid and gas, thus decreasing the solid yield. The temperature is the main factor affecting the occurrence of the decomposition reactions [28], playing a pivotal role in kinetics, as can be seen in the strong effect on the product's yields even with an increase of only 30 °C. By increasing the temperature from 220 to 250 °C, the solid yield decreased from 65.8 to 49.7 wt%. Water was the second most abundant product after the torrefied solid and was obtained from either evaporation of moisture present in the material or dehydration reactions taking place with hydroxyl groups of carbohydrates (cellulose and hemicellulose) [28]. The water yield in AS torrefaction was 19.2 and 23.7 wt% at 220 °C and 250 °C, respectively. On the other hand, the yield of condensable organics with respect to biomass fed increased from 7.8 to 15.7 wt% when raising the temperature from 220 to 250 °C. The same upward trend was observed for non-condensable gas (from 5.4 to 10.4 wt %).

3.1.2. Characterization of torrefied solids

The product of interest in the torrefaction process is the torrefied solid, which should have better fuel properties than the raw material. The obtained solid (see its appearance in Figure S2 in the Supplementary Information Section) became darker with the increased temperature because of the caramelization of cellulose and hemicellulose components and the formation of quinones [31]. In addition, the high initial hardness of AS was noticeably reduced (the torrefied material was easily crushed). The results of ultimate and proximate analyses and the HHV of AS, TAS220, and TAS250 are summarized in Table 2. The HHV of AS increased from 18.6 MJ/kg to 22.7 MJ/kg in TAS220 and up to 27.0 MJ/kg in TAS250, meaning an increase of 22 % and 45 %, respectively. This energy density gain is ascribed to the release of volatiles [32] and increase in the fixed carbon content, and also consistent with the observed decrease in the O/C molar ratio in the torrefied solid due to the important release of CO_2 (section 3.1.3) and H_2O because of dehydration reactions. Table S2 in the Supplementary Information Section shows a comparison of AS torrefaction performance with other materials from the literature. For instance, in the study of Brachi et al. [33], the torrefaction of sugar beet pulp (smaller particle size between 1 and 2 mm and ash content up to 4 wt%) at 250 °C in a fixed bed reactor led to the same yield of solid product (49 wt%) but different production of gas (34.4 wt% for sugar beet pulp vs 10.4 wt% for AS) and liquid product (16.6 wt% for sugar beet pulp vs 39.4 wt% for AS) when operating at similar conditions but in different reactor type and particle size. For a shorter residence time (15 min vs 27 min in this work), higher torrefied solid yield (up to 83 wt% vs 49.7 wt% in this work) was reported in the study of Asadullah et al. [34] using palm kernel shell as raw material (bigger particle size between 7 and 15 mm and ash content of 3 wt%) in a fixed bed reactor. In contrast, in spite of using a woody material, whose behavior could be expected to be a priori far different from AS, Branchi et al. obtained a more similar value of solid yield (43 wt%) when torrefying pine (with closer particle size and ash content to AS) [35].

Table 2
Characterization results of AS, TAS220 and TAS250.

	AS	TAS220	TAS250
Proximate analysis (wt. %, ar. basis)			
Ash	0.20 ± 0.04	0.4 ± 0.1	0.73 ± 0.01
Moisture	8.74 ± 0.03	1.4 ± 0.4	2.0 ± 0.4
Volatile matter	74.6 ± 0.3	69 ± 2	52.6 ± 0.8
Fixed Carbon	16.5 ± 0.4	30 ± 2	45 ± 1
Ultimate analysis (wt. %, ar. basis)			
C	47.5 ± 0.2	59.8 ± 0.2	68.9 ± 0.1
H	6.55 ±	5.5 ± 0.1	4.75 ± 0.04
N	0.08	0.243 ±	0.33 ± 0.01
S	0.177 ±	0.005	0.040 ±
O[(a)]	0.003	0.040 ±	0.001
O/C ratio	0.044 ±	0.001	25.2 ± 0.1
H/C ratio	0.001	33.9 ± 0.3	0.28
	45.5 ± 0.2	0.43	0.43
	0.58	0.78	
	1.65		
HHV (MJ/kg)	18.61 ± 0.04	22.67 ± 0.04	26.97 ± 0.05
Macro-components composition (wt. %, ar. basis)			
Extractives	0.2 ± 0.1	0.4 ± 0.01	0.5 ± 0.1
Hemicellulose	21 ± 1	5 ± 0.2	0.60 ± 0.03
Cellulose	35 ± 2	31 ± 2	34 ± 2
Lignin	34 ± 2	61 ± 3	62 ± 3

(a) Calculated by difference (wt.%): O = 100—C—H—N—S—Ash.

Accordingly, the distribution of the products in the torrefaction process is impacted by many factors (reactor configuration, material nature, temperature, residence time, particle size and ash content) and extrapolating the results from one material to another does not result in good predictions if all the operational factors are not properly controlled.

Slight variations are also observed in the torrefied solid characteristics as, for example, HHV ranges between 22.7 and 26.2 MJ/kg and the carbon content between 60 and 70 wt%.

Table 2 also lists the results of the macro-components composition of the raw material and torrefied AS. The hemicellulose content dropped from 21 % in AS to 5 % in TAS220 and 0.6 % in TAS250. These results attest that hemicellulose was the major component decomposed during torrefaction, being almost totally degraded at 250 °C, which agrees with other results found in the literature [17]. The diminution of cellulose content was also significant in both cases: 41 % of cellulose in AS was degraded at 220 °C, and this rate increased to 51 % at 250 °C. These results highlight the high reactivity of this material even at this moderate temperature interval.

Regarding lignin, data in the literature show that its decomposition starts at around 200 °C [28]. Therefore, during torrefaction at 220–250 °C, lignin depolymerization should be expected to occur to some extent. In fact, as will be discussed below, the presence of some phenolic compounds in the torrefaction liquid points to the degradation of lignin. However, as shown in Table 2, the lignin content increased from 34 % in AS to 61 % in TAS220 and 62 % in TAS250. This increase was not only observed in terms of percentage but also in the net weight of lignin produced. This increase could be explained by the condensation and repolymerization processes of lignin itself during the torrefaction process [17] or due to the formation of new compounds from the decomposition of polysaccharides and subsequent condensation reactions, forming compounds that are insoluble in sulfuric acid (72 %) and therefore quantified as lignin by the Van Soest analysis procedure (considered as technical lignin).

The derivative thermogravimetry curves of AS, TAS220 and TAS250 are shown in Fig. 3. Different weight loss stages can be clearly distinguished in them. For the raw AS, the first low-intensity mass loss (up to 10 %) at the beginning of heating (T < 140 °C) corresponds to the removal of moisture (8.74 % according to the proximate analysis at

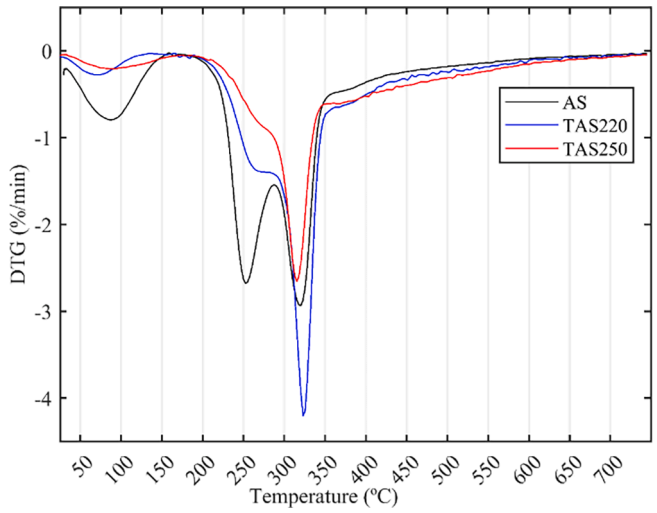

Fig. 3. DTG plots of AS before and after torrefaction at 220 and 250 °C.

105 °C); another stage of mass loss starts at around 200 °C, showing a strong intensity peak that continues up to around 350 °C. The slope change observed in this part of the mass loss curve may correspond to the simultaneous degradation of more than one constituent (hemicellulose, cellulose, or even lignin). Lignin decomposition starts from around 200 °C [28], but this does not always represent a clear shoulder peak different from hemicellulose and cellulose decomposition peaks. For higher temperatures (T > 350 °C), a slower mass loss corresponding to lignin degradation is observed. Overall, it can be concluded that the major part of pyrolysis conversion occurs at a temperature below 500 °C. The noticeable diminution and/or disappearance of peaks (Fig. 3) for TAS220 and TAS250 in the temperature interval between 30 and 300 °C can be correlated with the differences in moisture and hemicellulose contents. However, taking into account that Van Soest analysis of AS showed a hemicellulose content of 21 %, it can be stated that the second peak observed in the DTG of AS (from 200 °C to 280 °C in Fig. 3), which corresponds to around 30 % of mass loss in the TGA, may correspond not only to hemicellulose degradation but also to the beginning of cellulose or lignin depolymerization. This peak area was significantly reduced in TAS220 and TAS250, which agrees with the almost complete removal of hemicellulose in the torrefied material according to Van Soest analysis (degradation of 85 % and 98.6 % of hemicellulose in TAS200 and TAS250, respectively) [36]. On the other hand, according to some studies in the literature [37], the third peak (from 280 to 360 °C) in the DTG would a priori be mostly attributed to cellulose degradation. However, according to this statement, the third peak in the three solids should have a more similar size, as comparable cellulose contents were found in AS, TAS220 and TAS250 with the Van Soest analysis (Table 2). Hence, the noticeable differences observed in the area of these peaks (Fig. 3) highlight an overlapping of cellulose, hemicellulose and even lignin degradation processes in the temperature range of 220–340 °C [38].

The change in the composition of AS after torrefaction was also observed by ATR FTIR (Fig. 4). In general, the FTIR spectrum of AS changed significantly after torrefaction. The intensity of peaks #1 (wavenumber in the range of 3600–3100 cm^{-1}) and #2 (wavenumber in the range of 3000–2800 cm^{-1}) decreased with the increase of torrefaction temperature, showing the loss of hydroxyl groups by either dehydration reactions or sample drying and the disappearance of alkyl groups in the torrefied AS, respectively. The peak observed at wavenumbers in the range of 1760–1700 cm^{-1} (peak #3), corresponding to the C═O band (typical of acids, esters, aldehydes, and ketones), was especially reduced during the torrefaction of AS. This fact could be correlated with the important release of CO and CO_2 in the generated gas and the collection of acetic acid in the torrefaction liquid during the experiments, which may likely be due to the cleavage of acetyl radicals ($COCH_3$), especially from hemicellulose [28] (see section 3.1.3). Peaks at wavenumbers around 1640–1500 cm^{-1} indicate aromatic links (peak #4), and its intensity in TAS220 and TAS250 was slightly increased compared to the raw AS, which can be correlated with the increase in technical lignin content in the torrefied solids (from 34 to 61–62 wt%, Table 2). Finally, it should also be noted that the reduction of the peaks #6 (~1250 cm^{-1}) and #7 (~1050 cm^{-1}) after torrefaction corresponds to the reduction of hydroxyl groups and ether bonds (C—O—C) in lignin, xylan and cellulose [39].

3.1.3. *Characterization of liquid and gas torrefaction products*

The liquid produced in the torrefaction process mainly comprises water (71 and 60 % on a solvent-free basis at 220 and 250 °C, respectively) and oxygen-containing organic compounds. Hence, water yield reached 19 wt% (at 220 °C) and 24 wt% (at 250 °C) with respect to AS fed, and organic liquid yield (calculated by difference from the total liquid yield) was 8 wt% (at 220 °C) and 16 wt% (at 250 °C) (see Figure S1 in the Supplementary Information Section). The quantification via GC–MS/GC-FID (Table 3) allowed identifying and quantifying around 59–67 % of such mass of organic compounds. Methanol is known to be one of the most abundant organic products in the torrefaction

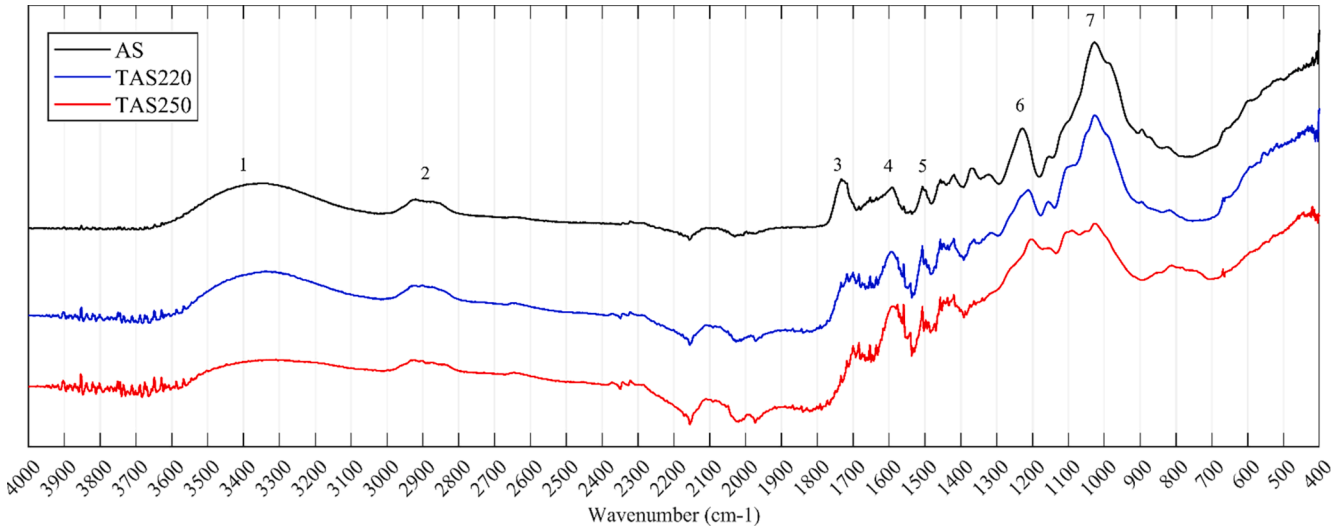

Fig. 4. FTIR spectra of AS before and after torrefaction at 220 and 250 °C.

Table 3
Concentration of organic compounds in the torrefaction liquids (mg/g liquid, quantified by GC-FID).

	Concentration in the torrefaction liquid (mg/g torrefaction liquid)*	
Compound	AS, 220 °C	AS, 250 °C
Furan, tetrahydro-2,5-dimethoxy-	–	1.9
Acetol	6	11
1-Hydroxy-2-butanone	9	11
Acetic acid	146	159
Furfural	14	14
Propanoic acid	5.90	9.3
5-methyl furfuryl	0.500	0.7
2-Furanmethanol	1.7	2.9
2-Cyclopenten-1-one, 2-hydroxy	0.6	1.30
2-Cyclopenten-1-one, 2-hydroxy-3-methyl-	0.6	1.80
Guaiacol	1.5	3.7
Creosol	0.6	2.3
4-Ethylguaiacol	0.5	1.4
Cyclopentanol	–	0.7
Eugenol	–	0.3
4-Vinylguaiacol	0.3	0.6
Phenol, 2,6-dimethoxy-	1.7	4.9
Trans-Isoeugenol	1	1.4
Methoxyeugenol	1	3.4
Benzene, 1,2,3-trimethoxy-5-methyl-	0.5	1.8
Vanillin	0.4	0.6
Guaiacylacetone	–	0.4
Total	191.8	234.4

*Concentration data are expressed on a solvent-free basis.

liquid product [40] due to the degradation of xylan or from the methoxyl groups of uronic acid [41]. Methanol was clearly identified in our chromatograms, but as it had been used as a solvent for recovering the liquid from the condensers, its real production during torrefaction could not be estimated. This fact, together with the presence of oligomeric compounds (with high molecular weight) undetectable by GC [42,43], may fit the remaining fraction of organics that could not be properly explained by GC–MS-FID. Most of the identified organic compounds belong to the families of acids, alcohols, ketones, aldehydes, furans, and phenols (Figure S3 in the Supplementary Information Section). Acids, alcohols, ketones, and furans are typical products of thermal degradation of hemicellulose [44], but they can also be produced during cellulose degradation [41]. More specifically, acids have been found to be produced as soon as the temperature threshold for the thermal decomposition of cellulose (around 270 °C in the case of some woody biomass) is exceeded [45]. On the other hand, the production of phenols is known to result from lignin decomposition.

Table 3 presents the individual GC-FID quantification results of the main compounds identified in the torrefaction liquids. As can be seen, the most abundant compound was acetic acid. Its concentration increased slightly with the torrefaction temperature from 146 to 159 mg/g liquid. Several studies relate the formation of acetic acid in torrefaction with the thermolysis of acetyl radicals linked to the hemicellulose pentosans [28,41]. On the other hand, furfural content, which was also one of the major compounds in the torrefaction liquids, was not affected by the torrefaction temperature. Its formation is related to the dehydration of the xylose unit (hemicellulose component) [46] or to the degradation of cellulose via the dehydration of the formed levoglucosan followed by formaldehyde degradation [47]. Phenols with the highest concentrations in AS torrefaction liquids (essentially methoxy- and dimethoxy- phenols) were derived from coniferyl alcohol (G) and sinapyl alcohol (S), respectively. Temperature promoted the production of most of the identified phenols.

Non-condensable gas was the minority product (by weight) in the torrefaction of AS (Figure S1 in the Supplementary Information Section). On a N_2-free basis, CO_2 (62–65 vol%) and CO (25–30 vol%) were the main gases produced, while CH_4 (6–7 vol%) and H_2 (1 vol%) were detected in smaller percentages. The formation of CO_2 (at this temperature range) is due to the decarboxylation reaction of the carboxyl group in hemicellulose [48,49], while CO is the result of carbonyl, carboxyl and ether groups cracking [49]. Such volumetric concentration data match with the following mass yields calculated with respect to the mass of AS fed: 4–8 wt% for CO_2, 1–2 wt% for CO, 0.2–0.3 wt% for CH_4 and 0.003–0.005 wt% for H_2 (the higher torrefaction temperature, the higher yield).

3.2. Gasification results

3.2.1. Thermodynamic equilibrium model results

As commented, the gasification model described above was run under a wide range of operational conditions (T = 750–1100 °C and S/C = 0–1.1) to determine the ER required for auto-thermal gasification and to evaluate the gas composition once chemical equilibrium was reached for the studied materials (AS, TAS220 and TAS250). Fig. 5 shows the results of these simulations for the raw AS and the torrefied materials at different temperatures and S/C values. The higher the temperature, the higher the ER required for operation. ER for auto-thermal and chemical equilibrium conditions ranges between 30 % and 45 %. Note that the equilibrium calculation in the case of TAS250 has shown lower ER values, especially at the lowest studied temperatures, thus pointing to incomplete solid conversion.

The gas quality is evaluated through the H_2/CO ratio. As expected, the increase of the S/C ratio leads to a higher H_2/CO ratio in all cases, regardless of the temperature evaluated, due to the shift of the water–gas shift reaction (R1), one of the most representative reactions of the gasification process, to the products side. H_2/CO ratio is reduced with increasing temperature (shift of R1 towards left side because of its exothermic character), and this reduction is even more pronounced with the incorporation of steam in the gasification atmosphere due to the enhancement of the water–gas shift reaction. Although higher S/C ratios lead to improved H_2/CO ratios in the producer gas, syngas production (considering this as the joint production of CO and H_2) is not always favored at such conditions, as higher ER is in turn required to reach auto-thermal conditions, which negatively affects the effective use of the raw material due to the conversion of more C into CO_2 (complete combustion, R2).

Water-gas shift (WGS):

$$CO(g) + H_2O(g) \leftrightarrow CO_2(g) + H_2(g)\ \Delta H_{r,\ 298K} = -41.16\ kJ/mol \quad (R1)$$

Oxidation:

$$C(s) + O_2(g) \leftrightarrow CO_2(g)\ \Delta H_{r,\ 298K}\ -393.509\ kJ/mol \quad (R2)$$

Fig. 6 shows the production of CO + H_2 and CO_2 at different temperatures and S/C values for both the raw and torrefied materials. The production of CO + H_2 is enhanced at lower S/C ratios and lower temperatures (both involving lower ER), this occurring at the expense of CO_2 generation. This trend is not observed for TAS250 gasification at the lowest S/C ratios (S/C < 0.5) and temperatures (<900 °C), as a total conversion of the carbonaceous material is not reached. For example, syngas production in AS gasification at 850 °C falls from 1.12 to 1.04 m^3_{STP}/kg when the S/C ratio varies from 0.184 to 1.1, while CO_2 production almost doubles its value (Fig. 6A). A similar effect of S/C is observed for TAS220 (Fig. 6B), even though higher syngas production (1.43 m^3_{STP}/kg TAS220 at S/C of 0.024) and lower CO_2 generation with

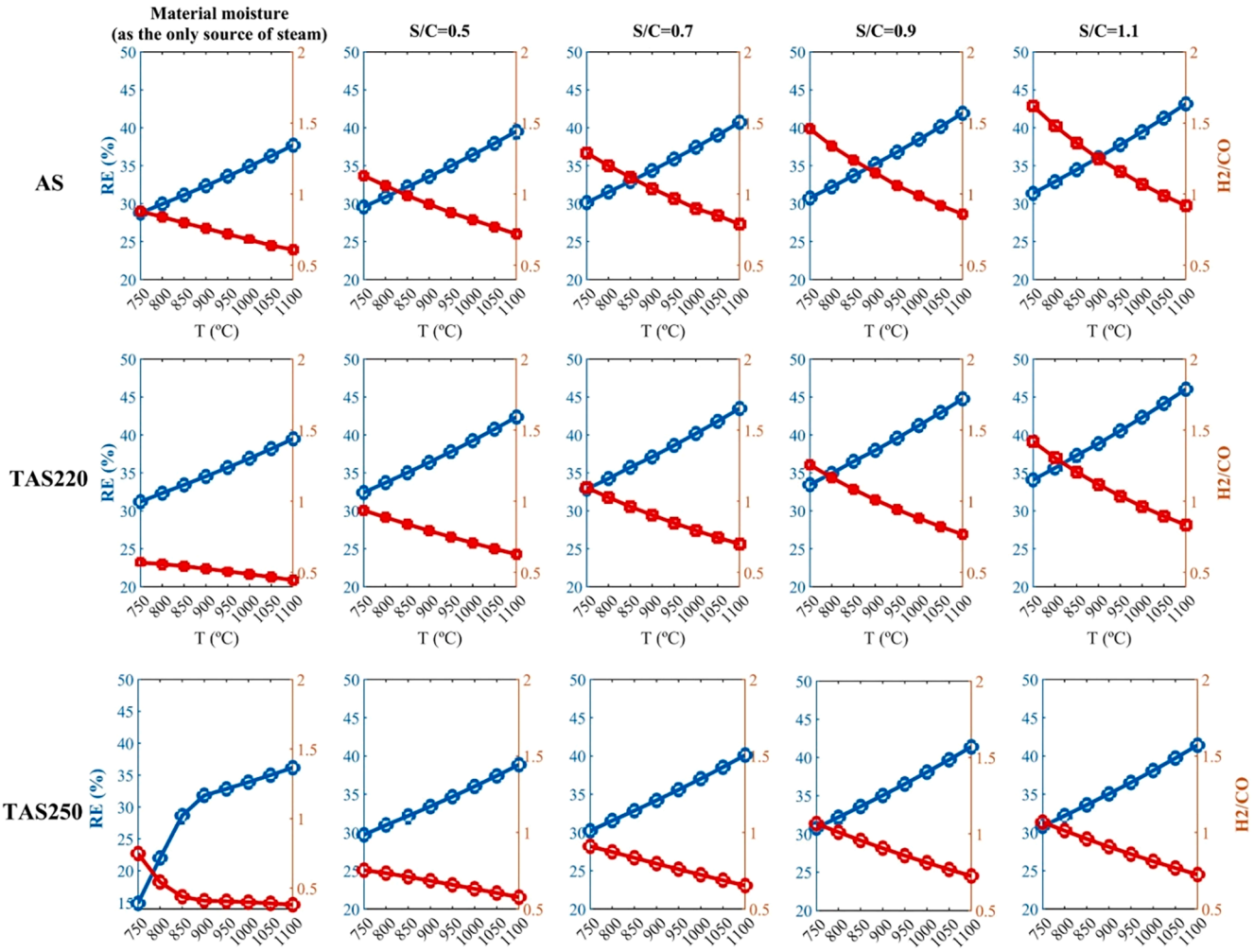

Fig. 5. General view of AS, TAS220 and TAS250 gasification simulation results.

respect to the gasification of raw AS are found. Syngas production is even higher in TAS250 gasification when operating at temperatures above 850 °C and with enough amount of gasifying agent (1.76 m^3_{STP}/kg a S/C = 0.5). Hence, if taking into account the elemental composition of the three materials, it can be concluded that the production of syngas at auto-thermal and equilibrium conditions is favored by lower O/C and H/C ratios in the feedstock (as long as the material can be gasified entirely), not so the H_2/CO ratio in the syngas, which follows the opposite trend.

In summary, these theoretical results from the equilibrium model have pointed out that increasing the S/C ratio is favorable for a higher H_2/CO in the produced gas (Fig. 5), but not for maximizing syngas production (Fig. 6). In addition, too low temperatures could leave behind unconverted solid, especially in the case of torrefied AS. Hence, an intermediate value of S/C ratio (0.5) was set for the gasification experiments, as an agreement between the studied parameters is required to obtain a syngas rich in H_2. Moreover, kinetic aspects usually hinder reaching chemical equilibrium in the process, so tar formation and uncomplete conversion of solid carbon may be expected from real gasification processes. This motivated us to set the gasification temperature for the experiments at a value of 850 °C. Such a combination of temperature and S/C ratio allowed operating at an ER lower than 35 % in all cases, which is favorable for syngas (CO + H_2) production and CO_2 minimization.

3.2.2. Product distribution

Mass balance closed fairly well, between 92 % and 97 %, in all the experiments.

Experimental results for the distribution of gasification products, either from AS or TAS220, are summarized in Table 4. A significant increase in the generation of char (solid product) was observed in the case of TAS220 gasification if compared with the raw AS (10.6 vs 2.3 wt % when using only air and 7.5 vs 1.8 wt% when using air–steam). As the ash content is even lower in the char obtained from TAS220 (Table 4), this noticeable increase in the amount of char could be justified by a reduced reactivity of the raw material after torrefaction. A similar finding has already been reported in the study of Fisher et al. [50] using raw and torrefied short rotation coppice willow. In fact, the carbon content in the remaining solid after TAS220 gasification was found to be significantly higher, while oxygen content was much lower, thus leading to a reduced O/C ratio. Using a mixture of air and steam as the gasifying agent instead of only air slightly decreased the production of char in both cases (AS and TAS220) due to the enhancement of the water–gas reaction (R3) that could further generate CO and H_2, but also due to favored combustion of char (R2), as the addition of steam involves higher ER for auto-thermal operation.

Water-gas reaction:

$$C(s) + H_2O(g) \leftrightarrow CO(g) + H_2(g)\ \Delta H_{r,\ 298K} = 131.30\ kJ/mol \quad (R3)$$

The yield of liquid product (including tar and condensed water) was found to increase when adding steam as gasifying agent (from 22 to 30 wt% for AS gasification and from 17.9 to 34 wt% for TAS220). Such a rough increase in the liquid yield may not necessarily mean a higher tar

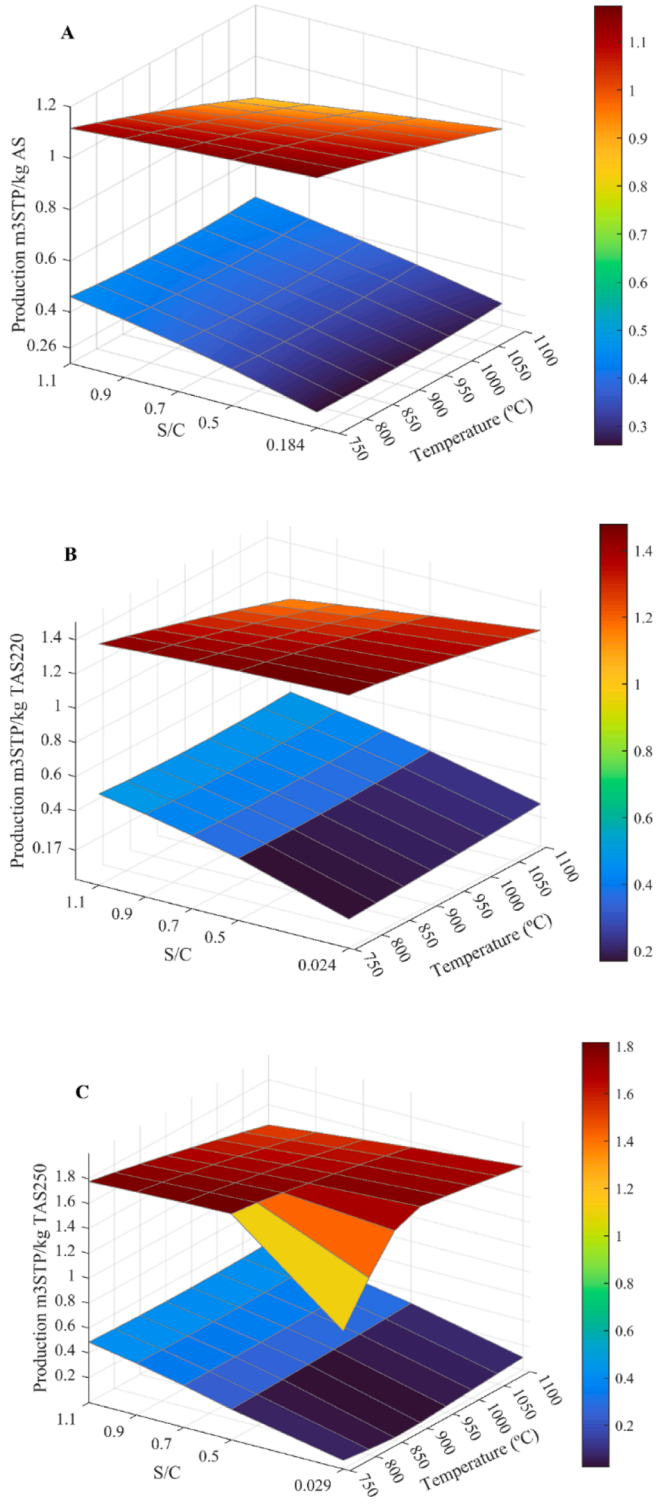

Fig. 6. Theoretical production of CO + H_2 (red surface) and CO_2 (blue surface) at different temperatures and S/C ratios for AS (A), TAS220 (B) and TAS250 (C) gasification.

formation (see section 3.2.4), as un-converted or produced water is also included in this yield.

On the other hand, the fact of having "strange" gas yields above 100 % is only a matter of the calculation basis (the reference is only biomass).

The volumetric gas production is usually defined in the gasification studies as a more representative factor of syngas generation. As shown in

Table 4
Experimental results from the gasification at 850 °C of AS and TAS220.

Run Material	1 & 2 AS	3 & 4 AS	5 TAS220	6 TAS220
Reaction medium	Air	Air-steam	Air	Air-steam
Product yield (wt. %)				
Char	2.3 ± 0.4	1.8 ± 0.6	10.6	7.5
Liquid (tar + water)	22 ± 1	30.24 ± 0.02	17.9	34
Gas (N_2 free basis)	135 ± 2	133 ± 7	138	148
Syngas composition (vol. %)				
H_2	9.4 ± 0.9	11 ± 2	6.9	9.4
CO	14 ± 1	12 ± 1	11	10
CO_2	17.3 ± 0.2	18.2 ± 0.3	17	18
CH_4	0.3	3.9 ± 0.4	3.1	3.0
C_2H_6	4.0 ± 0.2	0.12 ± 0.03	0.1	0.1
C_2H_4	0.14 ± 0.02	0.9 ± 0.1	0.6	0.6
C_2H_2	0.9 ± 0.1	0.08 ± 0.01	0.1	0.03
H_2S	0.07 ± 0.05	0.10 ± 0.01	0.01	0.1
N_2	0.1 ± 0.05	54 ± 3	62	59
	54 ± 2			
H_2/CO ratio	0.69 ± 0.04	0.90 ± 0.04	0.64	0.94
CO/CO_2 ratio	0.81 ± 0.04	0.7 ± 0.1	0.63	0.57
Cold gas efficiency (%)	66 ± 4	66 ± 9	45.3 (37)	48.7 (40)
LHV_{gas} (MJ/m^3_{STP})	4.7 ± 0.3	4.5 ± 0.5	3.6	3.6
Gas production(m^3_{STP}/kg material)	2.37 ± 0.01	2.4 ± 0.1	2.7 (1.8)	2.9 (1.9)
Gas production N_2-free basis (m^3_{STP}/kg material)	1.1 ± 0.4	1.1 ± 0.1	1.1 (0.7)	1.2 (0.8)
Carbon yield to the gas phase (%)	100 ± 2	97 ± 7	79	83
Concentration of tar in syngas, g/m^3_{STP} (GC–MS)	0.7 ± 0.1	0.6 ± 0.1	0.7	0.3
Char characterization (elemental analysis and ash content, wt. %)				
C	83 ± 7	79.9	92.8	92.6
H	2 ± 1	1.3	0.9	1.1
N	0.7 ± 0.1	0.8	1	0.9
O	8.1	11.1	2.9	2.8
Ash	6.2 ± 0.1	6.9	2.4	2.5

The values shown in brackets for TAS220 gasification represent the analogous results obtained if considering for the calculations the original amount of AS that was torrefied instead of the amount of TAS220 that was gasified.

Table 4, this factor has shown values of around 2.4 m^3_{STP}/kg for AS, while increased up to 2.7–2.9 m^3_{STP}/kg for TAS220. These gas production data include N_2 coming from air and, as TAS220 gasification involved highest values of ER (see Table 1), it means that N_2 feeding was also greater. By considering a N_2-free basis for gas production, such differences between the raw AS and the torrefied material practically disappear (1.1–1.2 m^3_{STP}/kg material). As expected, if gas production in TAS220 gasification is calculated with respect to the original amount of AS previously torrefied, it falls by around 25 % (0.7–0.8 m^3_{STP}/kg AS). The N_2-free gas produced in the torrefaction stage (0.08 m^3_{STP}/kg AS) does not offset such a difference.

3.2.3. Syngas composition and properties

Besides the reactions previously commented, a wide range of exothermic and endothermic reactions occur during the different stages

taking place in the gasification process:

Partial oxidation:

$$C(s) + 1/2O_2(g) \leftrightarrow CO(g)\ \Delta H_{r,\ 298K} = -110.53\ kJ/mol \quad (R4)$$

Boudouard:

$$C(s) + CO_2(g) \leftrightarrow 2CO(g)\ \Delta H_{r,\ 298K} = 172.45\ kJ/mol \quad (R5)$$

Methanation:

$$C(s) + 2H_2(g) \leftrightarrow CH_4(g)\ \Delta H_{r,\ 298K} = -74.85\ kJ/mol \quad (R6)$$

Steam reforming:

$$C_xH_y(g) + xH_2O(g) \leftrightarrow xCO(g) + (y/2 + x)\ H_2(g)\ \Delta H > 0 \quad (R7)$$

Dry reforming:

$$C_xH_y(g) + xCO_2(g) \leftrightarrow 2xCO(g) + (y/2)\ H_2(g)\ \Delta H > 0 \quad (R8)$$

Cracking:

$$C_xH_y(g) \leftrightarrow xC(s) + (y/2)\ H_2(g)\ \Delta H > 0 \quad (R9)$$

According to the results exposed in Table 4, the gasification of AS and TAS220 produced significant amounts of H_2, CO, CO_2, light hydrocarbons (predominantly CH_4) and H_2S (detected and quantified by micro-GC). As predicted by the equilibrium calculations, the experimental data confirmed that adding steam to the gasifying agent improved the quality of the gas. H_2 concentration was increased from 9.7 % vol. to 11 % vol. when adding steam (S/C = 0.5) in the case of AS gasification. Lower H_2 concentrations were obtained in the case of TAS gasification: 6.9 % vol. when gasifying with only air and 9.4 % vol. at S/C = 0.5. The opposite behavior was found for CO concentration, which decreased when steam was added. This reverse relation between H_2 and CO concentrations directly affects the H_2/CO ratio, which was enhanced by adding steam from 0.69 to 0.9 in the case of AS and from 0.64 to 0.94 for TAS220. Therefore, the torrefaction of AS did not further improve the H_2/CO ratio in the syngas. These H_2/CO values were greater than those reported in the literature for the gasification of similar materials, such as almond shells gasification in an updraft reactor at 850 °C, for which the H_2/CO ratio ranged between 0.46 (S/C = 0) and 0.75 (S/C = 0.2) [11]. The torrefaction stage neither played an important role in the production of CO_2 during the subsequent gasification, as it was maintained around 17 % vol. in all cases when gasifying with only air. A slight increase was observed when adding steam, which could boost either the water–gas shift reaction or combustion reactions because of the simultaneous increase of the ER (needed to keep the reaction at 850 °C). As expected, the production of light hydrocarbons during gasification was significantly affected by the previous torrefaction stage.

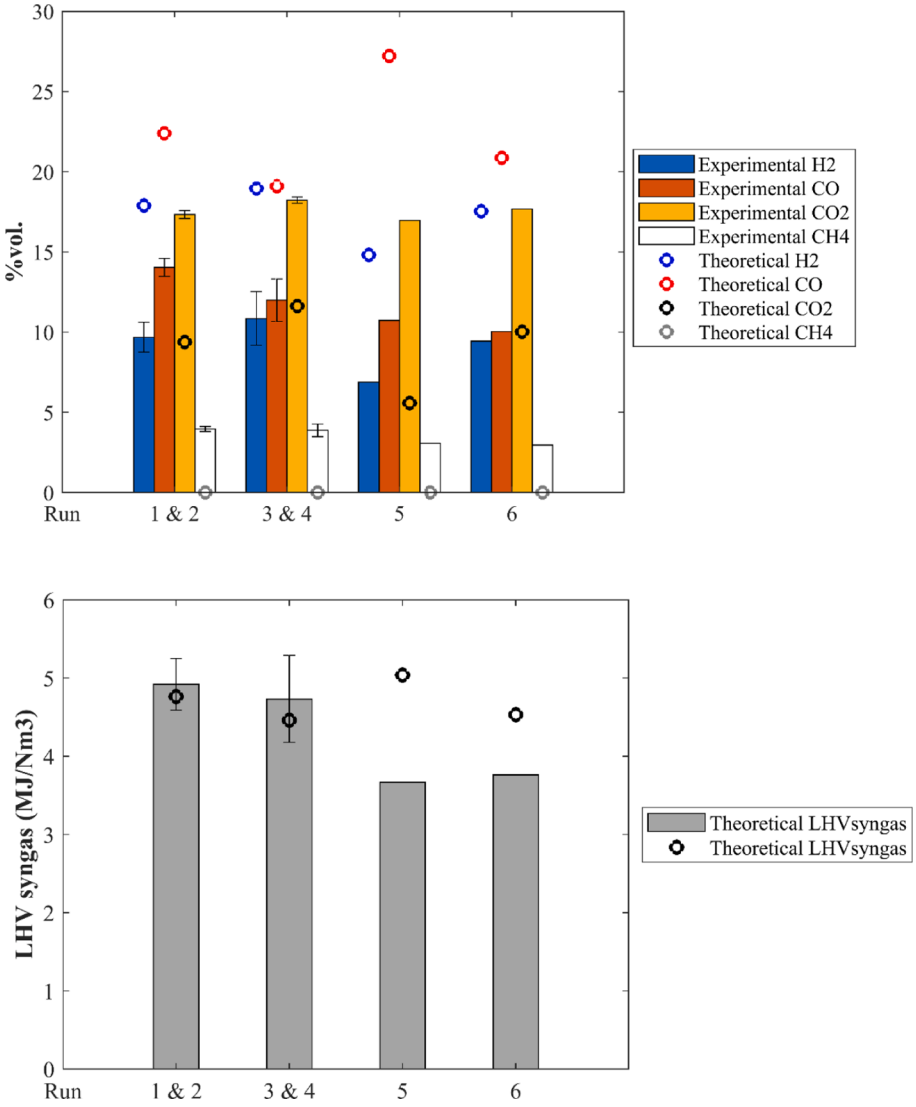

Fig. 7. Theoretical and experimental concentrations of CO, H_2, CO_2 and CH_4 (% vol.) in the gasification gas and corresponding LHVs.

The concentration of CH_4 was around 25 % lower in TAS220 gas. This fact seems to be directly related to the volatile matter released during the torrefaction process. As a result, the volatile matter content in the raw material was significantly reduced: 75 wt% in AS vs 69 wt% in TAS220. A similar trend was observed by Strandberg [51], who compared the gasification of raw and torrefied woody residues. As mentioned in that work, the main reason for CH_4 presence in the gasification syngas is an unconverted fraction of pyrolysis products coming from the volatile components in the raw biomass. It is to highlight that the CH_4 content was not affected by the composition of the gasifying agent for both materials (no significant effect of steam addition was observed).

Fig. 7 compares the experimental gas composition obtained at the different operating conditions with the theoretical data predicted by the equilibrium model (only including the four main gas products). Theoretical and experimental data are noticeably different. The equilibrium calculations predicted higher concentrations of H_2 and CO (approximately double) than those experimentally obtained in the lab setup, while the experimental content of CO_2 almost doubled the simulation prediction in some cases. The model expected only traces of CH_4 (<0.01 % vol.), while real concentrations obtained in the gasification experiments were between 3 and 4 % vol. This divergence between the theoretical and experimental data means that the equilibrium was not reached during the experiments at these operational conditions.

Besides composition, other important characteristics of the produced syngas, such as its lower heating value (LHV_{gas}), the carbon conversion to the gas phase and the cold gas efficiency are also included in Table 4. The addition of steam to the gasification atmosphere did not significantly affect the LHV of the gas obtained from any of the two materials gasified. Typical values between 3 and 5 MJ/m^3 are reported in the literature for the LHV of the syngas obtained in the air gasification of many lignocellulosic materials (woody, herbaceous or fruit-shells [17,52,53]). For instance, in the study of Kulkarni et al. [17], the LHV of the syngas was 5.2 MJ/Nm^3 for pine gasification. For walnut and pistachio shells, the study of Karatas and Akgun [52] reported LHV values of up to 5 MJ/m^3 at lower ER values. The ER plays a significant role in the LHV of the gas because of the N_2 dilution effect. However, significant differences were found in the LHV_{gas} when comparing the gas from AS and TAS220, as it was reduced by around 1 MJ/m^3_{STP} when feeding the torrefied material. This reduction may be related to the lower content of combustible gases such as CH_4, H_2 and CO and the increased fraction of N_2 in the syngas from TAS220. A similar trend was observed in other work in the literature for the gasification of raw and torrefied switchgrass (at 230 and 270 °C), for which the LHV_{gas} decreased in 0.4 and 0.6 MJ/m^3, respectively [53]. Kulkarni et al. reported a decrease of up to 0.7 MJ/Nm^3 in LHV_{gas} after the gasification of torrefied pine [17].

As shown in Fig. 7, the equilibrium-based model used to simulate the gasification of AS and TAS220, either with air or air–steam, predicted minor differences between the values of LHV_{gas} obtained from both materials, all of them ranging between 4.5 and 5.1 MJ/m^3_{STP}. The experimental values of LHV_{gas} obtained in the case of AS gasification were quite similar to the model estimations, while in the case of TAS220, the theoretical values were higher. The theoretical model does not consider the nature of the chemical bonds in the original materials. However, the kinetics of the gasification process has been experimentally proved to be affected by the chemical transformations occurring in the previous torrefaction stage (as shown by the higher char yield obtained in the gasification of TAS220), which in turn results in important differences in the composition and the LHV of the syngas.

The LHV of the syngas directly affects the cold gas efficiency (Equation (3)). The gasification of AS showed a cold gas efficiency higher than 60 %, while in the case of TAS220 gasification, it reached 49 % as the maximum value. This difference is explained by the lower energy density in the gas from TAS220. The cold gas efficiency for the gasification of the torrefied material is even lower (37–40 %) if considering the initial amount of AS that was torrefied as the calculation reference. However, gas from torrefaction (LHV = 0.6 MJ/m^3_{STP}) could also be considered to calculate a global cold gas efficiency for the two-stages process, obtaining a result of 40–43 %. From this point of view, the two-stages process is less efficient than the direct gasification of the raw AS.

Another interesting parameter to assess the gasification performance is the carbon yield to the gas phase, which is the ratio between the mass of carbon contained in the syngas and the mass of carbon in the material fed (fraction of carbon converted to gaseous compounds). At equilibrium conditions, this ratio was estimated to be 100 % in all cases. However, lower values were obtained experimentally (Table 4), especially for TAS220 (79 and 83 %). This difference points to slower kinetics for the gasification of the torrefied material.

3.2.4. Production of tar

The production of tar in the gasification runs was quantified by GC–MS-FID analysis. Table 4 exposes the concentration of tar in the produced syngas, which was quite similar in most cases (between 0.6 and 0.7 g/m^3_{STP}), except when gasifying TAS220 at a S/C ratio of 0.5, for which a decrease of 50 % was observed. This was also confirmed in terms of tar yield with respect to the material fed, which ranged around 1.5–1.7 g/kg in the case of AS and dropped from 1.9 to 0.9 g/kg in the case of TAS220 gasification (Table 5). Kulkarni et al. [17] observed that the gasification of torrefied pine (at a temperature of 935 °C and ER of 25 %) reduced by half the production of tar compared to the original material (from 8 to 3.9 g/kg dried biomass). In the present work, we used calcined dolomite as bed material, which has been proved to be efficient in tar cracking at analogous operating conditions (temperature and use of steam) [29], which might be the reason for such low values of tar production.

Tar is mainly composed of polycyclic aromatic hydrocarbons (PAHs). Table 5 summarizes the composition of the identified tar (mass fractions), including 11 different PAHs detected in the condensed liquids. As shown, naphthalene, acenaphthylene and phenanthrene were the main tar compounds, accounting for 55–65 % of the produced tar. The formation of these aromatic tar species without substituent groups is favored in the temperature range of 750 to 900 °C [54]. According to Devi et al., such types of aromatics are considered the most challenging tar fraction to destroy because of their stability [54]. Steam addition to

Table 5
Production of tar in the gasification experiments and composition of tar samples (GC/MS/FID).

Run	1 & 2	3 & 4	5	6
Material, S/C	AS, 0.184	AS, 0.5	TAS220, 0.024	TAS220, 0.5
Production of tar (g/kg material)	1.7 ± 0.2	1.5 ± 0.2	1.9	0.9
Tar composition (wt.%)				
Naphthalene	42 ± 6	35 ± 6	43.2	34.9
Acenaphthylene	13 ± 2	11 ± 2	12.9	12.1
Acenaphthene	2.1 ± 0.1	2.9 ± 0.1	2.6	3.9
Fluorene	5.4 ± 0.4	5.7 ± 0.6	6.1	6.5
Phenanthrene	9 ± 1	9 ± 2	9.2	10.3
Anthracene	3.7 ± 0.3	4.2 ± 0.5	4.1	4.9
Fluoranthene	3.8 ± 0.4	4.3 ± 0.5	4.2	5.2
Pyrene	3.6 ± 0.4	4.2 ± 0.6	4.2	5.1
Benz[*a*]anthracene	3.5 ± 0.08	5.0 ± 0.4	4.7	5.9
Chrysene	3.5 ± 0.1	4.8 ± 0.3	4.5	5.8
Benzo[*b*]fluoranthene	3.0 ± 0.2	4.5 ± 0.3	4.2	5.4

the gasification atmosphere contributed to decreasing the individual production of these PAHs. For example, naphthalene yield dropped from 0.8 to 0.6 g/kg in the case of AS and from 0.8 to 0.3 g/kg in the case of TAS220 by increasing the S/C ratio up to 0.5. Steam reforming reactions (R7) may be involved in such observed reduction [55]. In summary, tar production during the gasification of AS or TAS220 with air was hardly affected by the torrefaction stage previously undergone by the solid, while a reduction in tar production was observed when adding steam to the TAS220 gasification atmosphere. However, tar composition was hardly impacted by the torrefaction stage, as the same PAHs (naphthalene, acenaphthylene and phenanthrene) were identified as the majority ones.

4. Conclusions

The torrefaction of argan nutshells (AS) has been experimentally studied at lab-scale as a potential process to improve its properties as fuel. This biomass showed a very reactive behavior even at moderate torrefaction temperatures (220–250 °C). Compared to the raw material, the torrefied solid product (yield between 49.7 and 65.8 wt%) was richer in fixed carbon and showed a lower O/C ratio and an important increase in the HHV (from 18.6 MJ/kg for the argan nutshells up to 27 MJ/kg for the material torrefied at 250 °C). Hemicellulose was almost totally removed from argan nutshells after torrefaction.

The gasification experimental study (planned for operating at auto-thermal conditions), as well as the chemical equilibrium theoretical model implemented for such auto-thermal operation, revealed that adding steam to the gasification atmosphere has a beneficial effect on the syngas composition by improving its H_2/CO ratio. The theoretical model pointed out that the lower O/C and H/C ratios found in the torrefied solid (TAS220) should leave behind a higher production of syngas ($CO + H_2$) and a lower H_2/CO ratio in the syngas, but this result was not observed experimentally, pointing that chemical equilibrium was not achieved in the experimental runs. The H_2/CO ratio was slightly higher for the torrefied material (0.94 for TAS220 vs 0.9 for AS), while the lower heating value of the gas from TAS220 was reduced mainly because of its lower CH_4 content (4.7 MJ/m^3_{STP} for AS gasification vs 3.6 MJ/m^3_{STP} for TAS220 gasification).

Tar reduction was one of the major expected advantages of including torrefaction as a pretreatment step before argan nutshells gasification. However, in the presence of dolomite, tar reduction was only slightly observed when adding steam into the gasification atmosphere (0.7 g/m^3_{STP} for AS gasification vs 0.3 g/m^3_{STP} for TAS220). On the other hand, argan nutshells turned less reactive after torrefaction, thus resulting in higher char formation and lower conversion of carbon to the gas phase, also with a lower CO/CO_2 distribution ratio. Hence, torrefaction as a pretreatment stage has not brought many benefits in terms of syngas production and quality for the gasification of argan nutshells.

CRediT authorship contribution statement

Zainab Afailal: Methodology, Investigation, Writing – original draft. **Noemí Gil-lalaguna:** Methodology, Investigation, Writing – review & editing. **Isabel Fonts:** Writing – review & editing. **Alberto Gonzalo:** Writing – review & editing, Project administration. **Jesús Arauzo:** Supervision, Project administration, Funding acquisition. **José Luis Sánchez:** Writing – review & editing, Supervision, Funding acquisition.

Declaration of Competing Interest

The authors declare that they have no known competing financial interests or personal relationships that could have appeared to influence the work reported in this paper.

Data availability

E-supplementary data of this work can be found in the paper's online version.

Acknowledgments

The authors express their gratitude to Agencia Estatal de Investigación in Spain (project PID2020-114936RB-I00) and Aragón Government (Research Group Ref. T22_20R) for providing frame support for this work. I. Fonts acknowledges the MINECO, European Social Fund, AEI and Unizar for the post-doctoral contract awarded (RYC2020-030593-I).

Appendix A. Supplementary data

Supplementary data to this article can be found online at https://doi.org/10.1016/j.fuel.2022.125970.

References

[1] Huber GW, Iborra S, Corma A. Synthesis of Transportation Fuels from Biomass: Chemistry, Catalysts, and Engineering. Chem Rev 2006;106(9):4044–98. https://doi.org/10.1021/cr068360d.
[2] Dahbi M, Kiso M, Kubota K, Horiba T, Chafik T, Hida K, et al. Synthesis of hard carbon from argan shells for Na-ion batteries. J Mater Chem A 2017;5(20):9917–28. https://doi.org/10.1039/c7ta01394a.
[3] Rahib Y, Boushaki T, Sarh B, Chaoufi J, Ihlal A, Bonammy S, et al. Combustion Analysis of Fixed Beds of Argan Nut Shell (ANS) Biomass in a Batch Type Reactor. In: in 2019 7th International Renewable and Sustainable Energy Conference (IRSEC); 2019. https://doi.org/10.1109/irsec48032.2019.9078217.
[4] Rahib Y, Elorf A, Sarh B, Ezahri M, Rahib Y, Bonnamy S. Experimental Analysis on Thermal Characteristics of Argan Nut Shell (ANS) Biomass as a Green Energy Resource. International Journal of Renewable Energy Research 2019;9(4):1606–15.
[5] Afailal Z, Gil-Lalaguna N, Torrijos MT, Gonzalo A, Arauzo J, Sánchez JL. Antioxidant Additives Produced from Argan Shell Lignin Depolymerization. Energy Fuels 2021;35(21):17149–66. https://doi.org/10.1021/acs.energyfuels.1c01705.
[6] Demirbaş A. Calculation of higher heating values of biomass fuels. Fuel 1997;76(5):431–4. https://doi.org/10.1016/S0016-2361(97)85520-2.
[7] Rapagnà S, Latif A. Steam gasification of almond shells in a fluidised bed reactor: the influence of temperature and particle size on product yield and distribution. Biomass Bioenergy 1997;12(4):281–8.
[8] Roger M. Rowell R.P., Mandla A. Tshabalala. Cell Wall Chemistry. In Handbook of Wood Chemistry and Wood Composites, Rowell, R.M., Editor CRC Press (2012). p.
[9] Nguyen NM, Alobaid F, May J, Peters J, Epple B. Experimental study on steam gasification of torrefied woodchips in a bubbling fluidized bed reactor. Energy 2020;202:117744. https://doi.org/10.1016/j.energy.2020.117744.
[10] Ahrenfeldt J, Knoef H. GasNet. Netherlands: Handbook biomass gasificationBTG Biomass Technology Group Enschede; 2005.
[11] Cerone N, Zimbardi F, Contuzzi L, Baleta J, Cerinski D, Skvorčinskienė R. Experimental investigation of syngas composition variation along updraft fixed bed gasifier. Energy Convers Manage 2020;221:113116. https://doi.org/10.1016/j.enconman.2020.113116.
[12] Dayton DC, Turk B, Gupta R. Syngas Cleanup, Conditioning, and Utilization. In Thermochemical Processing of. Biomass 2019:125–74.
[13] P.L. Spath D.C.D., ed. Preliminary Screening – Technical and economic assessment of synthesis gas to fuels and chemicals with emphasis on the potential for biomass-derived syngas. ed. report, T.2003: United States. doi: 10.2172/15006100.
[14] Gil-Lalaguna N, Sánchez JL, Murillo MB, Rodríguez E, Gea G. Air–steam gasification of sewage sludge in a fluidized bed. Influence of some operating conditions. Chem Eng J 2014;248:373–82. https://doi.org/10.1016/j.cej.2014.03.055.
[15] Cerone N, Zimbardi F, Villone A, Strjiugas N, Kiyikci EG. Gasification of Wood and Torrefied Wood with Air, Oxygen, and Steam in a Fixed-Bed Pilot Plant. Energy Fuels 2016;30(5):4034–43. https://doi.org/10.1021/acs.energyfuels.6b00126.
[16] Chen W-H, Chen C-J, Hung C-I, Shen C-H, Hsu H-W. A comparison of gasification phenomena among raw biomass, torrefied biomass and coal in an entrained-flow reactor. Appl Energy 2013;112:421–30. https://doi.org/10.1016/j.apenergy.2013.01.034.
[17] Kulkarni A, Baker R, Abdoulmomine N, Adhikari S, Bhavnani S. Experimental study of torrefied pine as a gasification fuel using a bubbling fluidized bed gasifier. Renewable Energy 2016;93:460–8. https://doi.org/10.1016/j.renene.2016.03.006.
[18] Li M-F, Chen L-X, Li X, Chen C-Z, Lai Y-C, Xiao X, et al. Evaluation of the structure and fuel properties of lignocelluloses through carbon dioxide torrefaction. Energy Convers Manage 2016;119:463–72. https://doi.org/10.1016/j.enconman.2016.04.064.

[19] Rahib Y, Boushaki T, Sarh B, Chaoufi J. Combustion and pollutant emission characteristics of argan nut shell (ANS) biomass. Fuel Process Technol 2021;213:106665. https://doi.org/10.1016/j.fuproc.2020.106665.
[20] Cazaña F, Afailal Z, González-Martín M, Sánchez JL, Latorre N, Romeo E, et al. Hydrogen and CNT Production by Methane Cracking Using Ni–Cu and Co–Cu Catalysts Supported on Argan-Derived Carbon. ChemEngineering 2022;6(4):47.
[21] Barco-Burgos J, Carles-Bruno J, Eicker U, Saldana-Robles AL, Alcántar-Camarena V. Hydrogen-rich syngas production from palm kernel shells (PKS) biomass on a downdraft allothermal gasifier using steam as a gasifying agent. Energy Convers Manage 2021;245:114592. https://doi.org/10.1016/j.enconman.2021.114592.
[22] Zubair YA, Rao SM, Muchtar A, Anwar SS, Daud RW, W.. Effects of temperature on the chemical composition of tars produced from the gasification of coconut and palm kernel shells using downdraft fixed-bed reactor. Fuel 2020;265:116910. https://doi.org/10.1016/j.fuel.2019.116910.
[23] Menon SD, Sampath K, Kaarthik SS. Feasibility studies of coconut shells biomass for downdraft gasification. Mater Today: Proc 2021;44:3133–7. https://doi.org/10.1016/j.matpr.2021.02.813.
[24] Yahaya AZ, Somalu MR, Muchtar A, Sulaiman SA, Wan Daud WR. Effect of particle size and temperature on gasification performance of coconut and palm kernel shells in downdraft fixed-bed reactor. Energy 2019;175:931–40. https://doi.org/10.1016/j.energy.2019.03.138.
[25] Macrì D, Catizzone E, Molino A, Migliori M. Supercritical water gasification of biomass and agro-food residues: Energy assessment from modelling approach. Renewable Energy 2020;150:624–36. https://doi.org/10.1016/j.renene.2019.12.147.
[26] Godin B, Agneessens R, Gofflot S, Lamaudière S, Sinnaeve G, Gerin PA, et al. Revue bibliographique sur les méthodes d'analyse des polysaccharides structuraux des biomasses lignocellulosiques. Biotechnologie, Agronomie, Société et Environnement 2011;15(1):165–82.
[27] Scanlon JT, Willis DE. Calculation of Flame Ionization Detector Relative Response Factors Using the Effective Carbon Number Concept. J Chromatogr Sci 1985;23(8):333–40. https://doi.org/10.1093/chromsci/23.8.333.
[28] Nunes LJR, De Oliveira Matias JC, Da Silva CJP. Chapter 3 - Biomass Torrefaction Process. In: Nunes LJR, De Oliveira Matias JC, Da Silva Catalão JP, editors. Torrefaction of Biomass for Energy Applications. Academic Press; 2018. p. 89–124.
[29] Berrueco C, Montané D, Matas GB, del Alamo G. Effect of temperature and dolomite on tar formation during gasification of torrefied biomass in a pressurized fluidized bed. Energy 2014;66:849–59. https://doi.org/10.1016/j.energy.2013.12.035.
[30] Gil-Lalaguna N, Afailal Z, Aznar M, Fonts I. Exploring the sustainable production of ammonia by recycling N and H in biological residues: Evolution of fuel-N during glutamic acid gasification. J Cleaner Prod 2021;282:124417. https://doi.org/10.1016/j.jclepro.2020.124417.
[31] Boonstra M., A two-stage thermal modification of wood, (2008), Editor˚Editors, Ghent University.
[32] Grigiante M, Antolini D. Experimental Results of Mass and Energy Yield Referred to Different Torrefaction Pathways. Waste Biomass Valorization 2014;5(1):11–7. https://doi.org/10.1007/s12649-013-9205-3.
[33] Brachi P, Riianova E, Miccio M, Miccio F, Ruoppolo G, Chirone R. Valorization of Sugar Beet Pulp via Torrefaction with a Focus on the Effect of the Preliminary Extraction of Pectins. Energy Fuels 2017;31(9):9595–604. https://doi.org/10.1021/acs.energyfuels.7b01766.
[34] Asadullah M, Adi AM, Suhada N, Malek NH, Saringat MI, Azdarpour A. Optimization of palm kernel shell torrefaction to produce energy densified bio-coal. Energy Convers Manage 2014;88:1086–93. https://doi.org/10.1016/j.enconman.2014.04.071.
[35] Brachi P, Chirone R, Miccio M, Ruoppolo G. Fluidized Bed Torrefaction of Commercial Wood Pellets: Process Performance and Solid Product Quality. Energy Fuels 2018;32(9):9459–69. https://doi.org/10.1021/acs.energyfuels.8b01519.
[36] Kizuka R, Ishii K, Ochiai S, Sato M, Yamada A, Nishimiya K. Improvement of Biomass Fuel Properties for Rice Straw Pellets Using Torrefaction and Mixing with Wood Chips. Waste Biomass Valorization 2021;12(6):3417–29.
[37] Chen W-H, Kuo P-C. A study on torrefaction of various biomass materials and its impact on lignocellulosic structure simulated by a thermogravimetry. Energy 2010;35(6):2580–6. https://doi.org/10.1016/j.energy.2010.02.054.
[38] Di Blasi C. Modeling chemical and physical processes of wood and biomass pyrolysis. Prog Energy Combust Sci 2008;34(1):47–90. https://doi.org/10.1016/j.pecs.2006.12.001.
[39] Shi J, Xing D, Lia J. FTIR Studies of the Changes in Wood Chemistry from Wood Forming Tissue under Inclined Treatment. Energy Procedia 2012;16:758–62. https://doi.org/10.1016/j.egypro.2012.01.122.
[40] Medic D, Darr M, Shah A, Potter B, Zimmerman J. Effects of torrefaction process parameters on biomass feedstock upgrading. Fuel 2012;91(1):147–54. https://doi.org/10.1016/j.fuel.2011.07.019.
[41] Demirbaş A. Mechanisms of liquefaction and pyrolysis reactions of biomass. Energy Convers Manage 2000;41(6):633–46. https://doi.org/10.1016/S0196-8904(99)00130-2.
[42] Fonts I, Atienza-Martínez M, Carstensen H-H, Benés M, Pinheiro Pires AP, Garcia-Perez M, et al. Thermodynamic and Physical Property Estimation of Compounds Derived from the Fast Pyrolysis of Lignocellulosic Materials. Energy Fuels 2021;35(21):17114–37. https://doi.org/10.1021/acs.energyfuels.1c01709.
[43] Pinheiro Pires AP, Arauzo J, Fonts I, Domine ME, Fernández AA, Garcia-Perez ME, et al. Challenges and Opportunities for Bio-oil Refining: A Review. Energy Fuels 2019;33(6):4683–720. https://doi.org/10.1021/acs.energyfuels.9b00039.
[44] Zheng A, Zhao Z, Chang S, Huang Z, He F, Li H. Effect of Torrefaction Temperature on Product Distribution from Two-Staged Pyrolysis of Biomass. Energy Fuels 2012;26(5):2968–74. https://doi.org/10.1021/ef201872y.
[45] Melkior T, Jacob S, Gerbaud G, Hediger S, Le Pape L, Bonnefois L, et al. NMR analysis of the transformation of wood constituents by torrefaction. Fuel 2012;92(1):271–80. https://doi.org/10.1016/j.fuel.2011.06.042.
[46] Demirbas A. Pyrolysis of ground beech wood in irregular heating rate conditions. J Anal Appl Pyrol 2005;73(1):39–43. https://doi.org/10.1016/j.jaap.2004.04.002.
[47] Van der Stelt MJC. Chemistry and reaction kinetics of biowaste torrefaction 2011. https://doi.org/10.6100/IR695294.
[48] Atienza-Martínez M, Mastral JF, Ábrego J, Ceamanos J, Gea G. Sewage Sludge Torrefaction in an Auger Reactor. Energy Fuels 2015;29(1):160–70. https://doi.org/10.1021/ef501425h.
[49] Yang H, Yan R, Chen H, Lee DH, Zheng C. Characteristics of hemicellulose, cellulose and lignin pyrolysis. Fuel 2007;86(12):1781–8. https://doi.org/10.1016/j.fuel.2006.12.013.
[50] Fisher EM, Dupont C, Darvell LI, Commandré JM, Saddawi A, Jones JM, et al. Combustion and gasification characteristics of chars from raw and torrefied biomass. Bioresour Technol 2012;119:157–65. https://doi.org/10.1016/j.biortech.2012.05.109.
[51] Strandberg M. From torrefaction to gasification Pilot scale studies for upgrading of biomass. Department of Applied Physics and Electronics. Umeå University; 2015. Vol. Doctoral Thesis.
[52] Karatas H, Akgun F. Experimental results of gasification of walnut shell and pistachio shell in a bubbling fluidized bed gasifier under air and steam atmospheres. Fuel 2018;214:285–92. https://doi.org/10.1016/j.fuel.2017.10.061.
[53] Sarkar M, Kumar A, Tumuluru JS, Patil KN, Bellmer DD. Gasification performance of switchgrass pretreated with torrefaction and densification. Appl Energy 2014;127:194–201. https://doi.org/10.1016/j.apenergy.2014.04.027.
[54] Devi L, Ptasinski KJ, Janssen FJJG. Pretreated olivine as tar removal catalyst for biomass gasifiers: investigation using naphthalene as model biomass tar. Fuel Process Technol 2005;86(6):707–30. https://doi.org/10.1016/j.fuproc.2004.07.001.
[55] Yu H, Zhang Z, Li Z, Chen D. Characteristics of tar formation during cellulose, hemicellulose and lignin gasification. Fuel 2014;118:250–6. https://doi.org/10.1016/j.fuel.2013.10.080.

- Afailal, Zainab; Gil Lalaguna, Noemí; Torrijos, Maria; Gonzalo, Alberto; Arauzo Pérez, Jesús María; Sánchez, José Luis (2021). "*Antioxidant additives produced from argan shells lignin depolymerization*". **Energy and fuels journal,** 35, 21, 17149–17166, DOI: 10.1021/acs.energyfuels.1c01705.

energy&fuels

pubs.acs.org/EF

Article

Antioxidant Additives Produced from Argan Shell Lignin Depolymerization

Zainab Afailal, Noemí Gil-Lalaguna, María Teresa Torrijos, Alberto Gonzalo, Jesús Arauzo,* and José Luis Sánchez

Cite This: *Energy Fuels* 2021, 35, 17149–17166

Read Online

ACCESS | Metrics & More | Article Recommendations | Supporting Information

ABSTRACT: The present work summarizes the results of an experimental study focused on producing antioxidant additives for biofuels from argan shell lignin. The generation of this waste has noticeably increased in specific regions of Morocco as a result of the upward trend in the production of argan oil. Lignin extracted from argan shells via a semi-chemical pulping process was depolymerized under hydrothermal conditions in a stirred autoclave reactor at a temperature range of 250−350 °C. Lignin conversion to phenolic compounds was conducted in subcritical water together with different reaction medium (H_2, CO_2, and HCOOH). The organic fraction in the aqueous liquid product was extracted and blended with biodiesel at a dosage of 1 wt % to evaluate its antioxidant potential. According to the obtained results, the biodiesel oxidation stability time was drastically improved up to 400%. The depolymerization temperature was observed as a critical factor in the antioxidant potential of the additives, showing a maximum value at 300 °C, regardless of the reaction medium. An extensive characterization of the produced additives was performed. The phenolic monomers present in the produced additives were identified using gas chromatography−mass spectrometry, finding a notable presence of catechol, especially in the additives obtained at 300 °C, which led to the best results of biodiesel oxidation stability. Gel permeation chromatography analyses of the additives also showed a well dissolution of relatively big molecules (up to 7000 Da) in biodiesel. More efforts are required to verify the actual antioxidant potential of these types of molecules.

1. INTRODUCTION

Lignin is considered one of the most abundant biopolymers in the world (up to 40% of the dried weight in some types of lignocellulosic biomass[1−3]). Lignin is an amorphous polymer with a complex structure that consists principally of three different monomer units: *p*-coumaryl alcohol (H), coniferyl alcohol (G), and sinapyl alcohol (S),[2−4] linked together with condensed linkages, such as 5−5, *β*−*β*, *β*−5, and *β*−1, and/or ether linkages, such as *α*−O−4, 5−O−4, and *β*−O−4.[5−7] The proper cleavage of these chemical bonds (depolymerization) may result in bio-based aromatic chemicals with an important additive value.

In the industrial processes, lignin can be extracted from the lignocellulosic biomass by classical chemical methods (kraft and sulfite processes) and semi-chemical methods (organosolv and soda processes), in addition to the new promising methods, such as pretreatments using ammonia[8] or imidazole.[9] However, as a result of its complicated structure, the extraction of an unaltered state of the native lignin is still not yet possible.[4] A semi-chemical pulping process using soda has been a historically typical process in the production of pulp and paper from non-wood materials, such as some crops (*Miscanthus* and kenaf) or agricultural residues (straw and bagasse).[10] This process entails separating pulp with a high cellulose content from the original lignocellulosic material, living behind a black liquor, rich in lignin content, as a problematic byproduct to be managed.[10,11]

Lignin conversion could be considered a potential alternative to the petrochemical industry, especially for fuel and chemical production.[4] For its chemical valorization, lignin fragmentation can be implemented via various technologies, such as biological depolymerization, homogeneous and heterogeneous catalysis, and thermochemical treatments.[12] Generally, the main depolymerization products in thermochemical treatments are a gas stream (mainly CO_2), small organic compounds, up to 10 wt % phenolic monomers, and between 45 and 70 wt % oligomers.[13]

Special Issue: 2021 Pioneers in Energy Research: Javier Bilbao

Received: June 2, 2021
Revised: August 5, 2021
Published: September 3, 2021

Downloaded via UNIV DE ZARAGOZA on February 1, 2022 at 11:40:39 (UTC).
See https://pubs.acs.org/sharingguidelines for options on how to legitimately share published articles.

ACS Publications

© 2021 The Authors. Published by American Chemical Society

Among thermochemical treatments, hydrothermal processes are defined as chemical and physical transformations at a high pressure[14] and moderate temperature (200−400 °C)[15] in an aqueous solution. These processes are considered as an effective and environmentally friendly technology for the chemical valorization of lignocellulosic biomass,[14−17] with the conveniences of a high conversion rate and short holding time.[15] Several studies were dedicated to lignin fragmentation by hydrothermal treatment for chemical production.[18,19] During this treatment, the oxygen content in the organic material can decrease from 40 to 15% through its release in the form of CO_2, H_2O, and CO.[20] Additionally, many reactions occur during the hydrothermal process, such as demethoxylation, alkylation, condensation, and fracture of ether and carbon−carbon bonds.[15,21] With regard to the reaction medium, some works were focused on the performance of H_2 and hydrogen donors (such as formic acid and alcohols) on the stability of the free radicals formed during the hydrothermal depolymerization of lignin[22] and its effectivity in increasing the yield of depolymerized lignin,[7,23] halting repolymerization reactions and promoting demethoxylation.[24] Other gaseous reaction medium have been studied, such as CO_2,[15] whose incorporation in the aqueous solution leads to carbonic acid formation, which enhanced the quality of the resulting substrates during enzymatic hydrolysis reactions.[25] Furthermore, other studies were focused on the effect of base catalysts [such as $Ca(OH)_2$, K_2CO_3, LiOH, KOH, and NaOH] on lignin depolymerization.[26−28] This reaction medium prevents coke formation and favors the monomer and dimer production. The type of base catalyst used affects the nature of the phenolic products obtained and the organic compound yields.[29] According to Toledano et al., NaOH was considered as the best option to catalyze the hydrothermal depolymerization of lignin.[30]

The lignin-derived chemical products from hydrothermal depolymerization are mainly based on phenolic compounds. In general, phenolic compounds as a whole are usually considered to have good antioxidant properties.[31] In this field, some research works have already tested the production of antioxidants from renewable phenolic sources destined more specifically to improve the oxidation stability of biodiesel.[5,21]

Biodiesel is an environmentally friendly fuel composed of fatty acid esters, usually synthesized through triglyceride transesterification with short-chain alcohols.[32] Biodiesel can replace fossil diesel in conventional engines (decreasing the unburned carbon monoxide and smoke emissions by 30 and 50%, respectively[33]) while keeping in mind essential issues related to the low storage stability of biodegradable fuels. Biodiesel is less resistant to oxidative degradation as a result of the instability caused by the unsaturation of fatty acid chains.[34] Its oxidation process begins by forming a peroxyl radical (from a fatty acid radical in the presence of O_2). Then, this unstable radical starts the self-sustaining chain reaction, abstracting the most reactive hydrogen atoms. To avert this problem, synthetic antioxidants are usually incorporated into the biofuel with the role of interrupting the subsequent chain reaction of peroxyl radicals by substituting them with new and less reactive radicals (such as phenolic radicals) to stop and retard the chain degradation.[32,34,35] According to several studies, the use of commercial antioxidants, such as butylated hydroxytoluene (BHT), *tert*-butylhydroxyquinone (TBHQ), and 3-*tert*-butyl-4-hydroxyanisole (BHA), shows an efficient way to improve biodiesel oxidation stability.[36,37] However, the production of antioxidant additives using renewable materials could be a promising alternative to fossil-based additives for biodiesel and biolubricants.[21,35,38]

During the last years, the Thermochemical Processes Research Group (University of Zaragoza, Spain) has been focused on using different lignocellulosic feedstocks[5,38−41] for the production of natural antioxidant additives for biodiesel. The incorporation of bio-based antioxidant additives, such as bio-oil fractions, has led to excellent biodiesel oxidation stability improvements.[38] The present study continues in the same investigation field by processing a non-explored agro-industrial residue: argan shells. Argan shell (AS) is a waste coming from the fruit of *Argania spinosa* (L.) Skeels. The main current interest of this fruit lies in the production of argan nut oil, an increasingly widespread cosmetic oil. The extraction of this oil leaves behind 20 tons of non-valorized waste (shells) per ton of oil produced. As far as the authors are aware, no studies about the production of chemicals from AS have been published before.

Taking into account the great social and economic impact that the valorization of agricultural wastes will take in a biorefinery concept,[42] the present work focuses on the valorization of lignin contained in AS, which was extracted through a semi-chemical process.[10] The resulting black liquor contained a high amount of lignin as well as hemicellulose and inorganic matter (in the form of ash[4]) from the chemicals used in the treatment (NaOH).[5] The solid contained in the black liquor (from now on, ASL_f, lignin-rich fraction from argan shells) was depolymerized under hydrothermal conditions (aqueous solution) at a temperature interval between 250 and 350 °C, involving different reaction medium: formic acid (HCOOH) and H_2 and CO_2 (both gases being the decomposition products of HCOOH in hydrothermal conditions). The impact of those factors on the hydrothermal treatment performance was investigated. The lignin degradation product was tested as an antioxidant additive for biodiesel to improve its oxidative stability.

2. MATERIALS AND METHODS

2.1. Material. Argan shells were provided by a Moroccan cooperative in the region of Essaouira (southwest of Morocco, 31° 30′ 47″ N, 9° 46′ 11″ W). It was crushed and characterized. Table 1 summarizes the results of the ultimate and proximate analyses, the higher heating value (HHV), and the extractive, hemicellulose, cellulose, and lignin contents. Analytical standards and methods used in the material characterization are also detailed in Table 1. As seen, AS is a material rich in lignin (up to 34 wt %) with a low ash content (0.3 wt %) and considerable HHV (19 MJ/kg). Carbon and oxygen contents are pretty similar.

2.2. Extraction and Characterization of the Lignin Fraction. Before extraction of the lignin fraction, AS was washed to remove dust and impurities and dried at room temperature overnight. Then, lignin was extracted via a semi-chemical pulping process, in which the material was digested for 4 h in an aqueous solution of sodium hydroxide (9.5 wt % NaOH with respect to the dry weight of the material) in a batch stirred reactor of 50 L at 98 °C and atmospheric pressure.[5,10,11] The produced black liquor was separated from the remaining shells by filtration (mesh size of 100 μm) and kept in an oven at 105 °C until obtaining a dried solid, which was maintained at such a temperature during storage to prevent rehydration. The dried lignin-rich fraction (ASL_f) was characterized in terms of the molecular weight distribution, acid-insoluble lignin content, ash content, HHV, and elemental analysis. Acid-insoluble lignin was gravimetrically quantified after precipitation of the raw solid dissolved in water.[13] HCl (0.5 N) was added to the aqueous solution to decrease the pH to

https://doi.org/10.1021/acs.energyfuels.1c01705
Energy Fuels 2021, 35, 17149−17166

Table 1. Ultimate and Proximate Analyses, HHV, and Chemical Composition of AS

parameter	average value (±standard deviation)	analytical standard/methods or equipment
Proximate Analysis (wt %, As-Received Basis)		
ash	0.30 ± 0.01	EN 14775:2010
moisture	6.5 ± 0.1	EN 14774-3:2010
volatile matter	75.7 ± 0.1	EN 15148:2010
fixed carbon	17.5 ± 0.2	by difference
Ultimate Analysis (wt %, As-Received Basis)		
C	47.5 ± 0.2	LECO CHN628
H	6.5 ± 0.1	LECO CHN628
N	0.177 ± 0.003	LECO CHN628
S	<0.05	LECO CHN628-628-S add-on
O	45.5 ± 0.2	by difference
HHV (MJ/kg)	18.98 ± 0.02	calorific bomb IKA C2000 basic
Chemical Composition (wt %, As-Received Basis)		
extractives	0.2 ± 0.1	Soxhlet extraction using CH_2Cl_2
hemicellulose	21 ± 1	Van Soest digestion
cellulose	35 ± 2	Van Soest digestion
lignin	34 ± 2	Van Soest digestion

2. The solution was heated to approximately 70 °C during 20 min and then filtered with a Büchner funnel to separate acid-insoluble lignin.

The molecular weight distribution was measured by gel permeation chromatography (GPC) using high-performance liquid chromatography (HPLC) Agilent 1200 equipment. The equipment consists of two columns (Ultrahydrogel 250 by Waters) and ultraviolet−visible (UV−vis) (280 and 250 nm)/refractive index (RI) detectors. The columns and detectors were maintained at 40 °C under operation. An aqueous solution (pH 12) of NaOH/methanol (1:1, by weight) with 0.1 vol % LiBr and 0.05 vol % NaN_3 was used as the mobile phase (flow rate of 0.8 mL/min). For the analysis, the solid was dissolved at a concentration of around 1 g/L. A total of 13 different polyethylene glycol standards ranging from 106 to 100 900 Da were used for calibration (more information is shown in Figure S1 of the Supporting Information). The results of GPC were expressed in terms of the average molecular weight in number (M_n) and in weight (M_w) and polydispersity.

2.3. Lignin Depolymerization Experiments: Hydrothermal Treatment. The depolymerization experiments were carried out in a 500 mL Parr reactor (Parker, Inc., U.S.A.) operating in a discontinuous system (Figure 1). In a typical run, an aqueous solution of 200 g with 7 wt % ASL_f was homogeneously prepared and loaded to the reactor. Different liquid and gas medium were selected for the depolymerization process. On the one hand, HCOOH was added to the aqueous solution (under a N_2 atmosphere) as a hydrogen donor. On the other hand, H_2 and CO_2 atmospheres were also tested, aiming at evaluating their individual effect on the product distribution and antioxidant activity, because these gases are the major products of HCOOH decomposition under the experimental conditions set.[7]

In the HCOOH experiments, the selected amount (14 or 28 g, leading to a mass ratio between HCOOH and ASL_f of 1 or 2, respectively) was slowly added to the aqueous mixture before closing the reactor. The pH of the reactional mixture and the final mixture after the experiment were measured with a Thermo Orion Star A215 pH/conductivity benchtop multiparameter meter.

Once the reactor was sealed, the air was evacuated using a vacuum pump and purged with pressurized N_2 (a common step in all experiments to check leakage and remove air). Moreover, in the experiments using H_2 or CO_2, some further purges involving the pressurized reagent gas were required. After the purge stage, the reactor was finally loaded with the selected pressure of H_2 or CO_2 (25 or 50 bar) just before starting the heating. The reactor temperature was raised to the specified temperature (250, 300, or 350 °C) at a heating rate of 5 °C/min and then held constant for 1 h. The stirring was fixed at 1000 rpm throughout the experiment and also during the reactor cooling. Once the experiment had finished, the reactor was quickly cooled by moving tap water into the built-in cooling coil. The produced gas phase was collected in a gas bag and analyzed with a microgas chromatograph (Agilent 3000A).

The aqueous liquid product was recovered from the reactor, and the reactor walls and stirrer were washed with methanol, filtering both liquids together under vacuum conditions (using a pre-weighed filter paper). Methanol was used as washing solvent to ensure the recovery of the water-insoluble organic phase that remained stuck on the walls, stirrer, and cooling coil. The solid remaining in the filter was dried at 105 °C overnight and weighted to determine the yield of insoluble solid (Y_{IS}) according to eq 1. An aliquot of the filtered liquid was also dried at 105 °C (three replicates) to determine the yield of soluble solid (Y_{SS}, eq 2). Although some volatile organics can be lost during drying, the organic compounds considered of interest as an antioxidant (mainly phenolics) have vapor pressures that are low enough to be hardly affected

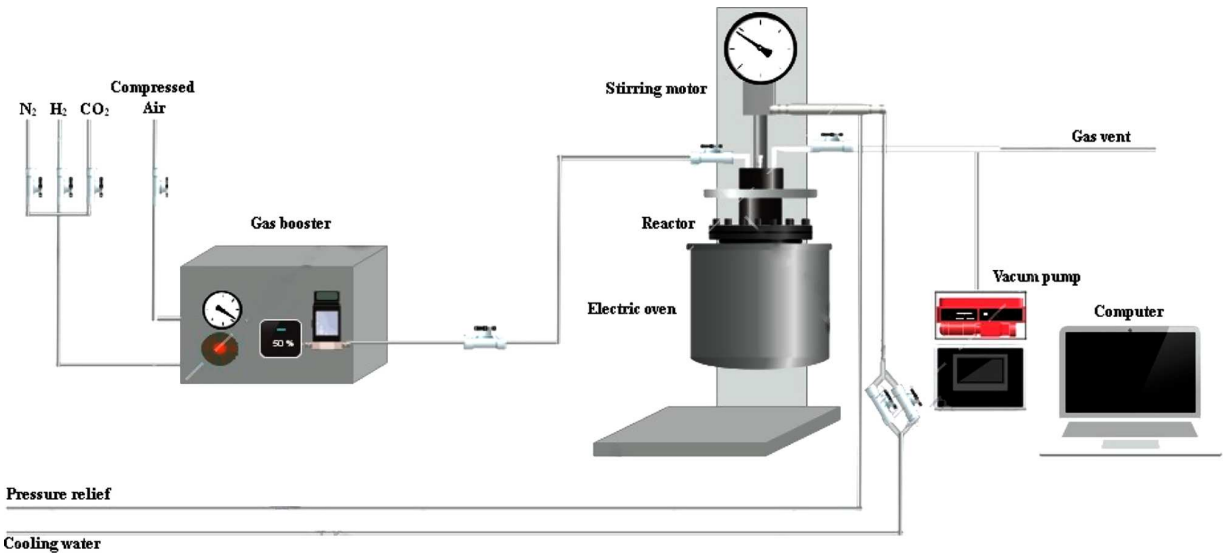

Figure 1. Hydrothermal experimental plant (Parr reactor).

https://doi.org/10.1021/acs.energyfuels.1c01705
Energy Fuels 2021, 35, 17149−17166

$$Y_{IS}\ (\text{wt}\,\%) = \frac{W_{IS}}{W_{ASL_f}} \times 100 \quad (1)$$

$$Y_{SS}\ (\text{wt}\,\%) = \frac{X_{SS}W_{FL}}{W_{ASL_f}} \times 100 \quad (2)$$

where W_{IS} is the weight of the insoluble filtered solid (g), W_{ASL_f} is the weight of the dried lignin-rich fraction initially loaded in the rector (g), W_{FL} is the weight of the total filtered liquid (aqueous reaction product + washing methanol) (g), and X_{SS} is the content of soluble solid in this liquid (wt %).

A full factorial design 2^k with two factors and two levels was established for each reaction medium (H_2, CO_2, and HCOOH) to study the influence of the temperature (250−350 °C) and the initial amount of reagent (0−50 bar of H_2 or CO_2 and 0−28 g of HCOOH) on the production and characteristics of the antioxidant additives. Three replicates in the central point of the factor levels (300 °C, 25 bar of H_2 or CO_2, or 14 g of HCOOH) were carried out for evaluating the experimental error. In the end, a total of 17 runs were performed. Table 2 summarizes the experimental conditions tested (factors and levels).

Table 2. Experimental Design Planned for the Depolymerization Experiments

experiment number	reaction medium	T (°C)	initial gas (H_2/CO) pressure (bar)/HCOOH weight (g)
1	inert atmosphere experiments	250	0
2		350	0
3	H_2 experiments	250	50
4		350	50
5		300	25
6		300	25
7		300	25
8	CO_2 experiments	250	50
9		350	50
10		300	25
11		300	25
12		300	25
13	HCOOH experiments	250	28
14		350	28
15		300	14
16		300	14
17		300	14

Some experimental data, such as the production of insoluble solid (eq 1) and soluble solid (eq 2) after ASL_f depolymerization, the C/H ratio in each solid, the additive yield (see section 2.4), the solubility of the additives in biodiesel (see section 3.4), and the performance as antioxidants for biodiesel (see section 2.5), were analyzed through analysis of variance (ANOVA) with a confidence level of 90%, and the least significant difference was calculated. Hence, the significant effects of the factors as well as their interactions were highlighted.

2.4. Additive Preparation and Characterization. An aliquot of the filtered liquid (about half of it) was extracted using twice the weight of isopropyl acetate (chosen as the extracting solvent according to a previous study, in which a large variety of solvents were evaluated[41]). The mixture was shaken for 10 min in a funnel and then left to decant at room temperature. The decanted aqueous phase was separated and discarded, while the organic phase (OP) was filtered using silicone-treated filter paper to remove aqueous-phase particles that remained in suspension. Three aliquots of OP (15 g each) were dried during 48 h at 50 °C to determine the concentration of extracted compounds, and from this value, the additive yield ($Y_{additive}$) was calculated according to eq 3 (from now on, the dried OP will be referred to as "additive" throughout this paper)

$$Y_{additive}\ (\text{wt}\,\%) = \frac{X_{OP}W_{OP}W_{FL}}{W_{EL}W_{ASL_f\ (\text{ash-free})}} \times 100 \quad (3)$$

where X_{OP} is the concentration (wt %) of the lignin-derived compounds in the OP, W_{OP} is the weight (g) of OP obtained after the extraction, and W_{EL} is the weight (g) of the aqueous liquid subjected to extraction. Here, W_{ASL_f} is expressed on an ash-free basis involving only the organic fraction present in the raw material.

For chemical characterization, the additives were redissolved in methanol and analyzed by gas chromatography (GC) with an Agilent 7890A gas chromatograph equipped with a flame ionization detector (FID) and combined with an Agilent 5975C mass selective detector (MSD) (operating parameters were detailed in Table S1 of the Supporting Information). For the calibration of the FID signal, eight standard solutions, including the most abundant phenolic components in the samples (guaiacol, creosol, 2,4,6-trimethylphenol, phenol, 4-ethylguaiacol, 2,5-dimethylphenol, *p*-creosol, eugenol, 4-ethylphenol, 2,6-dimethoxyphenol, 3-methoxycatechol, 4-allyl-2,6-dimethoxyphenol, vanillin, apocynin, guaiacylacetone, catechol, homovanillyl alcohol, and hydroquinone), were prepared using dichloromethane/methanol (1:1, by volume) as the eluent. The concentration of each compound in the standard solutions ranged between 50 and 3000 μg/mL. Moreover, the concentrations of the compounds that were identified by mass spectrometry (MS) but not included in the standards was calculated from the response factor of the most similar standards used, applying to it a correction factor according to a methodology based on the effective carbon number (ECN).[25,43,44]

The structural composition of the additives was also investigated using a Fourier transform infrared (FTIR) spectrometer, Agilent Cary 630 FTIR.

For further characterization, the molecular weight distribution of the additives as well as their biodiesel-insoluble fractions (see section 2.5), was measured by GPC following the same procedure detailed for the raw lignin.

2.5. Blend of Biodiesel and Additives and Measurement of Oxidation Stability. The biodiesel used in this study was synthesized in the laboratory using sunflower oil and methanol as reagents (molar ratio of methanol/oil of 6:1) and potassium hydroxide as the catalyst (1% of oil mass). The biodiesel production process has been described in greater detail elsewhere.[5,38,39,41]

To start the procedure of incorporating the additives to biodiesel, a portion of the OP extracted was evaporated in a rotary evaporator at 60 °C and vacuum conditions (10 mbar absolute pressure). The remaining dried solid (i.e., the additive itself) was weighed; therefore, the appropriate amount of neat biodiesel could be added to the same flask, adjusting it to an initial additive dosage of 1 wt %. To enhance the additive dissolution in the biodiesel, methanol was used as a co-solvent (with a mass ratio of methanol/biodiesel of 1:1) and the mixture was sonicated for several minutes in an ultrasound bath. Then, methanol was removed in a rotary evaporator. The final mixture of biodiesel and additive was centrifuged to separate the additive-insoluble fraction. The homogeneous mixture of doped biodiesel was recovered from the upper part of the centrifugation tube, while the insoluble fraction remaining at the bottom was thoroughly washed with hexane (with sonication) to remove biodiesel traces. Then, the washed solid was dried overnight at 50 °C and weighed to determine the fraction of insoluble additive and, by difference, the dosage of additive that was really dissolved in biodiesel. As commented before, GPC analyses were conducted on these insoluble fractions of the additive.

The oxidation stability of both neat and doped biodiesel samples was measured according to EN 16091 and ASTM D7545 methods through a PetroOXY tester device (Petrotest Instruments GmbH & Co.). The oxidation stability was measured as the time required by the biodiesel samples (5 mL) to reduce by 10% the oxygen pressure initially established in the measurement vessel.

Figure 2 summarizes all of the steps in the experimental procedure developed in this work, from the initial stage of lignin extraction from AS to the last step of measurement of the oxidation stability of biodiesel after incorporating the antioxidant additives.

https://doi.org/10.1021/acs.energyfuels.1c01705
Energy Fuels 2021, 35, 17149−17166

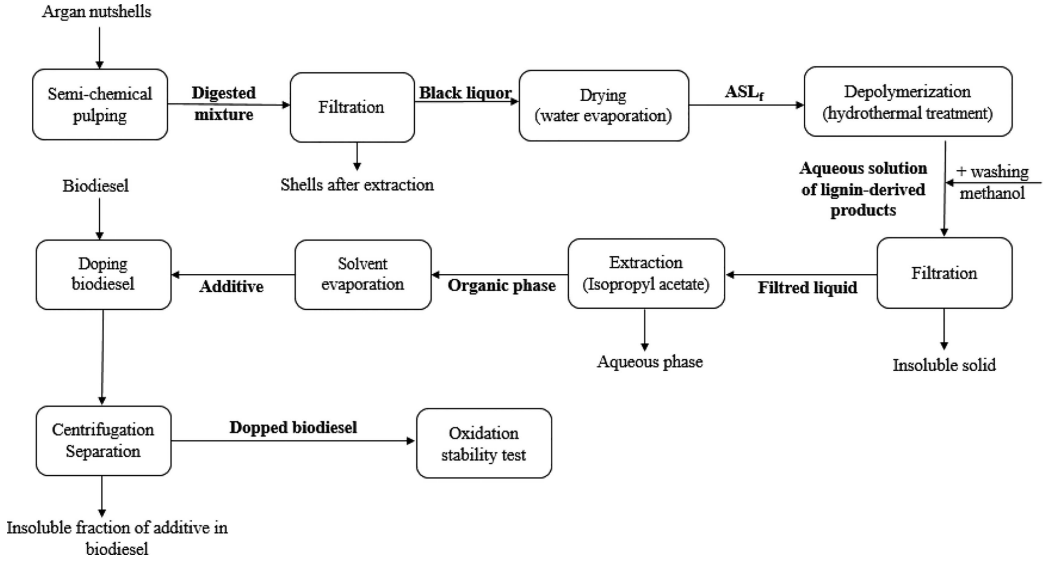

Figure 2. Experimental steps: lignin extraction, lignin depolymerization, additive preparation, and mixture with biodiesel and oxidation stability tests.

3. RESULTS AND DISCUSSION

3.1. Characterization Results of the Lignin-Rich Fraction Extracted from Argan Shells. The yield of the lignin fraction extracted from AS by the semi-chemical pulping treatment was up to 22% with respect to the initial lignin contained in the raw material (ash-free basis). As commented before, the content of acid-insoluble lignin in this extracted fraction was determined gravimetrically, accounting for 43 wt % of the organic fraction in the solid (ash-free basis). Table 3

Table 3. Characterization of the Lignin-Rich Fraction Extracted from AS

parameter	average value
C (wt %)	75.2 ± 0.1
H (wt %)	7.78 ± 0.04
N (wt %)	0.58 ± 0.02
S (wt %)	<0.05
O (wt %)[a]	16.4 ± 0.2
HHV (MJ/kg)	10.33 ± 0.04

[a]By difference.

shows other characterization results of the extracted and dried ASL_f (ash-free basis). The ash content in ASL_f was much higher (up to 60 wt %) than the initial ash content in AS (0.3%). This high ash content could be explained by the presence of much of NaOH used in the pulping treatment,[4,5] which will benefit the subsequent depolymerization process, because NaOH could be considered a base catalyst in the hydrothermal process.[19] According to Toledano et al.,[29] NaOH is a suitable base catalyst for lignin depolymerization in terms of conversion and fractionation to phenolic monomers.

With regard to the molecular weight distribution of ASL_f, M_w was found to be 37 900 Da, M_n was 24 200 Da, and polydispersity was 1.6.

3.2. Product Distribution in the Hydrothermal Treatment. During depolymerization, ASL_f has been mainly converted to water-soluble and -insoluble solid compounds (or liquids in the case of some specific soluble compounds). Only a minimal amount of gases was generated in the process. Mass balance (without including the few produced gases) was closed fairly well (between 86 and 100.8%). With regard to the produced gas, Figure S2 of the Supporting Information shows the residual gas pressure in the reactor after cooling (at 20 °C). As shown, at the inert atmosphere reaction medium, only up to 0.4 bar of gas was generated after the experiment at 250 °C, a value that increased to 2 bar at 350 °C. In both cases, the gas product was essentially composed of CO_2 and traces of H_2. In the case of the H_2 experiments conducted at 350 and 300 °C, the amount of residual gas was lower than the initial pressure loaded in the reactor, which points to a net consumption of H_2 during the reaction. However, a slight increase in the total amount of gas was detected at 250 °C as a consequence of higher CO_2 production, thus hiding H_2 consumption. In the case of CO_2 experiments, generation of residual gas (around 5 bar) was only observed when initially loading the highest pressure of CO_2 in the reactor (at both 250 and 350 °C). As expected, the composition of this residual gas was essentially CO_2 (between 90 and 98 vol %). Lastly, a drastic increase in pressure was observed in HCOOH experiments as a result of the formic acid decomposition into H_2, CO_2, and CO at this temperature range according to two possible pathways (reactions R1 and R2).[45]

$$HCOOH \leftrightarrow CO_2 + H_2 \quad \Delta G = -48.4\ kJ\ mol^{-1} \qquad (R1)$$

$$HCOOH \leftrightarrow CO + H_2O \quad \Delta G = -28.5\ kJ\ mol^{-1} \qquad (R2)$$

Table S2 of the Supporting Information shows the maximal pressures reached during each experiment. As shown, these pressures were varied from one reaction medium to other and, obviously, depending upon the temperature.

With regard to other products formed in the hydrothermal treatment of ASL_f, the joint yield of soluble and insoluble solids (Y_{SS} + Y_{IS}) (shown in Figure S3 of the Supporting Information) ranged between 88 and 96% in most experiments, except on some of those experiments carried out with HCOOH, in which this joint yield exceeded 100%, reaching

https://doi.org/10.1021/acs.energyfuels.1c01705
Energy Fuels 2021, 35, 17149−17166

Table 4. Product Distribution, C/H Ratio in the Solids, and Additive Yields

reaction medium	T (°C)	initial gas (H_2/CO) pressure (bar)/HCOOH weight (g)	Y_{IS} (wt %)	Y_{SS} (wt %)	C/H ratio		$Y_{additive}$ (wt %)
					C/H$_{(IS)}$	C/H$_{(SS)}$	
inert atmosphere	250	0	0.86	93.58	9.2 ± 0.1	8.0 ± 0.6	6.42
	350	0	2.01	86.18	15.1 ± 0.1	9.1 ± 0.3	21.29
H_2	250	50	0.81	92.70	9.8 ± 0.1	7.6 ± 0.1	13.18
	350	50	1.38	86.88	12.9 ± 0.1	7.4 ± 0.4	20.50
	300	25	1.04	92.27	12.13 ± 0.04	7.5 ± 0.3	13.49
	300	25	0.80	95.17	12.3 ± 0.05	6.89 ± 0.02	19.13
	300	25	0.76	92.20	12.3 ± 0.2	7.9 ± 0.1	17.94
CO_2	250	50	3.90	92.10	13.4 ± 0.2	8.5 ± 0.1	18.48
	350	50	3.92	88.17	16.3 ± 0.6	9.4 ± 0.4	24.38
	300	25	3.26	89.24	16.0 ± 0.2	8.36 ± 0.01	14.49
	300	25	3.32	89.44	15.8 ± 1.4	9.3 ± 0.2	17.54
	300	25	3.58	91.78	16.1 ± 0.1	8.7 ± 0.3	17.09
HCOOH	250	28	2.98	102.60	10.4 ± 0.1	6.8 ± 0.3	38.80
	350	28	2.46	90.63	10.6 ± 0.2	7.1 ± 0.2	28.08
	300	14	2.72	112.16	11.3 ± 0.5	4.6 ± 0.2	18.24
	300	14	3.36	109.60	10.9 ± 0.2	4.5 ± 0.1	24.11
	300	14	3.58	99.24	11.2 ± 0.1	5.828 ± 0.001	21.06

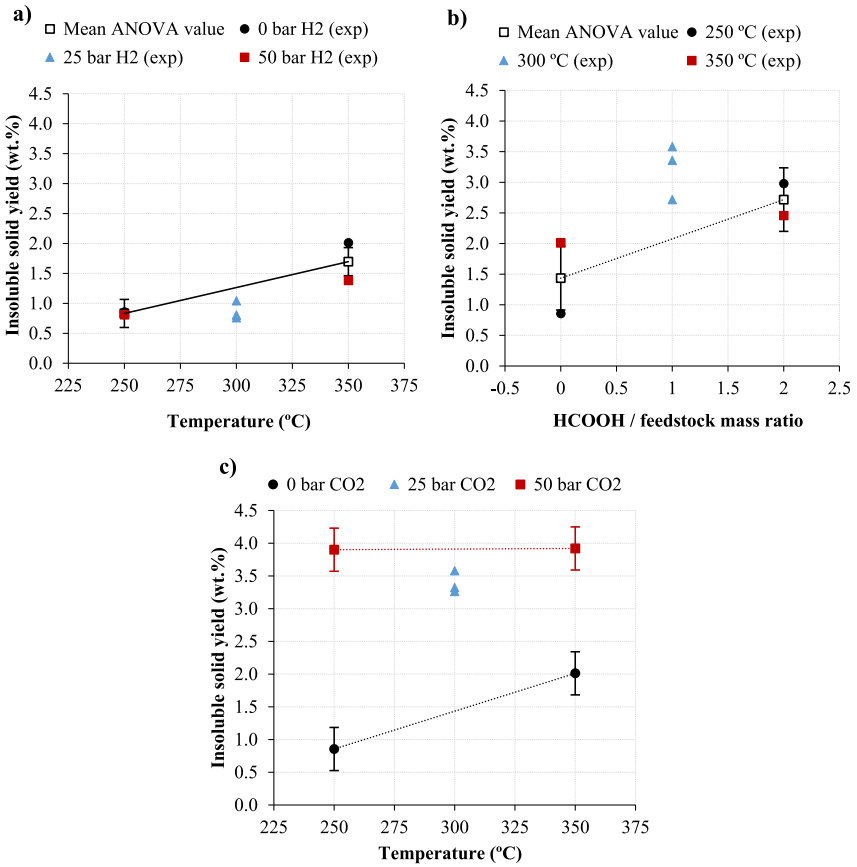

Figure 3. Effect of the temperature and reagent amount used in the depolymerization experiments on the yield of insoluble filtered solid (wt %): (a) H_2 experiments, (b) HCOOH experiments, and (c) CO_2 experiments.

values even up to 110%. Such high values could be due to the precipitation of sodium bicarbonate ($NaHCO_3$), which may be formed in the reaction between dissociated CO_2 from HCOOH decomposition and Na^+ from NaOH present in ASL_f. It should be highlighted that the initial pH of the reactional mixture decreased from 10.5 to around 3 with the addition of HCOOH, which indicates neutralization of NaOH by HCOOH before heating the reaction system.

The influence of the operational factors on the production of soluble and insoluble solids is detailed more specifically below.

3.2.1. Insoluble Solid Yield. Among other results, Table 4 shows the yield of insoluble solid obtained under the different

https://doi.org/10.1021/acs.energyfuels.1c01705
Energy Fuels 2021, 35, 17149−17166

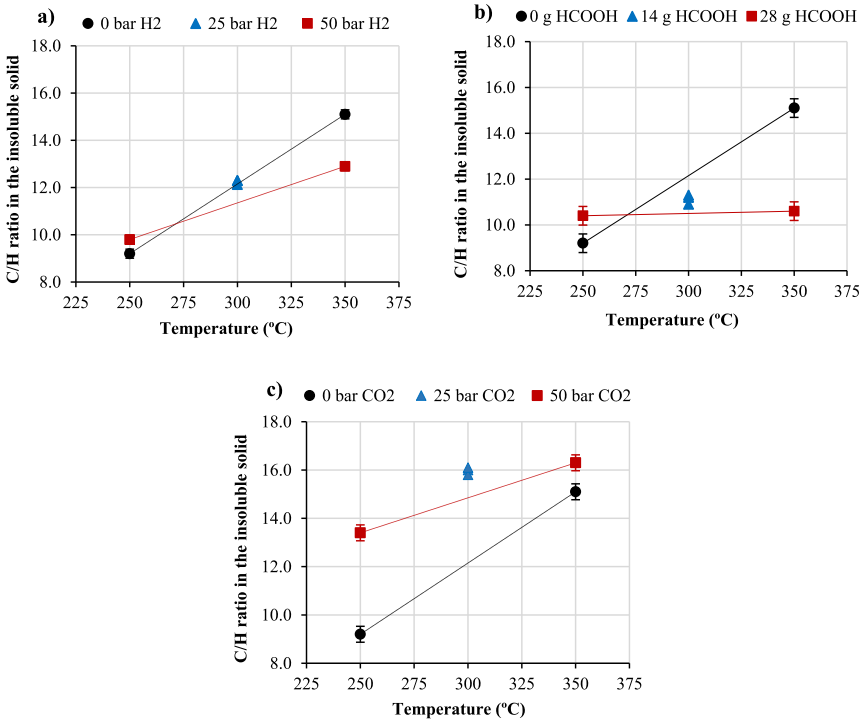

Figure 4. Effect of the temperature and reagent amount used in the depolymerization experiments on the C/H ratio of the insoluble filtered solid (wt %): (a) H_2 experiments, (b) HCOOH experiments, and (c) CO_2 experiments.

operational conditions. For a better interpretation of the results, Figure 3 plots the ANOVA statistical analysis of this response parameter (error bars correspond to the least significant difference at a confidence level of 90%). Both the experimental data (denoted in the figures as filled symbols and named) and the theoretical values resulting from the one-way ANOVA (denoted in the figures as "mean ANOVA value") have been represented in the figures, thus giving a first approach of the good or bad fitting of the models in the high and low levels of the experimental design. If the mean ANOVA value does not appear in a figure, it means that experimental and theoretical values are just the same.

As seen in Figure 3a, the depolymerization temperature showed a significant positive effect on the production of insoluble solid in the case of operating under an inert atmosphere or with H_2 as a reaction medium. This increase in the insoluble solid yield was interpreted according to many studies by the condensation or repolymerization reactions that could occur at temperatures higher than 300 °C.[7,46,47] The repolymerization/condensation reaction has been reported by several studies and explicated as the reaction between unstable lignin fragments and original lignin.[29,48] According to Li et al.,[49] the key point of these reactions is the carbenium ion generated at the α-carbon atom. After the ether bond cleavage, this ion can be attacked by an adjacent aromatic ring forming a stable carbon−carbon bond that increases the molecular weight[28,29] and could change the molecular structure. Contrary to what was expected, the presence of H_2 did not show a significant impact on the insoluble solid yield with respect to the experiments carried out under the initial inert atmosphere (Figure 3a). According to various studies in the literature, some H-donating reaction medium (in the presence of alcohols or acetone) have been proven to reduce char formation.[18,50] However, this effect was not observed in the present work. In fact, the addition of HCOOH as a H donor to the reaction medium even showed the opposite effect, because the production of the insoluble yield was augmented in comparison to the inert atmosphere results (Figure 3b). That seems to be correlated with the generation of CO_2 from HCOOH, as in the case of CO_2 experiments (Figure 3c). The presence of CO_2 had a remarkable effect on the increase of the insoluble solid yield, which was maintained stable (around 4%) throughout all of the temperature range (and P_{CO_2} = 50 bar). A significant interaction between both factors has been observed: the temperature showed a positive effect on the production of the insoluble yield in the absence of CO_2, while that effect disappeared by initially feeding CO_2 or HCOOH.

In short, the most unfavorable operating conditions from the point of view of the generation of such an insoluble solid, which is an undesirable byproduct for the purpose of the process, involves high amounts of CO_2 in the reaction medium. To minimize its production, the optimal working conditions would be the most moderate reaction temperature (250 °C) and either inert or H_2 atmospheres (Y_{IS} of around 0.8 wt %).

The C/H ratio in both the insoluble and soluble solids was calculated using the elemental analysis data summarized in Table S3 of the Supporting Information. These data are included in Table 4. The ANOVA of the C/H ratio in the insoluble solid is shown in Figure 4. The temperature, the reaction medium, and the interaction between them had a significant effect on this C/H ratio. The presence of CO_2 had a positive effect on the C/H ratio in the entire temperature interval, while the presence of H_2 or HCCOH contributed to increase the fraction of H in the solid formed at the highest temperature.

https://doi.org/10.1021/acs.energyfuels.1c01705
Energy Fuels 2021, 35, 17149−17166

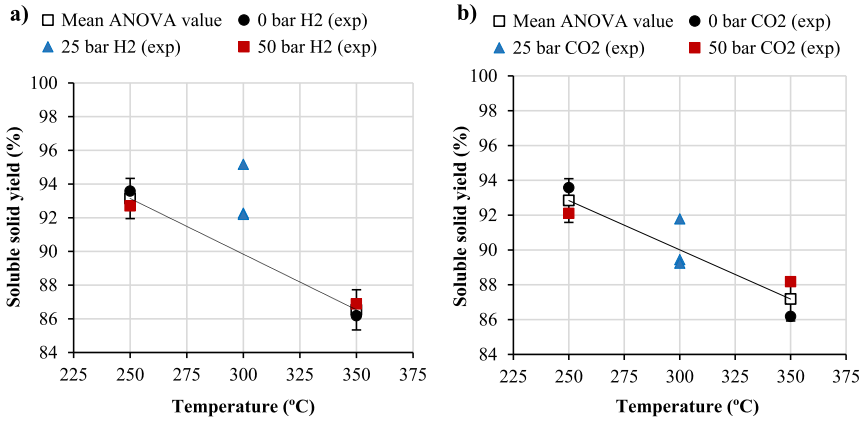

Figure 5. Effect of the temperature and reagent amount used in the depolymerization experiments on the yield of soluble filtered solid (wt %): (a) H_2 experiments and (b) CO_2 experiments.

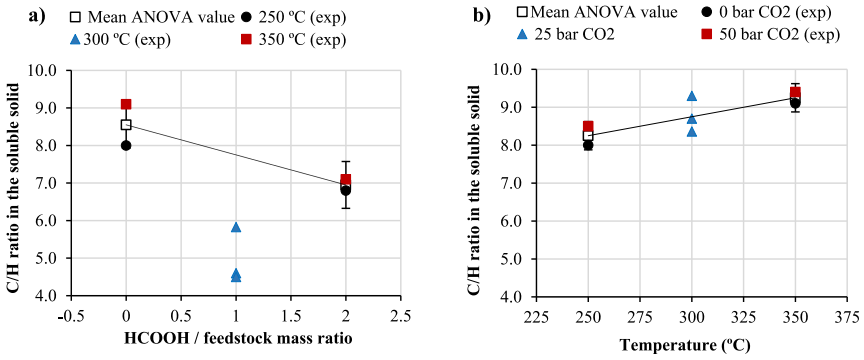

Figure 6. Effect of the temperature and reagent amount used in the depolymerization experiments on the C/H ratio of soluble filtered solid (wt %): (a) HCOOH experiments and (b) CO_2 experiments.

3.2.2. Soluble Solid Yield. Figure 5 shows the ANOVA of the results obtained for the yield of soluble solid produced under the different reaction medium and temperatures (Table 4). The operational factors did not affect this response parameter in HCOOH experiments (no significant effect was detected). However, according to ANOVA, the treatment temperature had an apparent negative effect on the yields of soluble solid in the presence of H_2 and CO_2, while the initial pressure of gas loaded in the reactor did not show a significant effect on either of the two reaction medium. In the case of H_2 experiments, data did not fit a linear model (significant curvature), which may be related to the temperature profile, because the amount of H_2 present in the reaction medium was found to have a non-significant effect.

It should be noted that the distribution of the solid product into the soluble or insoluble fractions was really affected by the amount of methanol used in washing the reactor and the filtered solid, because methanol plays a co-solvent role and can enhance the dissolution of some water-insoluble compounds in the aqueous methanol phase. Therefore, the amount of methanol used for washing was similar in all of the experiments.

Figure 6 shows the ANOVA of the C/H ratio in the soluble solid. No significant effect of the operational factors was detected for this response parameter in H_2 experiments. In the presence of CO_2 (Figure 6b), a slightly positive and linear effect of the temperature was observed. In the case of HCOOH experiments (Figure 6a), data showed a non-linear model (with significant curvature).

As shown in Table S4 of the Supporting Information, the fraction of these three elements yielding soluble compounds was found to be significantly higher than that producing insoluble compounds, regardless of the experimental conditions.

3.3. Additive Yields. Table 4 reports the yields of the produced additives under the different experimental conditions. The ANOVA of the results (Figure 7) shows that both the temperature and reaction medium had a significant effect on the additive yield obtained as a whole. A linear trend in the additive production relative to the temperature was observed, with a clear positive effect in the case of H_2 experiments and CO_2 experiments and a slight negative effect in the case of HCOOH experiments. With regard to the influence of each reaction medium, no significant effect of H_2 presence has been found. In contrast, in the presence of CO_2, a positive effect of the initial pressure of gas was observed in the entire temperature interval, which means that the additive production when 50 bar of CO_2 was initially fed in the reactor was greater than that obtained in the initial inert atmosphere. The same occurred in the case of HCOOH experiments, although this drastic positive effect was only reported at the lowest temperature (250 °C), because the interaction between both factors was found to be significant in this reaction medium. The use of HCOOH was the most favorable reagent from the point of view of maximizing the production of additives,

https://doi.org/10.1021/acs.energyfuels.1c01705
Energy Fuels 2021, 35, 17149−17166

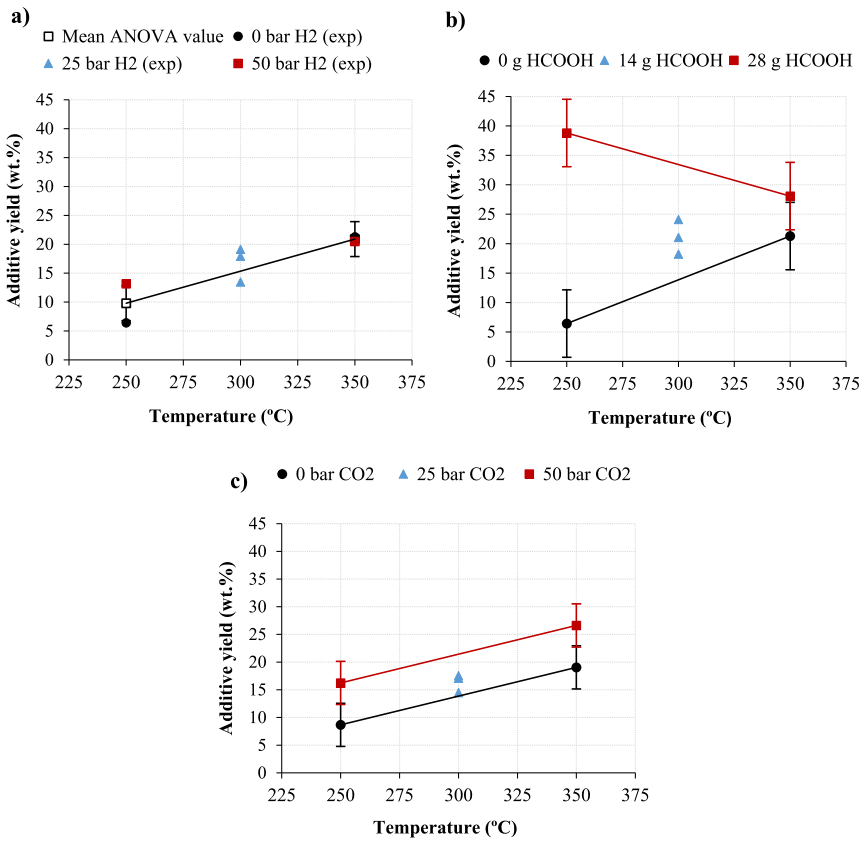

Figure 7. Effect of the temperature and reagent amount used in the depolymerization experiments on the additive yield (wt %): (a) H_2 experiments, (b) HCOOH experiments, and (c) CO_2 experiments.

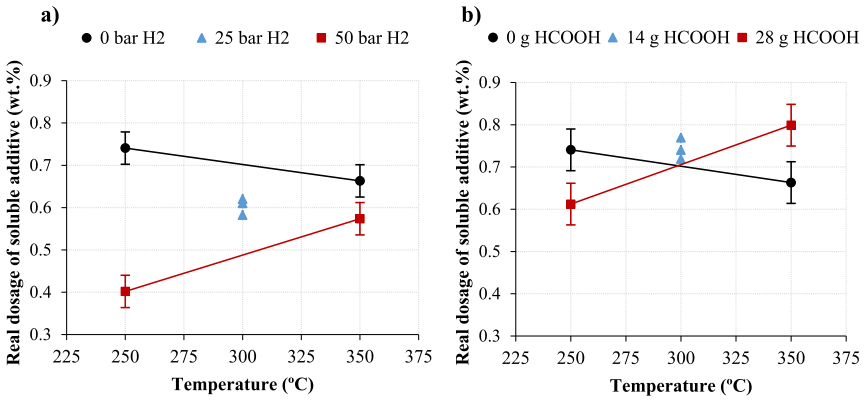

Figure 8. Effect of the temperature and amount of H_2 and HCOOH used in the depolymerization experiments on the additive solubility in biodiesel (wt %): (a) H_2 experiments and (b) HCOOH experiments.

especially operating at 250 °C and with an initial amount of 28 g of HCOOH (HCOOH/ASL_f mass ratio of 2), which led to a maximum additive yield of around 39 wt %.

3.4. Additive Solubility in Biodiesel. The dried additives were individually mixed with biodiesel at an initial dosage of 1 wt %. However, after centrifugation, it could be observed that the entire additive was not homogeneously dissolved in biodiesel. The real dosage of soluble additive was determined after centrifugation and separation of the insoluble fraction according to eq 4

$$\text{real dosage of soluble additive (\%)} = \frac{W_{\text{initial additive}} - W_{\text{insoluble additive}}}{W_{\text{biodiesel}} + (W_{\text{initial additive}} - W_{\text{insoluble additive}})} \times 100 \quad (4)$$

where $W_{\text{initial additive}}$ is the weight (g) of the additive initially added to biodiesel, $W_{\text{insoluble additive}}$ is the weight (g) of the insoluble additive quantified after centrifugation, hexane washing, and drying, and $W_{\text{biodiesel}}$ is the weight (g) of neat biodiesel used for the mixture.

https://doi.org/10.1021/acs.energyfuels.1c01705
Energy Fuels 2021, 35, 17149−17166

Table 5. Concentration of Monomeric Phenolic Compounds in the Additives Produced at Different Conditions

	concentration in the dried additives (mg/g)																
	inert atmosphere experiments		H_2 experiments					CO_2 experiments					HCOOH experiments				
compound	250 °C	350 °C	250 °C, 50 bar	350 °C, 50 bar	300 °C, 25 bar			250 °C, 50 bar	350 °C, 50 bar	300 °C, 25 bar			250 °C, 28 g	350 °C, 28 g	300 °C, 14 g		
guaiacol	18	1	24	1	2	3	3	8	0.3	11	4	2	0.2	6	1	1	3
2,6-dimethylphenol			0.5	1	0.5	0.3	0.5						0.1	0.4	0.3		
creosol	2	0.3	2		1	1	1	0.3	0.2	3	1	1	0.1	1	0.5	0.4	1
1,2,3-trimethoxybenzene	2	0.1	2				0.2	0.3	0.2				0.3				
2,4,6-trimethylphenol				0.5					0.1				0.2	0.2	0.5		
phenol	2	0.4	3	6	1	1	2	1	1	5	1	1	1	3	1	0.5	1
4-ethylguaiacol	2	0.1	2		0.4	0.5	0.4	1	0.03	2	1	0.3		2	1	1	2
3-ethylphenol		1		0.5					0.1								
p-cresol		3		3	0.2	0.4	0.3		1	1	0.3	0.1	1	0.4		0.1	0.3
2-methoxy-4-propylphenol								0.2		1		0.3	0.3	2	1	1	1
4-ethylphenol			0.2	1	0.5	0.4	0.3	0.1	0.5	1		0.2	1	1	0.2	0.2	0.4
3,4-dimethylphenol				0.5				0.2	1	1	1	0.2	0.3				
syringol	148	0.2	71	0.4	1	1	1	27		3	2	1	5	3	6	4	9
3,5-dimethoxy-4-hydroxytoluene	39	0.1	20		0.5	0.3	0.4	2		1	1	1		1	0.5	0.3	1
1,2,3-trimethoxy-5-methylbenzene	16	0.4	8		0.3	1	0.2	3		1	0.5	0.2		4			
m-guaiacol	1	1	0.4			0.3		0.1	0.3								
2-allyl-4-methylphenol													0.3				
vanillin	4		1	1	0.5		1	0.3	0.4		0.5	0.2					
4-butyl-1,2-dimethoxybenzene	4		2	1	0.3	0.3		1	1				0.5				
apocynin	8		4		2	1	2	1		1	2	0.6		0.5			
guaiacylacetone	8	0.5	5					4	0.4		1	0.4		15	2	1.2	
catechol	35		18	30	51	64	36	16		54	32	19		11	15	12	24
3-methylcatechol					6		13			12	9		3				13
homovanillyl alcohol	2	0.2						1						9	5	3	4
4-ethylcatechol															4	3	6
4-hydroxy-3-methoxybenzenepropanol			9	1	1	0.5	0.3	5		1	2	1		4	3	2	3
4-hydroxybenzeneethanol													0.3	1	4	3	3
desaspidinol	4		3					1			1	1		4			
hydroquinone										1	1	0.2		2	5	3	6

https://doi.org/10.1021/acs.energyfuels.1c01705
Energy Fuels 2021, 35, 17149−17166

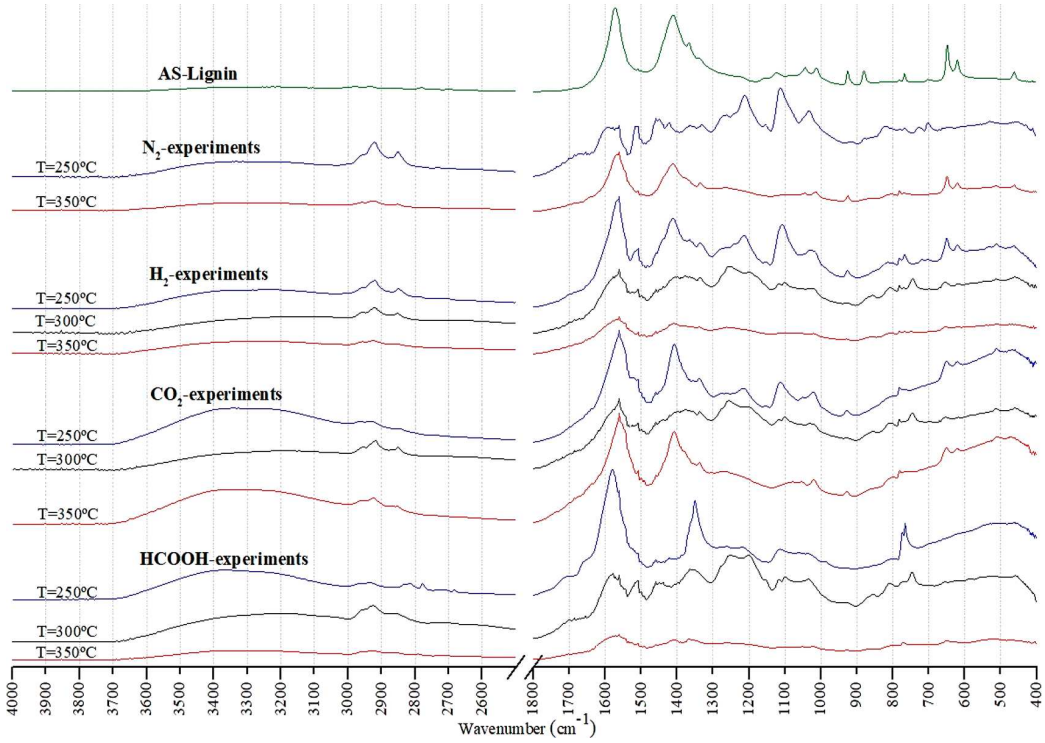

Figure 9. FTIR spectra of the additives prepared at different operational conditions and ASL_f.

Figure 8 shows the effect of both the temperature and amount of H_2 or HCOOH used in the depolymerization experiments on the additive solubility in biodiesel. As shown, at the lowest temperature (250 °C), the presence of H_2 (50 bar initially) led to a much less soluble additive than that obtained in the case of operating with an inert atmosphere. This difference in the solubility of both additives was considerably reduced at 350 °C. Moreover, the solubility of the additives produced under an inert atmosphere was damaged with the temperature, while it improved under H_2 medium (significant interaction between both factors). The same trend was observed for solubility of the additives obtained under HCOOH medium, although these data were noticeably better than those obtained for H_2 medium. The most soluble additive (real additive dosage incorporated to biodiesel of 0.8 wt %) was obtained under HCOOH medium at 350 °C. Concerning the CO_2 presence during the additive production and according to ANOVA, the additive solubility was not significantly affected by the operational factors, ranging between 0.52 and 0.67 wt %, irrespective of the temperature and initial pressure of CO_2 loaded.

3.5. Additive Characterization. *3.5.1. GC−FID−MS Analysis of the Additives.* The GC−FID−MS analysis revealed the presence of a wide variety of monomeric phenolic compounds as well as acetic acid, aldehydes, and furans. Table 5 shows the concentration of the monomeric phenolic compounds expressed as milligrams per gram of the dried additive. As shown, some of the major phenolic compounds identified were phenol, guaiacol, syringol, and catechol as well as their alkyl- and methoxy-substituted derivates. Catechol was identified as the predominant compound at 300 °C, regardless of the reaction medium, while syringol was the main phenolic product at 250 °C, especially in the case of using an inert medium. In general (except for the HCOOH medium), the increase in the depolymerization temperature led to a reduction in the concentration of syringol and guaiacol, while catechol and catechol derivatives increased their concentrations. However, using HCOOH as a reaction medium, only traces of guaiacol were detected in the additive produced at 250 °C, which increased proportionally with the temperature, while no apparent effect of the temperature was detected on the syringol concentration. In this reaction medium (HCOOH), a wider variety of phenolic monomers was observed in the produced additives, especially at high temperatures. In addition to catechol and catechol derivatives, the presence of other monomers, such as hydroquinone, 4-hydroxybenzeneethanol, 4-hydroxy-3-methoxybenzeneethanol, and homovanillyl alcohol, has been found at a level comparable to guaiacol or syringol.

According to several studies in the literature,[29,30,48] at severe conditions of temperature (at least 300 °C) and in the presence of base catalysts, both guaiacol and syringol directly coming from lignin fragmentation are intermediate products that could undergo demethylation, demethoxylation, and dealkylation reactions to produce advantageous products, such as phenol, catechol, catechol derivatives, and creosol. This finding is in agreement with the observations found in this work for inert, H_2, and CO_2 atmospheres, because ASL_f contains an important amount of NaOH used for the extraction of lignin from AS. Trends were not so clear for the HCOOH medium, which could be due to the acidic character of this reactional mixture. As shown in Table S5 of the Supporting Information, an alkaline reaction medium was maintained throughout the experiments in the cases of an initial inert atmosphere and H_2 medium, while in the case of the CO_2 experiment, the pH of the reactional mixture was neutralized. However, different pH values were measured after the experiments in the case of HCOOH medium: 4.8, 6.3, and

https://doi.org/10.1021/acs.energyfuels.1c01705
Energy Fuels 2021, 35, 17149−17166

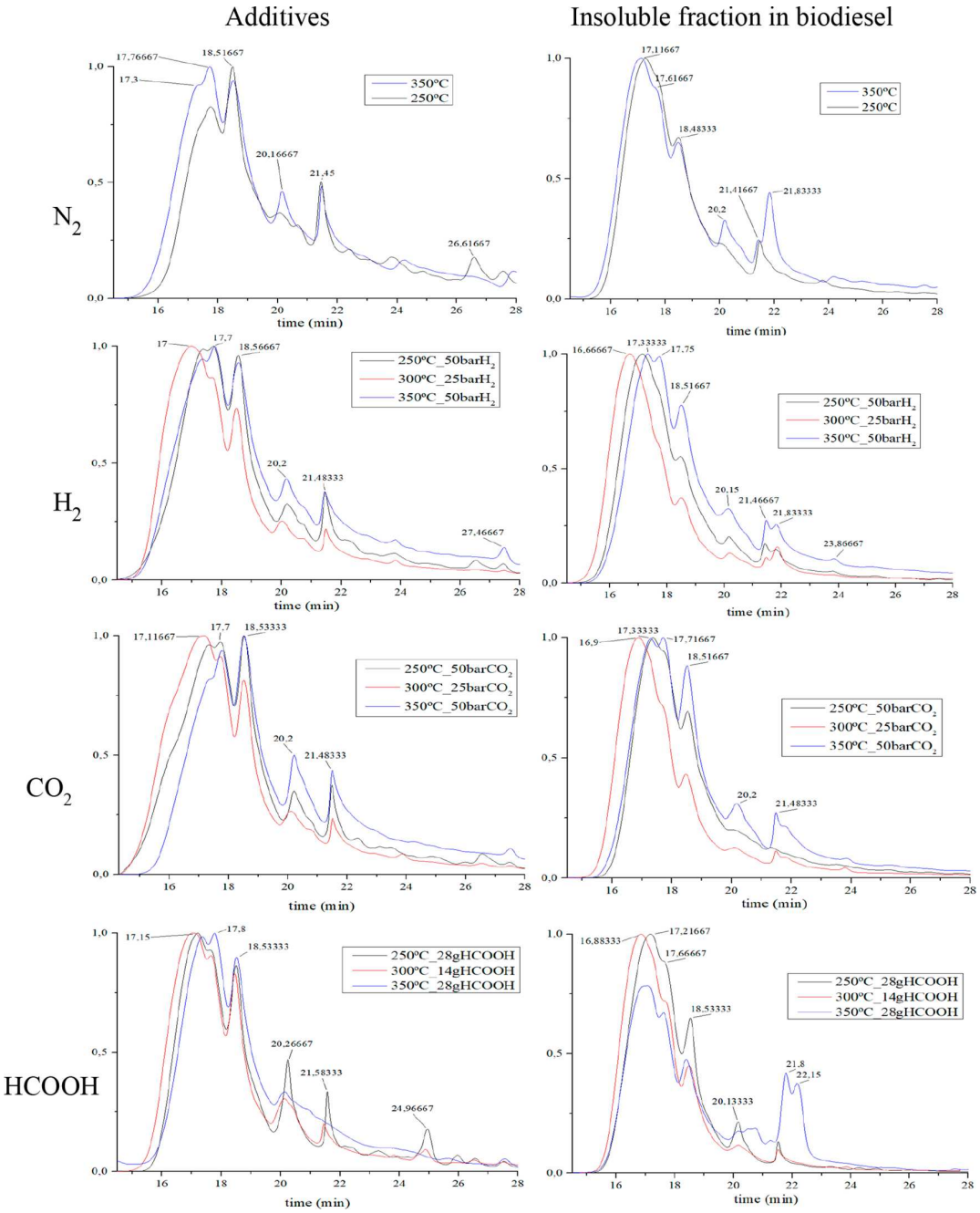

Figure 10. Molecular weight distribution (GPC plots) of the additives and their insoluble fractions in biodiesel.

7.6 at 250, 300, and 350 °C, respectively, which correlate with the decomposition extent of HCOOH.

It should be stressed that the GC−FID−MS analysis allowed for identifying and quantifying around 47% of the organic mass of the additive produced in the case of the inert atmosphere at 250 °C, a value that dropped to only 5% at 350 °C. The identified and quantified additive fraction obtained in the H_2 experiments dropped from 20% at 250 °C to 10% at higher temperatures and did not exceed 10% in the remaining cases. The identified fraction of additives constituted phenolic compounds (Table 5) and non-phenolic compounds, such as hexadecanoic acid methyl ester, acetic acid, and cyclopentenone derivatives.

The most important part of the GC−FID unquantified components could be related to undetectable phenolic dimers, trimers, and oligomers with a mass-to-charge index (m/z) higher than 500, also including repolymerized fractions of lignin with a very high molecular weight. For further characterization, the molecular weight distribution of the additives was analyzed (section 3.5.3).

3.5.2. FTIR Analysis of the Additives. FTIR spectra of the produced additives and that of the original raw material are represented in Figure 9. In general, the spectra show some significant differences in the function of the reaction medium and the lignin processing temperature. The peak intensity corresponding to the hydroxyl group (at wavenumbers in the

https://doi.org/10.1021/acs.energyfuels.1c01705
Energy Fuels 2021, 35, 17149−17166

Table 6. Molecular Weight (M_n, M_w, and M_w/M_n) of the Whole Additives and Their Insoluble Fractions in Biodiesel

			whole additives			insoluble fraction of the additives in biodiesel		
	T (°C)	initial gas pressure (bar)/HCOOH weight (g)	M_n (Da)	M_w (Da)	M_w/M_n	M_n (Da)	M_w (Da)	M_w/M_n
inert atmosphere experiments	250	0	6700	13000	1.9	10600	16800	1.6
	350	0	8200	15900	2.0	10700	18600	1.8
H_2experiments	250	50	10000	18900	1.9	11800	18500	1.6
	350	50	9200	18400	2.0	9200	15900	1.7
	300	25	13200	22000	1.7	15600	23600	1.5
CO_2experiments	250	50	12600	24700	2.0	9800	14600	1.5
	350	50	8100	16300	2.0	9300	15400	1.6
	300	25	15200	27300	1.8	14200	20700	1.4
HCOOH experiments	250	28	10000	16400	1.6	12600	17800	1.4
	350	28	9300	15100	1.6	10800	18700	1.7
	300	14	12000	19600	1.6	14600	20600	1.4

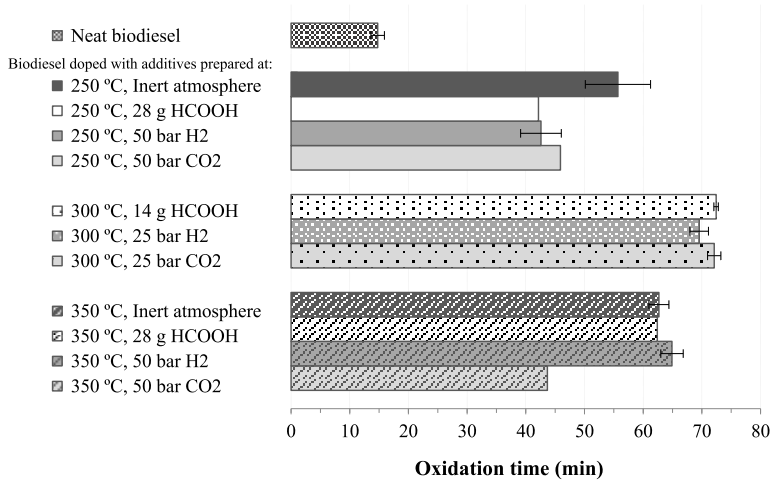

Figure 11. Oxidation stability times of neat and doped biodiesels.

range of 3600−3100 cm^{-1}) was not strongly affected by the medium and/or the temperature but was more pronounced in the case of CO_2 and HCOOH medium. Peaks corresponding to alkyl groups (wavenumber between 3000 and 2900 cm^{-1}) almost completely disappeared in the additives obtained at 350 °C, regardless of the reaction medium. No peaks were detected throughout the interval of 3600−2900 cm^{-1} in the spectra of the original raw material. On the other hand, the two clear peaks observed in the original raw material at wavenumbers in the range of 1700−400 cm^{-1} have undergone several changes compared to the spectra of the additives obtained at 250 °C. Some of these peaks were reduced or disappeared, while others appeared when increasing the depolymerization temperature up to 300 °C, thus indicating the ASL_f depolymerization by cleavage of many functional groups and restructuration into other bonds. At 350 °C, the spectra of all of the additives became similar to char and activated carbon plots, with fewer peaks representing functional groups, which could indicate the condensation of phenolic compounds forming a residual or repolymerized lignin at this severe treatment temperature. It is noteworthy that, in the additives produced at 250 and 300 °C (regardless of the reaction medium), an important peak appeared at wavenumbers of around 1300−1150 cm^{-1}, with a significant shoulder at 1250 cm^{-1}. The peaks at these wavenumbers are usually attributed to aromatic links and tertiary/secondary alcohols, which could be explained by the presence of catechol, alkyl catechol, syringol, guaiacol, and hydroquinone in the additives prepared at 300 °C (Table 5). The intensity of the peak observed in the spectra of ASL_f at a wavenumber of around 1400 cm^{-1} (corresponding to O−CH_3 links) started to decrease in the additives prepared at 250 °C in the presence of H_2 and CO_2 and almost completely disappeared at 300 °C. According to Li et al.,[49] the β−O−4 linkages are the first to be cleaved during the hydrothermal treatment. This peak was observed to reappear again in the additives produced at 350 °C under a CO_2 medium and inert atmosphere, which might be due to repolymerization reactions involving linkages between phenolic rings, similar to those present in the original feedstock. No peaks were detected at this wavenumber (1400 cm^{-1}) in the additives produced at the highest temperature in the presence of HCOOH and H_2, which seems to indicate that these H-donating reaction medium led to other types of products and could also be more efficient in preventing repolymerization reactions to avoid the formation of residual lignin. As commented, this effect on the insoluble solid yield was hindered because of experimental measurement uncertainty.

3.5.3. Molecular Weight Distribution of the Additives. The GPC chromatograms of both the entire additives and the insoluble fractions in biodiesel are reported in Figure 10. Table 6 summarizes final results, such as the number-average molecular weight (M_n), weight-average molecular weight

https://doi.org/10.1021/acs.energyfuels.1c01705
Energy Fuels 2021, 35, 17149−17166

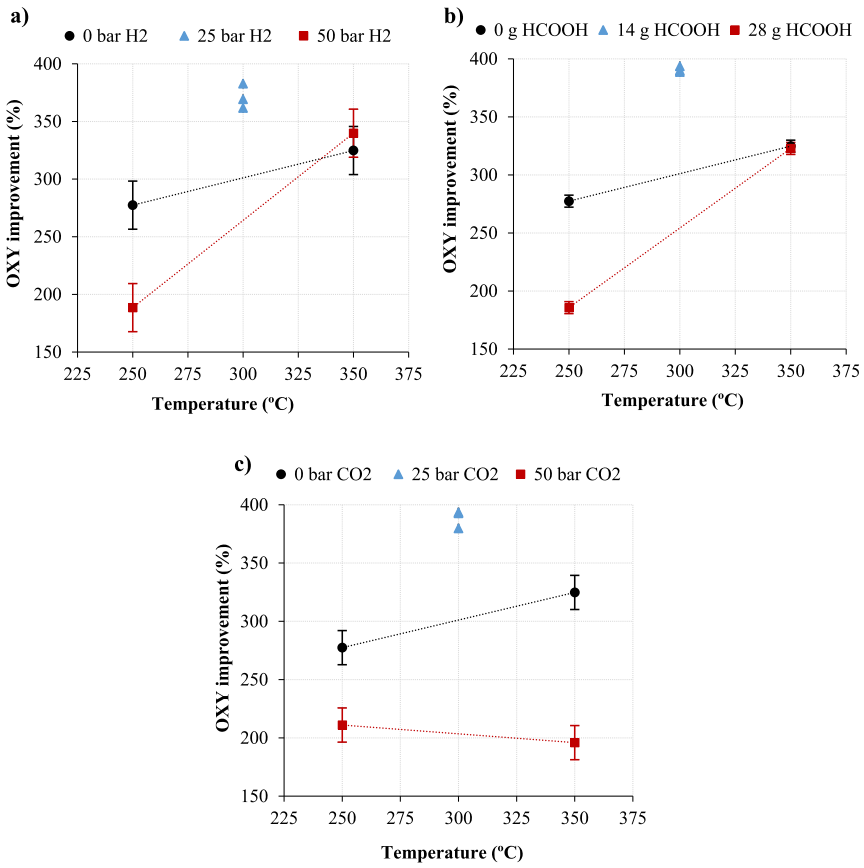

Figure 12. Effect of the temperature and reagent amount used in the depolymerization experiments on the improvement of biodiesel oxidation stability: (a) H_2 experiments, (b) HCOOH experiments, and (c) CO_2 experiments.

(M_w), and polydispersity (M_w/M_n) of the analyzed samples. As shown in Figure 10, up to four different peaks (or shoulders) were observed for the additives. The peaks that eluted at lower retention times could be related to a part of unconverted lignin, higher molecular weight fragments of lignin, and repolymerized lignin, while the peaks observed at a higher retention time (from 21 min) are associated with a lower molecular weight (<1400 Da), thus meaning that the depolymerization reaction had occurred to a greater or lesser extent.[29] Noteworthy is the significant increase in peaks at a retention time of around 17 min in the additives produced at 300 °C, regardless of the reaction atmosphere, which indicates a higher molecular weight compared to those obtained at 250 and 350 °C. This tendency was also observed in the non-soluble additive fraction (probably because of repolymerization reactions). The comparison of the GPC plots of the entire additives and their respective insoluble fractions in biodiesel highlights a noticeable decrease in the intensities of the peaks at retention times of 18.5, 20.2, and 21.48. This reduction is related to the fraction of the additive that was mainly dissolved in biodiesel. These soluble compounds include molecules with a molecular size of <1400 Da and a heavier fraction with a molecular weight of around 7000 Da (more noticeable in the additives obtained at 300 °C under all reaction medium).

Concerning the global data of M_n and M_w, higher values were obtained for either the entire additive or the fraction insoluble in biodiesel depending upon the depolymerization operating conditions. The better solubility of the additives has been correlated with a higher molecular weight of the insoluble fractions compared to the entire additive, thus pointing to a prevalence of the smaller molecules in the fraction of the additive soluble in biodiesel. Moreover, it should be noted that the incorporation of H_2, CO_2, or HCOOH to the reaction medium had a noticeable effect on increasing the molecular weight of the additives, especially at 350 °C.

3.6. Oxidation Stability of Biodiesel. Figure 11 shows a visual comparison of all of the results of biodiesel oxidation stability time (PetroOXY tests). The average oxidation stability time (OXY) of neat biodiesel was 14.8 ± 1.1 min. As a general result, doping biodiesel with AS lignin-based additives has been demonstrated to achieve an excellent improvement of the OXY time. More specifically, increasing the depolymerization temperature from 250 to 300 °C resulted in a significant increase in the OXY time, while only slight differences were observed as a result of the reaction medium for ASL_f depolymerization at this temperature. However, the results obtained at 250 and 350 °C were more affected by the reaction medium. To examine the impact of the factors on this response, the ANOVA statistical analysis was performed on the improvement rate of the OXY time (eq 5).

$$\text{OXY improvement (\%)} = \frac{\text{OXY doped biodiesel} - \text{OXY neat biodiesel}}{\text{OXY neat biodiesel}} \times 100 \quad (5)$$

https://doi.org/10.1021/acs.energyfuels.1c01705
Energy Fuels 2021, 35, 17149−17166

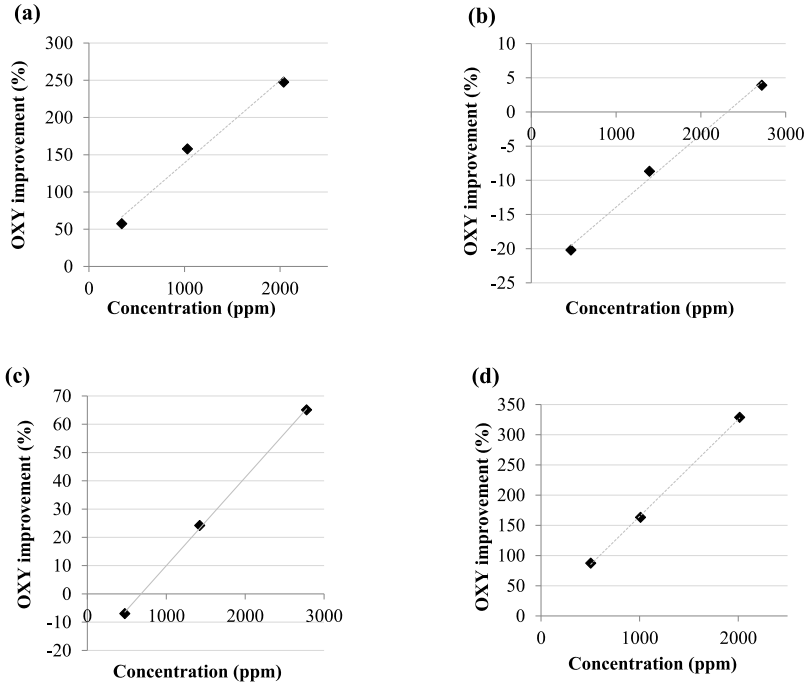

Figure 13. Improvement of biodiesel oxidation stability as a function of the concentrations of (a) catechol, (b) guaiacol, (c) syringol, and (d) BKF dimer.

The results from ANOVA (Figure 12) indicate that both the temperature and the reaction medium and the interaction between them were significant terms in all cases. The increase in the reaction temperature from 250 to 350 °C had a positive impact on the biodiesel oxidation stability achieved with the additives obtained under an inert atmosphere or H_2 and HCOOH medium but not in the case of the CO_2 medium (similar results for both temperatures). However, experimental data did not fit a linear model, but a strong curvature was detected at 300 °C, regardless of the nature of the reagent incorporated (quadratic effect of the temperature). On the other hand, introducing H_2 or HCOOH in the process was not an advantage for this studied variable. No substantial differences were found at the highest temperatures (300−350 °C), obtaining similar oxidation stability values in the three cases (with or without adding H_2 or HCOOH). However, at a temperature of 250 °C, a negative effect of the presence of H_2 (50 bar) or HCOOH (28 g) was even observed when comparing to the result obtained in the inert atmosphere. These results seem to be connected with the observed decrease in the additive solubility in biodiesel, which dropped from a real soluble dosage of 0.74 wt % for the additive produced under an inert atmosphere to 0.4 and 0.61 wt % for the additives produced under H_2 and HCOOH medium, respectively. On the other hand, adding 50 bar of CO_2 to the reaction medium led to additives that achieved lower OXY improvements than those obtained in the N_2 inert atmosphere. Concretely, the improvement of oxidation stability decreased dramatically from 334% (with the additive obtained in a N_2 atmosphere at 350 °C) to 196% (with the additive produced at 350 °C and 50 bar of CO_2), while in H_2 and HCOOH medium, such variation was not observed (OXY improvement of 340 and 323%, respectively). Therefore, the most favorable operating conditions from the point of view of maximizing the improvement of biodiesel oxidation stability were those corresponding to the central points of the experimental design: 391% (300 °C and 28 g of HCOOH), 389% (300 °C and 25 bar of CO_2), and 371% (300 °C and 25 bar of H_2).

The composition of the additives analyzed by GC−FID−MS (Table 5) can partially help to explain the trends observed in the antioxidant potential of the additives. For instance, the highest concentration of catechol was obtained at a treatment temperature of 300 °C, regardless of the reaction medium. This finding could also be related to obtaining the maximum improvement rate of the oxidation stability with the additives produced at 300 °C. Catechol has been reported to show a high antioxidant potential, even at lower dosages,[35,51] much higher than other phenolic monomers derived from lignin, such as guaiacol or alkylated guaiacols, that not only do not have an antioxidant effect but, instead, have a pro-oxidant effect.[35] That means that the presence of guaiacols could play a role in the dilution of the antioxidant activity of other active components present in the additives, such as catechol.

Additionally, Larson et al. reported that not only monomers but also dimers and oligomers obtained from lignin fractionation have a great antioxidant activity,[35] even though they were hard to determine, which is the nature of these components by GC−MS analysis. Hence, the antioxidant capacity of the additives produced in this study could be affected too by the presence of dimers and oligomers undetected by GC−MS, especially because the results of the GPC tests showed that the M_w of the additives produced were in the order of 15 000 Da and the size of the fraction soluble in biodiesel was mainly lower than 7000 Da. Dimer potential candidates in ASL_f depolymerization could be based on monomers of catechol or guaiacol, such as α,ω-dicatechols or diguaiacols, and both proved to have an important antioxidant activity.[35]

https://doi.org/10.1021/acs.energyfuels.1c01705
Energy Fuels 2021, 35, 17149−17166

With the aim to study the individual effect of some phenolic compounds in the oxidation stability of biodiesel, biodiesel was blended with catechol, syringol, guaiacol, and a dimer commercially named as the BKF antioxidant [2,2′-methylenebis(4-methyl-6-*tert*-butylphenol, whose structure is shown in Figure S4 of the Supporting Information] at different concentrations, and OXY tests were conducted according to the same methodology used before. Figure 13 shows the biodiesel OXY improvement as a function of the phenolic compound concentration. As shown, both catechol and the BKF antioxidant positively and linearly affect the oxidation stability, even at a low concentration. In contrast, the inverse trend was shown in the case of guaiacol, negatively affecting the oxidation, which confirms the pro-oxidant effect of this component. Similar to guaiacol, syringol negatively affects the oxidation stability of biodiesel at a low concentration but slightly improves it at higher dosages. These results correlate with the finding that the additives with a higher catechol content and lower guaiacol/guaiacol derivate content led to the most remarkable OXY improvements.

CONCLUSION

Depolymerization of lignin extracted from argan shells to produce added-value chemicals, specifically antioxidant additives, has been studied. Lignin from argan shells was processed in hydrothermal conditions under N_2, H_2, CO_2, or HCOOH as the reaction medium at temperatures ranging from 250 to 350 °C. For the purpose of producing antioxidant additives for biofuels, such as biodiesel, the depolymerization temperature was a critical factor in both the production and antioxidant potential and solubility of the additives. In general, a significant increase in the biodiesel oxidation stability time was obtained at a small dosage of additive (<1 wt %). Under the best operating conditions (300 °C), the process yielded 15−20% of additive and the improvement of the oxidation stability of biodiesel doped with these additives was close to 400%, regardless of the reaction medium. The presence of catechol and catechol derivates in the additives obtained at 300 °C could be partially responsible for these good results of oxidation stability. This experimental study has shown the technical feasibility to produce efficient antioxidant additives from an underused waste, such as argan shell. However, more effort is required to develop a simpler process that could be economically feasible at a larger scale in the context of a biorefinery process focused on argan uses.

ASSOCIATED CONTENT

Supporting Information

The Supporting Information is available free of charge at https://pubs.acs.org/doi/10.1021/acs.energyfuels.1c01705.

Operating and method parameters used in the GC−FID−MS analysis of the produced additives (Table S1), maximal pressures reached during the depolymerization experiments in a Parr reactor at different operational conditions (Table S2), elemental analysis of the insoluble and soluble solids (Table S3), distribution of C, H, and N in soluble and insoluble solids (Table S4), pH values of the reaction mixture before and after each experiment (Table S5), GPC standards and calibration curve (Figure S1), residual gas pressure in the reactor (measured at 20 °C) (Figure S2), joint yield of soluble and insoluble solids from depolymerization experiments (Figure S3), and structure of the BKF antioxidant (Figure S4) (PDF)

AUTHOR INFORMATION

Corresponding Author

Jesús Arauzo − *Thermochemical Processes Group, Aragón Institute of Engineering Research (I3A), University of Zaragoza, 50018 Zaragoza, Spain;* orcid.org/0000-0002-5959-3168; Email: jarauzo@unizar.es

Authors

Zainab Afailal − *Thermochemical Processes Group, Aragón Institute of Engineering Research (I3A), University of Zaragoza, 50018 Zaragoza, Spain*

Noemí Gil-Lalaguna − *Thermochemical Processes Group, Aragón Institute of Engineering Research (I3A), University of Zaragoza, 50018 Zaragoza, Spain;* orcid.org/0000-0002-8704-9274

María Teresa Torrijos − *Thermochemical Processes Group, Aragón Institute of Engineering Research (I3A), University of Zaragoza, 50018 Zaragoza, Spain*

Alberto Gonzalo − *Thermochemical Processes Group, Aragón Institute of Engineering Research (I3A), University of Zaragoza, 50018 Zaragoza, Spain*

José Luis Sánchez − *Thermochemical Processes Group, Aragón Institute of Engineering Research (I3A), University of Zaragoza, 50018 Zaragoza, Spain;* orcid.org/0000-0002-9705-2207

Complete contact information is available at: https://pubs.acs.org/10.1021/acs.energyfuels.1c01705

Author Contributions

Zainab Afailal, investigation and writing the original draft and editing; Noemí Gil-Lalaguna, methodology and writing reviewing and editing; María Teresa Torrijos, investigation; Alberto Gonzalo, technical support and writing reviewing and editing; Jesús Arauzo, supervision; and José Luis Sánchez, scientific work and writing reviewing and editing.

Notes

The authors declare no competing financial interest.

ACKNOWLEDGMENTS

The authors express their gratitude to the Aragón government (Research Group T22_20R), co-funded by FEDER 2014−2020 "Construyendo Europa desde Aragón", and MINECO (Project ENE2017-85040-R: Renewable Additives for Biofuels) for providing the frame support of this work.

REFERENCES

(1) Effendi, A.; Gerhauser, H.; Bridgwater, A. V. Production of renewable phenolic resins by thermochemical conversion of biomass: A review. *Renewable Sustainable Energy Rev.* **2008**, *12* (8), 2092−2116.

(2) Pandey, M. P.; Kim, C. S. Lignin Depolymerization and Conversion: A Review of Thermochemical Methods. *Chem. Eng. Technol.* **2011**, *34* (1), 29−41.

(3) Amen-Chen, C.; Pakdel, H.; Roy, C. Production of monomeric phenols by thermochemical conversion of biomass: A review. *Bioresour. Technol.* **2001**, *79* (3), 277−299.

(4) Gillet, S.; Aguedo, M.; Petitjean, L.; Morais, A. R. C.; da Costa Lopes, A. M.; Łukasik, R. M.; Anastas, P. T. Lignin transformations for high value applications: Towards targeted modifications using green chemistry. *Green Chem.* **2017**, *19* (18), 4200−4233.

(5) Lavoie, J.-M.; Ghislain, T.; Bahl, E.; Arauzo, J.; Gonzalo, A.; Gil-Lalaguna, N.; Sánchez, J. L. Renewable antioxidant additive for biodiesel obtained from black liquor. *Fuel* **2019**, *254*, 115689.
(6) Tolbert, A.; Akinosho, H.; Khunsupat, R.; Naskar, A. K.; Ragauskas, A. J. Characterization and analysis of the molecular weight of lignin for biorefining studies. *Biofuels, Bioprod. Biorefin.* **2014**, *8* (6), 836−856.
(7) Huang, S.; Mahmood, N.; Tymchyshyn, M.; Yuan, Z.; Xu, C. Reductive de-polymerization of kraft lignin for chemicals and fuels using formic acid as an in-situ hydrogen source. *Bioresour. Technol.* **2014**, *171*, 95−102.
(8) da Costa Sousa, L.; Jin, M.; Chundawat, S. P. S.; Bokade, V.; Tang, X.; Azarpira, A.; Lu, F.; Avci, U.; Humpula, J.; Uppugundla, N.; Gunawan, C.; Pattathil, S.; Cheh, A. M.; Kothari, N.; Kumar, R.; Ralph, J.; Hahn, M. G.; Wyman, C. E.; Singh, S.; Simmons, B. A.; Dale, B. E.; Balan, V. Next-generation ammonia pretreatment enhances cellulosic biofuel production. *Energy Environ. Sci.* **2016**, *9* (4), 1215−1223.
(9) Morais, A. R. C.; Pinto, J. V.; Nunes, D.; Roseiro, L. B.; Oliveira, M. C.; Fortunato, E.; Bogel-Łukasik, R. Imidazole: Prospect Solvent for Lignocellulosic Biomass Fractionation and Delignification. *ACS Sustainable Chem. Eng.* **2016**, *4* (3), 1643−1652.
(10) Gonzalo, A.; Bimbela, F.; Sánchez, J. L.; Labidi, J.; Marín, F.; Arauzo, J. Evaluation of different agricultural residues as raw materials for pulp and paper production using a semichemical process. *J. Cleaner Prod.* **2017**, *156*, 184−193.
(11) Marín, F.; Sánchez, J. L.; Arauzo, J.; Fuertes, R.; Gonzalo, A. Semichemical pulping of Miscanthus giganteus. *Bioresour. Technol.* **2009**, *100* (17), 3933−3940.
(12) Ragauskas, A. J.; Beckham, G. T.; Biddy, M. J.; Chandra, R.; Chen, F.; Davis, M. F.; Davison, B. H.; Dixon, R. A.; Gilna, P.; Keller, M.; Langan, P.; Naskar, A. K.; Saddler, J. N.; Tschaplinski, T. J.; Tuskan, G. A.; Wyman, C. E. Lignin Valorization: Improving Lignin Processing in the Biorefinery. *Science* **2014**, *344* (6185), 1246843.
(13) Beauchet, R.; Monteil-Rivera, F.; Lavoie, J. M. Conversion of lignin to aromatic-based chemicals (L-chems) and biofuels (L-fuels). *Bioresour. Technol.* **2012**, *121*, 328−334.
(14) Kang, S.; Li, X.; Fan, J.; Chang, J. Hydrothermal conversion of lignin: A review. *Renewable Sustainable Energy Rev.* **2013**, *27*, 546−558.
(15) Cao, L.; Yu, I. K. M.; Liu, Y.; Ruan, X.; Tsang, D. C. W.; Hunt, A. J.; Ok, Y. S.; Song, H.; Zhang, S. Lignin valorization for the production of renewable chemicals: State-of-the-art review and future prospects. *Bioresour. Technol.* **2018**, *269*, 465−475.
(16) Garrote, G.; Domínguez, H.; Parajó, J. C. Hydrothermal processing of lignocellulosic materials. *Holz als Roh- und Werkstoff.* **1999**, *57* (3), 191−202.
(17) Akhtar, J.; Amin, N. A. S. A review on process conditions for optimum bio-oil yield in hydrothermal liquefaction of biomass. *Renewable Sustainable Energy Rev.* **2011**, *15* (3), 1615−1624.
(18) Gosselink, R. J. A.; Teunissen, W.; van Dam, J. E. G.; de Jong, E.; Gellerstedt, G.; Scott, E. L.; Sanders, J. P. M. Lignin depolymerisation in supercritical carbon dioxide/acetone/water fluid for the production of aromatic chemicals. *Bioresour. Technol.* **2012**, *106*, 173−177.
(19) Otromke, M.; White, R. J.; Sauer, J. Hydrothermal base catalyzed depolymerization and conversion of technical lignin—An introductory review. *Carbon Resources Conversion.* **2019**, *2* (1), 59−71.
(20) He, W.; Li, G.; Kong, L.; Wang, H.; Huang, J.; Xu, J. Application of hydrothermal reaction in resource recovery of organic wastes. *Resour., Conserv. Recycl.* **2008**, *52* (5), 691−699.
(21) Chandrasekaran, S. R.; Murali, D.; Marley, K. A.; Larson, R. A.; Doll, K. M.; Moser, B. R.; Scott, J.; Sharma, B. K. Antioxidants from Slow Pyrolysis Bio-Oil of Birch Wood: Application for Biodiesel and Biobased Lubricants. *ACS Sustainable Chem. Eng.* **2016**, *4* (3), 1414−1421.
(22) Davoudzadeh, F.; Smith, B.; Avni, E.; Coughlin, R. W. Depolymerization of lignin at low pressure using lewis acid catalysts and under high pressure using H_2 donor solvents. *Holzforschung* **1985**, *39* (3), 159−166.
(23) Kleinert, M.; Gasson, J. R.; Barth, T. Optimizing solvolysis conditions for integrated depolymerisation and hydrodeoxygenation of lignin to produce liquid biofuel. *J. Anal. Appl. Pyrolysis* **2009**, *85* (1), 108−117.
(24) Kim, K. H.; Brown, R. C.; Kieffer, M.; Bai, X. Hydrogen-Donor-Assisted Solvent Liquefaction of Lignin to Short-Chain Alkylphenols Using a Micro Reactor/Gas Chromatography System. *Energy Fuels* **2014**, *28* (10), 6429−6437.
(25) Scanlon, J. T.; Willis, D. E. Calculation of Flame Ionization Detector Relative Response Factors Using the Effective Carbon Number Concept. *J. Chromatogr. Sci.* **1985**, *23* (8), 333−340.
(26) Mahmood, N.; Yuan, Z.; Schmidt, J.; Xu, C. Production of polyols via direct hydrolysis of kraft lignin: Effect of process parameters. *Bioresour. Technol.* **2013**, *139*, 13−20.
(27) Toledano, A.; Serrano, L.; Labidi, J. Improving base catalyzed lignin depolymerization by avoiding lignin repolymerization. *Fuel* **2014**, *116*, 617−624.
(28) Erdocia, X.; Prado, R.; Corcuera, M Á; Labidi, J. Base catalyzed depolymerization of lignin: Influence of organosolv lignin nature. *Biomass Bioenergy* **2014**, *66*, 379−386.
(29) Toledano, A.; Serrano, L.; Labidi, J. Organosolv lignin depolymerization with different base catalysts. *J. Chem. Technol. Biotechnol.* **2012**, *87* (11), 1593−1599.
(30) Zabaleta, A. T. Lignin extraction, purification and depolymerization study. Ph.D. Thesis, Departamento de Ingeniería Química y del Medio Ambiente, Universidad del País Vasco, San Sebastián, Spain, 2012.
(31) Kähkönen, M. P.; Hopia, A. I.; Vuorela, H. J.; Rauha, J.-P.; Pihlaja, K.; Kujala, T. S.; Heinonen, M. Antioxidant Activity of Plant Extracts Containing Phenolic Compounds. *J. Agric. Food Chem.* **1999**, *47* (10), 3954−3962.
(32) Yaakob, Z.; Narayanan, B. N.; Padikkaparambil, S.; Unni, K. S.; Akbar, P. M. A review on the oxidation stability of biodiesel. *Renewable Sustainable Energy Rev.* **2014**, *35*, 136−153.
(33) Tabatabaei, M.; Aghbashlo, M. The critical role of advanced sustainability assessment tools in enhancing the real-world application of biofuels. *Acta Innovations* **2020**, *37*, 67−73.
(34) Pullen, J.; Saeed, K. An overview of biodiesel oxidation stability. *Renewable Sustainable Energy Rev.* **2012**, *16* (8), 5924−5950.
(35) Larson, R. A.; Sharma, B. K.; Marley, K. A.; Kunwar, B.; Murali, D.; Scott, J. Potential antioxidants for biodiesel from a softwood lignin pyrolyzate. *Ind. Crops Prod.* **2017**, *109*, 476−482.
(36) Domingos, A. K.; Saad, E. B.; Vechiatto, W. W. D.; Wilhelm, H. M.; Ramos, L. P. The influence of BHA, BHT and TBHQ on the oxidation stability of soybean oil ethyl esters (biodiesel). *J. Braz. Chem. Soc.* **2007**, *18*, 416−423.
(37) Focke, W. W.; van der Westhuizen, I.; Grobler, A. B. L.; Nshoane, K. T.; Reddy, J. K.; Luyt, A. S. The effect of synthetic antioxidants on the oxidative stability of biodiesel. *Fuel* **2012**, *94*, 227−233.
(38) Gil-Lalaguna, N.; Bautista, A.; Gonzalo, A.; Sánchez, J. L.; Arauzo, J. Obtaining biodiesel antioxidant additives by hydrothermal treatment of lignocellulosic bio-oil. *Fuel Process. Technol.* **2017**, *166*, 1−7.
(39) Palomo, J.; Moles, S.; Salafranca, J.; Gil-Lalaguna, N.; Gonzalo, A.; Sánchez, J. L. Production of antioxidants for biodiesel from straw black liquor depolymerization. *WIT Trans. Ecol. Environ.* **2019**, *237*, 97−108.
(40) Botella, L.; Stankovikj, F.; Sánchez, J. L.; Gonzalo, A.; Arauzo, J.; Garcia-Pérez, M. Bio-Oil Hydrotreatment for Enhancing Solubility in Biodiesel and the Oxydation Stability of Resulting Blends. *Front. Chem.* **2018**, *6*, 83−83.
(41) García, M.; Botella, L.; Gil-Lalaguna, N.; Arauzo, J.; Gonzalo, A.; Sánchez, J. L. Antioxidants for biodiesel: Additives prepared from extracted fractions of bio-oil. *Fuel Process. Technol.* **2017**, *156*, 407−414.

https://doi.org/10.1021/acs.energyfuels.1c01705
Energy Fuels 2021, 35, 17149−17166

(42) Manzanares, P. The role of biorefinering research in the development of a modern bioeconomy. *Acta Innovations.* **2020**, *37*, 47−56.
(43) Kállai, M.; Balla, J. The effect of molecular structure upon the response of the flame ionization detector. *Chromatographia* **2002**, *56* (5), 357−360.
(44) Jorgensen, A. D.; Picel, K. C.; Stamoudis, V. C. Prediction of gas chromatography flame ionization detector response factors from molecular structures. *Anal. Chem.* **1990**, *62* (7), 683−689.
(45) Tedsree, K.; Li, T.; Jones, S.; Chan, C. W. A.; Yu, K. M. K.; Bagot, P. A. J.; Marquis, E. A.; Smith, G. D. W.; Tsang, S. C. E. Hydrogen production from formic acid decomposition at room temperature using a Ag-Pd core-shell nanocatalyst. *Nat. Nanotechnol.* **2011**, *6* (5), 302−307.
(46) Yuan, Z.; Cheng, S.; Leitch, M.; Xu, C. Hydrolytic degradation of alkaline lignin in hot-compressed water and ethanol. *Bioresour. Technol.* **2010**, *101* (23), 9308−9313.
(47) Long, J.; Xu, Y.; Wang, T.; Shu, R.; Zhang, Q.; Zhang, X.; Fu, J.; Ma, L. Hydrothermal Depolymerization of Lignin: Understanding the Structural Evolution. *BioResources* **2014**, *9* (4), 7162−7175.
(48) Miller, J.; Evans, L.; Mudd, J.; Brown, K. *Batch Microreactor Studies of Lignin Depolymerization by Bases. 2. Aqueous Solvents*; Sandia National Laboratories: Albuquerque, NM, 2002; Technical Report SAND2002-1318,.
(49) Li, J.; Henriksson, G.; Gellerstedt, G. Lignin depolymerization/repolymerization and its critical role for delignification of aspen wood by steam explosion. *Bioresour. Technol.* **2007**, *98* (16), 3061−3068.
(50) Kleinert, M.; Barth, T. Phenols from lignin. *Chem. Eng. Technol.* **2008**, *31* (5), 736−745.
(51) Botella, L.; Bimbela, F.; Martín, L.; Arauzo, J.; Sánchez, J. L. Oxidation stability of biodiesel fuels and blends using the Rancimat and PetroOXY methods. Effect of 4-allyl-2,6-dimethoxyphenol and catechol as biodiesel additives on oxidation stability. *Front. Chem.* **2014**, *2*, 43.

https://doi.org/10.1021/acs.energyfuels.1c01705
Energy Fuels 2021, 35, 17149−17166

APPENDIX II: Complementary information of Chapter 2.

- **Instruction for determining the macro-component distribution in biomass: simplified method from Van Soest procedure[1].**

This method consists of succeeding digestion steps using three different detergents (neutral detergent, acid detergent, and sulfuric acid 72 %). The biomass sample was crushed and sieved to a particle size between 1 and 2 mm. For each sample, it is recommended to start with four repetitions, as in each step, one of them is kept to determine the elemental and ash contents. Before starting the digestion, the dissolutions (detergents) were prepared previously (to be used at most two weeks after preparation).

– **Reactants preparation**

Neutral detergent

In a 1 liter volumetric flask, 30 g of sodium dodecyl sulfate (SDS: $C_{12}H_{25}NaSO_4S$) was dissolved in 400 ml of warm water. 18.61 g of EDTA Na, 6.81 g of decahydrate sodium tetraborate (Borax) and 4.56 g sodium hydrogen phosphate (PO_4HNa_2) were weighed separately (in a beaker), and 400 ml of distilled water were added. The solution was dissolved by heating lightly, then let cool and transferred into the volumetric flask containing the SDS solution. Then 10 ml of triethylene glycol was added (to limit the foam formation) before completing the volume with distilled water. The pH of this solution should be between 6.9 and 7.1 (possibly readjusted by adding some drops of NaOH solution).

Acid detergent

This solution consists of a cetylmethylammonium bromide solution (CTAB) at 2 % (weight/volume) in H_2SO_4 (1N).

Sulfuric acid solution

A solution of sulfuric acid at 72 %.

– **Digestion**

Neutral detergent step (using NDF solution)

In a round-bottom flask of 250 ml, around 2 ± 0.001 g of sample P_0 (dried sample) was weighed. 100 ml of neutral detergent solution (NDF) was added, and the flasks were transferred to the hot extraction unit (consisting of a heating magnetic stirrer and cooling

[1] Godin, B., Agneessens, R., Gofflot, S., Lamaudière, S., Sinnaeve, G., Gerin, P. A., & Delcarte, J. 2011. Revue bibliographique sur les méthodes d'analyse des polysaccharides structuraux des biomasses lignocellulosiques. Biotechnologie, Agronomie, Société et Environnement, 15(1), 165-182.

system, as shown in the picture below). The system's heat was adjusted and kept boiling for 1 h (moderate and constant degree of boiling).

When the time finished, the magnetic stirring bar was removed and rinsed with boiling distilled water; then, the solution was filtered using a glass microfiber filter (previously weighed) suitable for a vacuum Buchner. The solid was washed with boiling distilled water until the total disappearance of the soapy aspect of the filtrate, and then it was washed twice with acetone.

The glass microfiber filter containing the sample was transferred to a glass crucible (previously weighed) and dried overnight at 105 °C. The crucible was placed into the desiccator and weighed after cooling P_1. One repetition after this step was saved to determine the elemental and ash content.

Acid detergent step (using ADF solution)

The NDF residue was placed in a round-bottom flask of 250 ml, 100 ml of acid detergent solution (ADF) was added, and the same steps were followed. The dried sample was weighed P_2, and one repetition was kept for the elemental and ash content determination.

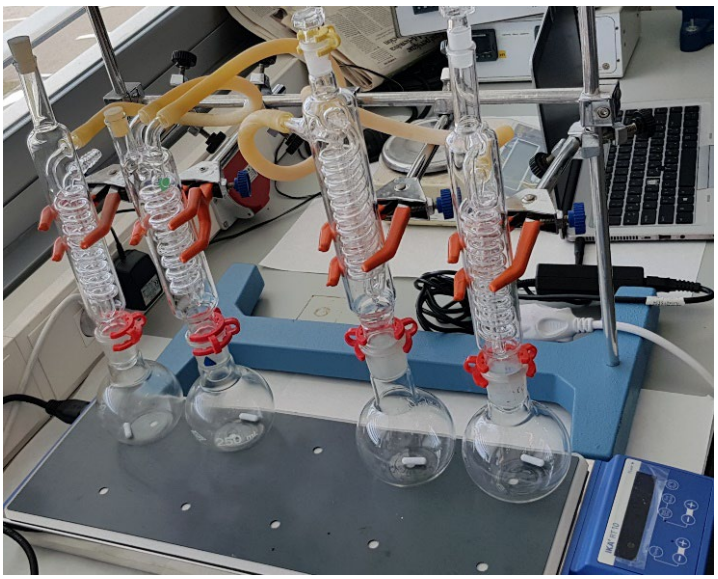

Sulfuric acid step (using ADL solution)

The ADF residue was placed in an 80 ml centrifuge tube, and 50 ml of acid detergent (ADL) was added. The sample was kept in contact with the acid solution for 3 h, then centrifuged for 5 min (3200 rpm). The solution was carefully filtered and washed with boiling distilled water until neutralizing the filtrate, then washed twice with acetone. The dried sample was weighed P_3, then transferred to a porcelain crucible where it was calcinated at 550 °C for 3 h and weighed after cooling P_4.

– **Calculation (dry and ash-free basis)**

All the weights should be expressed on a daf-basis.

% Easily-digestible proteins, lipids and pectins: $(P_0-P_1)/100$.

% Hemicellulose: $(P_1-P_2)/100$.

% Cellulose: $(P_2-P_3)/100$.

% Lignin: $(P_3-P_4)/100$.

- **Soxhlet extraction**

The soxhlet extraction process involves intimate contact of the sample with the extraction solvent. The solid sample was crushed and sieved to a particle size of up to 1 mm. Two glass wool plugs were placed on the bottom of a glass fiber extraction thimble. Then around 3 g of the dried solid sample was mixed with anhydrous sodium sulfate, and two glass wool plugs were placed on the top of the thimble. The latter was placed into the Soxhlet extractor and assembled with a preweighted flask containing 200 mL of the extraction solvent (the experimental setup shown in the picture). The system's heat was adjusted to have between 4 and 6 cycles per hour. The extraction time ranged between 16 and 24 h (until obtaining a clear solvent). Once the time finished, the solvent was evaporated, and the extractives content was determined gravimetrically.

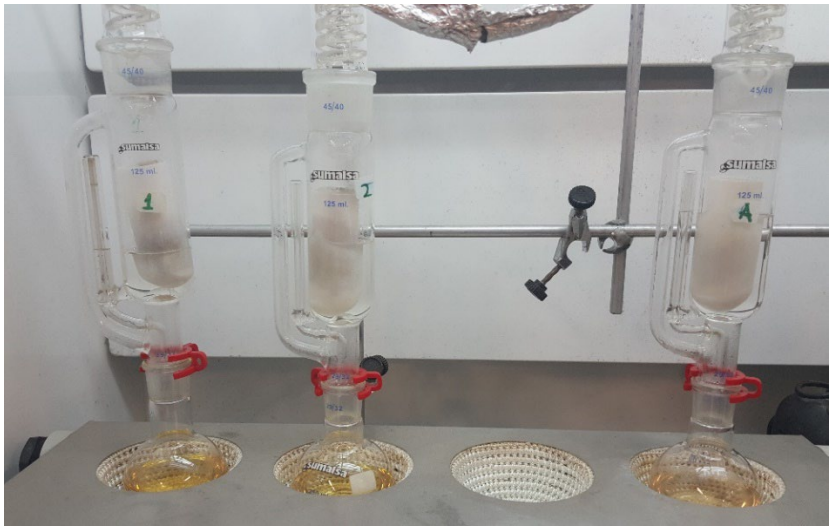

APPENDIX III: Complementary information of Chapter 3.

- Operating and method parameters for GC/MS/FID analysis of torrefaction liquids.

Column	HP-FFAP (Polyethylene Glycol), 50 m x 200 µm x 0.33 µm
Injection volume	1 µL
Injector	300 °C, splitless
Carrier gas	Helium (constant flow: 1 mL/min in column)
Oven program	60 °C (4 min); then to 80 °C (5 min) at 1.5 °C /min; then to 100 °C (10 min) at 3.5 °C /min; then to 240 °C (15 min) at 1.8 °C /min.
Detector	(i) Front Detector FID (300 °C; H_2/air) (ii) MSD analyzer (Trace Ion Detection; electron ionization)
Library program of MS signal	NIST MS Search Program 2.2

- Determination of the FID response factor for the compounds present in the analyzed oils but not comprised in the standard calibration solutions.

(Methodology based on the Effective Carbon Numbers**)**

The FID response factors of the compounds identified by GC/MS but not calibrated as standards were calculated according to the following equations reported in the Scanlon and Willis work[2].

$$F(R-wt) = \frac{RF_i}{RF_ref}$$

$$F(R-wt) = \frac{MW_i * ECN_ref}{MW_ref * ECN_i}$$

where:

F(R-wt): Relative weight response factor.

RF_i: FID response factor of any compound "i" identified by GC/MS and not included in the standard used in the FID signal calibration.

RF_ref: FID response factor of the compound chosen as a reference for the compound "i", experimentally obtained from the calibration of FID signal (compounds present in the standard solutions). The reference compound was chosen according to chemical similarity with the compound "i".

MW_ref and MW_i: Molecular weights of the reference compound and the compound "i", respectively.

ECN_ref and ECN_i: Effective Carbon Number of the reference compound and the compound "i", respectively.

[2]Scanlon J.T., Willis D.E. (1985), Calculation of Flame Ionization Detector Relative Response Factors Using the Effective Carbon Number Concept. Journal of Chromatographic Science. 23(8): 333-340.

- List of ECN values used to calculate the compounds' response factor that was not included in the standard calibration solutions.

Compound name (formula)	MW ($g\ mol^{-1}$)	ECN	Compound name (formula)	MW ($g\ mol^{-1}$)	ECN
Compounds ref			**Compounds i**		
Acetic acid ($C_2H_4O_2$)	60.05	1	**Benzene, 1,2,3-trimethoxy-5-methyl ($C_{10}H_{14}O_3$)**	182.22	7
Eugenol ($C_{10}H_{12}O_2$)	164.20	8.4	**Butanoic acid, anhydride ($C_8H_{14}O_3$)**	88.11	3
Phenol (C_6H_6O)	94.11	5.5	**Cyclopentanol ($C_5H_{10}O$)**	86.13	4.5
Syringol ($C_8H_{02}O_3$)	154.16	5.5	**Furan, tetrahydro-2,5-dimethoxy ($C_6H_{12}O_3$)**	132.16	3
2-Furancarboxaldehyde, 5-methyl ($C_6H_6O_2$)	110.11	3.8	**Guaiacylacetone ($C_{10}H_{12}O_3$)**	180.20	7.5
4-Ethylguaiacol ($C_9H_{12}O_2$)	152.19	7.5	**Methoxyeugenol ($C_{11}H_{14}O_3$)**	194.23	8.4
			Propanoic acid ($C_3H_6O_2$)	74.08	2
			1-Hydroxy-2-butanone ($C_4H_8O_2$)	88.11	2.5
			2-Cyclopenten-1-one, 2-hydroxy ($C_5H_6O_2$)	98.10	3.4
			2-Cyclopenten-1-one, 2-hydroxy-3-methyl ($C_6H_8O_2$)	112.13	4.4
			4-Vinylguaiacol ($C_9H_{10}O_2$)	105.18	7.4

- Comparison of AS and P torrefaction with other materials in the literature.

	AS (220 °C, 27 min) Auger reactor Current study	AS (250 °C, 27 min) Auger reactor Current study	P (250 °C, 27 min) Auger reactor Current study	Sugar Beet Pulp (250 °C, 30 min) Fixed bed reactor Brachi et al. 2017	Wood Pellets (250 °C, 15 min) Fluidized bed reactor Brachi et al. 2018	Palm kernel shell (250 °C, 15 min) Batch reactor Asadullah et al. 2014
Torrefied solid characterization						
C	59.8	68.9	58.5	58.6[b]	62.3	68.2[b]
H	5.5	4.75	5.26	5.9[b]	5.4[c]	4.9[b]
N	0.24	0.33	0.21	2.3[b]	0.1	0.6[b]
O[a]	33.9	25.2	31.0	33.1[b]	29.6	26.0[b]
HHV (MJ/kg)	22.67	26.97	23.20	22.71[c]	24.20[c]	26.16[c]
Fixed Carbon (wt.%)	30	45	28	36[b]	-	47.2
Product distribution (wt.%, ar)						
Torrefied Solid	65.8	49.7	61.8	49.1	42.9	82.6
Liquid	27	39.4	28.3	16.6	17.4	12.8
Gas	5.4	10.4	12.3	34.4	5.04	4.6

[a] by difference
[b] dry and ash-free basis
[c] dry basis

- Energy distribution calculation of torrefaction products.

HHV of the produced liquid:

$$HHV_{liquid} = 8{,}140 \,.\frac{\%C}{100} + 34{,}400 \,.\left(\frac{\%H}{100} - \frac{\%O}{800}\right) + 2{,}220 \,.\frac{\%S}{100}$$

Composition of the produced tar and HHV calculated using Dulong's formula.

	AS, 220 °C	**AS, 250 °C**	**P, 220 °C**	**P, 250 °C**
C (wt. %)	52.3	51.3	41.4±0.4	47±2
H (wt. %)	4.2	3	6.8±1.4	10.8±0.6
O (wt. %)	43.6	45.7	51.9±1.1	42.6±1.3
HHV (MJ/kg)	15.9	13.6	14.5	23.8

HHV of torrefaction gas:

$$HHV_{gas} = LHV_{gas} + 2.257 \,.\,(9 \,.\, H\,)$$

where H is expressed in (kg of H/Nm^3 gas)

$$LHV_{gas} = 10.789 \,.\left(\frac{\%vol.\,H_2}{100}\right) + 12.63 \,.\left(\frac{\%vol.\,CO}{100}\right) + 35.812 \,.\left(\frac{\%vol.\,CH_4}{100}\right) + 63.744 \,.\left(\frac{\%vol.\,C_2H_6}{100}\right) + 59.033.\left(\frac{\%vol.\,C_2H_4}{100}\right) + 56.088 \,.\left(\frac{\%vol.\,C_2H_2}{100}\right) + 23.113 \,.\left(\frac{\%vol.\,H_2S}{100}\right)$$

Using the gas composition and the equations above, we obtain:

LHV and HHV of the produced gas

	AS, 220 °C	**AS, 250 °C**	**P, 220 °C**	**P, 250 °C**
LHV (MJ/m$^3_{STP}$)	6.3	6.6	5.8 ± 0.8	5.6 ± 0.9
HHV (MJ/m$^3_{STP}$)	6.6	6.9	5.9 ± 0.8	5.7 ± 0.9

APPENDIX IV: Complementary information of Chapter 4.

- Operating and method parameters for GC/MS/FID analysis of gasification liquids.

Column	DB-17ms (50%-phenyl)- methylpolysiloxane), 60 m x 250 µm x 0.25 µm
Injection volume	1 µL
Injector	250 °C, splitless
Carrier gas	Helium (constant flow: 1 mL/min in column)
Oven program	50 ºC (5 min); then to 80 ºC (15 min) at 1.5 ºC/min; then to 200 ºC at 1.5 ºC/min, then to 236 ºC at 3 ºC/min; then to 250 ºC (5 min) at 1.5 ºC/min; then to 320 ºC at 5 ºC/min
Detector	(i) Front Detector FID (250 °C; H_2/air) (ii) MSD analyzer (Trace Ion Detection; electron ionization)
Library program of MS signal	NIST MS Search Program 2.2

APPENDIX V: Complementary information of Chapter 5.

- Operating and method parameters for GC/MS/FID analysis of organic phases extracted from bio-oil and bio-oil hydrothermally treated.

Column	DB-17ms ((50%-phenyl)- methylpolysiloxane). 60 m x 250 μm x 0.25 μm.
Injection volume	1 μL.
Injector	300 °C; split 1/10.
Carrier gas	Helium (constant flow: 1 mL/min in the column)
Oven program	80 °C (10 min); then to 130 °C (5 min) at 3 °C/min; then to 180 °C (10 min) at 2°C/min. then to 250 °C (0 min) at 10 °C/min. then to 320 °C (15 min).
Detector	(i) Front Detector FID (300 °C; H_2/air) (ii) MSD analyzer (Trace Ion Detection; electron ionization)
Library program of MS signal	NIST MS Search Program 2.2

- Composition of the synthetic additives (using as a reference the composition of the additives prepared from the original bio-oils obtained at 550 °C)

	Concentaration of each component in the additive (wt.%)	
	WS bio-oil	AS bio-oil
Phenol	1.8	1.0
p-Cresol	0.8	0.8
Guaiacol	3.8	5.1
3-ethylphenol	1.5	1.0
Creosol	1.0	3.9
Catechol	1.7	5.4
4-ethylguaiacol	1.0	2.1
3-methoxycatechol	1.5	2.6
4-vinylguaiacol	16.0	6.9
Eugenol	0.5	2.3
Syringol	1.4	6.6
Vanillin	0.3	0.7
Apocynin	0.1	0.02
Guaiacylacetone	0.1	0.8
OXY time (min)	27 ± 1	36 ± 2
ΔOXY (%)	89 ± 8	144 ± 15

APPENDIX VI: Complementary information of Chapter 7.

Table A. GPC standards and calibration curve.

Standard	Time (min)	Mp	log Mp
13	14.48333	100900	5.00389
12	14.8	69100	4.83948
11	15.5	44000	4.64345
10	16.23333	25200	4.4014
9	17.48333	12600	4.10037
8	18.55	6690	3.82543
7	19.35	4290	3.63246
6	21.08333	1400	3.14613
5	21.66667	1030	3.01284
4	22.53333	633	2.8014
3	23.28333	430	2.63347
2	24.95	202	2.30535
1	26.3	106	2.02531

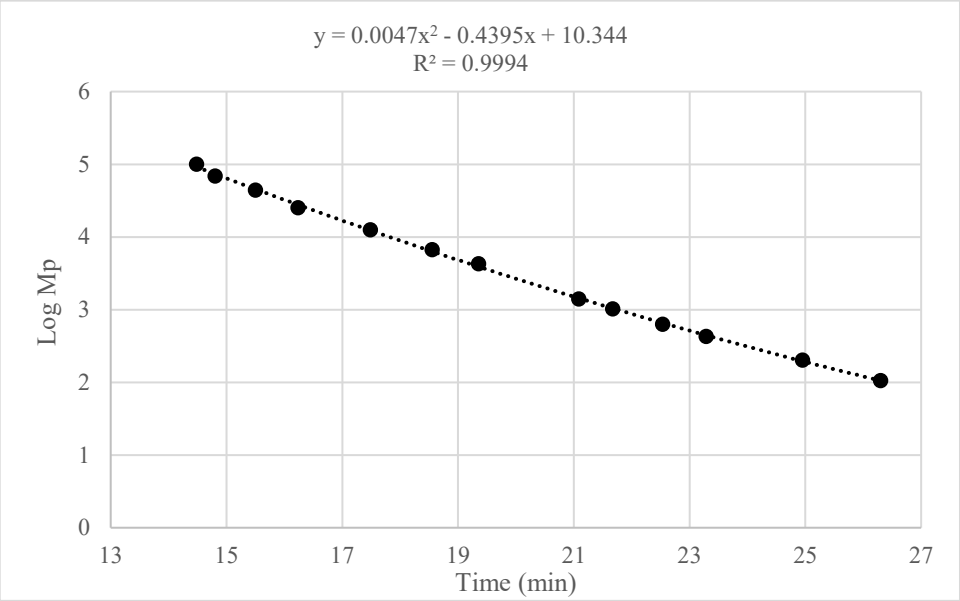

- Operating and method parameters for GC/MS/FID analysis of the redissolved antioxidant additives produced from AS lignin.

Column	HP-FFAP (Polyethylene Glycol), 50 m x 200 µm x 0.33 µm.
Injection volume	1 µL.
Injector	300 °C, splitless.
Carrier gas	Helium (constant flow: 1 mL/min in column)
Oven program	60 °C (4 min); then to 80 °C (5 min) at 1.5 °C/min; then to 100 °C (5 min) at 3.5 °C/min; then to 160 °C (5 min) at 1 °C/min, then to 180 °C (5 min) at 1 °C/min, then to 210 °C (5 min) at 1 °C/min, then to 230 °C (20 min) at 1 °C/min.
Detector	(i) Front Detector FID (300 °C; H2/air) (ii) MSD analyzer (Trace Ion Detection; electron ionization)
Library program of MS signal	NIST MS Search Program 2.2

- Elemental analysis of the insoluble and the soluble solid.

	T (°C)	Initial gas pressure (bar) / HCOOH weight (g)	Elemental analysis of the insoluble solid (wt.%)			Elemental analysis of the soluble solid (wt.%)		
			%C	%H	%N	%C	%H	%N
Inert atmosphere Experiments	250	0	34.9±0.4	3.8±0.1	0.52±0.01	26±2	3.31±0.02	0.26±0.02
	350	0	64.2±0.3	4.25±0.05	0.55±0.02	24.3±0.9	2.67±0.02	0.10±0.03
H_2 Experiments	250	50	37.2±0.1	3.78±0.02	0.52±0.03	25.8±0.2	3.407±0.001	0.23±0.03
	350	50	62.5±0.2	4.9±0.1	0.66±0.02	24.4±0.2	3.3±0.04	0.22±0.01
	300	25	46.6±0.2	3.84±0.03	0.601±0.005	25±1	3.306±0.004	0.21±0.02
	300	25	47.2±0.1	3.824±0.004	0.60±0.03	25.78±0.13	3.741±0.006	0.233±0.001
	300	25	44.5±0.2	3.6±0.1	0.60±0.01	27.22±0.04	3.46±0.03	0.24±0.03
CO_2 Experiments	250	50	61.9±0.3	4.6±0.1	0.57±0.04	26.0±0.2	3.06±0.01	0.173±0.004
	350	50	73.9±0.2	4.5±0.2	0.63±0.02	24.5±0.1	2.6±0.1	0.10±0.03
	300	25	69±1	4.289±0.001	0.63±0.04	25±1	2.9±0.1	0.12±0.02
	300	25	69±4	4.4±0.1	0.75±0.02	26±1	2.82±0.04	0.23±0.13
	300	25	67.6±0.2	4.20±0.02	0.62±0.02	26±1	3.0±0.1	0.16±0.02
HCOOH Experiments	250	28	66.0±0.1	6.37±0.04	0.67±0.03	22±1	3.18±0.02	0.17±0.01
	350	28	49.4±0.1	4.7±0.1	0.55±0.04	27±2	3.7±0.1	0.19±0.02
	300	14	58.1±0.4	5.2±0.2	0.83±0.02	24±1	5.13±0.07	0.17±0.01
	300	14	63.1±0.1	5.8±0.1	0.83±0.02	22±1	4.96±0.03	0.13±0.02
	300	14	60.9±0.1	5.44±0.03	0.84±0.01	25.2±0.5	4.32±0.08	0.156±0.003

- **Structure of the BKF antioxidant.**

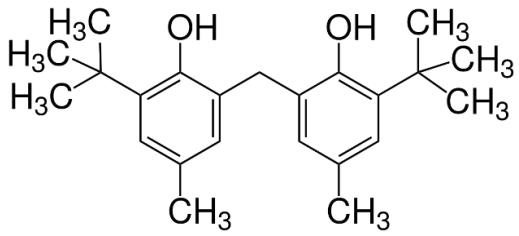

2,2′-Methylenbis(4-methyl-6-tert-butylphenol)

APPENDIX VII: Complementary information of Chapter 8.

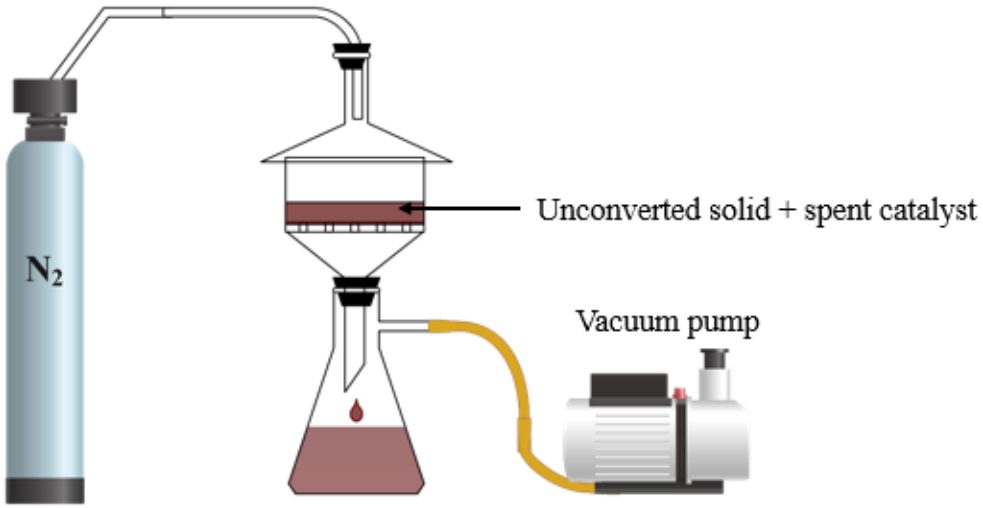

- Filtration setup.

- Operating and method parameters for GC/MS/FID analysis of the organic liquids from RCF of AS.

Column	DB-17ms ((50%-phenyl)- methylpolysiloxane). 60 m x 250 µm x 0.25 µm.
Injection volume	1 µL.
Injector	300 °C; splitless.
Carrier gas	Helium (constant flow: 1 mL/min in column)
Oven program	40 °C (4 min); then to 80 °C (5 min) at 2.5 °C/min; then to 130 °C (5 min) at 2.5 °C/min; then to 180 °C (5 min) at 2.5°C/min. then to 250 °C (1 min) at 2.5 °C/min. then to 300 °C (2 min) at 10 °C/min.
Detector	(i) Front Detector FID (300 °C; H_2/air) (ii) MSD analyzer (Trace Ion Detection; electron ionization)
Library program of MS signal	NIST MS Search Program 2.2

Table A. Response factor from GC/FID calibration curves (RF_ref), values of the effective carbon number (ECN_ref for reference compounds and ECN_i for compounds "i") and calculated response factors for compounds"i" (RF_i).

Reference compound	RF_ref	MW	ECN	Compound i	MW	ECN	RF_i
Acetic acid	3.00E-05	60.05	1	**5-(3-Hydroxypropyl)-2,3-dimethoxyphenol/4-n-propanolsyringol***	212.24	8	7.2453E-06
Guaiacol	7.00E-06	124.14	5.5	**3,5-Dimethoxy-4-hydroxytoluene**	168.19	6.5	8.6659E-06
Creosol	1.00E-05	138.16	6.5	**Benzenepropanol, 4-hydroxy-3-methoxy**	182.22	8	9.1364E-06
Phenol, 2,4,6-trimethyl-	3.00E-06	136.19	8.5	**Phenol, 3-methyl**	108.14	6.5	4.8954E-06
Phenol	6.00E-06	94.11	5.5	**Phenol, 2-methoxy-4-propyl**	166.22	8.5	4.1648E-06
Phenol, 4-ethyl-2-methoxy-	6.00E-06	152.19	7.5	**Benzene, 1,2,3-trimethoxy-5-methyl**	182.22	7	8.6141E-06
Phenol, 2,5-dimethyl-	5.00E-06	122.16	7.5	**5-tert-Butylpyrogallol**	182.22	7.5	1.1536E-05
p-Cresol	6.00E-06	108.14	6.5	**Benzoic acid, 4-hydroxy-3-methoxy-, methyl ester**	182.17	5.5	6.1747E-06
Eugenol	5.00E-06	164.20	8.4	**Homovanillic acid**	182.18	6	6.3305E-06
Phenol, 4-ethyl-	5.00E-06	122.16	7.5	**Benzeneacetic acid, 4-hydroxy-3-methoxy-, methyl ester**	196.20	6.5	6.7757E-06
Phenol, 2,6-dimethoxy-	8.00E-06	154.16	5.5	**3-(p-Hydroxyphenyl)-1-propanol**	152.19	8	5.3969E-06
3-methoxycatechol	1.00E-05	140.14	5	**3,5-Dimethoxy-4-hydroxyphenethylamine**	197.23	7.5	7.9134E-06
4-Allyl-2,6 dimethoxy phenol	9.00E-06	194.23	8.4	**3-(3,4-Dimethoxyphenyl)-1-propanol**	196.24	8.5	8.3256E-06
Vanillin	1.00E-05	152.15	5.5	**Benzaldehyde, 4-hydroxy-3,5-dimethoxy**	182.17	5.5	6.1747E-06
Apocynin	8.00E-06	166.17	6.5	**Ethanone, 1-(4-hydroxy-3,5-dimethoxyphenyl)**	196.20	6.5	6.7757E-06
Guaiacylacetone	8.00E-06	180.20	7.5	**Propan-2-one, 1-(4-isopropoxy-3-methoxyphenyl)**	222.28	10	8.6475E-06
Homovanillyl alcohol	8.00E-06	168.19	7	**Desaspidinol**	210.23	8	7.3147E-06
Orcinol	9.00E-06	124.13	6	**1-(2-Hydroxy-4-methoxyphenyl)propan-1-one**	180.20	7.5	7.7495E-06
Catechol	9E-06+279.38	110.11	5	**3,5-Dimethoxy-4-hydroxyphenylacetic acid**	212.20	6	5.435E-06
Hydroquinone	1.00E-05	110.11	5	**Phenol, 2-methoxy-4-(1-propenyl)-,(Z)**	164.20	8.4	6.2285E-06
1,2 propanediol	4.00E-05	76.09	2.25	**Benzoic acid, methyl ester**	136.15	6	9.0131E-06
2-cyclopenten-1-one	1.00E-05	82.04	4.9	**1-Hydroxy-2-butanone**	88.11	2.5	3.8383E-05
2-Ethyl-1-Hexanol	9.00E-06	130.23	6.5	**4-Hydroxy-3-hexanone**	116.16	3.5	4.0759E-05
Furfural	2.00E-05	96.08	2.8	**2,5-Hexanedione**	114.14	4	4.7404E-05

Ethylene dimethcrylate	9.00E-06	198.22	5.9
n-butyl acetate	2.00E-05	116.16	5
Furfuryl alcohol	3.00E-05	98.10	3.3
2,5-dimethylfuran	2.00E-05	96.13	4.8
Butanoic acid, methyl ester	1.10E-05	102.13	3
Hexanoic acid, methyl ester	8.56E-06	130.18	5
Octanoic acid, methyl ester	7.08E-06	158.24	7
Methyl tetradecanoate	5.72E-06	242.40	13
Pentadecanoic acid, methyl ester	5.67E-06	256.42	14
Methyl stearate	2.82E-06	298.50	17
9,12-Octadecadienoic acid (Z,Z)-, methyl ester	1.05E-05	294.47	16.8

meso-3,4-Hexanediol	118.17	5.25	6.0095E-05
1,2-Butanediol	90.12	3.25	4.8782E-05
Butanoic acid, 4-hydroxy	104.10	2.5	4.3263E-05
Octadecanoic acid	284.48	17	2.9553E-06
Cyclopentanone	84.12	4	7.9618E-06
Cyclopentanone, 2-methyl	98.14	5	8.5298E-06
Cyclohexanone, 2-hydroxy	114.14	4.5	6.6008E-06
2-Cyclopenten-1-one, 2-methyl	96.13	4.9	8.5345E-06
1,2-Cyclopentanedione, 3-methyl	112.13	4	5.9728E-06
2-Cyclopenten-1-one, 2-hydroxy-3,4-dimethyl	126.15	5.4	7.1668E-06
2-Cyclopenten-1-one, 2-hydroxy-3-methyl	112.13	4.4	6.5701E-06
2-Cyclopenten-1-one, 2,3-dimethyl	110.15	5.9	8.9677E-06
2-Acetonylcyclopentanone	140.18	6	7.1663E-06
2-Furanol, tetrahydro-2-methyl	102.13	4.5	1.7648E-05
2-Furancarboxaldehyde, 5-methyl	110.11	3.8	2.3685E-05
Methyl 2-furancarboxylate	126.11	2.8	1.5238E-05
5-Hydroxymethylfurfural	126.11	3.3	2.3337E-05
Butane, 1,1-dibutoxy	202.33	10	2.2964E-05
Butyl ether	130.23	7	2.4975E-05
Acetic acid, hydroxy-, methyl ester	90.08	0.5	1E-05
Propanoic acid, 2-hydroxy-, methyl ester	104.10	1.5	6.0569E-06
Butanoic acid, 2-hydroxy-, methyl ester	118.13	2.5	7.9001E-06
Butanoic acid, butyl ester	144.21	7	7.7728E-06
Acetic acid, hydroxy-, butyl ester	132.16	4.5	7.5847E-06
Propanoic acid, 2-hydroxy-, butyl ester	146.18	4.5	1.1491E-05
Pentanoic acid, 4-oxo-, methyl ester	130.14	6	7.3827E-06
Butanedioic acid, dimethyl ester	146.14	2	3.3004E-06

Pentanedioic acid, dimethyl ester	160.17	3	6.992E-06
Pentanoic acid, 4-oxo-, butyl ester	172.22	6	5.5789E-06
Butanedioic acid, dibutyl ester	230.30	8	5.5626E-06
Hexadecanoic acid, methyl ester	270.45	15	2.7429E-06
9-Octadecenoic acid, methyl ester, (E)	296.49	16.9	1.0495E-05
Hexadecanoic acid, butyl ester	312.53	18	2.8483E-06
Octadecanoic acid, butyl ester	340.60	20	2.9039E-06
.alpha.-d-Ribopyranoside, methyl	164.16	2.5	4.2683E-06
.beta.-D-Ribopyranoside, methyl	164.16	2.5	4.2683E-06

*It is worth highlighting that according to GC/MS identification (by the NIST14 library), it was detected (with a probability of 93%) the presence of the phenolic monomer 5-(3-Hydroxypropyl)-2,3-dimethoxyphenol (an unusual compound in this kind of studies), an isomer of 4-n-propanolsyringol. As both isomers have the same m/z characteristic peaks due to the same way of ionization at m/z 212, 168, 153, 137 and 77, there is no evidence that this identification is reliable. Hence, according to the literature and the indications obtained by NMR results, the compound was identified as 4-n-propanolsyringol in the present work.

Table B. Yields (wt. % with respect to lignin in AS) of the main phenolic compounds identified (by NIST.14 library) in the produced oils (MSO and BSO before drying).

	Phenolic monomers yield (wt.% total lignin)									
Exp.#	**1**	**2**	**3**	**4**	**5,6,7**	**8**	**9**	**10**	**11**	**12,13,14**
Phenol	0.4	0.4	0.1	0.4	0.15 ± 0.02	-	-	-	-	-
3-methylphenol	0.1	0.2	0.1	0.1	0.088 ± 0.003	-	-	-	-	-
Benzoic acid, methyl ester	-	-	-	-	-	0.04	0.2	-	-	-
Guaiacol	0.2	2.5	0.5	0.7	0.50 ± 0.01	1.0	2.3	0.3	0.5	0.53 ± 0.01
4-ethylphenol	-	0.04	-	-	-	0.01	0.03	-	-	-
4-methylguaiacol (Creosol)	0.1	2.0	0.2	1.1	1.03 ± 0.05	0.1	0.7	0.4	0.8	0.55 ± 0.04
Catechol	1.0	1.9	1.1	1.3	1.4 ± 0.4	-	-	-	-	-
4-ethylguaiacol	0.1	1.2	0.5	2.7	1.7 ± 0.1	0.4	1.1	1.3	0.9	0.8 ± 0.1
4-propylguaiacol	0.02	0.3	1.4	6.2	3.51 ± 0.03	0.1	0.5	0.8	0.7	0.8 ± 0.1
4-allylguaiacol	-	-	-	-	-	0.1	0.1	-	-	-
Methylhydroquinone	0.1	0.3	0.1	0.2	0.07 ± 0.01	-	-	0.1	0.5	0.45 ± 0.01
Syringol	0.3	2.9	1.0	1.5	0.99 ± 0.03	1.7	3.3	0.4	0.8	0.63 ± 0.01
cis-4-propenyl guaiacol	-	-	-	-	-	0.1	0.1	-	-	-
trans-p-propenylguaiacol	0.04	0.2	-	-	-	0.8	0.5	-	-	-
Vanillin	0.3	0.6	-	-	-	0.2	0.1	-	-	-
4-methylsyringol	0.01	1.1	0.2	0.6	0.5 ± 0.2	0.3	0.8	1.9	0.4	0.34 ± 0.01
Homovanillic acid	-	-	-	-	-	-	-	-	0.1	0.038 ± 0.004
5-tert-Butylpyrogallol	0.2	1.8	1.0	0.4	0.8 ± 0.1	-	-	-	-	-
3,4,5-Trimethoxytoluene	-	-	2.4	4.2	2.3 ± 0.2	0.7	0.1	1.6	1.5	1.2 ± 0.1
Apocynin	0.1	0.3	-	-	-	0.1	1.4	0.1	0.1	0.13 ± 0.05
Benzoic acid, 4-hydroxy-3-methoxy-methyl ester	-	-	-	-	-	0.2	0.2	-	-	-
Guaiacylacetone	0.1	0.7	0.2	0.1	0.17 ± 0.01	0.3	0.3	0.4	0.5	-
Homovanillic acid methyl ester	-	-	-	-	-	0.1	-	-	-	0.2 ± 0.1
Benzenepropanol,4-hydroxy	-	-	-	-	-	-	-	0.3	0.2	0.33 ± 0.01
3,5-Dimethoxy-4-hydroxyphenethylamine	-	0.5	4.2	10.8	6.9 ± 0.3	0.2	1.4	2.1	1.9	1.9 ± 0.3

4-allylsyringol	-	-	-	-	-	0.2	0.2	-	-	-
1-(2-Hydroxy-4-methoxyphenyl)propan-1-one	-	-	-	-	-	-	-	0.3	0.3	0.34 ± 0.01
4-n-propanolguaiacol	0.1	0.8	11.3	11.3	11.2 ± 0.4	0.5	0.5	21.2	20.1	23 ± 1
trans-4-propenylsyringol	0.1	0.1	-	-	-	0.7	0.5	-	-	-
3-(3,4-Dimethoxyphenyl)-1-propanol	-	-	-	-	-	-	-	0.02	0.2	0.37 ± 0.02
Syringaldehyde	0.2	0.2	-	-	-	0.1	0.05	-	-	-
4-acetylsyringol	0.04	0.4	-	-	-	0.2	0.2	0.1	0.1	-
Propan-2-one, 1-(4-isopropoxy-3-methoxyphenyl)	-	-	-	-	-	0.1	0.2	-	-	-
Desaspidinol	0.1	0.3	0.1	0.2	0.18 ± 0.02	0.3	0.6	-	-	-
Homosyringic acid	-	-	-	-	-	-	-	0.1	0.05	-
4-n-propanolsyringol	0.1	0.4	8.2	6.2	6.2 ± 0.4	0.5	0.5	16.1	13.7	17 ± 1

Table C. Yields (wt. % with respect to holocellulose in AS) of the carbohydrate-derived compounds identified (by NIST.14 library) in the produced oils (MSO and BSO before drying).

	Carbohydrate-derived compounds yield (wt.% with respect to holocellulose in AS)									
Exp.#	**1**	**2**	**3**	**4**	**5,6,7**	**8**	**9**	**10**	**11**	**12,13,14**
Acetic acid, hydroxy-, methyl ester	-	-	-	-	-	0.4	3.4	0.1	0.6	0.32 ± 0.02
Propanoic acid, 2-hydroxy-, methyl ester, (±)-	-	-	-	-	-	0.1	0.2	0.1	0.3	0.15 ± 0.01
Butanoic acid, 2-hydroxy-, methyl ester	-	-	-	-	-	0.5	2.2	0.4	1.0	0.40 ± 0.03
Pentanoic acid, 4-oxo-, methyl ester	-	-	-	-	-	0.03	0.3	0.03	0.1	0.06 ± 0.02
Pentanoic acid, 5-oxo-, methyl ester	-	-	-	-	-	-	-	0.1	0.2	0.15 ± 0.01
Butanedioic acid, dimethyl ester	-	-	-	-	-	0.1	0.2	0.1	0.1	0.074 ± 0.002
Butanedioic acid, methyl-, dimethyl ester	-	-	-	-	-	0.02	0.1	-	-	-
Pentanedioic acid, dimethyl ester	-	-	-	-	-	0.1	0.3	0.3	0.01	-
Hexadecanoic acid, methyl ester	-	-	-	-	-	0.1	0.1	0.1	0.1	-
9-Octadecenoic acid, methyl ester,(E)	-	-	-	-	-	0.8	0.3	-	-	-
9,12-Octadecadienoic acid, methyl ester	-	-	-	-	-	0.6	0.4	-	-	-
Methyl stearate	-	-	-	-	-	-	-	0.4	0.4	0.44 ± 0.01
Acetic acid, butyl ester	8	45	25	33	28 ± 1	-	-	-	-	-
Butanoic acid, butyl ester	0.1	0.3	0.3	0.7	0.4 ± 0.1	-	-	-	-	-
Acetic acid, hydroxy-, butyl ester	0.5	2.1	0.4	0.3	1.19 ± 0.02	-	-	-	-	-
Propanoic acid, 2-hydroxy-, butyl ester	0.5	1.7	-	-	-	-	-	-	-	-
Pentanoic acid, 4-oxo-, butyl ester	0.05	0.4	-	-	-	-	-	-	-	-
Butanedioic acid, dibutyl ester	0.02	0.1	0.1	0.1	-	-	-	-	-	-
Hexadecanoic acid, butyl ester	0.01	0.04	0.03	0.1	0.037 ± 0.003	-	-	-	-	-
Octadecanoic acid	-	-	0.1	0.2	0.19 ± 0.02	-	-	-	-	-
Octadecanoic acid, butyl ester	-	-	0.05	0.2	0.15 ± 0.01	-	-	-	-	-
1-Hydroxy-2-butanone	-	-	1.2	0.5	4 ± 1	0.6	0.4	7	12	15 ± 1

4-Hydroxy-3-hexanone	-	-	0.7	-	-	-	-	0.3	1.4	0.9 ± 0.1
2,5-Hexanedione	0.3	1.6	1.2	2.1	1.4 ± 0.1	-	-	-	-	-
meso-3,4-Hexanediol	-	-	-	-	-	-	0.2	2.6	4.2	4 ± 1
1,2-Butanediol	-	-	-	-	-	-	-	0.4	2.0	1.1 ± 0.1
Butanoic acid, 4-hydroxy-	-	0.1	1.1	0.4	-	-	-	-	-	-
Furfural	1.3	-	-	-	-	0.3	0.3	-	-	-
2-Furanmethanol	-	-	1.2	0.3	0.3 ± 0.1	0.3	0.5	0.2	2.4	0.7 ± 0.1
2-Furanol, tetrahydro-2-methyl	-	-	1	-	-	-	-	-	4.0	0.70 ± 0.04
2-Furancarboxaldehyde, 5-methyl-	0.2	-	-	-	-	-	-	-	-	-
Methyl 2-furancarboxylate	-	-	-	-	-	0.1	0.3	0.4	0.3	0.29 ± 0.03
Butyl ether	0.7	0.6	-	-	-	-	-	-	-	-
Butane, 1,1-dibutoxy	3	16	8	7	7 ± 1	-	-	-	-	-
.alpha.-d-Ribopyranoside, methyl	-	-	-	-	-	0.02	0.05	0.01	0.01	0.010 ± 0.001
.beta.-D-Ribopyranoside, methyl	-	-	-	-	-	0.01	0.4	0.1	0.1	0.03 ± 0.01
2-Cyclopenten-1-one, 2-methyl	0.03	0.4	-	-	-	0.01	0.2	-	0.3	-
Cyclopentanone	-	-	0.03	0.2	-	-	-	0.04	0.2	0.072 ± 0.002
Cyclopentanone, 2-methyl-	-	-	1.5	0.9	0.6 ± 0.2	-	-	0.03	0.8	0.23 ± 0.01
Cyclohexanone, 2-hydroxy-	-	-	0.1	0.1	0.07 ± 0.01	-	-	0.01	0.1	0.08 ± 0.01
1,2-Cyclopentanedione, 3-methyl-	0.1	-	-	-	-	0.005	0.3	-	-	-
2-Cyclopenten-1-one, 2-hydroxy-3,4-dimethyl-	-	-	0.01	0.1	0.024 ± 0.004	0.004	0.3	-	-	-
2-Cyclopenten-1-one, 2-hydroxy-3-methyl-	0.01	0.2	-	-	-	-	-	-	-	-
2-Cyclopenten-1-one, 2,3-dimethyl-	0.3	0.2	0.1	-	0.11 ± 0.01	-	-	-	-	-
2-Acetonylcyclopentanone	0.002	0.1	0.3	0.3	0.29 ± 0.01	-	-	-	-	-

- HSQC-NMR spectroscopy

HSQC-NMR spectroscopy has been widely used during the last years to characterize lignin, providing valuable information for its structural characterization.[3][4][5][6][7]

Quantitative HSQC experiments were run using by Two-Dimensional Extrapolated Time-Zero $^{1}H-^{13}C$ HSQC ($HSQC_0$) experiment running the pulse programs downloaded from the National Magnetic Resonance Facility at Madison University[8], according to Hu et al.[9] Samples for HSQC experiments were prepared at *ca.* 10 %w/v. DOSY was run using the *stebpgp1s* pulse program in QF acquisition mode. Diffusion delay (*d20*) in *stebpgp1s* was optimized using residual DMSO signal keeping gradient pulse length (*p30*) constant at 1000 □s, resulting in 160 - 170 ms. Each pseudo-2D experiment consisted of a series of 16 spectra. DOSY experiments were done in DMSO-d_6 at 300 K and fixed low concentrations, 1 % w/v. The accuracy of the gradient was checked by the determination of the diffusion coefficient of residual DMSO in DMSO-d_6. DOSY analyses were processed using TOPSPIN 3.6.2 software from Bruker. Once F2 was phased, automatic baseline correction was run using a 5th-grade polynomial function. Using the T1/T2 relaxation module installed in the module permitted FID for the first spectrum (2 % gradient) to be extracted and to perform manual integration. The integration regions were exported to the relaxation module, where decay values were fitted by area using the *vargrad* preinstalled function with a 5.35 G/mm gradient calibration constant. Graphical processing was run using Bruker's 'Dynamic Center v. 2.6.1' software. Unless otherwise stated, the Stejskal-Tanner equation was fitted using the intensity obtained after the peak peaking of the first spectrum corresponding to a 2 % gradient.

[3] Wen, J. L., Sun, S. L., Xue, B. L., & Sun, R. C. (2013). Recent advances in characterization of lignin polymer by solution-state nuclear magnetic resonance (NMR) methodology. Materials, 6(1), 359–391. https://doi.org/10.3390/ma6010359

[4] Rencoret, J., Marques, G., Gutiérrez, A., Nieto, L., Santos, J. I., Jiménez-Barbero, J., Martínez, Á. T., & del Río, J. C. (2009). HSQC-NMR analysis of lignin in woody (Eucalyptus globulus and Picea abies) and non-woody (Agave sisalana) ball-milled plant materials at the gel state. Holzforschung, 63(6), 691–698. https://doi.org/10.1515/HF.2009.070

[5] Zeng, J., Helms, G. L., Gao, X., & Chen, S. (2013). Quantification of wheat straw lignin structure by comprehensive NMR analysis. Journal of Agricultural and Food Chemistry, 61(46), 10848–10857. https://doi.org/10.1021/jf4030486

[6] Kuznetsov, B. N., Chesnokov, N. v., Sudakova, I. G., Garyntseva, N. v., Kuznetsova, S. A., Malyar, Y. N., Yakovlev, V. A., & Djakovitch, L. (2018). Green catalytic processing of native and organosolv lignins. Catalysis Today, 309(December 2017), 18–30. https://doi.org/10.1016/j.cattod.2017.11.036

[7] Hu, G., Cateto, C., Pu, Y., Samuel, R., & Ragauskas, A. J. (2012). Structural characterization of switchgrass lignin after ethanol organosolv pretreatment. Energy and Fuels, 26(1), 740–745. https://doi.org/10.1021/ef201477p

[8] https://nmrfam.wisc.edu/pulse-programs-bruker/

[9] Hu, K., Westler, W. M., & Markley, J. L. (2011). Simultaneous Quantification and Identification of Individual Chemicals in Metabolite Mixtures by Two-Dimensional Extrapolated Time-Zero 1H−13C HSQC (HSQC0). Journal of the American Chemical Society, 133(6), 1662-1665. doi: 10.1021/ja1095304.